THROUGH DRYING OF PAPER

by

Osman Polat

A Thesis submitted to the Faculty of Graduate Studies
and Research in partial fulfillment of the
requirements for the degree of
Doctor of Philosophy

Department of Chemical Engineering
McGill University
Montreal

April 1989

To

Suna, Barış Erinç and Ayşe Bikem

ABSTRACT

The first comprehensive set of measurements is obtained for rates of through drying paper with all drying conditions measured and controlled Complete pressure drop-drying rate curves are determined for 235 handsheets of kraft paper of basis weights 25-150g/m^2 dried in air over a wide range of temperatures and throughflow rates

The previous procedure of calculating permeability by Darcy's law is substantially in error at relevant throughflow rates. A new characteristic dimension for flow through both dry and moist paper is determined by application of fundamental momentum transport principles. During through drying the value of this d_f drops substantially from an upper to a lower asymptotic limit, shown to correspond to known water-fibre relations A theoretically based Re-f-d_F treatment is shown to be a more powerful method than those used previously

A comprehensive, tested correlation for through drying rates in the constant rate period is reported Through drying is demonstrated to start with an increasing rate period during which, for industrial conditions, about half the water is removed An original treatment, "drying period diagrams", shows the extent of the increasing, constant and falling rate periods as a function of drying conditions The concept of an increasing-constant-falling rate triple point, X_{ICF}, shows that typically there will be no constant rate period for industrial conditions of through drying light weight paper of low moisture content.

Sherwood number is calculated for the constant rate period of drying using the characteristic dimension and interfacial transfer area for moist paper determined by momentum transfer analysis. Sherwood number is related to drying conditions and to transport phenomena within the sheet.

Through drying rates are successfully predicted by a model which treats the process as three drying periods, i.e. increasing, constant and falling rate, with a variable specific surface of paper.

RESUME

La premiere serie comprehensive de mesures est obtenue pour le taux de sechage de papier par air traversant, toutes les conditions de sechage etant mesurees et controlees Les courbes completes de perte de charge et de taux de sechage sont determinees pour 235 feuilles de papier kraft de grammage 25-150g/m^2, en utilisant une vaste gamme de temperature et de debit d'air

La methode anterieure utilisant la loi de D'Arcy pour le calcul de la permeabilite est considerablement erronee pour les debits pertinents Une nouvelle dimension caracteristique, d_p, pour l'ecoulement traversant le papier humide ou sec est determinee en appliquant les principes fondamentaux du transport de la force vive Durant le sechage, la valeur de d_p decroit considerablement d'une haute à une basse limite asymptotique, limites qui correspondent aux relations connues entre les fibres de papier et l'eau Un traitement theorique avec la relation Re_f-d_p s'avere plus efficace que les methodes anterieures

Pour les taux de sechage durant la periode de taux constant, on presente une correlation comprehensive et verifiee On demontre que le sechage par air traversant commence par une periode de croissance de taux Dans les conditions de sechage industriel, presque la moitie de l'eau serait enlevee pendant cette periode Un traitement original nomme "diagramme des periodes de sechage" montre l'etendue des periodes de croissance, de constance et de decroissance du taux de sechage en fonction des conditions le concept d'un point triple de la croissance-constance-decroissance du taux de sechage, X_{ICF}, montre que typiquement il n'y aura pas de periode de taux constant avec les conditions utilisees dans les sechoirs industriels par air traversant pour le papier ouate avec faible humidite

Le nombre de Sherwood est calcule pour la periode de taux constant en utilisant la dimension caracteristique et la surface specifique de transfert interfaciel pour le papier humide, celles-ci etant determinees par une analyse de transfert de la force vive. Le nombre de Sherwood est relie aux conditions de sechage et aux phenomenes de transfert à l'interieur de la feuille

Les taux de sechage par air traversant sont predits correctement avec

un modèle comprenant trois périodes de séchage, celles de croissance, constance et décroissance de taux, avec la surface spécifique de papier qui est variable

ACKNOWLEDGEMENTS

I would like to express my gratitude to Dr W J.M Douglas for his constructive advice, financial support, continuous encouragement and enthusiasm during the course of this work

I would also like to thank my co-supervisor Dr. R H. Crotogino for his expert advice, guidance intresting discussions and suggestions throughout all stages of this project

Special thanks must go to my research group committee members· Dr. A.S Mujumdar, Dr. A R P. van Heiningen, Dr Bing Huang, Cemal Ercan and Ian Journeaux for their useful suggestions, stimulating discussions and friendship

I am particularly indepted to

Mr A. Krish, Mr D P W Pounds, machine shop personnel in the Department of Chemical Engineering and Pulp and Paper Research Institute of Canada for their help in construction of the experimental facility

Dr A M Scallan for fibre saturation point measurements

Ms G. de Silveira for the scanning electron micrographs.

Mr W Bichard for his assistance and advice during sample preparation

Mr L. Heffell for supplying the laboratory kraft pulp.

The Pulp and Paper Research Institute of Canada for the use of their facilities and services, and for financial support through S.G. Mason, 1981-82, F L Mitchell, 1982-83 and 1983-84, fellowships and a merit award, 1986

Paper Industries Management Association for their scholarship, 1982, support.

A special word of thanks goes to many friends especially Dr. A. Jeff Giacomin, Gunter Lohfink, A Turgut Mutel, Lorraine J Pelletier and Tony Samurkas for their sincere friendship

Last, but not least, I would like to thank my mother, my late father, my wife-colleague-friend, Suna, and my children, Barış Erinç and Ayşe Bikem, for their love, patience, understanding and continuous moral support.

TABLE OF CONTENTS

LIST OF FIGURES

LIST OF TABLES

NOMENCLATURE

A	surface area, m^2, also a constant defined in Table 4.13
A'	a constant
A_f	wall effect factor in f definition
a, a'	constants
a_P, a_P'	specific surface, m^2/m^3 and m^2/g respectively
Ar	Archimedes number, $d_P^3 g\rho(\rho_P-\rho)/\mu^2$
B	a constant defined in Table 4 13
b, b'	constants
C	inertial constant, also a constant
C_P	specific heat capacity, kJ/kgK, C_a, C_{PY}, C_v, C_W dry air, moist air, water vapor and water heat capacities
c	a constant, also c_o, c', c_1, c_2 constants
D	column or channel diameter, m
$\mathcal{D}$	molecular diffusion coefficient, m^2/s
D_x	axial dispersion coefficient, m^2/s
D_P	pore diameter, m
Da	Darcy number defined in Table 4 11
d, d'	constants
d_{eq}	Hagen-Poiseuille equivalent channel diameter, m
d_f	fibre diameter, m
d_P	characteristic dimension, m; d_P^* characteristic dimension used in Fanning friction factor definition
E	elastic modulus of fibers, Pa
F	force, N
f	friction factor; f^* Fanning friction factor; f_{fk} kinetic

	friction factor defined in Eqn. 2 14; f_v viscous friction factor defined in Eqn 2.13
f_1, f_2	ε and N_e functions in Eqn 2 15
G	mass flow rate, kg/m^2s
H_G	height of a transfer unit, m
h	heat transfer coefficient, W/m^2K
Δh	latent heat of vaporization, kJ/kg, Δh_o at 0°C
Δh_A	heat of adsorption of water on fibres, kJ/kg
j_D	Chilton-Colburn j-factor for mass transfer, $Sh/(Re\ Sc^{1/3})$
j_H	Chilton-Colburn j-factor for heat transfer, $Nu/(Re\ Pr^{1/3})$
j_m	dimensionless mass transfer coefficient
K	kinetic energy per unit volume, N/m^2
k	permeability, m^2, k' Darcy permeability
k_f	thermal conductivity of solid
k_G	mass transfer coefficient, m/s; k_G' molar transfer coefficient, $moles/m^2s$, $k_G'^*$ transfer coefficient corrected for high mass transfer rates
k_m	mass transfer coefficient based on external area, m/s
k_o	shape factor
L	bed or paper thickness, m
L_e	actual pore length, m
M	molecular weight, kg/kg moles
M_B	basis weight, g/m^2
m	average hydraulic radius of the medium, m; m_i hydraulic radius of the individual capillaries; also a constant in Eqn. 4.1
N	number of sheets tested
N	mass flux, kg/m^2s

N_d deflection number defined in Eqn. 2.15

N_e effective pore number

N_G number of transfer units

Nu Nusselt number

n number of moles and also a constant

n molar flux, moles/m²s. n_w, n_a water vapor and air respectively; and also unit normal vector

P pressure, Pa

ΔP pressure drop, Pa

p a constant

p_v partial pressure, Pa; p_v^* vapor pressure

Pe Peclet number, ReSc, Pe_x, axial dispersion Peclet number, $Pe(D/D_x)$

Pr Prandtl number

q a constant, q_1 size distribution parameter

R drying rate, kg/m²h, R_c constant drying rate, R_s maximum attainable drying rate, i.e. at saturation conditions; also gas constant, kgm²/s²kgmolK

Re Reynolds number, Re^* defined using d_p^*

Sc Schmidt number

Sh Sherwood number

T temperature, °C; T_A air, T_i throughflow inlet, T_S and T_{WB} wet bulb, T_P paper temperatures

ΔT temperature driving force, K, ΔT_i at inlet conditions, i.e. $T_i - T_S$

t time, s

Δt elapsed time, s

u velocity, m/s, u_S superficial velocity, Std. m³/m²s

V averaging volume, m³, V_b bulk volume

V_S volumetric flow rate, Std. m^3/min

v interstitial velocity vector, m/s

v' fluctuating component of the interstitial velocity vector, m/s

W a parameter used by Pfeffer[1964]

X paper moisture content, kg/kg dry fibre; X_o initial moisture content; X_{eq} equilibrium moisture content; X_C, X_{C_i}, X_{Cf} critical, initial and final critical moisture contents respectively; X_{ICF} triple point

Y air humidity, kg/kg dry air; Y_i, Y_o at the inlet and exit of the sheet respectively, Y_s at saturation; Y_W^*, $Y_{W\infty}$ at surface and in the bulk phase respectively

ΔY humidity driving force, kg/kg dry air, ΔY_i, ΔY_o, ΔY_M at the inlet, exit and log mean respectively

y_W mole fraction of water, moles/moles dry air, y_W^*, $y_{W\infty}$ at surface and in the bulk phase respectively

z z coordinate

α viscous parameter in momentum equation, $1/m^2$

α' viscous parameter for moist sheet in momentum equation, 1/m

β inertial parameter in momentum equation, 1/m

β' inertial parameter for moist sheet in momentum equation

Γ system time constant defined in Appendix 1, s

γ a constant

ε porosity

κ Kozeny constant

μ dynamic viscosity, Pa s; μ_o at the temperature of the solid surface

ν	kinematic viscosity, m^2/s
ξ	ratio of average channeling length to particle diameter
ρ	density, kg/m^3; ρ_a air density; ρ_b bulk density; ρ_f fibre density; ρ_p apparent paper density
σ	standard deviation
τ	tortuosity
Φ	shape factor in Eqn 2.17
ϕ	mass transfer rate factor
ψ_1	particle shape parameter
ω	vapor pressure depression factor

CHAPTER 1

INTRODUCTION

Interest in the through drying of paper is stimulated by the potential for higher drying rate-lower drying cost for light weight grades of paper. Maximum removal of water in the press section is advantageous economically through reduction in the amount of water removed by drying, but produces a stiffer paper, undesirable for some product grades. "Soft" sanitary grades of paper can be produced by sending the wet sheet from the forming fabric directly to drying. Through dryers facilitate the production of soft or creped grades of tissue paper. Thus the technique of through drying is becoming a preferred method of drying light weight grades of paper, Villalobos [1986].

The high rate of through drying derives from the drying medium being in contact with the wet material throughout the bed or web, rather than only at the external surface Flow of drying medium through the moist material reduces both the distance through which heat must be transferred to the wet solid and that moisture must diffuse before evaporating into the drying medium Applicability of through drying is evidently limited by the permeability of the porous wet material. For the case of a web of limited permeability, drying rates may be enhanced by combination of other drying processes with through drying. The "Papridryer" technique proposed by Burgess *et al.*[1972a, b] for drying newsprint would constitute such a dual process, i.e. combined impingement and through drying.

Although the concept of through drying is simple, the interrelation

between the several physical processes governing the drying rate is not yet established. The few attempts to develop a basic understanding of the through drying of permeable webs such as paper and textiles provide incomplete and contradictory results

Chu and Kuo[1967] for tissue paper, Walser and Swenson[1968] for 86g/m^2 paper, and Martin[1972] for 100 g/m^2 handsheets reported drying rates from their laboratory through dryers Because their experimental techniques permitted large charges in air throughflow rates, interpretation of these results is difficult The drying rate curves of Chu and Kuo reflect a combination of drying and mechanical dewatering. In mill trials Walser and Svenson could not detect a basis weight effect on drying rates of paper in the range 52-147g/m^2, evidently due to shortcomings of the measurement technique required with the industrial installation. Raj and Emmons[1975] dried paper of 13-64g/m^2 basis weight with ambient temperature air in their laboratory through dryer but as their analysis of through drying contains several errors, the results do not clarify this process

In development of their through drying models Rohrer and Gardiner [1976] considered air flow through the web as analogous to turbulent flow through ducts, while Wedel and Chance[1977] analysed it as an external flow over a cylinder, neither of which is realistic. Neither study documented any experimental data

Although he used tissue paper without significant change in a key variable, basis weight, Gummel[1977] came closest to providing laboratory through drying rates with throughflow rate controlled rather than variable as in the other investigations. Gummel's experimentally measured transfer coefficients are lower than those he calculated from

empirical relations developed for laminar flow with entrance effects, a discrepancy which he explained in terms of pore size distribution and uneven drying due to permeability variation His results do however clearly indicate that the throughflow air leaves the sheet at a humidity substantially below saturation. In spite of the evidence from Gummel's study that throughflow air remains significantly below saturation, the absence of precise information and reliable correlations in this regard has resulted in continued use of the assumption of saturated exit throughflow by all those who have attempted to model this process. Crotogino and Allenger[1979] and Soininen[1987].

Rates of through drying have yet to be analyzed in terms established for heat and mass transfer in packed beds Even for beds of particles as simple as spheres, when the particle size becomes very small and the Reynolds number correspondingly low, experimental Sherwood and Nusselt number measurements are anomolously low. Various researchers have been observed this decrease in Sh or Nu with decreasing particle size - decreasing Re There is as yet no proven quantitative model which explains this effect. and which could be applied to predict heat and mass transfer rates reliably for the through drying of paper

Work to date on the through drying of paper is then characterized by oversimplified approaches and contradictory results. Because of shortcomings in the design of the previous laboratory experiments, there exists no reliable set of experimental data on through drying rates of paper and the associated momentum transport. A fundamental analysis of through drying paper requires a data set measured over a

significant range of the relevant parameters of the throughflow, i.e. its temperature and flow rate, and those of the paper, i.e. its basis weight and initial moisture content. Nor is there available a quantitative, tested description of the combined momentum, heat and mass transport phenomena involved in through drying, as the basis of fundamentally based, reliable design procedures for through dryers. Because of the increasing industrial importance of through drying of paper, alone or potentially in combination with other drying techniques, the present study was undertaken with the following objectives:

1. To design a laboratory through dryer experimental facility with which the momentum, heat and mass transfer aspects of through drying can be measured simultaneously, under conditions where all relevant variables are controlled and monitored throughout such transient experiments, with the capability to vary these parameters over a wide range.

2. With this equipment, to obtain an extensive and reliable set of through drying measurements under wide-ranging conditions, as the basis for an analysis of the simultaneous transport phenomena involved.

3. To analyze the rate of through drying paper in terms of the simultaneous momentum, heat and mass transport phenomena involved, with the objective of obtaining a fundamentally based rate model.

CHAPTER 2

LITERATURE REVIEW

2.1 INTRODUCTION

Major improvements in the technology of drying paper are more likely if the fundamental aspects of the associated flow, heat and mass transfer processes are understood The objective of this work is to contribute to this understanding for the case of through drying With this ultimate objective, the current technology of papermaking is first summarized In through drying paper the momentum, heat and mass transport occur in a porous media of great complexity Thus the porous structure of paper is reviewed, as are aspects of flow, heat and mass transfer in porous media

2 2 PAPERMAKING

2.2.1 Papermachine Operations

The four primary papermaking operations occuring in a fourdrinier paper machine, Fig. 2 1, are (i) formation and drainage, involving the headbox and fourdrinier screen (ii) pressing (iii) drying (iv) calendering. In sheet formation a fibre-water suspension of 0.2-1.0% fibres is delivered to a forming screen or fabric where, with the combined action of gravity, suction, pressure and/or centrifugal forces, water is drained and a web of about 18-23% fibres is formed. More water is removed mechanically in the pressing section where, with about 33-55% fibres, web consolidation starts. Drying to a final moisture content of 6-9% is most frequently achieved by contact heat transfer from a series of steam heated cylinders. Drying is the key process in conso-

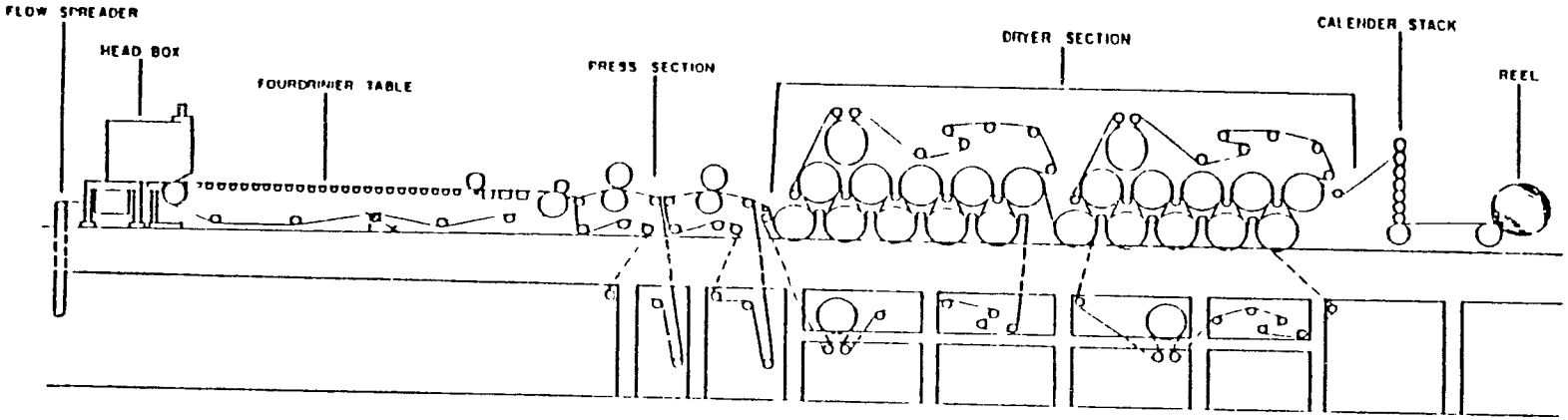

Figure 2.1 Fourdrinier paper machine.

lidation of the fibre mat, during which the properties of the sheet are developed. The surface properties of the sheet are improved by compressing it in the nips of calender rolls, generally the final operation of papermaking except for winding on a reel. For some grades of paper there are additional finishing operations such as off-machine coating and/or supercalendering prior to the paper being cut to the desired width and rewound for shipment.

Through drying and impingement drying are drying processes alternate to the most common method, contact drying over steam heated cylinders. For light weight tissue paper, the web is taken off the forming fabric at a much lower fibre content, typically 10% When pressed to the surface of an impingement dryer after the presses, such paper will contain about 40% fibres On some paper machines for soft tissue, the sheet is not pressed but is taken from the forming fabric directly onto a through dryer, in which case the sheet enters the dryer at a fibre content of only 15-20%.

2.2.2 The Dryer Section

As drying is the most energy-intensive, costly step in papermaking, there is great economic incentive for drying system improvement. The steam-heated cylinder technique has remained the primary drying process since 1817, when John Dickinson built a steam-heated cylinder for drying paper continuously. The trend to higher paper machine speeds, lower basis weights and less expensive raw materials is pushing the multi-cylinder dryer beyond its limits, Crotogino[1975]. The production capacity of tissue machines is now frequently dryer limited.

Two drying processes in which heat transfer is primarily by convec-

tion, i.e. impingement drying and through drying, Fig. 2.2, have been developed as alternatives to cylinder drying where the sheet receives heat by contact heat transfer. Drying rates of ~100kg/m^{2}h can be achieved by a modern high-velocity (u_j>100m/s), high-temperature ($T_i \geq 420°C$) impingement dryer. Impingement dryers are widely accepted in two important applications, the drying of coatings and drying of tissue and machine-glazed(MG) papers in conjunction with Yankee and MG cylinders. Fig. 2.3a shows a tissue machine with creping drying for sanitary papers, and Fig 2 3b, a paper machine with an impingement dryer for MG 18-55g/m^2 packing paper In such applications, i.e combined impingement and steam-heated cylinder drying, drying rates may be as high as 175-200 kg/m^{2}h The other use of convection heat transfer is for through drying, in which the hot drying air flows through a permeable web. Soft tissue may be made by some combination of through drying and contact/impingement drying Burgess *et al.*[1972a,b] investigated the possible combination of impingement drying and through drying for newsprint, but this did not lead to a commercial process.

Current through dryers are of two configurations, rotary through dryers and flat bed dryers. The rotary type has an open, perforated, cylinder enclosed in a hood, with air flow either into or out of the cylinder. For the configuration with the air drawn through the web and into the cylinder by vacuum, no sheet support is needed For the alternate configuration with air flow from a pressurized cylinder, the sheet must be held on the cylinder with a very open fabric.

In the flat bed design of through dryer there is a fabric support, conveying structure and top and bottom air chambers. The supply air can be applied through either chamber depending upon the design and process

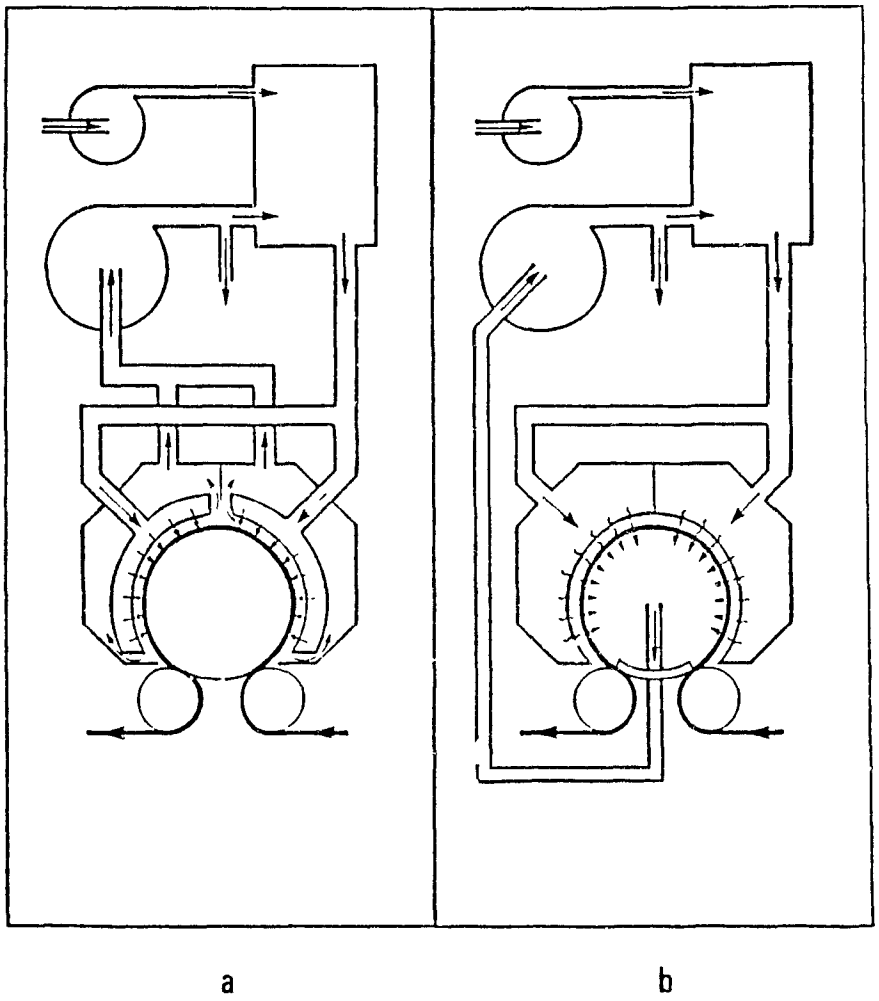

Figure 2.2 Convective paper dryers: a) impingement dryer, b) through dryer.

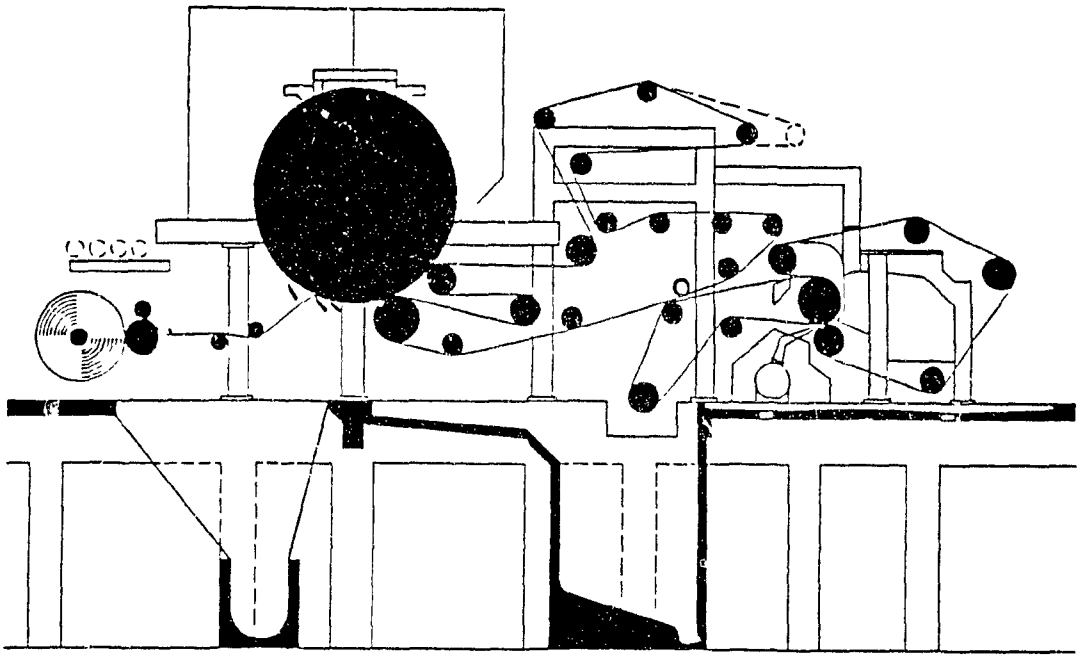

a

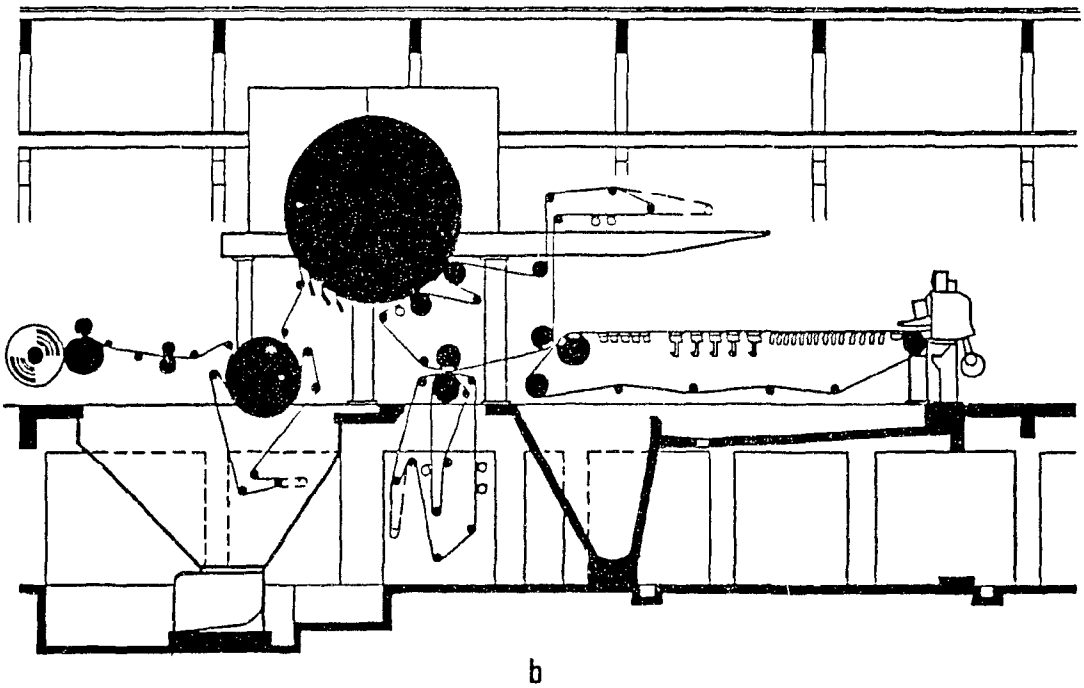

b

Figure 2.3 Paper machine with: a) creping dryer for sanitary paper b) Yankee impingement dryer for MG paper.

conditions. The flat bed arrangement is particularly suited to highly permeable products for which the pressure differential required is low, Villalobos[1975].

High throughflow rates for permeable sheets make high drying rates possible, at the same time virtually eliminating "one-sidedness" and cross-machine variations in the product. Through dryer thermal efficiencies have been increased to 80% with the use of several drying stages and air recycling or cascade systems. Vacuum cylinders of diameter to 6.7m and width to 7.6m operate at paper machine speeds to 30m/s and air temperatures of 370-430°C in recent applications. Villalobos[1986] reports through drying rates of 100-200kg/m^{2}h for normal operation, and to as high as 350-500kg/m^{2}h.

2.3 STUDIES ON THROUGH DRYING OF PAPER

In through drying, higher drying rates derive from the drying medium being in contact throughout the wet web rather than only at the external surface. Flow of the drying medium through the moist material reduces the distances through which heat must be transferred and that moisture must diffuse before evaporating into the drying medium. The interrelation between the several physical processes governing the drying rate is not yet established The few attempts to develop a basic understanding of the through drying of permeable webs such as paper and textiles have provided contradictory results.

In their laboratory study, Chu and Kuo[1967] proposed different mathematical models for each of the three drying periods they distinguished according to the mechanism controlling water movement, i.e., simultaneous two phase flow (mechanical dewatering), capillary action,

and diffusion. The proposed models agreed reasonably well with their experimental data on through drying of tissue paper at T_1=21° and 82°C for the throughflow rate range of $0.8 \leq G \leq 3.3 kg/m^2 s$. However their drying rate curves reflect a combination of drying and mechanical dewatering at these high throughflow rates An energy balance around their drying systems reveals that the effect of mechanical dewatering was present at moisture contents as low as 25%. Because their experimental technique permits a large change, >40%, in air throughflow rate, interpretation of these results is difficult

Walser and Swenson[1968] reported through drying rates from both laboratory scale equipment and mill trials Their laboratory results, limited to single basis weight, $86 g/m^2$, obtained with two $43 g/m^2$ sheets, have the same interpretation problem as Chu and Kuo's work due to a change of air throughflow rate by more than 100%. In their experimental range, i.e. $60 \leq T_i \leq 260$°C and $0.05 \leq u_s \leq 0.25 m/s$, they found that air leaves the $86 g/m^2$ sheet saturated during the constant rate period of drying. In mill trials with filter paper, toweling and open kraft grades of basis weight $52\text{-}147 g/m^2$, they could not detect basis weight effect, which may have been obscured by the additional drying from air swept over the sheet in the draws

Martin[1972] measured rates of through drying of $100 g/m^2$ handsheets in his laboratory dryer by applying constant vacuum across the sheet. The throughflow rate therefore changed 3-5 fold during each experiment and, moreover, the rates measured were simply averages over the entire drying cycle.

Raj and Emmons[1975] investigated the through drying of paper of basis weight $13\text{-}65 g/m^2$ and high porosity, 0.86-0.89, at ambient tempe-

ratures. Whether they maintained the rate of throughflow air constant in their laboratory scale through dryer is not specified. The accuracy of their measurements, i.e. monitoring the weight of sample and holder, was substantially reduced by a high noise to signal ratio, 0.1, and corrections needed for the time lag introduced by the spring dashpot system used to damp the noise They reported a correlation for a non-dimensional mass transfer coefficient, defined as $k_G \rho_a / G$, as a function of Peclet number to the power -0.8 As the Peclet number characteristic dimension, they used the square root of Darcy permeability of the dry sample, a choice which subsequent work establishes is too small by about a factor of 10. On this basis they concluded that the flow through paper was laminar.

Rohrer and Gardiner[1976] went to the other extreme in considering air flow through the web as analogous to turbulent flow through ducts. In an industrial through dryer, they measured only the parameters needed in their model and claimed, without any supporting evidence, that their derived heat transfer expression agreed well with their experimental data for highly permeable products

Wedel and Chance[1977] analysed the flow of air in through drying as an external flow over a cylinder, a model which bears little relation to the role of the complex structure of the pores through which flow occurs. They claimed that their calculations agreed well with their laboratory experimental data, which they did not document, as well as with those of Walser and Swenson[1968]. However, for their experimental conditions the exiting throughflow air became saturated, which provides a very insensitive test of any model.

The through drying rates measured by Gummel[1977] for 20 and

$23 g/m^2$ paper at a constant throughflow rate of air in his laboratory through dryer are considerably lower than would correspond to the exiting throughflow reaching adiabatic saturation. In contrast to the turbulent duct flow model of Rohrer and Gardiner, Gummel explained his experimental findings for textiles and very thin tissue products in terms of a laminar internal flow with entrance effects. However, theoretically predicted drying rates for that type of flow were substantially higher than those he measured experimentally. Gummel explained this discrepancy in terms of the pore size distribution of the material and uneven drying due to permeability variations.

The diverse and oversimplified approaches of studies to date, and the inconclusive and contradictory results from these investigations have not led to an understanding of the basic transport processes involved in the through drying of paper Raj and Emmons[1975], Rohrer and Gardiner[1976] and Gummel[1977] analysed the through drying phenomena as analogous to an internal flow through ducts, but as either pure viscous flow or pure turbulent flow, while Wedel and Chance[1977] chose the model of external flow over smooth cylinders. None of these simplifications seems warranted. Also, deficiencies in the design of the various laboratory experiments are such that not a single, reliable set of experimental data exists in which through drying rates have been documented over a significant range of conditions of the throughflow, i.e. its temperature and flow rate, and conditions of the paper, i.e. its thickness and initial moisture content.

2.4 FLOW THROUGH POROUS MEDIA

2.4.1 Viscous Flow

Flow through paper can be described by general relations applicable to porous media, but a controlling factor in their use is the exceptional complexity of the flow channels provided by the porous structure of paper. Rigorous analytical solutions for flow through porous media of a simple, regular and rigid structure are unrealistic for the case of paper, where the individual fibres are of great irregularity and are of dimensions highly dependent on moisture content. In his treatment of pore space models for transport coefficients such as permeability and effective diffusion coefficient, van Brakel[1975] critically reviews the one, two and three dimensional models as well as the non-pore space models such as discrete particle, statistical dynamics, irreversible thermodynamics, and continuum models. Jackson and James[1986] reviewed experimental and theoretical studies of permeability of fibrous porous media but, because of their interest in highly porous media (ε>0 90), the models cited are based on drag theories which are variants, extensions or generalizations of Stokes' law. The extensive review of single phase flow through porous media by Dullien [1975] is more relevant to the range of porosities in paper.

Of the two fundamentally different approaches to modelling this phenomena, i.e. as a flow inside conduits or flow around solid objects, the former has found more success for packed beds, Bird *et al.*[1960]. There are also so-called phenomenological models, e.g. Rumpf and Gupte [1971], derived by empiricism aided by dimensional analysis and other theoretical considerations, that are equally applicable to internal or external flows, whichever is the more appropriate. There are three

variants of theconduit flow approach: (i) geometrical models, (ii) statistical models, (iii) models utilizing the complete Navier-Stokes equation. Statistical models are not reviewed because the knowledge of the complex paper pore structure, necessary for this theoretical approach, is not available. Only models closely related to the present work, i.e. geometrical models, because of their wide applicability to porous media, and some models using solutions of the Navier-Stokes equation, because of their sound theoretical basis, are summarized. Broader treatments are available in the review articles of van Brakel [1975] and Dullien[1975], and in the standard reference books, Carman [1956], Bear[1972], Scheidegger[1974]

The resistance of a porous medium to the passage of a single-phase fluid is customarily expressed by Darcy's law (Darcy[1856])

$$u = - (k'/\mu) \frac{\Delta P}{L} \tag{2.1}$$

where u is superficial velocity, L bed thickness and k' is generally referred as to specific permeability, Darcy permeability or simply permeability. Barring unusual effects, for sufficiently low flow rate k is uniquely determined by pore geometry

Kozeny[1927] introduced his well known hydraulic radius theory for viscous flow through tortuous tubes, which was later corrected by Carman[1937] to relate permeability to porosity and to the internal specific surface of the porous structure as

$$k' = \frac{\varepsilon^3}{k_o (L_e/L)^2 (1-\varepsilon)^2 a_p^2} \tag{2.2}$$

The combined variable $\kappa = k_c (L_e/L)^2$ is often referred as the Kozeny constant and L_e/L as tortuosity. According to Carman, 5.0 is the best value for κ to fit most experimental data.

Kozeny theory for viscous flows represents the porous medium by an

assemblage of channels of variable cross-section but of a definite length. It is further assumed that in a cross-section normal to the channels there is no tangential component of fluid velocity, a restriction strongly criticized by Scheidegger[1974]. Other restrictions inherent to all hydraulic theories including this one, (Carman [1941, 1948]), include the assumptions that all pores are open to flow and are randomly distributed, that diffusion (slip) phenomena are absent, and that the porosity is not too high, $\sim\varepsilon\leq 0.80$,

The Kozeny-Carman equation is particulary useful in measuring the surface area of powders Dullien[1975] notes that the Kozeny-Carman equation should be applied only with caution for particles that deviate strongly from spherical, for wide particle size distributions and for consolidated media, a set of specifications which describe paper eminently well. One reason for lack of agreement between permeabilities predicted by this equation and experimental values relates to the aspect of tortuosities, but adjustment of the tortuosity factor to make the equation fit is also unsatisfactory

Carman[1956] claimed that even though pore size distribution is nonuniform, two points favoring the Kozeny equation are:

(i) if the range of pore size is not too great, say less than 2:1, alternate averages lead to much the same result. In $k=\varepsilon m^2/\kappa$, m being the average hydraulic radius of the medium, Kozeny's approach gives $1/m=\langle 1/m_i\rangle_{av}$. However if pore sizes are taken as non-uniform, then $\langle m_i^2\rangle_{av}>1/\langle 1/m_i\rangle_{av}^2$, where m_i is the hydraulic radius of the individual capillaries. Carman notes the small difference between these two averages.

(ii) even if the pore size distribution is wide, the same type of

distribution leads always to the same ratio between the two average values, hence it does not matter if the value of κ is wrong provided it has always about the same value.

The factors most frequently criticized in the Kozeny theory are the omission of the excess viscous dissipation due to convergent-divergent flow (Scheidegger[1974]), failure to indicate the anisotropic permeability due to the non-uniformities present in nature (Childs and Collis George[1950]), and dependence of Kozeny constant, κ, on porosity at higher porosities, i.e. $\varepsilon>0$ 90, (Kyan *et al*[1970]). In spite of these rather severe objections on various theoretical bases, Kozeny's work remains today a widely accepted equation relating the permeability to flow with geometrical parameters of a porous medium.

In their study of flow of air through randomly packed plugs of cotton, wool, rayon, and glass wool, Fowler and Hertel[1940] found excellent agreement between experimental results and Eqn.2.2 using κ=5.55. This value has been adopted in various studies of flow through beds of cellulose fibres, i e for water permeability by Robertson and Mason[1949], Mason[1950], Ingmanson[1953] and Gren[1972], and for air permeability by Garner and Kerekes[1978] and Knauf and Doshi[1986].

In order to improve the Kozeny-Carman relation for low Reynolds flow through porous media others have put forward porosity functions different than the $(1-\varepsilon)^2/\varepsilon^3$ term proposed by Blake[1922], Kozeny[1927] and Carman[1937]. Summaries of these porosity functions are reported by Rumpf and Gupte[1971], Dullien[1975] and Knauf and Doshi[1986]. However these porosity functions generally give $\kappa\cong$5.55 for the intermediate level of porosities, $0.6\leq\varepsilon\leq0.7$, encountered with paper.

2.4.2 Inertial Effects

Air flow through paper or pulp pads is widely expressed in terms of purely viscous resistance following the early work of Darcy[1856]. Carson[1934] appears to have been the first to note that, for paper sufficiently thin that pin holes become evident, the flow is not purely viscous. Rather than try to treat this reality, Carson and subsequent researchers have instead tried to eliminate or minimize this problem by increasing thickness or decreasing flow rate, and have continued to use the Darcy's law approximation of pure viscous flow Such a restrictive approach is contrary to the ultimate objective, either theoretical or for industrial relevance

At higher flow rates Darcy's law obviously breaks down. Experiments for determination of the 'critical' Reynolds number above which Darcy's law is not valid, show great discrepancies. One problem is the variety of choices for the characteristic dimension needed Scheidegger [1974] notes that the range of values for this critical Reynolds number lies between 0.1 (Nielsen[1951]) and 75 (Plain and Morrison[1954]), a broad range indeed. This uncertainty relates to differences in pore structure of materials and to the choice of a characteristic dimension.

The breakdown of Darcy's law is often interpreted as the transition to turbulent flow. However, as pointed out by Scheidegger[1960] and reaffirmed by Happel and Brenner[1965], failure of Darcy's law results when distortions in the streamlines owing to changes in direction of motion are sufficiently great for inertial forces to become significant compared with viscous forces. The incidence of turbulence should occur at much higher Reynolds numbers yet, if indeed such a phenomenon occurs at all in porous media of small particulates

The contribution of inertial effects can be expressed mathematically in several ways The simplest form is to regard inertial and viscous resistance as additive, as first proposed by Reynolds[1900],

$$\frac{\Delta P}{L} = au + b\rho u^2 \qquad (2.3)$$

Forchheimer[1901] suggested similar modifications to Darcy's law by including a second-order term in the velocity as did Reynolds, and later a third-order term, as

$$\frac{\Delta P}{L} = au + bu^2 + cu^3 \qquad (2.4)$$

Although the second-order term is postulated from semi-theoretical reasoning by analogy with the phenomena occuring for flow in tubes, the third-order term was added simply to make the equation fit experimental data. Although proposed first by Reynolds, Eqn 2.3 is widely known as Forchheimer relation Later Polubarinova-Kochina[1952] further generalized the Forchheimer relation by including a time dependent term, but this term is found to be small

Missbach[1937] proposed the relationship.

$$\frac{\Delta P}{L} = a'u^n \qquad (2.5)$$

He had generalized the relationship found by White[1935] for air flow through dry packed towers. White's results yielded an exponent of n=1.8

In general the value of the exponent n lies between 1 and 2. At n=1, Eqn. 2.5 is simply Darcy's law Dudgeon[1966] found a region with n somewhat less than one. but presented no satisfactory explanation or interpretation of these results, which therefore appear doubtful.

The Eqn. 2 5 coefficient a' has a clearly identifiable physical meaning only at the limits for which n is 1 or 2. At n=1, a' becomes the Eqn. 2.3 coefficient a, and is related to the Darcy permeability. At n=2, a' relates to the pressure loss due to pure inertial effects.

At intermediate values of n, the parameters a' and n are simply regression coefficients.

Eqn. 2.5 is a simplest relationship to check whether inertial effects are appreciable For example, Gummel[1977] described his pressure drop measurements across tissue paper of basis weight in the range 20-23g/m^2 in terms of two regression equations, an initial viscous part and an inertial part with a coefficient n=1.5, although his data do not appear to require this split.

The Forchheimer relation, Eqn 2 3, or its modified versions have been applied extensively and successfully to describe flow through porous media. The best known form of this relation is the equation of Ergun[1952].

$$\frac{\Delta P}{L} = \frac{150}{d_p{}^2} \frac{(1-\varepsilon)^2}{\varepsilon^3} \mu u + \frac{1.75}{d_F} \frac{(1-\varepsilon)}{\varepsilon^3} \rho u^2 \qquad (2.6)$$

The viscous term in the Ergun equation is the well known Kozeny-Carman equation. However, why Ergun took the Kozeny constant as 4.16 instead of widely accepted value of 5 is not known Ergun adopted the constant of the inertial term as 1 75 from Burke and Plummer[1928]. The results of the extensive experimental test of the Ergun equation by Macdonald *et al.*[1979] can be summarized as. (i) the physical basis of the Forchheimer equation is accurate, (ii) a wide variety of unconsolidated media are adequately represented by the modified Ergun equation, i.e. with the viscous term constant replaced by 180 as Carman suggested , and the inertial constant given a value of 1.8 for smooth particles and 4.0 for rough ones, iii) the Ergun equation is superior to others for a wide porosity range, and replacing the ε^3 term with $\varepsilon^{3.6}$ gives an even better porosity function, and (iv) different parameter values, approximately 15% higher than the suggested ones, give better aggree-

ment for non-spherical particles

The applicability of this type of equation to consolidated media has also been shown by Green and Duwez[1951], Ahmed and Sunada[1969] and by Macdonald *et al.*[1979] with the data of Fancher and Lewis[1933]. In a series of studies, Beavers and co-workers successfully applied the Forchheimer equation to water flow through beds of foamed nickel fibers with no free ends, a wire screen assembly, and a compressed mat of stainless-steel fibers, Beavers and Sparrow[1969]; for highly deformable polyurethane foams with air flow, Beavers *et al.*[1975] and Beavers *et al* [1981a], and for this media with water flow, Beavers *et al*[1981b] The Forchheimer relation was also used by Nilson[1981] in his numerical analysis of the inertial-dominated to viscous-dominated transition in porous media for gas or liquid flows

Two fundamentally different types of application of the complete Navier-Stokes equations have been used In one approach the equations have been solved numerically for flow channels of different geometries, e.g. the application by Payatakes *et al* [1973] of the stream function-vorticity method to the case of periodically constricted tubes. In the alternate approach Whitaker[1969] and Slattery[1972] averaged the equations over a representative part of the porous medium Using the momentum equation with the volume averaging theorem of Slattery[1972] and Whitaker[1967], Dullien and Azzam[1973] obtained the Forchheimer equation in the following form,

$$\nabla P = \alpha\mu u + \beta\rho u^2 \qquad (2.7)$$

where α and β are determined from the volume and area integrals

$$\alpha = \frac{1}{D_P^2 V} \iiint \nabla^2 \mathbf{v}\, dV \quad ; \quad \beta = \frac{1}{D_P V} \left(\iiint \mathbf{v}\, \nabla \mathbf{v}\, dV + \iint \frac{P}{\rho u^2}\, \mathbf{n}\, dA \right)$$

where D_P is pore diameter, V averaging volume, **v** interstitial velocity

vector, **n** unit vector, u superficial velocity and A the surface area bounding the averaging volume.

Ahmed and Sunada[1969] have also derived Eqn. 2.7 by averaging the Navier-Stokes equation and accounting for the average and fluctuating components of velocities and pressures, similar to turbulent fluctuations. The viscous and inertial terms, in their solution, are

$$\alpha = \frac{1}{D_p^2 \varepsilon V_b} \iiint \nabla^2 \mathbf{v} \; (\varepsilon dV_b) \quad , \quad \beta = \frac{1}{D_p \varepsilon V_b} \left(\iiint (\mathbf{v} \nabla \mathbf{v} - \mathbf{v}' \nabla \mathbf{v}')(\varepsilon dV_b)\right)$$

where ε is the porosity of the medium, V_b the bulk volume and $\mathbf{v}'$ the fluctuating component of the interstitial velocity vector. They were able to represent a large number of data of both consolidated and unconsolidated beds by a single curve in the following form,

$$\frac{\Delta P/L}{\beta \rho u^2} = \frac{\alpha \mu}{\beta \rho u} + 1 \tag{2.8}$$

Although it was proposed rather heuristically by Reynolds[1900] and Forchheimer[1901], the later empirical and theoretical studies summarized above confirm the correctness of the momentum transport relation expressed originally as Eqn. 2 3 and most recently as Eqn 2 8 The viscous term parameter, α, is the reciprocal of permeability, and the inertial term parameter, β, also known as the Forchheimer constant, is defined as $C/\sqrt{k}$ where C is the inertial constant.

A great variety of bases have been used for the characteristic length, d_p, required in Reynolds number, $Re=d_p \rho u/\mu$ Apart from widely used dimensions based on particle diameter for unconsolidated beds, the reciprocal of specific surface and the square root of permeability are widely used as the characteristic dimension for consolidated beds. A variety of empirical definitions exists. For example, Geertsma[1974] found a good correlation between porosity and the nondimensional ratio $\beta/\sqrt{\alpha}=0.005/\varepsilon^{5.5}$. This value is based on his data on flow through uncon-

solidated and consolidated sands as well as the data for porous metals of Green and Duwez[1951], and for consolidated sands of Cornell and Katz[1953]. From Eqn. 2 8 of Ahmed and Sunada, their Reynolds number definition, $Re=(\beta/\alpha)\rho u/\mu$, becomes $Re=0\ 005\rho u\sqrt{k}/\mu\varepsilon^{5.5}$, and Darcy's law holds up to Re=0.1 for all samples, Geertsma[1974]. Interestingly, Rumpf and Gupte[1971] have also suggested, by a phenomenological approach, the same porosity function, i.e. $\varepsilon^{-5.5}$, rather than $(1-\varepsilon)^2/\varepsilon^3$ as Kozeny and Carman proposed, to describe flow through randomly packed spheres over a wide range of porosities. $0\ 35\leq\varepsilon\leq 0\ 70$.

2.4.3 Friction Factor

A widely used method to express pressure drop is in terms of the non-dimensional friction factor, f Because numerous studies indicated friction losses to be proportional to the kinetic energy of the fluid, $\rho u^2/2$, and to the surface area of the solid in contact with the fluid, A, the resistance force, F, was expressed by Knudsen and Katz[1958] as,

$$F = f\ \frac{\rho u^2}{2}\ A \tag{2.9}$$

As Eqn. 2.9 is a definition of the proportionality constant, f, not a law of fluid mechanics, definitions of f may vary.

The friction factor for packed beds is generally defined analogous to that for flow in conduits

$$f^* = \frac{\Delta P}{L}\ \frac{d_p}{2\rho u^2} \tag{2.10}$$

with f^* usually referred to as the Fanning friction factor. Friction factor definitions for packed beds vary from the Eqn. 2.10 form due to the problem of definition of characteristic dimension, d_p, for the Reynolds number For example White[1935] introduced an empirical correction factor, dependent on particle size, in his attempt to correlate

data of other investigators for packed beds of rings and saddles.

In their study of the flow of air, water and petroleum through beds of sand, sandstone and lead shot Fancher and Lewis[1933] employed the Eqn. 2.10 definition. Using a weight mean diameter as d_p, they found that these data, which were principally in the viscous range, could be represented as $f^*=A'/Re$ where A' varies with the porous media.

Chalmers *et al.*[1932], using the Dupuit relation, replaced superficial velocity, u, in Eqn 2.10 with interstitial velocity, u/ε, while Bakhmeteff and Feodoroff[1937] used $u^2/\varepsilon^{4/3}$ instead of u^2/ε^2. For packed beds in columns of relatively small diameter, D, Chilton and Colburn[1934] introduced into the f definition the "wall effect factor, A_f", as a function of d_p/D Blake[1922] used $1/a_p$ for d_p in the Re definition, while defining f as $\frac{\Delta P_f \varepsilon^3}{LG^2 a_F}$. Later Kozeny [1927] derived the mean hydraulic radius to be ε/a_F for the flow channels in granular beds. Burke and Plummer[1928] used a modified Re definition equivalent to $G(1-\varepsilon)/\mu a_p$. In a series of papers Carman[1937, 1938, 1939] correlated the pressure drop data of others using the relation

$$f = \frac{\Delta P \varepsilon^3}{L\rho u^2 (a_p + 4/D)} = C \left(\frac{\mu a_F}{\rho u}\right)^{0.1} \qquad (2.11)$$

where C is a parameter depending on particle shape. Brownell and Katz [1947] used $d_p \varepsilon^n$ instead of d_p in Eqn 2.10, with n dependent on particle shape and bed porosity All earlier studies are summarized by Leva *et al.*[1951].

Ergun[1952] combined the works of Blake, Kozeny, Burke and Plummer, and Carman to propose his widely recognized relationship applicable to both viscous and inertial dominated flows

$$f = \frac{\Delta P}{L} \frac{d_p}{2\rho u^2} \frac{\varepsilon^3}{1-\varepsilon} = 1.75 + 150 \frac{1-\varepsilon}{Re} \qquad (2.12)$$

He also defined a new friction factor, f_v, which could be called a

viscous friction factor,

$$f_v = \frac{\Delta P}{L} \frac{d_p^2}{\mu u} \frac{\varepsilon^3}{(1-\varepsilon)^2} = 1\ 75\ \frac{Re}{1-\varepsilon} + 150 \qquad (2.13)$$

By rearranging the Forchheimer relation Ahmed and Sunada[1969] proposed yet another friction factor, $f=\Delta P/L\beta\rho u^2$, with $d_p=\beta/\alpha$ for the Reynolds number characteristic dimension, Eqn. 2.8. They showed that their data as well as those for various authors are represented extremely well by Eqn. 2 8

Other studies have focussed mostly on finding an appropriate porosity function to use in the definition of f in order to fit most of the experimental data. For example Kyan *et al.*[1970] modified the f definition given by Eqn. 2 12 for fibre beds as

$$f_{fk} = \frac{\Delta P}{L} \frac{d_f}{\rho u^2} N_e^4 (1-\varepsilon)^2 \qquad (2.14)$$

where f_{fk} is the kinetic friction factor for fibrous beds, d_f is fibre diameter and N_e is the effective pore number. The final form they report is

$$f_{fk} = \frac{1-\varepsilon}{Re} f_1(\varepsilon) + N_d f_1(\varepsilon) f_2(\varepsilon) \qquad (2.15)$$

where $Re=d_f\rho u/\mu(1-\varepsilon)$, N_d is deflection number, $\mu^2/Ed_f^2\rho$, E modulus of elasticity of fiber, f_1 and f_2 are complicated functions of ε and N_e.

Macdonald *et al.*[1979] have proposed to replace the constants in Ergun equation, Eqn. 2 11, with more appropriate ones in order to better fit the existing data, as summarized in Section 2.4.2.

2.5 HEAT AND MASS TRANSFER IN FINE PARTICLE POROUS MEDIA

2.5.1 The Ranz and Marshall Model

Most heat and mass transfer studies have used beds of packing of relatively large size. Thus relationships for heat and mass transfer in porous media are based on empirical data mainly for Re>10, substan-

tially above the Reynolds numbers typical for flow across paper in through drying.

Correlations of the nondimensional heat and mass transfer coefficients, Nu and Sh, have been based on the form suggested by Ranz and Marshall[1952]

$$Sh(Nu) = 2.0 + aRe^{b}Sc^{1/3}(Pr^{1/3}) \qquad (2.16)$$

This form assumes that, as Reynolds number decreases, the Sherwood or Nusselt number for packed beds approaches the limiting value of two which applies for single sphere in stagnant fluid. Ranz and Marshall gave a=0.6 and b=0.5. Specific forms include:

for single cylinders,

$Nu = 0.32 + 0.43\ Re^{0.52}$ McAdams[1954]

$Nu = (0.4\ Re^{1/2} + 0\ 06\ Re^{2/3})\ Pr^{0.4}\ (\mu/\mu_c)^{1/4}$ Whitaker[1977]

for single spheres,

$Nu = 2 + (0.4\ Re^{1/2} + 0.06\ Re^{2/3})\ Pr^{0.4}\ (\mu/\mu_o)^{1/4}$ Whitaker[1977]

for packed beds.

$Nu = (0.4\ Re^{1/2} + 0.2\ Re^{2/3})\ Pr^{0.4}$ Whitaker[1977]

In their review of mass transfer in packed beds, Wakao and Kaguei [1982] found that a=1.1 and b=0.6 in Eqn. 2.16 would be more consistent with the data now available. However the Reynolds number range of the supporting data is higher than 1, generally higher than 10 for the relations of McAdams, Whitaker, and Wakao and Kaguei.

Most of the experimental work on heat or mass transfer in packed beds for gas flow at low Reynolds numbers, i.e. Re<10, are presented in Fig. 2.4 and summarized in Table 2.1 The results show that transport phenomena are quite different for beds of small and large particles. Various studies of heat and mass transfer establish that, even for beds

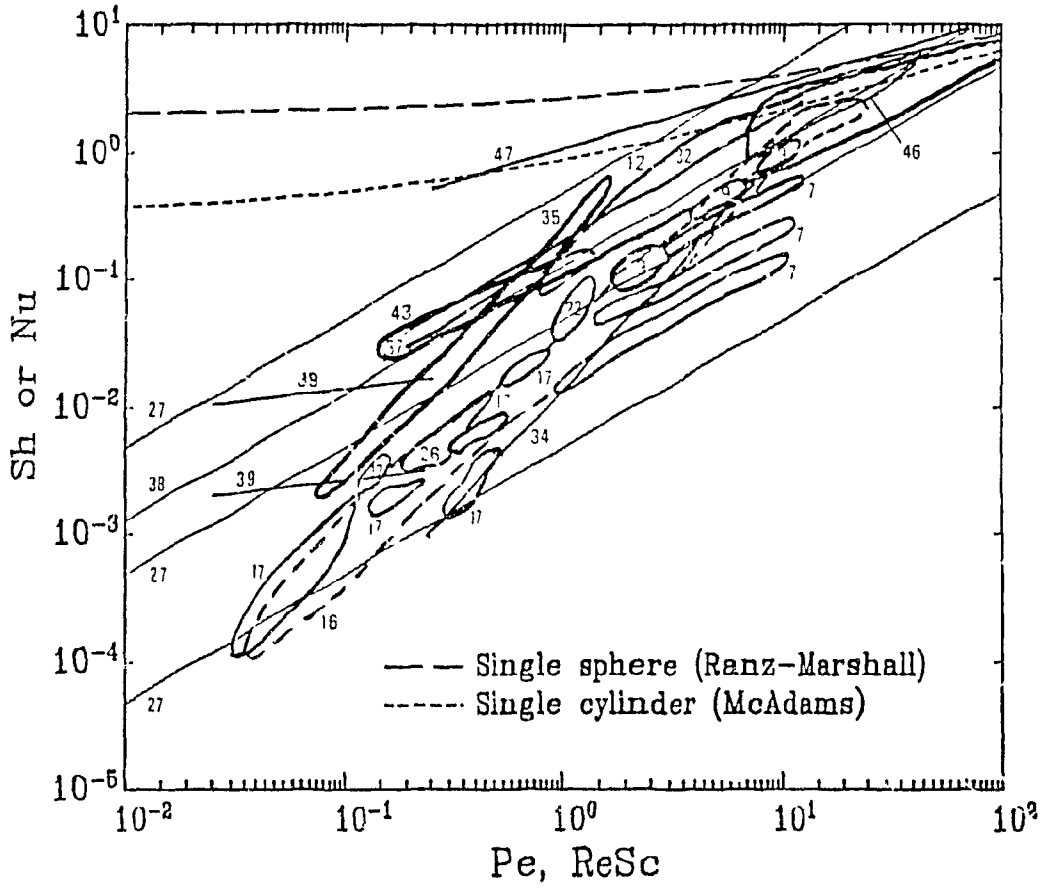

Figure 2.4 Heat and mass transfer in fixed beds of fine particles.

Numbers correspond to those given on Table 2.1

Table 2.1 Heat and mass transfer studies in fixed beds of fine particles

	Investigator	Experimental Method	Fluid	Fluid Dispersion	Particles in Bed Material	Shape	Size mm	Structure	Characteristic Dimension	Reynolds number Definition	Range	Sc (Pr)	Correlation‡	Remarks
1	Gamson *et al.* [1943]	water evaporation steady state heat-mass transfer	air	not considered	calite	spheres cylinders	2 1-11 6 4 1×4 8 to 18 1×16 9	UC†	equivalent sphere diameter	Gd_p/μ	60-3750	0 61 (0 72)	$j_D \propto Re^{-1}$ Re<40 $j_D \propto Re^{-0.41}$ Re>350	j_H/j_D=1 076 particle temp assumed to be T_{WB}
2	Hurt [1943]	water evaporation naphthalene sublimation steady state heat-mass transfer	air H_2	not considered	silica gel naphthalene	cylinders cylinders irregular	9 5×9 5 4 8×4 8 9 5×9 5 2 0-5 6	UC	particle diameter	Gd_p/μ	140-380 7-e70	0 61 (0 72) 2 5 4 05		particle temp measured, data presented in tables & graphs
3	Wilke and Hougen [1945]	water evaporation steady state heat-mass transfer	air	not considered	calite	cylinders	3 1×3 1 to 18 2×16 9	UC	equivalent sphere diameter	Gd_p/μ	45-250	0 60	$j_D \propto Re^{-0.51}$ Re<150	particle temp assumed to be T_{WB} Data available for h calculations too
4	Resnick and White [1949]	naphthalene sublimation steady state mass transfer	air CO_2 H_2	not considered	naphthalene	granules	0 3-1 1	UC	average particle diameter	Gd_p/μ	0 83-25	2.39 1 47 4 02	$j_D \propto Re^{-0.26} d_p^{1.4}$	criticized by Bar Ilan and Resnick[1957]
5	Taecker and Hougen [1949]	water evaporation steady state heat mass transfer	air	not considered	clay-kieselguhr mixture	Raschig & partition rings, Berl saddles	8 1-84 6	UC	square-root of particle external area	$G/A_p/\mu$	30-14600	0 61 (0 72)	$j_D \propto Re^{-0.41}$ for rings 100<Re<20000 $j_D \propto Re^{-0.34}$ for saddles 50<Re<3000	j_H/j_D=1 073-1 076 particle temp measured
6	Gamson [1951]	review of previous heat and mass transfer data	air H_2O	not considered	various	spheres cylinders flakes	2 3-16 0	UC	equivalent sphere diameter	$6G/a_p\phi\mu$	5-10000	0 6 to 1500	$j_D \propto Re^{-1}(1-\epsilon)^{0.2}$ Re<10 $j_D \propto Re^{-0.41}(1-\epsilon)^{0.2}$ Re>100	j_H/j_D=1 076 ϕ is the shape factor
7.	Grootenhuis *et al* [1951]	steady state heat transfer	air	not considered	metal	spheres	0 05-0 4	UC	sphere diameter	Gd_p/μ	1-30	0 72	$Nu \propto Pe^{1/3}$	*Nu decreases* with d_p
8	Hobson and Thodos [1951]	water and organic solvent evaporation steady state mass transfer	air N_2 CO_2 H_2	not considered	porous packing	spheres	9 4	UC	sphere diameter	Gd_p/μ	8 5-330	0 61 to 5 06	$j_D \propto Re^{-1}$ Re<50 $j_D \propto Re^{-0.45}$ Re>150	particle temp measured shallow beds of large particles
9	Eichorn and White [1952]	high frequency dielectric heating steady state, heat cr	air CO_2	not considered	Dowex-50	spheres	0 1-0 7	UC	sphere diameter	Gd_p/μ	2-19	0 7 0 8	$j_H \propto Re^{-0.30}$ j_H decreases with d_p	particle temp mass criticized by Littman *et al*[1968]
10	Chu *et al* [1953]	naphthalene sublimation steady state mass transfer	air	not considered	glass, lead calite rapeseed	spheres cylinders	0 7-14 0	UC	equivalent sphere diameter	$Gd_p/\mu(1-\epsilon)$	10-12000	2 57	$j_D \propto Re^{-0.78}$ 1<Re<30 $j_D \propto Re^{-0.44}$ 30<Re<10000	both fixed and fluidized bed data
11	Satterfield and Resnick [1954]	decomposition of H_2O_2 steady state heat and mass transfer	mixture of H_2O_2, H_2O vapor	not considered	polished catalytic metal	spheres	5 1	UC	sphere diameter	Gd_p/μ	15-160	0 7 0 9 (1 0)	$j_D \propto Re^{-0.34}$	particle temp measured j_H/j_D=1 37

Table 2.1 continued

	Investigator	Experimental Method	Fluid	Fluid Dispersion	Particles in Bed: Material	Shape	Size mm	Structure	Characteristic Dimension	Reynolds number: Definition	Range	Sc (Pr)	Correlations‡	Remarks
12	Bar Ilan and Resnick [1957]	naphthalene sublimation steady state mass transfer	air	not considered	naphthalene	granules pellets	0 37 8 2	UC	equivalent sphere diameter	$Gd_p/\mu(1-\ )$	0 2 →20	2 57	$j_D \propto Re^{-\ \ **}$ 1 5<Re<300	j_D decreases with d_p for granules j_D max at Re~1 0
13	Galloway *et al* [1957]	water evaporation steady state heat and mass transfer	air	not considered	celite	spheres	17 1	UC	sphere diameter	Gd_p/μ	150-1200	0 61 (0 72)	$j_D \propto Re^{n}$ and $j_H \propto Re^{n}$ 0 64<n<0 01 -0 72 n< 0 02	particle temp mass assumption of perfect mixing also considered
14	DeAcetis and Thodos [1960]	water evaporation steady state heat and mass transfer	air	not considered	celite	spheres	15 9	UC	sphere diameter	Gd_p/μ	15-2100	0 61 (0 72)	$j_D = 1/(Re^{0\ **}\ 0\ 15)$	particle temp measured j_H/j_D=1 51
15	Bradshaw and Bennett [1961]	naphthalene sublimation steady state mass transfer	air	considered Pe_p=2	naphthalene	cylinders spheres	6 3-12 4 9 5	UC	effective particle diameter	Gd_p/μ	500-10000	2 57	$j_D \propto Re^{*\ 51}$	Chu *et al* [1953] and Hobson & Thodos[1951] data used in correlation
16	Donnadieu [1961]	steady state heat transfer	air	not considered	sand	granules	0 13-1 1	UC	particle diameter	Gd_p/μ	0 04 40	0 72	$Nu \propto Pe^{1\ **}$	
17	Kunii and Smith [1961]	steady state heat transfer	air, He CO_2, H_2O	not considered	glass sand	spheres	0 1-1 02 0 1 0 24	UC	sphere diameter	Gd_p/μ	0 001-1		$Nu \propto Re^{1\ *}$ and decreases with d_p	Littman *et al*[1968], Gunn & deSouza[1974] criticized
18	SenGupta & Thodos[1962]	review of previous heat-mass transfer data		not considered	various	various	0 8-16 0	UC	particle diameter	Gd_p/μ	0 4-2100		$cj_D = a + \frac{b}{Re^{0\ **}\ c}$ Re>1	j_H/j_D=1 076
19	Yoshida *et al* [1962]	review of previous mass transfer data	air water	not considered	celite 2-naphthol	spheres cylinders	2 3-11 6 3 1-18 0	UC	reciprocal of specific surface	$G/a_p^2\mu$	0 4-4000	0 6 to 1760	$j_D \propto Re^{-0\ **}$ 0 01<Re<50 $j_H \propto Re^{0\ **}$ 50<Re<1000	ϕ is the shape factor
20	Bradshaw and Myers [1963]	water evaporation steady state heat and mass transfer	air	not considered	kaolin AMT kaosorb celite	spheres cylinders	4 7-8 8 4 0x4 1 6 2x4 9	UC	particle diameter	$Gd_p/(1-\epsilon)\mu$	400-6500	0 6 (0 72)	$j_D \propto Re^{*\ **}$ fixed and fluidized $j_D \propto Re^{*\ **}$ fixed beds	particle temperature measured
21	McConnachie and Thodos [1963]	water evaporation steady state heat and mass transfer	air	not considered	celite	spheres	15 9	UC	sphere diameter	$Gd_p/(1-\epsilon)\mu$	70-2500	0 61 (0 72)	$j_D \propto 1/[Re^{0\ **}\ 1\ 52]$ fixed fluidized and distended beds	particle temperature measured
22	Mimura[1963]	steady state heat tr	air	not considered		spheres	3 7	UC	particle dia	Gd_p/μ	1-3	0 72	$Nu \propto Pe^{1\ *}$	
23	SenGupta and Thodos [1963]	water evaporation steady state heat and mass transfer	air	not considered	celite	spheres	15 9	UC	sphere diameter	Gd_p/μ	100-2000	0 61 (0 72)	$cj_D \propto Re^{*\ 378}$ $j_H = j_D$	particle temperature measured
24	Pfeffer[1964]	theoretical solution, "free surface model of Happel			combined with "thin layer boundary layer solution" of Levitch					applicable for low Re-high Pe range			$Sh=1\ 26\left(\frac{1-(1-\epsilon)^{5/3}}{u}\right)^{1/3}(ReSc)^{1/3}$	
25	SenGupta and Thodos [1964]	water evaporation steady state heat and mass transfer	air	not considered	celite	spheres	15 9	UC	sphere diameter	Gd_p/μ	2000 6000	0 61 (0 72)	a cj_D max at at Re~800	particle temperature measured

Table 2.1 continued

	Investigator	Experimental Method	Fluid	Fluid Dispersion	Particles in bed: Material	Shape	Size mm	Structure	Characteristic Dimension	Reynolds number: Definition	Range	Sc (Pr)	Correlation‡	Remarks
26	Suzuki[1964]	steady state heat tr	air	not considered		spheres	1 1	UC	particle dia	Gd_p/μ	0 1-1 0	0 72	$Nu \propto Re^n$, n>1	
27	Kunii and Suzuki[1967]	theoretical model using "channeling" concept								for ξ being the channeling length to d_p ratio			$Sh = \frac{\phi}{6(1-\epsilon)\xi} Pe$	ϕ shape factor
28	Malling and Thodos [1967]	water evaporation steady state heat and mass transfer	air	considered	celite	spheres	15 7-15 9	UC	sphere diameter	Gd_p/μ	185-8500	0 61 (0 72)	$\epsilon^{1.18} j \propto Re^{-0.44}$ $\epsilon^{1.18} j \propto Re^{-0.47}$	without fluid dispersion with fluid dispersion
29	Littman et al[1968]	frequency response unsteady heat transfer	air	considered Pe_s=2 0	copper lead glass	spheres	0 5-2 0	UC	sphere diameter	Gd_p/μ	2-100	0 7	$Nu \propto Re^n$, n~1 0	criticized by Kaguei et al[1977]
30	Petrovic and Thodos [1968]	heavy hydrocarbons and water evaporation steady state mass transfer	air	considered Pe_s=2 0	celite	spheres	1 8-9 4	UC	sphere diameter	Gd_p/μ	3-230	0 60 to 5 45	$\epsilon j_D \propto Re^{-0.38}$	
31	Wilkins and Thodos[1969]	n-decane evaporation steady state mass transfer	air	considered	celite	spheres	2 6 3 1	UC	sphere diameter	Gd_p/μ	150-260	3 7	$\epsilon j_D \propto Re^{-0.43}$	both fixed and fluidized beds
32	Kato et al [1970]	naphthalene sublimation steady state mass transfer	air	not considered	naphthalene	spheres	0 16 - 0	UC	sphere diameter	Gd_p/μ	0 1-100	2 57	$Sh \propto [Re(d_p/L)^{0.6}]^{0.66} Sc^{1/3}$, $0 \le Re(d_p/L)^{0.6} \le 5$ $Sh \propto [Re(d_p/L)^{0.6}]^{0.43} Sc^{1/3}$, $5 \le Re(d_p/L)^{0.6} \le 10^3$	
33	Kato and Wen[1970]	review of previous heat transfer data	air H_2, CO_2	not considered	various	various	0 24-21 7	UC	particle diameter	Gd_p/μ	0 1-1000	0 67 to 0 75	$Nu \propto [Re(d_p/L)^{0.6}]^{1.1} Sc^{1/3}$, $0 \le Re(d_p/L)^{0.6} \le 2.5$ $Nu \propto [Re(d_p/L)^{0.6}]^{0.43} Sc^{1/3}$, $2.5 < Re(d_p/L)^{0.6} < 10^3$	
34	Gunn and deSouza[1974]	frequency response unsteady heat transfer	air	considered	glass steel lead	spheres	0 1-6 3	UC	sphere diameter	Gd_p/μ	0 05-330	0 7	$Nu = \epsilon(RePr)^2/((1-\epsilon)D_s/k_f)$	Nu at Re<1 were not calculated
35	Wakao and Tanisho [1974]	pulse response non adsorption unsteady mass transfer	H_2	not considered	vanadium diatomaceous earth	cylinders granules	3 1×4 7 1 1	UC	equivalent sphere diameter	$Gd_p\epsilon/\mu$	0 05-1 8	1 5	$Sh \propto Re^2$ $0.05 \le Re \le 1.0$	criticized by Wakao[1976]
36	Bhattacharyya and Pei[1975]	microwave heating steady state heat tranfer	air	not considered	ferric oxide	spheres cylinders	3 2 7 6 5 1×5 1	UC	particle diameter	$Gd_p/\mu^*(1-\epsilon)$	110-830	0 7	$j_H \propto [Ar\ Re^{-3}]^{0.28}$ $Ar = d_p^3 g \rho_f (\rho_p - \rho_f)/\mu^2$	particle temp measured
37	Cybulski et al [1975]	radial heat conduction steady state	air	not considered	silicon-copper	irregular	0 1	UC	mean particle diameter	Gd_p/μ	0 24-0 63	0 7	$Nu \propto Re$	criticized by Wakao et al [1977]
38	Nelson and Galloway[1975]	theoretical model, potential flow solution using a			synthesis of boundary layer theory and Danckwert's penetration theory								$Sh = \frac{1}{(1-\epsilon)^{1/3}} \left\{\frac{1}{(1-\epsilon)^{1/3}} - 1\right\} Re\ Sc^{1/3}$	as Re→0
39	Raj and Emmons[1975]	water evaporation steady state mass transfer	air	not considered	paper			C	square root of permeability/	$G/k/\mu$	0 04-0 4	0 61 (0 72)	$j_H \propto k_1^{0.2} (ReSc)^{-0.8}$ $j_D = \frac{k_1^{0.2} k_2^{0.8}}{6}$	correlation includes sheet thickness
40	Appel and Newman [1976]	cathodic reduction limiting current steady state mass tr	aq soln KNO_3, ferricyanide & ferrocyanide	not considered	stainless steel	spheres	3 97	UC	reciprocal of specific surface	$G/a_p\mu$	0 002-0 05	1400		

Table 2.1 continued

	Investigator	Experimental Method	Fluid	Fluid Dispersion	Particles in Bed Material	Shape	Size mm	Structure	Characteristic Dimension	Reynolds number Definition	Range	Sc (Pr)	Correlation‡	Remarks
41	Miyauchi et al [1976]	pulse response, unsteady chemical reaction	C_3H_8, N_2 H_2, He	considered	porous packing	spheres	0 7-1 4	UC	hydraulic diameter d_h	Gd_h/μ	3-200	0 5-2 0	Sh=d 33 , Pe≥100	
42	Rohrer and Gardiner[1976]	water evaporation steady heat mass transfer	air	not considered	paper			C	charc linear dim of sheet	Gd_p/μ		0 61 (0 72)	$h = b\,G^{0.8}$ 0 11≤b≤0 16	experimental results not documented
43	Wakao et al [1976]	pulse chromacography unsteady adsorption	H_2	considered	activated carbon	spheres	2 2	UC	sphere diameter	$Gd_p\varepsilon/\mu$	0 1-1 0	1 5	$Sh \propto Re^{0.8}$	criticized by Wakao[1976]
44	Cano and Bohm[1977]	electrochemical steady mass transfer	aq NaOH ferro and ferricyanide	considered	nickel-plated bronze	screens	0 3<d<2 0 1 2<D 5 0	C UC	d wire dia and D, wire wire dia	$Re=Gd/\nu$ $Re=GD/\nu\varepsilon$	0 25-20 1-75	1050 1290	$j \propto Re^{-0.44}$ $j \propto Re^{-0.44}(\frac{D}{d})^{1/2}$	
45	Dwivedi and Upadhyay[1977]	review of previous mass transfer data	various	not considered	various	various	0 4-22 2	UC	equivalent sphere diameter	Gd_p/μ	1-10^4	0 6-5 5	$j_D\varepsilon \propto Re^{-0.407}$ Re>10	
46	Gummel [1977]	water evaporation steady mass transfer	air	found not important	paper		0 13 0 17	C	Hagen Poiseuille equivalent diameter	$Gd_{eq}/\varepsilon\mu$	10-100	0 57	no correlation	strong ΔT_1 effect on Sh observed
47	Hsiung and Thodos[1977]	naphthalene sublimation steady heat transfer	air	considered $Pe_h \propto Pe^{0.33}$	naphthalene	spheres	0 25-2 0	UC	average particle diameter	Gd_p/μ	0 1-100	2 57	$j_D \propto Re^{-0.40}$ $j_D \propto Re^{-0.39}$	bed temp and conc profiles measured
48	Kumar et al [1977]	benzoic acid dissolution steady mass transfer	water 60% prop glycol	not considered	benzoic acid	cylinders pellets	5 5×2 5 12 8×4 9	UC	equivalent sphere diameter	Gd_p/μ	0 01-600	767-42400	$j_D \propto Re^{-0.72}$ Re<10 $j_D \propto Re^{-0.44}$, Re>10	
49	Fedkiw and Newman[1978]	asymptotic behaviour of the mass transfer coefficients at low Pe is found using a singular perturbation approach								they demonstrated that			i) film mass transfer coefficient → Const at low Pe ii) average mass transfer coefficient ∝ Pe at low Pe	
50	Wakao and Funazkri[1978]	previously published mass transfer data are corrected for the axial fluid dispersion								$Ud_p\varepsilon/\mu$	3-10000		$Sh = 2 + 1\,1\,Sc^{1/3}\,Re^{0.6}$	
51	Fedkiw and Newman[1982]	cathodic reduction steady mass transfer	$CuSO_4$ soln acidic(1M H_2SO_4)	not considered	SS, copper plated	spheres	3 18	UC	reciprocal of specific surface	$U/a_p\nu$	0 002-0 2	1900 8880		strong a_pL effect on Sh observed
52	Kehinde et al [1983]	pulse chromatography unsteady mass transfer	benzene tracer in He carrier	considered	coated glass	spheres	0 7	UC	sphere diameter	Ud_p/ν	0 025-0 25		$Sh = 2\,13$	
53	Huber and Jones[1988]	frequency response unsteady heat transfer	gas	considered	alumina	spheres	3 3 to 19 8	UC	sphere diameter	Ud_p/ν	0 7-16		$Nu \propto Re^{1.48}$	

‡ some regression equations are calculated here from the original data
‡‡ C - consolidated bed UC - unconsolidated bed

of spherical particles, the theoretically derived limiting value of two for Sh or Nu is not valid as particle size decreases. This decrease in Sh or Nu with decreasing particle size has been observed in mass transfer studies by Hurt[1943] with cylinders and irregular shape flakes, Resnick and White[1949] and Bar Ilan and Resnick[1957] with granules, Wakao and Tanisho[1974] with cylinders and granules, and in heat transfer studies with spheres by Grootenhuis *et al.*[1951], Eichorn and White [1952] and Kunii and Smith[1961]

Regression equations of the Eqn 2 16 form are consistent with experimental data only in the turbulent flow range Fluid turbulence may degrade the effects of adjacent particles and boundary layers should develop on the particle surfaces in a manner similar to that for an isolated particle. At low Reynolds number, however, boundary conditions describing heat or mass transfer are quite different from those for an isolated particle system, as Cornish[1965] has noted Therefore the theoretical value, 2, for a single sphere in a stagnant medium has no physical meaning in very low Reynolds number flow through porous media. For this case the minimum theoretical value of Nusselt number, according to Cornish, approaches zero

2 5.2 Alternate Models

Kunii and Suzuki[1967] proposed a channeling model due to the inhomogeneities in a bed, at low Re or Pe, to explain the drop in heat or mass transfer far below what would otherwise be expected. In their equation:

$$Sh = \frac{\Phi}{6(1-\varepsilon)\xi} Re\ Sc \qquad (2.17)$$

Φ is a shape factor and ξ the ratio of average channeling length to

particle diameter. The main assumptions in the derivation of Eqn. 2.17 are: (i) in the stagnant region, the temperature or concentration of the fluid is in equilibrium with that of the interspersed solid , (ii) transfer of heat and mass can be described in two-dimensional coordinates and the channeling fluid flow is assumed to be plug flow; (iii) heat or mass transfer is restricted to molecular diffusion in the direction perpendicular to flow Martin[1978] showed that many, but not all, reported data fit Eqn. 2 17, if it is assumed that the average channeling length is equal to the thickness of the bed, as would be the case for the pin holes present in thin paper

In extension of the work of Cornish[1965], Nelson and Galloway [1975] point out that any attempt to derive expressions for heat and mass transfer for an assembly of spheres based on theories of a single sphere in an infinite medium are doomed to fail at low Reynolds number because of an incorrect boundary condition They proposed a potential flow solution for flow in arrays of spheres and, using a synthesis of the results of boundary layer theory and Danckwerts' penetration theory, they obtained a mathematical model for heat and mass transfer in dense (low porosity) systems of fine particles Their model at infinite dilution, $\varepsilon=1$ i.e. the single sphere case, yields the Ranz-Marshall equation. As $Re \to 0$, the model reduces to

$$Sh = \frac{0.18}{(1-\varepsilon)^{1/3}} \left(\frac{1}{(1-\varepsilon)^{1/3}} - 1 \right) Re\, Sc^{2/3} \qquad (2.18)$$

These two theoretical models for mass transfer at low Reynolds number, i.e. Kunii and Suzuki[1967], Eqn 2 17, and Nelson and Galloway [1975], Eqn. 2.18, give $Sh \propto ReSc$ and $Sh \propto ReSc^{2/3}$. Moreover in their rigorous singular perturbation approach coupled with heuristic arguments, Fedkiw and Newman[1978] found that for packed bed reactors the volumet-

ric mass transfer coefficient decreases linearly with Peclet number as Peclet number approaches zero. These Reynolds or Peclet dependencies of Nu or Sh differ considerably from any of the classical creeping flow solutions that yield $Sh \propto (ReSc)^{1/3}$ Nelson and Galloway claim that this is a result of finite radius boundary conditions used in their solution.

According to Schlunder[1977], the linear dependency of Sh to Re in both the Kunii-Suzuki and Nelson-Galloway models is a consequence of their transfer coefficient definitions, based on the difference of inlet temperature (or concentration) instead of the mean driving force. He proposed to include pore size distribution in the overall mass transfer coefficient calculations. Schlunder represented the packed bed as a bundle of capillaries with nonuniform diameters and divided the total flow rate among these capillaries according to their size. The mass transfer equation for laminar pipe flow with entrance effects, Eqn 2.19,

$$Sh = (49 + (4.2 + 0.293 (Re \frac{d}{L})^{1/2}) Sc Re \frac{d}{L})^{1/3} \qquad (2.19)$$

was then employed to predict the transfer coefficients in each capillary, and the overall mass transfer coefficient was found as a result of the mixing of these flow streams. However, the measured drop in Sh shown in Fig 2.4 would require a complicated, and probably unrealistic, pore size distribution function.

Krischer and Loos[1958] and Krischer[1963] used a variety of geometric shapes for the particles in beds of small particles in a theoretical treatment which led to values of Nu much higher than those measured.

Web consolidation and the presence of pin holes in paper correspond to the channelling model of Kunii and Suzuki[1967]. Martin[1978] found that, with an appropriately chosen channelling length, most of

the previous experimental data could be represented by this model. The Nelson and Galloway[1975] model should not apply for paper since it is derived for dense beds Inclusion of the effect of pore size distribution, the model of Schlunder[1977], is not applicable to paper due to the complexity of its structure Thus for heat and mass transfer in through drying of paper the evidence does not yet permit recommendation of a specific model which is theoretically sound and practically applicable As has been observed by van Brakel[1980], reference to the broad band of experimental data, presented here in Fig 2.4, remains to date the best guide available

2.6 POROUS STRUCTURE OF PAPER

Paper is a complex matrix of wood fibres in a highly anisotropic porous structure. The fibres are oriented with their axes approximately parallel to the web surface, and in that plane are to some extent randomly oriented Pore spaces range in size from interfibre gaps to interstices of molecular dimensions Paper porosity can be the most important single structural feature of the end product, for example high porosity is required for filter and sanitary paper Low porosity is obtained for other products by coating, impregnation or lamination.

The porous structure of paper is affected by the raw material (type of wood, type of pulping process) and by the papermaking process. Papermaking processes are in turn governed by the porous structure of the web while this structure is being developed. Drainage of a freshly formed web is a function of its water permeability. Dewatering by suction and pressing depends on both the water and air permeability of the web. The complex heat and mass transfer processes in drying depend on

air permeability, water transport characteristics, porosity, specific surface area and pore size distribution of the paper. In through drying the flow rate of air across the paper, governed by the air permeability of the paper, is the primary variable governing drying rate. Rates of heat and mass transfer between the throughflow air and the fibres are governed by the specific surface area of the fibre matrix. The movement of moisture within the fibres is a function the capillary microstructure of fibres

Porosity, specific surface area, pore size and pore size distributions are parameters which describe the porous structure of paper Porosity, ε, is the ratio of pore volume to total volume. The interfacial area of particles is generally normalized to the volume of a porous medium and is termed specific surface area, a_p As the basis weight of paper (weight per unit area) can be measured with more precision than its thickness or volume, a mass based specific surface area is usually preferred with paper Average pore size contains essentially the same information as specific surface area, in that it describes how finely distributed pore volume is within the fibre matrix. Pore size distribution provides information about the character of the pores, e.g. an estimate of the relative number of interfibre to intrafibre pores. A more detailed geometrical characterization of the pore network through use of parameters describing the shape or tortuosity of the pores appears to be unrealistic for a porous structure of the complexity of paper.

2.6.1 Porosity

Porosity is defined as the ratio of pore volume to total volume,

$$\varepsilon = \frac{\text{pore volume of paper}}{\text{total volume of paper}} = 1 - \frac{\rho_b}{\rho_f} = 1 - \frac{M_B}{\rho_f L}$$

where ρ_b is the bulk density, ρ_f the fibre density, M_B the basis weight and L the thickness of paper Fibre density, ρ_f, is obtained either by the classical fluid displacement technique or by mercury intrusion. Thickness is measured by a caliper under standard conditions because of the compressibility of paper. Basis weight is a precise measurement. Alternately, bulk density, ρ_b, is determined directly by mercury pycnometry , the mercury buoyancy technique, the non-polar liquid displacement technique using heptane, benzene or toluene, or the gas displacement method, typically with helium Porosity values vary slightly due to the compressiblity of paper and surface effects, depending on the method (Murakami and Imamura[1984])

2.6.2 Specific Surface

Solution adsorption, optical methods, and gas adsorption, generally with N_2, are the main techniques for measurement of the specific surface of paper, in each case in conjuction with the B.E.T. method, Brunauer, Emmett and Teller[1938] A widely accepted method to measure internal total surface area of paper is from the adsorption isotherm at liquid nitrogen temperature, then calculation of a_p from the BET equation Alternately, the amount of gas adsorbed may be measured by conventional thermal conductivity cells, Nelsen and Eggertsen[1958] and by Stone and Nickerson[1963], instead of the earlier volume or mass measurements. Although very accurate, especially for materials of low specific surface area, $<1 m^2/g$, the method is quite tedious and applicable to dry paper only Inverse Gas Chromatography, IGC, described by Gurnagul and Gray[1987], is similar to the N_2-adsorption techniques but

is applicable to both wet and dry paper, and the measurements are made at ambient temperature and pressure The principle for the solution adsorption method, in which a solute is adsorbed from a nonswelling solvent, is the same as for the gas adsorption method.

Optical methods are based on reflectance. The specific scattering coefficient is calculated from reflectance using the Kubelka-Munk equation Haselton[1955] showed that for pulp sheets the scattering coefficient is proportional to the BET surface area. This method is widely used for relative comparisons of internal area between pulp sheets.

The internal surface area of pulp mats or paper have also been determined from gas or liquid permeation using some form of the Kozeny-Carman equation. The hydrodynamic surface area is the external area of fibres that are immersed in water The surface area of water swollen fibres by the air permeation measurement could be much smaller than the hydrodynamic surface area due to the surface area of internal pores.

A less common method for specific surface determination is the silvering technique devised by Clark[1942], later modified by Browning [1950], based on the catalytic decomposition of hydrogen peroxide at the silvered surface of wetted fibers in paper or pulp mats.

2.6.3 Pore Size and Pore Size Distribution

Although there is no direct experimental measurement to describe the geometrically irregular shape of the pore space, pore radius (or diameter) is a widely used characterization. As pore radius does not describe the actual pores, pore size and pore size distribution are functions of the experimental techniques used for the measurement. The generally applied techniques are X-ray small angle scattering; gas

sorption, such as N_2; vapor sorption, e.g. benzene; mercury intrusion; and the dioxane gas drive method There is also the unique technique of Banacki and Bowers[1962] which involves passing through the specimen a nonswelling liquid suspension of spherical beads of known size distribution and determining the size distribution of the beads which pass through.

The measurements of paper characteristics noted in Sections 2.6.1, 2.6.2 and 2.6.3 are detailed by Corte[1982] and by Murakami and Imamura [1984].

2.6.4 Permeability

The gas permeability of paper, a measure of the relation between rate of gas throughflow and the pressure driving force, is an integrated measure of the structure properties discussed above. According to Scheidegger[1974] and Dullien and Batra[1970], pore spaces can be classified as interconnected, dead-end or noninterconnected depending on whether they are accessible from both ends, one end and not at all. Only the interconnected part of the pore system is open to fluid flow, and is therefore called the effective pore space. Permeability, then, relates the effective pore space

The principal studies on permeability, internal specific surface, pore size, and pore size distribution summarized in Tables 2.2 and 2.3, show a wide range of values depending on the pulp, preparation technique and measurement method For example adsorption methods, the silvering method, and permeability methods do not give the same values for specific surface, yet all may be correct measures of a different interfacial area. As the interest of the present study is with proces-

Table 2.2 Specific surface of paper and pulp pads

Method	Pulp	a'_p m^2/g	Remarks	Reference
N_2 adsorption	bleached Sulphite	0.66 0.81	65 g/m² handsheets, dried spray dried pulp	Haselton [1955]
N_2 adsorption	Kraft Fibres Paper	230 1.2 0.5-1.0	swollen, unbleached‡ oven dried, unbonded oven dried	Stone & Scallan [1965]
N_2 adsorption	Sulphate unbeaten Sulphite unbeaten	0.62 1.12 0.48 1.02	unbonded area, 100g/m² total area unbonded area, 100g/m² total area	Hartler & Rennel [1969]
IGC(mesitylene) IGC(n-decane) Kr sorption	bleached Kraft unbeaten	0.67 0.68 0.80	60 g/m² handsheets same same	Gurnagul & Gray [1987]
Silvering technique	unbeaten beaten groundwood	0.7-1.5 1.0-4.0 1.5-2.5	pulp pulp pulp	Browning [1950]
Hydrodynamic	Kraft Sulphite Sulphite	0.91-0.95 1.02-1.06 1.14-1.33	never dried pulp same rewetted pulp	Robertson & Mason [1949]
Hydrodynamic	bleached Sulphite unbeaten	0.62-0.69	porosity range 0.7-0 74	Ingmanson *et al.* [1959]
Hydrodynamic	bleached Sulphite unbeaten	0.66		Ingmanson & Andrews [1963]
Hydrodynamic	Sulphate unbeaten	1.16	Kappa number 17 fibre diameter ~28μm	Gren [1972]
Hydrodynamic	bleached Sulfite	0.42	2350 g/m² handsheet wet pressed at 345 kPa	Bliesner [1964]
Hydrodynamic	bleached Kraft	0.70 0.88	200 g/m² handsheet, CSF 725 same , CSF 685	Knauf & Doshi [1986]
Aerodynamic	Sulfite unbeaten	0.40	21 g/m² handsheets k_{σ}‡ taken as 3	Brown [1950]
Aerodynamic	bleached Sulfite	0.87-1.6	100 g/m² handsheets refined	Sanborn [1962]

Table 2.2 continued

Method	Pulp	a_p m^2/g	Remarks	Reference
Aerodynamic	bleached Sulfite unrefined	0.71 0.90 1.15	100g/m², wet pressed @172 kPa same 345 kPa same 690 kPa	Bliesner [1964]
Aerodynamic	Kraft	0.46	air dried, dry refined pulp	Garner & Kerekes [1978]
Aerodynamic	Groundwood TMP Sulphite	1.2-1.5 1.0-1 4 0 41	beaten beaten beaten	Nevalainen *et al.* [1983]
Aerodynamic	bleached Kraft	0 60 0.69	200 g/m² handsheet, CSF 725 same , CSF 685	Knauf & Doshi [1986]
Calculation	bleached Kraft	0.65-0.84	cell wall thickness 1.1-1.5μm lumen/fibre width ratio 0.8-0.9 lumen collapse 66-69%	Scallan & Borch [1976]

‡ solvent exchange dried
‡‡ k_o in Kozeny-Carman eqn. see Eqn 2.2

Table 2.3 Permeability and pore size of paper and pulp pads

Method	Pulp	pore size μm	k m^2	Remarks	Reference
Aerodynamic	blotting paper	-	$2\ 10\times10^{-13}$	{ calculated from his	Carson [1934]
	newsprint	-	0.07	{ original data	
Aerodynamic	various paper	0.2-1.2	-	various samples of book papers to bond papers	Carson [1940]
Air and oil Permeability	bleached Sulfite	0.1-1 3	1.1×10^{-15}	0.09 mm thick sheets of beaten fibres, effective pore radius is quoted	Bublitz, Dappen & van der Akker [1948]
Aerodynamic	bleached Sulfite	3-7	$0.1\text{-}6\times10^{-14}$	100 g/m^2 sheets of refined fibres	Sanborn [1962]
Hydrodynamic	blotting paper	4-100+	$1\text{-}6\times10^{-7}$ ‡	pore sizes quoted are the	White &
	filter paper	10-100+	$1\text{-}3\times10^{-6}$ ‡	controlling pore diameters during dewatering, X>1	Marceau [1962]
Aerodynamic	blotting paper	4-100+	$1\text{-}5\times10^{-10}$ ‡	270-340 g/m^2 wet samples	White &
	filter paper	10-100+	$1\text{-}2\times10^{-9}$ ‡	80-245 g/m^2 wet samples	Marceau [1962]
Aerodynamic	bleched	4.7∓1 1	1.4×10^{-12}	100g/m^2, wet pressed @172kPa	Bliesner
	Sulfite	3.6∓0.9	$5\ 8\times10^{-13}$	same 345kPa	[1964]
	unrefined	2.8∓0.8	$2\ 7\times10^{-13}$	same 690kPa	
Aerodynamic	Kraft	-	$0.9\text{-}6\times10^{-10}$ ‡	47 and 85 g/m^2, never dried	Brundrett
	Kraft	-	0.9×10^{-10} ‡	77 g/m^2,calendered rewetted	& Baines
	Newsprint	-	$0\ 9\times10^{-10}$ ‡	52 g/m^2, never dried	[1966]
	Newsprint	-	$1\ 3\times10^{-10}$ ‡	52 g/m^2,calendered rewetted	
Aerodynamic, Hg Intrusion	bleached Kraft	7-8	$0.5\text{-}5\times10^{-12}$ ‡‡	60 g/m^2 sheets of unbeaten fibres, equivalent pore dia. of freeze dried samples are measured	Murakami & Yamauchi [1981]
Aerodynamic, Hg Porosimetry	Kraft	3-4	2×10^{-14} ‡‡	120-180 g/m^2 sheets of	Yamauchi
		8-9	$2\text{-}5\times10^{-13}$ ‡‡	unbeaten fibres from	&
		12-13	$1\text{-}2\times10^{-12}$ ‡‡	different species	Murakami [1983]
Hg Porosimetry	TMP	4	-	median pore radius is	Ohtake
	Kraft	1.5	-	quoted	*et al* [1984]

‡ k/L values in m

‡‡ effective permeability coefficient, i.e. k divide by the product of the porosity and the mercury retraction volume ratio

ses occuring during through drying, it is effective pore space which is of relevance here.

2.7 SUMMARY

1) Measurements of rate of through drying of paper: Previous investigations of through drying have produced contradictory results due to shortcomings in the design of the laboratory through dryers used and to the limited range of experimental variables studied. Thus there is no reliable set of appropriately controlled measurements of through drying rate which are documented over a significant range of conditions of the throughflow, i e its flow rate and temperature, and conditions of the paper, i e. its thickness and moisture content.

2) Momentum transport in flow through paper For air throughflow across paper, the general neglect of the inertial contribution to pressure drop and the use of unjustifiable choices as the characteristic dimension for Reynolds number are fundamental deficiencies of previous studies.

3) Transport phenomena in porous media of fine particles: The subject of heat and mass transfer for fluid flow through porous media of fine particles remains a challenging area filled with disagreement and uncertainty. A key obstacle for the case of flow through paper is the lack of a theoretically sound characteristic dimension for the Reynolds, Sherwood and Nusselt numbers.

The present study of the through drying of paper attempts to make a contribution by appropriate response to the above analysis of this field

CHAPTER 3

EXPERIMENTAL APPARATUS

3.1 EXPERIMENTAL STRATEGY

An experimental facility was designed and constructed for the study of transport phenomena involved in throughflow drying of light to medium grades of paper. The objective was to obtain simultaneously the instantaneous values of momentum, heat and mass transport data, i.e , pressure drop across the web, humidity and temperature of the drying air out of the sheet, moisture content of the wet web and drying rate, while maintaining constant the controlling conditions of flow rate and inlet temperature of the air throughflow. The basic experimental design involves transient drying for experiments with total drying time as low as 15 seconds. As full-scale changes in value of some variables may occur within a second during these transient experiments, achieving very fast measurement times was an overriding requirement.

A basic design constraint adopted was that the air throughflow rate remain constant during each transient experiment in spite of very large changes in sheet permeability from wet to dry. With this constraint, the drying rate curve for each transient experiment would be associated with a known, constant throughflow rate. The design requirement for determination of instantaneous exit air humidity, which may have a full-scale change within seconds, was met by monitoring this humidity continuously with a fast-response IR analyzer.

Thus a facility was developed for the through drying of paper of a range of basis weights, in transient experiments conducted at constant mass throughflow air rate, with continuous measurement of the exit air

moisture content, exit air temperature and pressure drop across the drying sheet. In consideration of the time scale of these transient experiments, complete data acquisition was with a dedicated micro-computer

3 2 EQUIPMENT

A flow sheet of the experimental set-up is shown as Fig. 3.1, with a photograph as Fig. 3.2 A constant mass rate of throughflow air across the drying sheet of greatly varying permeability was achieved by maintaining sufficient pressure drop across the manual control valve (Whitey Union Bonnet regulating valve model SS-6LRF4) (1), to assure critical flow. For air the limiting pressure ratio to achieve critical flow is approximately 0 53 The rate of throughflow air was measured by a rotameter (Schutte and Koerting Co model 4-HCFB) (2), upstream of the electrical heater (3), comprising four individually controlled stages The air volume contained between the critical flow valve (1), and the paper sample holder (4), was minimized so that during an experiment the difference between the mass flow rate of air through the paper and the selected constant value of flow rate across the critical flow valve was not significant If this system volume were large, then variation of the mass inventory of air in this section, caused by variation of permeability and hence ΔP for the paper, would cause the paper throughflow rate to deviate from the controlled rate at the critical flow valve. Proof that this objective was achieved is detailed in Appendix 1. Air from the paper sheet passed through the measurement cell (6), of IR detector-analyzer (5), (7) Air temperature was measured with Omega fine wire (76μm) copper/constantan thermocouples,

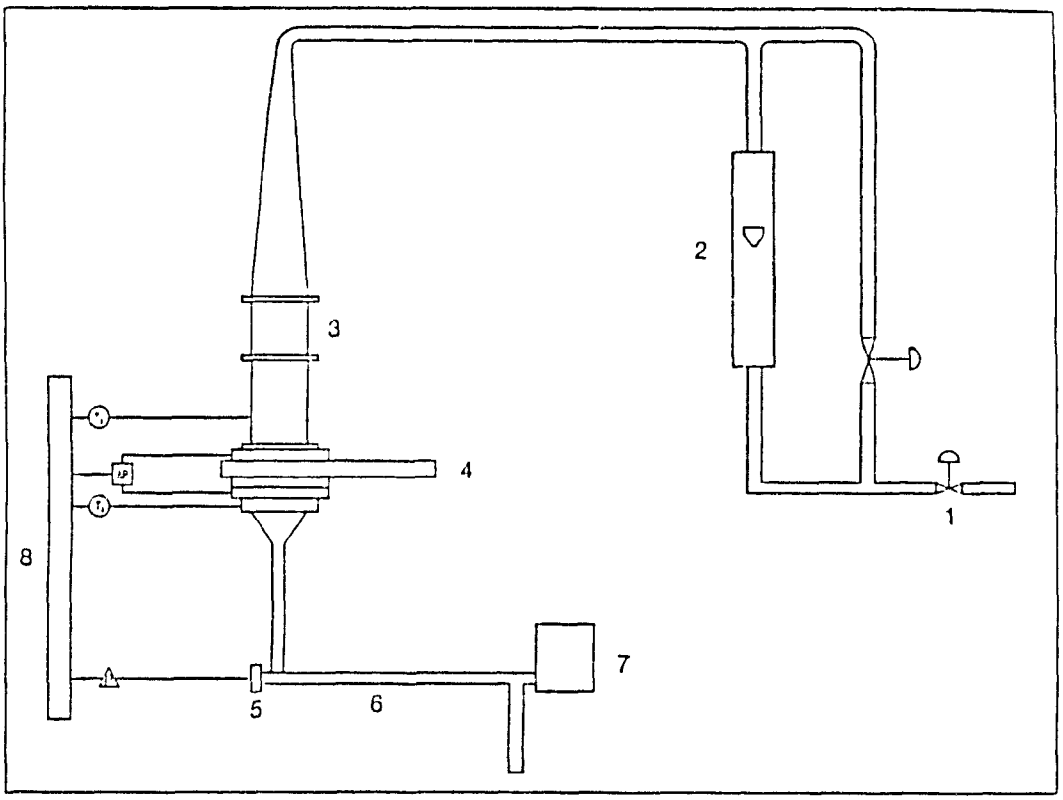

Figure 3.1 Laboratory through drying facility, (1) Critical flow valve, (2) Rotameter, (3) Heater, (4) Sliding sample holder assembly, (5) IR detector, (6) IR measuring cell, (7) IR source, (8) A/D board and microcomputer.

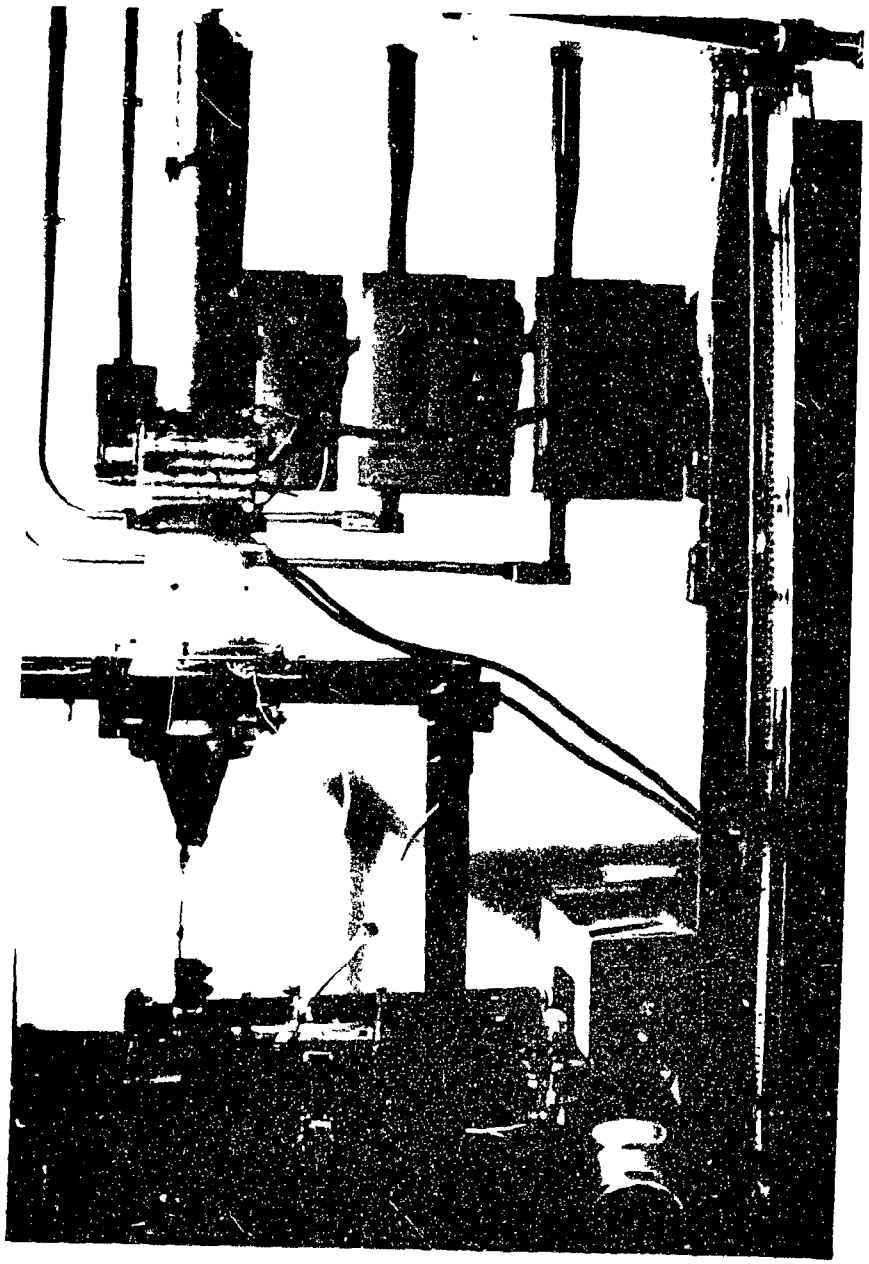

Figure 3.2 Experimental facility

pressure drop across the sheet with a strain-gage type differential pressure transducer (Statham Laboratories model PL96TCd 3-350) The data acquisition microcomputer (8), monitored this temperature and pressure drop as weel as the exit air humidity

The wet sheet was held in a plexiglas sample holder designed for very quick insertion into and removal from the drying system. The complete sample insertion assembly is shown as Fig 3.3, the sample holder as Fig 3.4, and the components of the sample holder as Fig 3 5 The diameter of the paper samples was fixed at 104mm because this size, easily cut from standard 158mm diameter handsheets, is sufficiently large to permit accurate determination of drying rates. Of the four principal elements shown on Fig 3 3, the top and the bottom rings carry the pressure taps, while the largest component is the insertion-withdrawal sliding section which is secured in position by a quick turn of the long handles of the tightening ring immediately below it. The insertion-withdrawal section is shown in its position during a transient drying experiment Prior to and following a drying experiment this sliding section remains in its alternate position, i.e. with the paper sample holder outside the drying system

The paper sample holder element of the insertion-withdrawal unit is shown in Fig 3 4 in its assembled state, in Fig 3 5 with its four rings detailed The 104mm diameter paper sample was clamped between the 1mm wide surfaces of the lip on the upper ring and the mating ledge on the adjacent ring, as shown on Fig 3 5. The third component shown on Fig 3.5 is the paper support, a 4 2mm thick section of aluminum honeycomb (hexagonal size 4 7mm) of open area greater than 90%, supported by the bottom ring shown Two O-rings, one on each side of

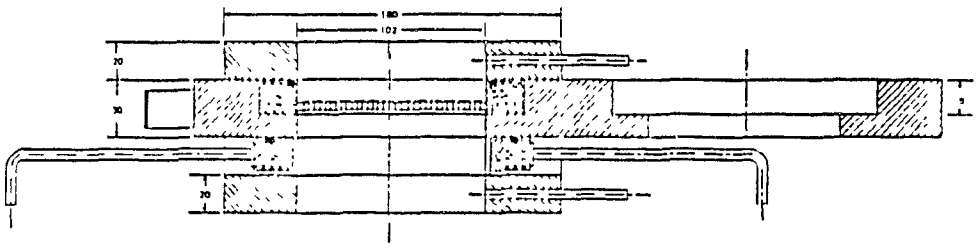

Figure 3.3 Sample insertion assembly (dimensions in mm).

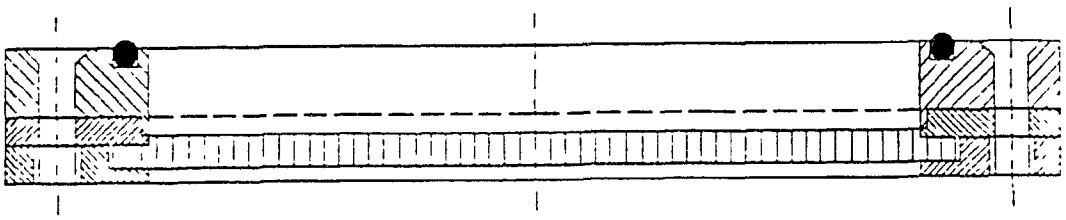

Figure 3 4 Sample holder

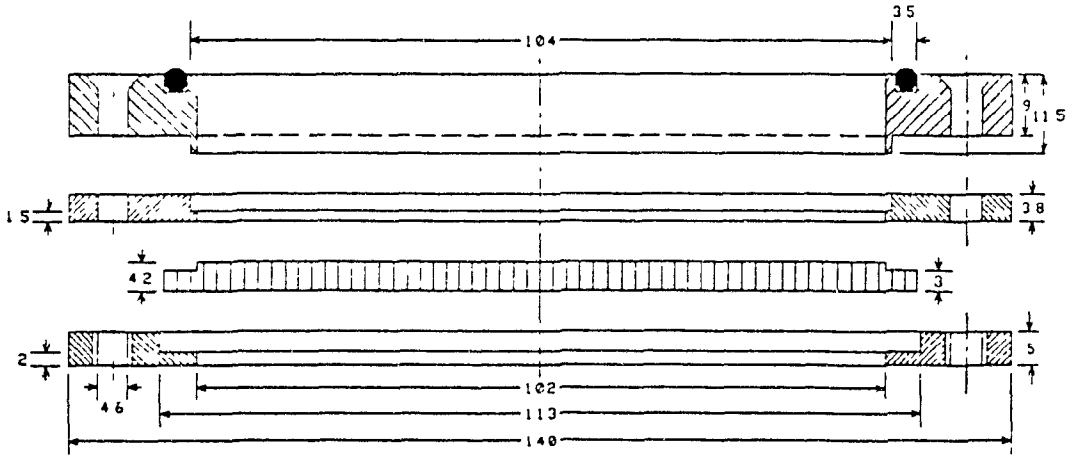

Figure 3.5 Sample holder components (dimensions in mm)

the sliding mechanism where leakage would otherwise occur, serve to prevent drying air from by-passing the paper. At the moment the sample is inserted into the drying system a perfect seal is obtained by pressing these O-rings tightly to the sliding section by means of a quick throw lever

3.3 MONITORING THE EXIT AIR HUMIDITY

The throughflow air exiting the sheet passes through the measurement cell of a Wilks Miran-1 infrared spectrophotometer for determination of humidity The instantaneous values of drying rate and paper moisture content can be calculated by mass balance from the throughflow air humidity and flowrate This indirect technique to measure drying rate was first used by Zabeschek[1977] for free-flowing granular materials in fluid beds and was later applied to the through drying of textiles by Gummel[1977] and to fluid bed drying of NPK fertilizer granules by Hallstrom[1985] Maintainence of drying conditions undisturbed by any measuring device, and very rapid response, are advantages of this technique which are critical for transient through drying experiments of very short duration

The Wilks-Miran spectrophotometer was adapted to the present use with a measurement cell of length 500mm and set to measure the absorbance of water vapor at a wavelength of 2.70μm. In the fundamental infrared spectrum range, i e excluding the near and far IR regions, water vapor has several strong absorbance bands, including at 2.55, 2.60, 2 66, 2.70 and 2 74μm The IR spectrophotometer was calibrated against a cooled-mirror dew-point meter (EG&G Model 660) using saturated salt solutions of known vapor pressure at all five of

those wavelengths. The calibration procedure is given in Appendix 2. Although the 2.66μm band is the strongest, sharpest peak in this range, 2.70μm was chosen because calibration curves at this wavelength displayed better reproducibility, perhaps due to this being a wider peak. The calibration between absorbance at 2.70μm and air moisture concentration, ρ, g/m^3, Fig 3 6, shows a non-linear dependency, represented here by a second-order polynomial The non-linearity of absorbance for long measurement cells has been discussed in detail by Houghton and Smith [1966].

The choice of length of IR measurement cell involves a balance between considerations of instrument sensitivity and of residence time for flow through the cell A measurement cell 100mm long, desirable for the latter requirement, was found to give an insufficiently accurate measurement of humidity The final choice, a pyrex glass measurement cell of length 500mm, diameter 25mm, gave good humidity accuracy while representing a mean residence time in the range of only 0.07 to 0.30s. These values should be viewed in the context that the IR instrument time constant was 0 15s

3.4 DATA ACQUISITION

The thermocouples, IR-Analyzer and pressure transducer outputs were connected to a data acquisition system based on an IBM-PC microcomputer. Each output was connected to a signal conditioning unit, Data Translation, Inc. Model DT6701 or DT6702 depending on the input voltage level, equipped with a low pass filter. The A/D board was Data Translation, Inc. Model DT2801-A with 16 single-ended channels. Typical sampling frequencies for data acquisition were in the range of 5-10 Hz

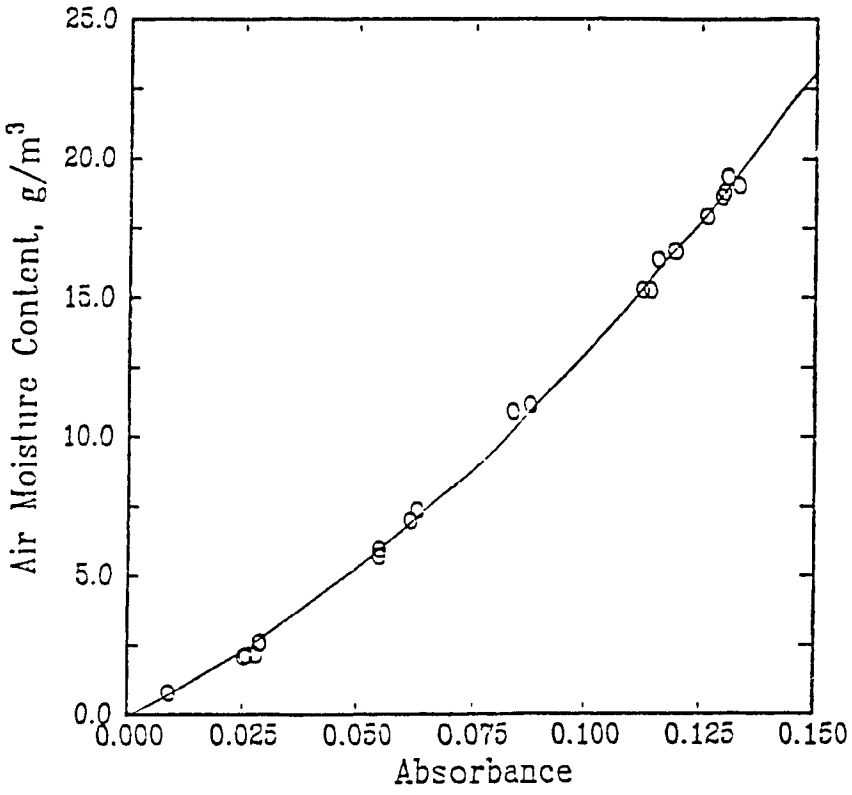

Figure 3.6 Calibration curve for IR absorbance

depending on the experimental conditions. The data acquisition program incorporated subroutines of the PC-LAB software of Data Translation, Inc. for this type of A/D board. All acquired data were stored for subsequent calculation and data processing, and were also printed out via a 3-pen recorder, Yokogawa Electric Works, Ltd. YEW Model 3660, for visual inspection of the pressure drop, exit air temperature and exit air humidity transients. Graphical output of calculated data was obtained with a Hewlett Packard Model HP7470A plotter using a modified version of MGPP (McGill University Plotting Package).

3.5 DEMONSTRATION RESULTS

3.5.1 Experimental Data

Raw experimental data, i.e , pressure drop, ΔP, exit air temperature, T_A, and exit air humidity, ρ, were plotted for visual inspection prior to further processing of the results Fig. 3.7 shows such a record for drying a handsheet made from unbleached kraft pulp, of basis weight 95g/m^2, initial moisture content about 2.0kg/kg (dry basis), dried by air of about 40°C and less than 2% relative humidity, with a superficial throughflow velocity of 0.08m/s. At time zero on Fig. 3.7 the data acquisition system starts to monitor the drying conditions, while the actual drying run starts with insertion of the wet paper sample into the system, at t=90s for the case shown. Upon insertion of the wet, low permeability sample there is an abrupt spike on the record for pressure drop, which eventually becomes steady at the much lower value corresponding to the dry paper. Exit air moisture also jumps immediately, quickly levelling off at a value which reflects the constant rate drying period. Exit air moisture then drops during the falling

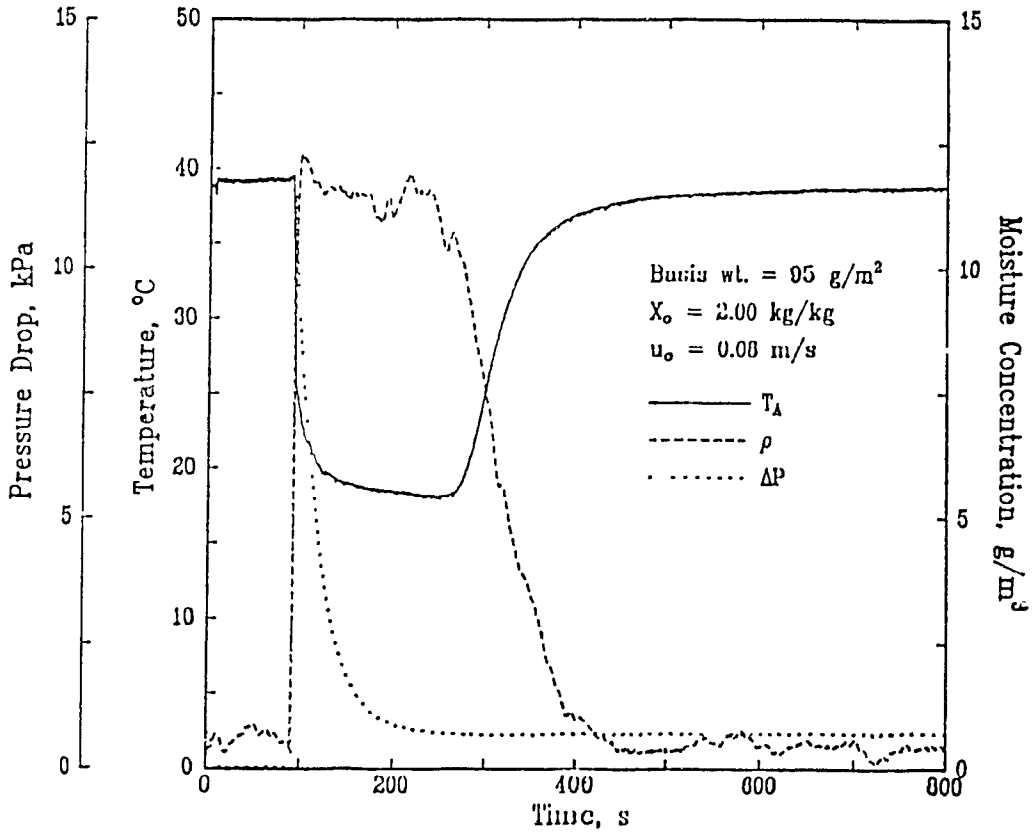

Figure 3.7 Printout of raw experimental data

rate period, reaching the inlet air humidity when drying is complete. The exit air temperature record corresponds to that for exit humidity.

From subsequent computer processing of the data, calculated results such as the paper moisture, drying rate and mass transfer coefficients were obtained and plotted

The detailed descriptions of the experimental procedures employed are given in Appendix 3, and the characteristics of the pulp used in Appendix 4.

3.5.2 Accuracy Checks

The continous monitoring of air humidity and temperature enables two checks to be made on the accuracy of the measurements

1 the total amount of water removed from paper, determined gravimetrically, may be compared with that determined by integrating the drying rate curve,

2. the continuously measured exit air temperature may be compared with that temperature as calculated via continuous heat and mass balances from the continuously measured exit air humidity.

As to the first of these checks, the total amount of water evaporated during an experiment is known accurately from the paper sample weight at the beginning and end of the run. For all experiments the amount of water evaporated, as determined by integrating the calculated drying rate curve, gave excellent checks, to within 2-3% of the value determined gravimetrically.

With respect to the other check, a comparison of the calculated and measured exhaust air temperatures is shown on Fig. 3.8 for the

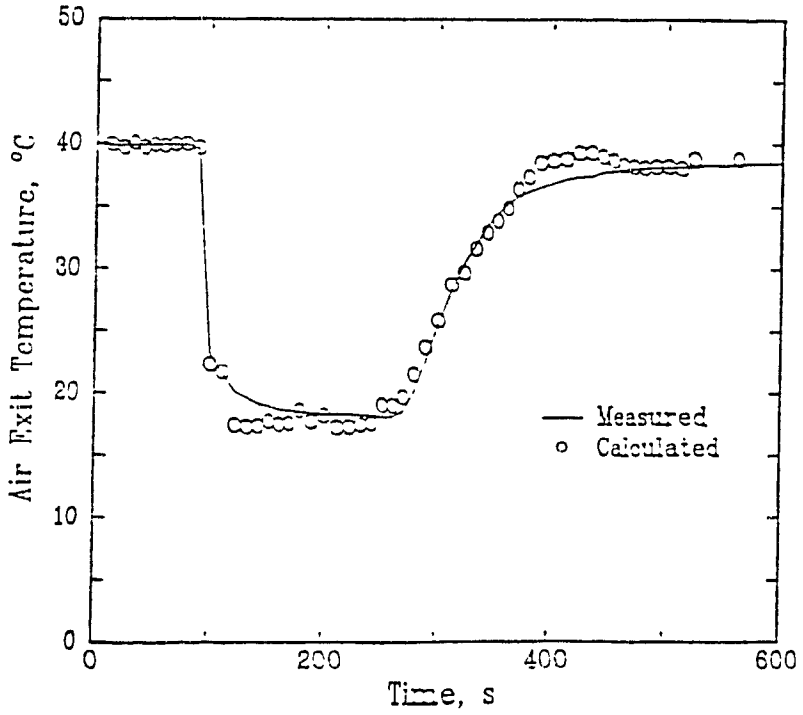

Figure 3.8 Accuracy check by heat and mass balance

experiment displayed on Fig. 3 7 Accounting for the change in paper temperature in these heat and mass balances required some auxiliary experiments. Drying experiments in the same equipment for samples with fine thermocouples embedded in the paper established that the paper reaches the adiabatic saturation temperature of the drying medium Thus paper temperature quickly drops, or rises, from its initial value, ambient temperature, to the adiabatic saturation temperature After the steady temperature assumed by the paper during the constant rate period, paper temperature rises rapidly with the drying medium temperature during the falling rate period In these heat and mass balances, the paper temperature transients, before and after the constant drying rate period, were taken as exponential functions The excellent agreement apparent in the case displayed on Fig 3 8 was typical of the results. The success of both of these accuracy checks indicates that all significant heat losses were eliminated and that the overall experimental method produced consistent and accurate measurement of the through drying rate for paper

The details of all the temperature measurements are presented in Appendix 5.

3.5.3 Calculated Data

As noted, the values of calculated variables such as drying rate and paper moisture content may be plotted relative to drying time, analogous to Fig. 3.7. More interestingly, the present experimental facility permits direct representation of calculated results, instantaneous drying rate or mass transfer coefficient, as a function of the corresponding instantaneous values of the controlling variables. Fig.

3.9 provides such a display for drying rate as a function of the corresponding moisture content of the paper for the case of handsheets of basis weight approximately 100g/m^2, dried by throughflow of 24°C air at superficial throughflow velocities ranging from 0.08 to 0.43m/s.

For any transient experiment there is an initial period of either heating or cooling of the paper For the series of experiments shown on Fig 3.9, for which the adiabatic saturation temperature is below the initial paper temperature, this initial period is one of cooling the paper, hence the initial high drying rates while the paper is cooling to the temperature it assumes during the constant drying rate period which follows When the adiabatic saturation temperature is above the initial paper temperature, the opposite effect prevails

The length of the constant drying rate period naturally decreases as air throughflow rate or inlet temperature increases, or as paper basis weight or paper initial moisture content decreases. All runs end with a falling rate period, the length of which is a function of the drying conditions

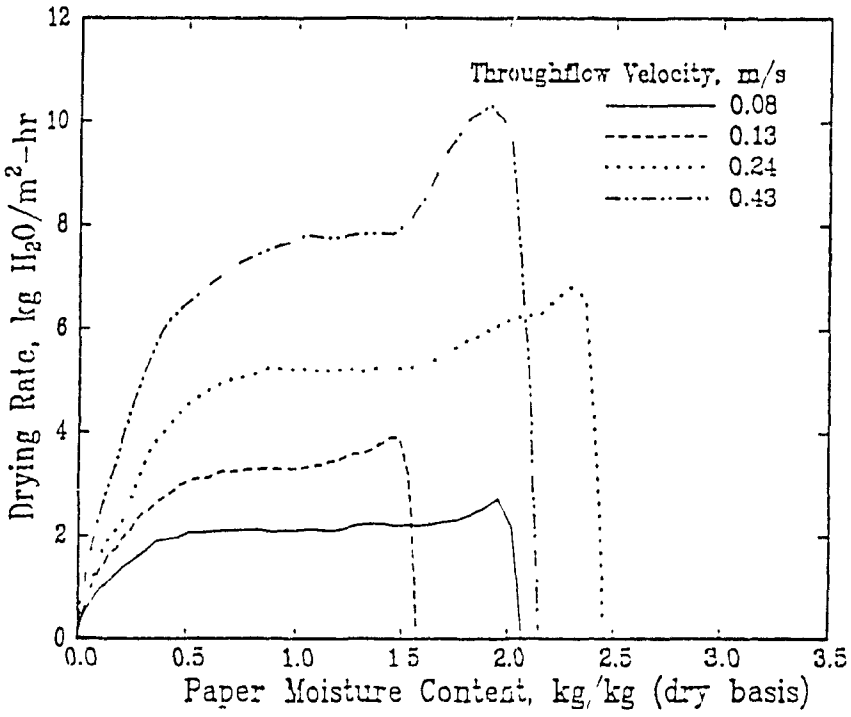

Figure 3.9 Through drying rate dependence on throughflow air velocity

CHAPTER 4

THROUGHFLOW ACROSS MOIST AND DRY PAPER

4.1 INTRODUCTION

A transport phenomena analysis for any process involving air flow across paper, such as through drying, requires characterization of the porous structure of paper As there is a choice of experimental techniques for characterizing porous media, the method used must relate directly to the processes concerned in throughflow

For dry paper, results of the numerous studies of permeability and specific surface differ considerably, depending on the type of pulp and the measurement technique The dependance of specific surface on the measurement technique derives from the complexity of the microstructure of paper Thus quite divergent values of specific surface can be correct measures of different types of fibre interfacial area Although there are numerous investigations of the permeability and specific surface of dry paper of medium to heavy grades, there are none at basis weights as low as our interest, 25g/m^2

For wet paper, the only studies to have made even limited measurements of the effect of paper moisture content on its permeability to air flow are those of White and Marceau[1962], Brundrett and Baines[1966], Burgess *et al* [1972a,b]. Those investigations are incomplete and contain contradictions. The experimental plan for our associated study of through drying rates provided the opportunity for a simultaneous study of momentum transport in air flow through paper over a wide range of basis weight and for moisture content over the full span from wet to dry Although the intended transport phenomena analysis of through drying rates required a

full momentum transport study, the latter subject, of intrinsic interest beyond this specific use, is the focus of this chapter.

4.2 EXPERIMENTAL

The equipment for permeability-through drying experiments was designed to permit simultaneous measurement of the transient values of pressure drop and drying rate, and of the controlling variables - moisture content and thickness of the paper, humidity and temperature of the throughflow air Each such experiment was conducted at a fixed value of mass flow rate of throughflow air across 104mm diameter sheets A description of the experimental technique was recently published (Polat *et al* [1987]), and additional details are provided in Chapter 3

Paper of basis weight 25, 50, 100 and 150g/m^2 from a standard handsheet apparatus was prepared, wet pressed at 345kPa and dried, all according to CPPA Standard C 4 Most handsheets were prepared from standard dry laboratory kraft pulp (unbeaten, unbleached, 100% black spruce, ~18-19 kappa number, CSF 685ml) which had not previously been formed The sheets when dry were of apparent density ~0 5g/cm^3 A few experiments were made with newsprint prepared on a Papriformer from reslushed mechanical pulp Sheets of 250g/m^2 were standard pulp testing blotters, of thickness 0 508±0.013mm, from a Quebec mill of DOMTAR Pulp and Paper Inc.

For a particular sheet and set of throughflow conditions, each experiment involved obtaining simultaneously the complete momentum transport and drying rate history of that sheet over the entire range from wet to dry In order to determine the extent of change of through-flow characteristics when a sheet is subjected to a complete wetting-

drying cycle, ΔP measurements were also made prior to a through drying experiment. After these tests the sheet was moistened to the desired initial moisture content for a complete permeability-through drying experiment Measurement of throughflow characteristics of the same sheet when moist and when dry, both before and after a wetting-through drying cycle. identifies conditions which change paper microstructure and those for which microstructure remains unchanged

4 3 PERMEABILITY OF DRY PAPER BEFORE A WETTING-THROUGH DRYING CYCLE

4 3 1 Permeability from Darcy's Law

Preliminary tests showed that at industrially relevant rates, air flow through paper is not a purely viscous flow but has a significant inertial component Therefore experiments with throughflow rates of 0.08-0.70kg/m^{2}s (0 07-0 60m/s superficial velocity) with air were supplemented with a fluid of much higher kinematic viscosity, helium, at throughflow rates of 0 02-0 20kg/m^{2}s (0 12-1 20m/s) These throughflows, all at ambient temperature, were repeated in triplicate, i.e. with three handsheets. The measurements, when correlated as

$$\Delta P = m\, G^n \qquad (4.1)$$

gave the values for the exponent, n, listed in Table 4 1, with correlation coefficients, r^2, in every case better than 0.999.

TABLE 4.1. Values of the exponent n for dry paper before a wetting-through drying cycle

Basis weight, g/m^2	25	50	100	150	250
Air flow	1.240	1.072	1.051	1.016	1.011
Helium flow	1.079	1.010	0.999	0.998	1.000

Flow through paper is customarily treated as a viscous flow, which in the form known as Darcy's law, is

$$\frac{\Delta P}{L} = \frac{\nu}{k'} G \qquad (4.2)$$

where L is paper thickness and k' the Darcy permeability Table 4.1 shows that for air flow through paper the assumption of viscous flow, i.e of Darcy's law, which implies n=1 in Eqn. 4 1, is never fully satisfied but is approached for the thickest paper, i.e. that of the highest basis weight With decreasing basis weight a growing inertial contribution to pressure drop with air is apparent

The value n=1 24 for 25g/m^2 paper agrees with the value n=1 21 which may be determined from the data of Gummel[1977] for tissue paper of basis weight 20 and 23g/m^2 Gummel in fact split his data at an air velocity, u=0 1m/s, and for his correlations below and above this value obtained the values of n of 1 and 1 5, respectively However his results can also be correlated well with a single regression as $\Delta P=mG^n$ with n=1 21

The results with helium, Table 4.1, indicate a more viscous flow than with air. This difference reflects the decrease in Reynolds number caused by the 7 5 times larger kinematic viscosity of helium An inertial contribution to pressure drop is none the less evident even for helium with lighter weight paper

4.3.2 Permeability from the Momentum Transport Equation

Momentum transport for the general case of flow through porous media, i.e. including both the viscous and inertial terms, is represented as

$$\frac{\Delta P}{L} = \alpha\mu u + \beta\rho u^2 \qquad (4.3)$$

The first and second terms represent the viscous and inertial contributions to ΔP, where u is superficial velocity and α and β are complex viscous and inertial term parameters. The applicability of this form, commonly referred to as the Forchheimer relation, has been established

for both consolidated and unconsolidated media. By solving the momentum equation using Slattery's averaging theorem, Dullien and Azzam[1972] found the theoretical definitions of α and β to be as follows:

$$\alpha = \frac{1}{D^2 V} \iiint \nabla^2 \mathbf{v} \, dV \quad : \quad \beta = \frac{1}{D\ V} \left(\iiint \mathbf{v} \nabla \mathbf{v} \, dV + \iint \frac{P}{\rho u^2} \mathbf{n} \, dA \right)$$

where D is the characteristic length of flow, V the averaging volume, **v** the velocity vector, **n** the unit vector, u the superficial velocity and A the surface bounding the averaging volume The volume and area integrals are on the associated fluid volume and solid-fluid interface in the averaging volume The α-β definitions of various authors differ slightly due to differences in the simplifying assumptions used and in the solution technique employed, but all involve complex volume and area integrals. The equation parameters are also related to permeability as α=1/k and β=C/$\sqrt{k}$ where C is an inertial flow constant For β=0, the equation reduces to Darcy's law

For determination of permeability, k, and the inertial constant, C, from ΔP data as a function of mass flow rate, G, Eqn. 4.3 may be rearranged to the form of the so-called Forchheimer plot

$$\frac{\Delta P}{\nu G L} = \alpha + \beta \frac{G}{\mu} \qquad (4\ 4)$$

Appendix 6 provides a sample calculation and tabulation of permeability values Fig. 4 1 is a Forchheimer plot with ΔP-G data for air used for Table 4 1 The results, Table 4.2, appear as the "before wetting-drying" data of Fig. 4 2 The number of sheets of paper tested of each basis weight is indicated by N, and the values of the parameters listed are the best fit values for the data from N sheets. The coefficients of determination show that this theoretical relationship fits the data almost as well as the purely empirical Eqn. 4 1. The values of σ_α and σ_k, less than 2% of the respective variables, are excellent. Although

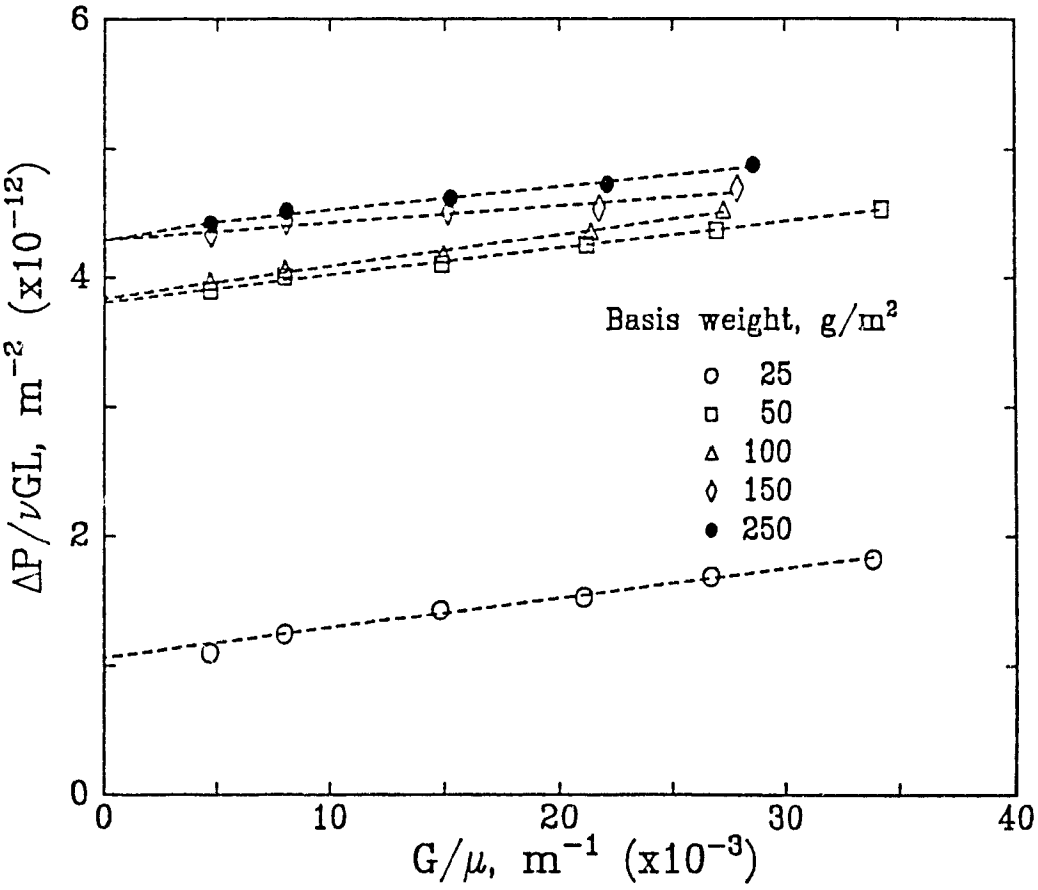

Figure 4.1 Momentum transport relation for permeability: dry paper before wetting-drying

TABLE 4.2. Momentum Transport Parameters for Dry Paper, before a Wetting-Through Drying Cycle

M_D, g/m²	N	α, m⁻²	σ_α, m⁻²	β, m⁻¹	σ_β, m⁻¹	r^2	k, m²	σ_k, m²	C
Air Flow									
25	3	1.06×10^{12}	2.5×10^{10}	2.29×10^{7}	9×10^{5}	0.993	9.43×10^{-13}	22×10^{-15}	22.2
50	3	3.81	2.0	2.09	8	0.998	2.62	1.4	10.7
100	3	3.84	2.6	2.46	16	0.996	2.60	1.8	12.5
150	3	4.29	0.8	1.33	11	0.968	2.34	0.44	6.4
250	3	4.34	1.8	1.82	17	0.994	2.30	0.96	8.7
Helium Flow									
25	3	1.07	2.0	2.43	15	0.974	9.35	18	23.5
50	3	3.49	2.0	2.57	17	0.977	2.87	1.6	13.8
100	3	3.70	0.8	0	-	-	2.70	0.58	0
150	3	3.80	0.9	0	-	-	2.63	0.62	0
250	3	3.90	0.95	0	-	-	2.56	0.63	0

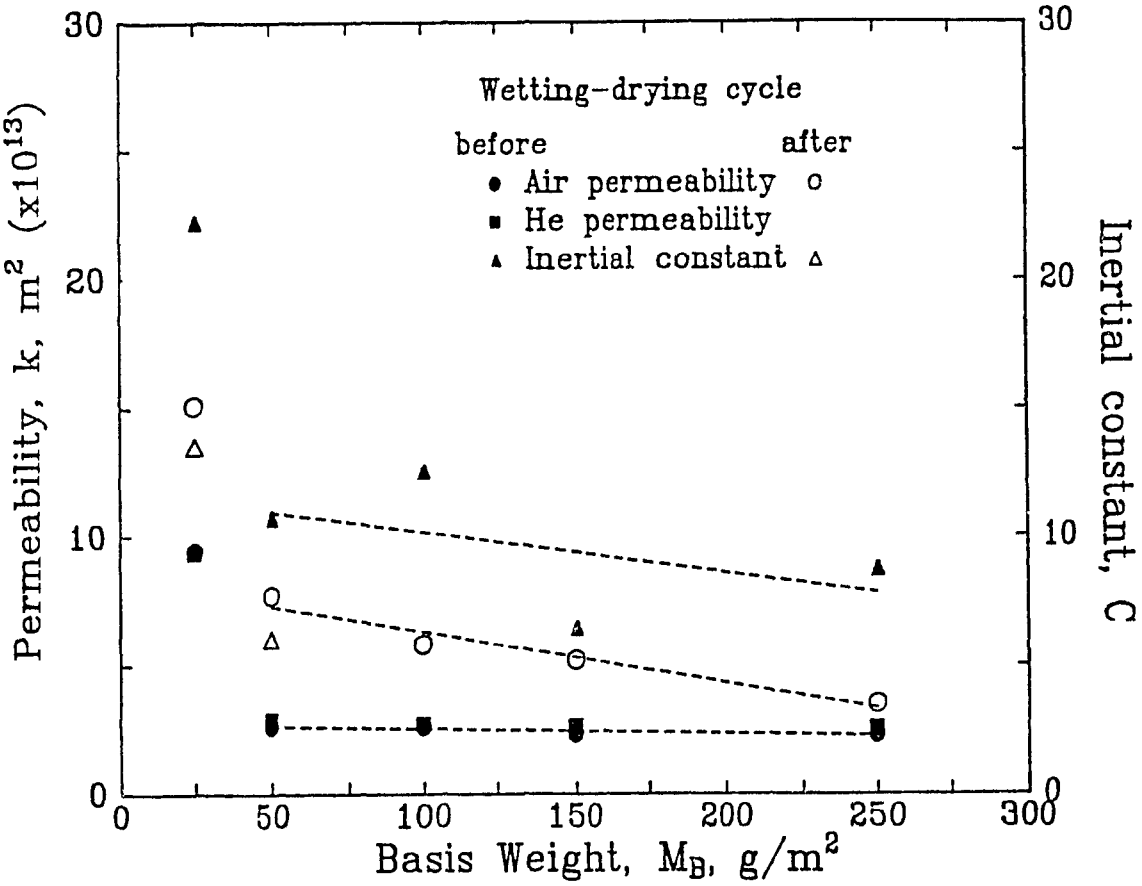

Figure 4.2 Effect of basis weight on permeability of dry paper

β is more difficult to measure accurately the values of σ_β in the range 4-9% are also very good. These values of σ derive primarily from the variation in formation between the different handsheets tested.

The inertial contribution to pressure drop, indicated by the parameter C, is maximum for the lightest weight paper, 25g/m^2, and becomes small or negligible for heavy paper. An inertial component in the flow is evidently detected much more sensitively with the momentum transport relation than by inspection of the exponent of the power law relationship, Eqn. 4.1. As shown in Fig 4.3, the fraction of pressure drop which derives from inertial effects, $(\beta G^2/\rho)/(\Delta P/L)$, approaches 50% for the combination of thinnest paper at the highest air throughflow rate. Even for heavier paper, of basis weight 50-100g/m^2, the inertial contribution to ΔP is in the range 15-20% for the maximum throughflow rates used here and would be substantially higher yet at the maximum throughflow rates used industrially.

4.3.3 Effect of Paper Basis Weight on Permeability

It might seem that permeability, being derived from $\Delta P/L$, should be independent of paper thickness or basis weight. The results, Fig. 4.2, indicate otherwise. With decreasing basis weight permeability increases, at first slightly, then with a big jump between 50 and 25g/m^2 paper. Thus straight lines are shown through Fig. 4.2 data over the basis weight range 50-250g/m^2, while the values for 25g/m^2 paper are simply shown as such. The small increase of k with decreasing M_B from 250g/m^2 to 50g/m^2 probably derives from small changes in pore size and pore size distribution. Based on the gas-drive technique of Corte[1958] to determine pore size distribution, the measurements of Bliesner[1964]

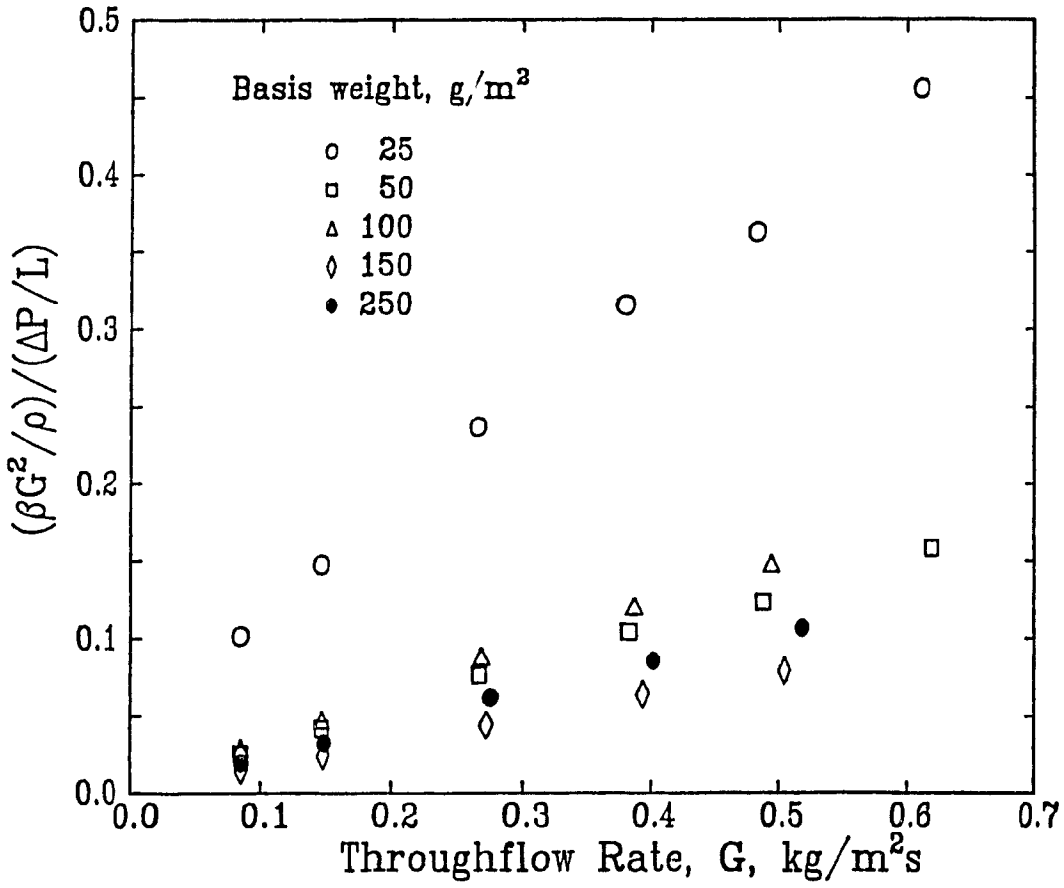

Figure 4.3 Effect of throughflow rate on inertial contribution to pressure drop: dry paper before wetting-drying

indicate that as paper thickness increases, mean pore size decreases and the pore size distribution becomes narrower. These trends are consistent with the decrease in permeability towards an asymptotic value, observed here, as basis weight increases.

The tripling in permeability for a reduction in basis weight from 50 to 25g/m^2 suggests a different mechanism. Corte and Kallmes[1962], Corte and Lloyd[1966], and Wiseman[1987] have noted that pin hole counts for commercial paper increase exponentially with decreasing basis weight. Pin holes accomodate disproportionately large flow rates. The large increase in permeability at such a low basis weight thus reflects a substantial fraction of flow occuring through pin holes.

4.3.4 Effect of Pulp Type on Permeability

With a furnish of bleached softwood kraft pulp, CSF 345ml, of apparent density ~0.72g/cm^3, Knauf and Doshi[1986] measured Darcy's law permeability to air about twice as high for handsheets of 60g/m^2 ($k=0.16\times10^{-13}m^2$) as for 200g/m^2 ($k=0.083\times10^{-13}m^2$). The basis weight below which permeability increases sharply would be expected to depend on the pulp used and on sheet formation techniques which affect pin hole formation. Knauf and Doshi employed a highly beaten pulp, CSF 345ml; the present study used an unbeaten kraft pulp of CSF 685ml. As the percentage of fines is much higher in beaten pulps, the retained fines decrease permeability appreciably below that measured here for paper from an unbeaten pulp. As sheet thickness increases, the percent fines retained also increases, giving much lower permeability. Therefore the steeper drop in air permeability of Knauf and Doshi with increasing basis weight over the 60-200g/m^2 range appears related to

differences in the pulp used.

4.3.5 Permeability Comparisons

Permeability values obtained from helium and air flow experiments (Table 4.2) agree remarkably well, averaging within 9% over the basis weight range 50-250g/m^2. This difference could be due to molecular flow effects. If the mean free path of molecules is an appreciable fraction of pore diameter, the phenomenon variously called slip flow, free molecular flow or Knudsen flow occurs at the pore walls. Although typically associated with low pressure flow, Corte[1982] claims that slip flow in paper may contribute appreciably even at atmospheric pressure. The pore size in paper has been reported to be in the range of about 0.1-10 microns, Carson[1940], Bublitz *et al.*[1948], Bliesner[1964]. As the mean free path of air and helium at 20^{0}C and 100kPa is about 0.09μm and 0.3μm, respectively, the slip effect could be present, particularly in helium permeation. This effect is consistent with the permeability being slightly higher for helium than air for heavier paper, of basis weight 50g/m^2 and above. The effect disappears with the larger pore size of 25g/m^2 basis weight paper, Table 4.2, for which permeability measured by air and helium flow is, within 1%, the same.

The air resistance values for the 250g/m^2 blotter paper, measured by Gurley densometer at the Pulp and Paper Research Institute of Canada according to CPPA Standard D14 prior to the shipment to our laboratory, gave permeabilities in the range of 1.8-2.2x10^{-13}m^2, very close to the Table 4.2 value, 2.3x10^{-13}m^2. Those permeabilities were calculated from Darcy's law because the method gives only the time elapsed during passage of a specified amount of air, generally 100cm^3, but the error

in k from this assumption is small for paper this thick.

The permeabilities measured here, Table 4.2, Fig. 4.2, agree well with those previously reported for similar paper. Carson[1934] reported $k=2.1x10^{-13}m^2$ for blotter paper. Knauf and Doshi[1986] used the Gurley densometer and Bendtsen porosimeter to measure air flow through $200g/m^2$ handsheets of apparent density $0.6g/cm^3$ made from unbeaten bleached softwood kraft pulp,of freeness CSF 725ml Their permeability, $2.38x10^{-13}m^2$, also agrees well with the present study. They observed that permeability increases as freeness (CSF) of the pulp increases and as apparent density of the paper decreases, with both effects quite important. The permeabilities of $5.75x10^{-13}m^2$ and $2.67x10^{-13}m^2$ reported by Bliesner[1964] for $100g/m^2$ sulfite handsheets wet pressed at 345 and 690 kPa respectively show the sensitivity of permeability to wet pressing conditions. The above permeabilities were all calculated by assuming Darcy's law.

When there is an inertial component to momentum transfer but permeability is determined assuming, incorrectly, Darcy's law, the permeabilities thus calculated are erroneously low. This error is small only for combinations of low throughflow rate-high basis weight. For the combination of maximum throughflow rate-minimum basis weight of the present study, the use of Darcy's law would result in an error in k of about 40%. Previous researchers either ignored the fact that the contribution to ΔP by inertial effects in gas flow through paper can be important, or tried to minimize this effect by restricting their studies to very thick paper and/or very low flow rates. The magnitude of the inertial constant, C, and the trends in C with paper thickness, Fig. 4.2, show that the factors which contribute to higher permeability con-

tribute also to higher inertial pressure drop. The present work is the first study of paper permeability which accounts for the inertial resistance. Thus permeability, correctly determined, has been documented for a wide experimental range of both air flow, $0.07<u<0.60$m/s, and basis weight, 25-250g/m^2, without this approximation of previous investigations.

4.4 PERMEABILITY OF DRY PAPER AFTER A WETTING-DRYING CYCLE

4.4.1 Experimental Results

Comparison of the above results with permeability measurements at the end of each permeability-through drying experiment indicates whether structural changes occuring during a complete wetting-drying cycle are irreversible. For each basis weight in the range 25-150g/m^2, the permeability at the end of a wetting-throughflow cycle was determined from 35 to 65 such experiments, each with a different handsheet, performed for various combinations of throughflow rate, G, 0.09-0 52kg/m^{2}s; throughflow inlet temperature, T_1, 20-90°C; and initial paper moisture content, X_o. For the associated through drying measurements T_1 and X_o are important variables, but simply provide replicate experiments for the ΔP of dry paper.

The experimental results, Table 4.3, Fig. 4.4, are analogous to those of Table 4.2, Fig. 4.1. At each basis weight the number of sheets tested is N. Forchheimer plots are shown only for the data of highest experimental scatter, i.e. for the two lowest basis weights. The greater scatter on Fig. 4.4 than Fig. 4.1 reflects the measurement of ΔP-G values for a much larger number of sheets, N. Thus for each basis weight, the line on the Forchheimer plot which determines a value of k

TABLE 4.3 Momentum Transport Parameters for Dry Paper, after a Wetting-Through Drying Cycle

M_B, g/m^2	N	α, m^{-2}	σ_α, m^{-2}	β, m^{-1}	σ_β, m^{-1}	r^2	k, m^2	σ_k, m^2	C
25	65	0.66×10^{12}	4.6×10^{10}	1.10×10^{7}	8×10^{5}	0.87	15.1×10^{-13}	110×10^{-15}	13.5
50	61	1.30	9.6	0.69	7	0.89	7.7	57	6.0
100	61	1.70	16.0	0	-	-	5.8	55	-
150	35	1.94	19.9	0	-	-	5.2	53	-
250	6	2.80	18.0	0	-	‡‡	3.5	23	-
45‡	9	13.0	25.0	4.70	33	0.995	0.78	1.5	130.0

‡ groundwood furnish, Papriformer newsprint, three flow rates only
‡‡ two flow rates only

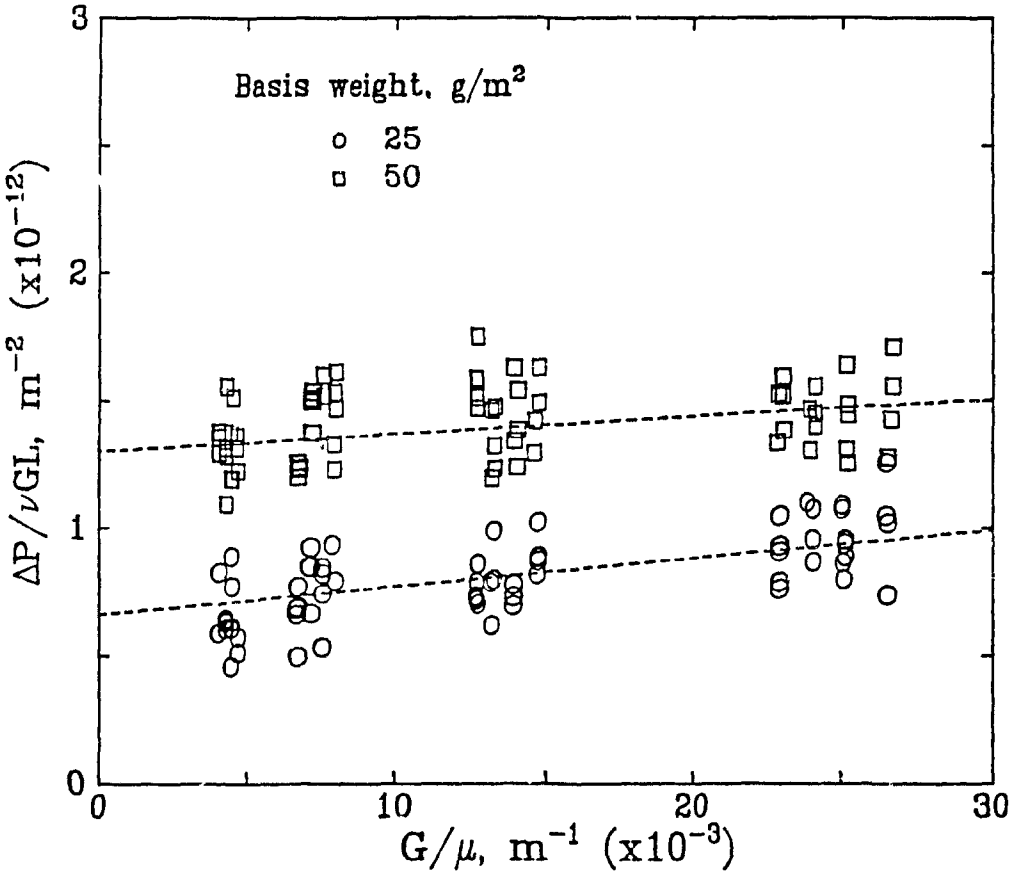

Figure 4.4 Momentum transport relation for permeability: dry paper after wetting-drying

and C is defined by ΔP-G measurement from as many as 65 sheets of paper after a wetting-drying cycle, Fig. 4 4, from 3 sheets for the measurements prior to this cycle, Fig. 4.1 In all cases the values of σ_α and σ_k are in the range 2-7% of the respective α and k, while σ_β is 7-10% of the value of β. These values of σ are similar to those noted for Table 4.2. Variation in structure between sheets is the source of essentially all scatter because of the very high precision of ΔP-G measurements. Analogous to Fig. 4.3, Fig. 4.5 shows $(\beta G^2/\rho)/(\Delta P/L)$, the fraction of pressure drop which derives from inertial effects. Even for low throughflow rates, $G \simeq 0.3$ kg/m^{2}s, $u_s \simeq 0.23$m/s, the inertial term accounts for 1/4-1/3 of ΔP.

For the same kraft paper before and after a wetting-through drying cycle the trends in the k-M_B relationship, Fig. 4.2, are similar but k is about twice as high after the wetting-drying operation. Over this complete cycle some changes in paper microstructure are evidently irreversible. Permeabilities measured after wetting-drying agree with results of the few previous comparable studies. Thus for paper after a wetting-drying cycle, White and Marceau[1962] reported $k \simeq 9 \times 10^{-13}$m^2 for 83g/m^2 filter paper of a southern kraft furnish, and 4.4×10^{-13}m^2 for 269g/m^2 blotting paper made from a furnish of 17% bleached soda, 32% bleached sulfite, 51% cotton linter, plus clay and starch(~70kg/ton fibre). As they assumed Darcy's law their results are somewhat lower than the correct values. Although their measurements were made at a sheet moisture content of approximately 0.25kg/kg, the observation that permeability does not change significantly with decreasing moisture content below $X \cong 0.3$, made initially by Brundrett and Baines[1966], was established more extensively in the present work, Section 4.5. For

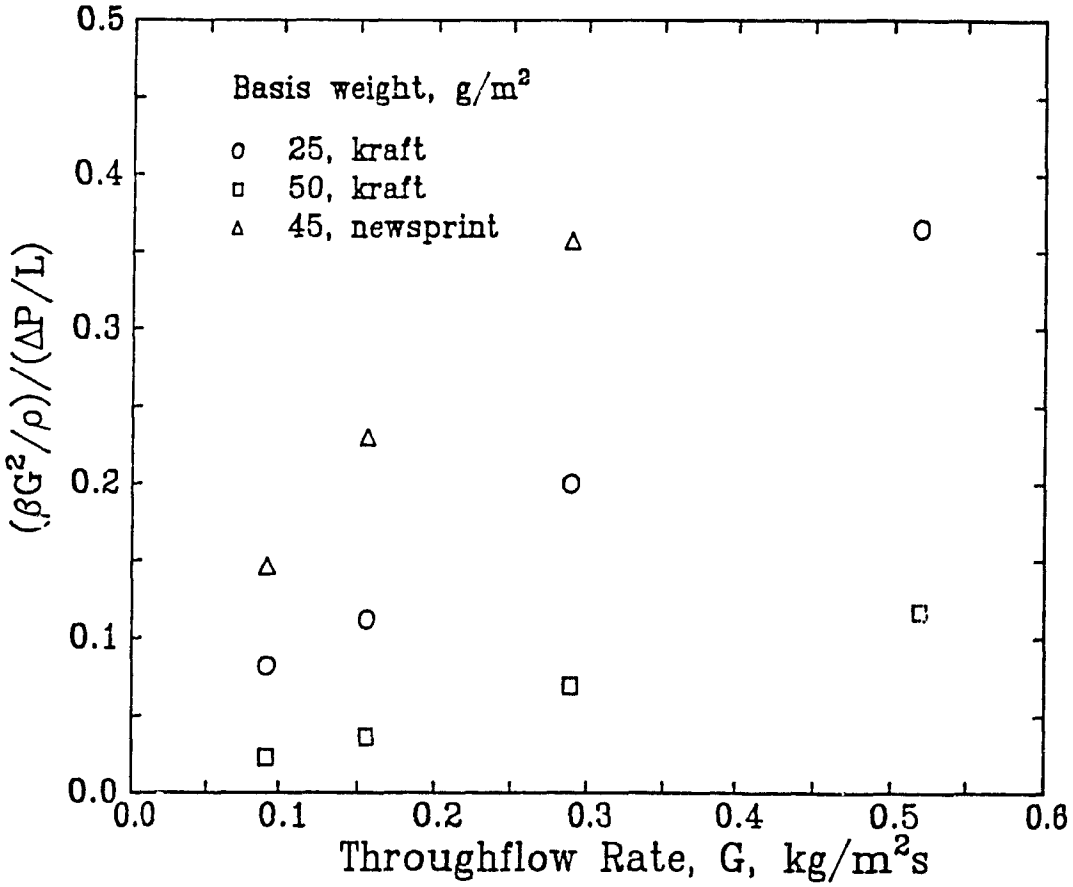

Figure 4.5 Effect of throughflow rate on inertial contribution to pressure drop: dry paper after wetting-drying

Papriformer newsprint, the permeability measured here after a wetting-drying cycle, $0.78 \times 10^{-13} m^2$, is two to three times that for the paper from never-dried stock measured by Burgess *et al.*[1972a,b], $0.2\text{-}0.3 \times 10^{-13} m^2$ (calculated assuming Darcy's law). Thus the present study indicates that for both newsprint and kraft paper, permeability increases substantially after paper is subjected to a wetting-drying cycle.

4.4.2 Permeability Changes during Wetting or Drying

A fundamental question is whether this substantial permeability increase when paper is subjected to a wetting-drying cycle is caused by irreversible changes occuring during the wetting, the drying, or both. The only previous measurement of permeability before and after a wetting-drying cycle is that of Brundrett and Baines[1966]. They reported flow and pressure drop measurements for commercial paper, both kraft and newsprint, produced from never-dried stock and, apparently, for other samples of the same paper after a wetting-drying cycle. Although they gave results only as the modified permeability, k/L, calculated assuming Darcy's law, and did not record sheet thickness, one may estimate the latter from their basis weight values and thereby estimate permeability from their measurements as follows:

	Before wetting-drying		After wetting-drying	
Pulp furnish	M_B, g/m^2	k, m^2	M_B, g/m^2	k, m^2
kraft press broke	85	0.36×10^{-13}	77	0.15×10^{-13}
newsprint	52	0.094×10^{-13}	52	0.135×10^{-13}

Thus their results for the effect of a wetting-drying cycle are contradictory, indicating a decrease in permeability of kraft paper but an increase for newsprint, in both cases by substantial amounts. They related this discrepancy to a higher percentage of fines retained by

commercial kraft paper which is wetted and dried compared to their laboratory formed sheet from press broke.

For newsprint formed in their laboratory, Brundrett and Baines obtained permeabilities almost an order of magnitude smaller than for machine made newsprint, a difference they attributed to their simple, non-standard laboratory formation technique Therefore the discrepancy between their newsprint permeabilities and those measured here, Table 4.3, appears due to their inappropriate sheet formation technique. Moreover as they did not change drying conditions, their data provide no indication as to the source of the large permeability change over a wetting-drying cycle Thus questions as to the change in permeability of dry paper that undergoes rewetting and drying, and the source of this change, were not clarified by the Brundrett and Baines study due to the shortcomings noted.

In the present study permeability of the same sheet is measured, before and after a wetting-drying cycle, in an experimental plan which also includes major variations in drying conditions, i.e. change of throughflow rate, G, by a factor of 5, Fig. 4.4, and change in through-flow air inlet temperature, T_1, between 20°C and 95°C. Drying rate is thereby changed enormously, by a factor of 20. However, permeability change over a complete wetting-drying cycle does not correlate with these very large changes in through drying conditions and drying rates. Thus the present study establishes that over a wetting-drying cycle the permeability of dry paper approximately doubles, and that it is irreversible changes in porous structure which occur during wetting that are the prime source of this doubling of permeability.

The values of the inertial constant, C, before and after a wetting-

drying cycle, Table 4.2 and 4.3, Fig. 4.2, show that over such a cycle the increase in permeability is accompanied by a decrease in the inertial constant. Some mechanism evidently links an increase in k with a decrease in the inertial contribution to ΔP.

4.4.3 Mechanisms of Permeability Change during Wetting

Relaxation of internal stresses during the wetting part of a wetting-drying cycle should increase permeability. During drying under restraint, stresses produced by lateral shrinkage pull fibre-fibre bonds apart, thereby generating fibrils at bond sites These bonds are of such strength that, when a sheet is dried free of restraint, micro-compressions form at the bond sites, as first observed by Page and Tydeman[1962]. When a sheet dried under restraint, stressed and fibrillated at the bond sites, is wetted, stress relaxation occurs because inter- and intra-fibre hydrogen bonds break and reform in the presence of water, thereby allowing fibrils to collapse back onto the fibre surface.

This collapse of stress induced fibrils, an irreversible process, is believed to be the main mechanism for the permeability increase over a complete wetting-drying cycle. In their interfacial area measurements of dry handsheets before and after a moistening-drying cycle, Gurnagul and Gray[1987] concluded that the specific surface decreases more from the collapse of stress-induced fibrillation than it increases due to fibre swelling. As fibre swelling on wetting and shrinkage on drying would continue over repeated cycles of wetting-drying, this is not a mechanism for the large irreversible change in permeability observed over such a cycle. Collapse of fibrils on the fibres increases permeability because of the decrease in inertial effects, i.e. the

irreversible flow processes from stalls, vortices and wakes in the channels. Reducing the number of obstacles, i.e. fibrils, in the flow channels reduces these irreversibilities in the flow, reflected in turn by the lower inertial constant and higher permeability. This aspect is discussed further in Section 4.7.

This wetting process should not be confused with reslushing, i.e. disintegrating a dry sheet to its constituent fibres and re-forming a sheet. As standard laboratory pulp is stored dry, the permeability measurements made "before a wetting-drying cycle" are necessarily preceded by wetting the pulp fibres when forming the sheet. On that initial wetting any changes in fibre microstructure would be small since the fibres were originally dried as a loose pulp, not as a restrained web. Reslushing involves quite different phenomena because on the larger scale, formation is set during drainage, while on the smaller scale, formation is modified during pressing. The effect of relushing on paper permeability has not been reported. What is relevant to the present study are the changes in fibre morphology which affect the microstructure of pores which participate in the throughflow process for sheets of already established formation.

4.4.4 Effect on Permeability of Pulp Type and Formation Technique

The permeability of dry paper is dependent not only on its thickness and on its wetting-drying history, but on the type of pulp and the technique used to form the web. The permeability of the 45g/m^2 Papriformer newsprint, Table 4.3, is about 1/10 of that of kraft handsheets of comparable basis weight. Although the forming technique would make the Papriformer sheets more permeable, the dominant effect

is evidently that of pulp type, as groundwood pulp produces a less permeable sheet. The scanning electron micrographs(SEM) of Fig. 4.6a illustrate the extensive fibrillation and high fines content of the mechanical pulp used for newsprint, compared to long clean fibres of unbeaten kraft. Further differences between the Papriformer newsprint and kraft handsheets of ~50g/m^2 are shown by the SEM photographs of the paper surface, Fig. 4.6b, and cross-sections, Fig. 4.6c. Thus the permeability of newsprint, lower by an order of magnitude than the equivalent sheet of kraft paper, results from more fibrillated fibres, Fig. 4.6a, in a web of higher bonded area, Fig. 4.6b, with more fines present in the interfibre pores, Fig. 4.6c.

4.4.5 Conclusions

The only previous attempt, Brundrett and Baines[1966], to determine the effect of wetting and drying on the permeability of paper formed in different ways from different pulps provides contradictory and inconclusive results. The work of Gurnagul and Gray[1987] focussed on the effect on specific surface which results when paper is remoistened, by humid air, up to a moisture content of only 20%. The present work provides the first comprehensive measurements of these effects on the permeability of paper and does so for a wide variety of experimental conditions and without the error associated with the use, by all previous workers, of the Darcy's law approximation. Important but little studied aspects of paper microstructure change during wetting and drying have thereby been revealed.

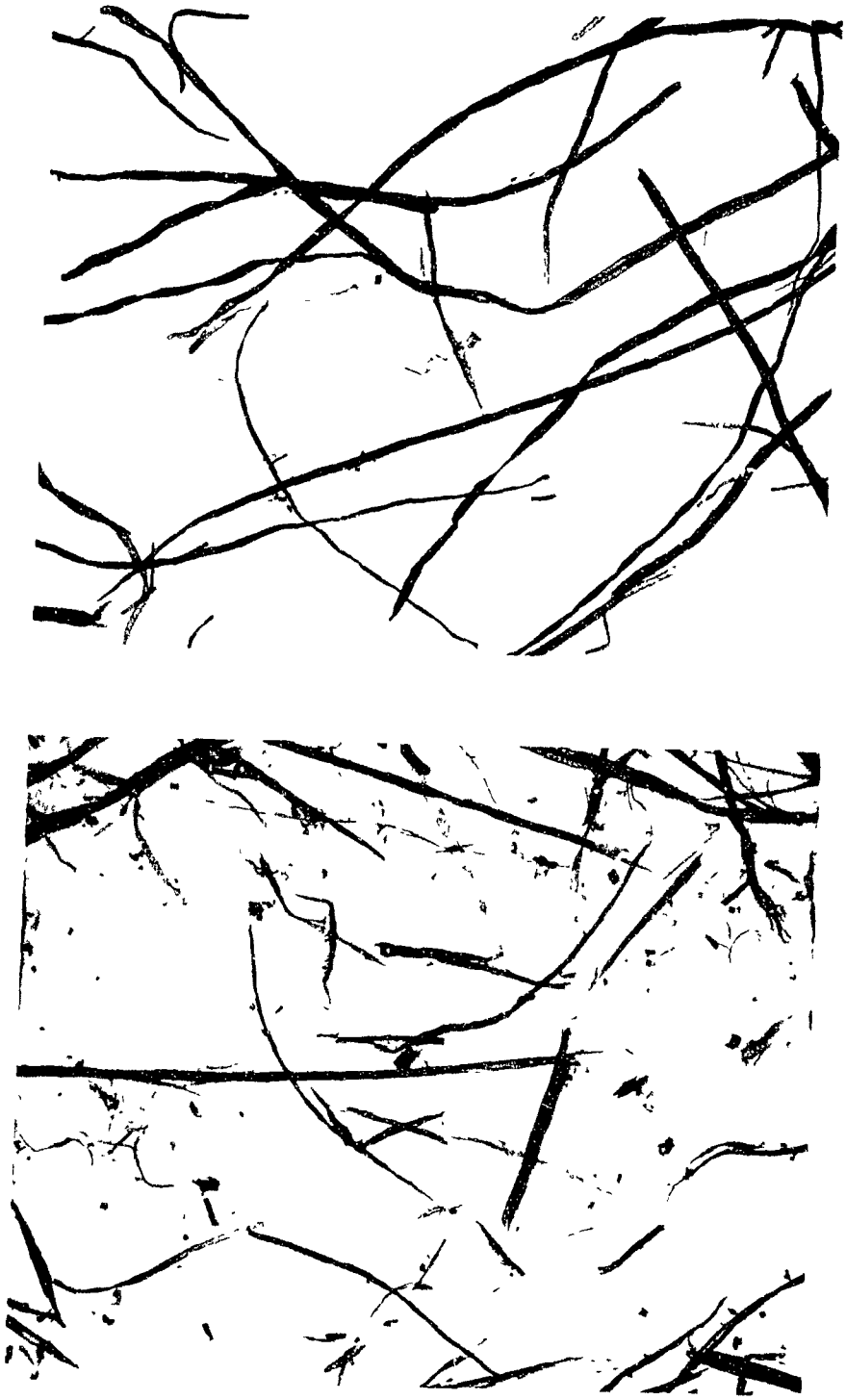

Figure 4.6 Scanning Electron Micrographs of 50g/m² kraft handsheet and 45g/m² Papriformer newsprint; a) individual fibres, b) sheet surface, c) cross-section.

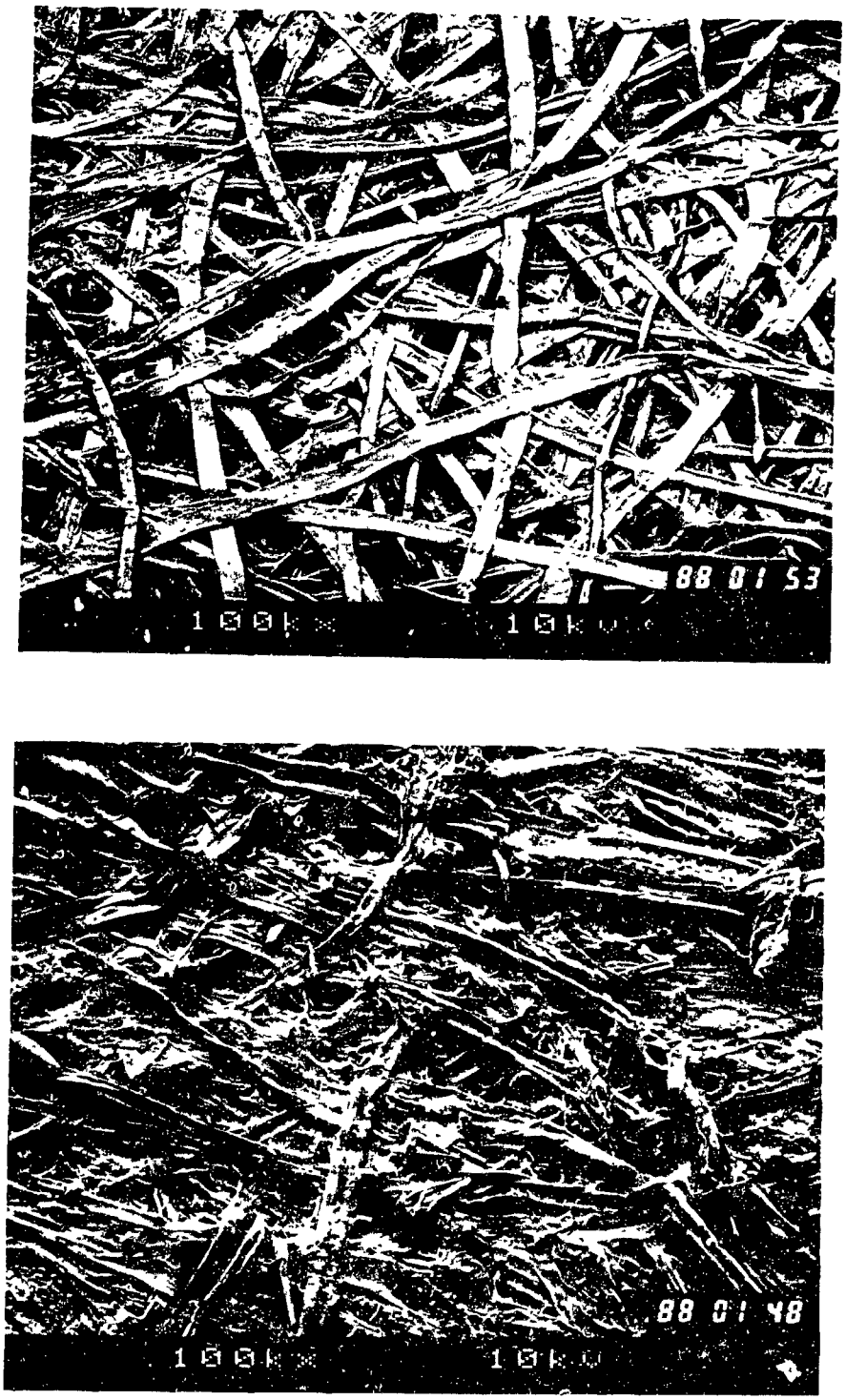

Figure 4.6b

The scale is indicated at the bottom of the photograph by the line which follows the three dashed lines. The length of the line corresponds to 100μm.

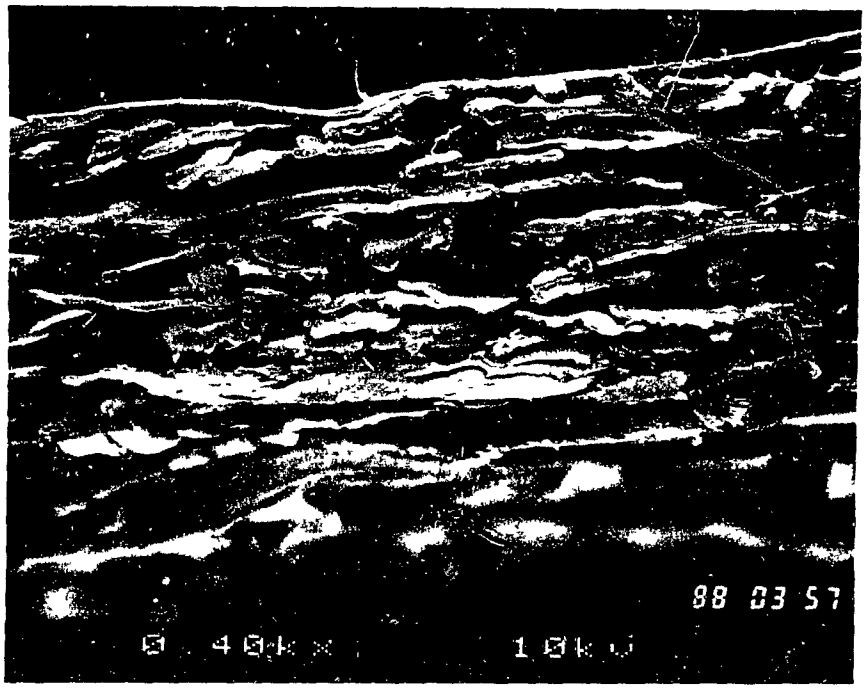

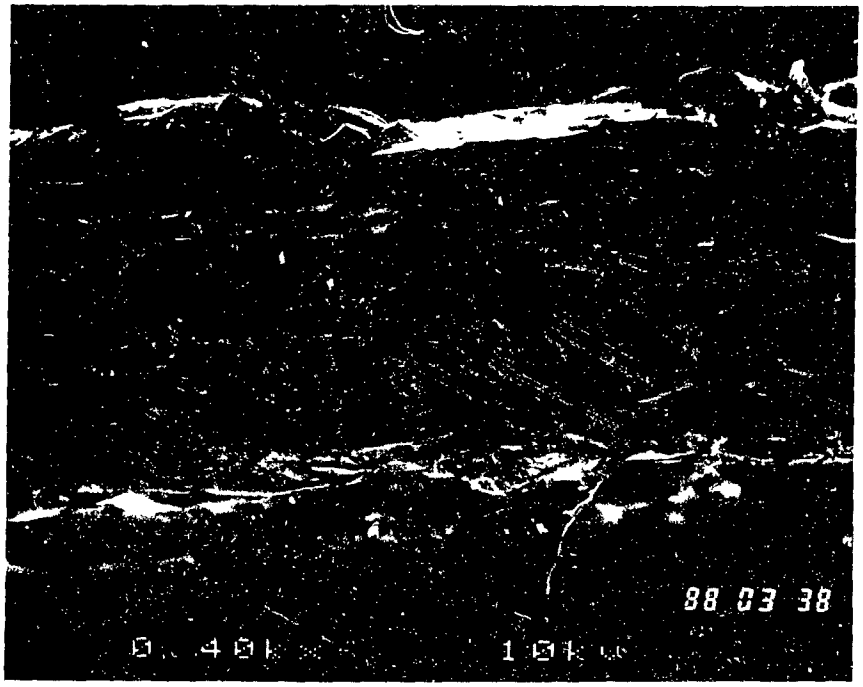

Figure 4.6c

The scale is indicated at the bottom of the photograph by the line which follows the two dashed lines. The length of the line corresponds to 10μm.

4.5 PERMEABILITY OF MOIST PAPER

4.5.1 Experimental Technique Valid with Inertial Effects

The experimental technique of these permeability-through drying experiments provides a continuous record of the pressure drop-paper moisture content history during drying, $\Delta P=f(X)$. Each such record applies for that sheet at a particular set of values of mass flow rate, G, and inlet temperature, T_i, of the throughflow air; of initial moisture content, X_o, and basis weight, M_B, of the paper. Variation of ΔP during experiments at constant G is large. With $25g/m^2$ paper for example, ΔP across the dry sheet is only 5-10% of that for the wet sheet at X=2.5kg/kg. The 4 levels of throughflow rate provided variation in G by about a factor of 5.

Examination of the Eqn. 4.4 form of the Forchheimer relationship used to determine permeability of dry paper indicates that the above information would be sufficient to determine k for moist paper if paper thickness, L, were known of function of its moisture content. In the absence of this information, the Forchheimer relation can however be rearranged to calculate a modified permeability, k/L, at a particular moisture content of the paper, X, as follows

$$\frac{\Delta p}{\nu G} = \alpha' + \beta' \frac{G}{\mu} \qquad (4.5)$$

where $\alpha'=L/k$, $\beta'=CL/\sqrt{k}$, and C the inertial constant.

White and Marceau[1962], Brundrett and Baines[1966] and Burgess *et al.*[1972a,b] determined a modified permeability, k/L, but only through assumption of Darcy's law, Eqn. 4.2. With respect to Eqn. 4.5 their procedure is equivalent to taking C=0, obtaining $k/L=\nu G/\Delta P$. The present study, Table 4.2, shows that for air flow through normal dry paper, i.e. paper which has not passed through a wetting-drying cycle, an

inertial component of pressure drop can be measured even for paper as heavy as basis weight 250g/m^2. The error in permeability of dry paper from use of the Darcy's law approximation is significant for basis weight below 100g/m^2, increasing to as much as 60% error for newsprint and tissue paper. As the present technique provides the data needed to avoid the Darcy's law approximation of neglecting the inertial component, this superior procedure was extended from dry to moist paper.

Relative to the procedure used for dry paper, Figs. 4.1 and 4.4, the addition is the variable paper moisture content, X. As the computer data acquisition system stored the measurements of ΔP and exit air humidity, Y_o, at a sampling frequency of 5-10Hz, values of ΔP for all handsheets tested could be obtained for selected common values of X. The initial moisture content, X_o, varied mainly over the range 1.5-3.0kg/kg, so 15 to 30 levels of X, at intervals of 0.1kg/kg, were selected to document the momentum transport behaviour of moist paper. Air viscosity was determined as a function of X at the average of inlet and outlet air humidity and temperature. A sample calculation and tabulation of values for modified permeability, k/L, for moist paper are provided in Appendix 6.

As 4 levels were used for each of the 3 variables, basis weight (25-150g/m^2), throughflow rate (0.09-0.52kg/m^{2}s) and throughflow inlet temperature (23°-88°C), the complete pressure drop history, $\Delta P=f(X)$, from wet to dry paper was determined typically for 64 combinations of M_B-G-T_i. For each such M_B-G-T_i combination, 2-4 values of X_o were used. As statistical analysis of the data confirmed that permeability is not a function of X_o or T_i, the 8-16 combinations of X_o and T_i, important variables for the associated drying rate measurements, constitute 8-16 replicates of any ΔP-G pair for each M_B in the permeability study. More

replicates were made for lower basis weight paper where the relative effect of sheet structure variability is greater.

4.5.2 Experimental Results

For M_B=25g/m^2 handsheets Figs. 4.7a and 4.7b show, on an Eqn. 4.5 type Forchheimer plot, the ΔP-G measurements for 35 sheets at a moisture content X=2.5kg/kg, and for 63 sheets at X=1.5kg/kg. The number of sheets corresponds to the use of 4 levels of T_1, 4 of G, 2-4 levels of X_o. As with dry paper, experimental scatter decreases with increasing basis weight. Therefore the sample Forchheimer plots shown, Fig. 4.7, are those of largest scatter, M_B=25g/m^2 As the measurements of ΔP, G, T_1 and X_o are of high accuracy, the scatter on Forchheimer plots reflects the variability in structure between handsheets.

Table 4.4 provides the key parameters, α' and β', and the permeability and inertial constant terms, k/L and C/L, which characterize throughflow across moist paper. Again N records the number of sheets tested. Although these momentum transport parameters were determined at moisture content intervals of 0.1kg/kg, Table 4.4 lists the results only at intervals 0.5kg/kg. The wide range in values of the inertial constant term, C/L, from large at M_B=25g/m^2 to negligible by M_B=100g/m^2, from large for wet paper to small for dry paper, indicates substantial changes in the relative importance of inertial effects in throughflow. Figs. 4.8a and 4.8b show the fraction of pressure drop that derives from inertial effects, $(\beta' G^2/\rho)/\Delta P$, which increases with decreasing paper thickness, as already shown for dry paper on Figs. 4.3 and 4.5, and increases strongly with increasing moisture content. The values of $\sigma_{\alpha'}$ and $\sigma_{k/L}$, in the range of 7-14% of the values of α' and k/L, and the values of

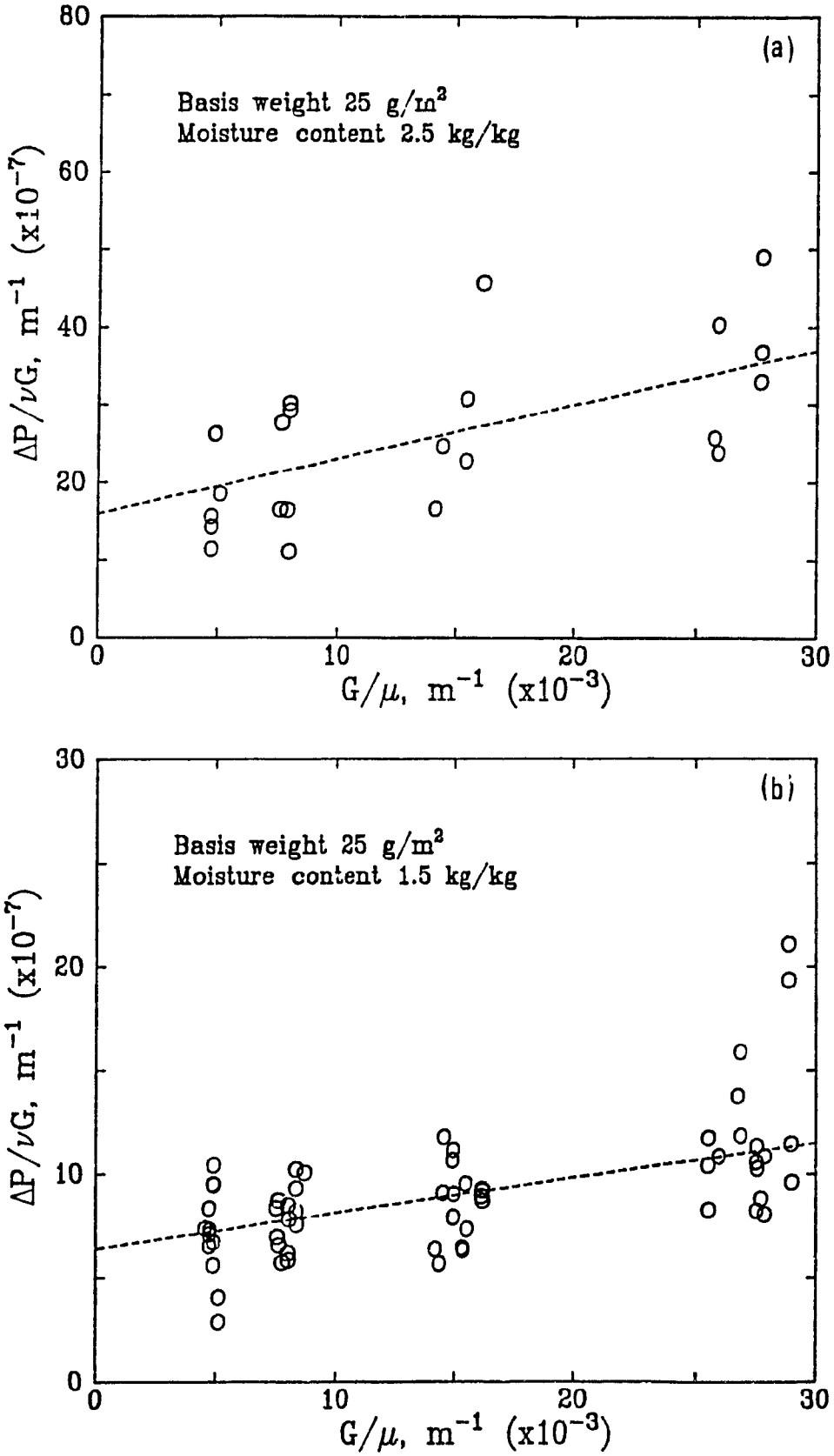

Figure 4.7 Momentum transport relation for permeablity: moist paper a) X=2.5kg/kg, b) X=1.5kg/kg

TABLE 4.4 Momentum Transport Parameters for Moist Paper

	X	N	α', m^{-1}	$\sigma_{\alpha'}$, m^{-1}	β'	$\sigma_{\beta'}$	k/L, m	$\sigma_{k/L}$, m	$C_f/L = \beta'/f\alpha'$
25g/m²	2.5	35	1.6×10^{8}	22×10^{6}	70×10^{2}	850	6.26×10^{-9}	86×10^{-11}	0.55
	2.0	55	1.0	14	43	410	9.79	130	0.43
	1.5	63	0.64	9	17	150	15.6	220	0.21
	1.0	65	0.47	5.8	7.6	85	21.5	260	0.11
	0.5	65	0.35	3.4	5.8	60	28.4	280	0.098
	0.1	65	0.34	3.1	5.6	51	29.6	270	0.096
50g/m²	2.5	33	10.6	95	100	1300	0.94	8.5	0.30
	2.0	57	5.7	68	75	920	1.76	21	0.31
	1.5	58	2.8	42	37	420	3.54	53	0.22
	1.0	61	1.9	21	16	200	5.23	58	0.12
	0.5	61	1.5	15.5	7.4	78	6.70	69	0.061
	0.1	61	1.4	10.7	5.8	61	6.90	54	0.049
100g/m²	2.0	27	22.5	230			0.444	4.6	
	1.5	57	12.4	190			0.808	12	
	1.0	61	6.1	98			1.64	26	
	0.5	61	4.4	54			2.26	27	
	0.1	61	3.8	43			2.62	29	
150g/m²	1.5	15	27.0	420			0.370	5.8	
	1.2	28	16.7	230			0.598	8.2	
	1.0	30	13.0	210			0.767	12	
	0.5	35	7.8	94			1.28	15	
	0.1	35	6.6	86			1.51	19	

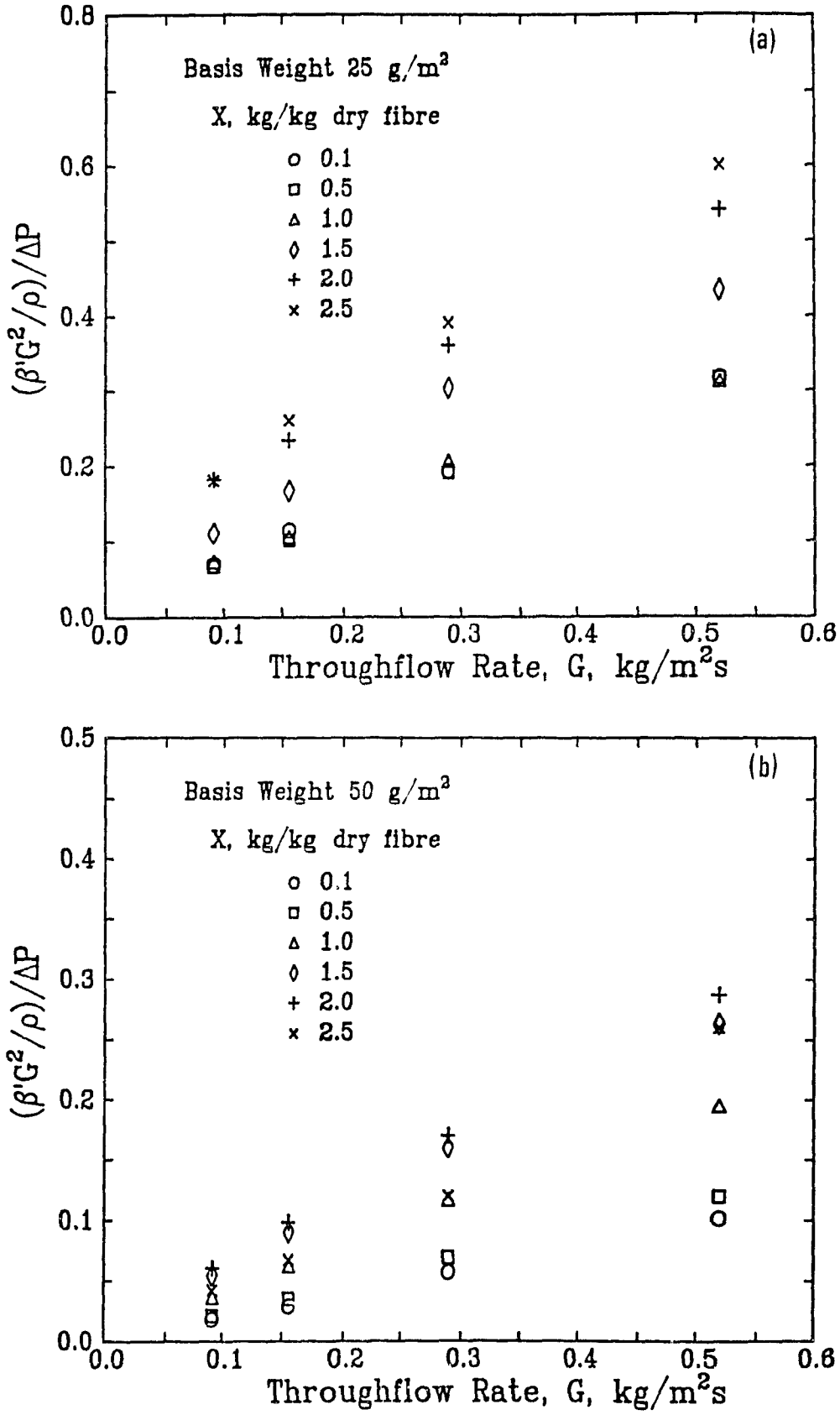

Figure 4.8 Effect of throughflow rate on inertial contribution to pressure drop: moist paper; a) 25g/m², b) 50g/m²

$\sigma_{\beta'}$, of 9-13% of β', are higher than the corresponding standard deviations for dry paper, Tables 4.2. and 4.3, and reflect primarily the variability in structure for the large number of sheets tested. Experimental variability of paper moisture content would be expected to result in larger values of σ for moist paper than for dry paper.

4.5.3 Analysis of Results

The approximately 6-fold decrease in the inertial constant term, C/L, from wet to dry paper, Table 4.4, is displayed for M_B=25g/m^2 on Fig. 4.9. For dry paper, Fig. 4.2 and Tables 4.2 and 4.3 documented the large increase in C as paper basis weight is decreased to M_B=25g/m^2. Fig. 4.9 and Table 4 4 record the similar increase in the inertial term, C/L, for decreasing thickness of moist paper, with the inertial term approximately doubling as basis weight is reduced from 50 to 25g/m^2 for all levels of moisture content from 2.5kg/kg to dry paper. Thus for light weight paper, whether dry or moist, high values of the inertial term reflect the large inertial effects which result from high velocity local flow at pin holes, or near-pin holes, i.e. with large local nonuniformities in throughflow rate. For wet paper, the throughflow at first opens only the bigger pores, in which the necessarily high local velocity produces the large values of the inertial effects term, C/L. As moisture content drops, smaller pores participate increasingly in the throughflow. With more pores open for flow at lower moisture content, the throughflow interstitial velocity decreases, therefore with less important inertial effects and a smaller value of C/L.

As moisture content drops over the range 2.5>X>0.5, modified permeability, k/L, increases greatly, by about a factor of 5-6. For

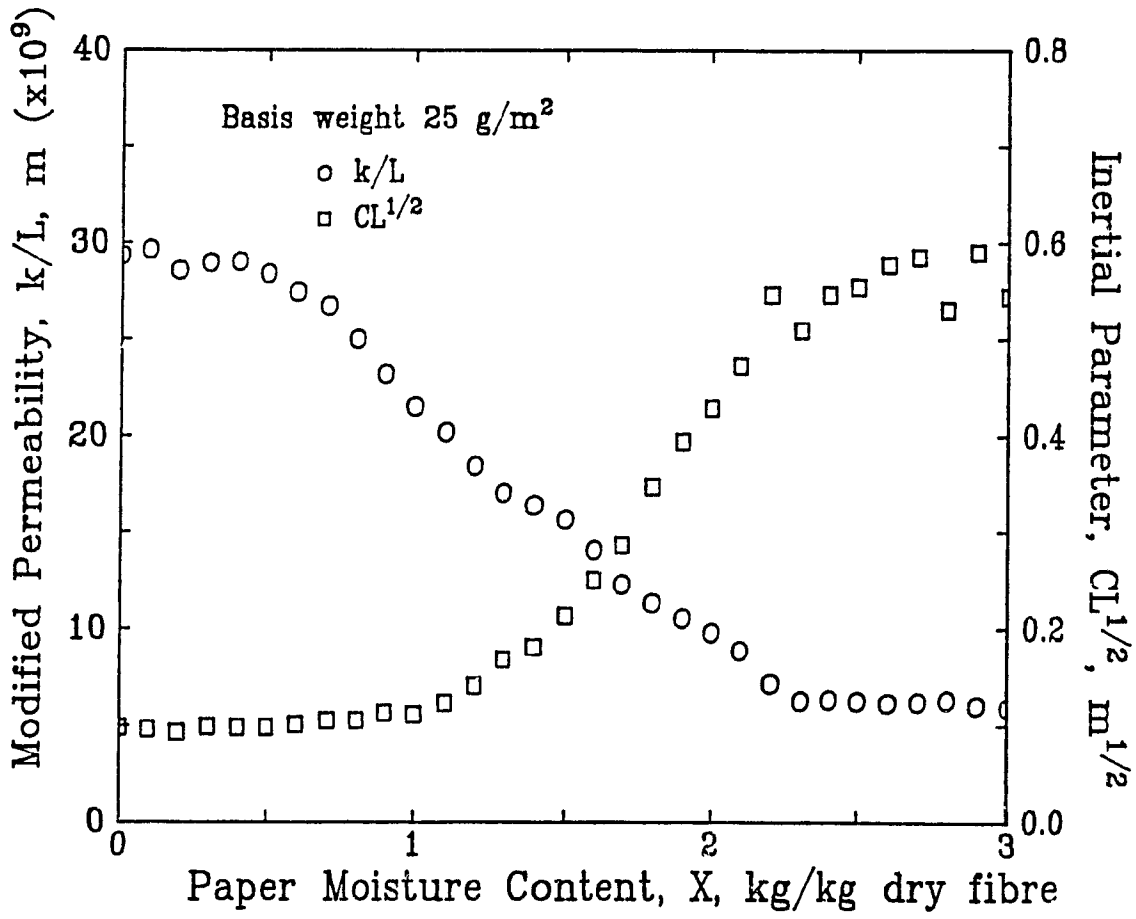

Figure 4.9 Effect of moisture content on modified permeability and inertial parameter

moisture contents of X<0.5, k/L approaches asymptotically the dry sheet value, as Fig. 4.9 illustrates for M_B=25g/m^2. The use of up to 16 replicate handsheets for each G at the lowest basis weight contributes to the considerable experimental scatter on Fig. 4.7 but leads to accurate permeability determinations with values of $\sigma_{k/L}$ in the range 7-14%, Table 4.4 and, correspondingly, with remarkably little scatter at even the lowest basis weight, Fig. 4.9. Complete k/L-X data for all four basis weights are shown subsequently, Figs. 4.10 and 4.11, with proposed correlations

These k/L-X relations illustrate an almost linear increase in permeability with decreasing moisture content. At low moisture content, water is sorbed in the smallest pores which, even when the water is removed, contribute little to permeability. Permeability at the final stages of drying would also be affected by fibre and sheet shrinkage. If the paper thickness-moisture content relation were known, enabling determination of k as well as k/L, then sheet shrinkage during the falling rate drying period would lead to a k-X relationship flatter for X<1kg/kg than the k/L-X curves of Figs. 4.9, 4.10 and 4.11.

4.5.4 Comparison with Other Studies

Brundrett and Baines[1966] attempted to measure the effect of moisture content on modified permeability, k/L, for laboratory handsheets of basis weight 47.5 to 85g/m^2 prepared from newsprint and chemical pulp furnishes. Their k/L values, determined by application of Darcy's law, are therefore somewhat too low. The present measurements make it possible to estimate their error for 50g/m^2 paper as ~25% for the highest G (0.518kg/m^{2}s) and X (2.5kg/kg), and ~10% for the same G but

at X=0.1. For newsprint their k/L values for laboratory formed paper were an order of magnitude lower than for commercial paper. Moreover for handsheets prepared from chemical pulps, their k/L-X results pass through a maximum at a moisture content of 1.0-1.5kg/kg. Such a maximum is not plausible, and no hint of such a maximum was observed in over 500 k/L-X determinations of the present study. With these anomalies it must be concluded that the Brundrett and Baines results do not provide reliable measurements of the effect of paper moisture content on permeability to air flow.

The measurements of White and Marceau[1962] show no effect of X on k/L, which is as expected because these data are limited to paper moisture contents less than 0.35kg/kg, a region of negligible change in k/L as documented in the present study. The k/L results of Burgess *et al.*[1972a,b], again including the error from use of Darcy's law, indicate k/L-X curves similar to those of Fig. 4.9. Their very limited data, obtained during the drying of three newsprint sheets from a moisture content of about 2kg/kg in a laboratory-scale combined impingement-through dryer, indicated the need for the present investigation into the sensitive permeability-moisture content relationship.

4.5 ɔ Correlation of Permeability with Moisture Content and Basis Weight

Two alternate relationships for the effect of paper moisture content on modified permeability are presented. The first form is suggested by the work of Nilsson and Larsson[1968] who, for water flow through paper webs in press nips, proposed that moisture content be related the flow resistance, defined as the inverse of Darcy law permeability,

$$L/k = p\, X^q \qquad (4.6)$$

This form of equation, not applicable at low moisture content, is extended here as

$$L/k = c_o + p\, X^q \qquad (4.7)$$

The three coefficients, determined by non-linear regression of the Table 4.4 results, are shown in Table 4.5.

TABLE 4.5 Parameters for Modified Nilsson-Larsson Equation for Effect of Moisture Content on Modified Permeability

M_B, g/m^2	25	50	100	150
$c_o x10^{-8}$	0.335	1.40	3.91	6.64
$p x10^{-8}$	0.126	0 496	2.55	6.54
q	2.40	3.06	2.82	2.50
r^2	0.998	0.999	0.999	0.999
σ	0.80	0.14	0.0065	0.0024

These coefficients correlate with basis weight as:

$$c_o x10^{-8} = -47.3 + 46.4 \exp (M_B/1000) \qquad r^2=0.999 \; ; \; \sigma=0.09$$

$$p\, x10^{-8} = 0.27 - 0.015\, M_B + 3.8x10^{-4}\, M_B^2 \qquad r^2=0.999 \; ; \; \sigma=0.03$$

$$q = 0.47\, M_B^{0.57} \exp(-0.0082\, M_B) \qquad r^2=0.999 \; ; \; \sigma=0.15$$

An alternate form for the permeability-moisture content relation is suggested by that for pore diameter-moisture content, and by concepts of the porous structure of paper. Measurements by White and Marceau [1962] of the controlling pore diameter for water flow through paper showed an exponential relationship for effect of moisture content. Studies of the porous structure of dry paper by Corte and Kallmes[1962] and Corte and Lloyd[1966], summarized recently by Corte[1982], show a Poisson distribution of fibres. Thus the probability of finding no fibres in a dry sheet, i.e. a pore space, at a given point is an exponential function of the number of fibres. For the exponential form of correlation tested for permeability

$$L/k = a + b\, e^{cX} \qquad (4.8)$$

the parameters, determined by non-linear regression of the Table 4.4 results, are shown in Table 4.6.

TABLE 4.6 Parameters for Exponential Form for Effect of Moisture Content on Modified Permeability

M_B, g/m^2	25	50	100	150
$ax10^{-8}$	0.25	1.24	3.24	5.63
$bx10^{-8}$	0.07	0.10	0.46	0.79
c	1.16	1.86	1.91	2.19
r^2	0.995	0.999	0.999	0.999
σ	1.34	0.20	0.006	0.004

The dependence of these coefficients on basis weight may be expressed as:

$$ax10^{-8} = -0.58 + 0.033\, M_B + 5.7\times10^{-5} M_B^2 \qquad r^2=0.999\ ;\ \sigma=0.06$$

$$bx10^{-8} = 3.7\times10^{-5}\, M_B^2 \qquad r^2=0.986\ ;\ \sigma=0.06$$

$$c = 0.042\, M_B - 1.86\times10^{-4}\, M_B^2 \qquad r^2=0.968\ ;\ \sigma=0.37$$

While showing the acceptability of both the Eqn. 4.7 and 4.8 correlations, Figs. 4.10 and 4.11 also complete the k/L-X records for all 4 levels of basis weight tested, shown in Fig. 4.9 for M_B=25g/m^2 only.

Inclusion of paper thickness in the modified permeability, k/L, requires any correlation to be a function of basis weight. However, even for dry paper the permeability, k, depends strongly on basis weight, Fig. 4.2. The k/L-M_B relation at various moisture contents, Fig. 4.12, parallels that for k-M_B at X=0, Fig. 4.2. The dry paper permeability data, reexpressed as k/L for inclusion on Fig. 4.12, complete the range of paper moisture content. The logarithmic scale of Fig. 4.12 accomodates the high sensitivity of permeability to both moisture content and basis weight. Moreover, Fig. 4.12 illustrates the remarkable precision

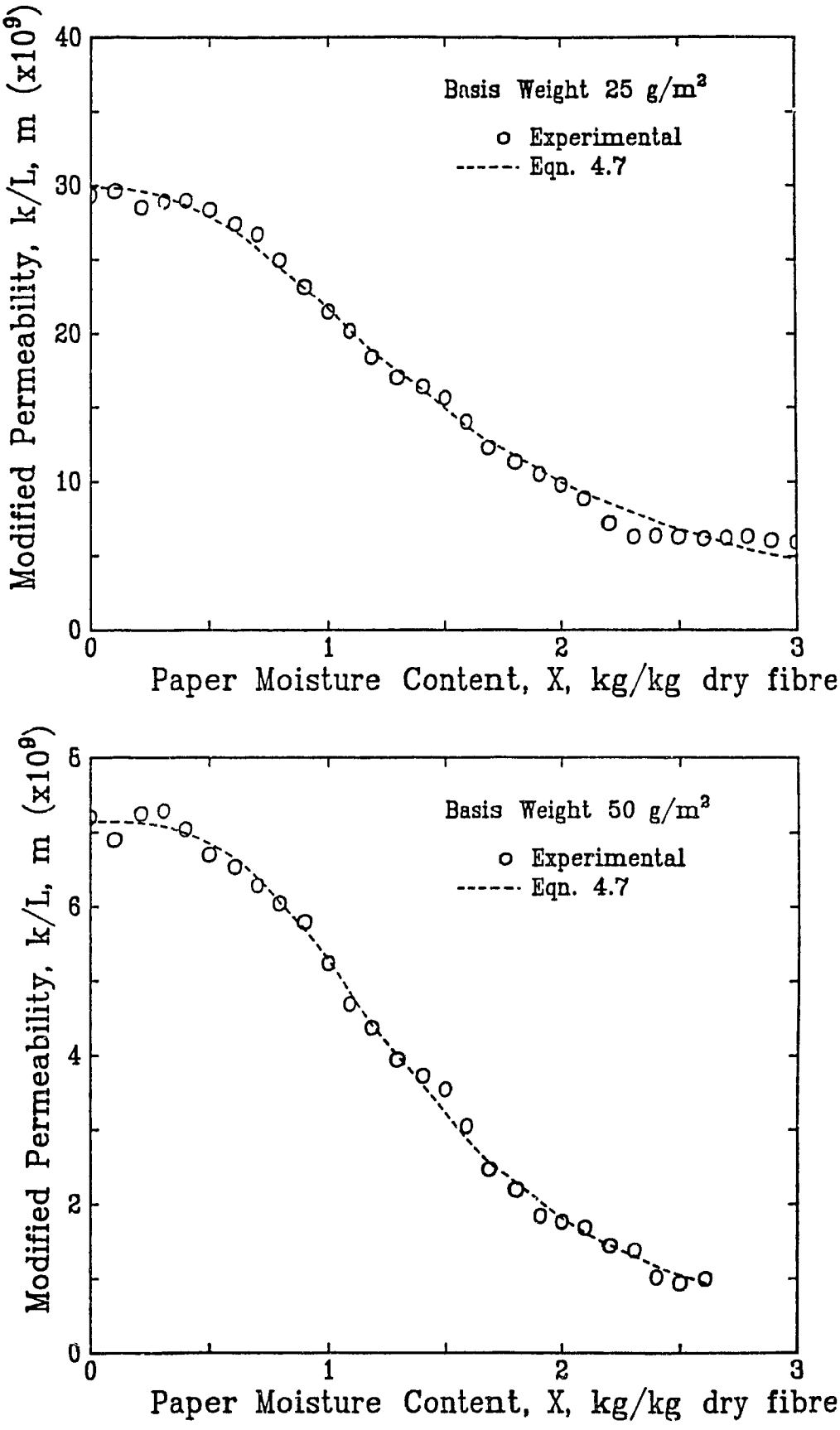

Figure 4.10 Effect of moisture content on modified permeability of paper
Modified Nilsson-Larsson equation

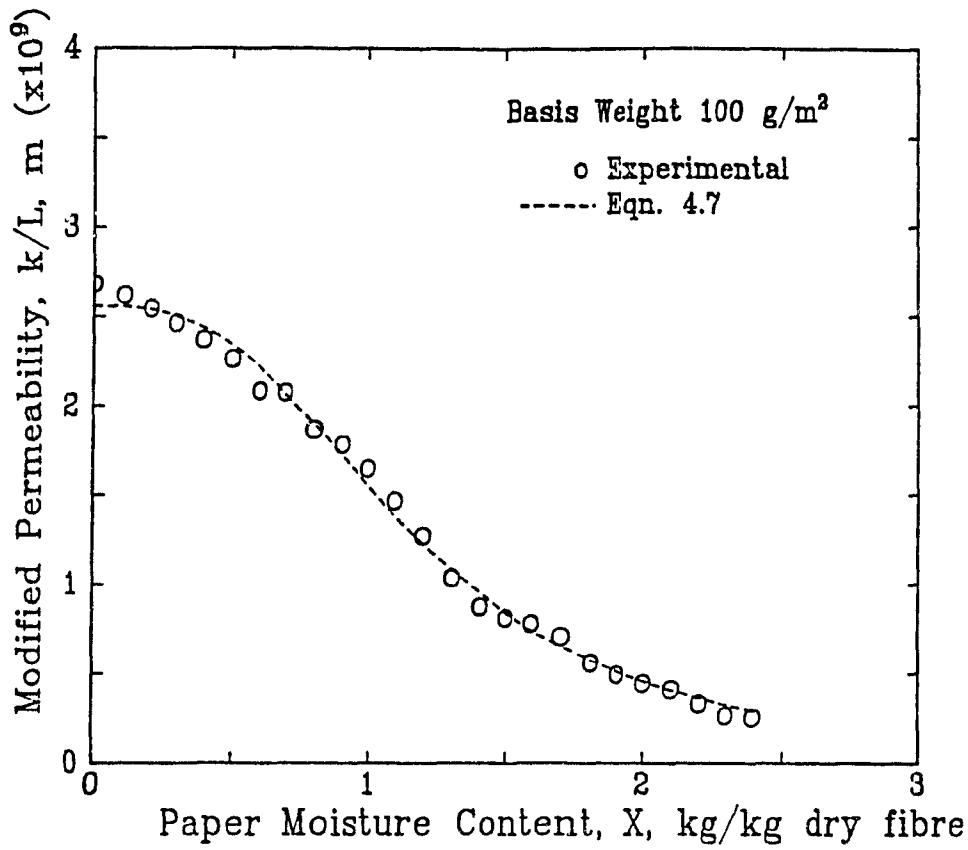

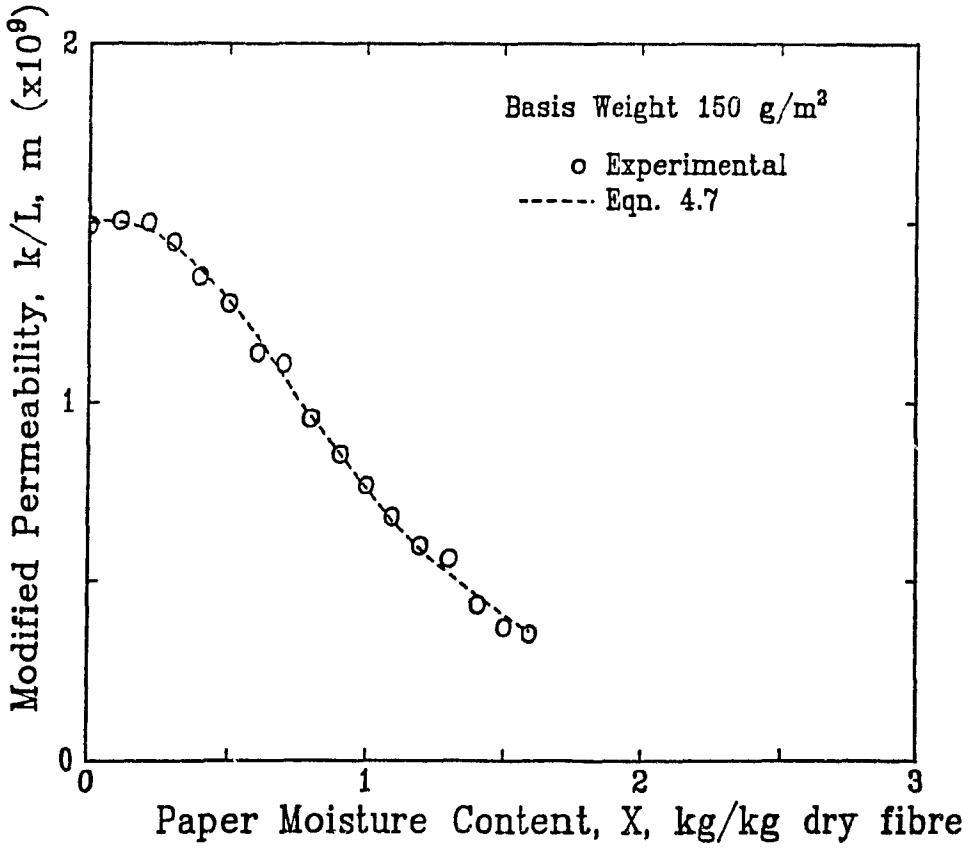

Figure 4.10 continued

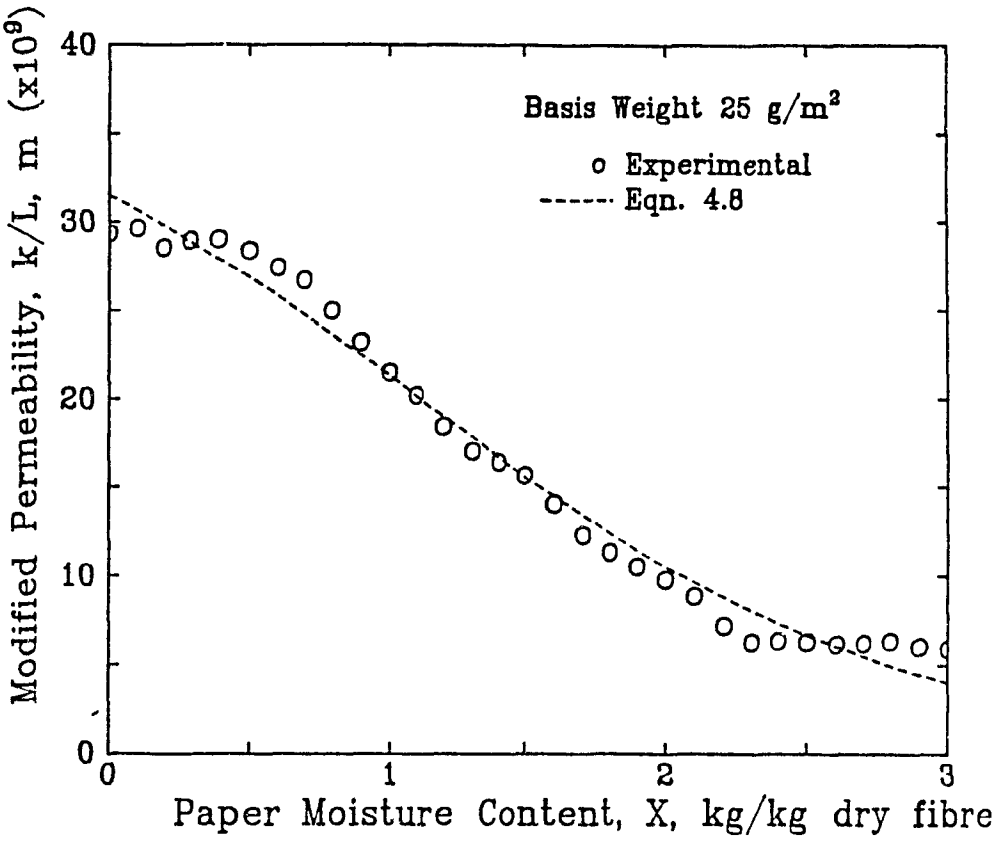

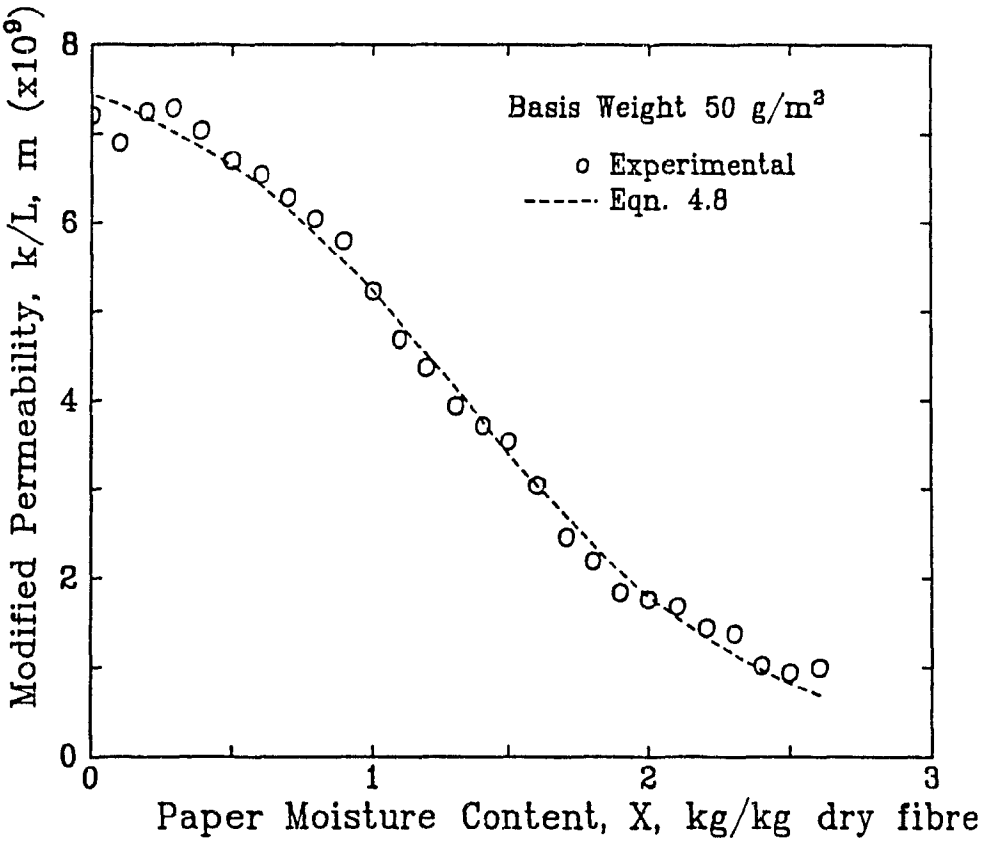

Figure 4.11 Effect of moisture content on modified permeability of paper: Exponential equation

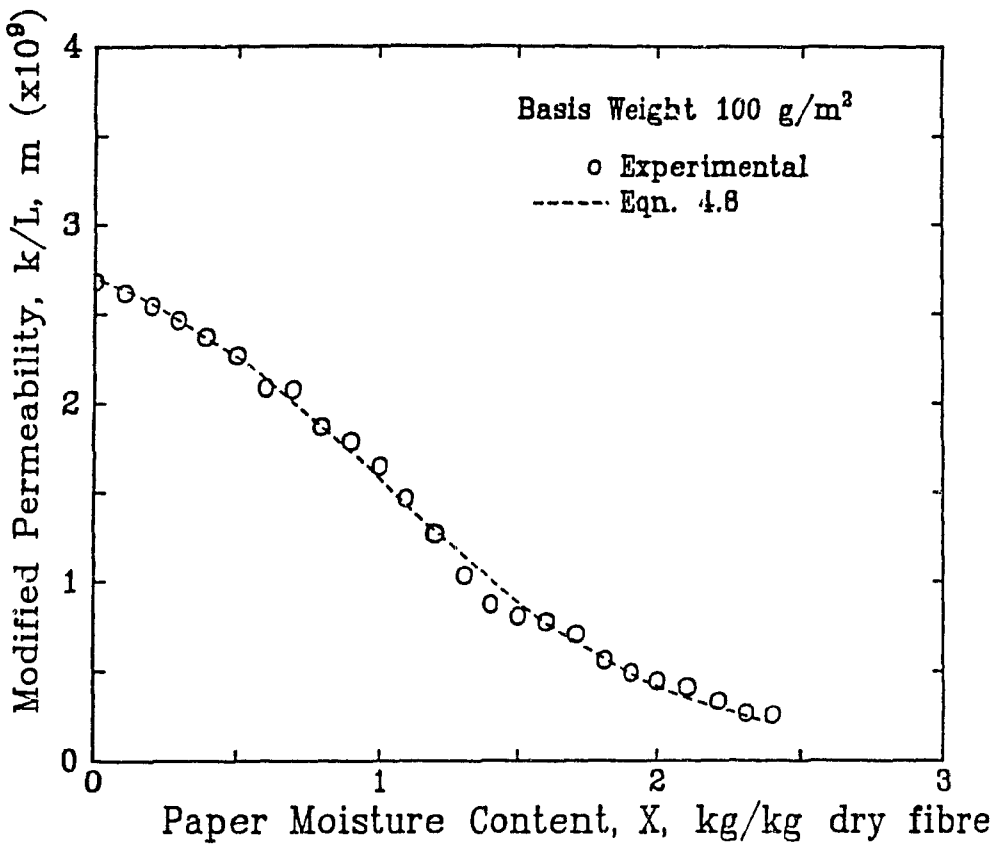

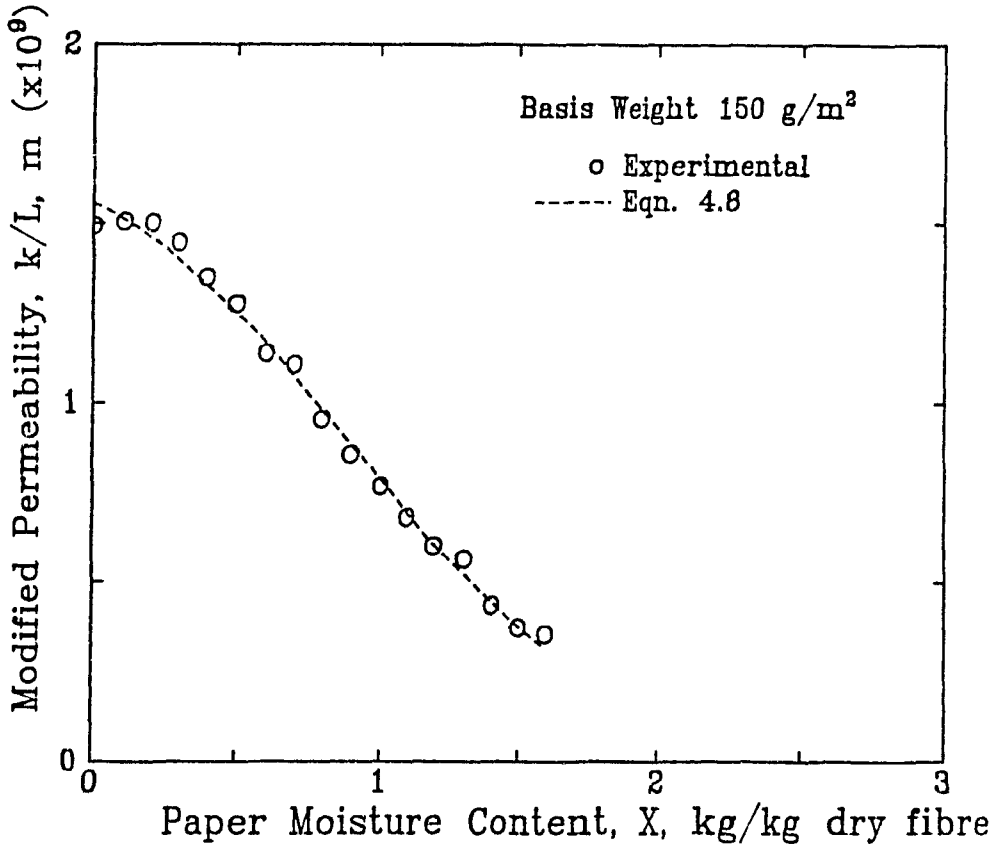

Figure 4.11 continued

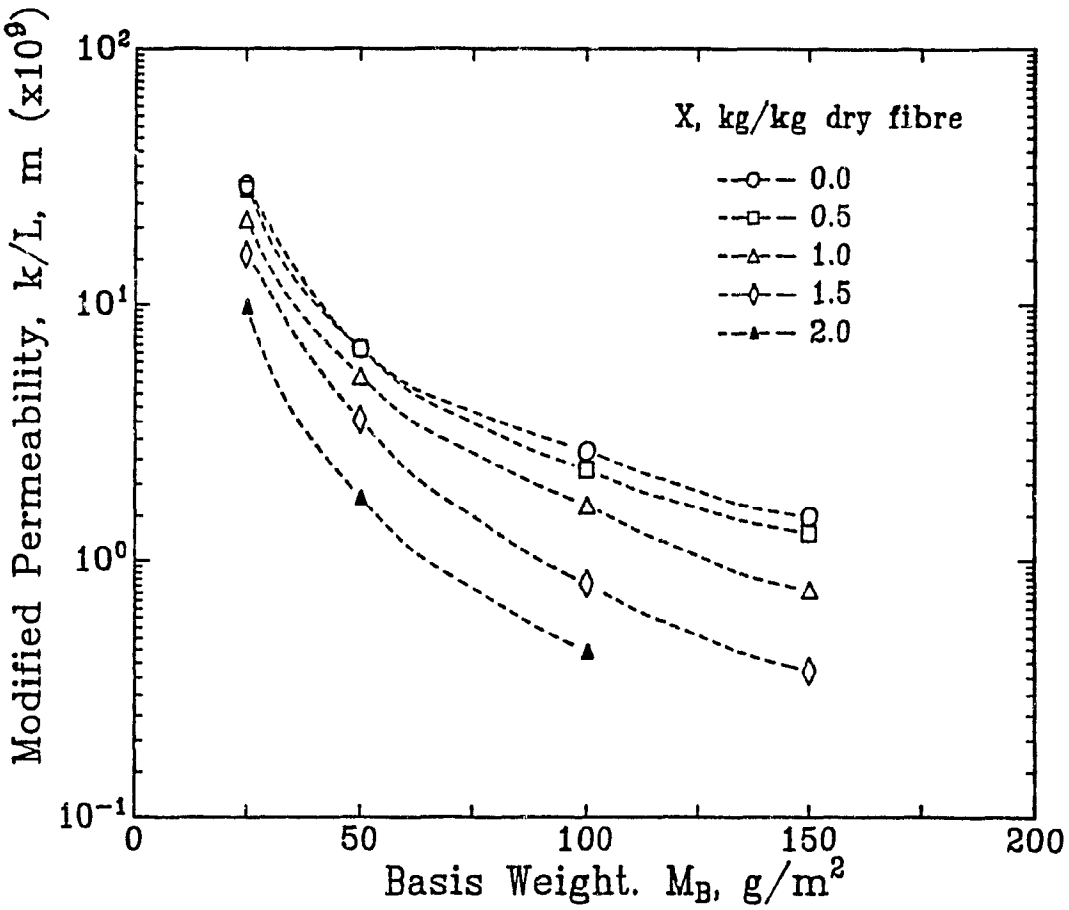

Figure 4.12 Effect of basis weight on modified permeability of moist paper

achieved in the measurement of permeability for paper, spanning more than two orders of magnitude from wet thick sheets to dry tissue paper.

4.5.6 Experimental Results without Inertial Effects

Where the inertial component of ΔP is demonstrated to be negligible, Table 4.4, it becomes legitimate to use Darcy's law, Eqn. 4.2, to calculate k/L-X values for each ΔP-G value. By contrast, the Forchheimer relationship permits determination of only one value of permeability for each set of ΔP-G values for paper of a specific basis weight. These additional results for 100 and 150g/m^2 paper appear on Figs. 4.13 and 4.14 as effectively continuous lines because the k/L-X results were calculated from the ΔP-X data at intervals of 1s. Figs. 4.13a and b show k/L-X curves for 8 sheets of 100g/m^2 paper, 6 sheets of 150g/m^2 paper, all at a single temperature, T_1=64°C. These k/L-X curves, each of which is for a particular sheet, vary randomly with the parameter, G, due to variation in structure of the paper from one sheet to another. The equivalent plots for the other 3 temperatures, T_i of 23°, 42° and 88°C, not shown, look similar.

When these k/L values for each level of T_1 are fitted to the Eqn. 4.8 type correlation, the resulting lines for 61 sheets of 100g/m^2 and 35 sheets of 150g/m^2 paper are as shown on Figs. 4.14a and b. Here the lines scatter randomly with respect to T_1. Thus Figs. 4.13 and 4.14 further confirm that throughflow rate and temperature have no significant effect on k/L.

A comparison of modified permeability by the Forchheimer relation, Table 4.4, and by Darcy's law, Figs. 4.13 and 4.14, is as follows:

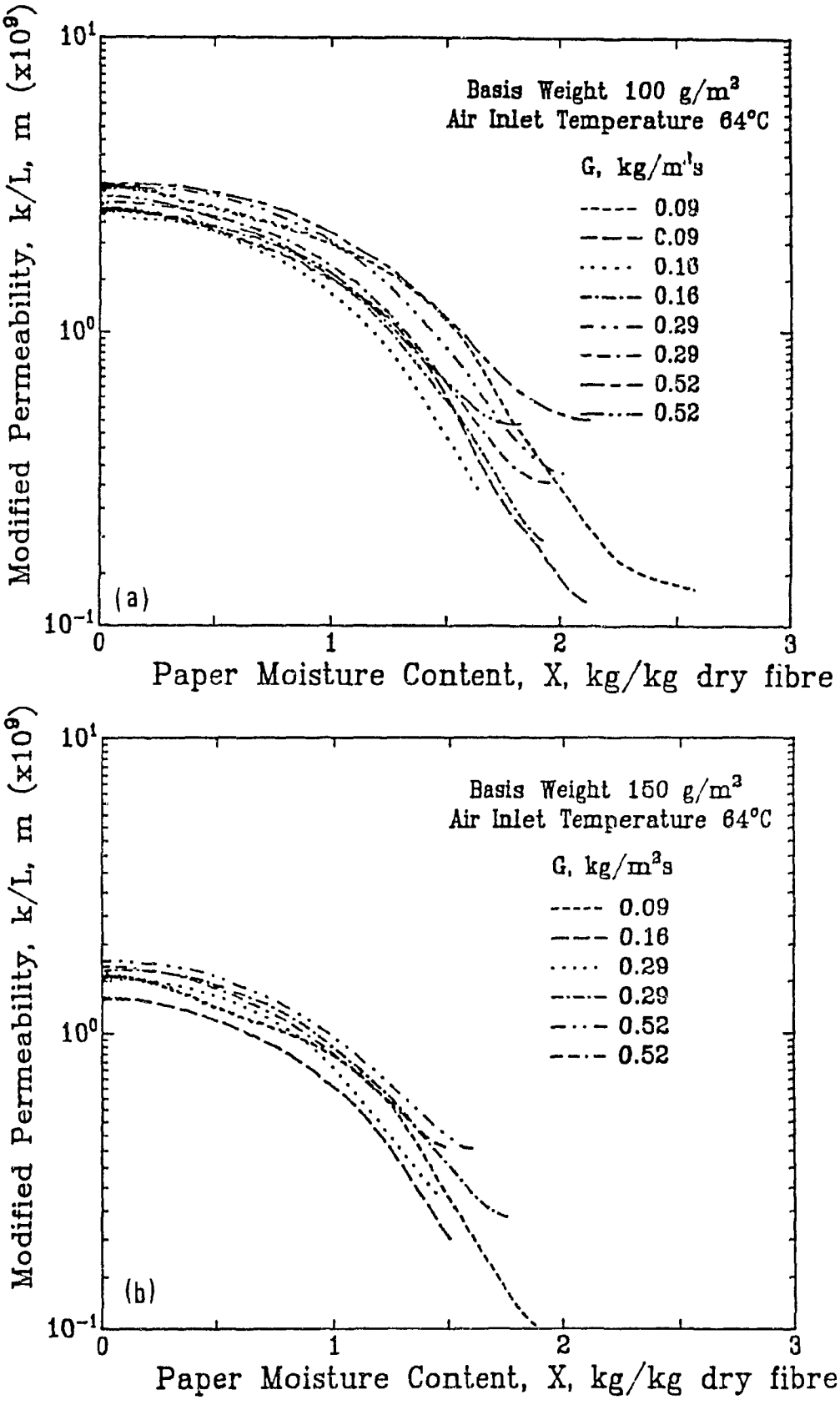

Figure 4.13 Effect of moisture content on modified permeability: Results without inertial effects; a) 100g/m², b) 150g/m²

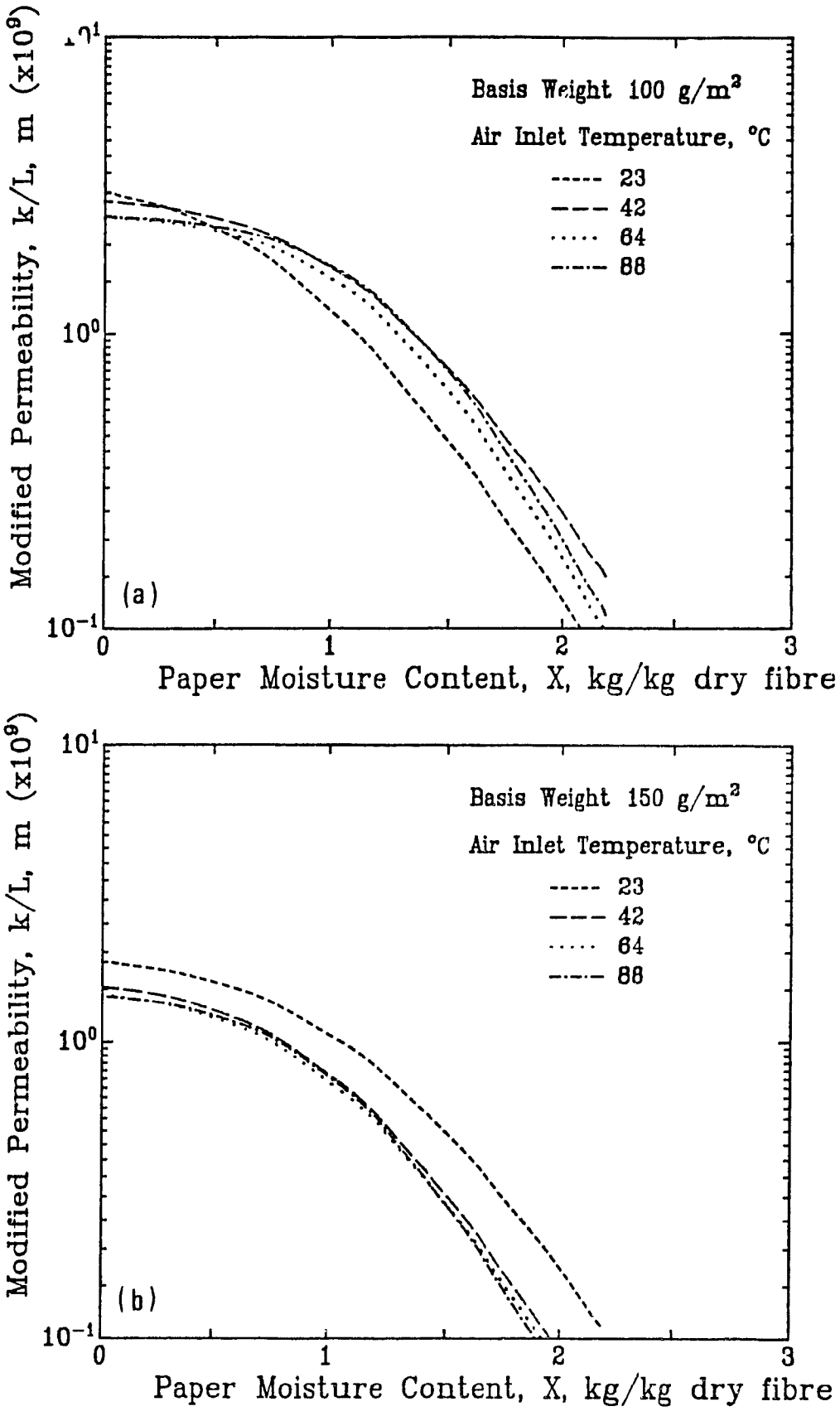

Figure 4.14 Effect of moisture content on modified permeability: Results without inertial effects using exponential equation; a) 100g/m², b) 150g/m²

	Modified Permeability, k/L, m (x10⁹)				
X, kg/kg	2.0	1.5	1.0	0.5	0.0
M_B=100g/m²					
Table 4.4	0.48	0.81	1.62	2.32	2.64‡
Figs. 4.13-4.14	0.15-0.52	0.45-1.10	1.35-2.10	2.10-2.50	2.40-2.95
M_B=150g/m²					
Table 4.4	-	0.39	0.57	1.26	1.54‡
Figs. 4.13-4.14	-	0.20-0.50	0.60-1.00	1.10-1.70	1.25-1.80

‡ calculated from Table 4.3

The excellent agreement confirms the validity of both procedures for moist paper, i.e. k/L from a Forchheimer plot when ΔP-X values are measured over a wide flow rate range, or k/L from Darcy's law for point values of ΔP-X-G when the inertial contribution to ΔP is negligible.

For basis weights of 100 and 150g/m², Eqn. 4.8 was fitted to the individual k/L values for drying conditions of over 100 combinations of G-T_i-M_B-X_o. Including replicates, over 3000 values of k/L were determined involving 96 sheets of these two basis weights, i.e. 61 of 100g/m² and 35 of 150g/m² (Table 4.3). Statistical analysis of these coefficients confirmed the expectation that k/L is not affected appreciably by rate, G, or inlet temperature, T_i, of the throughflow air or by the paper initial moisture content, X_o. This result extends the preliminary finding by Burgess *et al.*[1972a] of no effect of drying air temperature (~150-300°C) on modified paper permeability measured for their 3 sheets of newsprint dried from X_o=2kg/kg.

4.5.7 Conclusions

The finding that modified permeability is not significantly affected by velocity or temperature of throughflow air or by paper initial moisture content may be stated more generally as indicating that permeability is independent of drying conditions. Examination in Sections

4.3 and 4.4 of the change in permeability of dry paper between before and after a wetting-drying cycle established that the large permeability changes were associated with the wetting, i.e. that the structure of pores participating in the throughflow does not change significantly during drying. The agreement between these two independent types of experimental evidence adds further confidence to the conclusion that the aspects of microstructure which affect flow through paper do not change during drying.

Had modified permeability, k/L, for 25 and 50g/m^2 basis weight moist paper been calculated with the incorrect assumption of no inertial component to pressure drop, i.e. by Darcy's law as previously, such permeabilities would be erroneously low. This error varies greatly with conditions. At low moisture content, X<1.0, the error is small, about 10% for 25g/m^2 paper, 5% for 50g/m^2 paper. For wet paper, however, the error increases sharply to more than 70% at X=2.5 for both basis weights. The error would be larger yet for the higher throughflow rates used industrially. These levels of error are linked with the fraction of ΔP that derives from inertial effects, displayed for moist paper on Fig. 4.8. For the effect of moisture content of paper on its permeability to air flow, the measurements reported here are the first comprehensive set, are the first to be calculated without the Darcy's law approximation, and provide the first correlation for effective permeability as a function of basis weight and moisture content.

4.6 SPECIFIC SURFACE AND POROSITY OF DRY PAPER

4.6.1 Experimental Method

A widely accepted formulation for the relationship between perme-

ability and the geometrical properties of a porous medium, specific surface and porosity, is that of Kozeny[1927], modified by Carman[1937],

$$a_p^2 = \frac{1}{\kappa} \frac{\varepsilon^3}{(1-\varepsilon)^2} \frac{1}{k} \qquad (4.9)$$

Although some assumptions for the Kozeny-Carman relationship have been strongly criticized, Childs and Collis-George[1950], Kyan *et al.* [1970], Scheidegger[1974], its applicability to paper has been demonstrated for water permeability, Robertson and Mason[1949], Mason[1950], Ingmanson [1953], Gren[1972], and for air permeability, Garner and Kerekes[1978], Knauf and Doshi[1986]. The value of 5.55 proposed by Fowler and Hertel [1940] for the Kozeny-Carman parameter, κ, for fibrous media has been widely adopted for application to paper and webs of cellulose fibres

For moist paper, the transient values of thickness and hence porosity of moist paper during drying are not known as a function of moisture content, so the specific surface cannot be determined by the Kozeny-Carman equation. Because the $\varepsilon^3/(1-\varepsilon)^2$ term is quite sensitive to error in porosity, an approximate ε-X relation is not sufficient.

The porosity of dry paper is ~0.67, i.e. of apparent density ~0.5g/cm^3, for sheets formed by the standard handsheet making technique from the laboratory kraft pulp used here. The dry paper porosity was determined from its measured thickness, assuming a fibre density of 1550kg/m^3 (Stone *et al.*[1966]). For example the porosity of 25 g/m^2 paper, of average thickness 51μm before a rewetting-through drying cycle, is

$$\varepsilon = 1-\rho_b/\rho_f = 1-M_B/L\rho_f = 1-0.025/(5.1\times10^{-5}\times1550)=0.684$$

The complete listing of values in Table 4.7 indicates that paper porosity is larger by 5-10% after a rewetting-through drying cycle. This higher porosity, and the higher permeability noted earlier, are

consistent effects which are associated with the collapse of surface fibrillation during the wetting part of a wetting-drying cycle.

The specific surface of dry paper, determined using the Kozeny-Carman relation, Eqn. 4.9, with the above porosity and with permeability from Tables 4.2 and 4.3, is given in Table 4.7 on both a volumetric and a mass basis. Although generally given for other materials on the volumetric basis, a_p, for paper the mass based specific surface, a'_p, is often used because of the variability of paper thickness (or volume).

4.6.2 Analysis and Comparison of Results

Specific surface as determined by the present throughflow technique is compared on Fig 4.15 with that determined by sorption. The number of sheets used in each case is indicated by N, and the $\pm\sigma$ error bars are included on Fig. 4.15. Stone and Scallan[1965] did not report basis weight, so 60 g/m^2, the standard handsheet value, was assumed for their results. The particularly wide range of their results, 0.5-1m^2/g, could be due to variability of the paper, which was not documented. For bleached kraft handsheets Gurnagul and Gray[1987] report a standard deviation less than 0.03m^2/g for specific surface from their IGC measurements and 0.1m^2/g from Kr sorption. The good agreement between sorption technique measurements and those at 60g/m^2 basis weight obtained here by the Kozeny-Carman equation technique adds credibility to the new values at other basis weights. Not included in this figure are two sets of specific surface values obtained by the air permeability technique, i.e those of Garner and Kerekes[1978], because they used only unconsolidated pulp fibers, and of Knauf and Doshi[1986], because they used pulps of CSF considerably different than in the present study. Interpolation of Knauf and Doshi's

TABLE 4.7 Specific surface and porosity of dry paper before and after a wetting-through drying cycle

	Before				After			
M_B, g/m²	N	ε	a_p m²/m³	a'_p m²/g fibre	N	ε	a_p m²/m³	a'_p m²/g fibre
25	3	0.684	0.79×10^6	0.51	65	0.722	0.76×10^6	0.49
50	3	0.643	1.17	0.76	61	0.717	1.04	0.67
100	3	0.657	1.29	0.83	61	0.716	1.19	0.77
150	3	0.669	1.42	0.92	35	0.721	1.34	0.86
250	3	0.677	1.48	0.95	6	0.705	1.44	0.93
45‡	-	-	-	-	9	0.600	1.77	1.14

‡ groundwood furnish, Papriformer newsprint

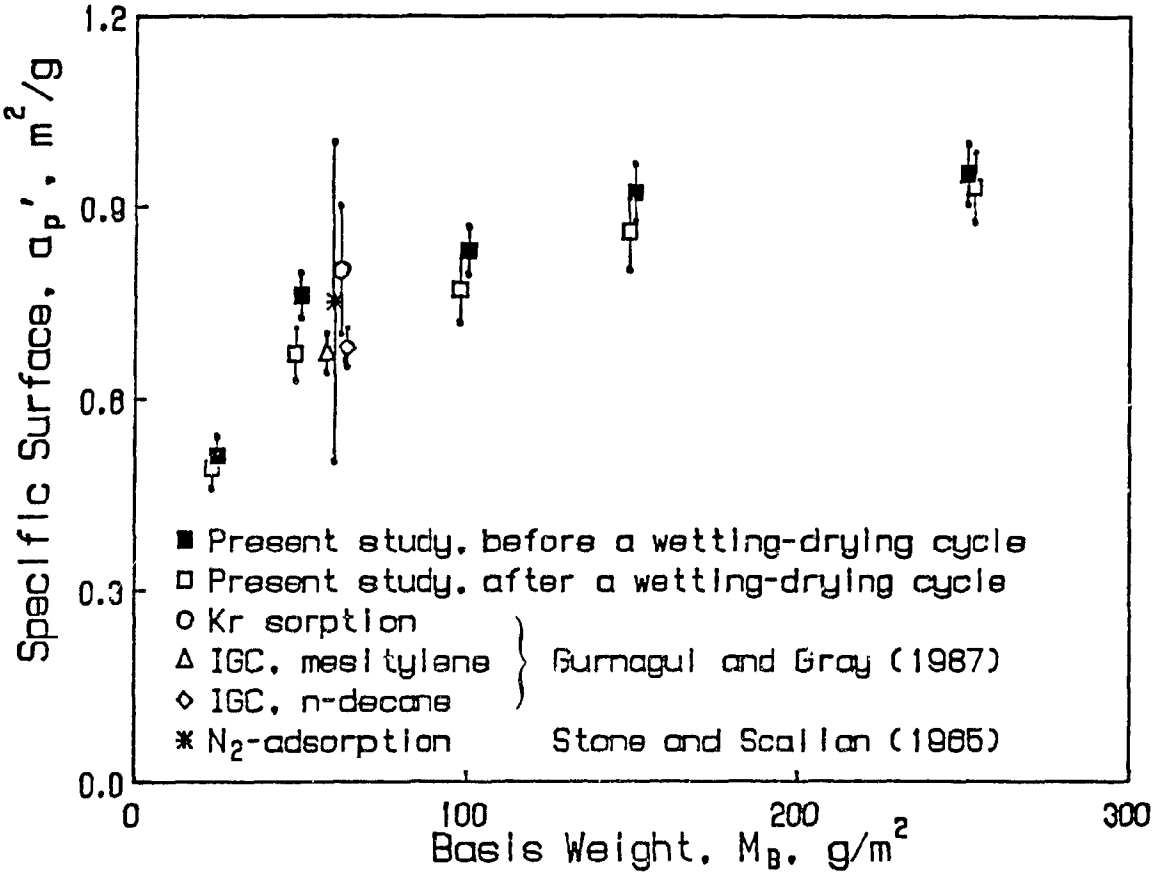

Figure 4.15 Effect of basis weight on specific surface of dry paper

data to the freeness of that used here, CSF=685ml, gives $a_p' \cong 0.7 m^2/g$ for their $200 g/m^2$ paper, approximately 25% lower than the present findings.

While specific surface determined by sorption is independent of basis weight, the fact that specific surface as measured by the gas permeation technique decreases as basis weight decreases shows that the latter method measures only that interfacial area which is effective in throughflow. This is the interfacial area which is relevant to transport phenomena in through drying. For the lowest basis weight paper, $25 g/m^2$, sorption techniques overestimate by about 50% the surface area that is effective for throughflow transport processes.

Specific surface drops by between 2-11% when paper is subjected to a wetting-through drying cycle, Table 4.7, Fig. 4.15. With their sorption technique Gurnagul and Gray[1987] measured a 16-19% drop in surface area of bleached kraft handsheets subjected to a moistening-drying cycle in which dry paper was moistened by humid air only up to about X≈17% (corresponding to 90% relative humidity) then oven dried at 105°C. The similarity in findings between these studies is remarkable in that entirely different measurement techniques were used. This agreement reinforces the conclusion, based on the present permeability measurements, that in a wetting-drying cycle it is the increase in paper moisture content that produces irreversible changes in the structural properties, which appear unaffected during the decrease in moisture content during drying. Moreover, the irreversible changes in microstructure which occur during wetting appear to occur for relatively small increases in paper moisture content.

4.6.3 Conclusions

Permeability, porosity, and specific surface are interconnected pro-

perties of a porous medium which, with some assumptions, may be related by the Kozeny-Carman equation. Any change in porous structure of paper, such as from remoistening or wetting, which decreases resistance to the flow, i.e. increases permeability, should also decrease the specific surface and increase porosity. Thus over a wetting-drying cycle the decrease in specific surface area and increase in permeability and porosity are attributed to the same mechanism, collapse of stress-induced surface fibrillation at bond sites. Sheet structure is very sensitive to irreversible changes occuring during the early stages of remoistening, so that the pore size, porosity, permeability and specific surface of dry paper all depend on such rearrangements which happen not only during wetting, but even in moderate remoistening from contact with high humidity air.

4.7 FLOW THROUGH MOIST AND DRY PAPER: A REYNOLDS NUMBER-FRICTION FACTOR-CHARACTERISTIC DIMENSION ANALYSIS

4.7.1 Basic Considerations for a Characteristic Dimension

An alternative to the standard procedure of analyzing pressure drop for flow through paper in terms of permeability would be to use the nondimensional Reynolds number-friction factor model. Of the various definitions of friction factor, that expressed by Bird *et al.*[1960] is

$$f = F/AK \tag{4.10}$$

where F is the force exerted by fluid motion, A the characteristic cross-sectional flow area, K the kinetic energy per unit volume. Thus F/A is the energy loss, i.e. ΔP. The friction factor, which is the nondimensional energy loss from flow, may be expressed as

$$f = f(Re) \tag{4.11}$$

where Reynolds number, Re, is $d_p \rho u/\mu$, with u the superficial velocity

and d_p the dimension characteristic of the flow.

For flow through packed beds the critical aspect of the nondimensional Re-f treatment of momentum transfer is specification of this characteristic length, d_p. Selection of d_p is straight-forward only for beds of rigid particles of simple shape, uniform size. For other cases a great variety of definitions of Reynolds number characteristic dimension have been used, including "effective" particle diameter, equivalent sphere diameter of the particle, pore size, Hagen-Poiseuille equivalent capillary diameter, reciprocal of specific surface, square root of permeability.

The degree of difficulty determining a characteristic dimension for paper is illustrated by the scanning electron micrographs of paper used in this study, Fig. 4.16. The porous structure of paper is determined by the bonding of flattened ribbon-like fibres, 4-8μm thick, 20-40μm wide, up to 3mm long. With the complexity of this porous structure it would be grossly unrealistic to model it as an assembly of rigid rods or any such oversimplified shape. For the paper used the property ranges are: porosity, ε, 0.65-0.70; basis weight, M_B, 25-250 g/m^2; paper thickness, L, 50-500μm. Thus these sheets are from about 10 to 100 fibres thick. In addition to the complexity of particle shape, the dimensions of pulp fibres, and hence of paper, vary with moisture content. Determination of an appropriate characteristic dimension for flow through paper of variable moisture content, of a structure indicated by Fig 4.16, is a problem of much greater difficulty than for the simple rigid particles of uniform dimensions involved in most studies of flow through packed beds. This degree of difficulty explains the lack of treatment of flow through paper by the Reynolds number-friction factor approach.

For transport phenomena in porous media a basic choice is between

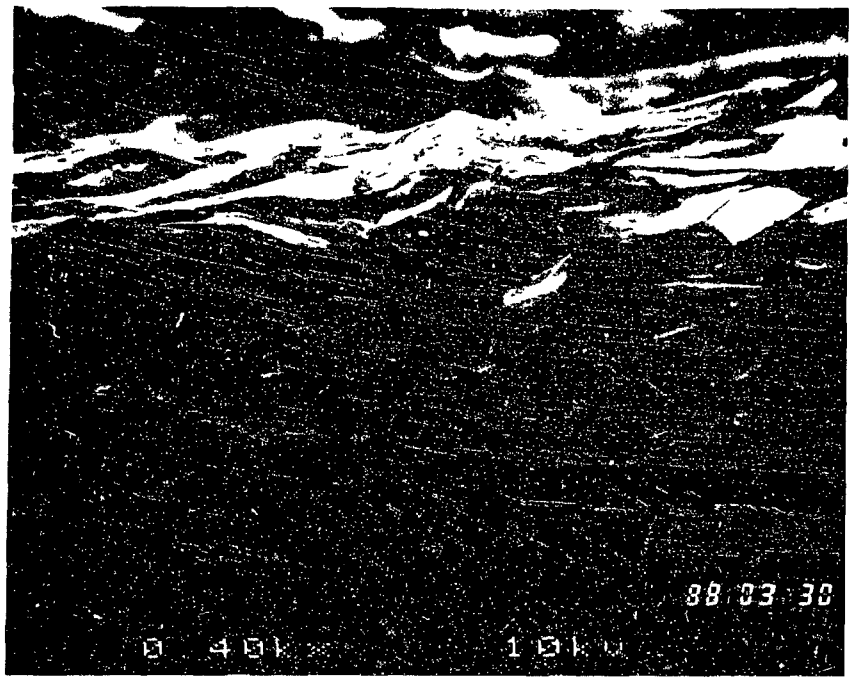

a

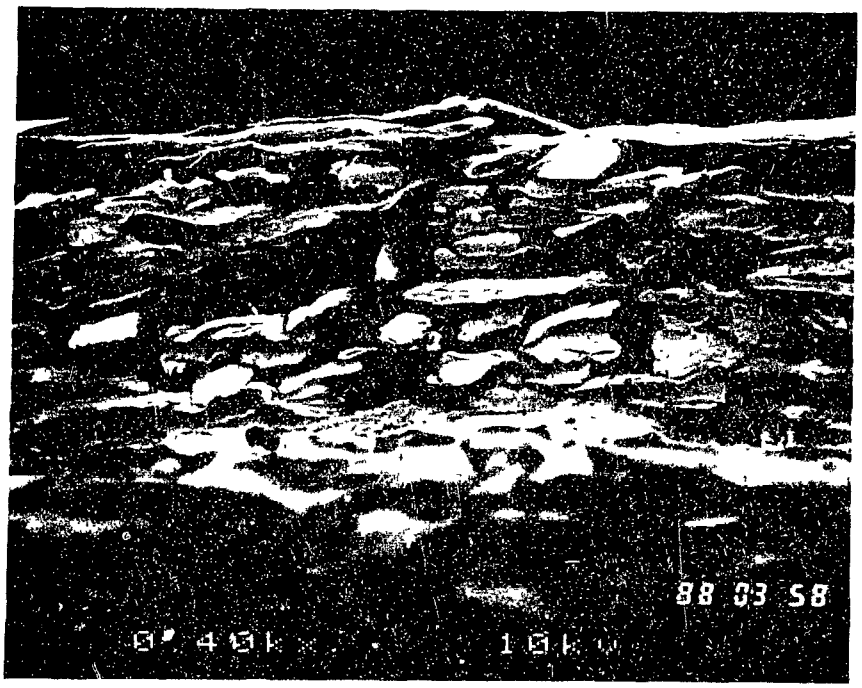

b

Figure 4.16 Scanning Electron Micrographs of paper cross-sections a) 25g/m², b) 50g/m², c) 100g/m², d) 150g/m²
The scale is indicated at the bottom of the photograph by the line which follows the two dashed lines. The length of the line corresponds to 10μm.

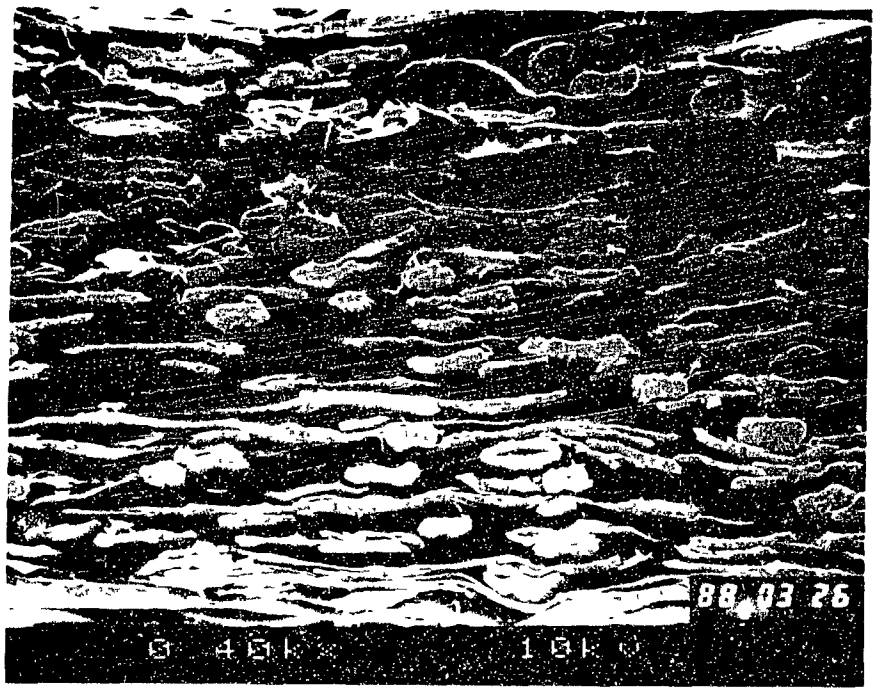

c

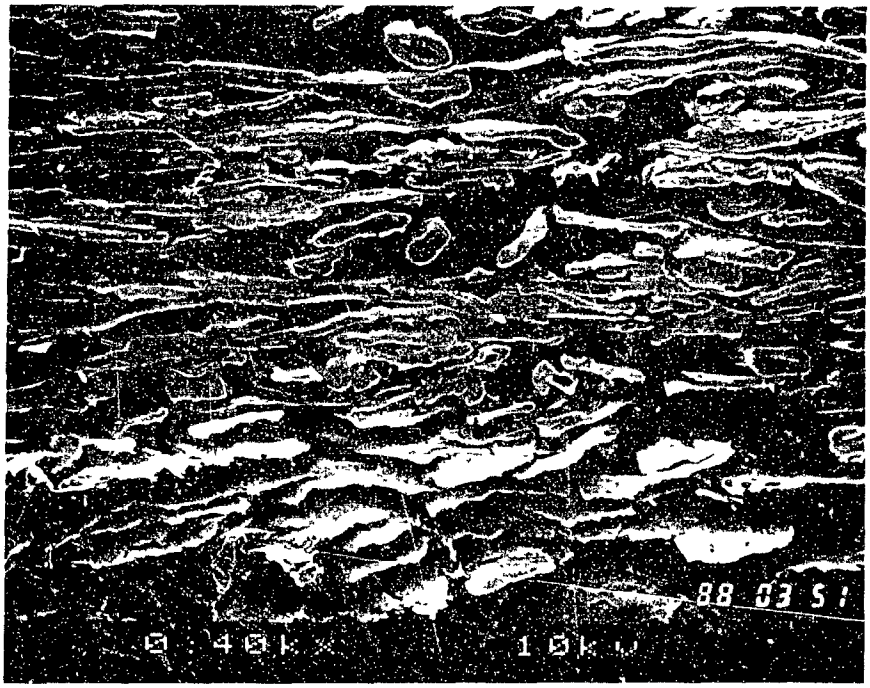

d

Figure 4.16 continued

analysis as an external flow around bodies of dimensions of the particles, or as an internal flow through pores, of shape and dimensions determined by the particles. Of various studies of through drying of paper only Wedel and Chance[1977] used the former approach. In a bed for which the porosity is as high as that of paper, 0.65-0.70, flow phenomena will be governed less by drag of the fibres which obstruct the flow, and more by the forces acting on a flow through the pores bounded by these fibres. Thus the choice of fibre diameter by Wedel and Chance[1977] is inappropriate because flow through paper is less an external flow around objects than an internal flow through an open porous structure.

4.7.2 Previously Used Characteristic Dimensions

For an internal flow through irregular pores in beds of complex particles, alternative characteristic dimensions have been based on permeability, k, on specific surface, a_p, on equivalent capillary tube diameter, d_{eq}. In view of the difficulty of any measurement for wet paper, all those choosing some characteristic dimension of paper with throughflow drying have used values for the dry sheet. As measurements of the present study indicate that both permeability and specific surface change substantially when paper is subjected to a wetting-through drying cycle, the choice of when the measurement is made is important. The present work establishes that these changes occur primarily during wetting, not drying. It follows therefore that any proposed characteristic dimension for dry paper should be based on measurements after drying, not before the wetting step that precedes a through drying measurement

(a) Square Root of Permeability

Square root of permeability has the correct dimensions and is some empirical measure of pore structure. $\sqrt{k}$ as the unique property representing the structure of a porous media is a view promoted by Spielman and Goren[1968] and in a series of papers by Beavers and co-workers, Beavers and Sparrow[1969], Beavers *et al.*[1975], [1981a], [1981b]. Spielman and Goren employed $\sqrt{k}$ in their treatment for pressure drop across fibrous filters, as did Beavers and co-workers for air and water flow through unconsolidated and consolidated beds of metal fibers, porous metal and polyurethane foam In a study of throughflow drying of paper Raj and Emmons[1975] used $\sqrt{k}$ for dry paper as the characteristic dimension for Pe, i.e. ReSc. They unfortunately did not specify whether permeability was measured prior to wetting the paper at the start of a drying experiment, or after completion of drying. The present results establish the substantial difference between these two dry paper conditions. Moreover they calculated $\sqrt{k}$ assuming Darcy's law, implying pure viscous flow with no inertial effects, an assumption which is proven in the present study to introduce substantial error for throughflow rates of practical interest.

(b) Hagen-Poiseuille Equivalent Capillary Diameter

Gummel[1977] calculated an equivalent pore diameter, d_{eq}, for flow through dry paper using the Hagen-Poiseuille equation. This procedure implies pure viscous flow with no inertial effects, which the present study establishes is an important error for some of the experimental conditions used by Gummel. He tried to minimize inertial effects by using superficial velocity as low as 0.02m/s. However, the inertial

contribution to total pressure drop could still be appreciable in those measurements even at this low velocity because his paper was extremely bulky, i.e ~260μm thick for 20g/m^2. Moreover, Gummel's flow experiments for d_{eq} were performed on dry paper before his wetting-through drying cycle, hence are for a paper microstructure substantially different from that during his through drying measurements. In addition to these problems, the equivalent channel diameter of Gummel is much too high, d_{eq} of 130μm to 170μm, because he used the surface porosity, i.e. pin hole area, of 10-15% whereas the porosity of the entire sheet for throughflow phenomena is higher than this by about a factor of 6 for dry paper. Even if the specific errors noted were avoided, Gummel's use of the Hagen-Poiseuille equation is fundamentally wrong because, with his d_{eq} values, his Reynolds numbers would all be greater than 0.2, which is higher than the Reynolds number limit for pure viscous flow given by various researchers, i.e. 0.02 (Ahmed and Sunada[1969]) or 0.1 (Scheidegger[1974]). In Gummel's range of Reynolds number the inertial effects would have been large, thus the Hagen-Poiseuille equation does not apply to his flow regime.

(c) Reciprocal of Specific Surface

Robertson and Mason[1949] used $1/a_p$ of dry paper as the Reynolds number characteristic dimension in their study of water flow through pulp pads, as did Knauf and Doshi[1986] for air flow. Knauf and Doshi calculated the specific surface of paper from air permeability data using the Kozeny-Carman relation. In order to minimize error due to inertial effects on ΔP, Knauf and Doshi used thick sheets, 200g/m^2, and very low throughflow velocities, <0.02m/s, a range far from that of

practical importance. As Reynolds numbers calculated using this a_p value were always less than 0.01 they concluded that Darcy's law was valid for their conditions.

4.7.3 Characteristic Dimension from Specific Surface and Permeability

As k and a_p were determined in the present study both before and after drying, the values of $\sqrt{k}$ and $1/a_p$ investigated as a characteristic dimension of paper for through drying, Table 4.8, are those obtained after the wetting-through drying cycle.

Table 4.8 Values of characteristic dimensions of dry paper based on permeability and specific surface

Basis Weight, g/m^2	$1/a_p$, μm	$\sqrt{k}$, μm
25	1.32	1.23
50	0.96	0.88
100	0.84	0.76
150	0.75	0.72
250	0.69	0.59

While the present work eliminates earlier errors, i.e. by now allowing for inertial effects in determining k and measuring only the interfacial area effective for transport phenomena, the question remains: is either $1/a_p$ or $\sqrt{k}$ is a valid characteristic dimension? The Table 4.8 values of $1/a_p$ and $\sqrt{k}$ are in the range of some very early measurements of effective pore radius for commercial paper, 0.2-1.2μm by Carson[1940] and 0.1-1.3μm by Bublitz *et al.*[1948], both by an air permeability technique. However these $1/a_p$ and $\sqrt{k}$ values are an order of magnitude lower than the mean pore diameter, 9-12μm, for handsheets measured by Bliesner[1964] using the gas drive technique which involves

the stepwise penetration of a gas through the sample above which there is a column of liquid.

Moreover, the scanning electron micrographs of paper used in the present study, Fig. 4.16, reveal a significant presence of much bigger pores, up to about 50μm for 25g/m^2 paper, and to 10·20μm for 150 g/m^2 paper. Thus any characteristic dimension in the order of a micron, as given by both $1/a_p$ and $\sqrt{k}$, bears no relation to the observed size of the flow channels. The values of $1/a_p$ and $\sqrt{k}$ are in fact in the range of intra-fibre pores, although the flow phenomena in the experiments used to determine k and a_p relate only to the inter-fibre channels. This contradiction indicates that it is invalid to simply manipulate a_p and k to obtain a term having the units of length and then treat such a term as the characteristic dimension for flow phenomena. Thus the present measurements indicate that, even when correctly determined, neither $1/a_p$ or $\sqrt{k}$ is a valid choice of characteristic dimension for flow processes through a porous media.

4.7.4 Characteristic Dimension from Momentum Transport Analysis: Theory

The approach adopted here is that the appropriate characteristic dimension should derive directly from the flow phenomena through paper. The Reynolds number, $Re=d_pG/\mu$, where d_p is the characteristic dimension of the porous media, is by definition the ratio of inertial to viscous forces. The inertial and viscous contributions appear explicitly in the momentum transport equation for flow through porous media, Eqn. 4.3 of Section 4.3.2,

$$\frac{\Delta P}{L} = \alpha\mu_1 + \beta\rho u^2$$

where $\alpha = \frac{1}{D^2V}\iiint \nabla^2\mathbf{v}\, dV$; $\beta = \frac{1}{D\,V}\left(\iiint \mathbf{v}\,\nabla\mathbf{v}\, dV + \iint \frac{P}{\rho u^2}\,\mathbf{n}\, dA\right)$

In the terms of this momentum transport equation, a true Reynolds number which is the ratio of inertial to viscous effects must be

$$Re = \beta\rho u^2/\alpha\mu u = \beta\rho u/\alpha\mu$$

Therefore the correct, theoretically based characteristic dimension for flow through porous media is

$$d_P = \beta/\alpha$$

which is a characteristic dimension derived directly from application of the momentum transport equation which yields the parameters α and β.

This definition of characteristic dimension, $d_P=\beta/\alpha$, has never been proposed or tested for paper. The characteristic dimension $d_P=\beta/\alpha$ was first proposed by Ahmed and Sunada[1969] for flow through beds of sand and other simple rigid particles. They employed this definition successfully with their experimental data and that of previous researchers for flow through sand, glass beads, metal saddles and granular absorbent beds. Macdonald *et al.*[1979] applied β/α as the characteristic dimension for correlation of ΔP across packed beds of a variety of simple, rigid particles, i.e. data for spherical glass beads from Rumpf and Gupte[1970]; cylindrical nylon, dacron and glass fibers from Kyan *et al.*[1970]; various sand, marble, gravel and metal mixtures from Dudgeon[1966]; and for various unconsolidated and consolidated media (ceramics, sandstone and oil sands) from Fancher and Lewis[1933].

Macdonald *et al.*[1979] gave the shortcomings of the $d_P=\beta/\alpha$ approach as: (i) α and β are functions of the bed which, not being based on dimensions of the media. must be determined experimentally, and (ii) ΔP must be measured over both the viscous and inertia dominated regimes in order to define α and β. The former restriction applies equally with any basis of characteristic dimension for beds of complex particle and

pore geometry, as for example d_p based on k, on a_p, or on application of the Hagen-Poiseuille equation for equivalent pore size. The latter restriction implies the need for a minimum of just two independent experimental measurements, i.e. not both in the pure viscous flow regime.

4.7.5 Characteristic Dimension from Momentum Transport Analysis: Experimental Results for Dry Paper

Table 4.9 gives the values of characteristic dimension, $d_p=\beta/\alpha$, for each basis weight of kraft paper as determined from the best fit values of the momentum transport parameters, α and β, given in Tables 4.2 and 4.3. Again N indicates the number of sheets of paper on which each d_p value is based. The results for 250 g/m² blotter paper extend the basis weight range while those for the 45g/m² Papriformer newsprint illustrate d_p for a quite different paper.

Table 4.9 Values of characteristic dimension of dry paper based on fundamental momentum transport relations

Basis weight	Before a wetting-drying cycle			After a wetting-drying cycle		
g/m²	N	$d_p=\beta/\alpha$, μm	σ, μm	N	$d_p=\beta/\alpha$, μm	σ, μm
25	3	21.6	1.0	65	16.8	1.7
50	3	5.5	0.2	61	5.4	0.6
100	3	6.4	0.4			
150	3	3.1	0.3			
250	3	4.2	0.4			
45‡				9	3.6	0.3

‡ groundwood furnish, Papriformer newsprint

As paper permeability approximately doubles after a wetting-drying cycle, a much higher throughflow rate is required to obtain an accurately measurable inertial contribution to pressure drop. For 100-250g/m² paper after a wetting-through drying cycle, β/α was indeterminant from

the permeability-through drying experiments because the throughflow rates used did not extend to values sufficiently high to obtain an inertial contribution to ΔP for paper this thick. Supplementary experiments were therefore made with the maximum throughflow rate increased to ~0.75kg/m^{2}s, a rate sufficient to give an inertial contribution to pressure drop of approximately 20% or higher for 100 and 150g/m^2 paper. At each basis weight over the range 25-150g/m^2, five of the same sheets used to obtain the Table 4.3 and 4.9 results were used again with the increased range of throughflow rate to obtain the additional results, Table 4 10. While these supplementary values of the characteristic dimension, $d_p=\beta/\alpha$, were obtained to complete the d_p values for 100 and 150g/m^2 paper, it is interesting to note that the additional values for 25 and 50g/m^2 paper

Table 4.10 Values of characteristic dimension of dry paper based on fundamental momentum transport relations: Supplementary measurements after a wetting-drying cycle

	M_B, g/m^2			
	25	50	100	150
N	5	5	5	5
α, m^{-2}	0.65×10^{12}	1.29×10^{12}	1.78×10^{12}	1.93×10^{12}
σ_α, m^{-2}	0.54×10^{10}	0.8×10^{10}	2×10^{10}	1.6×10^{10}
β, m^{-1}	1.01×10^{7}	0.69×10^{7}	0.89×10^{7}	0.91×10^{7}
σ_β, m^{-1}	5×10^{5}	3×10^{5}	7×10^{5}	8×10^{5}
k, m^2	15.3×10^{-13}	7.7×10^{-13}	5.6×10^{-13}	5.2×10^{-13}
σ_k, m^2	13×10^{-15}	4.8×10^{-15}	6.3×10^{-15}	4.4×10^{-15}
C	12.5	6.1	6.6	6.5
d_p, μm	15.4	5.3	5.0	4.7
σ_{d_p}, μm	0.8	0.3	0.4	0.4

agree closely with those obtained in the original permeability-through drying experiments, Table 4.9. At M_B=25g/m^2 these determinations of d_p differ by only 8%, the preferred value being that in Table 4.9, based on measurements for 65 sheets although with a somewhat narrower flow rate

range. The values of σ_{d_p} are all in the range 4-11% for the Table 4.9 and 4.10 results, i.e. in the same range as for σ_β in Tables 4.2 and 4.3 for the more sensitive of the two momentum transport parameters, β. Again it should be recalled that this spread in measured values of d_p derives mostly from the variation in formation between replicate handsheets.

The Table 4.9 and 4.10 values of characteristic dimension for standard handsheets of kraft paper are from 4 to 16 times higher than those determined at comparable basis weights from $1/a_p$ and $\sqrt{k}$, are 1/4-1/3 the Hagen-Poiseuille equivalent capillary diameter as determined by Gummel[1977], and are 1/3-1/2 the measurements of Bliesner[1964] for paper of basis weight 50g/m^2 and heavier. The results for the special case of 45g/m^2 paper is discussed subsequently. Reference to the scanning electron micrographs, Fig. 4.16, indicates that the Table 4.9 and 4.10 values of the $d_p=\beta/\alpha$ characteristic dimension are of a realistic magnitude, in contrast to the previously used $1/a_p$ and $\sqrt{k}$, which are much too small, and to the d_{eq} of Gummel and the Bliesner measurements, which are much too large. Thus the momentum transport based characteristic dimension is the first to be consistent with pore size as revealed by electron microscopy of paper.

4.7.6 Effect on Characteristic Dimension of Basis Weight, Wetting and Drying, and Pulp Type

The results for characteristic dimension of dry paper, Tables 4.9 and 4.10, are shown on Fig. 4.17, which includes $\pm 1\sigma$ error bars. The increase in the $d_p=\beta/\alpha$ characteristic dimension by a factor of 3-4 when basis weight is reduced from 50 to 25g/m^2 is believed to reflect the corresponding large increase in pin holes at low basis weight. The

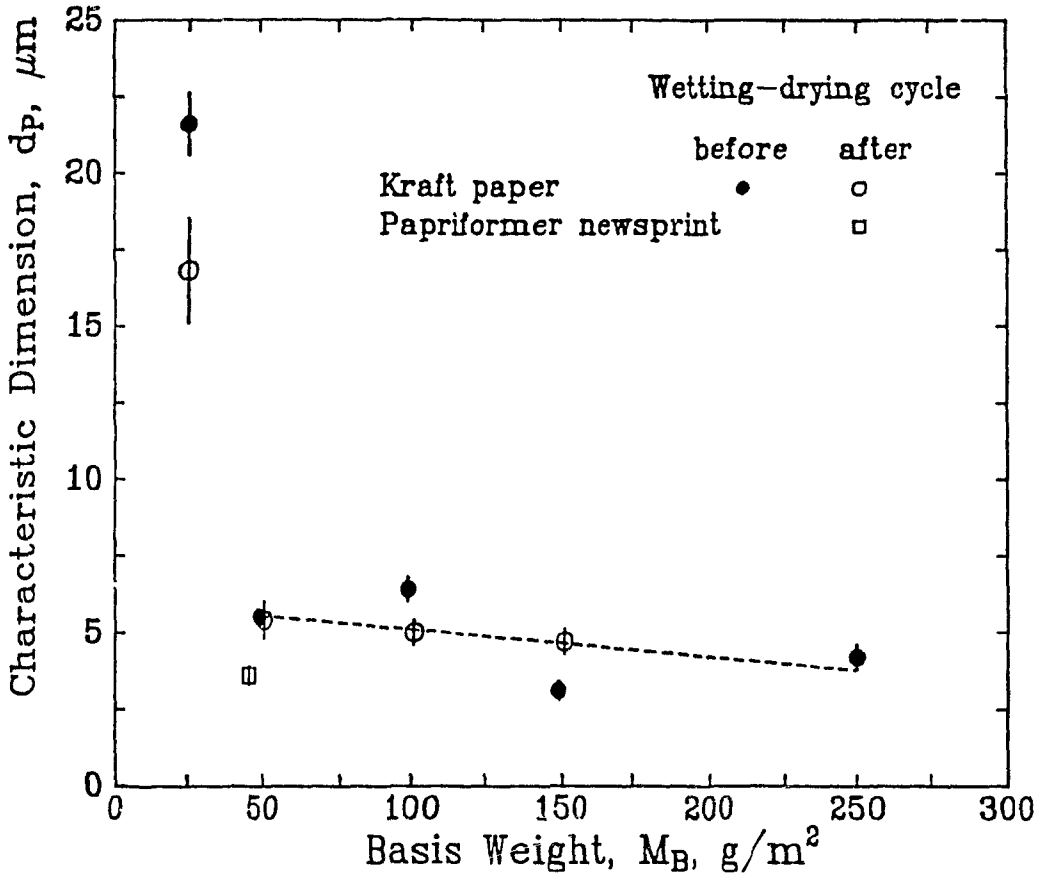

Figure 4.17 Effect of basis weight on characteristic dimension: dry paper, before and after a wetting-drying cycle

evidence concerning the pin hole-basis weight relationship was given in section 4.3.3. From paper basis weight 50g/m^2 (L≈100μm) to 250g/m^2 the characteristic dimension $d_p=\beta/\alpha$ scarcely changes, decreasing from about 5.5 to 4.2μm. Bliesner[1964] also observed little effect of basis weight on mean pore size of dry paper for $M_B \geq 100 g/m^2$. Over the basis weight range 50-250g/m^2 there is no statistical basis for differentiating between values of d_p obtained before and after a wetting-drying cycle, so a least squares straight line is shown over this range on Fig. 4.17. At $M_B=25 g/m^2$ the $\pm 1\sigma$ error bars shown on Fig. 4.17 indicate that the $\pm 2\sigma$ limits in fact overlap. Thus while there may be a decrease in d_p over a wetting-drying cycle for 25g/m^2 kraft paper, confirmation of this behaviour would require further study.

The data indicate that permeability and characteristic dimension for paper are affected somewhat differently by a wetting-drying cycle. Sections 4.3 and 4.4 establish that, over such a cycle, k approximately doubles, while here it is shown that, with the possible exception for 25g/m^2 paper, d_p remains unchanged. These findings might appear to be inconsistent. The characteristic dimension, d_p, according to the rigorous definition used here, is the ratio of inertial, β, and viscous, $\alpha=1/k$, parameters in the fundamental momentum transport equation. As the change in α (or k) and d_p over a wetting-drying cycle appears on Figs. 4.2 and 4.17, the effect of wetting-drying is completed with Fig. 4 18, which shows that β drops by half after such a cycle. Least square straight lines are shown on Fig. 4.18, along with $\pm 1\sigma$ error bars. Thus a wetting-drying cycle affects the α and β parameters in a similar way, i.e. both drop to about half of their value before such a cycle. Collapse of surface fibrillation, the main change in paper microstructure due to

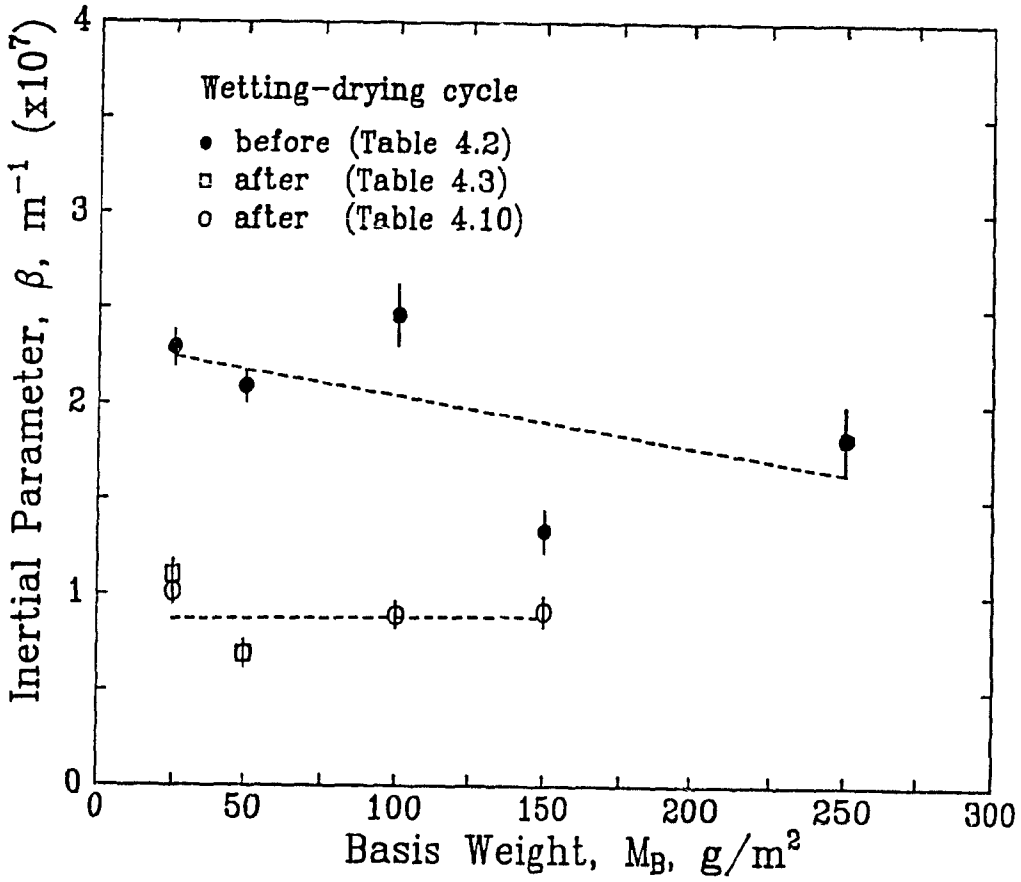

Figure 4.18 Effect of basis weight on inertial momentum transport term: dry paper, before and after a wetting-drying cycle

wetting as discussed in Section 4.4.3, reduces the obstacles in flow channels, and this is seen to result in about an equal reduction in the viscous and the inertial terms in the momentum transport equation. The mechanism of fibril collapse causes about the same percentage drop in α and β or percentage increase in k, so that $d_p=\beta/\alpha=k\beta$ stays about the same.

The characteristic dimension, d_p, of the 45g/m^2 Papriformer newsprint made from mechanical pulp, Table 4.9, is about 2/3 of that of handsheets of comparable basis weight made from chemical pulp. Relative to kraft paper, newsprint is made from more fibrillated fibres, Fig. 4.6a, in a web of higher bonded area, Fig. 4.6b, with more fines present in the interfibre pores, Fig 4.6c, which results in both lower permeability, discussed in Section 4.4.4, and smaller pores as defined by the momentum transport characteristic dimension, $d_p=\beta/\alpha$.

4.7.7 Reynolds Number-Friction Factor-Characteristic Dimension Relations

The momentum balance, Eqn. 4.4, may be rearranged to

$$\frac{\Delta P/L}{\beta G^2/\rho} = 1 + \frac{\alpha\mu}{\beta G} \qquad (4.12)$$

or, in terms of the new characteristic dimension for Reynolds number,

$$\frac{\Delta P/L}{\beta G^2/\rho} = 1 + 1/Re \qquad (4.13)$$

The left hand side of Eqns. 4.12 and 4.13, $(\Delta P/L)/(\beta G^2/\rho)$, is the ratio of total energy loss to the kinetic energy loss, which is precisely the friction factor definition of Eqn. 4.10. Thus Eqn. 4.13 can be written more simply as

$$f = 1 + 1/Re \qquad (4.14)$$

Comparison of the above definition of friction factor, $f=(\Delta P/L)/(\beta G^2/\rho)$, with the Fanning friction factor definition for flow through packed beds, $f^*=(\Delta P/L)d_p^*/(2G^2/\rho)$, indicates that the Fanning characte-

ristic dimension, $d_P^*=2d_P/C^2$, differs from that derived from the fundamental momentum transport equation, $d_P=\beta/\alpha$. Eqn. 4.10 is a definition for friction factor, not a law of fluid mechanics, and several definitions of Fanning friction factor exist, some corresponding to $2f^*$, others to $4f^*$. Because f^* for packed beds is defined analogous to flow in circular tubes, there is for the viscous flow range a linear f^*-Re relation, $f^*=A'/Re$, with the parameter A' dependent on the porous medium. For pipe flow, A'=16 from the Hagen-Poiseuille equation. Of the variety of porosity functions which have been introduced into the Fanning friction factor definition in attempts to obtain a universal f^*-Re relation, well summarized by Dullien[1975], the most widely adopted is that of Ergun[1952],

$$f^* = \frac{\Delta P/L}{G^2/\rho} d_P^* \frac{\varepsilon^3}{(1-\varepsilon)} = A \frac{(1-\varepsilon)}{Re} + B \qquad (4\ 15)$$

where A=150 and B=1.75 according to Ergun[1952]. Eqn. 4.15 shows that the Fanning friction factor definition for packed beds is a modified form of that for conduits, i.e. with the extra $\varepsilon^3/(1-\varepsilon)$ term.

Various Re-f-d_P relations are summarized in Table 4.11. Because the characteristic dimension, d_P^*, associated with the Fanning friction factor, f^*, differs from the characteristic dimension, d_P, based on momentum transport relations, it is important to note that even the Reynolds numbers in the two systems differ, i.e. $Re^*=(2/C^2)Re$. The Darcy number, Da, the ratio of total force to viscous force, is likewise included. With the present definition of friction factor, f, the total nondimensional pressure drop is represented as the sum of the reciprocals of Da and f, Table 4.11. In the context of the Table 4.11 compilation it is useful to recall that the Kozeny-Carman relation is $k=\frac{\varepsilon^3}{\kappa(1-\varepsilon)^2 a_p^2}$ while permeability may be expressed as $k=1/\alpha$

Table 4.11 Comparison of Reynolds number-friction factor relations

	Present Method	Fanning Friction Factor	
Momentum transport equation	$\frac{\Delta P}{L}=\alpha\mu u+\beta\rho u^2$ $=\frac{\mu}{k}u+\frac{C\rho}{\sqrt{k}}u^2$	$\frac{\Delta P}{L}=\frac{A}{d_p^{*2}}\frac{(1-\varepsilon)^2}{\varepsilon^3}\mu u+\frac{B}{d_p^*}\frac{(1-\varepsilon)}{\varepsilon^3}\rho u^2$	‡
Friction Factor	$f = F/AK$ $=(\Delta P/L)/\beta\rho u^2$	$f^* = (\Delta P/L)d_p^*/(2\rho u^2)$ $= (\beta^2/2\alpha)f$	‡‡
Characteristic dimension	$d_p=\beta/\alpha=C\sqrt{k}$	$d_p^*= (2/C^2)d_p = 2/\beta$	
Reynolds number	$Re=d_pG/\mu$	$Re^*=d_p^*G/\mu=(2d_p/C^2)G/\mu=(2/C^2)Re$	
General Re-f relation	$f =1+1/Re$	$f^*= \frac{A(1-\varepsilon)^2}{2\varepsilon^3Re^*}+\frac{B(1-\varepsilon)}{2\varepsilon^3}$	
Re-f relation for viscous flow	$f =1/Re$	$f^*= \frac{A(1-\varepsilon)^2}{2\varepsilon^3Re^*}=A'/Re^*$	
		$f^*= 16/Re^*$	‡‡‡
Re-f-Da relations	$Da=(\Delta P/L)/\alpha\mu u$ $Da= 1+Re$ $1/Da+1/f=1$		

‡ Ergun eqn. is used here due to its wide acceptance
‡‡ f^* definition analogous to flow through conduits (Bird *et al.*[1960])
‡‡‡ from Hagen-Poiseuille equation for pipe flow

The analysis of Rumpf and Gupte[1971] proposed that $\Delta P/\rho u^2$ be represented as a function of the nondimensional parameters $Re=uD_p/\nu$, L/D_p, ε, q_1, ψ_1, structure, where D_p is the surface average sphere diameter, and q_1 and ψ_1 are size distribution and particle shape parameters. Most previous researchers used the superficial velocity, u, or the Dupuit relation, u/ε, in the above relationship and tried to include the porosity, structure, size and shape parameters in the form of a porosity function In the present Re-f treatment of Eqn. 4.12 it is superficial not interstitial velocity which is employed and, significantly, no empirical porosity function is needed Definition here of a characteristic dimension, $d_p=\beta/\alpha$, based on basic transport phenomena relations eliminates the need for the various porosity, pore size distribution, particle or

pore shape empirical factors of earlier approaches. All these characteristics of the pore structure may be important, but in the present analysis they affect d_p through their effect on α and β.

Applicability of the Re-f model with $d_p=\beta/\alpha$ was successfully demonstrated by Ahmed and Sunada[1969] and Macdonald *et al.*[1979] for flow through porous media of simple, rigid particles. Thus this nondimensional form, Eqn. 4.14, of the fundamental momentum transport equation, Eqn. 4.3, is tested in the present study for the first time for flow through paper, a porous media of much greater complexity than any previously tested for this approach.

4.7.8 Reynolds Number-Friction Factor Experimental Results: Dry Paper

Fig. 4.19 shows the ΔP measurements for dry paper, calculated in terms of Reynolds number-friction factor with the characteristic dimension $d_p=\beta/\alpha$ The friction factor data on Fig. 4.19 derive from 120 ΔP measurements for 15 sheets made with both helium and air flow before a wetting-drying cycle (as for Table 4.2) and from the approximately 100 supplementary measurements of ΔP with 20 sheets after wetting-drying (as for Table 4.10). For Fig. 4.19 the Reynolds number value associated with each friction factor measurement was determined using an individual value of d_p for each sheet of paper tested Thus for paper before, and after, a wetting-drying cycle the single sheet values of d_p used to determine Re for Fig. 4.19 are not the best fit values of d_p for N sheets that are listed in Tables 4.9 and 4.10. The complete Re-f data are tabulated in Appendix 6.

For Fig. 4.20, by contrast, the values of Reynolds number derive from the best fit value of d_p for all the sheets of each basis weight.

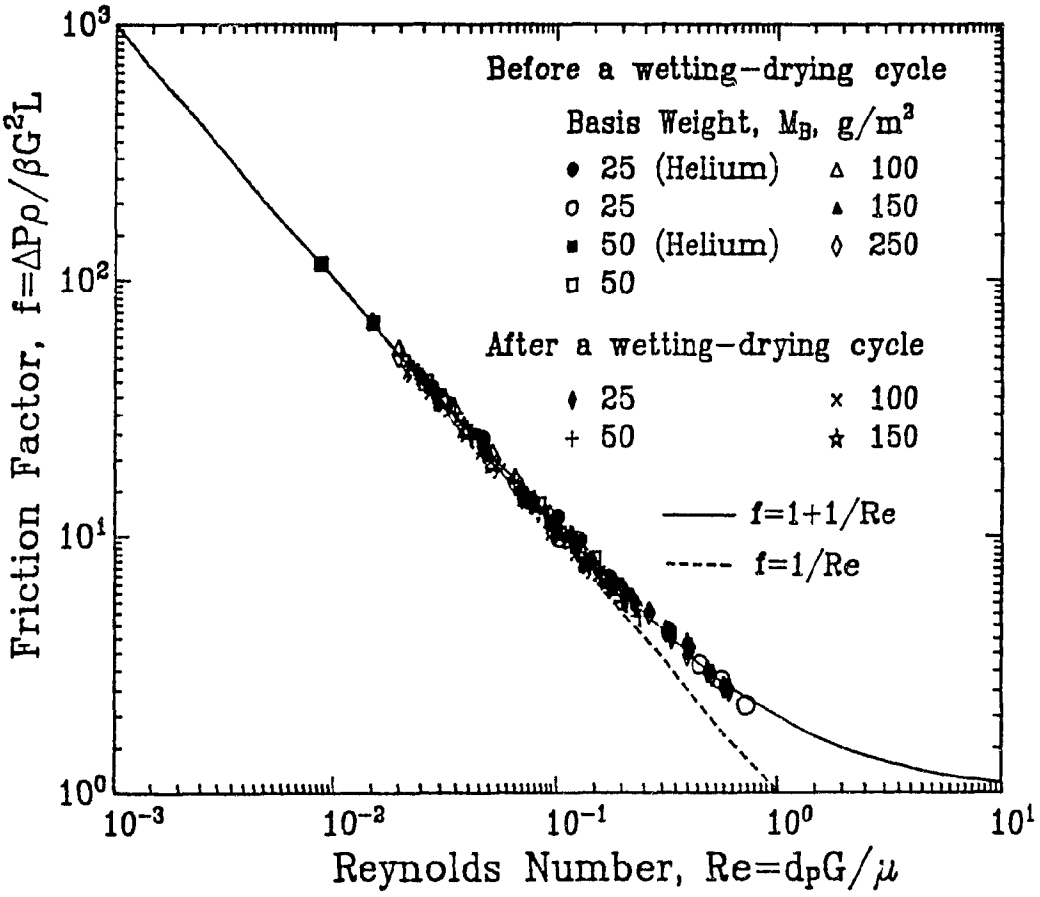

Figure 4.19 Pressure drop across dry paper: d_p for individual sheets

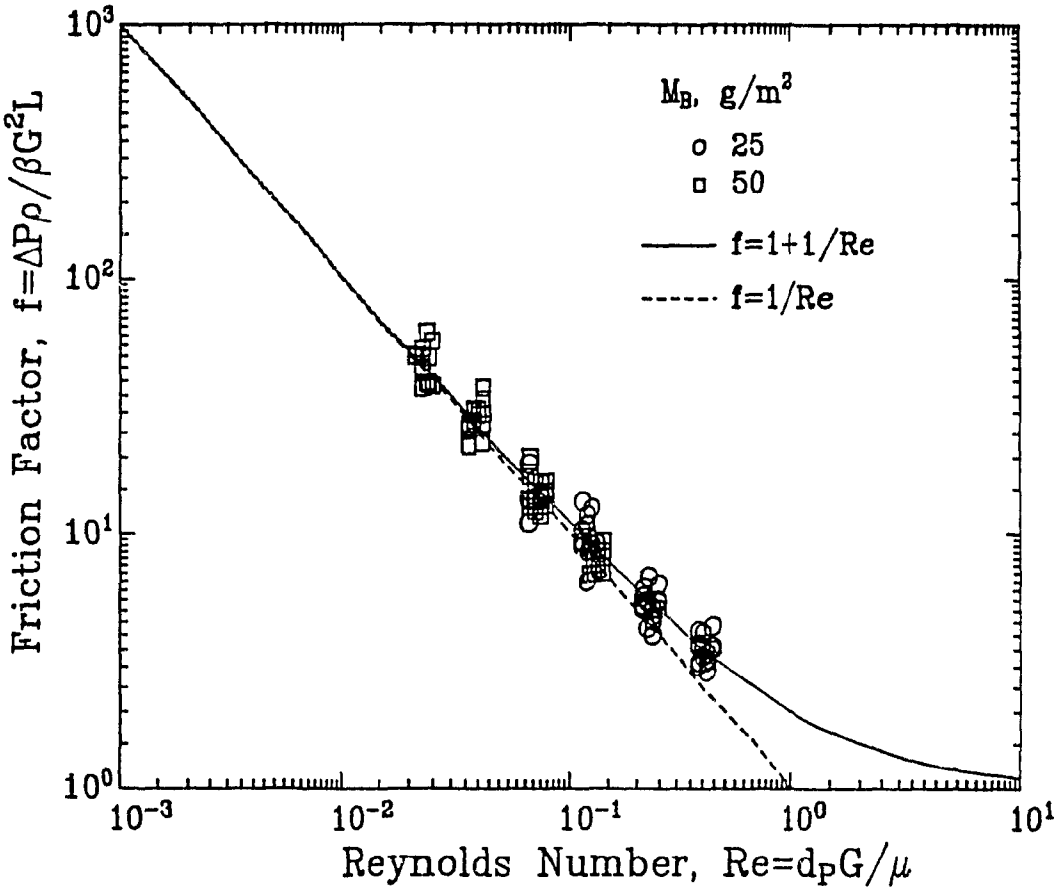

Figure 4.20 Pressure drop across dry paper: average d_p for each basis weight.

The Fig. 4.20 results represent about 500 ΔP-G measurements made after a wetting-drying cycle with 126 sheets, i.e. 65 sheets of basis weight $25 g/m^2$, 61 sheets of $50 g/m^2$, using only the two values of d_p given in Table 4.9.

Figs. 4.19 and 4.20 show all the ΔP data for dry paper obtained in the present study, some 700 measurements The amount of experimental scatter around the theoretical line f=1+1/Re is naturally greater for Fig. 4.20 because of the use of only one value of d_p representative of each basis weight, compared to an individual d_p value for each of the 35 sheets of the Fig. 4.19 results. The excellent agreement of the experimental results with the theoretical f=1+1/Re line, with surprisingly small scatter of the extensive data, Figs. 4.19-4.20, confirms the appropriateness of this new approach to the analysis of throughflow phenomena for dry paper. As this characteristic dimension for paper is also the first to give values of d_p consistent with observations from scanning electron microscopy of paper, these two types of confirmation validate the central feature of the analysis, i.e. definition of the characteristic dimension of paper, d_p, based rigorously on the momentum transport equation.

4.7.9 Characteristic Dimension from Momentum Transport Analysis: Experimental Results for Moist Paper

The success achieved with this Re-f-d_p approach for dry paper suggests testing whether it may be applied for moist paper as well. Application of the momentum transport equation, Eqn. 4.4, to the case for moist paper leads to the definition of the characteristic dimension as $d_p=\beta'/\alpha'$, equivalent to the $d_p=\beta/\alpha$ relation for dry paper. The experi-

mental technique of the present study provides the complete ΔP-X relation for a sheet of paper of a certain basis weight, M_B, dried from a known initial moisture content, X_o, with a throughflow of fixed rate and temperature, G and T_i. These ΔP-X relations are determined successively using a fixed throughflow rate, G, at four levels of G. The parameters X_o and T_i, important for the associated drying rate study, have been shown to have no effect on d_p, hence simply constitute additional replicate runs for the momentum transport part of the study considered here. Determination of α' and β' and thereby, d_p for moist paper, where d_p is expected to be a sensitive function of paper moisture content, X, therefore requires sets of ΔP-G data at constant X. Although the basic experimental data are determined as sets of ΔP-X measurements at constant G, the computer data acquisition at a real time frequency of 5-10Hz permits extraction of data in the required form of ΔP-G measurements at constant X at as many levels of moisture content, X, as desired. From each such ΔP-G data set, a value of α', β' and thereby d_p can be determined which applies for the basis weight, M_B, of that sheet and for the selected value of paper moisture content, X.

The results of this procedure appear in Table 4.12. In the Table 4.12 listing of experimental values of d_p for moist paper, N again represents the number of sheets tested. As ΔP for each sheet is normally measured at 4 values of G at each moisture content, X, each value of d_p is based on 4N sets of ΔP-G measurements. Although d_p was determined at moisture content intervals of 0.1kg/kg, for brevity only d_p values at every 0.5kg/kg are listed in Table 4.12 although the complete d_p-X data are shown on Fig. 4.21. Data are not available for $M_B \geq 100 g/m^2$ because the throughflow rates used were not sufficiently

high to give a measurable inertial contribution to pressure drop, hence the characteristic dimension, $d_p=\beta'/\alpha'$, could not be determined.

Table 4.12 Values of characteristic dimension of moist paper based on fundamental momentum transport relations

Moisture Content	Basis Weight, M_B=25g/m²			Basis Weight, M_B=50g/m²		
X, kg/kg	N	d_p, μm	σ_{d_p}, μm	N	d_p, μm	σ_{d_p}, μm
2.5	35	43.8	8.0	33	9.5	1.5
2.0	55	42.3	7.0	57	13.2	2.2
1.5	63	26.6	4.4	58	13.0	2.4
1.0	65	16.2	2.7	61	8.5	1.4
0.5	65	16.6	2.3	61	5.0	0 7
0.1	65	16.6	2.1	61	4.0	0.5

As moisture content decreases, the values of the characteristic dimension, $d_p=\beta'/\alpha'$, approach the corresponding values for dry paper after a wetting-drying cycle, Table 4.9, which come from the same complete set of ΔP-G-X measurements, and the dry paper d_p values of Table 4.10, which are from an independent series of ΔP-G measurements. With the addition of another variable, paper moisture content, it would be expected that σ_{d_p} for moist paper would be somewhat higher than for dry paper. Thus the values of σ_{d_p} of Table 4.12, in the range 12 to 18% of d_p, are higher than the corresponding range of 5-11% for σ_{d_p} for dry paper after a wetting-drying cycle, Tables 4.9 and 4 10. Recall however that most of this variability in d_p comes from the variability between the replicate handsheets.

4.7.10 Effect of Paper Moisture Content on Characteristic Dimension

Fig. 4.21 shows the first measurement of effect of paper moisture content on the characteristic dimension for paper with air throughflow. As moisture content decreases, ΔP decreases, and one typically associates

a decreasing ΔP with an increasing size of flow channels, d_p. However, the value of d_p for wet paper is 2 to 3 times that for the same paper when dry. As the moisture content of wet paper decreases, an increasing number of smaller pores participate in the flow, increasing the fraction of area open to air flow, decreasing the interstitial velocity in the pores so that both ΔP and d_p decrease. For wet paper, although the size of pores through which air flows is large, the fraction of the area open to throughflow is small, resulting in high ΔP for the high velocity flow in these channels.

For paper of basis weight 25 and 50g/m^2, the effective pore size for throughflow, d_p, becomes independent of moisture content below some value in the range 0.6-0.9kg/kg, while d_p reaches its maximum value at some moisture content around 1.7-2.1kg/kg. The plateau in d_p at low moisture content corresponds to water being present only in intra-fibre pores and in the smallest inter-fibre pores, through which there is negligible flow. Figs 4.9-4.12 show that permeability also becomes less sensitive to X at both high and low moisture contents, but the d_p-X relationships of Fig. 4 21 constitute a more fundamental representation of these phenomena

Electron micrographs of the paper used, Fig 4 16, indicate a maximum pore size of about 50μm and 10-20μm respectively for the 25 and 50g/m^2 basis weight paper. The agreement between the determination of maximum pore size visually by scanning electron microscopy and quantitatively by the new method of the present study is remarkable. Thus the maximum value of d_p found for wet paper, about 44 and 14μm at M_B of 25 and 50g/m^2, is controlled by the size of the largest pores in the sheet.

The lower d_p values for 50g/m^2 paper at X$\geq$2.3kg/kg may be due to

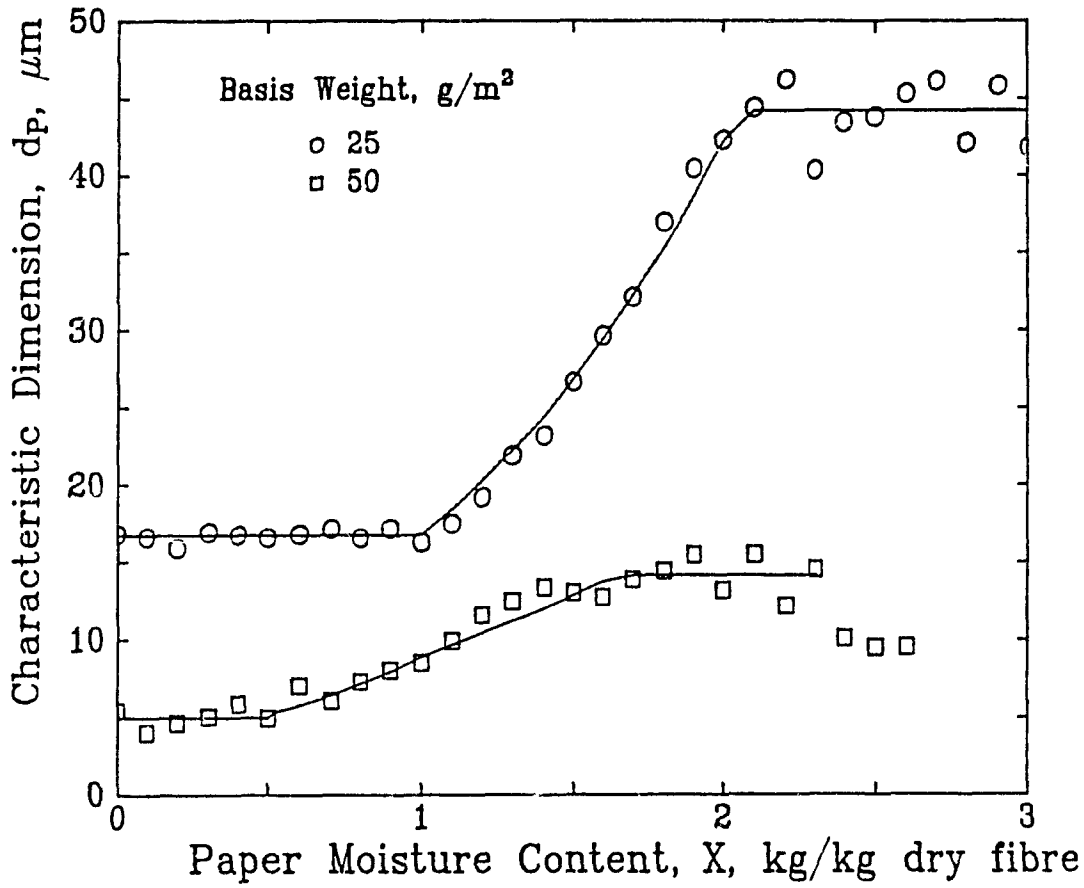

Figure 4.21 Effect of moisture content on characteristic dimension

compressibility of the sheet at the high ΔP values at these conditions. This possibility is illustrated by Fig. 4.22, for which the d_P-X data for M_B=50g/m^2 of Fig. 4.21 are shown together with ΔP-X data for M_B=50g/m^2 from a typical experiment at the highest level of throughflow rate. As moisture content decreases from X_o, ΔP drops rapidly from its maximum value, thereby reducing the compression force on the sheet. Testing the compressibility hypothesis would require a further study.

With these upper and lower physical limits on the variation with moisture content of d_P of paper, the d_P-X relation has three zones. Between the upper and lower plateau regions, zones I and III, the d_P-X relationship for the transitional region, zone II, may be represented as

$$d_P = 1/[c_1+c_2e^{-X}] \qquad (4.16)$$

This form is consistent with probabilistic studies of the porous structure of paper summarized by Corte[1982], Section 4.5. The results with the two parameters of Eqn. 4 16, determined by non-linear regression of the Fig. 4 21 data, are given in Table 4 13

Table 4.13 Parameters for the regression equations for effect of moisture content on characteristic dimension

Zone I : $d_P = A$		
M_B = 25g/m^2	A = 44 ± 2 μm	X≥2.1
M_B = 50g/m^2	A = 14 ± 1 μm	1.7≤X≤2.3
Zone II $d_P = 1/[c_1+c_2e^{-X}]$		
M_B = 25g/m^2	c_1= 0 0027 c_2= 0.16 r^2= 0.998 σ = 1.2 μm	0.9≤X≤2.1
M_B = 50g/m^2	c_1= 0.027 c_2= 0.23 r^2= 0 994 σ = 0.9 μm	0.6≤X≤1.7
Zone III: $d_P = B$		
M_B = 25g/m^2	B = 16.7 ± 0.3 μm	X≤0 9
M_B = 50g/m^2	B = 5.0 ± 0.5 μm	X≤0.6

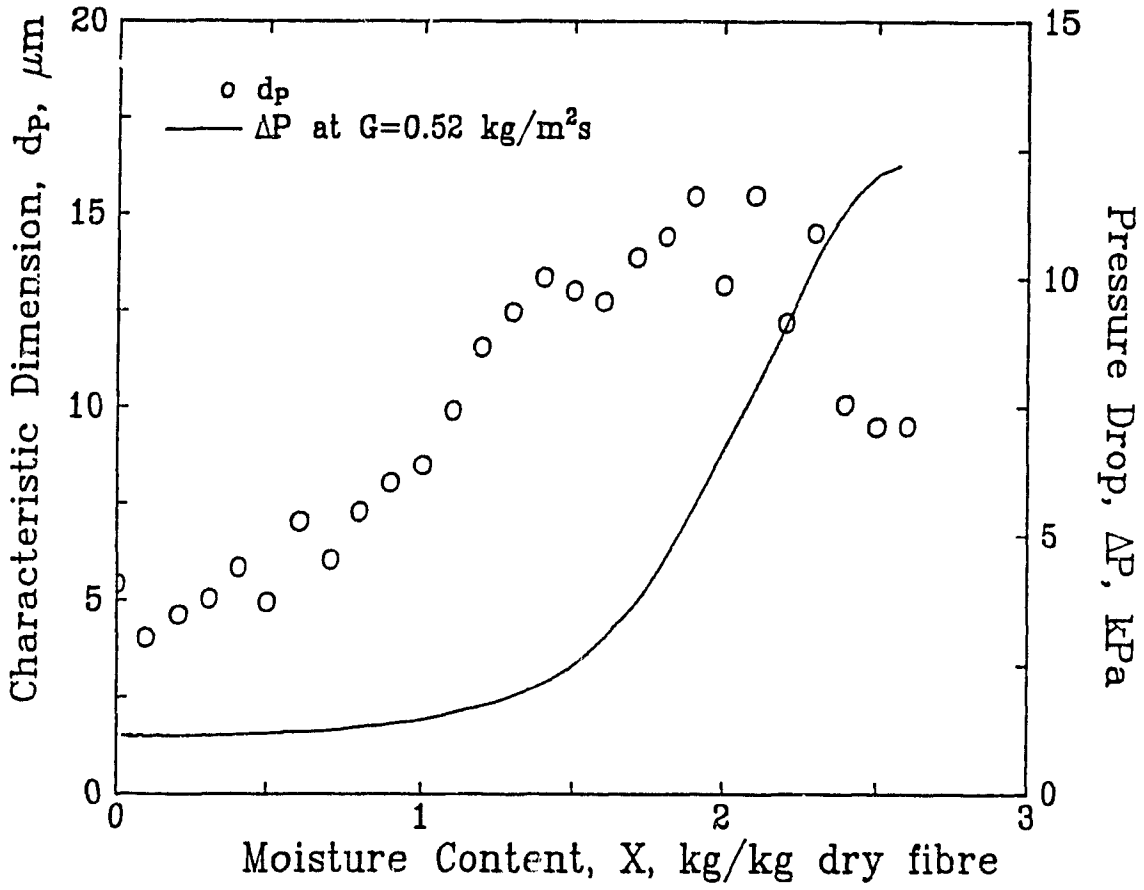

Figure 4.22 Effect of moisture content on pressure drop and characteristic dimension for 50g/m² paper

It is not possible to predict the moisture content which separates the first two zones, i.e. $X_{I/II}$, although finding $X_{I/II}$ to be higher for 25g/m^2 paper (2.1kg/kg) than for 50g/m^2 basis weight (1.7kg/kg) is as expected because of the wider pore size distribution in thinner paper. The moisture limit between the second and third zones, $X_{II/III}$, would be the point where all pores that participate in flow through dry paper become free of water and open to flow. With this remaining moisture absorbed in fibres and fibre agglomerates through which no flow occurs, the $X_{II/III}$ point should be very close to the fibre saturation point (FSP)

For the rewetted, unbeaten softwood kraft pulp used the fibre saturation point, determined here by the solute exclusion technique using 2% dextran solution, is 0 81kg H_2O/kg fibre for the original pulp and 0.72kg H_2O/kg fibre from the paper after a wetting-drying cycle. The $X_{II/III}$ limits of Table 4.12, 0.6-0.9 kg/kg, agree remarkably well with the fibre saturation point. It would again be expected that this limit would be slightly higher for 25g/m^2 paper because of the wider pore size distribution of the thinner sheet.

The d_p-X relation for 100 and 150g/m^2 paper is expected to be similar to that for 50g/m^2 because d_p for dry paper is effectively independent of basis weight over the range 50-150g/m^2, Table 4.10, Fig 4.17. This expectation could not be tested because the highest flowrate was insufficient for determination of d_p for paper this thick

4.7.11 Reynolds Number-Friction Factor Experimental Results: Moist Paper

Figs. 4.23a and Fig 23b are based on all the ΔP measurements of the present study for basis weight of 25 and 50g/m^2 over the wide range of moisture content, 2.5>X>0 1 kg/kg, at intervals of X=0.5. The

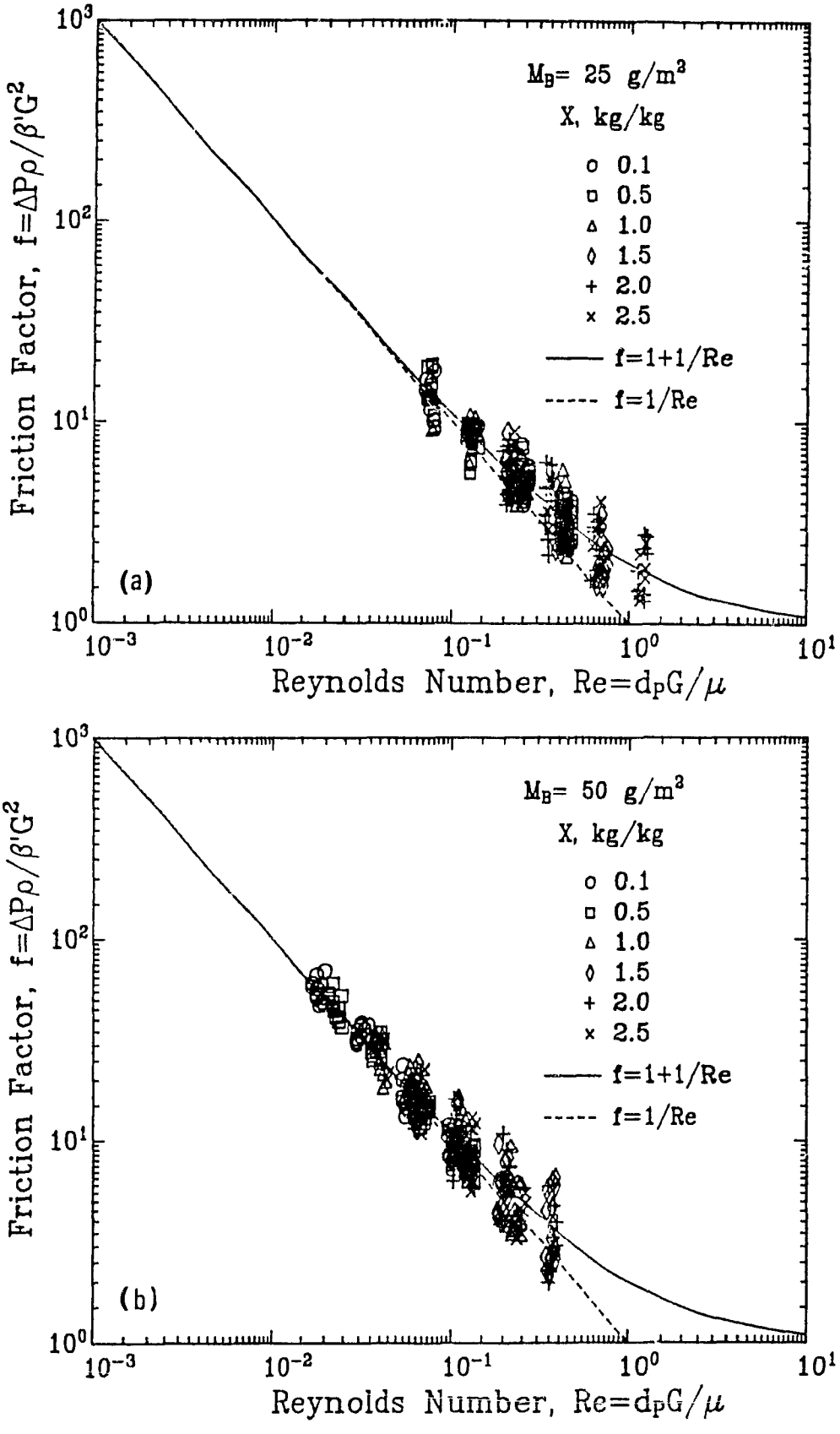

Figure 4.23 Pressure drop across moist paper: average d_p for each basis weight-moisture content, a) 25g/m², b) 50g/m²

ΔP-G-X data are converted to the Re-f form using one value of d_p for each of the 12 M_B-X combinations listed in Table 4.12. This data set, constituting about 3000 ΔP measurements on the 126 sheets, i.e. 65 sheets of 25g/m², 61 sheets of 50g/m² kraft paper, falls quite well around the theoretical line, f=1+1/Re. Comparison of Fig. 4.23 with Fig. 4.20 shows that the experimental scatter is larger for moist than dry paper, reflecting introduction of the additional key variable, paper moisture content. From wet to dry paper, ΔP varies by up to a factor of ~20, d_p by up to a factor of ~2 5. For moist paper no such comprehensive treatment of pressure drop has previously been available.

4.7.12 Flow Phenomena-Reynolds Number-Pressure Drop Relations

Velocity fields in a packed bed are complex, even at low Reynolds number. According to Scheidegger[1974], the transition from "laminar" to "turbulent" flow regime in a packed bed occurs over the Reynolds number range 0.1 to 75 Nelson and Galloway[1975] pointed out that this is a transition from reversible to irreversible flow phenomena, not from laminar to turbulent flow Flow irreversibilities result from stalls, vortices, or wakes forming in the interstitial flow passages between particles At high Reynolds number these vortices shed and consume energy as they degrade, while at low Reynolds number such vortices are time steady, hence conserve their energy The inertial resistance in paper measured here should be viewed in this context. In his interesting dye injection experiments Scheneebeli[1955] demonstrated that even when pressure gradient and velocity measurements indicated non-linear flow, the dye displayed laminar, stream-line flow Similarly, Ahmed and Sunada[1969] claim that energy loss by turbulence is negligible

for flow through porous media, but that non-linearity becomes important at Re≈0.02, i.e. at much lower Reynolds number than specified by Scheidegger. At a Reynolds number this low the Darcy's law assumption of neglecting inertial effects, i.e. equivalent to using f=1/Re rather than f=1+1/Re, introduces only ~2% error in the value of friction factor.

In the present analysis the characteristic dimension for Reynolds number for flow through moist and dry paper of a wide range of thickness has been defined without approximation, so that the Reynolds number obtained is rigorously the ratio of the inertial to the viscous contribution to momentum transfer Thus Reynolds number limits given, approximately as 0.02 by Ahmed and Sunada[1969] and 0 1 by Scheidegger[1974], may now be specified quantitatively for the case of paper as the porous media. As characteristic dimension for Reynolds number, Ahmed and Sunada used the same $d_p=\beta/\alpha$ as the present study while Scheidegger's choice, although unfortunately not specified, was probably the d_p^* definition of Table 4 11 for the Fanning friction factor, f^* For dry kraft paper of $M_B \geq 50$ g/m^2 the inertial term, C~6 5, is effectively independent of basis weight, Table 4 10. Thus for the presumed Re^* definition of Scheidegger and the Re-Re^* relation given in Table 4.11 his Reynolds numbers (Re^*) would be lower by a factor of $C^2/2$ than those on the basis of the present study (Re). For dry kraft paper Scheidegger's limiting Reynolds number of $Re^*=0.1$ would therefore correspond to $Re=0.1(C^2/2)$, i e. to Re=2 as defined here. Table 4 4 shows that for both 25 and 50g/m^2 paper, the inertial term C/L is higher for moist paper (X=2.5kg/kg) than for the dry sheet by about a factor 6, with most of this variation coming from C, not L Therefore for wet kraft paper, Scheidegger's $Re^*=0$ 1 limit would correspond to Re≈76. This demonstrates that although Scheidegger's limiting value $Re^*=0.1$ may be

applicable to the beds on which his work was based, a specific value of Re^* as a limit is not generally applicable to beds of different structures and is clearly not applicable to paper where the porosity to air flow increases from very low to very high in going from wet to dry paper. As the Re-f-d_P relation developed for paper here is derived directly from fundamental momentum transport relations, it is valid for all beds regardless of porosity or structure of the porous media, and reference values of Re are universally applicable.

The fact that Re^*, the form of Reynolds number definition used with the Fanning friction factor, is lower than $Re=d_P G/\mu$ with $d_P=\alpha/\beta$, the rigorously correct definition, is an observation of considerable practical significance for comparing results of various studies. For dry paper, $Re/Re^*\simeq 20$, while for wet paper, $Re/Re^*\simeq 760$. The same caution applies to the corresponding difference in the two friction factor definitions, i.e. $f^*=(\beta^2/2\alpha)f$. For $M_B=50 g/m^2$ dry paper, $f^*\sim 20f$.

From the Table 4.11 relations, the ratio of correct ΔP to that given by the Darcy's law approximation is simply $\frac{1+1/Re}{1/Re}$. If a limit of 5% error on ΔP were adopted, Re=0 05 would be the maximum allowable for neglect of inertial effects, a limit which is lower by a factor of 40 than that given by Scheidegger The present experimental data, Figs 4.19, 4.20, 4 23, extending between the Re values 0.02-1, cover a range for which the error i· ΔP from using the Darcy law approximation varies from 2-100%. With the rigorously correct basis of Reynolds number definition used here, the variety of arbitrary recommendations of earlier workers is now replaced by the exact error relationship, $\frac{1+1/Re}{1/Re}$, given above.

In industrial practice of through drying paper, throughflow rates may go up to $G=4 kg/m^2 s$ for tissue paper of $25 g/m^2$. With the characte-

ristic dimension $d_p=\beta/\alpha$, of the present study, the Reynolds number for this maximum throughflow rate would be about Re=6, corresponding to a flow condition for which the use of the Darcy's law approximation would give a value of ΔP too low by 600%.

4.7.13 Comparison of Models: Permeability vs. Reynolds Number-Friction Factor

Pressure drop has been expressed here in two ways. For flow through paper the permeability method, Sections 4.3-4.5, has been the standard procedure while the Reynolds number-friction factor approach, Section 4.7, has not previously been used. Permeability and Re-f relations are alternate procedures for momentum transfer in porous media. The permeability method has been widely adopted for porous media of complex particle shape because no characteristic dimension for the porous media is needed. The Fanning friction factor treatment as used for flow through other porous media has also discouraged applying the Reynolds number-friction factor model to paper because of the apparent need, Eqn. 4 15, for some complex porosity function and perhaps other pore structure parameters as well The empirical permeability approach which has been used for paper, even with elimination of the errors associated with the use of the Darcy's law approximation, does not permit the integration of momentum transfer work for paper with the large body of results using the nondimensional Re-f momentum transfer treatment for other porous media. Moreover, interpretation of ΔP measurements in terms of permeability has no relevance to other transport phenomena, i.e. heat or mass transfer, in the same porous media.

For throughflow phenomena in paper the importance of heat and mass

transfer in through drying provides a large incentive for the more fundamental, non-dimensional Reynolds number-friction factor treatment. The obstacle to the Re-f analysis for paper has been the lack of a soundly based characteristic dimension for throughflow across a porous media of porous structure as complex as paper. This obstacle has been removed by application in the present study of basic momentum transport principles to flow through paper. The result has been to obtain a physically meaningful characteristic dimension for paper which not only provides a more general treatment for momentum transfer in paper, but could be applied also for treatment of heat and mass transfer in the drying of paper. As one parameter in this technique, α, is the reciprocal of permeability, comparison of results by this alternative approach with previous studies is straightforward.

4.7.14 Application of the Re-f-d_p Method for Paper

In order to use the present Re-f-d_p method one needs in principle only two independent pieces of ΔP-G information, i.e. not both in the region of negligible inertial effects. With two such values of ΔP-G one may determine the characteristic dimension, d_p, for a given porous media. For the case of paper that implies specification of pulp type, formation technique, basis weight and moisture content With that d_p obtained from the minimum of two ΔP-G measurements, combined with the theoretical Re-f relation, Eqn 4.14, one may calculate ΔP for that paper at any G.

For the case of kraft paper over the range of basis weight 25-150 g/m^2 and moisture content 2.5kg/kg to dry, the results of the present study enable prediction of ΔP for any throughflow rate, moisture content

and basis weight. The characteristic dimension, d_p, required for Reynolds number is obtained from Eqn. 4.16 with the parameters listed in Table 4.13. For the Reynolds number corresponding to the throughflow rate with that value of d_p, the friction factor is obtained from Eqn. 4.14, and ΔP from Eqn. 4.13. As this value of pressure drop applies for paper formed in a standard laboratory handsheet former it may differ from that for commercial paper of the same basis weight and moisture content made from the same pulp. For each different type of pulp and sheet formation it is necessary to determine the $d_p=f(M_B, X)$ relation analogous to Eqn. 4.16 or Fig. 4.21, using the general procedure outlined above.

4.7.15 Conclusions

The characteristic dimension thus determined would apply for all nondimensional variables, i.e. Reynolds, Nusselt, Sherwood and Peclet numbers, relevant to treatment of the various transport phenomena involved for flow through the same paper. While constituting a much more powerful treatment than permeability, this analysis is also superior to the Fanning friction approach involving the Re^*-f^*-d_p^* definitions because no porosity function is needed, eliminating the substantial associated uncertainties. Thus for future transport phenomena work involving flow through paper, the characteristic dimension-Reynolds number analysis developed here for moist and dry paper is recommended due to its simplicity, its sound theoretical basis, and its applicability to related transport phenomena.

4.8 SUMMARY

1) The presence of an inertial component to pressure drop in through-flow across paper is detected more sensitively by application of the

momentum transport equation, the Forchheimer relation, than by inspection of the exponent in the power law relationship for pressure drop.

2) The permeability of both dry and moist paper was determined correctly for the first time by application of the momentum transport equation, i.e. without the commonly used approximation of Darcy's law which ignores inertial effects For the combination of minimum basis weight-maximum throughflow rate used, the permeability of dry paper calculated from Darcy's law is shown to be in error by about 40% with this error increasing up to 70% for wet paper.

3) The permeability of dry kraft paper of increasing thickness approaches an asymptotic value for high basis weight. Paper permeability increases gradually, approximately doubling, as basis weight is decreased from 250 to 50g/m^2, probably due to an associated widening of the pore size distribution. When basis weight is reduced from 50 to 25g/m^2, permeability increases sharply, by a factor of 2-3, believed due to the associated exponential increase in pin hole count.

4) Over the basis weight range 25-250 g/m^2, the permeability of dry kraft paper approximately doubles when subjected to a wetting-through drying cycle. This permeability increase is found to be associated with changes in paper microstructure during the wetting, not the drying.

5) For moist paper the modified permeability, k/L, determined from continuous monitoring of pressure drop across a sheet during permeability-through drying experiments, indicates that permeability is not significantly affected by any of the variables which control drying rate. Thus the permeability of moist paper during drying is essentially independent of the drying conditions.

6) A simple correlation relates the modified permeability of moist

kraft paper, k/L, as a function of only paper moisture content and basis weight, i.e. is independent of the moisture content at the start of drying and of the velocity and temperature of the through drying air.

7) The specific surface of dry kraft paper is 0.5-1m^2/g fibre, as determined from throughflow measurements using the Kozeny-Carman equation. Specific surface decreases moderately, by about 25%, as basis weight is reduced from 250 to 50g/m^2, then drops by about 1/3 for reduction to 25 g/m^2 basis weight. For paper of low basis weight, 25g/m^2, sorption techniques overestimate by about 50% the interfacial area that is effective for throughflow transport processes. Area associated with smaller pores, measured by sorption methods, scarcely affects the area measured by throughflow which, under these conditions, flows predominantly through large pores and pin holes, leaving the small pores essentially stagnant.

8) Over the basis weight range 25-250 g/m^2 the specific surface of dry kraft paper drops by 2-11% when it experiences a wetting-drying cycle This drop in specific surface occurs during the wetting, not the drying. The mechanism for this change in interfacial area is believed the result of the same irreversible mechanism, i.e collapse of fibre surface fibrillation, responsible for the associated doubling of paper permeability.

9) Over the basis weight range of 25-250g/m^2, the porosity of dry kraft paper increases from about 0.67 before a wetting-drying to about 0.72 after such a cycle, consistent with the same changes in paper structure that affect specific surface and permeability.

10) Because of the substantial changes in properties of paper during the wetting with which all reported drying studies begin, it is essential in drying research that all physical properties of dry paper used to describe the drying of paper be measured after drying, not before.

11) A new characteristic dimension was determined for flow through paper, $d_p=\beta/\alpha$, where α and β are complex parameters from the application of basic momentum transport analysis. This characteristic dimension was determined over the full range of moisture content from wet to dry paper for kraft paper of basis weight 25-250g/m^2 and, with a few exploratory measurements, for Papriformer newsprint.

12) With the new characteristic dimension, Reynolds number becomes rigorously the ratio of the inertial to the viscous contribution to momentum transport. The values of this theoretically based characteristic dimension, $d_p=\beta/\alpha$, are about an order of magnitude higher than given by two widely accepted empirical definitions of characteristic dimension for paper, square root of permeability and reciprocal of specific surface, and are about 1/4-1/2 of the values of the measurements of Bliesner[1964] and of the Hagen-Poiseuille equivalent pore diameter as determined by Gummel[1977].

13) For dry paper, d_p is essentially independent of paper thickness for basis weight above 50 g/m^2, while permeability, k, varies with paper thickness in this range. For 25g/m^2 dry paper. d_p is much higher, by about a factor of 3, due to pin holes, as affects permeability similarly With variation in paper moisture content the value of the characteristic dimension, $d_p=\beta/\alpha$, changes between two asymptotic limits. Above a paper moisture content of about 1.7-2.1kg/kg, d_p is limited by the maximum pore size. Below about 0.6-0.9kg/kg, the value of d_p for kraft paper does not change with paper moisture content. The latter moisture content agrees, as expected, with the values measured for the fibre saturation point, 0.72-0.81kg/kg, because for moisture contents lower than the FSP all water is held within the fibres. As moisture content decreases from

the upper to the lower asymptotic region, the d_p-X dependence reflects the opening of pores of progressively smaller size during through drying.

14) The maximum values of d_p for wet kraft paper, 44μm and 14μm for basis weights respectively of 25 and 50g/m^2, correspond to the maximum pore size as observed by scanning electron microscopy. The increase in the d_p of 50g/m^2 paper as moisture content decreases from 2.6 to about 2.3kg/kg may be due to compressibility of the sheet under the high ΔP across wet paper.

15) With $d_p=\beta/\alpha$, a theoretical relationship between friction factor, $f=(\Delta P/L)/(\beta G^2/\rho)$, and Reynolds number, Gd_p/μ, is shown to fit an extensive set of pressure drop measurements, about 700 ΔP measurements for dry paper of basis weight 25-250g/m^2, and about 3000 measurements for moist paper of two basis weights, 25 and 50g/m^2, for moisture contents covering the entire range from about 250% to dry paper. This analysis is the first treatment of air flow through dry and moist paper based on a fundamental, momentum transport relation.

16) This form of Reynolds number-friction factor definition, the most appropriate for beds of complex porous structure such as paper, also eliminates the need for the complicated and still unresolved porosity functions required in the Fanning friction factor definition The relations between the various friction factor and Reynolds number definitions have been provided as these are essential in comparing results of various studies

17) With the new definition for paper of $d_p=\beta/\alpha$ and $Re=d_pG/\mu$, the ratio between the correct ΔP and that given by the Darcy's law viscous flow simplification is determined to be $\frac{1+1/Re}{1/Re}$. Thus this error is 5% at Re=0.05 and 100% at Re=1 In industrial practice of through drying

of paper, Re=6 may be reached, where this error is now seen to be 600%.

18) As a theoretically based model, the β/α-d_p-Re-f treatment for air throughflow across moist and dry paper is a more powerful method than the traditional permeability approach, and does not suffer from the porosity function problem of the traditional Fanning friction factor Re^*-f^* treatment for flow through porous media. The Re-f-d_p analysis yields not only a fundamental fluid mechanics characterization of paper for momentum transport, but also provides the basis for theoretical analysis of other transport phenomena in paper such as heat transfer and mass transfer during through drying. This new approach is therefore recommended for application to paper and other complex media of fine particulates.

19) General procedures for application of the Re-f-d_p method to paper are given.

CHAPTER 5

THROUGH DRYING RATES FOR PAPER

5.1 INTRODUCTION

Although through drying of light weight grades of paper is an industrial practice, remarkably little information has appeared which relates the through drying process to four key variables: throughflow rate, temperature of the drying air, paper thickness or basis weight, initial moisture content of the paper The advantages of through drying are leading to its increasing adoption world-wide McConnell[1980] reported that about 15-20% of tissue paper in the United States was through dried. Higher drying rates, good specific energy consumption and perhaps beneficial quality effects for some products provide continuing growth potential for this process Application is currently limited to light weight grades, primarily tissue paper. As a developing technology, the economic limit for use of through drying with not such light weight grades may change. If in future it is found beneficial to combine through drying with other techniques, such as impingement drying for example, that would open other possibilities for application under new operating conditions.

Technical and economic studies aimed at achieving the full potential of through drying, either alone or in combination with other drying techniques, require accurate documentation of through drying rates and their relationship to the operating variables Such documentation is surprisingly limited. Chu and Kuo[1967] measured rates of drying tissue paper with throughflow, but their "drying rate" curves reflect a combination of drying and mechanical dewatering due to the

extremely high pressure drop used. On the basis of an energy balance they claimed that mechanical dewatering occured at moisture contents as low as 0.25kg/kg dry fibre. That claim is not plausible because this moisture contentan the fibre saturation point, FSP. Scallan and Carles [1972] determined the FSP to be about 1.6kg/kg for never-dried kraft pulp and approximately 0.85kg/kg for the reslushed pulp. For the present study, as noted in Chapter 4, the FSP was determined to be in the range 0.72-0.81kg/kg. Moreover, Ellis *et al.*[1983] showed that the water retention value of kraft pulp extrapolates to a value of about 0.5kg/kg at high values of centrifugal forces, $>10^5$g, which represents a limit for mechanical dewatering Interpretation of the Chu and Kuo results is also limited by their experimental technique which permitted a large change in mass flow rate of throughflow air during an experiment, a 40% change for the only data presented.

Walser and Swenson[1968] reported through drying rates from both laboratory equipment and paper mill trials. It is difficult to interprete their laboratory results, limited to a single basis weight ($86g/m^2$) obtained with two $43g/m^2$ sheets, because their technique permitted throughflow rate to double during an experiment Mill trial results, affected by air swept over the sheet in the draws, showed no effect of basis weight over the range $52-147g/m^2$.

There are problems also with all of the more recent laboratory studies reported Martin[1972] measured rates of through drying of $100g/m^2$ handsheets but, once more, the rate of throughflow air changed during each constant suction experiment, in this case by 3-5 fold As his quoted drying rates are simply averages over an entire run with such variable conditions, they provide no insight into the through

drying process. Raj and Emmons[1975] studied the through drying of 13-65g/m^2 basis weight paper of high porosity, 0.86-0.89, but reported neither rates nor drying rate curves. As it is not specified whether the air throughflow rate varied or was kept constant during these experiments with room temperature air, the results are of little use. For through drying of light weight paper, ~23g/m^2, Rohrer and Gardiner [1976] measured only those parameters necessary for their model. In reporting through drying rates for 24 and 48.8g/m^2 sheets Wedel and Chance[1977] claimed, incorrectly as is established by the present study, that their drying rates were for an adiabatic saturation process which is not affected by sheet basis weight. Neither Rohrer and Gardiner nor Wedel and Chance reported either experimental conditions or drying rates, in that only rates predicted by their respective through drying models were presented. In his study of the through drying of 20-23g/m^2 tissue paper Gummel[1977] measured drying rates considerably lower than would correspond to the exit air reaching adiabatic saturation Although Gummel kept the rate of throughflow air to the drying section constant, it appears that his drying rate measurements at high throughflow were reduced by by-passing of air around the sheet

The intimate contact between drying air and wet fibres is the source of the higher rate of through drying relative to the standard cylinder drying process where the paper receives heat successively at each surface and water leaves only after diffusing through the sheet. With the much improved contacting between fibres and drying air, and in the absence of reliable documentation of through drying rates, some analyses of through drying assume that the air leaves the wet web

saturated, Crotogino and Allenger[1979], Soininen[1987]. This condition of thermodynamic equilibrium at the exit would be achieved in through drying as, for example, in the analogous process of packed bed adsorption or desorption, with a low flow rate and a deep gas-solid contacting zone (thickness of the paper or the packed bed). These limits, quite well known for packed bed adsorption, are not established for through drying paper.

The objective of the present study of through drying paper is to measure instantaneous drying rates throughout this short duration process, while controlling and measuring all variables which affect drying rate. Production of a comprehensive set of precisely controlled measurements of through drying is the prerequisite for seeking a basic understanding of this process

5.2 EXPERIMENTAL

5.2.1 Objective

From start to finish of the through drying of a wet web the instantaneous values of drying rate, moisture content and permeability of the web, and the local values of temperature and humidity of the drying medium change greatly and, at times, very rapidly. The experimental program was designed to document transient through drying of paper so as to associate instantaneous drying rates with the corresponding transient conditions of the wet web and of the throughflow air inside the sheet This documentation focusses on the effects of the key parameters - basis weight and initial moisture content of paper, flow rate and inlet temperature of the throughflow drying air

5.2.2 Basic Considerations

A general deficiency of through drying investigations is variation of throughflow rate during the transient experiment. During the through drying of a sheet, lasting perhaps 15s, the permeability of paper may change by a factor of 20, from wet to dry. Martin[1972] conducted his transient experiments under the condition of constant pressure drop, i.e. highly variable throughflow rate. The equipment designs of Chu and Kuo[1967] and Walser and Swenson[1968] did not provide either constant ΔP or constant throughflow rate, with their throughflow rates varying greatly during a drying experiment Drying rates obtained under conditions of greatly changing throughflow rate are of limited significance because the sensitive relationship between drying rate and throughflow rate is obscured or lost. Only Gummel[1977], and possibly Raj and Emmons [1975], attempted to make through drying experiments at a constant rate of throughflow air.

Another fundamental choice for through drying experiments is the procedure for measuring drying rate. Direct methods involve continuously monitoring the sheet moisture content, while indirect methods monitor air humidity and flow rate Most early researchers employed direct methods. Chu and Kuo[1967] used a specially designed capacitance gauge requiring tedious calibration. Walser and Swenson[1968] employed a back scatter beta ray gauge in laboratory experiments, and intermittent weighing of web samples in mill trials. Raj and Emmons[1975] monitored the weight of the sample plus holder during drying, of low accuracy with their noise to signal ratio of 0.1 and the corrections needed for the time lag from the spring dashpot system that was required for noise damping. Martin[1972] recorded only the initial and final moisture

content of paper and total drying time, hence obtained only average rates. Only Gummel[1977] used the indirect method of monitoring exit air humidity by an infra-red analyzer. The advantage of this technique, the possibility of obtaining instantaneous drying rates, derives from its characteristics of rapid response, wide range and drying conditions undisturbed by the measuring device.

The indirect method was therefore chosen, with the exit air humidity monitored by an infrared spectrophotometer, a modified Wilks Miran I instrument. The choice of length of IR measurement cell involves a balance between competing considerations of instrument sensitivity and of residence time for flow through the cell. A short cell (100mm), desirable for the latter, had insufficient accuracy for humidity. The final choice, a 500mm long, 25mm diameter pyrex cell, gave good humidity accuracy with a mean residence time in the range of 0.07 to 0.30s.

The scale of the spectrophotometer, set to measure water absorbance at 2.70μm, was expanded by a factor of 20 to increase sensitivity, and the smallest time constant possible, 0 15s, was selected. Even at these limits of high sensitivity and fast response the signal noise level was sufficiently small that a simple smoothing technique was sufficient.

During a constant throughflow rate experiment, pressure drop may decrease by an order of magnitude At the highest pressure drop encountered, about 25 kPa, tests at first indicated some by-passing of throughflow air around a close-fitting sample holder designed for fast insertion into a tightly fitting drying position A positive seal with O-rings eliminated by-passing Analysis of published work indicates the presence of this source of error in some results

In experiments with substantial pressure variation, significant

error in the paper throughflow rate can derive from the unsteady state material balance. A dynamic analysis was made to select a drying system volume sufficiently small that this source of error was insignificant, a precaution not previously noted.

Because of the fast response of experimental variables and the short duration of these transient experiments, data acquisition was by a dedicated microprocessor based system. Data sampling frequencies of 5-10Hz provided, for the first time, continuous records of the instantaneous drying rate history for an extensive study of through drying. The same computer processed the raw data to the form of drying rate as a function of paper moisture content.

5.2.3 Experimental Conditions

The experimental design focussed on the effect of four parameters: for the paper, basis weight, M_B, and initial moisture content, X_o; for the throughflow air, inlet temperature, T_i, and mass flow rate, G (or superficial velocity, u_s) Inlet air humidity, about 0.0005kg/kg dry air, was not varied. Table 5.1 lists the range of these parameters for the experiments and in industrial practice.

TABLE 5.1 Range of parameters

	Experimental	Industrial Practice
T_i, °C	20-90	100-400
G, kg/m^2s	0.09-0.52	0.07-4
u_s, $Std.m^3/m^2s$*	0.07-0.41	0.05-3
M_B, g/m^2	25-150	15-100
X_o, kg/kg dry fibre	1.0-4.5	2-3

* at 0°C and 101.3kPa

There is very little use of industrial through dryers with paper as heavy as 100g/m^2, the typical use being for basis weight in the 15-35g/m^2 range. Paper up to 150g/m^2 was used here in order to extend the information to grades heavier than current industrial practice. The lower limit of throughflow temperature, i.e. ambient air, was chosen to achieve a close approach to the limiting condition of adiabatic saturation of exit air from the wet web. The highest air temperature, ~90°C, although lower than industrial practice, is as high as any laboratory study at constant throughflow rate yet published. The limitation is measurement accuracy At the higher throughflow temperatures used industrially, drying time could be a few seconds. Such measurements would require a faster response than is yet available from an infra-red moisture meter plus measurement cell. The upper limit of throughflow rate is likewise lower than industrial practice for reasons of measurement accuracy. The IR instrument time constant, 0.15s, the fastest available, limits the residence time in the measurement cell, hence limits the throughflow rate. Because of low paper permeability at the wet end of a dryer, the high industrial throughflow rates, Table 5.1, apply only to very low basis weight paper. For the upper range of basis weight, 100-150g/m^2, considerations of pressure drop, i.e. of power cost, would probably limit the economic range of throughflow rate to about that used here.

The choice of pulp was standard dry laboratory kraft (unbeaten, unbleached, 100% black spruce, ~18-19 kappa number, CSF 685ml). The only previous researchers to document pulp type, Walser and Swenson[1968], used kraft pulps. Presumably the other studies used paper from chemical pulps as this corresponds to industrial practice for the tissue paper

dried by through drying. Handsheets of 158mm diameter, prepared by CPPA Standard C.4, were dried under restraint at 25°C, 50% relative humidity, according to the CPPA Standard. Sheets for the 104mm diameter sample holder, cut from these handsheets, were moistened in the holder by an aerosol sprayer to the desired moisture content, and allowed to equilibrate in nearly saturated air. Total moisture evaporated during drying was determined by weighing the sample holder immediately before and after each experiment. The bone dry sample weight, determined subsequently by microwave drying, was used to calculate basis weight, initial and final moisture content.

The values of parameters are listed in Table 5.2.

TABLE 5.2 Levels of experimental parameters

Variable	Levels used	Variation around each level
T_i, °C	23, 42, 64, 88	~6%
G, kg/m^2s^1	0.09, 0.16, 0.29, 0.52	~1%
u_s, $Std.m^3/m^2s$	0.07, 0.12, 0.23, 0.42	~1%
M_B, g/m^2	26, 50, 100, 150	~5%
X_o, kg/kg	see below	

For these levels of T_i, the corresponding values of adiabatic saturation temperature, T_S, are ~8, 16, 23 and 29°C. From 2-4 values of initial moisture content of paper, X_o, were employed for each M_B-G-T_i combination, with generally more X_o values at lower values of M_B. For higher basis weights, $1<X_o<2$ was used for reasons of high ΔP, while for low basis weights, $2.5<X_o<4.5$ could be used. With 4 levels of M_B, G and T_i, 64 combinations of M_B-G-T_i were tested. With 2-4 values of X_o at each such M_B-G-T_i combination, the results are based on 235 combinations of M_B-G-T_i-X_o, an experimental program which, with its limitations, still constitutes the most comprehensive investigation of through drying yet undertaken.

5.2.4 Accuracy of Drying Rate Measurements

A high level of accuracy of drying rates was confirmed by using both a continuous heat and mass balance and an integral mass balance. The integral check involved comparing the total amount of water evaporated, determined gravimetrically, with that from integration of the exit air humidity and air flow rate. Agreement was always within 2-3%. In the continuous heat and mass balance the exit air temperature throughout the experiment, calculated allowing for all transient terms, agreed closely with that measured, as detailed in Section 3.3. The success of both checks establishes that the overall experimental method produces consistent and accurate measurement of the transient through drying rate for paper. Drying rate curves replicated well For conditions of maximum experimental variability, constant drying rates replicated to ±6.5%.

5.2.5 Basis for Drying Rates

Because through drying is a volumetric transport phenomena, as for example adsorption in a packed bed, transfer rates would logically be expressed per unit volume. Because paper shrinks during drying, the transient value of volume is not easily determined. Nearly equivalent are drying rates relative to the accurately known weight of dry fibre However, because paper is thin and throughflow air is customarily normalized with respect to the surface area of the web, a drying rate relative to sheet surface area is commonly used. Such an area-based drying rate likewise relates directly to the size of a dryer, hence its cost. Thus all results are expressed as the sheet surface area based water evaporation rate, R, kg/m^2h. The corresponding mass based drying

rate, kg/(kg dry fibre)(h), is simply the ratio of the area based drying rate to basis weight, i.e. R/M_B.

The three aspects considered are: the complete drying rate curves, Section 5.3; the constant drying rate period, Section 5.4; and the new concept of drying period diagrams, Section 5.5.

5.3 DRYING RATE CURVES AND DRYING RATE PERIODS

5.3.1 Determination of Drying Rate Curves

Documentation of a basic objective, the relation between transient through drying rate and the process variables, appears first in the form of drying rate curves, i.e. drying rate per unit throughflow area as a function of paper moisture content. Although the data acquisition frequency was 5-10Hz for throughflow exit temperature and humidity, data processing to drying rate and paper moisture content at intervals generally of 1s-2s was sufficient. The reproducibility of drying rate curves, checked by repeating experiments for two to six values of X_o for each T_i-G-M_B combination, is more difficult for lower basis weight paper where small differences in sheet formation have the largest relative effect. Thus only two values of X_o were used for conditions of low T_i-low G for M_B=150 g/m^2, for which there is little problem of variability in paper structure. Even for lowest basis weight paper, Fig. 5.1, replicate experiments show excellent reproducibility.

5.3.2 Effect of Drying Intensity on Drying Rate Curves

Two examples, Figs. 5.2 and 5.3, show drying rate curves between the extremes tested of low and high intensity drying conditions. For a throughflow of the lowest flow rate and air inlet temperature used,

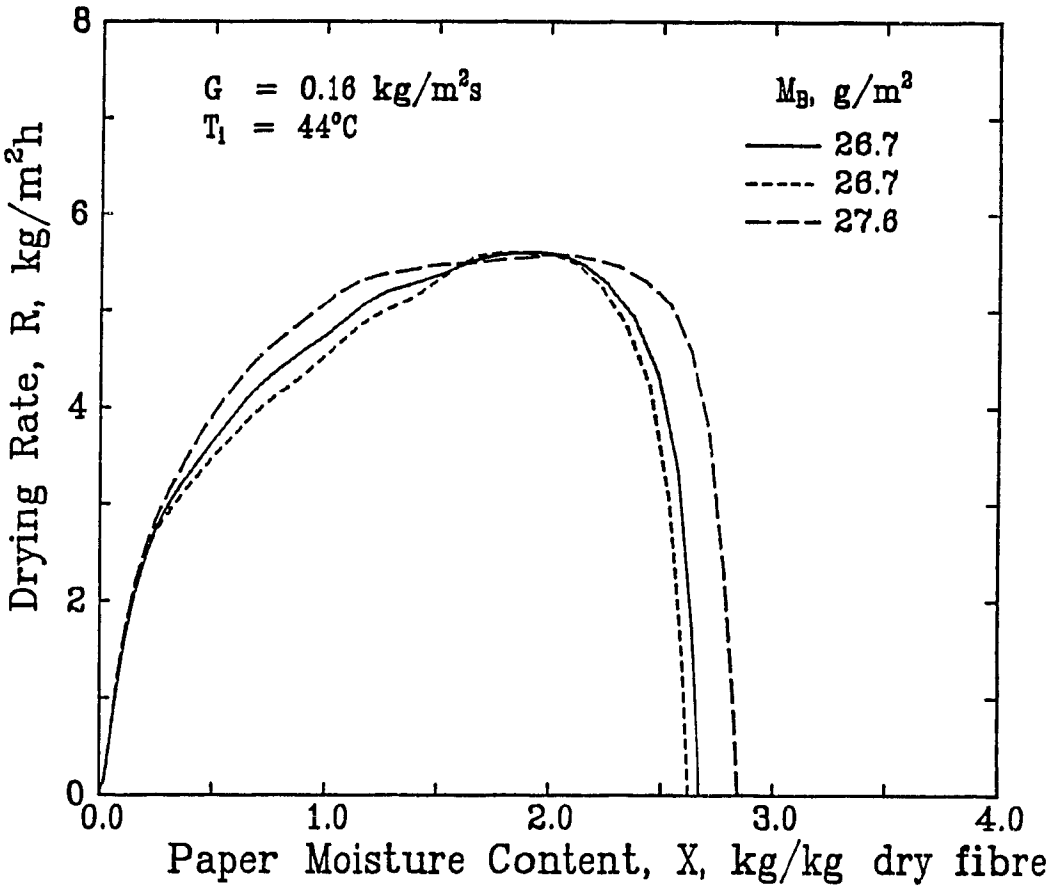

Figure 5.1 Reproducibility of drying rate curves

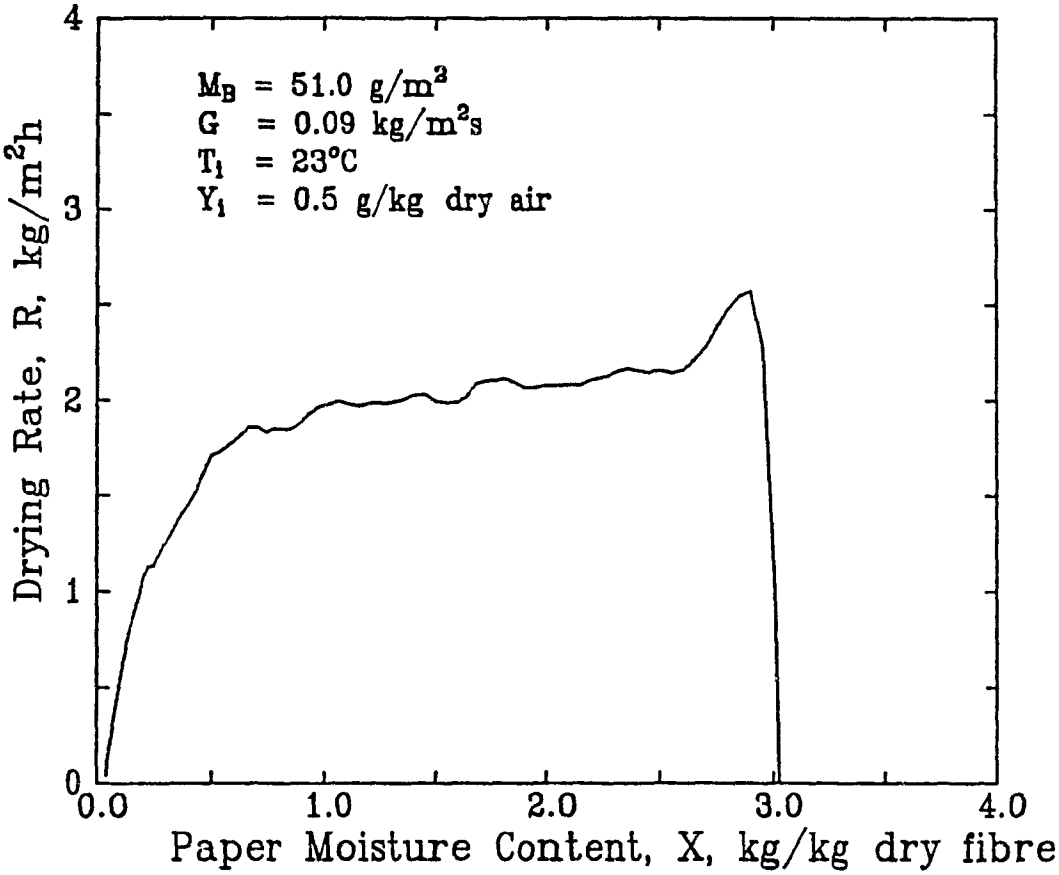

Figure 5.2 Drying rate curve for low intensity drying

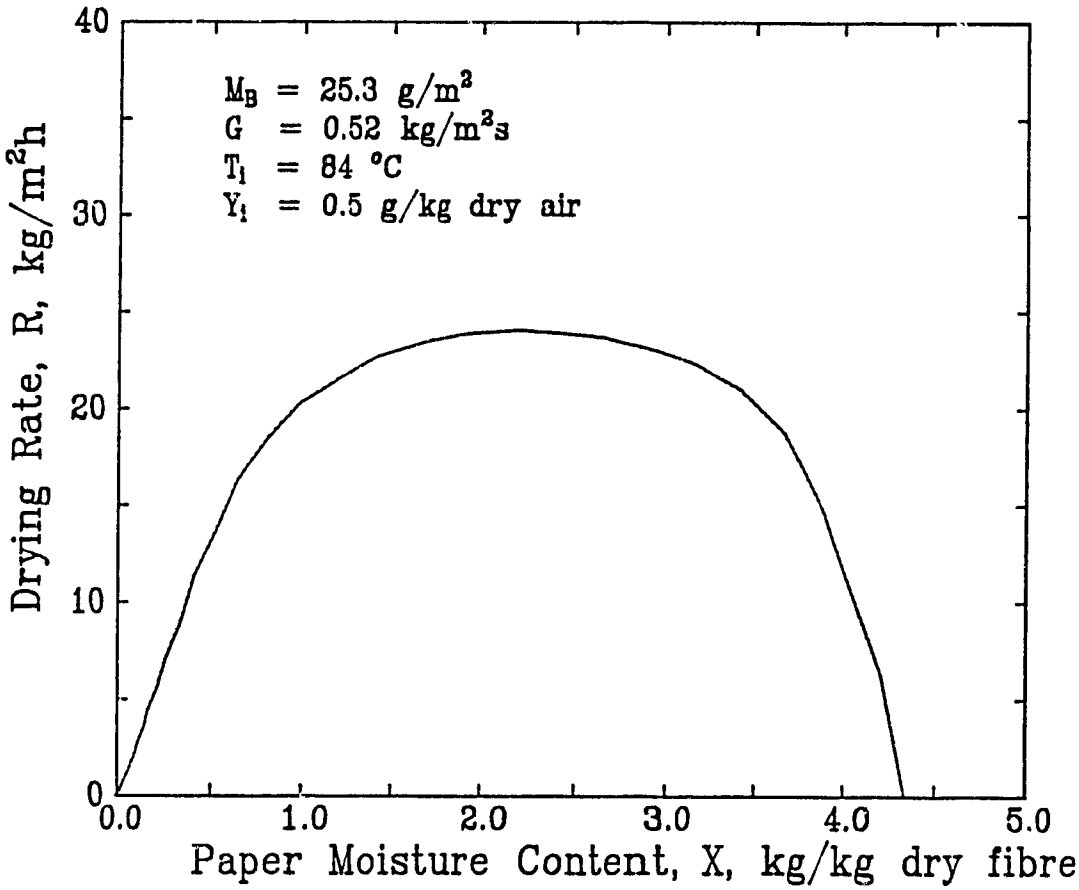

Figure 5.3 Drying rate curve for high intensity drying

Fig. 5.2 shows that the drying rate first passes through a sharp maximum before approaching a nearly steady value, that of the constant rate period. This decreasing rate after the early, sharp maximum occurs as the paper temperature is decreasing to approach the adiabatic saturation temperature, about 8°C in this case. The drying rate then remains relatively constant, Fig. 5.2, until the paper moisture content, X, drops to that for the start of the falling rate period. For the low intensity drying conditions of Fig 5.2, the throughflow air exiting the paper during the constant rate period is saturated.

Fig. 5.3 shows a more typical drying rate curve, i.e. high intensity drying of the lightest weight paper with a throughflow of the highest flow rate and highest inlet temperature of this study. As throughflow air at T_i=84°C and less than 0.5% relative humidity corresponds to an adiabatic saturation temperature of about 28°C, the paper temperature and hence drying rate simply increase continuously rather than display the unusual feature noted on Fig. 5.2 for the beginning of low intensity through drying. For Fig. 5.3 the paper moisture content was determined at intervals of 1s, the total drying time being ~35s for the high initial moisture content, X_o=4.3 kg/kg. For this case of high intensity drying, the maximum exit air humidity was substantially below saturation.

5.3.3 The Concept of Three Drying Rate Periods

The drying rate curves for 150, 50 and 25g/m^2 paper dried with a low throughflow rate at four levels of inlet air temperature, Figs. 5.4-5.6, demonstrate a perspective developed in the present study, namely, that through drying must be analyzed not in traditional terms of a paper

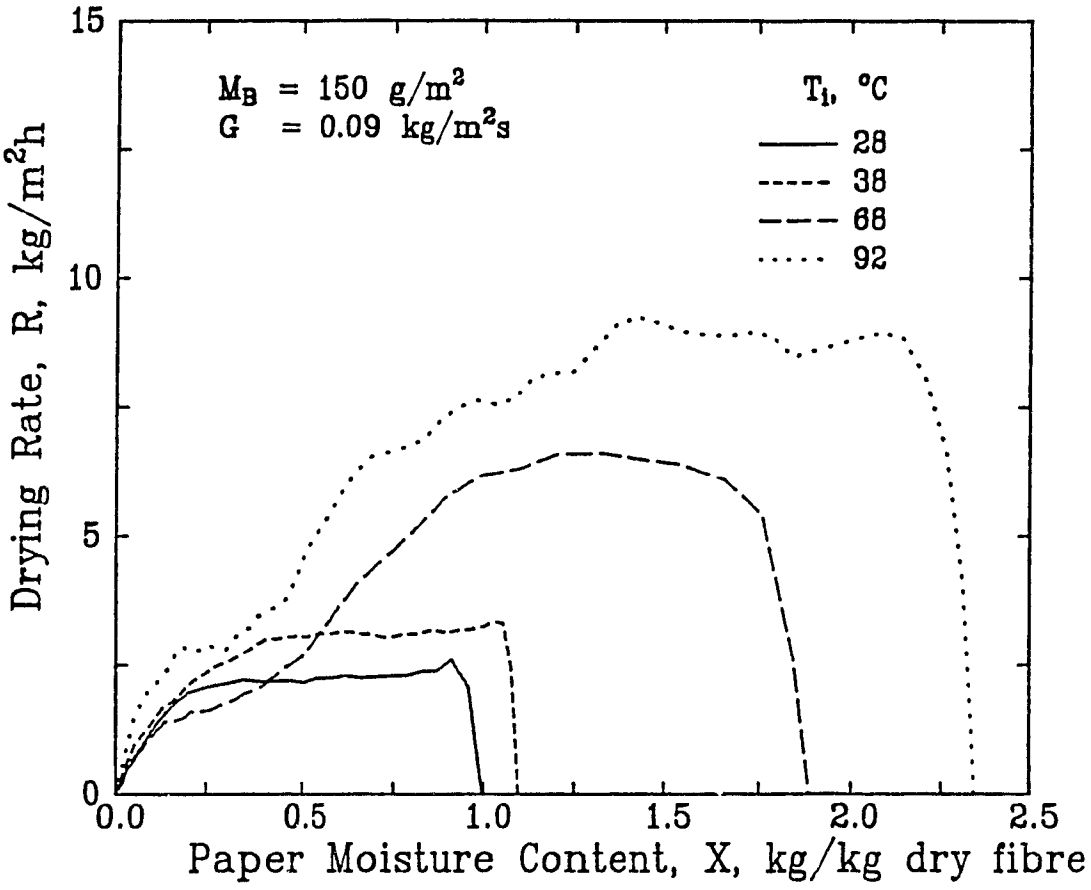

Figure 5.4 Effect of throughflow temperature on drying rate curve: Low throughflow rate-high basis weight

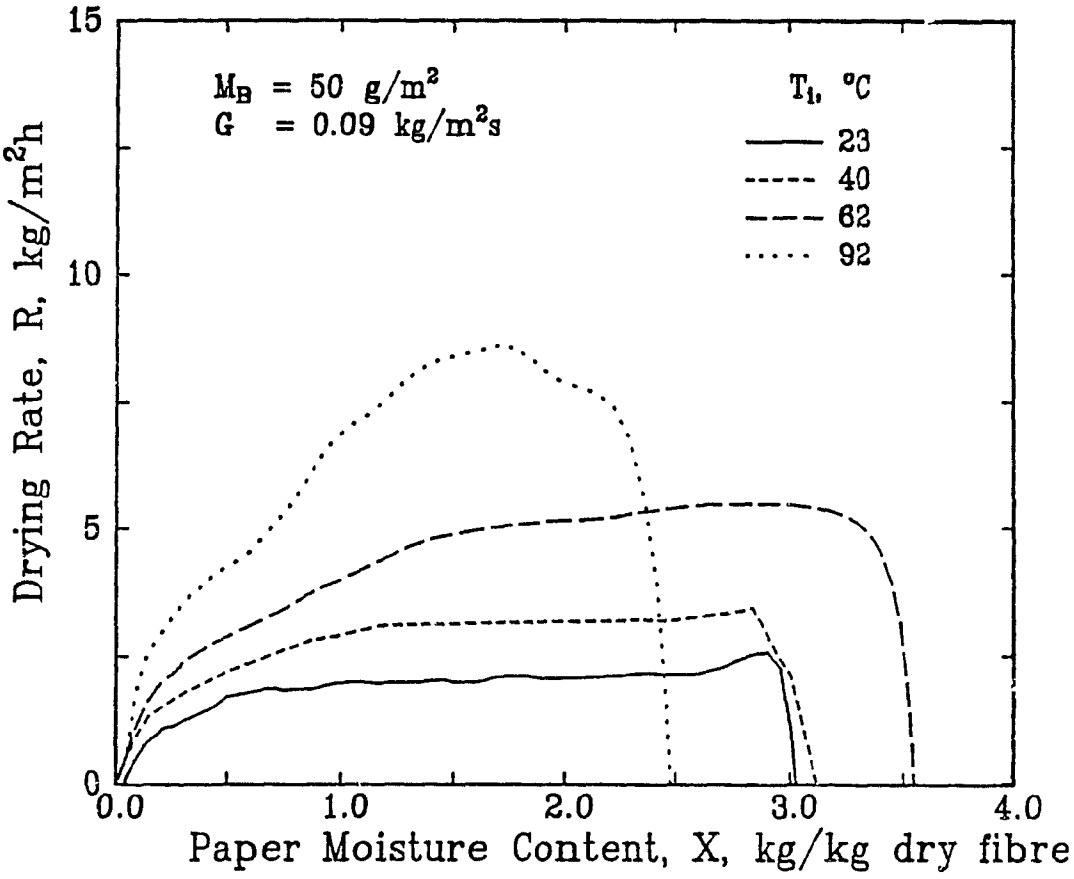

Figure 5.5 Effect of throughflow temperature on drying rate curve: Low throughflow rate-medium basis weight

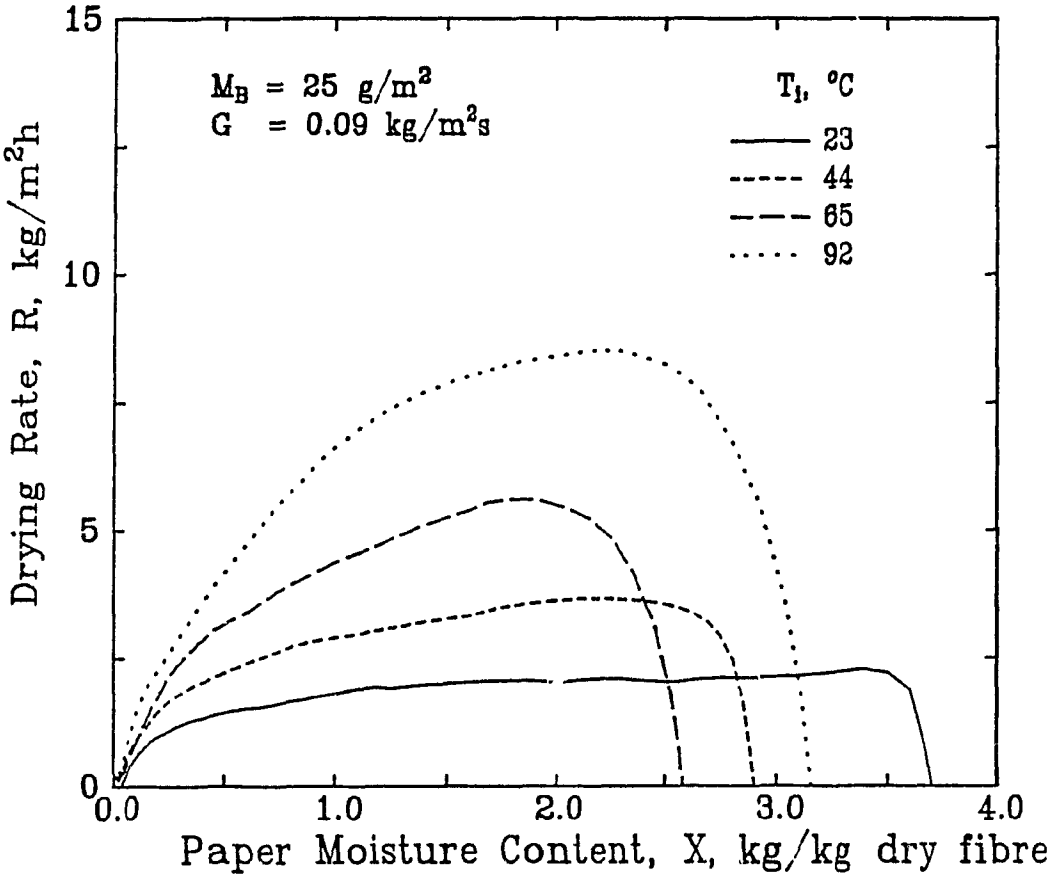

Figure 5.6 Effect of throughflow temperature on drying rate curve: Low throughflow rate-low basis weight

warm-up period followed by two drying periods, constart rate and falling rate drying, but with an additional period, that of "increasing rate" drying with which the process begins. The three periods -increasing rate, constant rate and faling rate- are most clearly seen for combinations of higher M_B-lower T_i where the drying times are longer. Thus for M_B=150g/m^2, Fig. 5.4, at all air temperatures a substantial fraction of the water is evaporated during the constant drying rate period which follows a short but not negligible increasing rate period. At M_B=50g/m^2, Fig. 5.5, there is a substantial period of constant rate drying for the three lower air temperatures but at the highest T_i constant rate drying is reached only momentarily, so that nearly all of the drying occurs during two periods, those of increasing rate and falling rate drying. Further shrinkage of the constant rate period and expansion of the increasing rate period is evident for the lowest basis weight paper tested, 25g/m^2, Fig 5.6. For the conditions of highest intensity drying displayed in Fig. 5.3, the amount of drying during the period defined here as that of increasing rate is seen to be comparable to that for the falling rate period, with the near disappearance of the period of constant rate drying

There are differences to be seen between drying rate curves at throughflow rates which are for this study the lowest, Figs. 5.4-5.6, and the highest, Figs. 5.7-5.9. The sensitivity of drying rate curves to initial moisture content, X_o, may be observed on Fig. 5.8 for two drying rate curves at T_i=88°C differing only as to X_o. For X_o=2.5kg/kg, about 0.3 kg water/kg fibre evaporates during a very short constant drying rate period. When initial moisture content is reduced by 0.5 kg/kg to X_o=2.0 kg/kg, the constant rate period disappears and the

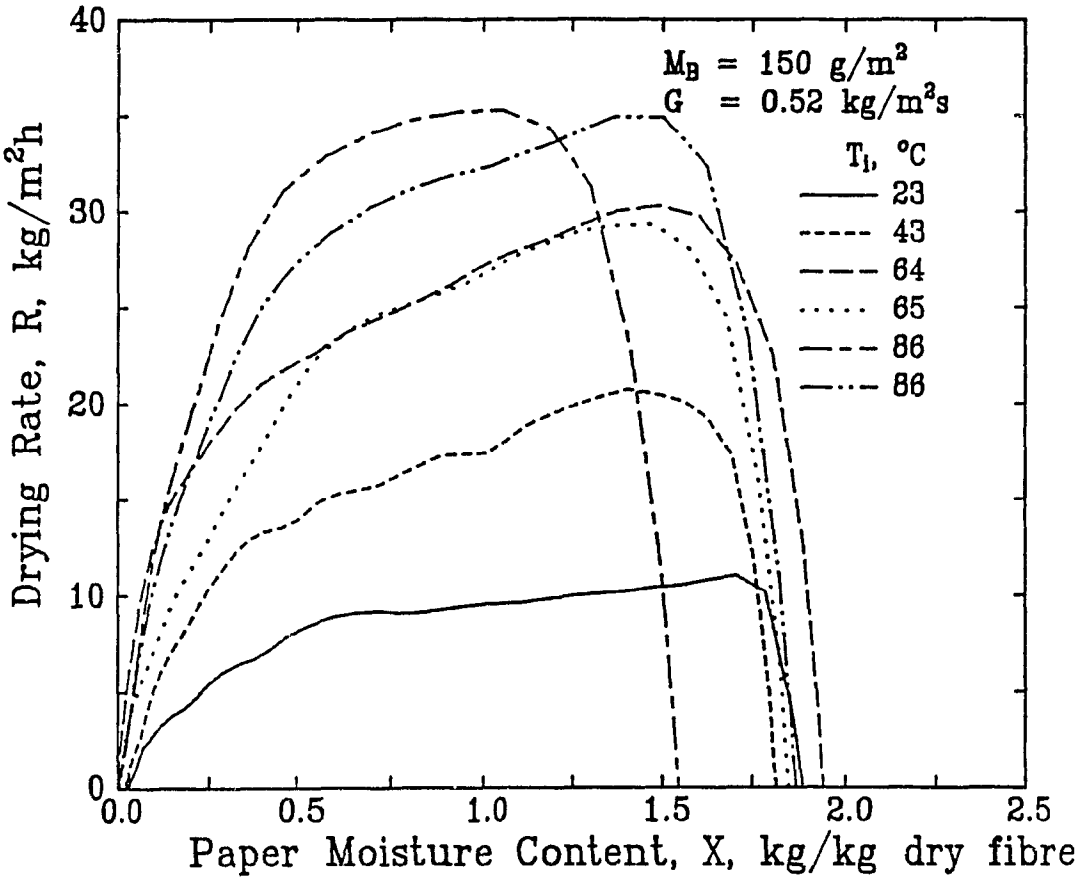

Figure 5.7 Effect of throughflow temperature on drying rate curve: High throughflow rate-high basis weight

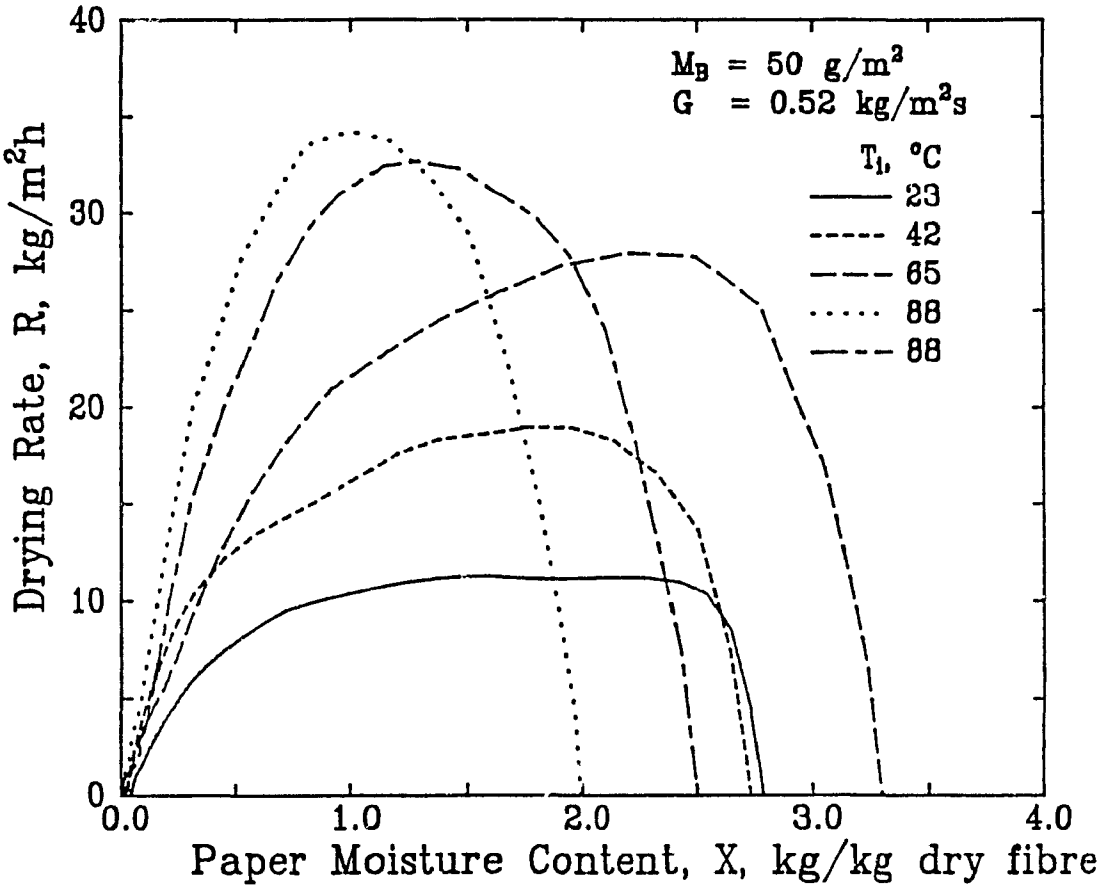

Figure 5.8 Effect of throughflow temperature on drying rate curve: High throughflow rate-medium basis weight

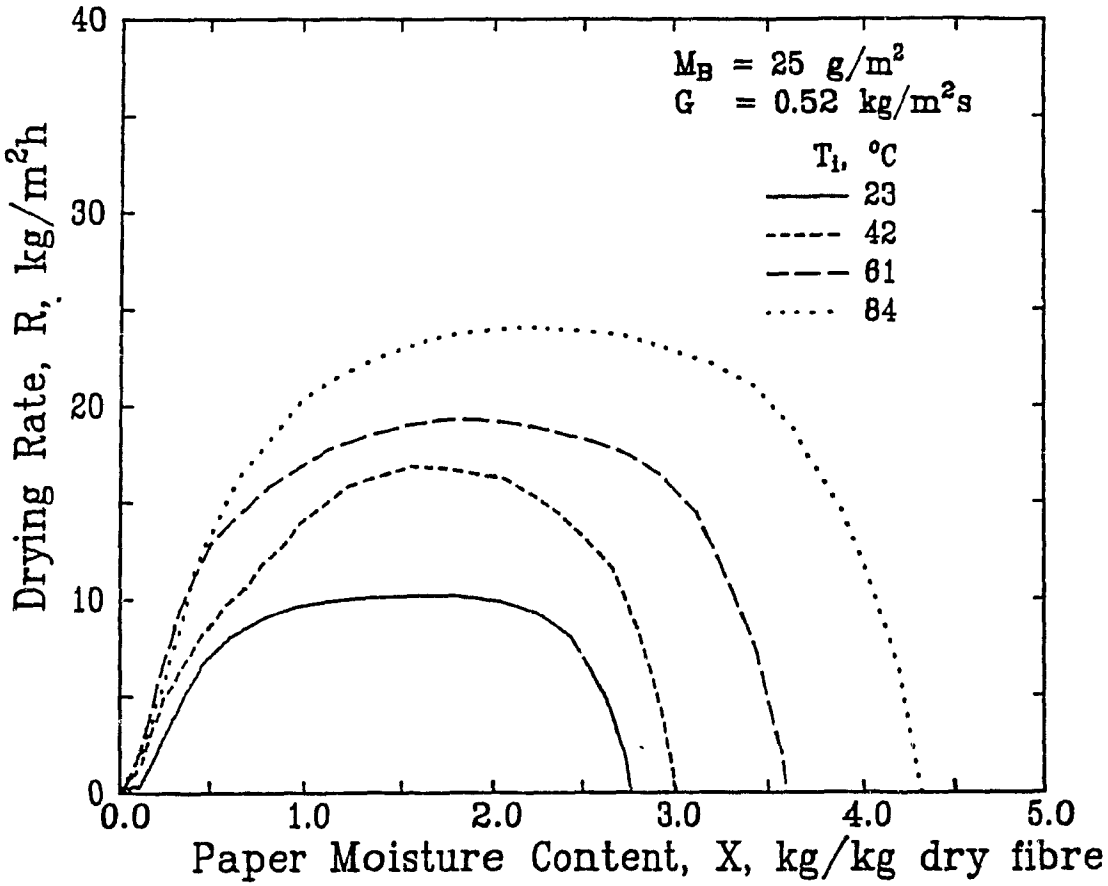

Figure 5.9 Effect of throughflow temperature on drying rate curve: High throughflow rate-low basis weight

increasing rate period terminates directly with the falling rate period. For the lightest weight paper tested, M_B=25g/m^2, Fig. 5.9 further demonstrates the greater importance assumed by the increasing rate period as T_i increases and as X_o decreases.

5.3.4 Increasing Rate Period of Drying

The drying literature has to date directed disproportionately little attention to the drying which occurs before the onset of the constant rate drying period.. This period has been generally treated as just a short transition before reaching conditions for constant rate drying. The initial period has been considered one of heat transfer from the drying medium to warm the moist material, but with an amount of evaporation negligible compared to that of the constant and falling rate periods of drying. However, the present results show that for through drying of beds of fine hygroscopic fibers there is an increasing rate period of drying which precedes the constant rate period and that an important fraction of the drying occurs during the increasing rate period. The complex combination of thermal and flow effects during this period of increasing rate thus warrants much greater attention.

It is proposed here that the increasing rate period derives from an increasing area for heat and mass transfer within the web, an increase resulting from a progressive opening of pores between the fibres. The effect of paper moisture content on effective pore size for throughflow, d_p, and on permeability, k, Chapter 4, supports this interpretation. The wide pore size distribution of paper becomes even wider for the light weight grades which are of greatest importance for through drying. For paper of 25g/m^2 basis weight a two order of

magnitude range in pore size, from less than 1μm to greater than 50μm, was demonstrated in Chapter 4. Also, local nonuniformities in flow derive from local nonuniformity in sheet structure. There may be fibre aggregates or flocs which, initially at high moisture content, may experience little throughflow. At the beginning of the increasing rate period only the largest pores are open for throughflow. However, the correspondingly low area for simultaneous heat and mass transfer is partially offset by the high local transfer coefficients for the high flow velocity through the low fraction of area open for flow. The relative importance of local variability in flow, caused by a wide pore size distribution and fibre agglomerates, would be expected to increase with thinner paper and with increasing intensity of drying, i.e. increasing temperature and rate of the throughflow air. Thus the extent of the increasing rate drying period could be expected to be larger for low basis weight paper dried with high flow rates of high temperature air. This expectation is subsequently demonstrated quantitatively.

The conditions for transition from the increasing rate period to that of constant rate are documented in Section 5.5. In the numerical simulation, Chapter 7, the effect of increasing internal specific surface of paper during the increasing rate period is applied to predict drying during this newly identified drying period.

5.3.5 Falling Rate Period of Drying

The period of falling drying rate for the case of surface drying, i.e. without throughflow, has been the subject of innumerable studies. Considerations invoked to explain this period of decreasing drying rate

include evaporation from a partly saturated surface, liquid diffusion, capillary driven liquid flow, combined vapour diffusion and liquid capillary motion, evaporation-condensation, evaporation from a submerged front, and theories based on irreversible thermodynamics. These concepts from surface drying have little applicability to through drying because throughflow eliminates the importance of most of the effects noted. In their simulation of through drying of paper Wedel and Chance[1977] obtained closer agreement with experiment by assuming negligible solid thermal conductivity This finding is consistent with the expectation that heat conduction and moisture diffusion through the solid are not factors for the falling rate period in through drying as is the case in surface drying of paper.

In their pioneering study of through drying of solids including fibrous materials such as excelsior, rayon and raw silk, Marshall and Hougen[1942] proposed, heuristically, an exponential relationship between moisture content and the rate of drying in the falling rate period, i.e. $X \propto e^{-at}$, an assumption found applicable to 2/3 of the materials tested. Rohrer and Gardiner[1976] adopted this idea for prediction of through drying rates of paper in the falling rate period. However the present extensive set of experiments shows that this is not a good approximation for paper during the falling rate period. Fig. 5.10 illustrates that this relationship is not followed for the highest intensity drying conditions tested, and the deviation is even larger for low intensity drying.

In their study of through drying of packed beds of non-porous materials, glass balls and crushed quartz, Allerton *et.al.*[1949] claimed that a narrow evaporation zone progresses through the bed, and

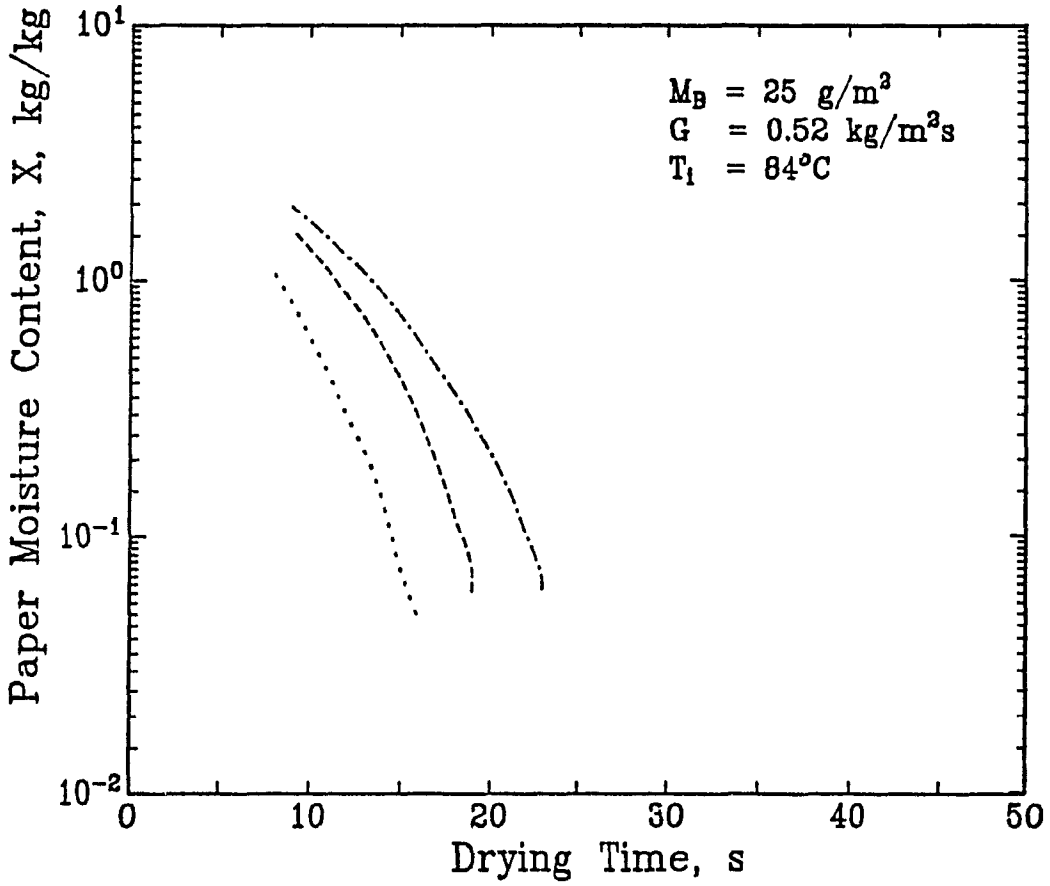

Figure. 5.10 Falling rate period: Test of exponential paper moisture content - drying time relation

that the falling rate period starts when this evaporation zone has passed completely through the bed. The extensive set of drying rate curves of the present study establish that for paper, a thin bed of small hygroscopic fibres, drying does not proceed by the mechanism noted above, except possibly under extremely mild drying conditions with the heaviest grades of paper, conditions not of relevance to industrial through drying of paper.

In their through drying simulation models Raj and Emmons[1975], Wedel and Chance[1977] and Crotogino and Allenger[1979] based their rates during the falling rate period on the decrease in partial pressure as documented for paper by Prahl[1968]. Other mechanisms for the falling rate period noted in these simulation models were the recession of moisture to smaller cavities and fibre shrinkage, Raj and Emmons; receding evaporation interface, Wedel and Chance; increasing heat of adsorption of water, Crotogino and Allenger. Randall[1984] used the polynomial relation between normalized drying rate, R/R_c, and moisture content, X/X_c, as determined experimentally for through drying of paper by Gottsching and Rhodus[1977].

In Section 5.5 the conditions for the onset of the falling rate period are analyzed. In Chapter 7 it will be shown that incorporating two thermodynamic aspects, i.e. vapor pressure depression and variable heat of adsorption, is sufficient to provide a reasonable modelling of the falling rate period in the through drying of paper.

5.3.6 Characterization of Through Drying Rate Curves

Various attempts have been made to generalize drying rate curves so that drying behaviour could be predicted from only a few bench-scale

tests. Keey and Suzuki[1974] and Schlunder[1976] proposed normalized plots of characteristic drying rate curves. Keey and Suzuki made a number of assumptions: critical moisture content invariant and independent of both initial moisture content and drying conditions; constant moisture diffusivity; receding evaporation front; geometrically similar drying rate curves independent of drying conditions. Van Brakel[1980] and Menon and Mujumdar[1987] have criticized these assumptions and choice of test cases considered inappropriate. The large number of drying rate curves of the present study and the results of the analyses of Sections 5.4 and 5.5 indicate that for through drying of a bed of small hygroscopic fibres such as paper, the Keey and Suzuki method fails because drying rate curves are not geometrically similar and some of their assumptions, i.e. receding evaporation front, critical moisture content independent of initial moisture content, do not apply.

Schlunder's model, a plot of R/R_c vs. $(X-X_{eq})/(X_c- X_{eq})$, consists of a normalized drying rate curve for which external conditions enter only as reflected by their effect on critical moisture content. This model holds well for molecular sieves but not for alumina-silica particles nor for paper. Although Gummel[1977] claimed that this method is successful for through drying of paper, the applicability of the temperature dependent normalized drying rate curves he reported is extremely limited because of lack of a means of extending them to throughflow conditions of industrial relevance.

A great diversity is apparent among the drying rate curves obtained in the precisely controlled experiments of the present study, as is evident even among the 17 curves displayed on Figs. 5.1-5.9, a small sample of the 235 drying rate curves documented in Appendix 8.

Conditions include those for which, with the disappearance of the constant rate period, drying passes directly from the period of increasing rate to that of falling rate. In view of these findings and of the limited success of the normalized drying rate approach, that approach is not used here. Rather, characterization of the present measurements is provided by analysis of the drying rate during the constant drying rate period, Section 5.4; by development of the relation between drying conditions and the extent of the periods of increasing, constant and falling rate drying, Section 5.5; by a transport phenomena analysis of through drying, Chapter 6; and by integration of mass and momentum transport in the modelling of the complete through drying process, Chapter 7.

5.4 CONSTANT DRYING RATE PERIOD

5.4.1 Experimental Results

(a) Definition and Reproducibility of R_c

For drying rate curves where there is a well defined period of constant drying rate, R_c, extending over an appreciable range of paper moisture content, and with a drying rate which is reasonably constant, there is no problem concerning the value of R_c. For drying rate curves where this is not the case, as is frequently seen on Figs. 5.1-5.9, R_c is the average drying rate over the moisture contents defined in Section 5.5 as marking the start and the end of the constant rate period. For R-X curves without a significant range of moisture content over which R remains relatively constant, R_c is taken as the maximum value on the drying rate curve.

The good reproducibility of R_c at varying X_o is shown in Fig.

5.11. As expected, the variability of replicates of drying rate curves increases with increasing temperature and flow rate of throughflow and with decreasing basis weight. Even for the extreme conditions of Fig. 5.11, i.e. highest T_i-highest G-lowest M_B, the reproducibility of R_c was within ±6.5%.

(b) Comparison of Results

The only comparable data are shown with the present results in Figs. 5.12 and 5.13. With the results of Gummel[1977] for 23g/m² paper, Fig. 5.12, the agreement is good only at his lowest air throughflow rate while at higher flow rates his drying rates are much lower than those measured here. His drying rates at G=0.43kg/m²s almost coincide with the present results at G=0.29kg/m²s. The difference in M_B is too small to be relevant to these large drying rate differences. The likely cause of Gummel's low drying rates at higher throughflows is by-passing of air around his sample holder which did not have a positive seal. As noted earlier the present study established that even a well machined, tightly fitting sample holder is inadequate and that a positive, O-ring seal, not used by Gummel, is essential to eliminate by-passing for experiments in the high G-high ΔP range.

Walser and Swenson[1968], Fig. 5.13, used two 43g/m² sheets to obtain 86g/m². In their experiments, not conducted at constant throughflow rate, they reported G increased 20% as the sheet dried from 150 to 90% moisture. The flow rates quoted are those measured at 120% moisture. The agreement between the two studies is as good as permitted by the differences in conditions.

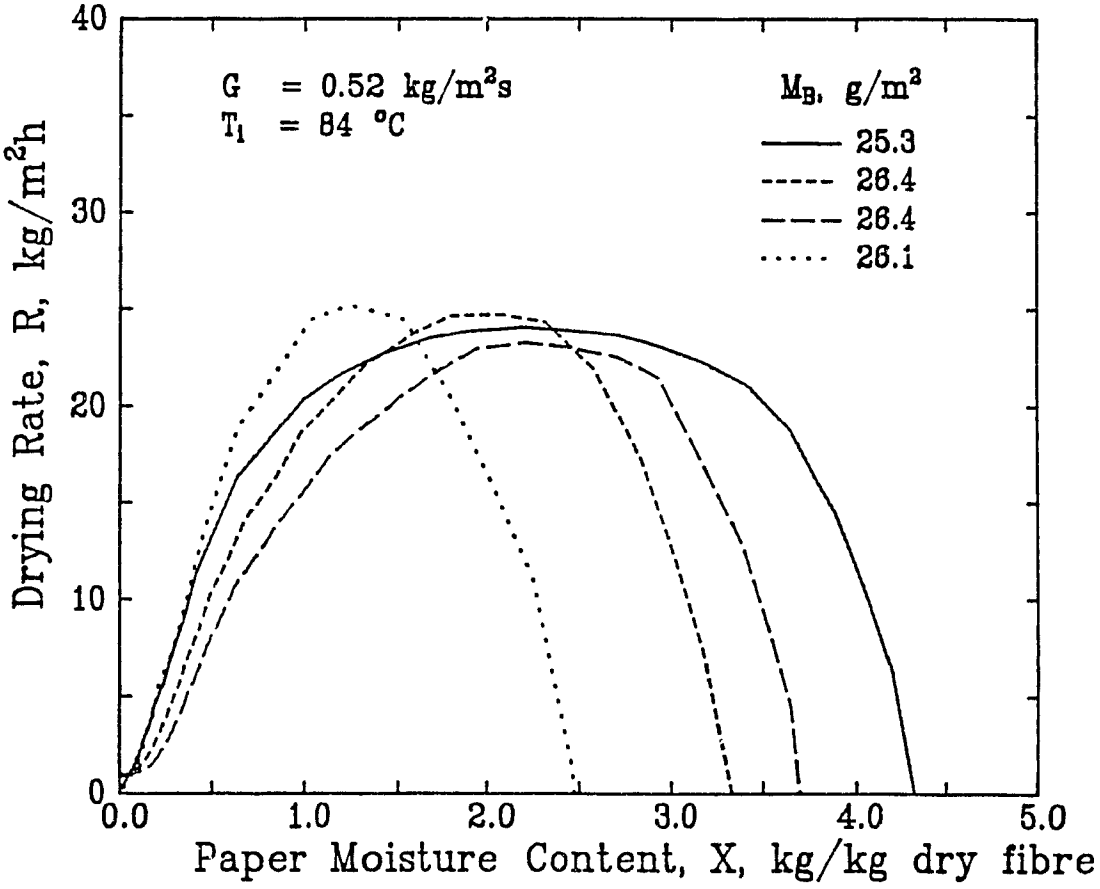

Figure 5.11 Reproducibility of constant drying rate

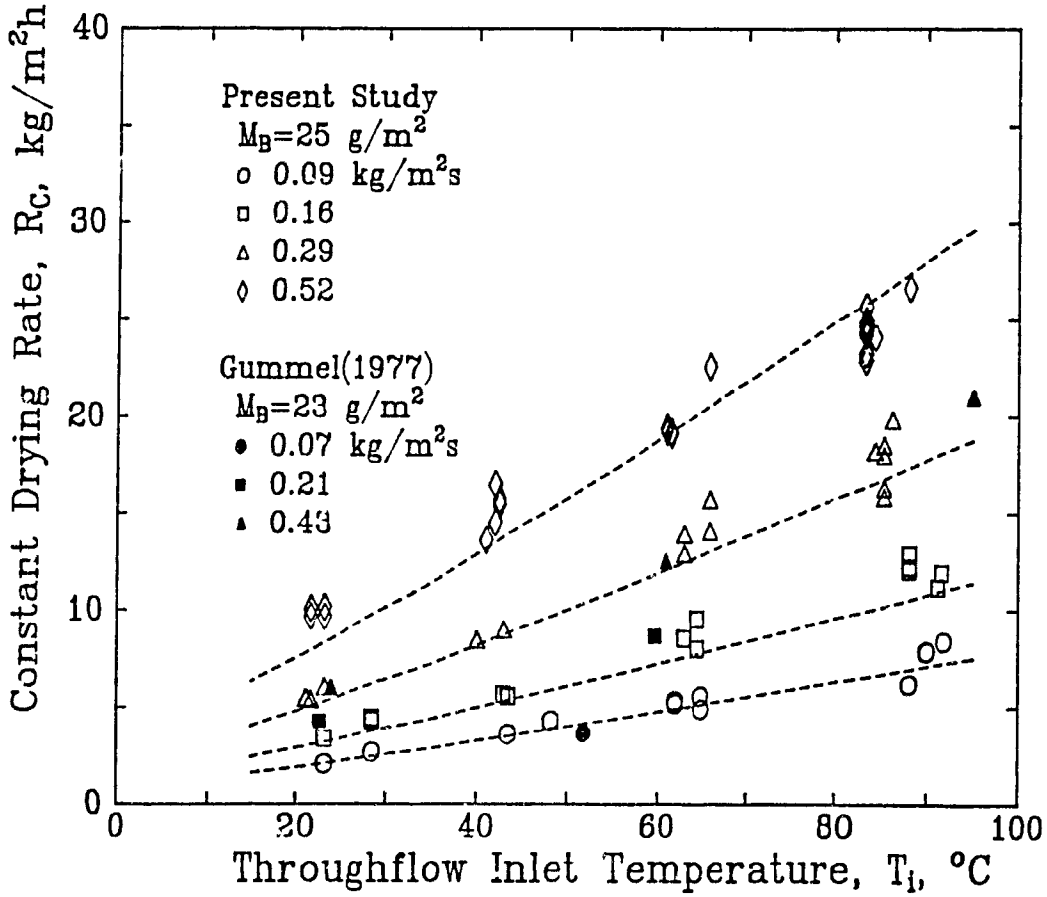

Figure 5.12 Effect of throughflow temperature on constant drying rate: low basis weight

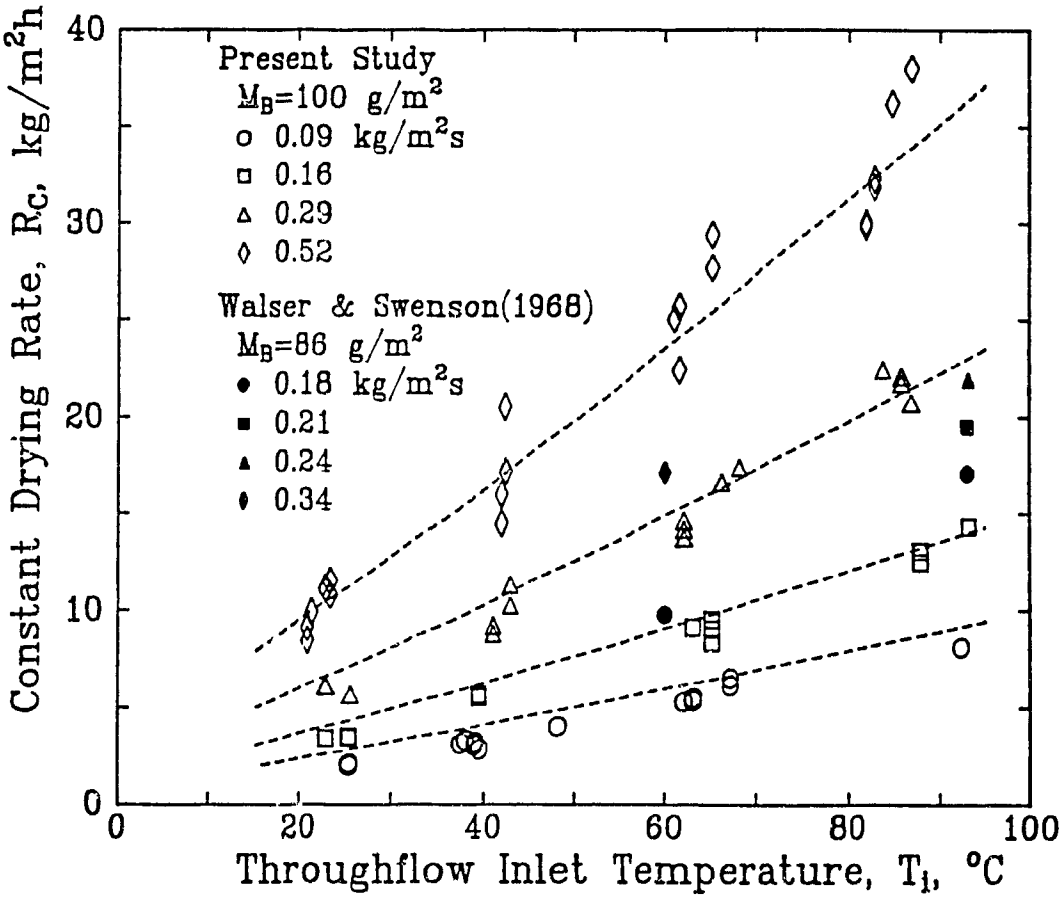

Figure 5.13 Effect of throughflow temperature on constant drying rate: medium basis weight

(c) Correlation of Drying Rate

The experimental data for R_C were correlated as

$$R_C = a\ (T_i - T_S)^b\ G^c\ (M_B)^d \qquad (5.1)$$

Initial moisture content of paper, X_O, was dropped from the correlation when found to be not statistically significant. The temperature term appears as the heat transfer driving force, the difference between dry and wet bulb temperature of inlet drying air, $T_i - T_S$. In the present study the range of T_i is about 23°-88°C, T_S about 8°-29°C. The extremes in the experimental values of ΔT_i were 14° and 64°C. Nonlinear correlation of 235 experimental R_C values, Table 5.3, gives a regression coefficient r^2=0.991 and a standard error for R_C of 1.13, about 6.5% of R_C for average drying conditions. The variation in R_C for the replicate experiments of Fig. 5.11 was likewise noted to be about ±6.5%. Fig. 5.14 illustrates the satisfactory fit of this regression equation. The good agreement of Eqn. 5.1 is also shown in Figs. 5.12 and 5.13, where the lines for the conditions of the present experimental data are those for Eqn. 5.1.

Table 5.3 Constant Drying Rate Correlation (Eqn. 5.1)

Variable	Exponent	Coefficient	Standard Error
	a	2.4	0.2
$T_i - T_S$	b	0.87	0.02
G	c	0.80	0.01
M_B	d	0.16	0.01

d) Correlation of Relative Drying Rate

For rate of through drying expressed per unit surface area of the sheet, the maximum attainable value, R_S, corresponds to the exit air being saturated. As knowledge of the exit air condition for through drying has been very limited, it has frequently been assumed that the

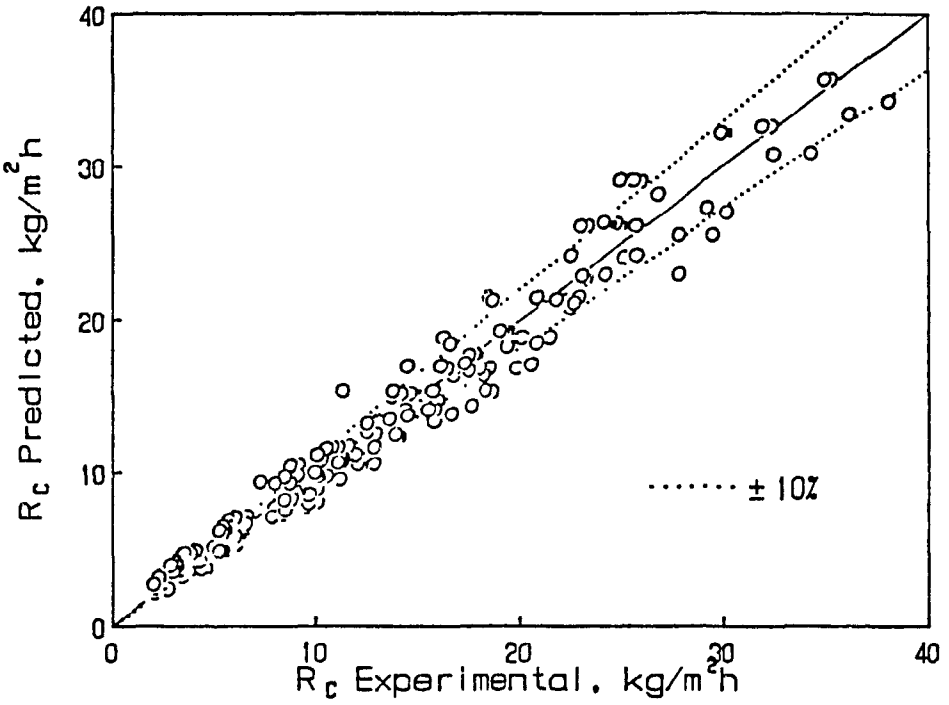

Figure 5.14 Comparison of constant drying rates: Experiment and correlation Eqn. 5.1

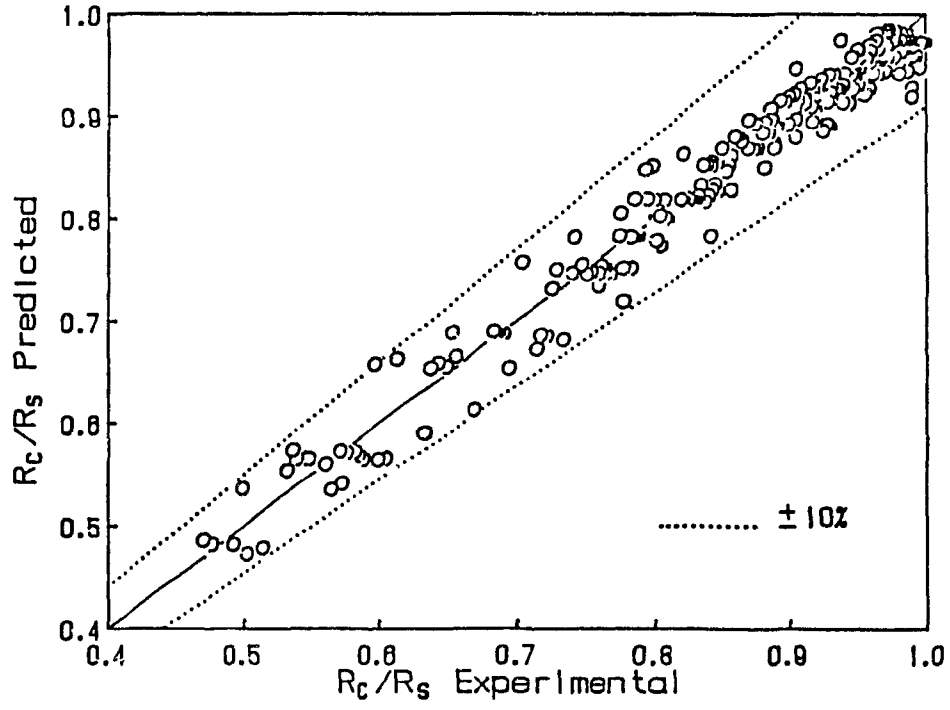

Figure 5.15 Comparison of relative drying rates: Experiment and correlation Eqn. 5.3

throughflow air leaves the sheet saturated, i.e., that $R_C=R_S$. This assumption is therefore now examined by expressing R_C relative to R_S, the maximum attainable rate for the limiting case of saturated exit air.

By definition, R_S is directly proportional to G, is independent of M_B, but the effect of temperature driving force on R_S is complicated because R_S relates to T_i via $R_S=f(Y_S)$, $Y_S=f(T_S)$ and $T_S=f(T_i)$. In fact $T_S=f(T_i,Y_i)$, but Y_i is constant in the present work. A heat and mass balance for the conditions of air to reach adiabatic saturation shows that $R_S=f(C_P\Delta T/\Delta h)$, where Δh is the latent heat, C_P the specific heat of air at inlet conditions. While C_P increases with T_i, expressed generally by a polynomial relation, Δh decreases with T_i, given as either as a power or exponential relation. Thus R_S should be proportional to ΔT^{γ} with γ slightly larger than 1 for the present experimental conditions. For R_S, therefore, the relation analogous to Eqn. 5.1 is:

$$R_S \propto (T_i-T_S)\ G\ (M_B)^0 \qquad (5.2)$$

The fractional decrease in R_C from R_S, i.e. $(R_S-R_C)/R_S=1-R_C/R_S$ where R_C/R_S is the relative drying rate, may be examined by fitting the experimental data to the regression equation

$$1-(R_C/R_S) = a'\ (T_i-T_S)^{b'}\ (G)^{c'}\ (M_B)^{d'} \qquad (5.3)$$

Nonlinear analysis of this representation of the same 235 experimental results, Table 5.4, gives a regression coefficient $r^2=0.99$, and a standard error for $1-R_C/R_S$ of 0.06. Fig. 5.15 illustrates the fit of this

Table 5.4 Relative Drying Rate Correlation (Eqn. 5.3)

Variable	Exponent	Coefficient	Standard Error
	a'	0.0083	0.002
T_i-T_S	b'	0.68	0.07
G	c'	0.92	0.08
M_B	d'	-0.50	0.03

regression equation.

From the correlations, Eqns. 5.1 and 5.3, the minimum and maximum limits of R_C and $1-R_C/R_S$ for the experimental conditions listed in Table 5.1 are:

$(R_C)_{max}$ = 39.5 kg/m²h at highest T_i-G-M_B

$(R_C)_{min}$ = 2.0 kg/m²h at lowest T_i-G-M_B

$(1-R_C/R_S)_{max}$ = 0.479 at highest T_i and G, lowest M_B

$(1-R_C/R_S)_{min}$ = 0.014 at lowest T_i and G, highest M_B

The latter two values indicate that the choice of operating conditions covered a good range, from those for which the experimental value of R_C was only 1.4% less than the limiting maximum for the throughflow exiting saturated, to conditions giving R_C less than half the limiting maximum rate of R_S.

Eqns. 5.1 and 5.3 may also be used to determine by what factors R_C and $1-R_C/R_S$ change for the experimental range of each of the three variables, as listed in Table 5.5. Thus the experimental ranges of T_i and G were in each case sufficient to vary R_C by about a factor of 4, but the wide range of M_B varied R_C only by 30% because R_C is not particularly sensitive to M_B, as indicated by the exponent d=0.16 in Eqn. 5.1. The range of each variable, T_i, G and M_B, was sufficient to produce large changes also in relative drying rate, $1-R_C/R_S$. This analysis indicates that the choice of range for each experimental variable was sufficient to determine its effect with good sensitivity.

Table 5.5 Effect of experimental variables on drying rate

Variable	Range	$(R_C)_{max}/(R_C)_{min}$	$(1-R_C/R_S)_{max}/(1-R_C/R_S)_{min}$
T_i-T_S	14-64	3.8	2.8
G	0.09-0.52	4.1	5.0
M_B	25-150	1.3	2.5

5.4.2 Effect of Throughflow Rate on Drying Rate

To isolate the effect of each independent variable, the results were calculated for the other independent variables at their average value. This was done for the effect of throughflow rate on drying rate, for example, by use of Eqns 5.1 and 5.3 as

$$(R_C)_{\Delta T, M_B} = R_C \ (\overline{\Delta T}/\Delta T)^b \ (\overline{M_B}/M_B)^d \tag{5.4}$$

$$\left((R_S - R_C)/R_S\right)_{\Delta T, M_B} = \left((R_S - R_C)/R_S\right) \ (\overline{\Delta T}/\Delta T)^{b'} \ (\overline{M_B}/M_B)^{d'} \tag{5.5}$$

where $(R_C)_{\Delta T, M_B}$ is the value of R_C adjusted according to Eqn. 5.1 to its value at $\Delta T = \overline{\Delta T}$ and $M_B = \overline{M_B}$, where $\overline{\Delta T}$ and $\overline{M_B}$ are the average values of these variables for all the experiments. Likewise, Eqn. 5.3 was used to obtain $\left((R_S - R_C)/R_S\right)_{\Delta T, M_B}$, the fractional decrease of R_C from R_S.

The results for R_C and R_C/R_S, appear in Figs. 5.16a and 5.16b with bars indicating $\pm 1\sigma$, with reference lines for the equations

$$R_C = a \ (\overline{\Delta T})^b \ (\overline{M_B})^d \ G^c \tag{5.6}$$

$$1 - (R_C/R_S) = a' \ (\overline{\Delta T})^{b'} \ (\overline{M_B})^{d'} \ G^{c'} \tag{5.7}$$

for the effect of throughflow rate, G, on R_C and R_C/R_S. As G is increased R_C of course increases, Fig. 5.16a, but R_C/R_S decreases, Fig. 5.16b. The strongest effect on R_C/R_S derives from throughflow rate, Table 5.4. As R_S is directly proportional to G, the value $c'=0.92$ indicates that R_C is proportional to a power less than one. The value of the coefficient $c'=0.92$ reflects the fact that heat and mass transfer coefficients increase with G to a power typically between 0.5 and 0.8, but at constant throughflow inlet temperature T_i, the mean driving force for heat and mass transfer also increases with G. The exponent found for G in the R_C correlation, Table 5.3, i.e. $c=0.80$, reflects the net effect of these two factors.

Each point on Fig. 5.16a represents the average of all experiments,

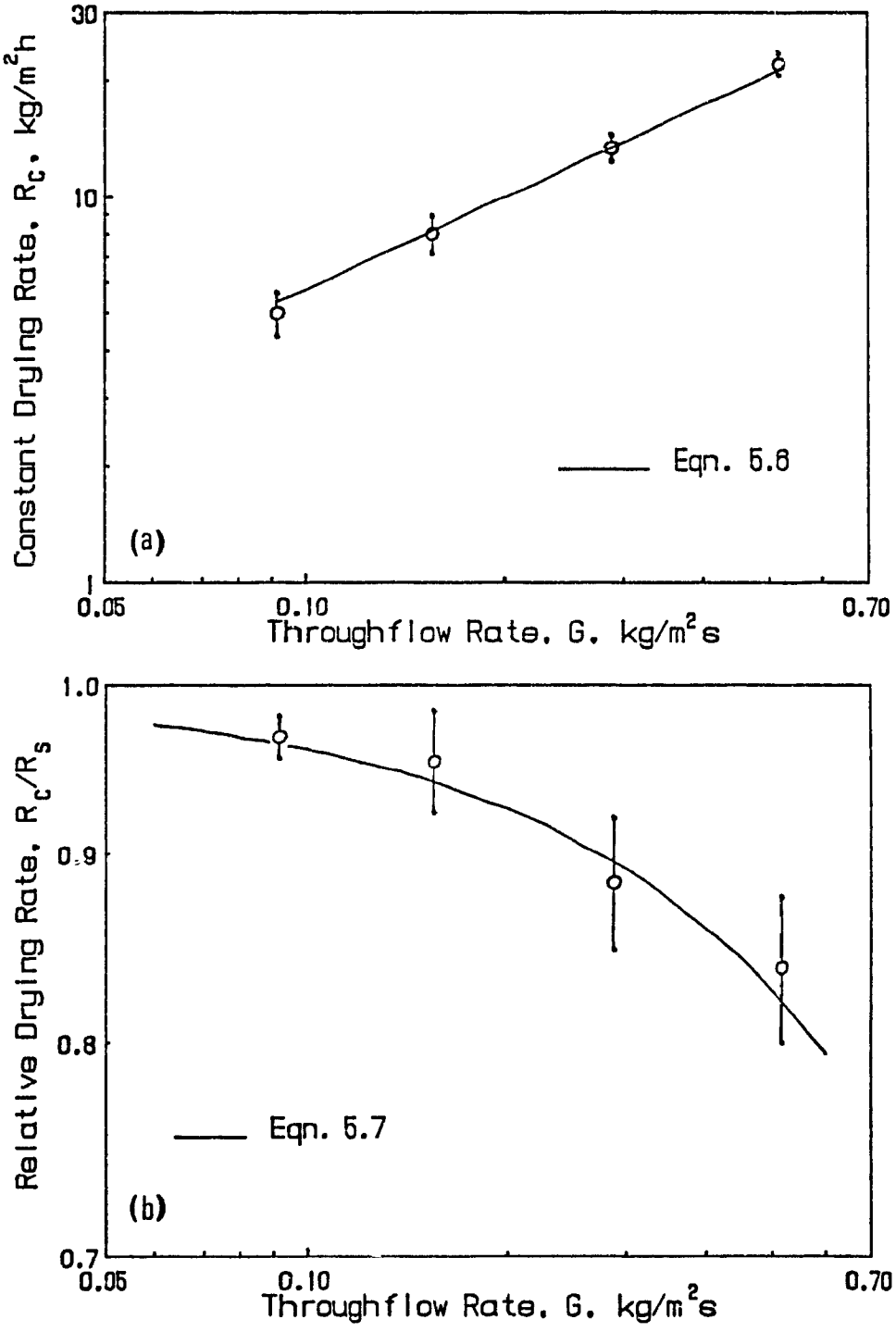

Figure 5.16 Effect of throughflow rate on drying rate: a) constant drying rate, b)relative drying rate

about 60, performed at that throughflow rate. The small deviations around the average values of R_C show the experimental precision of flow rate measurement and the adjustment procedure. The Eqn. 5.1 exponent of throughflow rate, 0.80, is consistent with those of previous studies of simultaneous heat and mass transfer in packed beds. Values obtained for the exponent of G include 0.81, Marshall and Hougen[1942]; 0.61, Taecker and Hougen[1949]; 0.8-0.9, Allerton *et al.*[1949]; 0.85-0.9, Hobson and Thodos[1951]; 0.72, De Acetis and Thodos[1960]; 0.75-0.81, McConnachie and Thodos[1963]; 0.69, Sen Gupta and Thodos[1964]; 0.85, Petrovic and Thodos[1968]. As to the effects of G, ΔT and M_B found by previous workers, most of the reference values reported above and in the two following sections were found by nonlinear regression of authors' original data because almost all have reported only correlations of mass transfer coefficient or Sherwood number.

Fig. 5.16b quantifies that the decrease in relative drying rate, R_C/R_S, with increasing throughflow rate. Wedel and Chance[1977] noted this trend in their laboratory results or through drying of paper, but provided no quantitative documentation. In their mill trials Walser and Swenson[1968] observed that at T_i of about 149°C and u_S=0.25 Std.m^3/m^2s, their measured drying rate was ~43kg/m^2h, 20% lower than R_S. Eqn. 5.3 would predict R_C/R_S= 0.77 for their G and T_i, assuming M_B=88g/m^2, an average of their experimental range, as they did not record basis weight. Their experimental drying rates may be enhanced slightly by additional drying from air swept over the sheet in the draws, an effect supplemental to the through drying. Although this agreement is excellent, its significance should not be exaggerated because of the uncertainties involved in comparing drying rates between

laboratory and paper mill.

5.4.3 Effect of Throughflow Temperature on Drying Rate

The effect of throughflow temperature, Fig. 5.17a-b, was isolated as described above for throughflow rate. Each point on Fig. 5.17 is again the average for all experiments, about 60, performed at that level of $\Delta T_i = T_i - T_s$. The $R_C - \Delta T_i$ relationship is not well documented in packed bed investigations, as in almost all studies for which experimental conditions are well documented the range for ΔT_i is small. As compared to the ΔT_i exponent of 0.87 for R_C, Table 5.3, the ΔT_i exponent calculated from the data of Allerton *et al* [1949] is 0.7, and from, that of Sen Gupta and Thodos[1964] is 0.83. As their ranges of ΔT were less than 10°C, compared to ΔT_i of 14°-64°C in the present study, the accuracy of those exponents is limited. Marshall and Hougen [1942] report an exponent of unity, but air inlet temperature was not varied in their study as they simply replaced the humidity driving force, ΔY, by $C_p \Delta T$, assuming linear wet bulb temperature lines.

Because R_S is directly proportional to ΔT_i in the present experimental range, Eqn. 5.2, the value of $b'=0.68$ indicates that the $(R_S - R_C)$ difference increases with ΔT_i with an exponent approximately 1.68.

From his tests on through drying of 100g/m² handsheets Martin[1972] reported that drying rate reaches to a plateau with increasing ΔT_i, and that increased throughflow rate delays the onset of this plateau. However the significance of his results is limited greatly by his measurement of only average evaporation rate, obtained using a technique that permitted 3 to 5-fold changes in throughflow rate during an experiment. From measurements on an industrial through dryer Rohrer and Gardiner[1976]

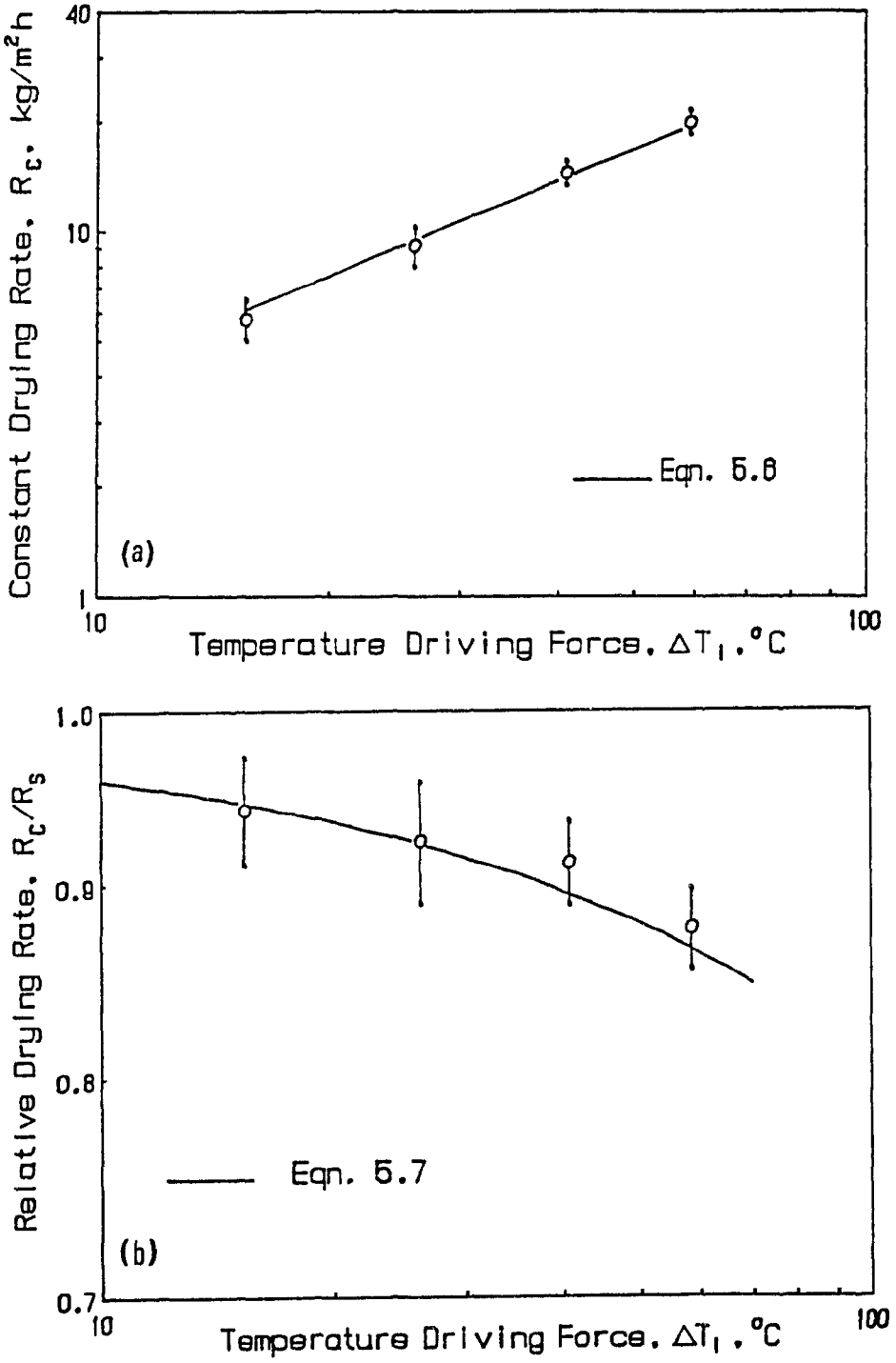

Figure 5.17 Effect of throughflow temperature on drying rate: a) constant drying rate, b)relative drying rate

reported that the drying rate-throughflow temperature relationship was not linear for T_i>150°C, but they provided no quantitative documentation.

For through drying of 20-23g/m^2 tissue paper at low throughflow rate the laboratory data of Gummel[1977] indicate an effect of T_i not noted by him. As he increased T_i from 22° to 87°C, his values of R_C/R_S drop from 0.90 to 0.66, an effect which is consistent with the trend observed in the present study, Fig. 5.17b. These R_C/R_S values from Gummel's data would correspond to values of 0.76-0.93 for b', the exponent of ΔT_i in Eqn. 5.3. Thus the trends with T_i which can be discerned in the data of Gummel, although not previously noted, are found to be similar to those obtained over the much more extensive range of through drying conditions in the present study

The limited data from previous studies for the effect of varying throughflow inlet temperature provide sketchy results, little analyzed and sometimes not even recognized No quantitative description has been given. The present study is the first to provide a quantitative treatment of this important effect in the throughflow drying of paper.

5.4.4 Effect of Basis Weight on Drying Rate

By definition, R_S is independent of basis weight, M_B. Therefore the effects of basis weight on R_C and on R_C/R_S, Fig. 5.18a-b, reflect alternate expressions of the same dependence. Although R_C approaches R_S for large M_B-small G, Fig. 5.18b indicates even for M_B as high as 150 g/m^2, R_C for the conditions shown is still about 5% below R_S.

There is again very little work reported for the effect of bed depth on transfer rates in packed beds, and the data is limited to generally two, or rarely, three values of nondimensional bed depth L/d_p. In most

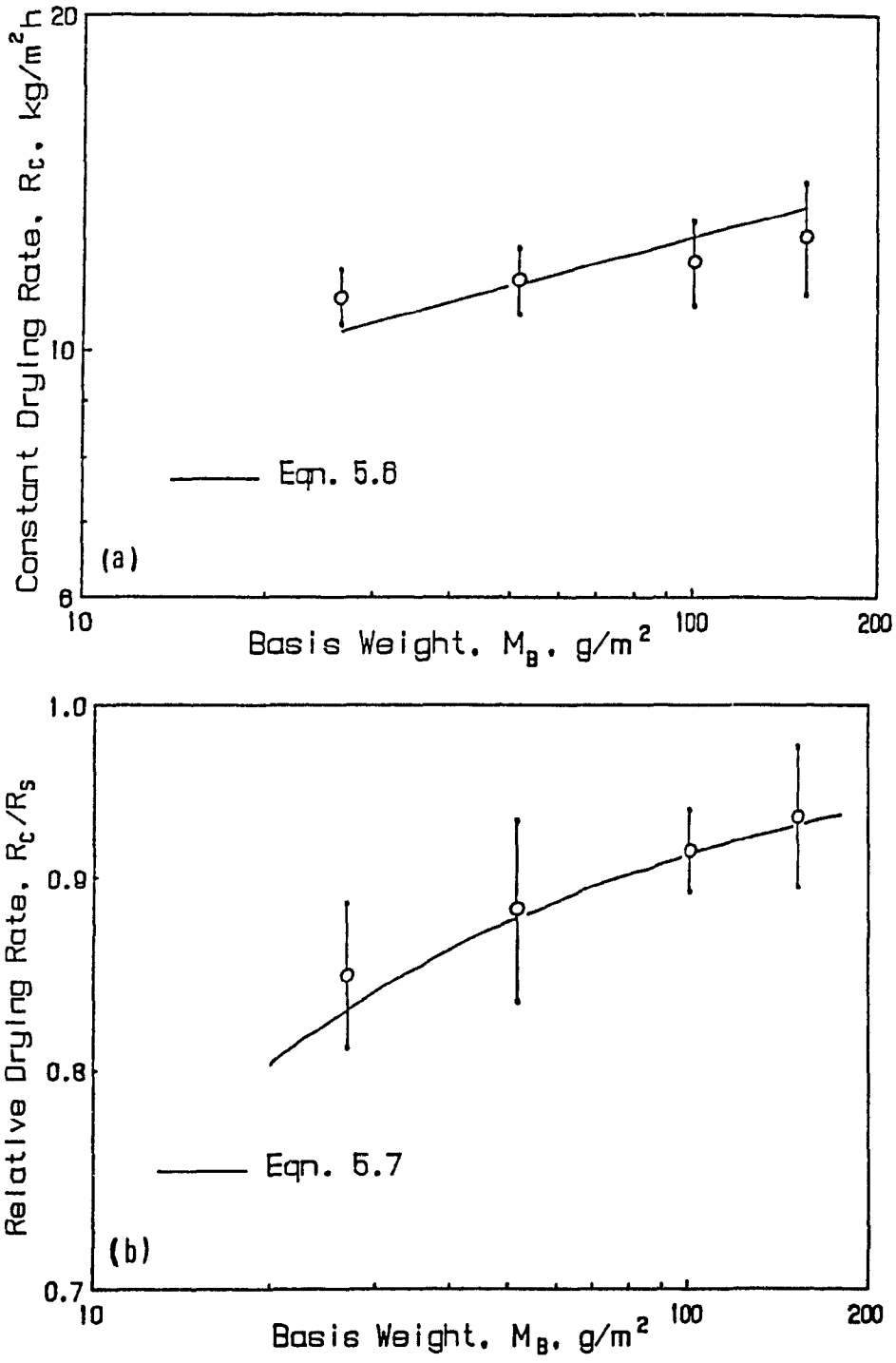

Figure 5.18 Effect of basis weight on drying rate: a) constant drying rate b)relative drying rate

studies bed depth, L, was kept constant and particle size, d_p, varied. The values reported for the transfer rate exponent of L/d_p vary considerably. The values of this exponent according to the data of Marshall and Hougen[1942] and Wilke and Hougen [1945] is ~0.5, from DeAcetis and Thodos[1960] is ~0.6, in both cases much larger than the exponent 0.16 for R_c found in the present study. Three other studies however obtained values of this exponent in the range found here, i.e. ~0.1 by Taecker and Hougen[1949]; ~0.12 by Allerton *et al*[1949]; 0.1-0.2 by Hobson and Thodos[1951].

For the more specific case of the effect of basis weight on the rate of through drying paper, there is again very limited reported work. Wedel and Chance[1977] reported only one case, almost a 25% drop in drying rate, from 520 to 390kg/m^{2}h, with a decrease in basis weight from 48 to 24g/m^2 for through drying at about T_1=205°C and throughflow velocity of about 3.7m/s. For their conditions the values of R_c predicted by Eqn. 5.1 are, respectively, 430 and 375kg/m^{2}h. It is especially significant that these predictions are so good in spite of the fact that the T_1 and G conditions are well outside the range for which Eqn. 5.1 was derived. The respective values of R_c/R_s, 0.61 and 0.44, would correspond to a basis weight dependence term for $1-R_c/R_s$ of about $M_B^{-0.52}$, which agrees well with Eqn. 5.3.

Because of constraints noted in Section 5.2.3, the drying rate correlations obtained in the present study are based on data which, although very extensive, are limited to lower levels of throughflow rate and temperature than used in industrial practice. Although the only comparisons possible are based on extremely limited measurements, the fact that good agreement is obtained for much higher levels of G

and T_1 than used here indicates that the correlation obtained here, Eqn. 5.1, provides a guide which is reliable well beyond the limits of the particular experimental throughflow conditions tested.

5.4.5 Overall Comparisons

For the only study which details all the experimental conditions, Gummel[1977], the correlation equations 5 1 and 5.3 predict values of R_C and R_C/R_S to within 2% of his reported laboratory results at low flow rates through paper. At high throughflow rates it is believed that Gummel's results are in error, as discussed earlier.

For through drying of crepe paper in industrial installations, drying rates of 90-100kg/m^{2}h at T_1=260°C, u_s=0.25m/s, M_B=146g/m^2, are reported by Macdonald and Franklin[1970], and rates of 150kg/m^{2}h for M_B=50g/m^2 at high T_1 and G by Fish[1975]. Eqn. 5.1 would predict a drying rate of 80kg/m^{2}h for the Macdonald and Franklin conditions. Fish does not specify the conditions for the drying rate he quotes, but the extreme conditions reported in his paper are T_1=288°C, V_s=700m^3/min for paper area of 14m^2, i.e. u_s=0.83m/s. For these values and T_S=88°C, Eqn. 5.1 predicts a drying rate of R_C=155 kg/m^{2}h. These two comparisons show that the drying rates predicted by Eqn. 5.1 agree remarkably well with the few measurements reported for industrial dryers.

Eqns. 5.1 and 5.3 are the first comprehensive empirical correlations reported for constant drying rate for the through drying of paper. Although the range of throughflow rates and temperatures used to determine these correlations is quite wide, the maximum values used were lower than industrial practice. There is however evidence that these correlations may apply well beyond the conditions for which they were derived. The

only studies reporting drying rates for industrial through drying installations are the measurements of Walser and Swenson[1968], Macdonald and Franklin[1970] and Fish[1975], and the predictions of Wedel and Chance [1977]. The good agreement between the drying rates reported by these authors and those predicted for their conditions by the correlations obtained in the present study indicates that these correlations may apply also at industrially used throughflow rates and temperatures for the through drying of paper.

5.5 DRYING PERIOD DIAGRAMS: INCREASING, CONSTANT, FALLING RATE PERIODS

5.5.1 Definition of Drying Period Diagrams

The relation between drying conditions and extent of the periods of increasing, constant and falling rate drying is presented through what are defined here as "Drying Period Diagrams", Figs. 5.19 and 5.22-5.25. Other than the $X=X_o$ diagonal, lines on these diagrams represent two key moisture contents. The upper series of lines marks the moisture content for transition from the increasing rate to the constant rate period of drying, with each line corresponding to a specific value of paper basis weight and throughflow rate and temperature. The lowest line marks the moisture content for transition from constant rate to falling rate drying. Here these two moisture contents are termed, respectively, the "initial" and the "final" critical moisture content, X_{ci} and X_{cf}. Although X_{cf} is the value generally referred to as "critical moisture content", the present analysis establishes that the initial critical moisture content, X_{c_i}, is equally important in the through drying of a web of small hygroscopic fibres, paper. The basis and construction of drying period diagrams is now described.

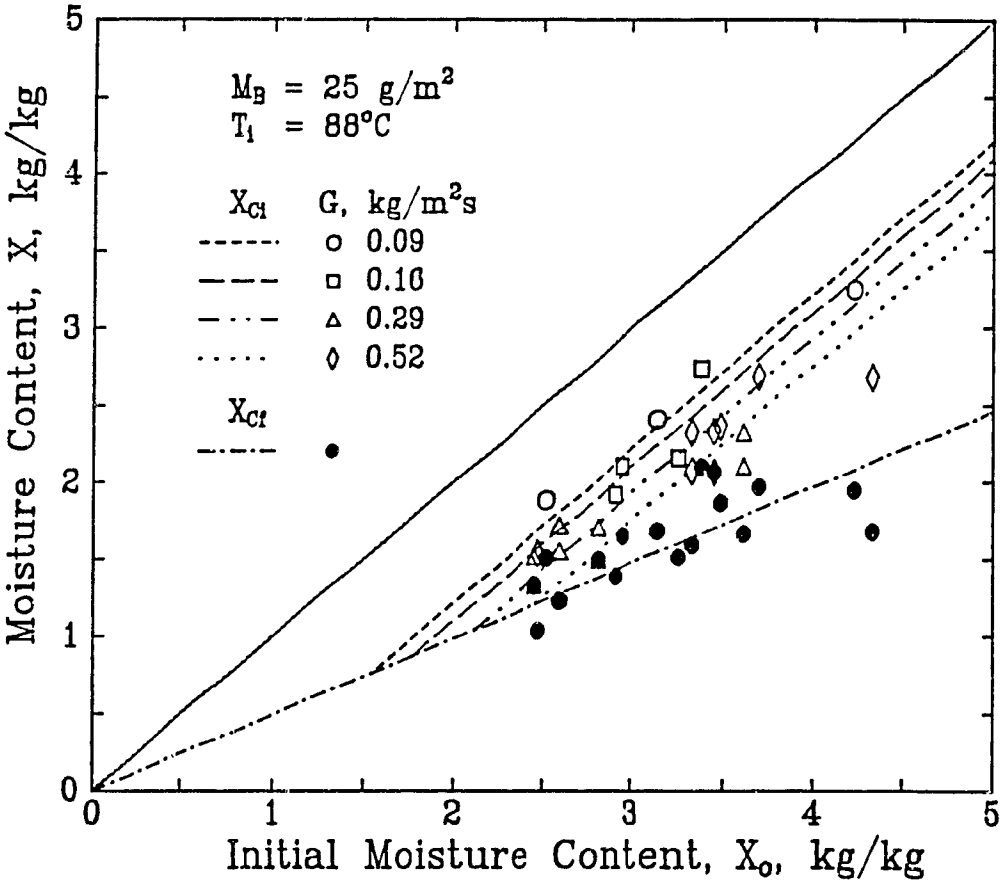

Figure 5.19 Drying period diagram: experimental results for M_B=25g/m², T_i=88°C

Because drying rate curves, Figs. 5.1-5.9, show such a variety of shapes depending on the T_i-G-M_B-X_o combination of drying conditions, the determination of the values of X_{Ci} and X_{Cf} at which the constant rate period starts and ends depends in some cases on how the constant rate period is defined In the frequently occuring case where there is a gradual change in slope of the drying rate curve, Figs. 5.2-5.9, the moisture contents at which the drying rate is 5% less than the maximum rate are defined as X_{Ci} and X_{Cf} on the respective sides of the constant rate period For drying rate curves where there are sharp slope differences between initial, constant and falling rate periods, X_{Ci} and X_{Cf} are taken as the moisture content at those points. With drying rate curves at low T_i for which the drying rate period passes through a maximum before the onset of the constant rate period, the end of that decreasing rate segment is defined as X_{Ci}. All X_{Ci} and X_{Cf} values were determined by a computer program from drying rate-paper moisture content data.

Four locus lines for X_{Ci} and the single lower line for X_{Cf} are shown on Fig. 5.19 for the case of 25g/m^2 paper dried at T_i of 88°C, i.e. the conditions of highest experimental scatter in present study. The drying of a sheet of paper would be represented on a drying period diagram by progression down a vertical line at the particular value of X_o. For a specific X_o, drying thus begins on the diagonal $X=X_o$ line, remains in the increasing drying rate period until X has dropped to the X_{Ci} line for the drying conditions used, remains in the constant rate period until $X=X_{Cf}$, after which paper moisture content decreases during the falling rate period. On Fig. 5.19 four X_{Ci}-X_o lines are shown, one for each of the four levels used for throughflow rate G. The

experimental data for all four throughflow rates are included on Fig. 5.19, an example of one of the 16 drying period diagrams obtained in the present study, i.e. one for each T_1-M_B combination used.

Statistical analysis of the X_{Cf} values from the 235 experiments of the present study shows that within the limit of experimental error, X_{Cf} is directly proportional to X_o. Thus X_{Cf}/X_o may be treated as a variable, greatly simplifying the analysis. Likewise, analysis of the 235 values of initial critical moisture content shows that for each value of T_1, G and M_B, one may represent X_{Ci} by a straight line parallel to the $X=X_o$ diagonal and displaced from it by an amount which depends on T_1, G and M_B. For any T_1-G-M_B combination there is a unique value of X_o below which no constant rate period exists. On the drying period diagrams this condition is the point at which the regions of the 3 drying periods intersect, hence it may be called the "triple point", X_{ICF}, of the increasing-constant-falling rate periods. Thus X_{ICF} is the value of X_o for which the constant rate condition is reached, but only momentarily, as drying passes directly from the increasing rate to the falling rate drying period. For $X_o<X_{ICF}$ there is no constant rate period, with the increasing and falling rate periods accounting for all the drying. Drying period diagram characteristics are now examined quantitatively.

5.5.2 Initial Critical Moisture Content, X_{Ci}

During the increasing rate period of drying the complex set of flow, heat and mass transfer effects occuring while conditions are approaching those of constant rate drying is determined by the opening of large pores and the change in temperature of the moist paper towards

that for constant rate drying. A simplified heat balance during the increasing rate period gives $(X_o - X_{Ci}) = f(G(T_i - T_S)\Delta t / M_B)$, where elapsed time, Δt, is also a function of G, M_B and ΔT. This relation suggests the following form of equation for the $X_{Ci} = f(T_i, G, M_B, X_o)$ relation:

$$X_{Ci} = X_o - (T_i - T_S)^a (G)^b (M_B)^c \qquad (5.8)$$

$X_o - X_{Ci}$ is the amount of water evaporated during the increasing rate period, i.e. until the conditions for transition from increasing to constant rate drying are reached at $X = X_{Ci}$, the initial critical moisture content. Eqn. 5.8 allows this amount of evaporation, $X_o - X_{Ci}$, to be function of ΔT, G and M_B. A proportionality constant, C_o, was dropped from Eqn. 5.8 when found to be not statistically significant. The results of nonlinear correlation, Table 5.6, give a regression coefficient $r^2 = 0.99$, and a standard error for X_{Ci} of 0.19kg water/kg dry fibre. Fig. 5.20a shows that this regression equation provides a satisfactory fit to the experimental data.

Table 5.6 Correlation for Initial Critical Moisture Content

Variable	Exponent	Coefficient	Standard Error
$T_i - T_S$	a	0.39	0.03
G	b	0.27	0.03
M_B	c	-0.37	0.03

As the temperature, T_i, and rate, G, of the throughflow increase, the drying rate of the constant drying rate period increases. Consequently there is an increase in the amount of water evaporated, $X_o - X_{Ci}$, while the drying rate is increasing to this higher value. Thus the positive values for the exponents a and b of Eqn. 5.8 are as expected. The negative exponent, c, for basis weight is likewise consistent with the expectation from the heat balance which led to the form of Eqn. 5.8.

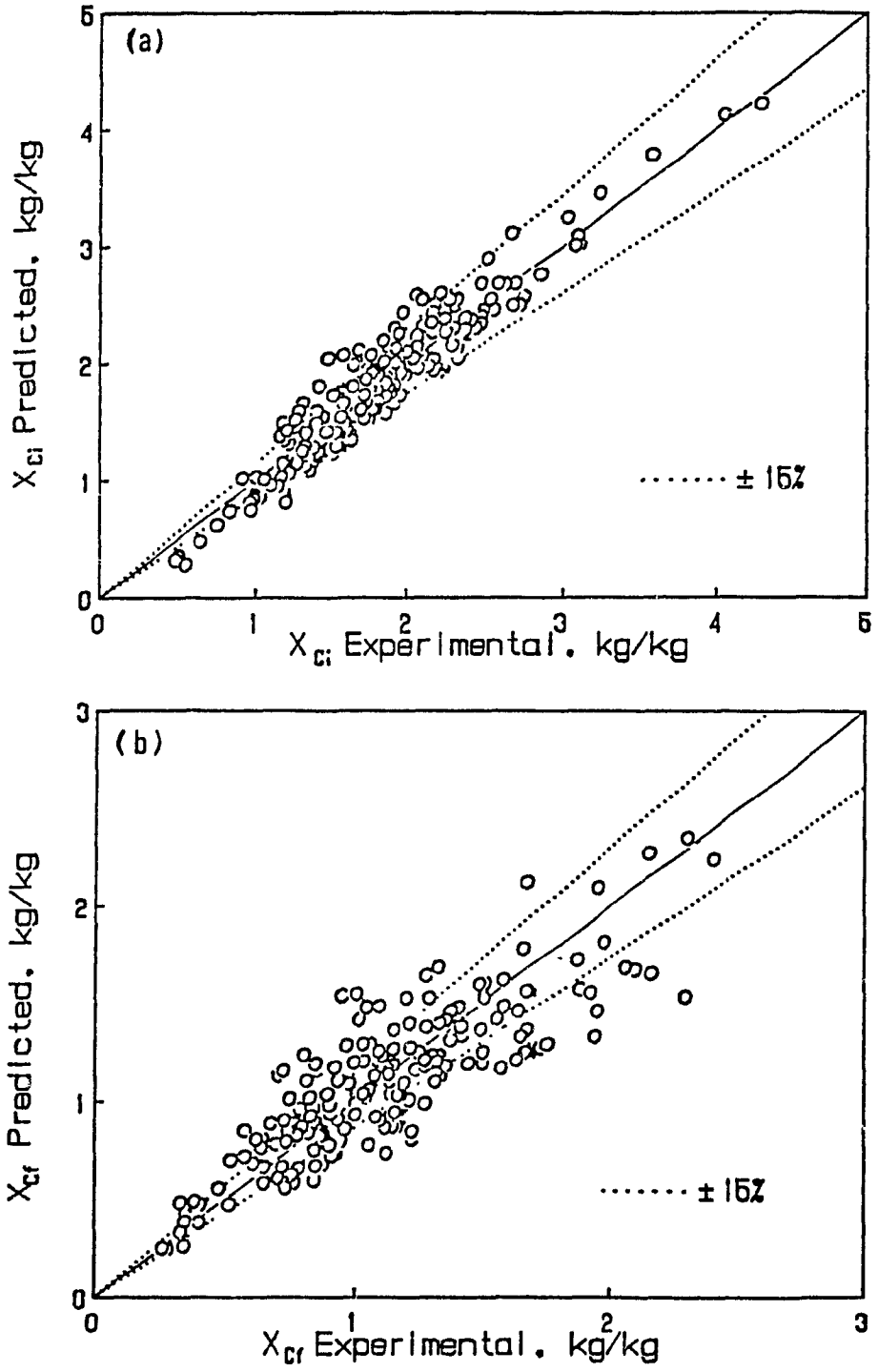

Figure 5.20 Comparison of critical moisture contents: Experiment and correlation; a) X_{ci}, b) X_{cf}

Some characteristics of the period of increasing rate are illustrated by Fig. 5.21 for the highest air throughflow rate. Each point is the average of 2 to 6 replicates at that drying condition. The effect of slight variations of T_i and M_B of these replicates are normalized according to the procedure described in Section 5.4.2. The bars indicate $\pm 1\sigma$ and the lines represent Eqn. 5.8. The amount of water removed during the increasing rate period, $X_o - X_{Ci}$, changes by more than a factor of five over the experimental range of drying conditions, i.e. between 0.24 kg water/kg dry fibre for the lowest T_i-lowest G-highest M_B condition (not shown), and 1.25kg/kg for the condition of highest T_i-highest G-lowest M_B. For the latter set of drying conditions and with, for example, $X_o = 2.5$, this shows that 50% of the drying would take place during the period of increasing drying rate. This large proportion of the drying underlines the central importance of the increasing rate period for the case of through drying of a web of small hygroscopic fibres such as paper.

Critical moisture content has sometimes been treated as a material property, i.e. as being not dependent on drying conditions. The initial critical moisture content defined here is shown not to be a material property, in that it is sensitive to all four of the variables tested, i.e. $X_{Ci} = f(T_i, G, M_B, X_o)$. When expressed as $X_o - X_{Ci} = f(T_i, G, M_B)$, Eqn. 5.8 indicates that for the range of T_i-G-M_B tested here there is a factor of 5 variation in the amount of water evaporated during the increasing rate period, $X_o - X_{Ci}$.

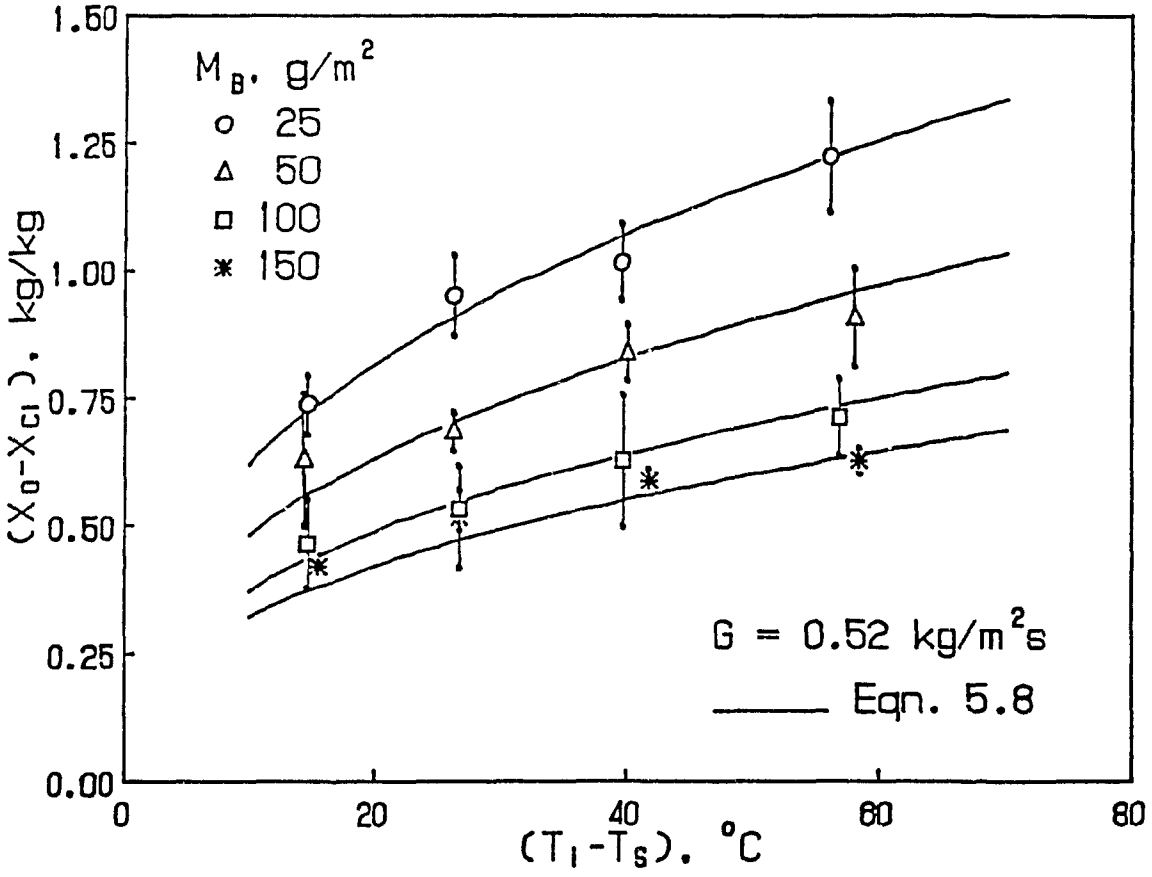

Figure 5.21 Water removal during increasing rate period: Effect of throughflow temperature and basis weight

5.5.3 Final Critical Moisture Content, X_{cf}

(a) X_{cf} Correlation

The definition used here for the final critical moisture content, X_{cf}, is that generally referred to in drying literature simply as the critical moisture content. This moisture content at the transition from constant to falling rates has traditionally been considered as the lowest moisture content at which the evaporating surface is maintained sufficiently wet, by diffusion and/or capillary action, to maintain constant rate drying. As the change from constant to falling drying rate is for most materials not sharp, the specific value depends on its definition. This value is sometimes taken as the intersection on the drying rate curve of straight lines representing the constant rate and the falling rate, a method not applicable to the variety of shapes of drying rate curves for through drying paper as documented in Figs. 5.1-5.9. The method used here to define X_{cf}, described earlier, was applicable to all through drying rate curves obtained.

The form of X_{cf} correlation for through drying paper bears no relation to that for surface drying because concepts relevant to the constant rate-falling rate transition are fundamentally different. Paper used in the present study consists of collapsed kraft fibres ~30μm wide, 4-8μm thick and a few mm long, Fig. 4.16. Kraft paper of basis weight 25-150g/m^2 is from 50-300μm thick. Thus this drying process involves flow through thin packed beds, of depth from less than 10 to about 60 fibres. In surface drying such paper, moisture must travel a distance of up to 10-60 fibres to reach the evaporating surface of the sheet. In through drying the moisture typically travels only half the thickness of fibre, about 2-4μm, to the surface of each

fibre before contacting the drying air. As local conditions within the web are incomparably different between surface and through drying, the respective concepts concerning X_{Cf} should have little in common. In particular, theories proposed in surface drying for relating X_{Cf} to properties affecting moisture transport through the solid relate to transport mechanisms not involved in through drying.

Investigation of the nature of the relationship between X_{Cf} and the system variables, $X_{Cf}=f(T_i, G, M_B, X_o)$, led to the particular form $X_{Cf}/X_o=f(T_i, G, M_B)$. Statistical analysis substantiated the finding that X_{Cf} is linearly proportional to X_o and that X_{Cf}/X_o may therefore be treated as the dependent variable, as first suggested by examination of Fig. 5.19 and the other 15 drying period diagrams produced. The effect of throughflow temperature, T_i, should appear in the form of the temperature driving force, ΔT_i, as in Eqn. 5.8, because the sheet remains at T_S to the end of the constant rate period of drying. The variables G and M_B were dropped from the regression when found not to be significant. Thus the final form of the relationship between X_{Cf} and system variables is simply

$$X_{Cf}/X_o = C_o\ (T_i - T_S)^a \qquad (5.9)$$

For the results of Table 5.7, r^2=0 967 and the standard error for X_{Cf} is 0.20, essentially the same as for X_{Ci} from Eqn. 5.8. Fig. 5.20b shows the satisfactory fit of the experimental data by Eqn. 5.9.

The low exponent for $T_i - T_S$, a parameter varied by a factor of 4

Table 5.7 Correlation for Final Critical Moisture Content

Variable	Exponent	Coefficient	Standard Error
	C_o	0.29	0.03
$T_i - T_S$	a	0.13	0.02

between 15° and 59°C, indicates that over the entire range of experimental values for T_i-G-M_B-X_o, the ratio X_{cf}/X_o in fact varies only between 0.41 and 0.49. Thus as an approximation, accurate to 10%, one could take

$$X_{cf}/X_o = 0.45 \qquad (5.9a)$$

as applying over the entire range of T_i-G-M_B-X_o variables tested in the present study. The best estimate of X_{cf}/X_o is of course with the regression equation 5.9.

(b) X_{cf} Comparison: Surface Drying and Through Drying

For the case of surface drying some theories, generally based on solutions of diffusion equations, have been developed to predict the final critical moisture content. For example the relationship of Suzuki *et al.*[1977] is of the form $\frac{X_{cf}}{X_o} = f(-\frac{RL}{X_o D})$ where R is drying rate, L is bed thickness and D is effective diffusivity of liquid water in the solid. The relevance of L, R and D for the case of the through drying of paper may be examined. Bed thickness, L, an important variable in the Suzuki model, has no effect on final critical moisture content for through drying paper, as discussed earlier. The relevance of drying rate to the value of X_{cf} for through drying paper may be seen by comparing the X_{cf} correlation, Eqn. 5.9, with that for constant drying rate, Eqn. 5.1, $R_c = 2.4(T_i - T_s)^{0.87}\ G^{0.80}\ M_B^{0.16}$. For through drying of beds of particles as small as paper fibres, final critical moisture content is clearly not dependent on drying rate. Effective diffusivity of liquid water appears in the theories of Suzuki and others for surface drying as $X_{cf} = f(D^{-1}) = f(T^{-1})$ because of the temperature dependence of the transport of liquid water in the solid. The effect of temperature

on X_{cf} found in the present study is not only different, but is moreover in the opposite direction to that found in surface drying and represented in the Suzuki correlation. In surface drying, temperature acts through its effect on increasing the rate of transport of water through the solid to the evaporating surface, hence X_{cf} decreases with increasing temperature. In through drying of small hygroscopic particles, temperature acts through its effect on increasing the rate of heat transfer to the particles and thereby on the rate of evaporation from the surface of the particles, hence X_{cf} increases with increasing temperature. Thus the effects of bed thickness, drying rate and temperature on final critical moisture content are totally different between surface drying and through drying.

(c) Interpretation of X_{cf} for Through Drying

The Eqn. 5.9 correlation throws some light on which processes affect the final critical moisture content in the through drying of paper, and which do not. Thus the role of M_B, T_i and G are now considered. The absence of paper basis weight from the correlation shows that X_{cf} is independent of paper thickness for through drying, which is not the case for surface drying, e.g. Suzuki *et.al.*[1977], Endo *et.al.*[1977]. In through drying, sheet thickness would not be expected to affect the onset of the falling rate period because the heat and mass transfer occurs at the level of individual fibres or fibre aggregates.

The fact that throughflow temperature but not throughflow rate appears in the correlation may seem inconsistent. The mechanism consistent with the increase of X_{cf} with increasing ΔT_i is the corresponding increase in rate of heat transfer to the fibres, thereby

increasing the rate at which moisture is removed from the fibre surface by evaporation into the througfhflow. This mechanism suggests that X_{cf} should increase also with increasing G. However by Eqn. 5.9 the dependence of X_{cf} on throughflow temperature is very small. Heat flux is linear with ΔT but for low Reynolds number flow through packed beds the fluid-particle heat flux may be proportional to only $G^{0.5}$. As Eqn. 5.9 shows $X_{cf} \propto \Delta T^{0.13}$, a marginal effect, this suggests that one might find $X_{cf} \propto G^{0.06}$. Thus the finding of no significant effect of G is as would be expected. The fact that the effect of ΔT_i is so small relates to the dimensions of the transport phenomena involved. For through drying of fibres as small as those in paper, only about 4-8μm thick, water moves a maximum distance of only half a fibre thickness, 2-4μm, in order to reach the evaporating surface. Hence changes affecting the rate of removal of water from the fibre surface affect X_{cf} to only a limited extent. Although the ΔT effect on X_{cf} is small, the direction of this effect is understandable, i.e. that the falling rate period should start at a somewhat higher moisture content with a higher temperature throughflow. With higher ΔT-higher intensity drying, those fibres adjacent to medium and large pores drop below the fibre saturation point before all the water from the smaller pores has evaporated, i.e. while the average moisture content, X_{cf}, for the sheet is at some higher value. Recall from the Table 5.7 discussion that the maximum change in X_{cf} due to ΔT_i variation is only 0.08kg/kg.

The X_{cf}-X_o relationship derives from through drying being a transient phenomena in a thin web which, on a micro-scale, has always some nonuniformity. The measured transient overall through drying rates are the spatial average of the local transient drying rates which

vary due to micro-scale nonuniformities in paper structure and therefore in local throughflow rate. As drying proceeds in this coupled transient process involving momentum, heat and mass transfer phenomena, any local nonuniformity at the start of through drying will inevitably become even more nonuniform. For example, areas of slightly higher porosity initially will dry faster due to a locally higher throughflow rate, thereby increasing in porosity faster than other areas. The falling rate starts with completion of evaporation of the unbound water at the surface of some local region of fibres in the web. With increasing X_o, drying time during both the increasing rate and constant rate periods increases, allowing initial local nonuniformities to become more developed, so that the condition of some local region of fibres dropping below the fibre saturation point occurs at a higher value of average sheet moisture content, X_{cf}. This mechanism of nonuniformity in local throughflow rate and local drying rate thus leads to the onset of falling rate shifting to higher moisture contents, i.e. to higher X_{cf}, as X_o increases.

A recurrent question is whether either the initial or final critical moisture content is a material property or is a function of drying conditions. For the through drying of paper the present study establishes that there is equal importance to the two critical moisture contents, X_{ci} and X_{cf}, at the start and end of the constant drying rate period. In Section 5.5.2 it developed that X_{ci} is far from being a material property. By contrast, X_{cf} is found to be independent of G and M_B, and only weakly dependent on T_i. As an approximation, accurate to within 10%, Eqn. 5.9a shows that $X_{cf}/X_o \simeq 0.45$. Thus for the through drying of paper, neither the initial nor final critical moisture

contents are material properties, but X_{c_1} and X_{cf} have very different sensitivities to drying conditions. The onset of the constant drying rate period (X_{c_1}) is highly sensitive to all drying variables, while the termination of the constant rate period (X_{cf}) is almost uniquely a function of the initial moisture content.

Previously only Chu and Kuo[1967] proposed correlations to predict X_{cf} in through drying of paper. They proposed relations for the various critical moisture contents that they defined, in each of which X_{cf} was assumed a function of water viscosity and capillary pressure. Thus their approach derived from the concept of X_{cf} for surface drying, an approach which the present study proves is totally inapplicable to the through drying of paper.

For the through drying of paper, the present study provides an experimentally verified correlation for the critical moisture content, X_{c_1}, at the transition from increasing rate to constant rate drying, a critical moisture content defined here for the first time. As for the other critical moisture content, that marking transition from the constant to falling rate period, X_{cf}, the only relation which has been subjected successfully to an extensive test is Eqn. 5.9. This correlation shows that X_{cf} is linearly dependent on initial moisture content, X_o, with a proportionality between 0.41 and 0.49 for the wide range of experimental variables tested. The final critical moisture content is found to be independent of paper thickness and air throughflow rate, and to increase only slightly with increasing throughflow temperature. More generally, it is shown that any theory developed for the surface drying is irrelevant and misleading for the case of through drying of webs of small hygroscopic fibres.

5.5.4 Extent of the Three Drying Periods

The set of drying period diagrams, Figs. 5.22-25, is prepared using Eqns. 5.8 and 5.9 for X_{Ci} and X_{Cf}. For each of four basis weights of paper used in the present experiments, 25, 50, 100 and 150g/m^2, a pair of drying period diagrams are presented, i.e. for the minimum and the maximum throughflow inlet temperature, T_i. Likewise on all drying period diagrams the lines for X_{Ci} are, for simplicity, shown only for two levels of throughflow rate, G, i.e. the minimum and maximum used in the present experiments. Thus for the four basis weights of paper tested, these 8 drying period diagrams show the effect of the extremes of throughflow rate and temperature tested. The drying period diagram for any other combination of T_i-G-M_B of interest may easily be generated with the regression equations 5 8 and 5 9 for X_{Ci} and X_{Cf}.

The fraction of moisture removed in each drying period is displayed visually on a drying period diagram. For example at X_o=3.0, Fig. 5.22b shows that for 25 g/m^2 paper dried at T_i=88°C, X_{Cf}=1.48kg/kg, so that almost 50% of its moisture is removed in the falling rate period. For this T_i-M_B-X_o combination, as G is increased from the minimum to the maximum value tested, X_{Ci} decreases from 2.22 to 1.75kg/kg. Thus the proportion of the drying that occurs in the constant rate period, $(X_{Ci}-X_{Cf})/X_o$, drops from about 25% to 9%, while that in the increasing rate period, $(X_o-X_{Ci})/X_o$, jumps from about 25% to 40%. At the highest G-highest T_i combination of the present experimental range, i.e. 0.518 kg/m^{2}s-88°C, these graphs show that as paper basis weight is decreased from 150g/m^2 to 100, 50 and 25g/m^2, the proportion of water removed in the constant rate period decreases from 29% to 26%, 18% and 9% while that for the increasing rate period doubles, from about 20% to 40%.

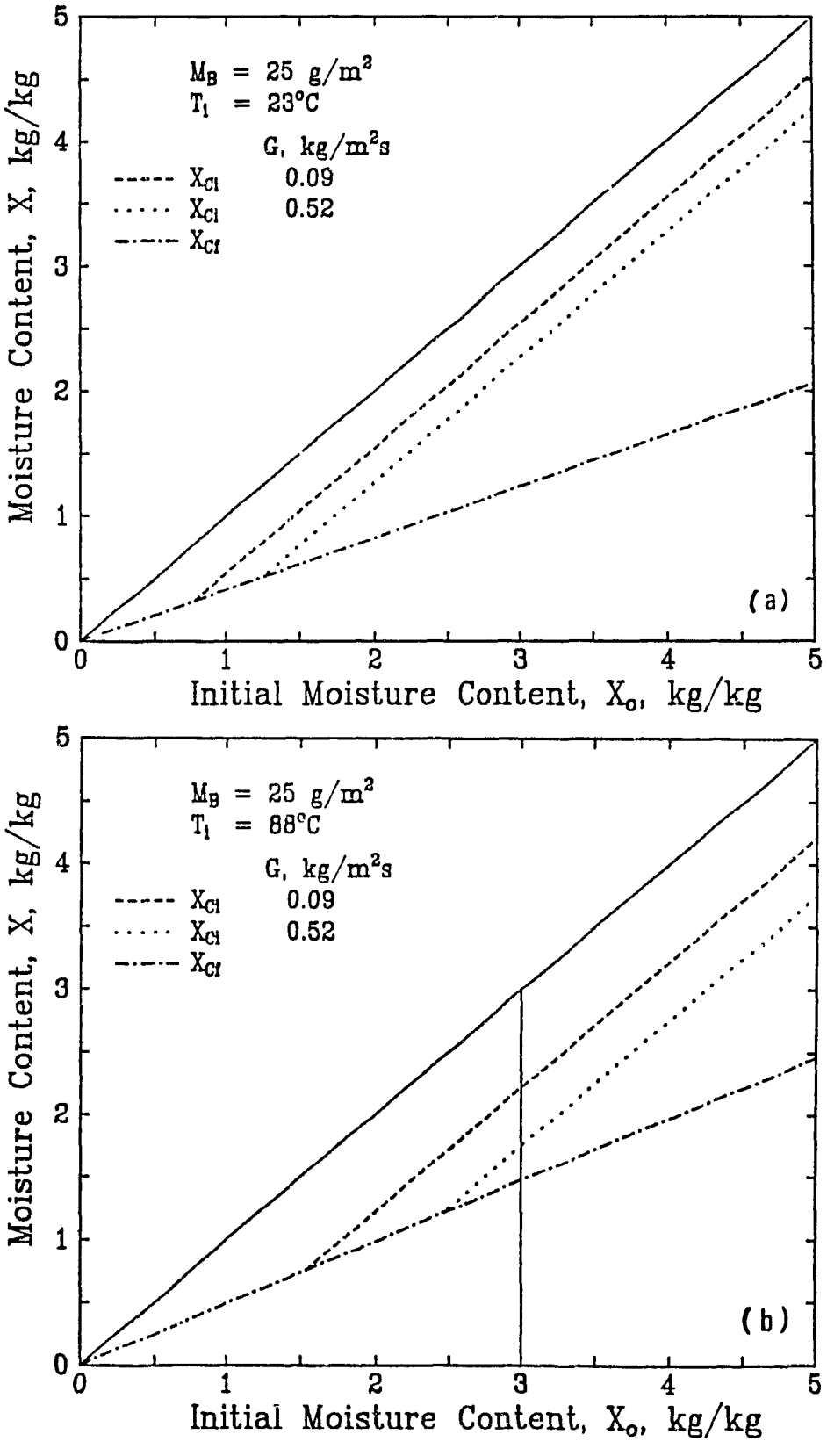

Figure 5.22 Drying period diagrams for 25g/m² paper: a) T_i=23°C, b) T_i=88°C

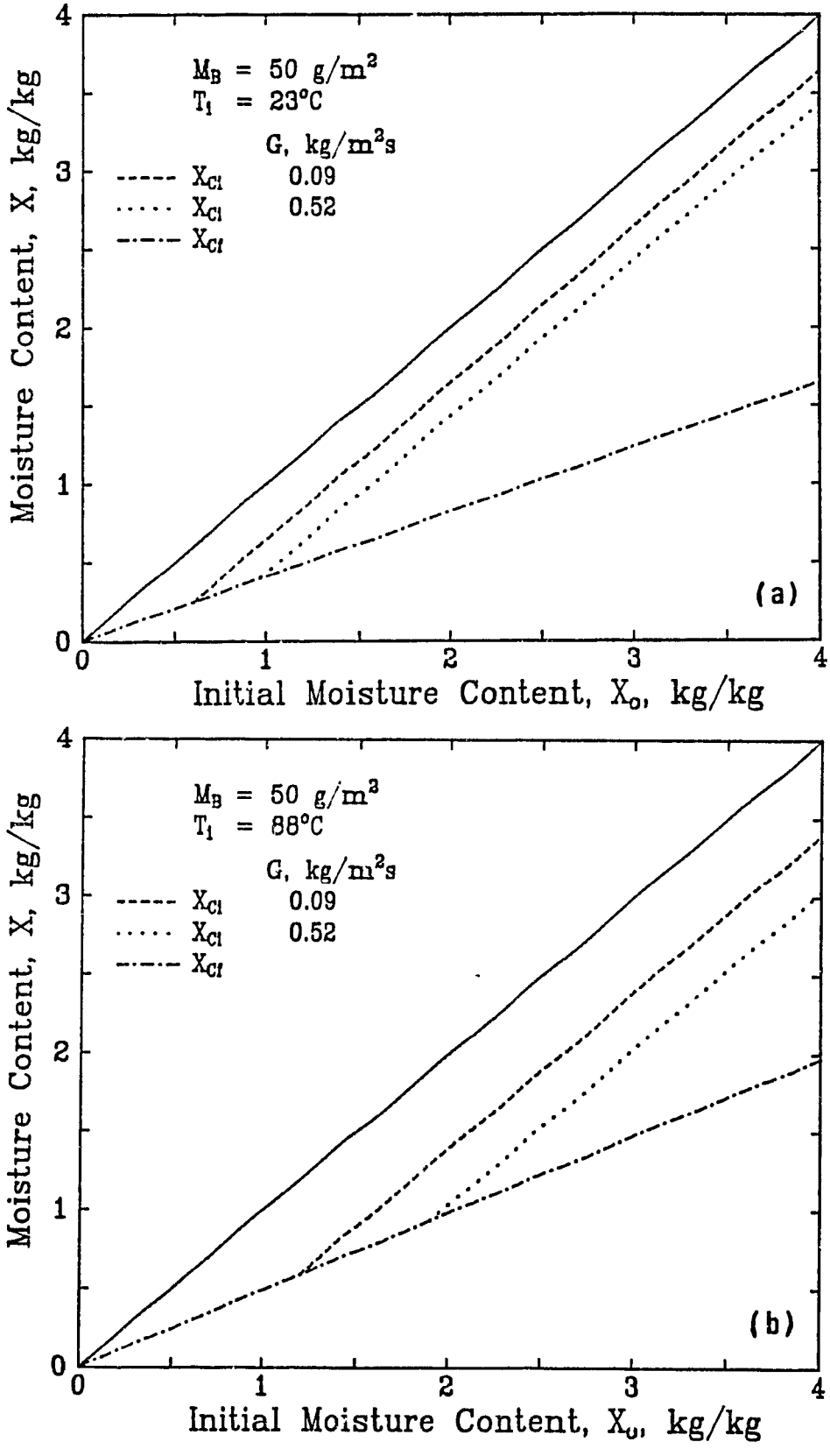

Figure 5.23 Drying period diagrams for 50g/m² paper: a) T_i=23°C, b) T_i=88°C

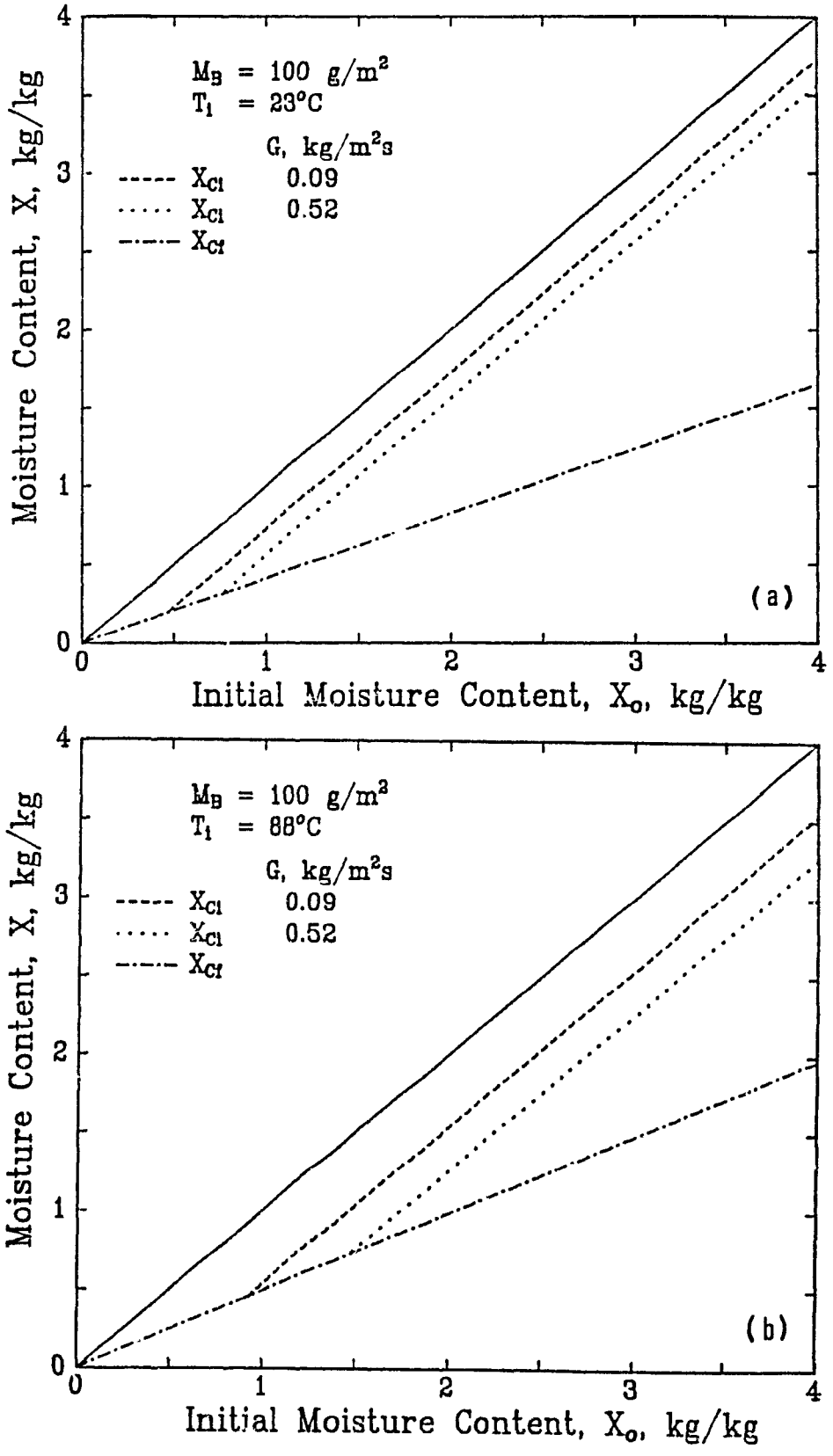

Figure 5.24 Drying period diagrams for 100g/m² paper: a) T_i=23°C, b) T_i=88°C

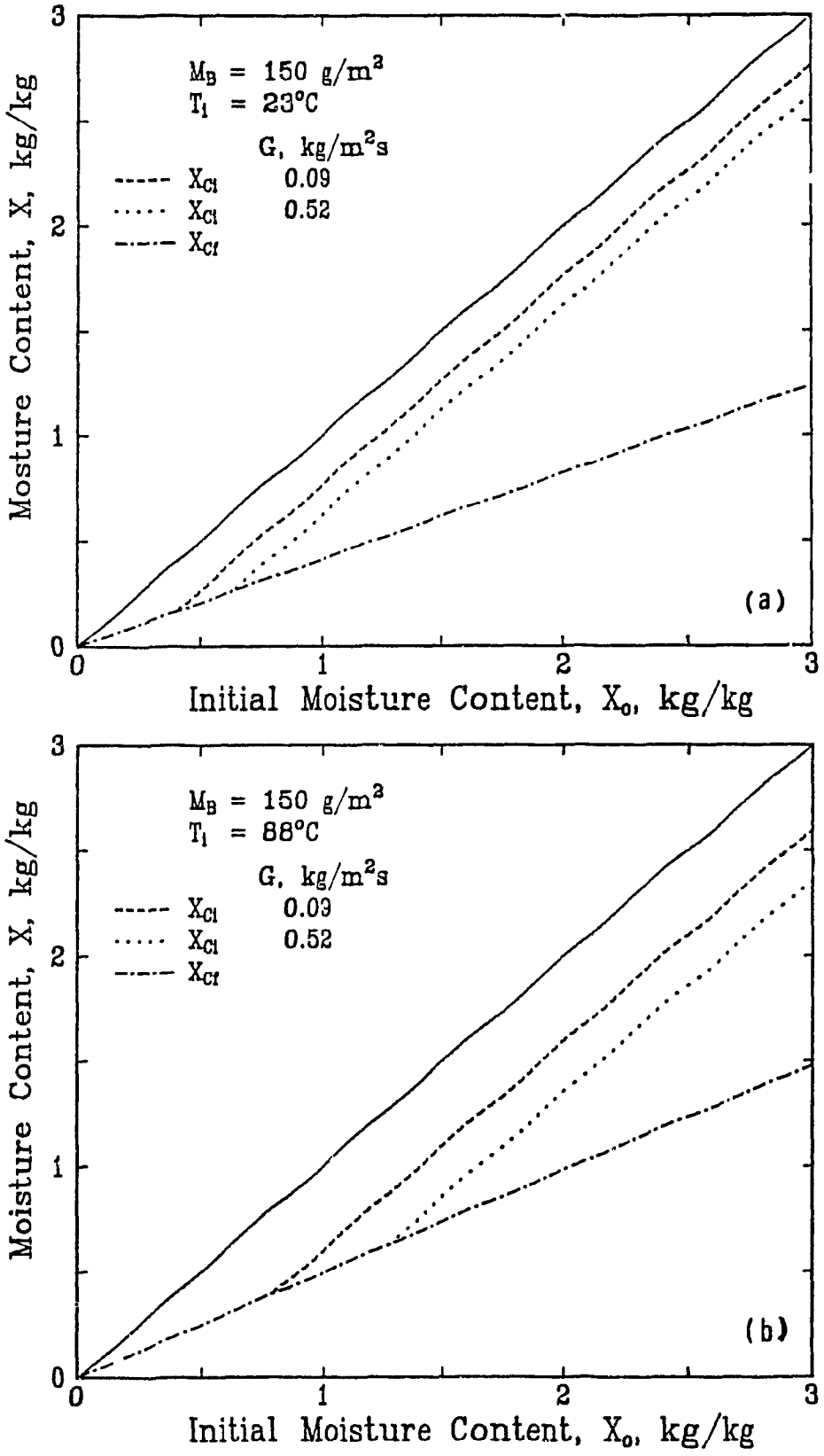

Figure 5.25 Drying period diagrams for 150g/m² paper: a) T_i=23°C, b) T_i=88°C

Thus for the highest intensity drying conditions used, even for the thickest paper tested always less than 30% of the water is removed during the constant drying rate period, while for the lightest paper dried up to 40% of the water is removed in the increasing rate period of drying.

The Figs. 5.22-5.25 set also portrays the shrinkage in extent of the constant rate period as X_o decreases. The increasing-constant-falling rate "triple point" $X_o=X_{ICF}$, is the value of X_o on each drying period diagram for which the constant rate drying condition is reached only momentarily as drying passes directly from the increasing rate to the falling rate period. A correlation for the triple point, X_{ICF}, derives from equating the X_{ci} and X_{cf} relations, Eqns. 5.8 and 5.9, as

$$X_{ICF} = \frac{(T_i-T_S)^{0.39}\, G^{0.27}}{M_B^{0.37}\,(1-0.29(T_i-T_S)^{0.13})} \qquad (5.10)$$

Thus the disappearence of the constant rate period occurs at higher values of X_o as drying intensity increases (higher G and T_i) and as basis weight decreases, as is intuitively evident. These effects of drying conditions on the value of X_{ICF} are shown explicitly in Fig. 5.26. The line for the highest temperature and rate of throughflow tested in the present study, T_i=88°C and G=0.518kg/m^{2}s, illustrates that for through drying 25g/m^2 paper, there is no constant rate drying period at all if $X_o \leq 2.5$kg/kg.

For the case of the highest G-highest T_i used, the relative importance of the three drying rate periods for water removal is illustrated explicitly on Figs. 5.27a and 5.27b for initial moisture contents, X_o, of 2.0 and 3.0kg/kg. These representations underline three basic characteristics: (1) the insensitivity of the fraction of the water which is removed during the falling rate period, a weak function

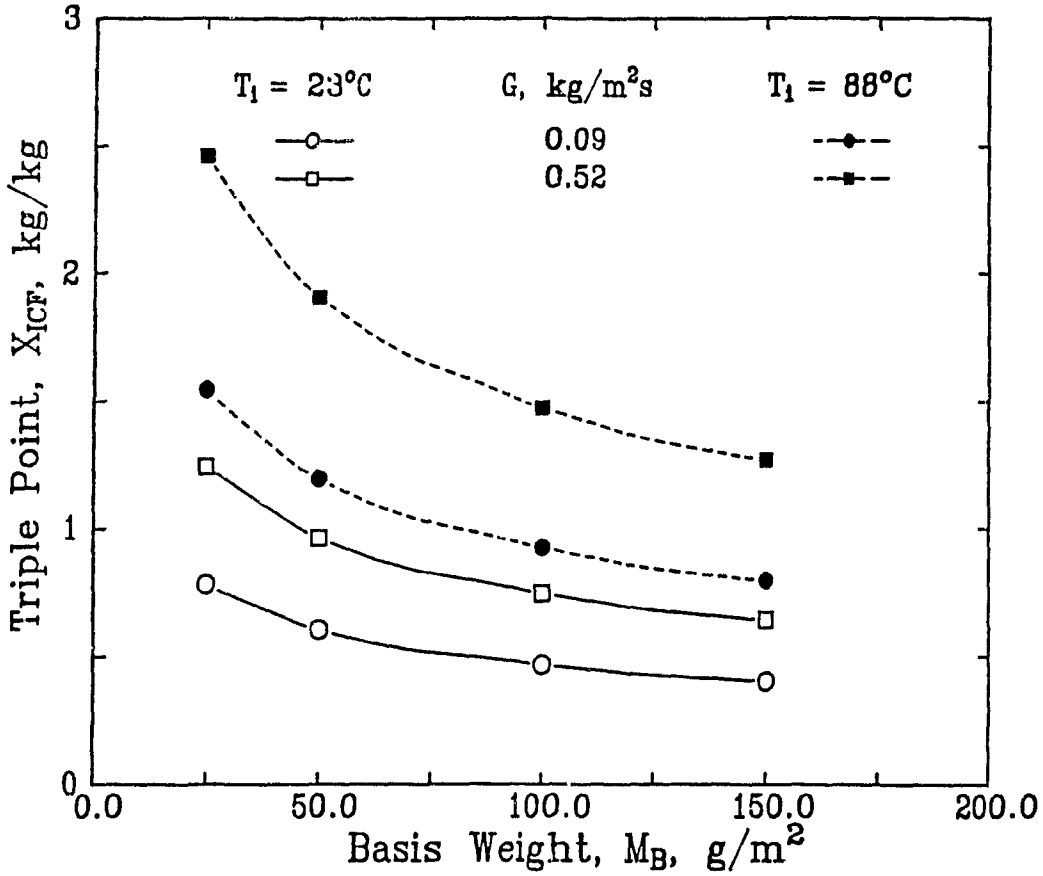

Figure 5.26 Effect of drying conditions on the triple point

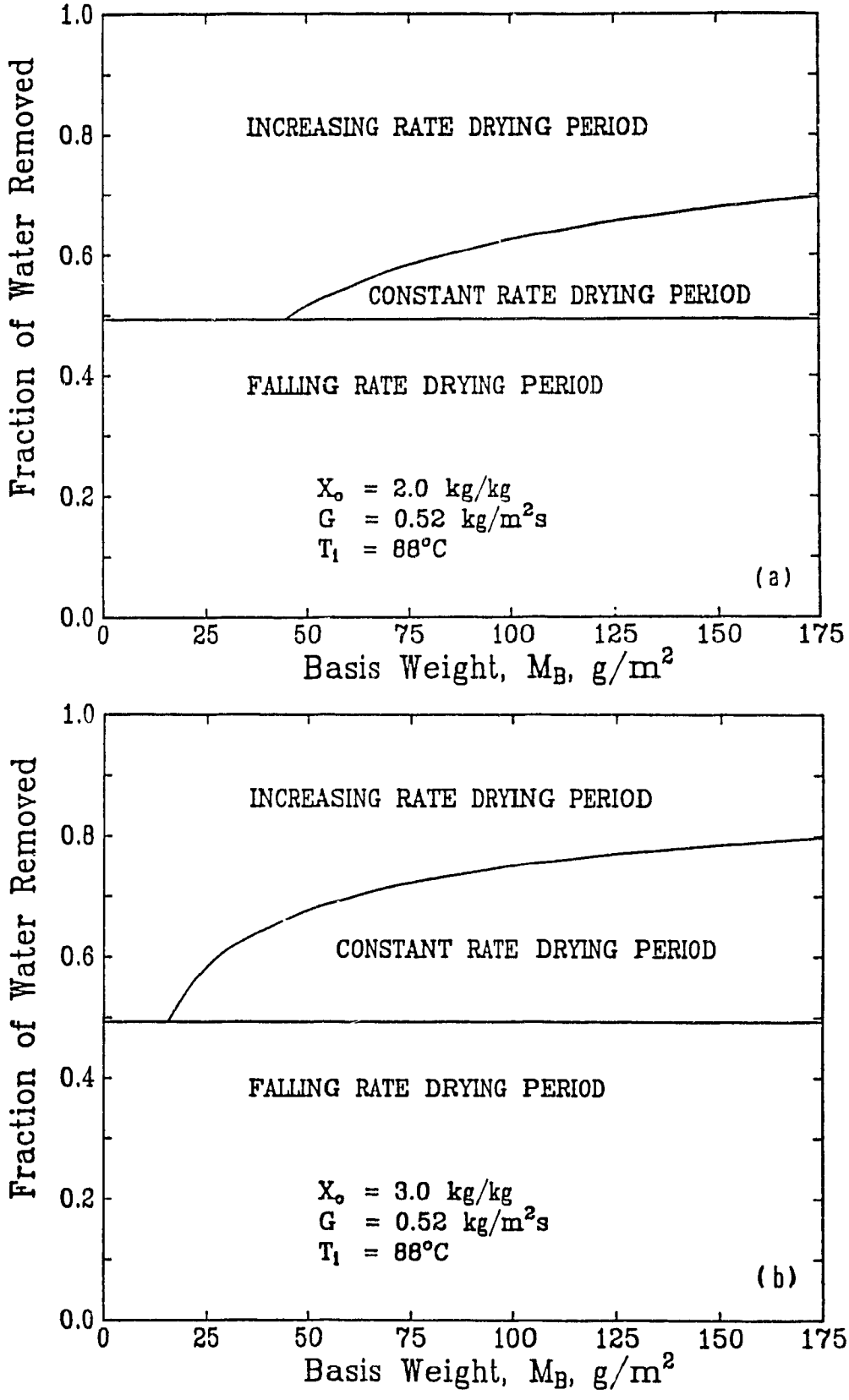

Figure 5.27 Extent of drying rate periods at high throughflow temperature: a) X_o=2.0kg/kg, b) X_o=3.0kg/kg

only of throughflow temperature, T_1, (2) the shrinking importance of the constant rate drying period at lower values of initial moisture content, X_o, and lower basis weight, M_B, and (3) the great importance, previously unrecognized, of the increasing rate period of drying. Plots equivalent to Figs. 5.27a and 5.27b for other drying conditions can readily be generated with the regression Eqns. 5.8 and 5.9.

For industrially used conditions of higher temperature and rate of throughflow air than tested in the present study it is evident from Figs. 5.26 and 5.27 that for tissue paper there would be no constant rate drying period. Inspection of Figs. 5.27a and b indicates that for industrially used conditions for through drying of tissue paper, essentially half the water is removed in the increasing rate period and half in the falling rate period of drying.

Although classical drying literature has focussed much attention on the constant rate period, for through drying at industrially relevant conditions for webs of hygroscopic fibres of the size in paper, there is typically no constant rate period. Attention should therefore be focussed where the action is, i.e. on the falling rate drying period, which has been studied extensively, and on the increasing rate drying period, the importance of which has not previously been recognized. One of the merits of the drying period diagram representation developed here is the highlighting of the relative importance of the three drying periods, directing attention on those of greatest significance. The use of drying period diagrams is therefore recommended as an aid to the analysis of through drying of paper or of any fine particulate.

5.6 SUMMARY

1) Complete drying rate curves were determined for the through drying of paper over a wide range of precisely controlled operating variables, i.e. for 235 combinations of drying conditions - temperature and rate of the through- flow, basis weight and initial moisture content of the paper. The present experimental program, with its limitations, constitutes the most comprehensive investigation of through drying yet reported.

2) This extensive set of drying rate curves indicates that through drying starts with an increasing rate period, recognized and named in the present study, which is shown to be of great importance in through drying. Thus the present study provides a new perspective on the through drying of paper as consisting of three drying periods, those of increasing, constant and falling rate drying.

3) The increasing rate period is associated with a progressive opening of pores which increases drying rate by increasing the area for heat and mass transfer within the web, as documented in the effect of paper moisture content on effective pore size and permeability in Chapter 4.

4) For light weight paper of typical initial moisture content,as through drying conditions become more intensive i.e. with higher values of throughflow rate and temperature, the constant drying rate period at first decreases, then disappears. For moderate to heavy paper of higher initial moisture content, the constant rate period retains an important role in water removal by through drying.

5) Through drying rates for the constant rate period, R_c, were measured for drying conditions which gave a wide range in R_c, from 2-40

kg/m^2h. For basis weights of 25 and 100g/m^2 the measured values of R_C agree as well as could be expected with the only comparable data available, those of Walser and Swenson[1968] and Gummel[1977].

6) The first comprehensive correlation for through drying rates of paper in the constant rate period, successfully tested for a wide range of drying conditions, is Eqn. 5.1,

$$R_C = 2.4\ (T_i - T_S)^{0.87}\ G^{0.80}\ M_B^{0.16}$$

R_C is quite sensitive to throughflow rate and temperature, only weakly dependent on basis weight, and independent of initial moisture content of the paper.

7) Through drying rates in the constant rate period, R_C, deviate by up to 50% from R_S, the maximum rate with the air exiting saturated. The extent of this deviation increases as the temperature and rate of throughflow increase, as paper basis weight decreases, but is independent of initial moisture content, according to the Eqn. 5.3 relation:

$$(R_C - R_S)/R_S = 0.0083\ (T_i - T_S)^{0.68}\ G^{0.92}\ M_B^{-0.50}$$

This finding shows that the assumption of throughflow air exiting saturated, made in some earlier work due to the lack of experimental measurements, is not appropriate because this assumption can lead to overpredicting drying rate by more than a factor of two for conditions of industrial relevance.

8) The correlations obtained in the present study for the through drying rates in the constant rate period are found to predict the drying rates reported for industrial through dryer applications remarkably well, despite the fact that the throughflow rates and temperatures used to derive these correlations are lower than industrial practice.

9) An original treatment of the relation between drying conditions and the extent of each drying period, i.e. increasing, constant and falling rate periods, was developed in a graphical form denoted "drying period diagrams".

10) The values of paper moisture content which mark the transition from the increasing to constant drying rate period, and from the constant to falling drying rate period, designated here as the "initial" and "final" critical moisture contents, X_{C_i} and X_{Cf}, are related to the drying conditions according to the Eqns. 5.8 and 5.9:

$$X_{C_i} = X_o - (T_i - T_S)^{0.39} G^{0.27} M_B^{-0.37}$$

$$X_{Cf} = 0.29 X_o (T_i - T_S)^{0.13}$$

11) The correlation for the initial critical moisture content, X_{C_i}, a drying parameter treated here for the first time, shows that for the through drying of paper, the onset of the constant rate period is sensitive to all drying variables.

12) By contrast, the final critical moisture content, X_{Cf}, for the through drying of paper is directly proportional to initial moisture content, X_o, with the proportionality, X_{Cf}/X_o, being independent of throughflow rate and basis weight and only weakly dependent on throughflow temperature. For the range of throughflow temperatures from 23° to 88°C, the final critical moisture content, X_{Cf}, varies only between 41 and 49% of X_o.

13) The drying period diagrams show that the amount of drying which occurs in the increasing drying rate period varies considerably with drying conditions, becoming higher with increasing throughflow temperature and rate and with decreasing basis weight. At the condition of highest T_i - highest G-lowest M_B tested, the amount evaporated during

the increasing drying rate period is large, about 1.25kg water/kg dry fibre. For the condition of highest intensity through drying tested, almost half the water present initially is evaporated during the increasing rate period, about half during the falling rate period.

14) The concept was introduced of an increasing-constant-falling rate triple point, X_{ICF}, where $X_{ci}=X_{cf}$. For an initial moisture content $X_o=X_{ICF}$, the constant rate drying condition is reached only momentarily as drying passes directly from the increasing rate to the falling rate period. For any X_o below X_{ICF} there is no constant rate period of drying. The demonstrated relation between drying conditions and the value of X_{ICF} was established as Eqn 5.10;

$$X_{ICF} = \frac{(T_i-T_s)^{0.39}\ G^{0.27}}{M_B^{0.37}\ (1-0.29(T_i-T_s)^{0.13})}$$

For the highest T_i-highest G-lowest M_B condition tested, X_{ICF}=2.5kg/kg, indicating no constant rate drying period for $X_o \leq 2.5$kg/kg.

15) According to present findings, there is typically no constant rate period for industrial conditions of through drying light weight grades of paper because for these conditions X_{ICF} is generally higher than X_o values used commercially.

16) The way in which critical moisture content at the end of the period of constant rate drying, X_{cf}, relates to paper properties and drying conditions is found to be completely different between through drying and surface drying. In surface drying, X_{cf} is reported to depend on paper thickness, on drying air temperature, on drying rate and on initial moisture content. In through drying of paper, X_{cf} is demonstrated here to be independent of paper thickness, and the dependence on drying air temperature is in the opposite direction from that for surface drying. With increasing air temperature, X_{cf} decreases in surface

drying because of the controlling rate of transport of water through the solid, while X_{cf} increases in through drying paper because of the effect of temperature on the rate of heat transfer from the throughflow to the fibres. Thus theories for surface drying are totally inapplicable to through drying of small hygroscopic particles such as the fibres in paper. The X_{cf} critical moisture content for paper, strongly dependent on drying rate conditions for surface drying, is nearly independent of throughflow conditions for through drying but is linearly proportional to initial moisture content

17) With respect to industrial practice, the present findings underline two important facts, that through drying rates are generally less than 50% of the maximum rate corresponding to the throughflow exiting saturated and, that typically the paper remains in the increasing rate period for about half the dryer, in the falling rate period for the remainder. This perspective dimensions the substantial potential there is for improvement of the efficiency of these dryers As the present study establishes that about half of such a dryer operates in conditions of the increasing rate period, and that those drying rates are limited by the development of pore area for heat and mass transfer within the web, the results of the present work point the way for work to increase the efficiency of through drying of paper

CHAPTER 6

TRANSPORT PHENOMENA IN THROUGH DRYING OF PAPER

6.1 INTRODUCTION

For the process of through drying there are two natural alternatives for expressing drying rate, i.e. either relative to the external surface area or to the amount of the material being dried. Drying rates normalized to external surface area relate directly to the area of the dryer and hence to its cost. This was the basis adopted in Chapter 5. However, because through drying takes place throughout the wet material, for a more fundamental analysis drying rate must be expressed relative to the amount of material. Thus rate of mass transfer for flow through packed beds and other porous media is normally expressed per unit volume. An additional complication arises in through drying if the bulk density of the porous media is a function of moisture content, as is the case for paper. With the variable paper thickness not known precisely as a function of moisture content during drying, an alternative is to normalize drying rate to the amount of dry fibre rather than to a variable volume. This factor may become important during the falling rate drying period during which the shrinkage occurs, but would not be a significant factor while the fibres are still wet, i.e. up to the end of the constant rate period.

Of the three periods of through drying paper - the increasing rate, constant rate and falling rate periods - only in constant rate period does the simplification of steady state conditions apply. The complication of variable volume of the paper during the falling rate period was noted above. For a transport phenomena analysis there are yet more formidable

difficulties for the increasing rate and falling rate periods. As sheet temperature may change substantially, this aspect complicates the energy balance during these unsteady state periods. The vapor pressure of water at the evaporating interface changes for this reason during both the increasing and falling rate periods, while it changes with paper moisture content as well during the falling rate period. Finally, there is the problem of obtaining a quantitative treatment for the rapid increase in interfacial area of heat and mass transfer between the throughflow and the moist paper during the increasing rate period In view of these obstacles to obtaining a rigorous transport phenomena treatment of the increasing rate and falling rate periods of through drying, the focus here is on the constant rate period, for which obtaining a transport phenomena analysis represents a challenge not previously solved.

Even if mass transfer coefficients could be determined for conditions of the constant rate period, there remains the need for a dimension which characterizes flow through paper, the characteristic dimension required for every nondimensional variable - Reynolds, Sherwood, Nusselt and Peclet number. The various empirical characteristic dimension definitions tested in Chapter 4 all gave values very different from those of the actual pore structure determined by scanning electron microscopy(SEM). On the basis of this evidence, all previously proposed empirical definitions of characteristic dimension must be rejected as invalid. In Chapter 4 a new characteristic dimension for flow through paper, $d_p=\beta/\alpha$, was determined from the application of a momentum transport analysis in which α and β are complex parameters. It was established that this theoretically based definition of d_p gives values consistent with the pore structure observations by SEM. The characteristic dimension $d_p=\beta/\alpha$

as developed for paper in this study was successfully applied in Chapter 4 to a nondimensional friction factor-Reynolds number analysis of momentum transport. This definition of characteristic dimension is now used in an attempt to obtain the first transport phenomena analysis of the constant rate period of through drying paper.

6.2 MASS TRANSFER COEFFICIENT

For a binary gas phase system, mass transfer film theory for unidirectional transport gives the local values of molar fluxes, expressed by Bird *et al.*[1960] as

$$1 + (y_W^* - y_{W\infty})/[n_W/(n_W + n_A) - y_W^*] = \exp\left((n_W + n_A)/k_G'\right) \qquad (6.1)$$

where n_W and n_A are the local values of the molar fluxes of water vapor and air at the mass transfer interface, y_W^* and $y_{W\infty}$ are the mole fractions of water vapor at this interface and in the bulk gas phase, and k_G' is the molar mass transfer coefficient, moles/m^{2}s. This equation has been applied for transfer coefficients in both surface and through drying, e.g. Schlünder *et al.*[1977]. For small values of the mole fraction of transferring component, y_W^* and $y_{W\infty}$, and because n_A=0 for air-water vapor system, Eqn. 6.1 may be linearized as

$$n_W = k_G' (y_W^* - y_{W\infty}) \qquad (6.2)$$

Converted from mole to mass flux, this equation becomes

$$N = k_G \rho_a (Y^* - Y) \qquad (6.3)$$

where **N** is the mass flux of water vapor, k_G the mass transfer coefficient, m/s, ρ_a the air density, and the absolute humidity of air is Y^* at the transfer surface and Y in the bulk gas phase, with all terms representing the local values within the sheet. The correct mass transfer driving force is considered to be the difference in water vapor partial

pressure rather than absolute humidity. However, for the present experimental conditions giving highest transfer rates the two driving forces differ, according to the relation of Keey[1972], but only about 1%.

The local differential mass balance at any point z within a sheet of paper being dried by throughflow is

$$G\ (\partial Y/\partial z) = a_p\ \mathbf{N} = k_G\ a_p\ \rho_a\ (Y^* - Y) \qquad (6.4)$$

where G is the mass throughflow rate of air, kg/m^2s, and a_p is the interfacial mass transfer area, i.e. the specific surface of paper, m^2/m^3. For the case of Y^*, a_p, ρ_a and k_G being independent of position within the sheet, and for plug flow within the sheet, integration of Eqn. 6.4 over the thickness of the sheet gives

$$k_G a_p \rho_a L/G = \ln [(Y^* - Y_i)/(Y^* - Y_o)] = (Y_o - Y_i)/\Delta Y_M \qquad (6.5)$$

where L is the thickness of paper, Y_i and Y_o are the absolute humidity of the throughflow air at the inlet and exit of the sheet, and ΔY_M is the log mean value of the mass transfer driving force, $\Delta Y = Y^* - Y$, between the evaporating surface and the throughflow air.

The values of **N**, Y_o, and Y^* vary during both the increasing rate and falling rate periods, a_p varies during the increasing rate period, while ρ_a and L vary during the falling rate period because of sheet shrinkage. Thus the information required for application of Eqn. 6.5 during the increasing rate or falling rate period does not exist. However Eqn. 6.5 may be applied to the period of constant rate drying during which **N**, ρ_a, L, Y_o and Y^* are at steady state values and Y^* is essentially constant across the sheet. As for interfacial area of mass transfer, if a_p for moist paper as a function of moisture content were not known, interfacial area could be combined with the area-based transfer coefficient, as is standard practice, to give a volumetric

mass transfer coefficient, $k_G a_p \rho_a$, per unit volume of wet sheet.

Eqn. 6.1 is not valid for very high transfer rates, for which the correction factor given by Bird *et al.*[1960] is

$$k_G'^* = k_G' \, \phi/(e^{\phi} - 1) \qquad (6.6)$$

where $k_G'^*$ is the corrected coefficient, and ϕ the mass transfer rate factor defined as $\phi=(\mathbf{n}_W+\mathbf{n}_A)/k_G'$. For small values of y_w and y_∞, the correction factor, $\phi/(e^{\phi}-1)$, approaches unity. In the present work the adiabatic saturation temperature of air at the highest throughflow air temperature used is ~30°C, for which $y^*\simeq 0.04$. When this, the highest possible driving force, is inserted into Eqn. 6.1, the value of ϕ thus calculated corresponds to a correction factor $\phi/(e^{\phi}-1)=0.98$. Thus no correction for high mass transfer rate is needed for the present study.

6.3 MASS TRANSPORT PARAMETERS FOR THE CONSTANT RATE DRYING PERIOD

6.3.1 Selection of Characteristic Dimension in Nondimensional Numbers

For a nondimensional analysis of transport phenomena occuring in through drying of a porous medium of the complexity of paper a key aspect is selection of the characteristic dimension for use in Reynolds, Sherwood, Nusselt or Peclet number. In the absence of reliable measurements with moist paper, those previous investigators who have used a characteristic dimension for momentum, heat or mass transport analysis of flow through paper have based such a dimension on measurements for dry paper, either before or after drying. Empirical definitions used for a characteristic dimension for flow through paper are reciprocal of specific surface, Robertson and Mason[1949], square root of permeability, Raj and Emmons[1975], fibre diameter, Wedel and Chance[1977], and equivalent diameter from the Hagen-Poiseuille

equation, Gummel[1977]. Moreover, all previous researchers have used the Darcy's law approximation which applies for purely viscous flow, ignoring the inertial contribution that the present study, Chapter 4, has shown to be a dominant component of pressure drop for air throughflow at industrially relevant rates for through drying. But even when permeability and specific surface are determined without the error associated with the Darcy's law approximation, Chapter 4 of the present study shows that the pore size distribution of dry paper extends to about 50μm whereas $\sqrt{k}$ and $1/a_p$, correctly determined, are in the order of a micron. Thus the empirical definitions of characteristic dimension which have been used for Re, Sh, Nu and Pe are not remotely consistent, even for dry paper, with the actual pore structure.

The present study has presented and validated for both dry and moist paper a definition of characteristic dimension which is based on fundamental momentum transport theory, Chapter 4. The range of values found for this theoretically based d_p coincide with those observed by scanning electron microscopy, Figs. 4.16 and 4.20. The relationship $d_p=f(X,M_B)$ for 25 and 50g/m^2 paper, from wet to dry, was documented in Fig. 4.21, Eqn. 4.16 and Table 4.12 The d_p determinations of the present work, Table 4.10 and Fig. 4.20, and the mean pore radius measurements of Bliesner[1964] by the gas-drive technique show that d_p for dry paper is essentially independent of basis weight for $M_B \geq 50$g/m^2. Moreover, the pore size shown by SEM cross-sections, Fig 4.16, is likewise similar for 50, 100 and 150g/m^2 sheets. As the best current estimate, therefore, the d_p-X relationship for 100 and 150g/m^2 kraft paper can be approximated as that determined here for 50g/m^2 basis weight.

Use of these d_p-X-M_B relations to determine d_p for Reynolds and

Sherwood number in the constant rate period of drying evidently requires the paper moisture content. In Chapter 5 the initial and final critical moisture contents, X_{Ci} and X_{Cf}, which mark the beginning and end of constant rate through drying, were defined and related to the determining variables. Thus the relations needed are:

$X_{Ci} = f(T_i, G, M_B, X_o)$ given by Eqn. 5.8,

$X_{Cf} = f(T_i, X_o)$ given by Eqn. 5.9, and

$d_P = f(M_B, X)$ given by Eqn. 4.16 and Table 4.12.

The moisture content, X, used for the d_P-X relation, is the average during the constant rate period, i e. $X=(X_{Ci}+X_{Cf})/2$. In this way, for each sheet dried the characteristic dimension, d_P, used in the nondimensional numbers, Re and Sh, depends on the conditions of the throughflow air, T_i and G, and those of the paper, M_B and X_o.

Each d_P value for the constant rate period given in Table 6.1 for the 64 experimental combinations of T_i-G-M_B was obtained by averaging the d_P values of from 2-4 experiments conducted with various values of X_o. Thus the effect of initial paper moisture content on d_P, through the effect of X_o on X_{Ci} and X_{Cf}, is present in the Table 6.1 although X_o does not appear explicitly.

For the kraft paper used in the present study the maximum and minimum values of d_P during the increasing rate and falling rate periods repectively, are 44μm and 16.7μm for 25g/m^2 sheets, and 14μm and 5μm for 50-150g/m^2 sheets, Fig. 4.21, Eqn. 4.16 and Table 4.12. Comparison of these limiting values with the d_P values given in Table 6.1 shows that the characteristic pore size for the constant rate drying period is closer to the maximum d_P of the increasing rate period than to the minimum d_P reached during the falling rate period. It should be appreciated that,

Table 6.1 Characteristic dimension of paper during constant rate period of through drying

G, kg/m²s	Throughflow temperature, T_1, °C 23	42	64	88	$\overline{d_P}$, μm
		M_E = 25 g/m²			
0.092	39.5	44.0	39.4	39.3	40.5
0.155	27.9	34.3	41.6	37.4	35.3
0.289	29.1	39 4	31.1	29.7	32.3
0.518	21.4	35 9	26.1	39.7	30.8
$\overline{d_P}$	29.5	38.4	34.5	36.5	34.7
		M_E = 50 g/m²			
0.092	9.9	12 9	14.0	12.3	12.3
0.155	12.6	12.3	13.0	14.0	13.0
0.289	12.7	12 8	13 6	12.3	12.9
0.518	11.4	12 5	13 5	12.0	12.4
$\overline{d_P}$	11 7	12 6	13.5	12.6	12.6
		M_E=100 g/m²			
0.092	8.9	10 2	14.0	10.3	10.9
0.155	10.4	9.1	11.1	12.6	10 8
0.289	11.4	9 6	11 8	10.3	10.8
0.518	10.4	8 9	12.0	12.4	10.9
$\overline{d_P}$	10.3	9.5	12 2	11.4	10.8
		M_E=150 g/m²			
0.092	5.8	6 4	11 0	14.0	9.3
0.155	6.7	9 5	9.9	11.7	9 4
0.289	9.0	8 8	9.5	9.8	9.3
0.518	9.2	9 6	11 3	9 9	10.0
$\overline{d_P}$	7 7	8 6	10 4	11 4	9.5

although d_P values are listed in Table 6.1 with respect to values of G and T_1, d_P is of course not a function of G and T_1. As $d_P=f(M_B, X)$, and the moisture content limits X_{C1} and X_{Cf} of the constant rate period are dependent on T_1, G, M_B and X_o, the Table 6.1 listing simply reflects the fact that the drying rates were measured for the 16 combinations of T_1 and G shown.

It may now be seen that previous researchers of through drying who have used a characteristic dimension based on one of the several empirical definitions listed earlier, Robertson and Mason[1949], Raj and Emmons

[1975], have reported values of Re, Sh or Pe which are between one and two orders of magnitude too low because their definitions of characteristic dimension give values which are too low to that extent. The error from these inappropriate definitions of characteristic dimension has been further increased because in all cases they used the value determined for dry paper while the present work shows that the characteristic dimension for moist paper may be 200-300% higher.

6.3.2 Determination of Transfer Area

Measurement or prediction of interfacial mass transfer area is a difficult aspect of the determination of mass transfer coefficient, k_G, Eqns. 6.4 and 6.5. In Chapter 4 the specific surface of dry paper was determined from the experimental measurements of permeability by using the widely accepted Carman-Kozeny equation The accuracy of such a_p values are very sensitive to the porosity function, $\varepsilon^3/(1-\varepsilon)^2$, of this equation. Due to the lack of a method for accurate determination of the ε-X relation, wet paper specific surface cannot be determined from the wet paper permeability measurements made, as discussed in Section 4.6, nor has any work been published on the effect of paper moisture on its porosity or specific surface.

If the pores were straight cylinders, i.e. of tortuosity $\tau=1$, with pore length equal to the paper thickness, L, then a_p would be inversely proportional to d_p. For cylindrical pores, the specific surface, a_p, equals $(n\pi\overline{d_p}L)/(n\pi\overline{d_p}^2L/4)=4/\overline{d_p}$. Table 6.2 shows this estimate of the transfer area of moist paper during the constant rate period of drying. Although individual d_p and $4/d_p$ values were calculated for each sheet dried, Table 6.2 shows for illustration purposes only the estimates with

the average value, $\overline{d_p}$, from Table 6.1. Dry paper comparative values are shown for a_p as correctly determined in Chapter 4 from the measured permeability and the Carman-Kozeny equation, and a_p as estimated from the relation $4/d_p$.

Table 6.2 Transfer area of moist paper during the constant rate drying period, and of dry paper

	Moist paper constant rate period		Dry paper			
M_B, g/m^2	$\overline{d_p}$, μm	$4/\overline{d_p}$, m^2/m^3	$4/d_p$, m^2/m^3	a_p, m^2/m^3	$\tau=a_p/(4/d_p)$	L, μm
25	34.7	0.12×10^6	0.25×10^6	0.76×10^6	3.0	58
50	12.6	0.32×10^6	0.76×10^6	1.04×10^6	1.4	114
100	10.8	0.37×10^6	0.80×10^6	1.19×10^6	1.5	227
150	9.5	0.42×10^6	0.85×10^6	1.34×10^6	1.6	350

For dry paper, the true specific surface is seen to be substantially larger than that given by the $4/d_p$ approximation. The values of tortuosity, $\tau=a_p/(4/d_p)$, in the range 1.4 to 3 are in fact quite acceptable for paper, Brown[1950]. No information is available as to the variation of tortuosity with paper moisture content. Going from wet to dry paper, τ will increase because the smallest pores have the highest tortuosity, but no quantitative basis for the τ-X relation exists. In the absence of such information, the tortuosity for moist paper during the constant rate period of drying is taken as $\tau=1$, and the mass transfer area for moist paper during the constant rate period, required for Eqn. 6.5, is approximated as $a_p=4/\overline{d_p}$, as listed in Table 6.2.

The only previous investigator of through drying paper whose treatment involved specific surface, Gummel[1977], used dry paper pressure drop to estimate the specific surface, assuming only pin holes are open to flow. Then he used this a_p for the constant rate period of

drying Although throughflow is mainly governed by the larger pores or pin holes during the constant rate period of drying, Gummel's a_p estimate using dry paper pressure drop is erroneous. In any case, the data in Table 6.2 indicate that the use of dry paper a_p instead of that for a moist sheet may correspond to the use of an a_p value too high by a factor of about 3-6.

6.3.3 Number of Transfer Units

The local differential mass balance for water vapor

$$dN_G = \frac{dY}{Y^*-Y} = \frac{dY}{\Delta Y} = \frac{k_G a_p \rho_a}{G} dz \qquad (6.7)$$

when integrated with the same constraints valid for the constant rate period as for Eqn 6.5, leads to the definition of integral number of transfer units for the constant rate period

$$N_G = \frac{k_G a_p \rho_a L}{G} = \frac{L}{H_G} = \ln \frac{Y^*-Y_1}{Y^*-Y_o} = \ln \frac{\Delta Y_1}{\Delta Y_o} = \frac{Y_o-Y_1}{\Delta Y_M} \qquad (6.8)$$

in which height of a gas phase transfer unit is $H_G = \frac{G}{k_G a_p \rho_a}$. The assumption of plug flow within the sheet used to derive Eqn. 6.8 is normally applied for through drying, Schlunder *et al.*[1977]. Moreover, as no measurement of gas phase axial dispersion for flow through paper has been reported, there is no alternative to using this standard assumption.

The number of transfer units is a nondimensional measure of the amount of mass transfer which occurs during the constant rate period in the continuous contacting of air and wet fibres from inlet to outlet of the sheet. One "transfer unit" of mass transfer occurs in a depth of porous media over which the gas stream composition, absolute humidity in this case, changes by an amount, Y_o-Y_1, equal to the mass transfer driving force, $\Delta Y_M=(Y^*-Y)_M$.

The transient exit air humidity, Y_o, is monitored during a through

drying experiment with a sampling frequency of 5-10Hz, Chapter 5. Thus from these values, N_G as a continuous function of paper moisture content, X, could be determined for each drying experiment, from which the value of N_G applicable for the constant rate period could be obtained. However, as such N_G-X drying rate curves would correspond to the R-X curves already available in Chapter 5 for the external surface area based drying rate, R, it is equivalent, and much simpler, to obtain the constant rate period values of N_G directly from R_C This procedure avoids duplicating the Chapter 5 procedure for identifying the constant rate period value from the complete record of drying rate for each experiment.

The external surface based drying rate at any time is

$$R = G\ (Y_o - Y_i) \tag{6.9}$$

The maximum rate of drying, i.e. with the air exiting saturated, is

$$R_S = G\ (Y^* - Y_i) \tag{6.10}$$

Combining equations 6 9 and 6 10 gives

$$\frac{R}{R_S} = \frac{(Y_o - Y_i)}{(Y^* - Y_i)} = 1 - \frac{(Y^* - Y_o)}{(Y^* - Y_i)} = 1 - e^{-N_G} \tag{6.11}$$

which may be expressed alternately as

$$N_G = \ln\left(\frac{R_S}{R_S - R}\right) \tag{6.12}$$

Therefore by use of Eqn 6.12 with $R=R_C$, the value of the volumetric drying rate expressed as the integral number of transfer units for the constant rate period can be calculated directly from the values documented in Chapter 5 for R_C, the external surface based drying rate during the constant rate period.

6.3.4 Mass Transfer Coefficients

For through drying of paper during the constant rate drying period the mass transfer coefficient, k_G, and its nondimensional equivalent,

Sherwood number, may be calculated from the corresponding N_G value from

$$N_G = \frac{k_G a_p \rho_a L}{G} = \frac{k_G d_p}{D} \quad \frac{\mu}{G d_p} \quad \frac{\rho_a D}{\mu} \; a_p L = \frac{Sh}{ReSc} \; a_p L \qquad (6.14)$$

Selection of values for specific surface, a_p, and thickness, L, is an important factor

Because sheet shrinkage takes place during the falling rate period of drying, L in Eqn. 6.14 is fairly constant in the paper moisture range between X_{c_i} and X_{cf}, the constant rate period limits. When completely swollen, never-dried fibres have a hollow cylindrical shape. As moisture leaves the fibre wall and lumen during the drying of never-dried fibres, they collapse, giving the ribbon like shape of dry fibres. Once collapsed, a fibre never returns to its original cylindrical shape upon rewetting. In laboratory drying studies, the present one and all previous investigations, handsheets are prepared from dry pulp, then wetted to the desired initial moisture content The thickness change during drying of paper made from the collapsed fibres of dried pulp is then much smaller than that with never-dried fibres. Thus approximating moist paper thickness, L, in Eqn. 6 14 as the thickness of dry paper at the end of through drying does not introduce appreciable error in mass transfer coefficient determination in laboratory drying studies.

For mass transfer in beds of complex internal structure with indeterminant interstitial transfer area, volume based transfer coefficients, i.e. $k_G a_p \rho_a$, are used. In the present work, however, the interstitial transfer area is determined as a function of drying conditions as described in Section 6.3.2. Thus the area-based mass transfer coefficient, k_G, and its nondimensional form, $Sh=k_G d_p/D$, can be calculated from Eqn. 6.14. A complete list of all experimental runs with corresponding M_B, G, T_i, R_C, R_S, N_G, k_G, Re and Sh values is given in Appendix 8.

6.4 MASS TRANSFER PHENOMENA DURING THE CONSTANT RATE PERIOD OF DRYING

6.4.1 Experimental Results

The amount of drying during the constant rate period, expressed nondimensionally as the number of transfer units, $N_G = \frac{k_G a_p \rho_a L}{G}$, includes specific surface, a_p, which in Section 6.3.2 was shown to be a function of the initial moisture content of paper, X_o. Specific surface introduces substantial variability in N_G because X_o was varied between 1.5 to 4.5kg/kg in the present study. As the alternate nondimensional representation of throughflow mass transfer, Sh, does not suffer from such an effect, mass transfer coefficients are reported here in the form of Sherwood number. N_G and Sh are related through Eqn. 6.14

Figs. 6.1 through 6.4 display the results expressed as Sh as a function of Re for the through drying of a total of 210 sheets of kraft paper. These four figures display the results of all sheets dried in the present study, with the exclusion of only those few cases where the exiting air was within 1% of saturation, for which the mass transfer driving force becomes too small for reliable determination of mass transfer coefficient. Each of Figs 6.1-6.4 presents all the results for one basis weight, 25, 50, 100 and 150g/m^2, with as a parameter the second key variable, the temperature driving force at the inlet, ΔT_i, in the nominal range of 15-59°C. The same Re and Sh scales are used for all four data sets so that the results can be seen in a common Re-Sh perspective.

For the present experiments ΔY_o at the exit of the sheet varied from ~1% to ~48% of that entering the sheet, ΔY_i. Correspondingly, ΔY_M varied from 1 to 16g/kg. In those experiments where exit air humidity approaches saturation a larger scatter in Sh data is expected because

the effect of the accuracy limit of humidity measurements is magnified as ΔY_o becomes extremely small. For example, for the heaviest paper ($150g/m^2$) dried with air of the lowest flow rate ($G=0.09kg/m^2s$) and lowest ΔT_i (15°C) air, ΔY_o is less than 0.1g/kg and ΔY_M is about 1g/kg. Even for these extreme conditions, the experimental scatter, displayed on Fig. 6.4 at low Re, is impressively small, thus confirming the high precision of the present humidity measurements and thereby, of mass transfer coefficients, k_G, and Sherwood number, Sh.

Only two investigations, Raj and Emmons[1975] and Gummel[1977], report mass transfer coefficients for through drying of paper. Both studies are incomplete as to the effect on throughflow mass transfer phenomena of two important variables, M_B and ΔT_i. Raj and Emmons varied the basis weight from 15 to $60g/m^2$, but only at a single, low value of ΔT_i, ~15°C. Gummel varied ΔT_i from ~15 to ~60°C, but only for a single basis weight of paper, $20g/m^2$ Other shortcomings of these studies are noted subsequently.

The results for the 210 M_B-ΔT_i-G-X_o combinations displayed on Figs. 6.1-6.4 thus cover a wide range of both M_B, 25-$150g/m^2$, and ΔT_i, 14-64°C, from experiments in which air throughflow rate, G, was varied from 0.09 to $0.52kg/m^2s$, with correspondingly wide variations in ΔY_o and ΔY_M, i.e. 0.03-11g/kg and 1-16g/kg. Therefore for the first time mass transfer coefficients for throughflow drying of paper are reported here over a wide range for all parameters, M_B-ΔT_i-Re-ΔY_i-ΔY_M.

6.4.2 Sh-Re-M_B-ΔT_i Relations

(a) Ceneral Correlation

The mass transfer coefficient, expressed nondimensionally as Sh,

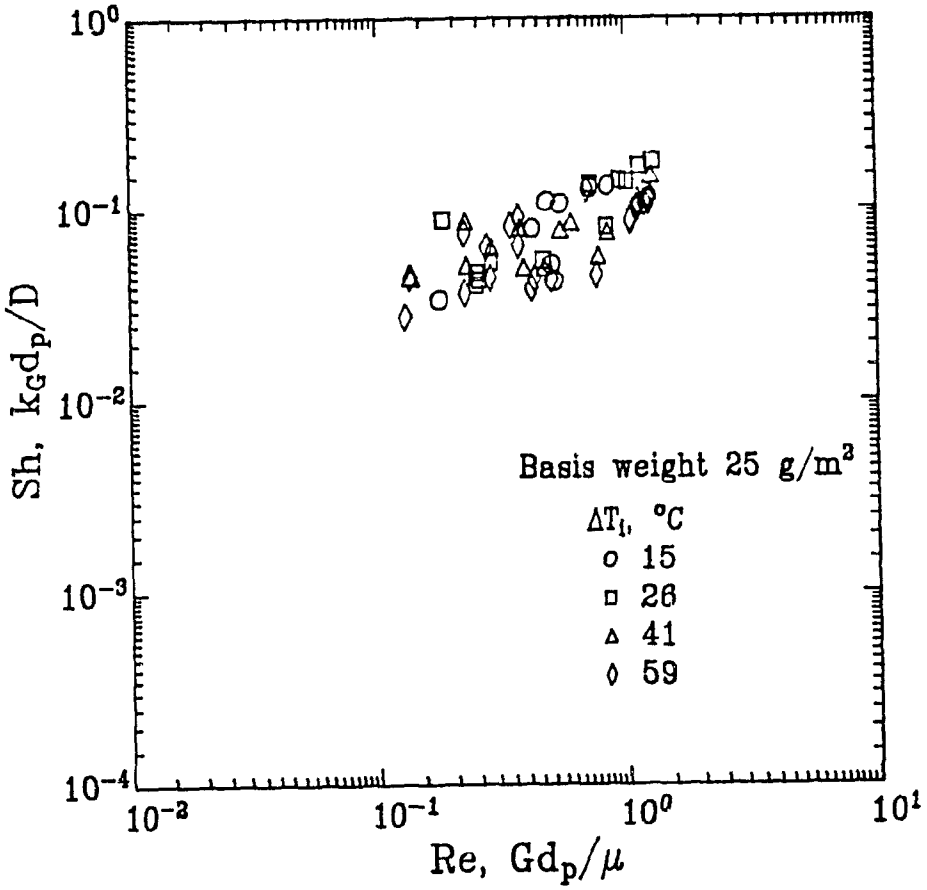

Figure 6.1 Mass transfer coefficients for through drying of paper: Experimental results, M_B=25g/m².

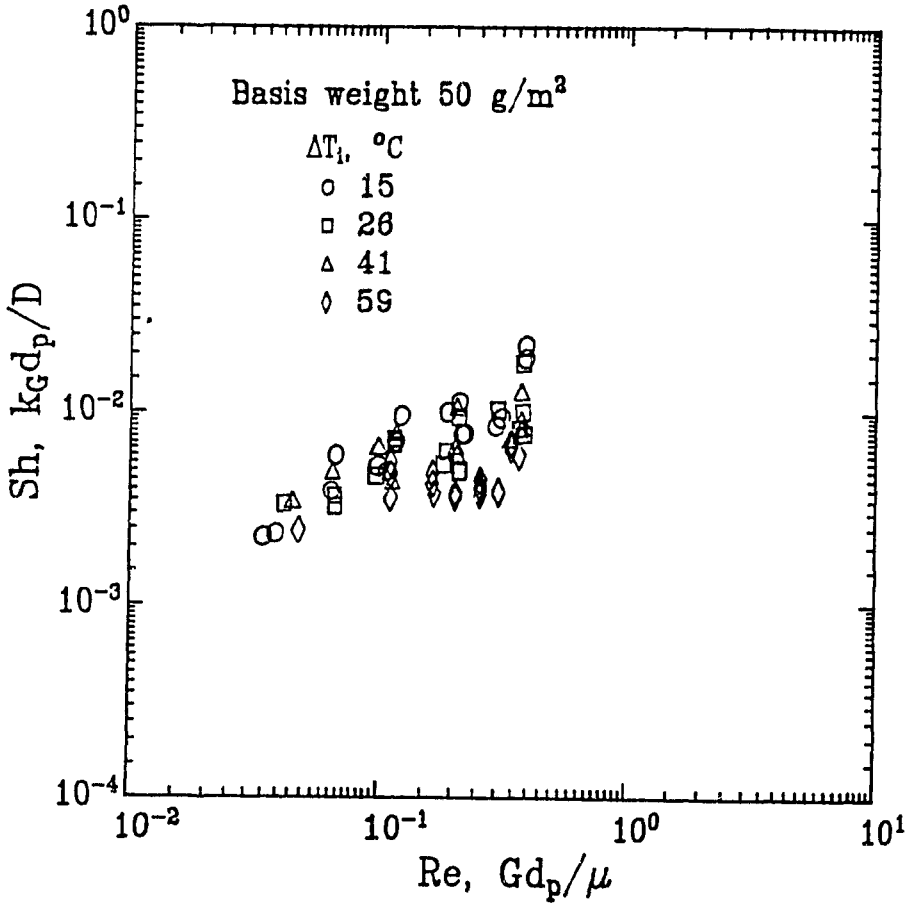

Figure 6.2 Mass transfer coefficients for through drying of paper: Experimental results, M_B=50g/m².

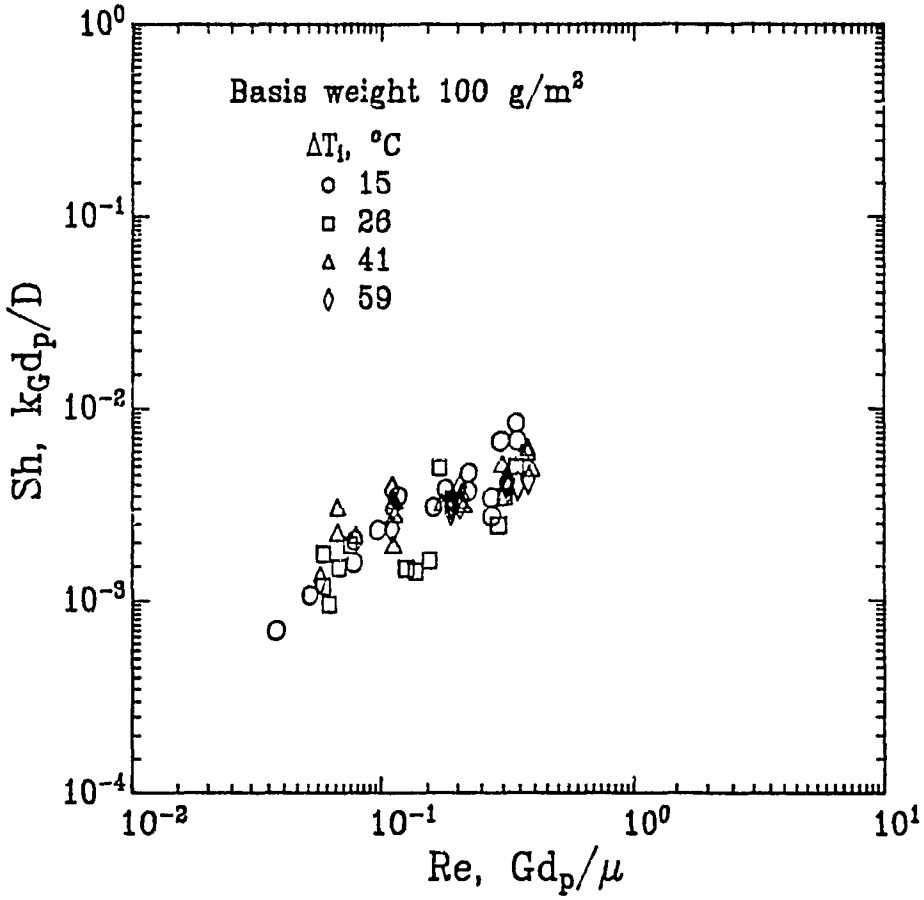

Figure 6.3 Mass transfer coefficients for through drying of paper: Experimental results, M_B=100g/m².

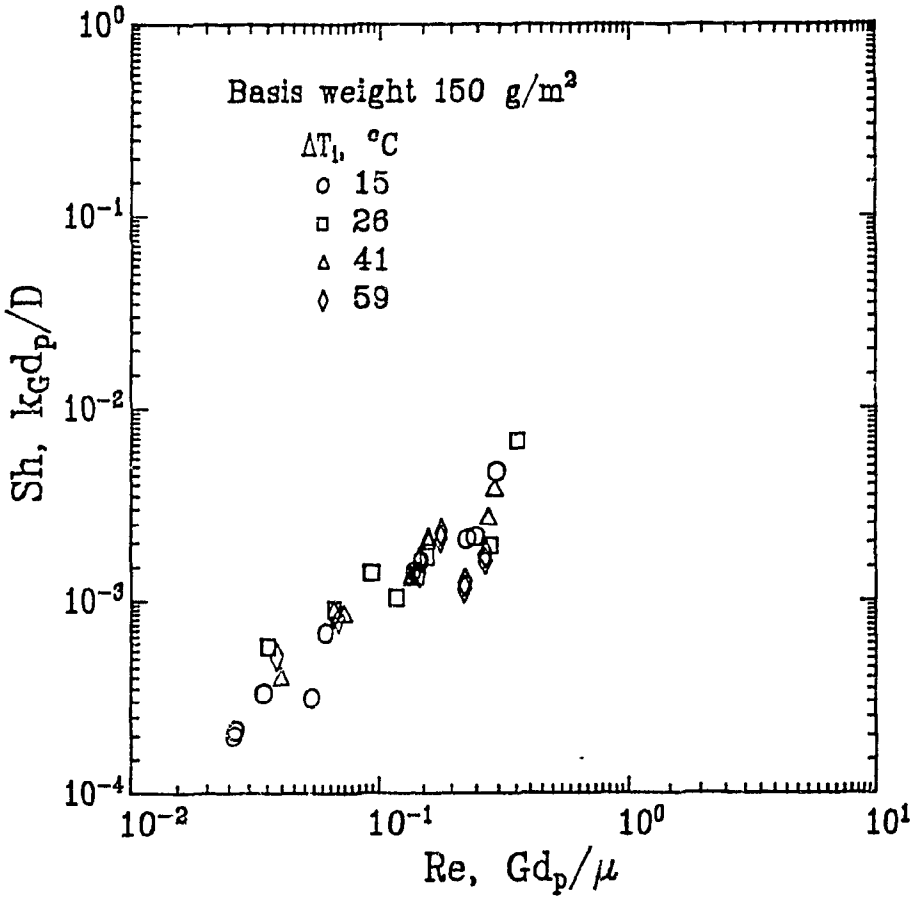

Figure 6.4 Mass transfer coefficients for through drying of paper: Experimental results, M_B=150g/m².

is represented as a function of Reynolds number,

$$Sh = a\ Re^n \qquad (6.15)$$

For comparison of results of different systems for which the physical properties represented by Schmidt number are variable, the preferred choice for nondimenional mass transfer representation is Peclet number, Pe=ReSc. However Re is used here because for the air-water vapor system within the present experimental range, Sc is effectively constant. Conversion of the present results to the ReSc form may be made using Sc=0.61. The Eqn. 6.15 regression results along with the standard error determinations are given in Table 6 3

Table 6.3 Parameters for Sherwood Number-Reynolds Number Correlation

M_B, g/m^2	ΔT_i, °C	a	n	σ_n	σ_{Sh}
25	15	0.143	0.86	0.12	0.021
	26	0 137	0.84	0 09	0.013
	41	0 101	0.47	0.12	0.017
	59	0.092	0.46	0.09	0.015
50	15	0.0314	0 75	0.09	0.0020
	26	0.0165	0 54	0.10	0.0018
	41	0.0134	0.38	0.09	0.0012
	59	0.0068	0.29	0.09	0.0010
100	15	0.0161	0.89	0.10	0.0010
	26	0.0070	0.60	0.12	0.0010
	41	0.0086	0.52	0.07	0.0006
	59	0.0068	0.46	0.07	0.0004
150	15	0.0081	0.97	0.08	0.00005
	26	0.0089	0.86	0.12	0.0010
	41	0.0106	0.95	0.08	0.0003
	59	0.0068	0.65	0.13	0.0004

The relative experimental error, σ_{Sh}/Sh, typically about 25%, increases with paper basis weight and, for a specific basis weight, increases as ΔT_i decreases. Both trends are consistent with the

associated closer approach to saturation for the throughflow leaving the sheet. For rate data of this kind these represent reasonable levels of experimental variability.

(b) Effect of M_B and ΔT_i on Reynolds Number Dependency

The strong dependency of n on both basis weight, M_B, and throughflow inlet temperature driving force, ΔT_i, apparent in Table 6.3 and displayed on Figs 6.5 and 6.6, is a central feature of the results. As for the effect of basis weight on the value of the Reynolds number exponent n, i.e. $(\partial Sh/\partial Re)_{\Delta T_i}$, Fig. 6.5 shows that with the exception of 25g/m^2 paper, n increases with M_B Thus over the 50-150g/m^2 range, as basis weight increases n approaches unity regardless of the temperature driving force. Tissue paper of basis weight 25g/m^2 forms a separate case as paper this thin cannot be treated as a packed bed, as is discussed subsequently. Fig. 6.6, analogous to Fig. 6.5, shows the effect of temperature driving force on the value of n, i.e. $(\partial Sh/\partial Re)_{M_B}$, for paper of basis weight 50-150g/m^2. In this case n approaches unity as ΔT_i becomes small. Thus the overall behaviour is that $\partial Sh/\partial Re$ approaches to unity as M_B increases and ΔT_i becomes small. When the results of various researchers for mass transfer at low Reynolds number in packed beds of small particulates are expressed in the Sh-Re form of Eqn. 6.15, the Re exponent is found to be unity, Martin[1978]. As Figs. 6.5 and 6.6 indicate a linear dependance for n as a function of both M_B and ΔT_i, the best-fit correlation for $n=f(M_B, \Delta T_i)$ was determined as follows:

$$n = 0.58 + 0.0037\ M_B - 0.0084\ \Delta T_i \qquad (6.16)$$

The lines shown on the two figures are those given by Eqn. 6.16. Although Figs 6.5 and 6.6 are presented with straight lines the

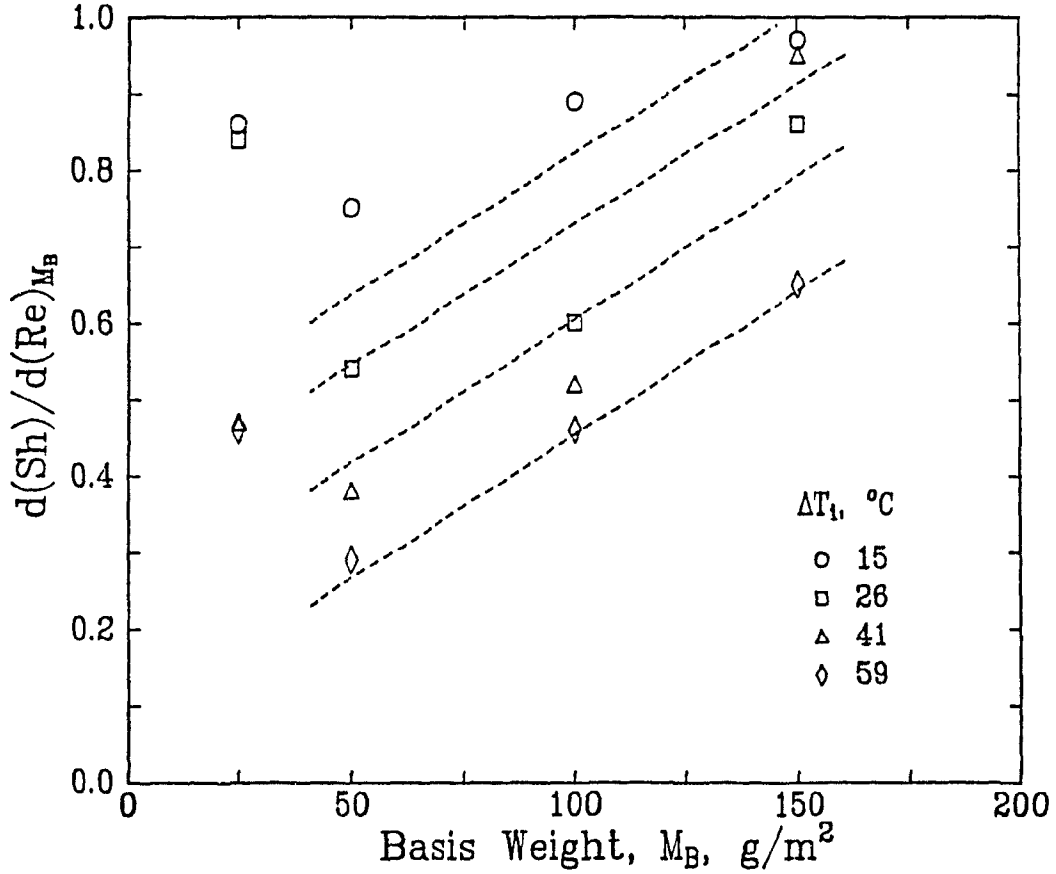

Figure 6.5 Effect of basis weight on the Re exponent of the Sh-Re relation

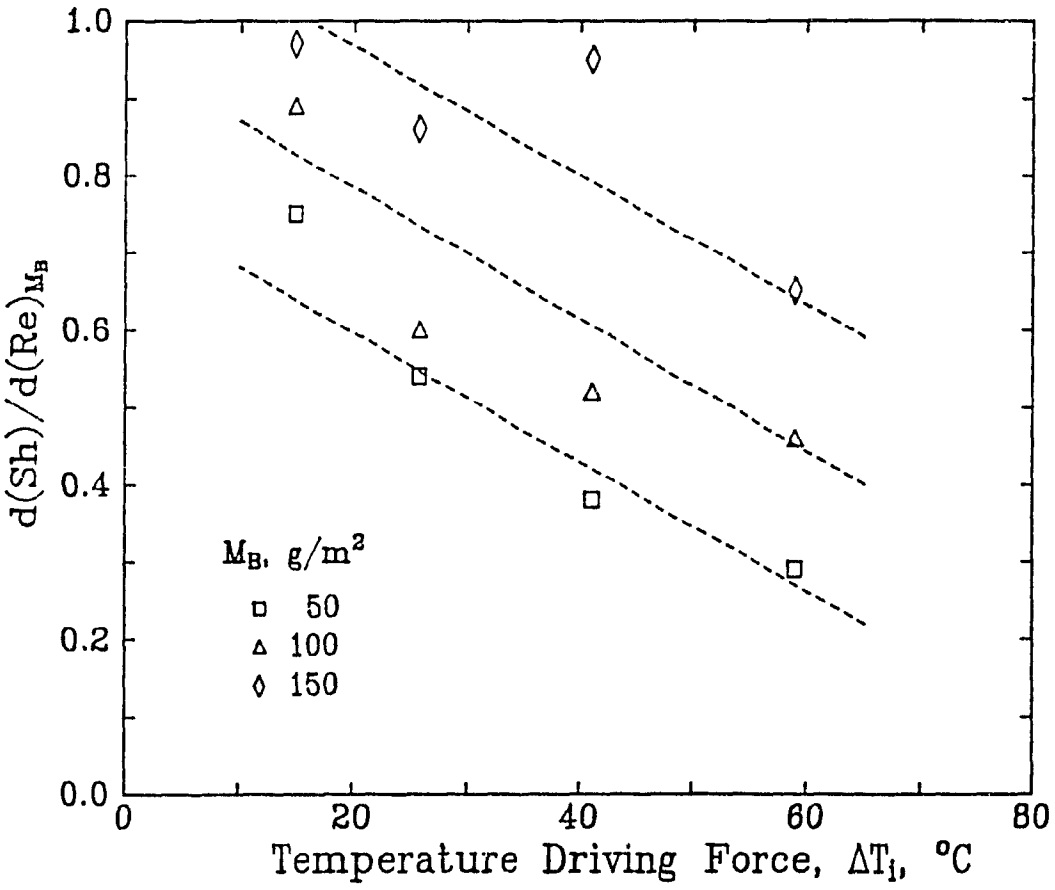

Figure 6.6 Effect of throughflow inlet temperature driving force on the Re exponent of the Sh-Re relation

expectation is that, if measurements had been made for $M_B > 150 g/m^2$ and $\Delta T_i < 15°C$, the corresponding Figs. 6.5 and 6.6 lines would curve to become asymptotic to a value of n of approximately unity.

(c) Effect of M_B on Sherwood Number

Figs. 6.7-6 10 are analogous to Figs. 6.1-6.4, except that instead of the original data, the corresponding regression lines are shown. For all four values of ΔT_i, the regression lines for the thinnest paper, $25 g/m^2$, stand clearly separate from those for all heavier grades When dried, this $25 g/m^2$ kraft paper is about 58μm thick Thus for the Table 6.1 values of $\overline{d_P}$, the $25 g/m^2$ sheet is only $1.7\overline{d_P}$ deep Transport processes for a porous media this thin are dominated by entrance and exit effects. In fact for $L=1\ 7\overline{d_P}$, this is effectively mass transfer with a screen, not in a bed. The acceleration and deceleration of flow with the corresponding sudden contraction and expansion at the entrance and exit of this "screen" account for the extra frictional losses and the enhanced heat and mass transfer rates measured in the present study for $25 g/m^2$ paper. Higher transfer rates in very short sections of whatever geometry are a well documented phenomena

For paper basis weights of 50, 100 and $150 g/m^2$, the sheet becomes $9\overline{d_P}$, $21\overline{d_P}$ and $37\overline{d_P}$ thick. As the end effect contribution would produce the same absolute enhancement in Nu and Sh, the relative importance of this effect decreases proportional to paper thickness. Figs. 6.7- 6.10 indicate that some basis weight effect on Sh is present over the basis weight range $50\text{-}150 g/m^2$, presumably becoming minimal for $M_B > 150 g/m^2$. Interestingly, for all experimental levels of ΔT_i, the Sh-Re regression lines for $50\text{-}150 g/m^2$ paper converge as Re increases, consistent with

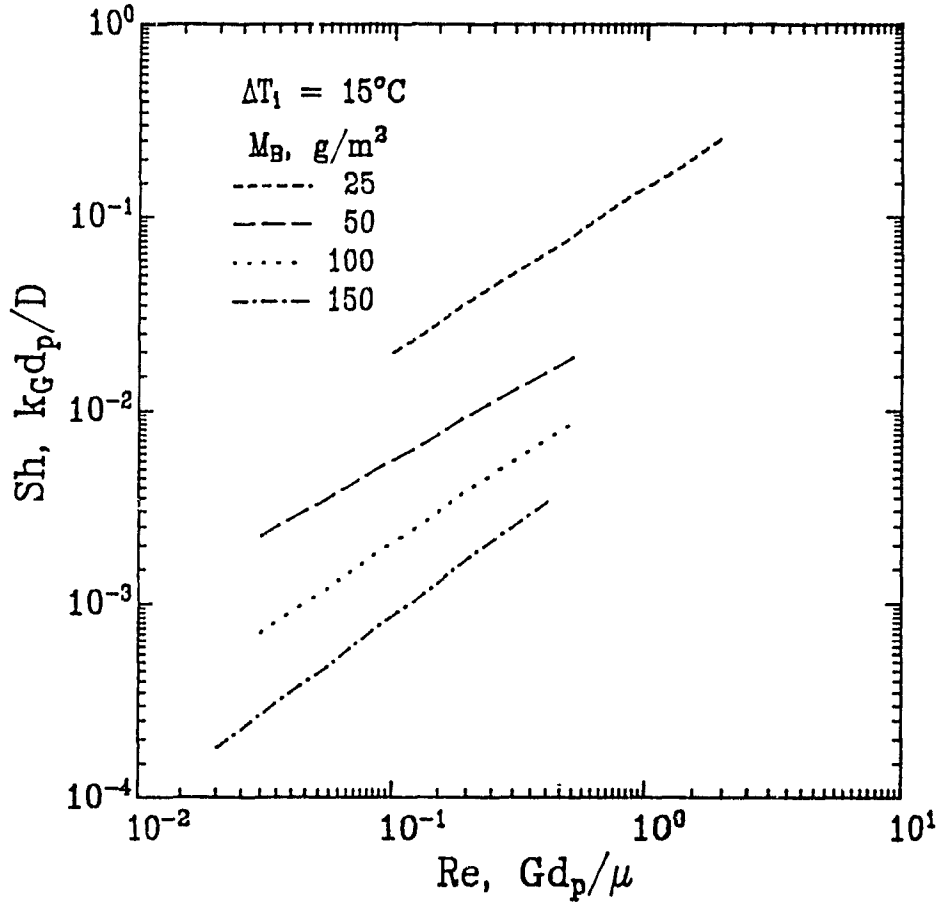

Figure 6.7 Mass transfer coefficients for through drying of paper: Regression results, ΔT_1=15°C

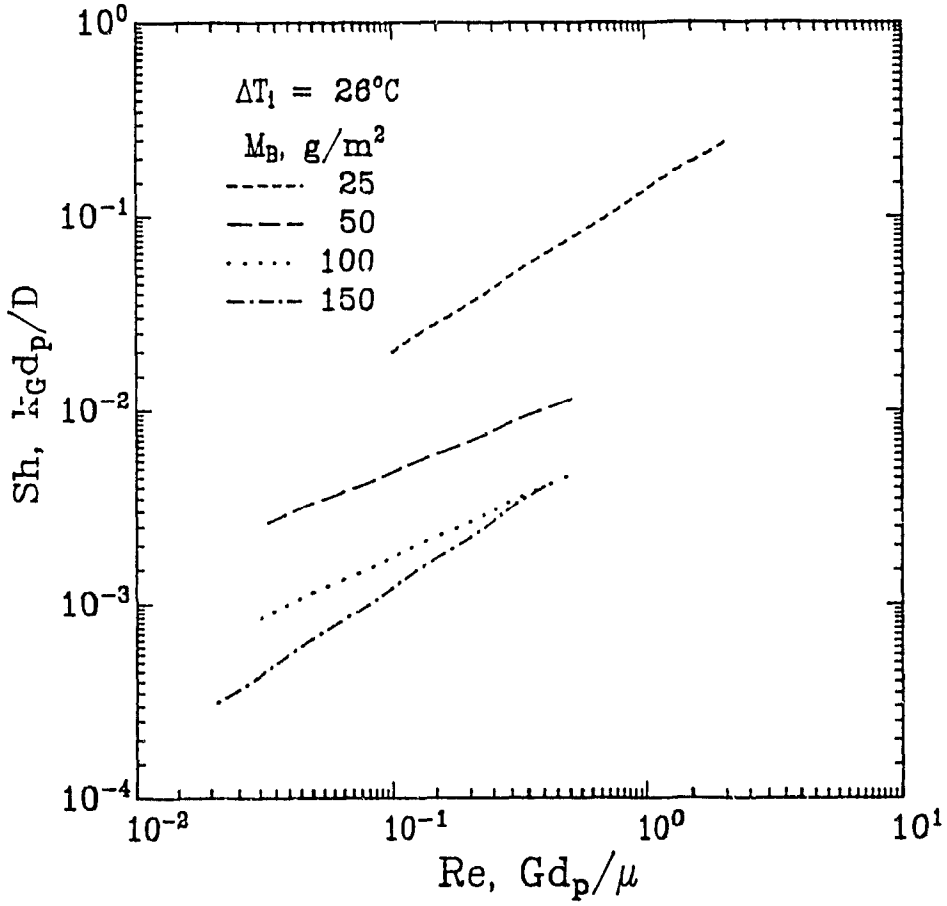

Figure 6.8 Mass transfer coefficients for through drying of paper: Regression results, ΔT_i=26°C

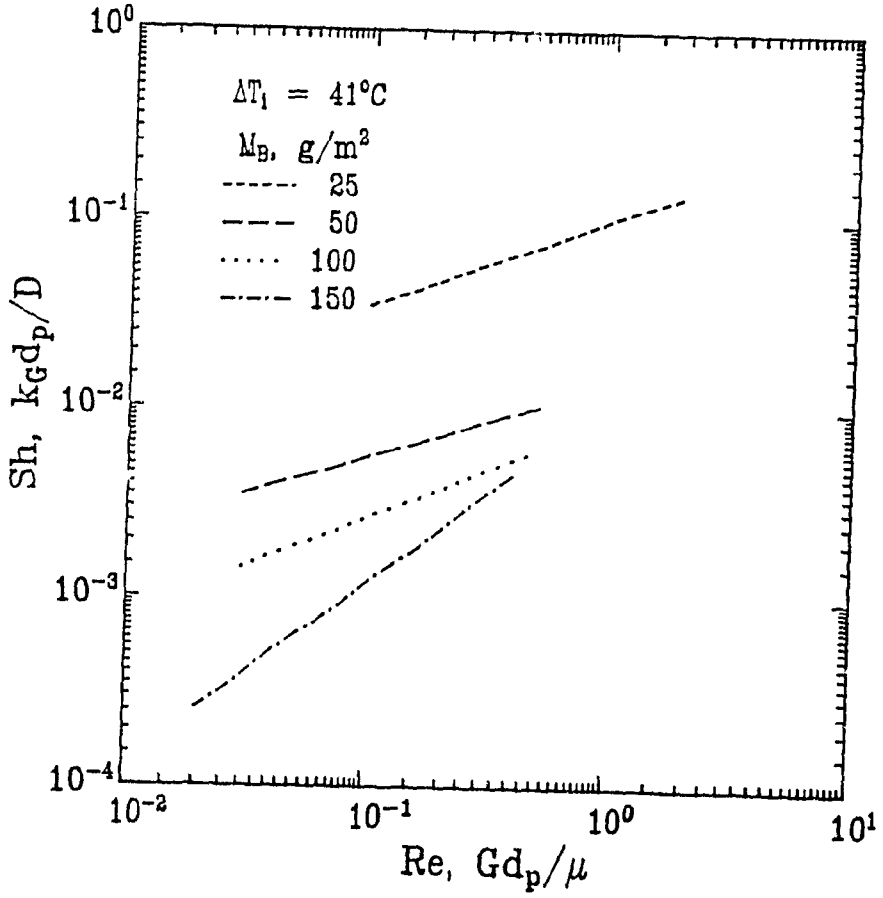

Figure 6.9 Mass transfer coefficients for through drying of paper: Regression results, ΔT_1 =41°C

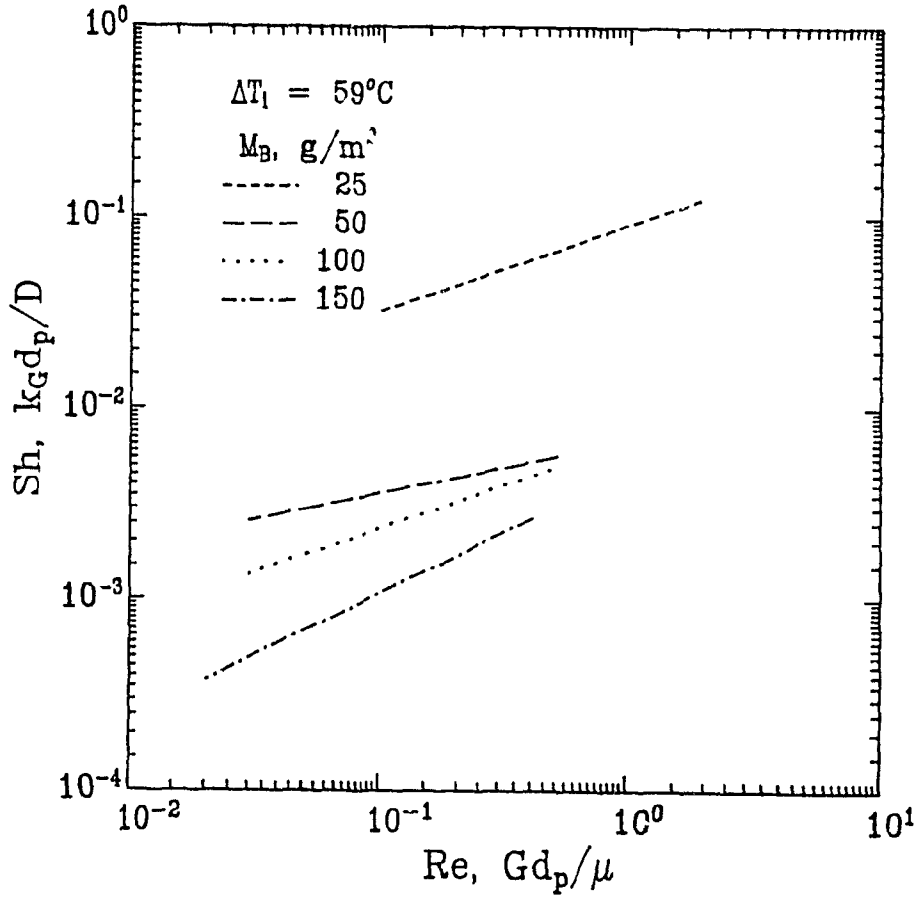

Figure 6.10 Mass transfer coefficients for through drying of paper: Regression results, ΔT_1 =59°C

the expectation that above some higher value of Re, the Sh-Re relation may become independent of M_B. The approach of the Reynolds number exponent of Sherwood number to a common value of about one at higher values of M_B, Fig. 6.5, further supports this expectation.

As mass transfer coefficients were determined here using the standard assumption of plug flow through the bed, the possible contribution of axial dispersion to the Sh-Re-M_B-ΔT_1 relations was investigated. Axial dispersion changes the temperature and concentration profiles in the flow direction so as to decrease the driving force for heat or mass transfer. To the extent that axial dispersion is present, values of Sh calculated with the assumption of plug flow would be correspondingly lower than the "true" values, i e those determined with the true driving force for the actual degree of axial dispersion. The effect of axial dispersion on mass transfer in a packed bed decreases sharply with increasing bed depth, Ercan[1989] As on Figs. 6.7-6.10 the trend is always for Sh to be higher for thinner paper for which the axial dispersion effect should be more important, axial dispersion is not the source of the segregation of results with respect to paper thickness observed here. In any case, no measurements of gas phase axial dispersion for flow through paper have been reported As Sherman[1964] pointed out, the axial dispersion characteristics of a fibre bed are determined by the web structure, the wide pore size distribution and the high porosity. As there is no geometrical similarity between the internal structure of paper, a consolidated bed of ribbon like fibres, and beds of rigid particles of simple shape, axial dispersion for paper cannot be predicted with any reliability from information available for beds of large, simple particles. Martin[1978] also found that the effect of

axial dispersion is not sufficient to explain the low transfer coefficients reported by various researchers.

A significant effect which has been ignored by previous researchers is the convective heat and mass transfer which cccurs before the throughflow enters the paper. The way transfer coefficients are always calculated attributes all the mass transfer to transfer within a packed bed, i.e. including whatever convective transfer occurs prior to the throughflow entering the bed. Thus the total amount of heat or mass transfer, the summation of transfer above and in the bed, is attributed entirely to transfer within the bed For a particular flow condition the convective transfer above a bed is independent of its thickness. Thus the relative contribution of this effect increases as the bed thickness decreases. The increase in Sh with decreasing M_B observed here could in part be due to such a convective effect. For the thickest paper used, $150 g/m^2$, this effect is probably negligible.

The trend of Sh decreasing with increasing bed thickness has also been observed by others. Kato *et al.*[1970] analyzed the bed thickness effect for their own data as well as that of others for naphthalene sublimation, decomposition of H_2O_2, evaporation of water and organic solvents; with throughflow fluids as varied as air, N_2, CO_2, H_2, and a mixture of H_2O-H_2O_2 vapor; with particle shapes of pellets, granules, spheres, cylinders; particle size $0.2<d_p<32mm$; and for a wide range of L/d_p, $0.3<L/d_p<25$. The results of studies appear in Table 2.1 and Fig 2.4. Their analysis indicated that $Sh\alpha(L/d_p)^{-0.6}$ at constant Reynolds number. They argued that according to theory, the fluid boundary layer thickness is inversely proportional to some power of Re, and that the ratio of mass boundary layer thickness to that of momentum is inversely

proportional to some power of Sc. Thus at low Re for gas-solid systems where Sc is rather small, these boundary layers overlap, reducing the effective mass transfer surface area. As a result, the surface area of the particles used to define the Eqn. 6 4 mass transfer coefficient is much larger than the effective surface area Kato *et al.* reasoned that this phenomenon becomes accentuated with increasing bed depth, with higher bulk concentration of the transferring component in the gas, or with increasing L/d_p.

Other researchers have attributed the decrease in Sh with increasing bed thickness to nonuniform flow distribution in the bed. With a model based on channeling through inhomogenous beds, Kunii and Suzuki[1967] showed that as the ratio of average channel length to particle diameter increases, the result is for Sh (or Nu) to decrease. Schlunder[1977] modelled the flow maldistribution resulting from pore size distribution using an array of tubes consisting of one large diameter capillary embedded in a matrix of smaller pores. Assuming plug flow through each capillary and using combined Graetz and Levesque solutions to predict the transfer coefficients, he showed that Sherwood number for the combined flow is less than that of individual capillaries.

Martin[1978] considered packed beds of uniform sized spheres with the section adjacent to the wall having a lower porosity. Again assuming plug flow in each section and basing the transfer coefficients on a Ranz-Marshall type equation, he predicted quite well the reported Nusselt number decrease with increasing L/d_p ratio. Martin also evaluated the influence of a small bypass, which he found to be negligible for large values of ReSc, >200, but which reduces overall Sh greatly in the range of small ReSc, <100. He also pointed out that in the range of ReSc of

2-20, the exponent n in $Nu \propto (ReSc)^n$ may even be greater than 1 because the by-pass flow ratio decreases with increasing Reynolds number.

In their mass transfer study for liquid flow, Sc=1900 and 8880, through packed beds of uniform sized spheres, Fedkiw and Newman[1982] demonstrated a clear decrease of Sh with increasing a_pL at lower values of Peclet number (ReSc), i.e. Pe<100 or Re<0.05. Again they found that this dependency diminishes as Peclet number increases, a trend also observed here with 50-150g/m^2 paper for which Sherwood number becomes more divergent the lower the Reynolds number. Fedkiw and Newman[1982] expanded Martin's approach using two sizes of tubes and predicting the transfer coefficients from the empirically combined asymptotic values, i.e. those for a low Pe-deep bed and for a high Pe-mixing region. They found that if plug flow were assumed through each tube and for a diameter ratio, large tube to small tube, of 1.56 and a porosity ratio of 0.015, their model predicts experimental behaviour quite well. They pointed out that at low Pe, the channeling effect will always be appreciable because the mass transfer is controlled predominantly by the larger channels.

All these researchers have shown that when there is plug flow through parallel flow channels of different resistance to flow, i.e. pores of different size or channels of different porosity, the effective overall mass transfer coefficient calculated by summing the contributions of each flow path is lower than that of the equivalent system without such flow nonuniformities. The simplified models of Martin[1978] and Fedkiw and Newman[1982] cannot be applied quantitatively to describe the effect on mass transfer coefficient of basis weight of paper with its complex pore structure of wide size distribution. However, the principle established by their analyses clearly explains qualitatively the observed

decrease of Sh with increasing M_B, an effect which becomes increasingly important at lower Re in the present study with paper, just has been found to be the case with porous media very different from paper.

There is considerable accumulated evidence from various previous investigations that heat and mass transfer in packed beds is sensitive to local nonuniformity of flow, with transfer coefficients always decreasing with increasing severity of local nonuniformity. Local nonuniformity of flow is also reflected in axial dispersion, but little can be said of this perspective because no researcher has measured axial dispersion for flow through paper.

(d) Effect of ΔT_i on Sherwood Number

In previous mass transfer studies on through drying of packed beds of particulates, inlet air temperature, and hence ΔT_i, was generally not varied. This lack has not been considered important because normally transfer coefficients are not a function of the driving force. Once the dependence of Sh, or Nu, on flow conditions is established for some ΔT or ΔY, the resulting transfer coefficients are taken as established. These coefficients are then used for other ΔT or ΔY conditions because for fixed hydrodynamics and bed characteristics (constant Re, a_p and L) the value of N_G is fixed and the system output, Y_o, responds to any change in Y_i or Y^* to maintain N_G invariant according to the Eqn. 6.8. However, in a through drying study of textiles and tissue paper Gummel [1977] observed a strong decrease in N_G and Sh when he increased T_i from 20°C to 90°C, i.e. ΔT_i increased from about 15°C to 60°C, at $Pe\frac{d_{eq}}{L}>4$ (or Re>2 using the Table 6.2 value of $\overline{d_p}$=34.7 for 25g/m^2 paper). He attributed this dependency to local nonuniformity of drying rate.

The present set of data provide the most comprehensive view yet of the complex relationship of $Sh=f(Re, M_B, \Delta T_i)$ for the through drying of paper or, by extension, for heat and mass transfer at low Reynolds number through thin beds of fine particulates. The Reynolds number dependency of Sherwood number is illustrated by Figs. 6.5 and 6.6 in terms of $\partial Sh/\partial Re$ dependency on M_B and ΔT_i. Fig 6.11 provides an additional perspective in displaying four pairs of the Eqn. 6.15-Table 6.3 regression lines for $Sh=f(Re, M_B, \Delta T_i)$. Each pair of lines on Fig. 6.11 shows, for a particular value of M_B, the Sh-Re relation for the minimum and maximum value of ΔT_i used in the present study, i.e. 15° and 59°C. Figs. 6.5 and 6.6 showed that the slope, n, of such lines increases towards a limiting value of unity as ΔT_i is decreased. Fig. 6.11 provides the additional perspective that while the slope of the Sh-Re lines increases as ΔT_i decreases, the Sh-Re lines shift so that each pair of lines cross within the experimental range of Re. Thus for each of the four basis weights of paper tested, from thin tissue paper to moderately thick paper of $M_B=150 g/m^2$, there is an upper Re region where Sh decreases as ΔT_i increases, and there is a lower Re region where Sh increases as ΔT_i increases. In the limited experiments of Gummel, only one of these two effects was observed, i.e. where Sh decreased with increasing ΔT_i. Thus where Gummel's results showed only one effect, Fig. 6.11 shows that Sh may either increase or decresase with increasing ΔT_i, depending on the level of Re.

(e) Micro-scale Transport Phenomena in Through Drying

As all the $Sh=f(Re, M_B, \Delta T_i)$ results recorded here are for the constant rate drying period, a reassesment of the nature of the constant rate period for the case of through drying paper may be in order. The

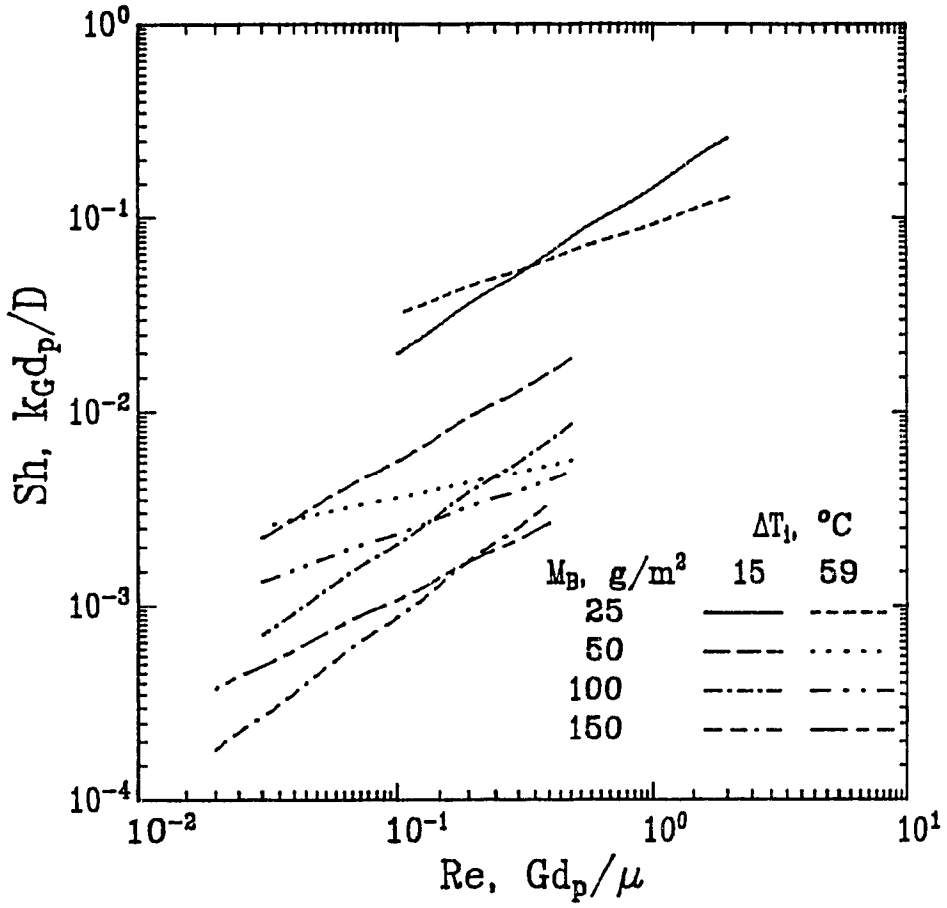

Figure 6.11 Comparison of mass transfer coefficients for minimum and maximum ΔT_i, 15° and 59°C

constant rate period has been characterized by uniform conditions throughout the drying medium. For through drying paper, the period of relatively constant rate drying may in fact not at all correspond to uniform drying conditions, but to conditions throughout the web which are nonuniform and which are changing. Thus the observation of a drying rate which, overall, is constant may be simply a result of mutually compensating changes in different parts of the drying web. As drying proceeds, progressively smaller pores become open to throughflow, hence increasing the overall drying rate by the associated increase in a_p. The evidence of Chapters 4 and 5 is that at the onset of the constant rate period, i.e. at $X=X_{C_i}$, d_p is at the upper plateau level of Fig. 4.21, while at the end of constant rate drying, i.e. at $X=X_{Cf}$, d_p is part way along the transition region toward the lower plateau level of Fig 4.21. As drying proceeds, the larger pores which have been opened earlier to throughflow may enter the falling rate period. These two processes act in compensating ways, i.e. the opening of smaller pores to throughflow simultaneously with some larger pores entering the falling rate conditions may be the micro-scale reality in the wet sheet during the period which, from macro-scale measurements, is identified as the constant rate period. There is as yet insufficient experimental evidence to identify precisely the micro-scale reality with macro-scale measurements of drying rate. However these complex micro-scale phenomena appear to be the source of the equally complex $Sh=f(Re, M_B, \Delta T_i)$ relationships documented more completely than previously by the present study of through drying of paper.

6.4.3 Comparison with the Previous Studies

Only two previous studies, Gummel[1977] and Raj and Emmons[1975], report mass transfer results on through drying of paper. First a comparison is in order of the present results with those on throughflow drying of tissue paper of Gummel[1977], who also varied T_1 in the same range as here. At $Pe\frac{d_{eq}}{L}=4$, where d_{eq} is the equivalent pore diameter calculated from dry sheet flow data using the Hagen-Poiseuille equation, Gummel[1977] reported values of number of transfer units, N_G, in the range 2-3 at 20°C, 0.9-1.5 at 60°C, and 0.7-1 at 90°C for thrcugh drying one thickness of paper, 20g/m^2. Gummel's value of $Pe\frac{d_{eq}}{L}=4$ may be converted to Re using his reported values of d_{eq} and L (~170μm and ~260μm respectively) along with the d_p value found for 25g/m^2 paper in the present study, Table 6.2. The result indicates that Gummel's experiments correspond to operation at Re≈2. At this value of Re the regression equation 6.15 with the parameters given in Table 6.3, predicts N_G of ~1.7 at 23°C, 0.85 at 64°C and 0.6 at 88°C, values which compare extremely well with Gummel's results.

Raj and Emmons[1975] dried paper samples of basis weight 15-65g/m^2, but always in ambient temperature air. They report results in the form of the j-factor $j_m=k_m\rho_a/G$, where k_m is the mass transfer coefficient based on sheet external surface area. As $k_m=k_G a_p L$, j_m as defined by Raj and Emmons is equivalent to the number of transfer units, N_G, used here. As Pe increased from 0.05 to 0.25 for 26g/m^2 paper, they found j_m decreased from 2-3 to 0.8. Because they defined $Pe=\frac{G\sqrt{k}}{D\rho_a}$, and did not report k, the dry sample permeability, their mass flow rates in the range 0.35-1.65 kg/m^{2}s can not be converted to Re. However for their lowest throughflow rate, G=0.35kg/m^{2}s, their value of N_G≈2.5 for 26g/m^2 paper compares well

with the value of N_G=2.3 predicted from Eqn. 6.15 using the Table 6.2 value of $\overline{d_p}$=34.7μm for 25g/m^2 paper throughdried at 23°C.

Raj and Emmons did not consider the wide spread in their j_m values significant although their paper thickness changed by a factor about 5 in their M_B range. They proposed a single correlation for their experimental data, j_m=0.226 $Pe^{-0.8}$. At their experimental ΔT_1, there is a significant difference between the Reynolds dependency of N_G as proposed by the Raj and Emmons correlation and that of Eqn. 6.15 of the present study, Table 6.3. However the Raj and Emmons analysis suffers from four fundamental errors: i) They used the square root of dry paper permeability as the characteristic dimension, shown here to be inappropriate, Chapter 4; ii) They applied to moist paper during the constant rate period this characteristic dimension found for dry paper, which is also inappropriate, Section 6.3.1; iii) They neglected the variability of a_p with X_o; iv) They ignored the proportionality that exists between j_m (or N_G) and paper thickness, L, (or basis weight, M_B). Thus their correlation is not valid.

The present data are compared on Fig. 6.12 with all available literature data for paper and for packed beds of particulates. The effects of L/d_p and ΔT_1 discussed earlier contribute significantly to the wide range of the Sh-Re relation on Fig. 6.12. The present results for each M_B value are shown in a band because of the observed effect of ΔT_1 on Sh, Section 6.4.2. Values of Sh for Raj and Emmons[1975] on Fig. 6.12 were calculated using their correlation for N_G along with k and a_p values as determined in the present study for 25g/m^2 and 50g/m^2 paper, as they did not supply these data. Experimental data for Sherwood number in packed beds at low Reynolds number are in general considerably

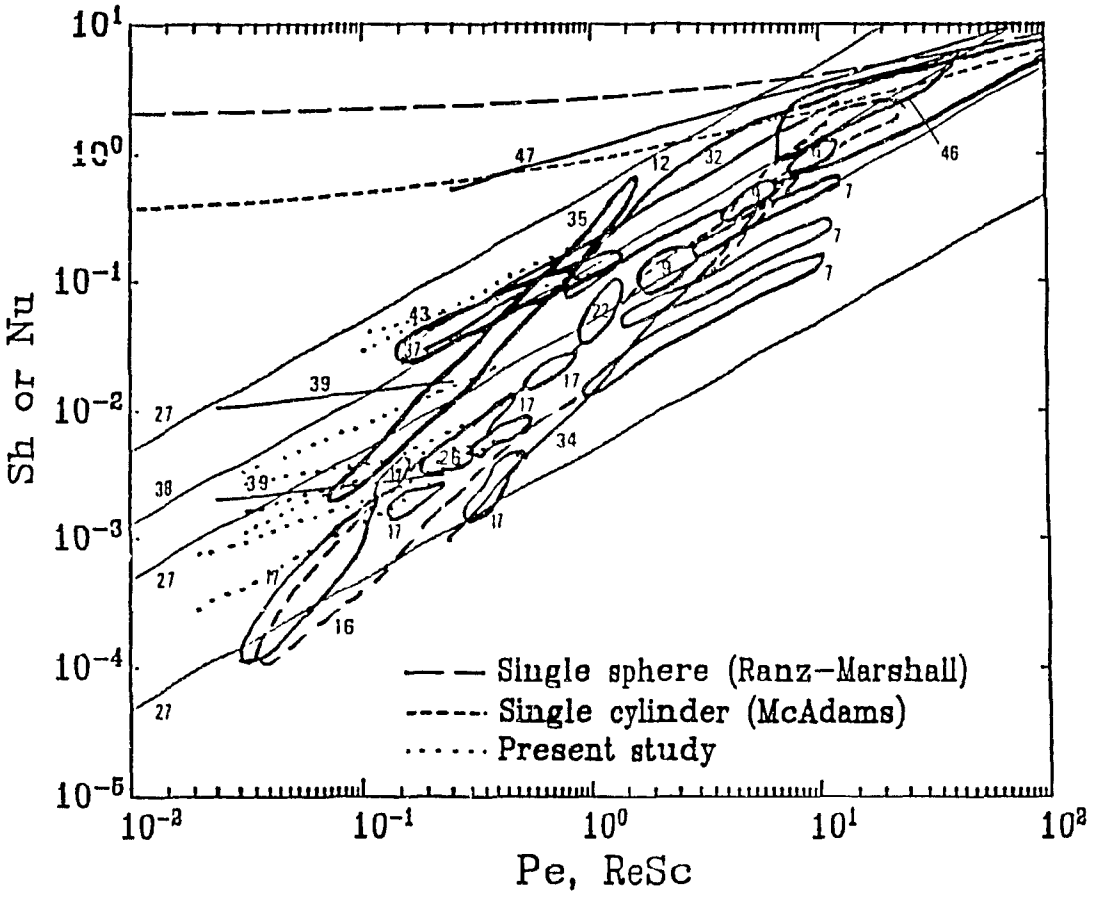

Figure 6.12 Comparison of mass transfer coefficients for through drying of paper with those for beds of small particulates

Numbers correspond to those given on Table 2.1

lower than given by correlations such as that of Ranz and Marshall[1952]. Fig 6.12 shows a general consistency in trend of the present results with those of previously published experiments at low Reynolds number.

6.4.4 Conclusions

The data and the correlations presented here are based on measurements over the most extensive range of paper thickness and throughflow rate and temperature yet published for through drying of paper or even for beds of small particulates. The wide range of M_B and ΔT_1 covered enabled demonstration of the complex $Sh=f(Re, M_B, \Delta T_1)$ relation. The scatter of the mass transfer results presented in Figs. 6.1-6.4 is impressively small considering the range of ΔY_o, <0.1 to 11g/kg, and ΔY_M, 1-16g/kg, thus confirming the accuracy and precision of the present experimental technique for measuring mass transfer coefficients for through drying paper.

The basis weight and temperature driving force effects on mass transfer coefficients presented in Figs. 6.1-6.11 are believed to originate from the various effects of channeling due to the nonuniform structure of paper, to overlapping of mass and momentum boundary layers, to the contribution of convective transfer above the sheet, and to uneven drying due to micro-scale nonuniformity of throughflow. For the through drying of paper, the first presentation of mass transfer coefficients in the form of a correlation, Eqn. 6.15, Table 6.3, valid for a wide range of parameters, M_B-ΔT_1-Re-ΔY_o-ΔY_M, provides the most quantitative description yet available of the constant rate period of this complex process. The rate of through drying of paper is believed to be controlled by interaction at the micro-scale between the

simultaneous momentum, heat and mass transfer phenomena in a media of structure inherently nonuniform at the micro-scale.

6.5 SUMMARY

1) The new characteristic dimension, derived here for paper for the first time from the fundamental momentum transport equation, is employed in the mass transfer analysis of the constant rate period of through drying paper.

2) The interstitial transfer area of paper during constant rate drying period is predicted from the characteristic dimension of moist sheet.

3) The nondimensional transfer coefficient, Sh, for through drying of paper presented here is the first to be calculated using the mass transfer coefficient, characteristic dimension and transfer area corresponding to the actual moisture content range in the constant rate period of through drying.

4) Experimental results, expressed as Sherwood number, are presented for the through drying of 210 sheets of kraft paper, of basis weight 25, 50, 100 and 150g/m^2, through dried from initial moisture contents ranging from 1.5 to 4.5kg/kg with air at 23°, 42°, 64° and 88°C, conditions for which the throughflow exits the sheet during the constant rate period at humidities varying from 48% to 99% of that for saturation.

5) The nondimensional mass transfer coefficient, Sh, for the constant rate period was found to be strongly affected by paper basis weight and throughflow inlet temperature driving force.

6) A regression equation of the form $Sh=aRe^n$ was developed, with the coefficients, a and n, functions of paper basis weight and

throughflow inlet temperature.

7) For 50-150g/m^2 paper, the Reynolds number exponent for Sherwood number, n, approaches unity as M_B increases and as ΔT_i decreases, consistent with previous studies for packed beds of small particles at low Reynolds number and with two studies of very limited scope of through drying of paper.

8) The constant rate period Sherwood number for tissue paper, 25g/m^2, is significantly higher than for thicker paper, believed the consequence of end effects for paper sufficiently thin to be effectively a screen, not a bed, being only $1.7d_p$ thick

9) The complex $Sh=f(Re, M_B, \Delta T_i)$ relationship documented here for paper is believed to result from the effects of channeling, the overlapping of mass and momentum boundary layers, the contributions of convective mass transfer above the sheet, and uneven drying due to micro-scale nonuniformities in momentum, heat and mass transfer in thin beds the structure of which is inherently nonuniform at the micro-scale.

CHAPTER 7

A MODEL FOR THROUGH DRYING OF PAPER

7.1 INTRODUCTION

Mathematical modelling provides a means for exploring comprehensive effects of system parameters on system behaviour. In drying, a model requires choices to be made in order to represent precisely the complicated relationships in moisture removal from wet material. Modelling complements experimental work by identifying incomplete areas of knowledge, and offers the opportunity for blending theoretical and empirical relationships to provide a low-cost tool for research and design.

The concept of mathematical modelling of drying was introduced by Lewis[1921], followed up by Sherwood[1929] Models in the drying literature deal mainly with surface evaporation. Drying modelling has attempted to represent realistically the complex phenomena of transport of moisture, both liquid and vapor, within the wet solid. In addition to general transport equations these treatments include model equations for capillarity, diffusion and multi-phase flow transport phenomena, and for water-substrate relationships such as adsorption behaviour and medium shrinkage. Such general models are so complex that both numerical solution and experimental testing is limited by the excessive number of parameters. Fortunately, several of these complex phenomena have little or no effect on the through drying of webs of small fibres due to the short distance of transport of moisture to the evaporating surface of the fibres.

7.2 PREVIOUS MODELS

Among the few simulation studies on through drying of paper, that of Raj and Emmons[1975] models only the falling rate period by solving numerically the heat and mass conservation equations for both the paper and the air. Their calculations are based on the relationship between vapor pressure of water and moisture content of the web determined by the measurements of Prahl[1968]. They proposed three models. Their first model included neither solid conduction nor fibre shrinkage; the second model included solid conduction but not fibre shrinkage; the third model included both effects. For moisture contents greater than 0.15 kg H_2O/kg dry fibre their first and third models were equally satisfactory. For lower moisture contents the third model gave better predictions. Their model which included only the solid conduction effect gave the poorest agreement with experiments.

The numerical analysis of through drying of Rohrer and Gardiner [1976] considered flow through paper as analogous to turbulent flow through ducts. For the constant rate drying period they correlated experimental heat transfer coefficients as $h \propto G^{0.8}$. For the falling rate period they assumed the rate of drying paper decreases linearly with moisture content, an assumption shown here to be invalid, Section 5.3.4. The claim of good agreement between their experimental and predicted drying rates was not substantiated by any data.

Wedel and Chance[1977] solved the heat and mass balance equations for through drying of paper allowing for solid heat conduction and decrease in vapor pressure of water in the falling rate period. They predicted the heat transfer coefficients from the correlation of Hilpert[1933] for flow over cylinders, an oversimplified basis quite

unlike the flow of air through paper. With the solid thermal conductivity term dropped, they claimed predictions agreed well with their experimental data and with those of Walser and Swenson[1968]. However, their use of data with the exiting throughflow air essentially saturated provides a very insensitive test of any model.

Due to the lack of reliable heat and mass transfer relationships Crotogino and Allenger[1979] in their mathematical model for combined impingement and through drying assumed the exiting throughflow air to be saturated during the constant rate period of drying. Crotogino and Allenger assumed no evaporation during the initial warm-up period, and calculated drying rates during the falling rate period by allowing for the decrease in vapor pressure and increase in heat of adsorption of water. In his model for this combined drying process, Randall[1984] used the approach of Rohrer and Gardiner[1976] for the constant rate period of drying, i.e. $h \propto G^{0.8}$. Although he characterized the warm-up period as one primarily of sensible heat convection to the web, he did not set the evaporation rate to zero during this period. He used an empirical relationship, Gottsching and Rhodus[1977], for modelling the falling rate period.

Soininen[1987] assumed thermodynamic equilibrium between air and the wet sheet in his through drying model which predicts the temperature and moisture profiles for the air stream in the vicinity of the sheet surface. His model did not include the falling rate period.

Previous models of through drying paper thus represent both accomplishments and shortcomings. For the constant rate period, transfer coefficients have been based on inadequate data or on inappropriate correlations with oversimplified flow models, or else the throughflow

has been assumed to exit saturated. The work reported here in Chapter 4 provides a more realistic basis for treating flow through moist paper according to fundamental momentum transport theory, while that of Chapters 5 and 6 documents the large deviations from saturation in the exiting throughflow. For the falling rate period, previous work has shown that the more complicated models including solid conduction and fibre shrinkage yield limited improvement. However the most serious deficiency of all previous attempts to model the through drying of paper has been treatment of the initial period as one of heat transfer to bring the paper temperature to that of the constant drying period. The extensive drying rate measurements of the present study, Chapter 5, establish that the neglect of drying during this initial period is most unrealistic. Thus the model of through drying of paper proposed here is the first to be based on three drying periods, i.e. increasing, constant and falling rate periods of drying. Moreover, the final version of this model incorporates a variable area of heat and mass transfer within the drying sheet, based on the momentum transfer aspects of Chapter4 of the present study. The model is first tested using measurements from the present extensive study of mass transfer coefficients for the through drying of paper, then is implemented for prediction using only general correlations for mass and momentum transport as developed in Chapters 4, 5 and 6.

7.3 NUMERICAL SIMULATION MODEL

7.3.1 Heat and Mass Balance Equations

This mathematical formulation of through drying of paper is one-dimensional in that all conditions affecting drying are taken as uniform

in the plane perpendicular to the direction of throughflow. This common assumption for such processes as heat and mass transfer with heterogeneous chemical reaction in granular beds, Chukhanov[1963]; drying of granular beds, Myklestad[1968]; drying beds of grain, Balazs [1979]; has been found satisfactory also for the through drying of paper, Raj and Emmons [1975], Wedel and Chance[1977]. Further assumptions are (i) pseudo-steady state, $\partial/\partial t \simeq 0$, for the air side, (ii) end effects negligible, and (iii) falling rate period attributed entirely to the decrease in vapor pressure and increase in heat of adsorption.

Based on the above approximations, the heat and mass balance equations become:

Air side mass balance

$$G\,(dY/dz) = N = k_G\ a_P\ \rho_a\ (Y^*-Y) \tag{7.1}$$

Paper side mass balance

$$-\rho_P\ (dX/dt) = N \tag{7.2}$$

Air side heat balance

$$G(C_a+C_V Y)(dT_a/dz)+G(\Delta h_o+C_V T_a)(dY/dz) = N(\Delta h_o+C_V T_P)-ha_P(T_a-T_P) \tag{7.3}$$

Paper side heat balance

$$\rho_P(C_P+C_W X)(dT_P/dt)+\rho_P(C_W T_P-\Delta h_A)(dX/dt) = ha_P(T_a-T_P)-N(\Delta h_o+C_V T_P) \tag{7.4}$$

The initial and boundary conditions used were:

$$\begin{aligned} &\text{at } t=0 \quad X(z,0) = X_o = \text{constant} \\ &\qquad\quad T_p(z,0) = T_{p_1} = \text{constant} \\ &\text{at } z=0 \quad Y(0,t) = Y_1 = \text{constant} \\ &\qquad\quad T_a(0,t) = T_{a_1} = \text{constant} \end{aligned} \tag{7.5}$$

7.3.2 Transfer Coefficients and Air-Water-Fibre System Properties

As the model requires both heat and mass transfer coefficients,

Eqns. 7.1, 7.3, 7.4, while mass transfer coefficients were measured in the present study, Chapter 6, the conversion between these coefficients was obtained using the Lewis relation

$$h/k_G = C_{PY} (Sc/Pr)^{2/3} \tag{7.6}$$

The mass transfer coefficient, k_G, for the constant rate period, determined from data given in Chapter 6, is assumed to be constant throughout drying. Other properties needed include saturation humidity, Y^*, heat of adsorption, Δh_A, and specific heat.

Absolute humidity was related to partial pressure of water by Dalton's law which, for the air-water system, is

$$Y^* = 0.622 (p_V/(P \cdot p_V))$$

At levels of paper moisture above the fibre saturation point, the vapor pressure exerted by water in the wet sheet, p_V, equals the saturation vapor pressure, p_V^*, at the web temperature, T_P. At lower levels of web moisture the heat of adsorption of water on fibres and the depression of vapor pressure should be taken into account. The decrease in vapor pressure was expressed in terms of a vapor pressure depression factor, ω, defined as

$$p_v = \omega\, p_V^* \tag{7.7}$$

The factor ω was evaluated using the experimental data of Prahl[1968] in the form suggested by Wedel and Chance[1976].

$$\begin{aligned} \omega &= 51.29\, X^{1.855} && 0 \le X \le 0.07 \\ \omega &= 1.0 - \exp(0.544 - 14.5\, X) && X > 0.07 \end{aligned} \tag{7.8}$$

The differential heat of adsorption, also taken from Prahl's data, was approximated in the form suggested by Crotogino and Allenger[1979],

$$\Delta h_A = 1320 \exp(-17.4\, X) \tag{7.9}$$

The saturation vapor pressure, p_V^*, in exponential form, and all

specific heats, as polynomial functions of temperature, were as used by Crotogino and Allenger[1979].

7.3.3 Numerical Solution Technique

The heat and mass conservation equations, Eqns. 7.1-7.4, with the conditions specified by Eqn. 7.5, can be solved numerically by the finite difference technique. A simple marching technique can be used in both time and space as the equations are one dimensional in both coordinates, Patankar[1980]. The finite difference equations were obtained by discretization of the mathematical model equations, Eqns. 7.1-7.4 as:

$$Y_I = (G/A1)\ Y_{I-1} + (k_G a_p \rho_a \Delta z/A1)\ Y_I^* \tag{7.10}$$

$$X_I^1 = X_I^0 + (G\Delta t/\rho_p \Delta z)\ (Y_{I-1} - Y_I) \tag{7.11}$$

$$T_{aI} = (1/(1+A2))\ T_{aI-1} + (A2/(1+A2))\ T_p^0 \tag{7.12}$$

$$T_{pI}^1 = T_{pI}^0 + (A3/A4)(X_I^1 - X_I^0) + (ha_p \Delta t/A4)(T_{aI} - T_{pI}^0) \tag{7.13}$$

where

$$A1 = G + k_G a_p \rho_a \Delta z \tag{7.14}$$

$$A2 = (C_V k_G a_p \rho_a \Delta z(Y_I^* - Y_I) + ha_p \Delta z)/(G(C_a + C_V Y_{I-1})) \tag{7.15}$$

$$A3 = \rho_p(\Delta h_o - \Delta h_A + (C_V + C_W)T_{pI}^0) \tag{7.16}$$

$$A4 = \rho_p(C_p + C_W X_I^0) \tag{7.17}$$

where T_{pI}^1 and X_I^1 are the future values of T_p and X at the grid point I at time $t+\Delta t$, and T_{pI}^0 and X_I^0 are the known values at time t.

A computer program in FORTRAN was written to solve the above equations iteratively using a Personal Computer.

7.3.4 Effect of Grid Size

The effects of grid size, both in time and space, were studied

separately by solving the discretization equations for the same drying conditions with a range of time and space steps.

Predictions varied with time steps larger than 0.001s but did not change with decreasing the time step from 0.001s to 0.0005s at the same space grid size. For example, for drying of a 100 g/m^2 handsheet with a flow of 0.22 kg/m^{2}s of 58°C air, when time steps of 0.001 and 0.0005s were used the model predicted exactly the same total drying time and drying rates, while air and paper temperature in the constant rate period differed by less than 0.1%. A time step of 0.001s was therefore used for all simulation runs.

The number of equally spaced grid points across the paper thickness was changed between 4 and 64. As the difference between results of simulations with 20 and 64 grid points was always less than 1%, 20 points were used in the simulation runs.

7.3.5 Conditions for Test of the Model

The model was tested using experimental measurements of the present study for the through drying of standard laboratory handsheets made from unbleached softwood kraft pulp, characterized in Chapter 5. In order to provide a critical test of a drying model the choice of drying conditions under which test data are obtained is of central importance. Results for drying conditions for which the exit throughflow is nearly saturated are insensitive to the model used. The claims of experimental validation of some earlier models are flawed by the use of experimental data with a nearly saturated exit throughflow.

The experimental study reported in Chapter 5 covered a range of T_1-G-M_B values for which the drying rate varied from 1.4% to 48% below

that corresponding to the throughflow exiting saturated. In order to provide sensitive tests of models, the T_i-G-M_B conditions chosen for model testing were those for which Chapter 5 established that the drying rates were from 23% to 46% below that for a saturated exit flow. Thus simulation tests avoided conditions favoring a saturated exit throughflow. i.e. low G, low T_i, high M_B.

7.4 MODEL IMPLEMENTED WITH TRADITIONAL ASSUMPTIONS

In all previous through drying modelling studies the initial period has been characterized mainly by heat transfer to the web until the conditions of the constant rate period of drying are reached, and most of them assumed no evaporation in this period. In view of this unanimity of approach in earlier work, the present model was first implemented with this standard assumption and tested using drying rates measured for unbleached kraft paper in the present study The basis for implementing this model is given in Table 7.1.

Table 7.1 Implementation of the through drying model with traditional assumptions: Model testing

1. Initial period
   - Paper moisture content:
     $X=X_o$
   - Evaporation rate:
     $N = 0 = dY/dz = dX/dt$ in Eqns. 7.1-7.4
   - Paper temperature:
     $T_P \leq T_P$ for constant rate period
2. Constant rate period
   - Paper temperature:
     T_P=adiabatic saturation temperature
   - Specific surface:
     $a_P=4/d_P$ as given in Chapter 6
   - Mass transfer coefficient:
     k_G as given in Chapter 6
3. Falling rate period
   - Volumetric mass transfer coefficient:
     $k_G a_P \rho_a$ as determined during the constant rate period

This through drying model was tested, Fig. 7.1, with the drying rate curve measured for a low basis weight paper ($M_B \cong 25 g/m^2$) initially at T_P=20°C, dried with a high throughflow (G=0.52kg/m²s) of $T_i \cong 63°C$ air. The most important conclusion from the test relates to the procedure of previous models that through drying begins with a period of pure heat transfer with N=0=R until T_P is raised to that of the constant rate period. The test displayed on Fig. 7.1 shows this to be an untenable assumption. The result of this assumption is to exaggerate greatly the extent of the constant rate period by projecting this drying period to start much too soon, i.e. at much too high a paper moisture content. Although only one test case is shown, the same conclusion applies for the large number of drying rate curves measured in the present study.

7.5 MODEL IMPLEMENTED WITH NEW TREATMENT FOR INCREASING RATE PERIOD

7.5.1 Introduction of Unique Features to the Model

The model test illustrated by Fig. 7.1, and supported by the analysis in Chapter 5 of the extensive set of drying rate curves determined in the present study, indicates that the start of through drying cannot be approximated as pure heat transfer but comprises a drying period of previously unrecognized importance, denoted in the present work as the increasing rate period. Thus an essential feature of the proposed model is the division of through drying into three periods, those of increasing rate, constant rate and falling rate, with demarcation between the increasing rate and constant rate periods at what is defined here as the initial critical moisture content, X_{C_1}. The general correlation for X_{C_1} developed in Chapter 5 is part of the new model.

The increasing rate of the initial drying period derives from a

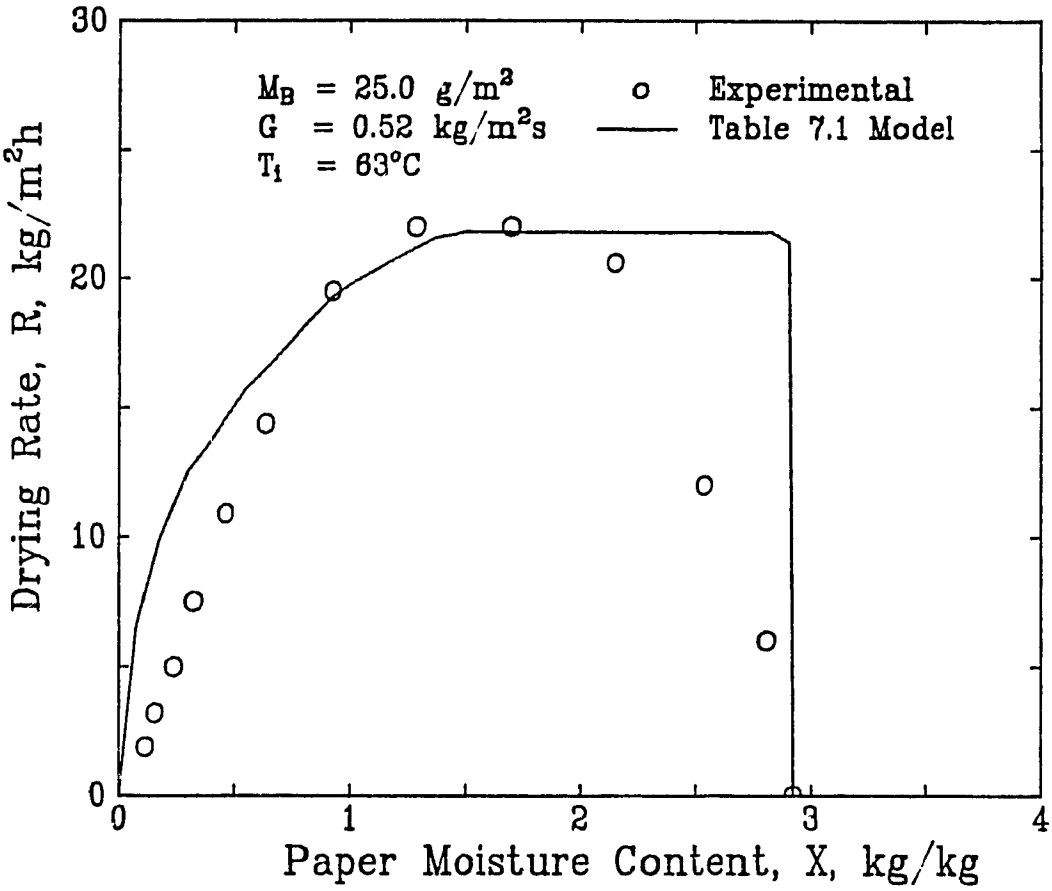

Figure 7.1 Comparison of drying rate curves: experimental and prediction with traditional assumptions

rapidly increasing interfacial area within the paper for heat and mass transfer between the throughflow and the wet sheet, an effect which predominates over the opposing effect of a decreasing heat transfer driving force as the paper warms to the adiabatic saturation temperature. For implementation the new through drying model requires some method for determining the specific surface of paper as a function of its moisture content, i.e. $a_p=f(X)$. As the present study is the first to document the transient measurements of ΔP during the through drying of paper, Chapter 4, these momentum transport measurements open the possibility of determining interfacial area, a_p, as a transient parameter during drying.

During the increasing rate period the ΔP across the paper decreases almost exponentially, Appendix 8, indicating a rapid increase in open area to flow. The Kozeny-Carman equation for the relationship between ΔP and a_p, internal specific surface area of paper, is:

$$a_p^2 = \frac{1}{\kappa} \frac{\varepsilon^3}{(1-\varepsilon)^2} \frac{1}{k} \qquad (7.18)$$

For a constant porosity bed, this equation shows the familiar relationship that ΔP decreases when a_p gets smaller, which is exactly the opposite of what occurs during through drying paper where ΔP decreases while a_p increases. During drying paper, porosity varies. The function, $\varepsilon^3/(1-\varepsilon)^2$, is very sensitive to porosity, for example increasing more than an order of magnitude for a doubling of porosity from 0.2 to 0.4. Hence Eqn. 7.18 cannot be employed to relate a_p for moist paper to ΔP because the ε-X relation is not known with sufficient accuracy.

In the relationship between pressure gradient and pore dimensions, the analysis of Chapter 4 showed that the absolute value of this relationship cannot be determined reliably by making the laminar flow assumption

of Darcy's law. In the present case, however, a_p for dry paper is determined in Chapter 4 using the Kozeny-Carman relation and for the constant rate period is determined as detailed in Chapter 6. For simply pro-rating the ΔP-a_p relationship during the increasing rate period, the Darcy's law approximation is satisfactory. Thus if throughflow occurs through n channels of radius r_i, it can be treated as flow through a circular channel of equivalent radius r, i.e. $r^2=nr_i^2$, and length equal to the thickness of the web. A proportionality between a_p and ΔP follows directly. According to the Hagen-Poiseuille equation, the ΔP-r relation is

$$r^2 = 8\nu GL/\Delta P \tag{7.19}$$

The specific surface of these pores can be expressed in terms of r as

$$a_p = \frac{\text{Circumferential area of the channels}}{\text{Volume of paper}}$$

$$= 2\pi rL/AL \tag{7.20}$$

where A is the nominal surface area of the paper. For the drying of a sheet of specific M_B with a throughflow of specific T_i and G, combining Eqns. 7.19 and 7.20 results in

$$a_p \propto r \propto (1/\Delta P)^{1/2} \tag{7.21}$$

Thus the interfacial area for heat and mass transfer in the paper during the increasing rate period of drying is estimated using Eqn. 7.21 and the corresponding a_p and ΔP values for the constant rate period, as

$$a_p = (a_p)_c\ [(\Delta P)_c/\Delta P]^{1/2} \tag{7.22}$$

The specific surface is assumed not to vary from the onset of the constant rate period through to dry paper.

The ΔP-X data for the drying of an individual sheet were fitted to an exponential form of relation, $\Delta P=a+be^{cX}$, similar to Eqn. 4.8. This relation is then incorporated into the solution scheme during the

increasing rate period of drying.

The essential features of the new model are given in Table 7.2.

Table 7.2 Implementation of the through drying model with new treatment for increasing rate period: Model testing

1. Increasing rate period
   - Paper moisture content:
     $X_o \leq X \leq X_{Ci}$
   - X_{Ci} is determined from the correlation in Chapter 5, Eqn. 5.8
   - $a_P = f(M_B, X)$ is determined from Eqn. 7.22, for which
   - $\Delta P = f(M_B, X, G, T_i)$ is that measured during the through drying of a specific sheet
   - k_G is determined for the same sheet during the constant rate drying period, as given in Chapter 6
   - Paper temperature.
     T_P is determined by the simultaneous solution of heat and mass balance equations given in Section 7.3.1
2. Constant rate period
   - Paper temperature:
     T_P=adiabatic saturation temperature, determined by the simultaneous solution of heat and mass balance equations given in Section 7.3.1
   - Specific surface:
     $a_P = 4/d_P$, with d_P for the specific sheet, as determined in Chapter 6
   - Mass transfer coefficient:
     k_G is for the same sheet, as determined in Chapter 6
3. Falling rate period
   - Volumetric mass transfer coefficient:
     $k_G a_P \rho_a$ is as determined for the same sheet during the constant rate period

7.5.2 Testing of the New Model

For through drying of 25g/m^2 paper initially at T_P=20°C with 0.52 kg/m^{2}s of 63°C air the experimental measurements are shown on Fig. 7.2 along with the predicted drying rate curves for the new model, Table 7.2, and for the model implemented with the traditional assumptions, Table 7.1, the latter curve reproduced from Fig. 7.1. The excellent agreement with experiments in the increasing rate period with this new model confirms the treatment of this as an important period of drying

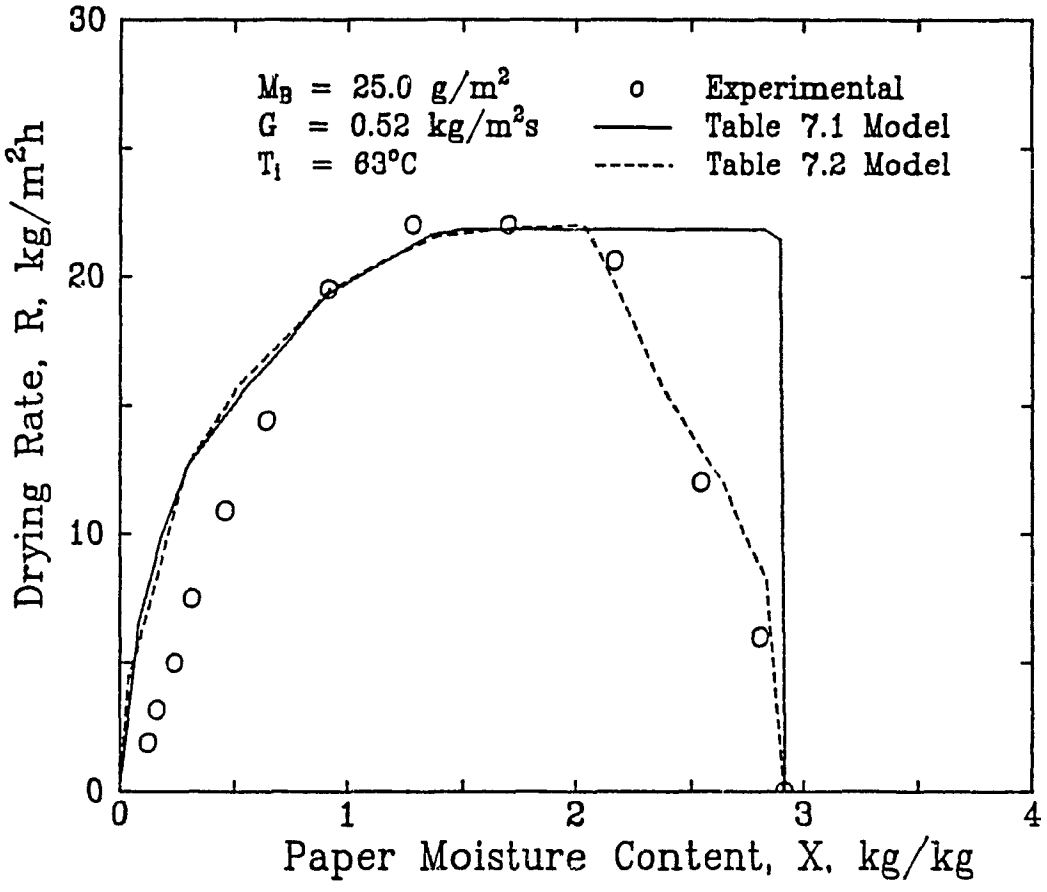

Figure 7.2 Comparison of drying rate curves: experimental and predictions with Table 7.1 and 7.2 models

during which the increasing rate derives from a rapidly increasing interfacial area for heat and mass transfer, with the latter determined satisfactorily in the model from the ΔP across the sheet.

The basic differences between the new model and those previously published are the accounting for evaporation during the increasing rate period and the linking of the increasing a_p with the decreasing ΔP during this newly identified drying period. Over the paper moisture content limits for the increasing rate period, Fig. 7.3 shows the associated T_p-X and a_p-X relationships. The value of T_p displayed is the average of all grid temperatures within paper. From Fig. 7.3 it is seen that paper temperature reaches the wet bulb condition quickly, when only about 5% of the initial water present has been evaporated. Thus, if the initial drying period were considered to be the heating of the sheet to its temperature during the constant rate period of drying, it is evident that the assumption of no evaporation during this period, as typically made by previous researchers, is not unreasonable. However, the associated assumption made in previous through drying models that as soon as paper temperature reaches that of the constant rate period the evaporation rate is likewise that of constant rate drying, is greatly in error. For the case illustrated the initial critical moisture content, X_{c_1}, is 1.70 kg/kg, i.e more than 40% of initial paper moisture is evaporated during increasing rate period of drying. Thus Fig. 7.3 further underlines the importance of the increasing rate period and of the rapidly changing specific surface, which is key to the new model, during that period.

For dryer design, accurate prediction of drying time is required. Therefore sheet moisture content, experimental and as predicted by the

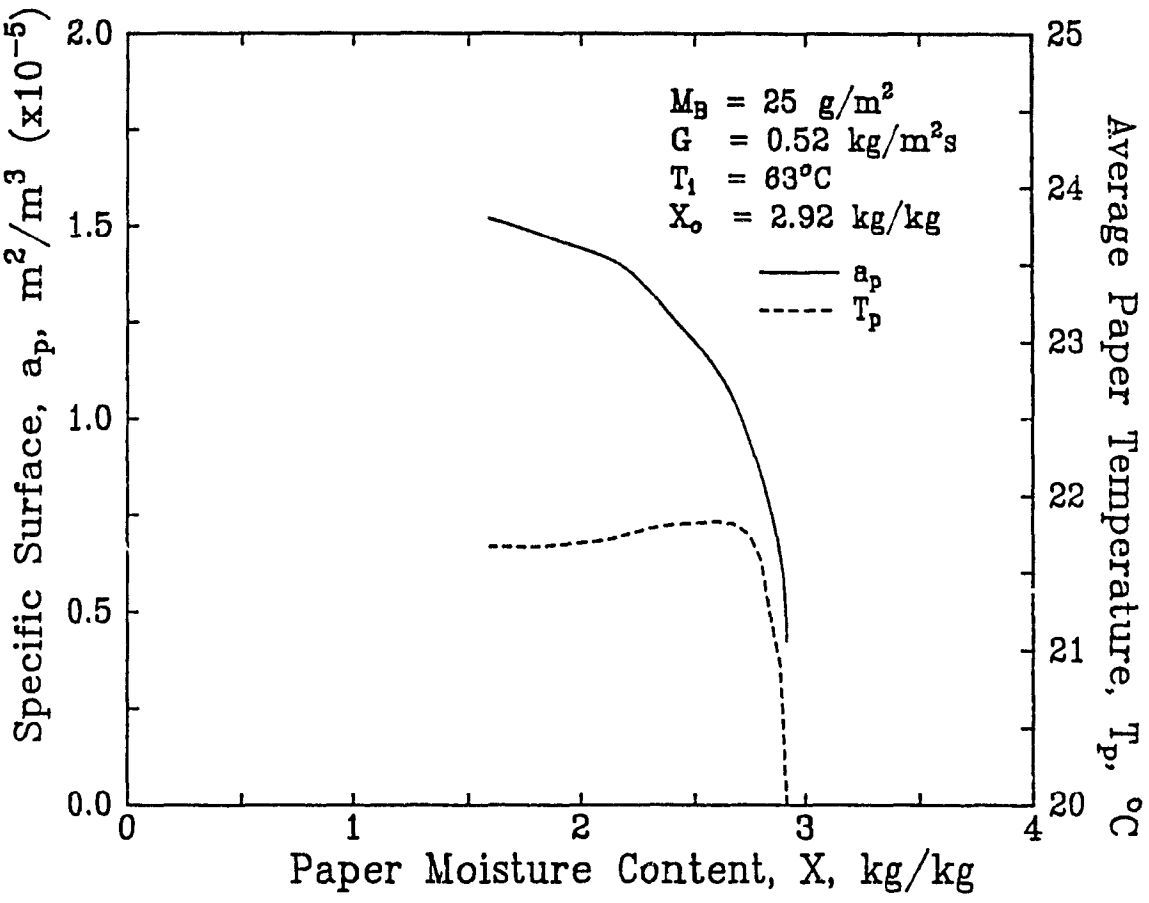

Figure 7.3 Specific surface and paper temperature increase during the increasing rate period of drying

new model and by the previously standard assumption of an initial period of pure heat transfer, are shown as a function of drying time in Fig. 7.4. Although the drying time predicted on the basis used in earlier models (Table 7.1) is substantially below the actual time, the new model (Table 7.2) follows the actual drying time curve accurately except in the final stage of drying where the model underpredicts drying time as it overpredicts drying rate, apparent on Fig. 7.2.

Improvements of this magnitude in the prediction of both drying rate and drying time curves with inclusion of the increasing rate period into the model suggest testing this model at other drying conditions. Therefore three additional simulation runs were performed. The drying conditions of the first run were for about the same M_B and G as the base case but with a higher air temperature, $T_1 \approx 84^\circ C$. The second and third runs were with this G and T_1 but for paper of 50 and 100g/m^2 basis weight. In all these simulation runs the ΔP data and mass transfer coefficients used in the model were those measured for the same individual sheet.

The drying rate and drying time curves, predicted and experimental, for these three runs are presented in consecutive pairs on Figs. 7.5-7.10. Overall good agreement in each of these figures between predictions and experimental measurements substantiates the validity of this model for through drying of paper.

7.6 NEW MODEL IMPLEMENTED FOR PREDICTION

7.6.1 Conversion of the Model to General Correlation Basis

With the successful testing of the new model with drying rates measured for individual sheets and with parameters of the model extracted from measurements with the same individual sheets, the final step is to

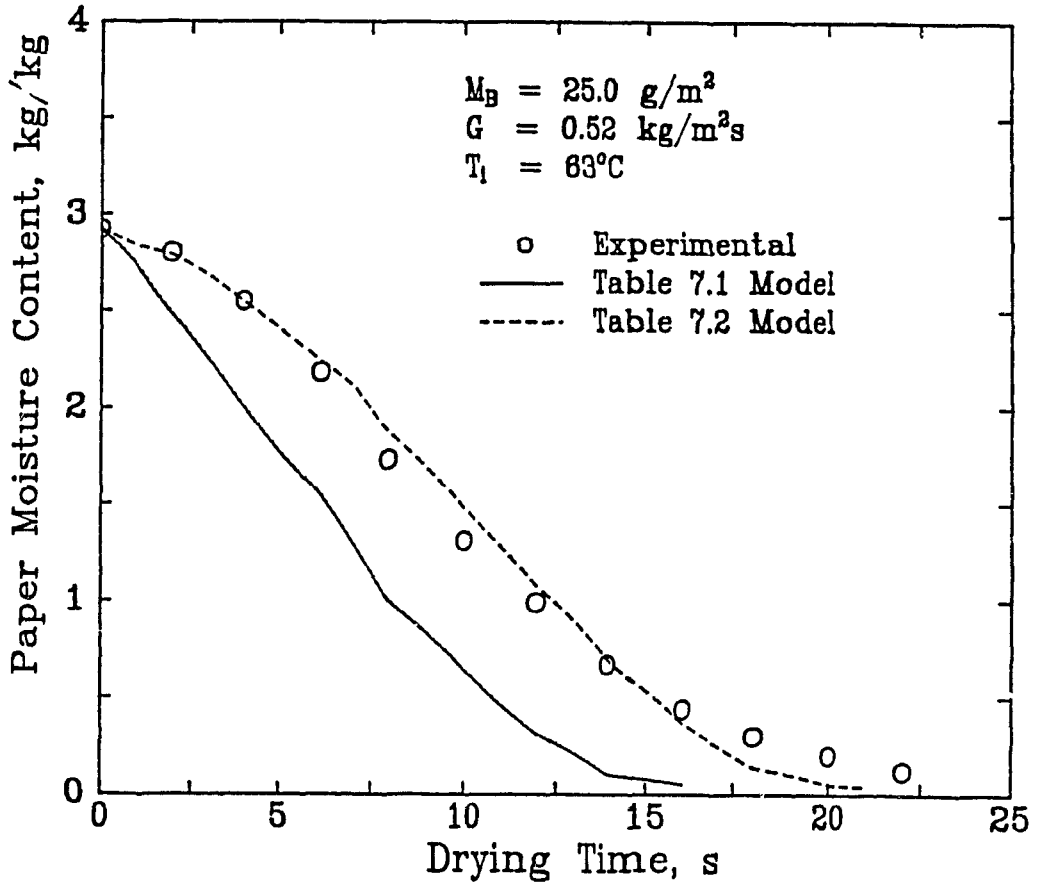

Figure 7.4 Comparison of drying time curves: experimental and predictions with Table 7.1 and 7.2 models

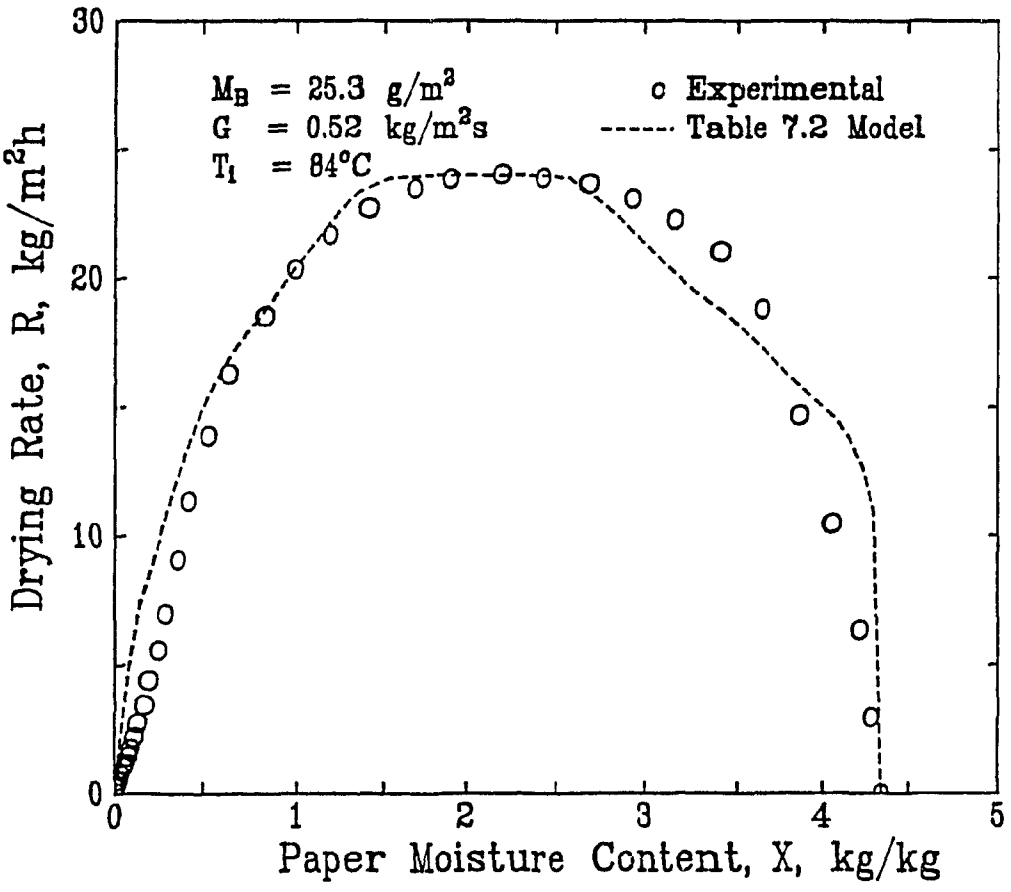

Figure 7.5 Comparison of drying rate curves: experimental and prediction with Table 7.2 model: 25g/m² paper

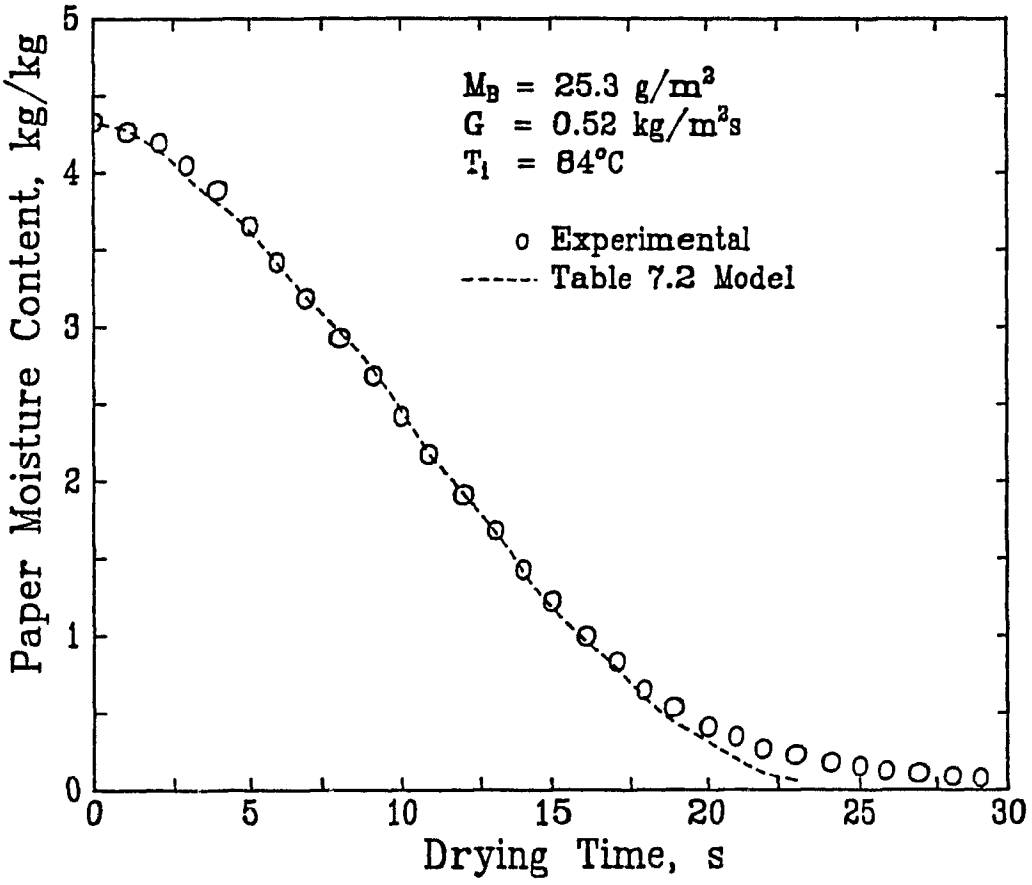

Figure 7.6 Comparison of drying time curves: experimental and prediction with Table 7.2 model: 25g/m² paper

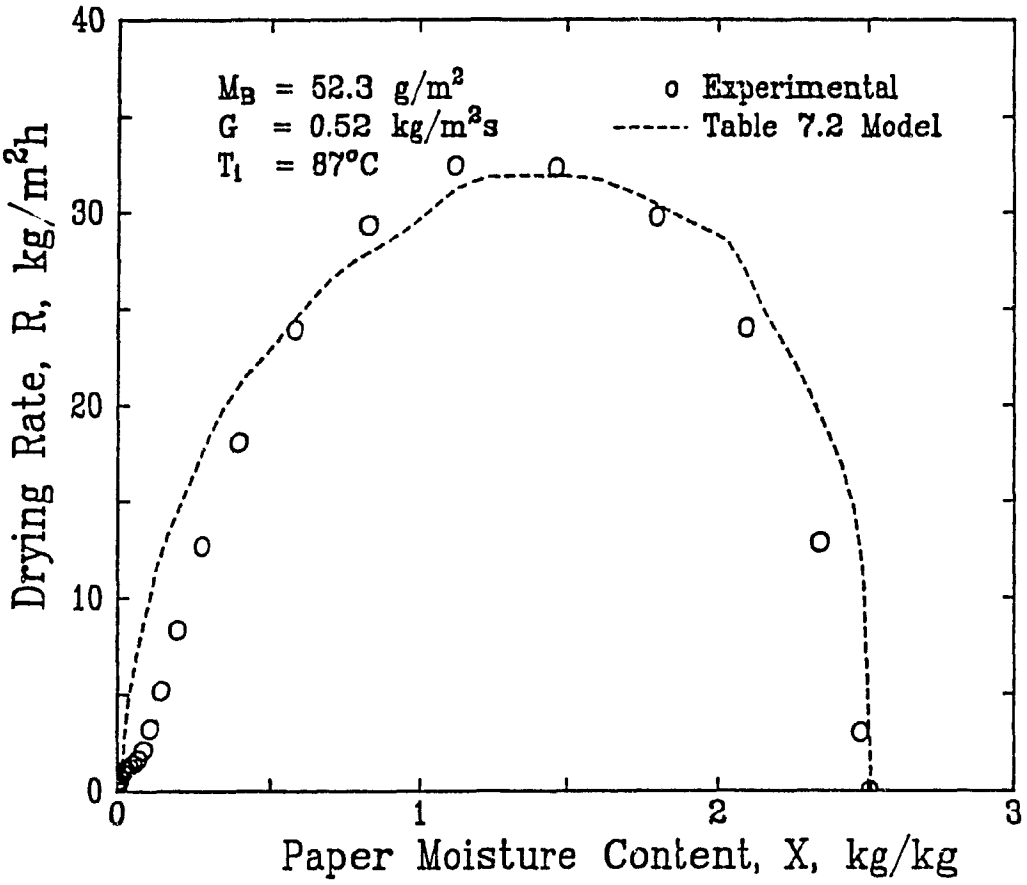

Figure 7.7 Comparison of drying rate curves: experimental and prediction with Table 7.2 model: 50g/m² paper

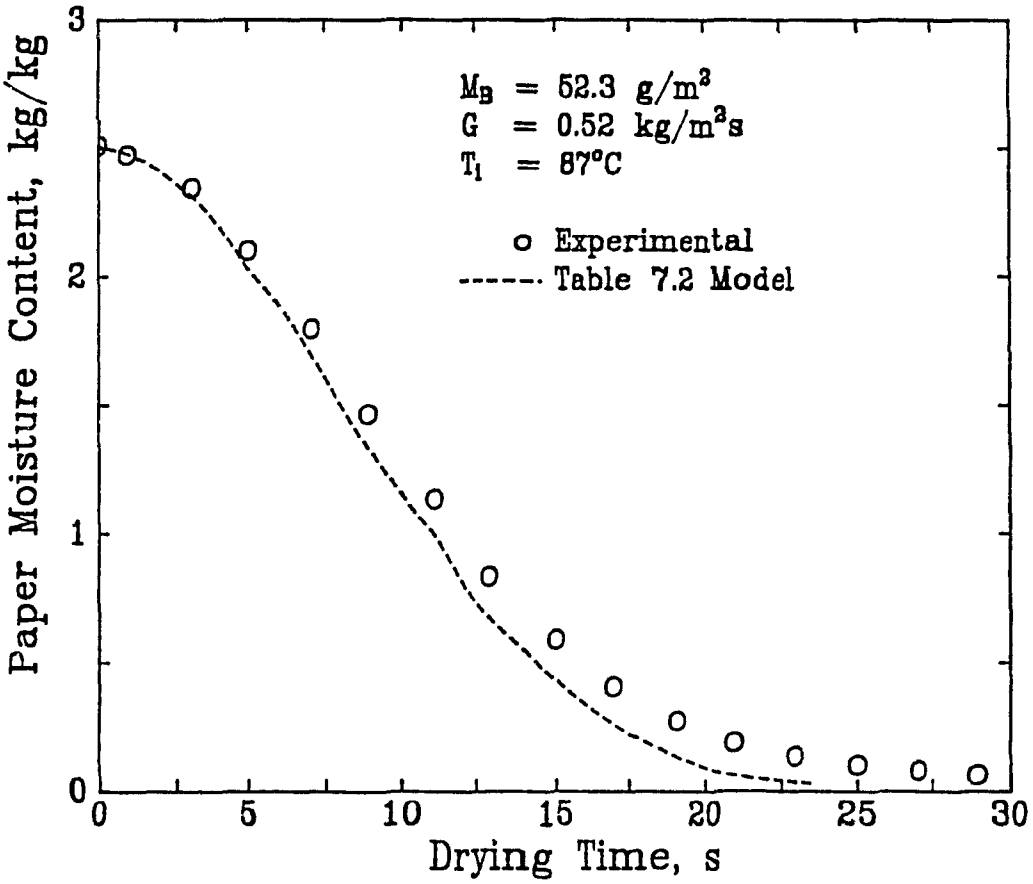

Figure 7.8 Comparison of drying time curves: experimental and prediction with Table 7.2 model: 50g/m² paper

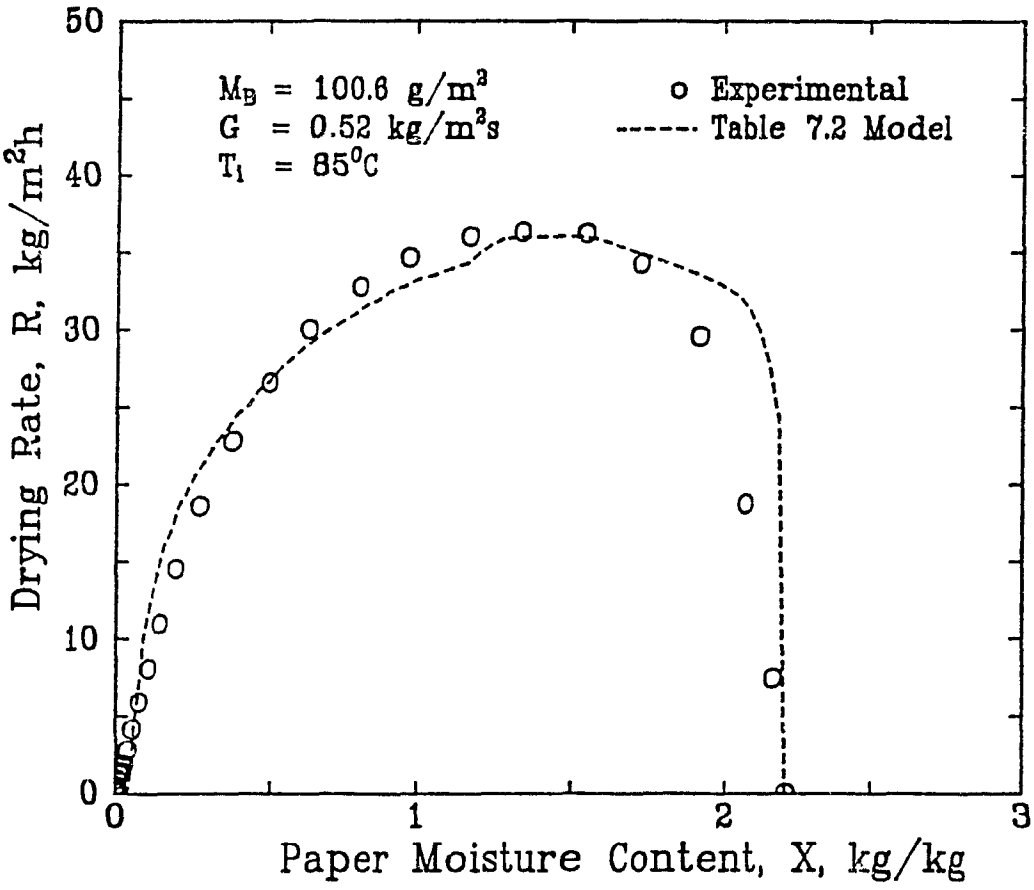

Figure 7.9 Comparison of drying rate curves: experimental and prediction with Table 7.2 model: 100g/m² paper

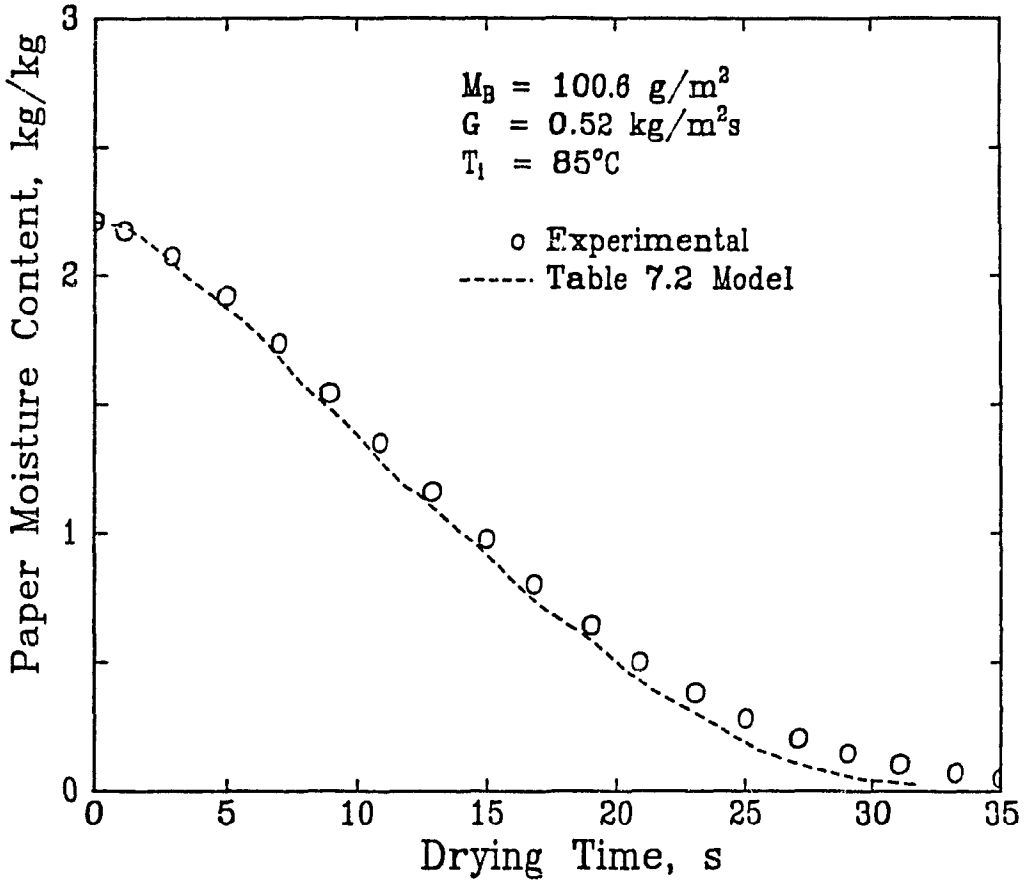

Figure 7.10 Comparison of drying time curves: experimental and prediction with Table 7.2 model: 100g/m² paper

implement the model for prediction. For this purpose the change that must be made concerns how the parameters of the model are determined. For testing the model, these parameters were determined using measurements of mass and momentum transfer. For prediction, the model parameters must be based on general correlations of mass and momentum transfer. The prediction form of this model is described fully in Table 7.3. The source of the general correlations derive entirely from Chapters 4, 5 and 6 of the present study, as itemized in Table 7.3. Details of implementation of the predictive form of the new model are provided in Appendix 9.

Table 7.3 Implementation of the new through drying model for prediction

1. Increasing rate period
   - Paper moisture content: $X_o \leq X \leq X_{Ci}$
   - X_{Ci} is determined from Eqn. 5.8
   - $a_P = f(M_B, X)$ is determined from Eqn. 7.22, for which
   - $\Delta P = f(M_B, X, G, T_i)$ is determined from Eqn. 4.14 and Fig 4.23, for which
   - $d_P = f(M_B, X)$, in $Re = Gd_P/\mu$, is determined from Eqn. 4.16, Table 4.13 and
   - $\beta' = f(M_B, X)$, in $f = (\Delta P/L)/(\beta' G^2/\rho)$, is determined from $d_P = \alpha'/\beta'$ for which $\alpha' = f(M_B, X)$ is determined from Eqn. 4.8, Table 4.6
   - $k_G = f(M_B, X, G, T_i)$ is determined from $Sh = f(Re)$ as given by Eqn. 6.15, Table 6 3
   - Paper temperature:
     T_P is determined by the simultaneous solution of heat and mass balance equations given in Section 7.3.1

2. Constant rate period
   - Paper temperature:
     T_P=adiabatic saturation temperature, determined by the simultaneous solution of heat and mass balance equations given in Section 7 3 1
   - Specific surface:
     $a_P = 4/d_P$ as described in Chapter 6, with d_P determined from correlations noted above
   - Mass transfer coefficient:
     k_G is determined as noted above

3. Falling rate period
   - Volumetric mass transfer coefficient:
     $k_G a_P \rho_a$ as determined during the constant rate period

Figs. 7.11 and 7.12 show the predicted drying rate and drying time curves for through drying with 0.52kg/m^{2}s of 84°C air for 25g/m^2 paper initially at 20°C and of four initial moisture contents, X_o, ranging from 2.45 to 4.3kg/kg dry fibre, along with experimental drying rates measured in the present study The conditions chosen are the most critical possible within the extensive range covered in Chapter 5 of the present work, i.e. for the lowest basis weight paper dried with the highest throughflow rate of the highest temperature air for which the correlations required have been tested.

7.6.2 Demonstration of the Model for Prediction

No direct comparisons of the present predictions can be made with those of previous models Wedel and Chance[1977] reported only two drying rate curves, both at higher air temperature and flow rate, T_1>200°C and u_s>3.5m/s. The general correlations for mass and momentum transport developed in the present study have not been validated for those drying conditions. The models of Crotogino and Allenger[1979] and Randall[1984] are for combined impingement and through drying. Rohrer and Gardiner[1976] did not report any drying rate curves. The model of Raj and Emmons[1975] treated only the falling rate period. Soininen[1987] assumed that the throughflow exits saturated, an assumption proved wrong by the present study.

The new model, based on general correlations, displays an impressive capability to simulate complete drying rate curves, curves which are subject to substantial fluctuations due to such factors as formation variability and local nonuniformity of paper structure, documented in Chapters 4, 5 and 6. Further work is required in the falling rate

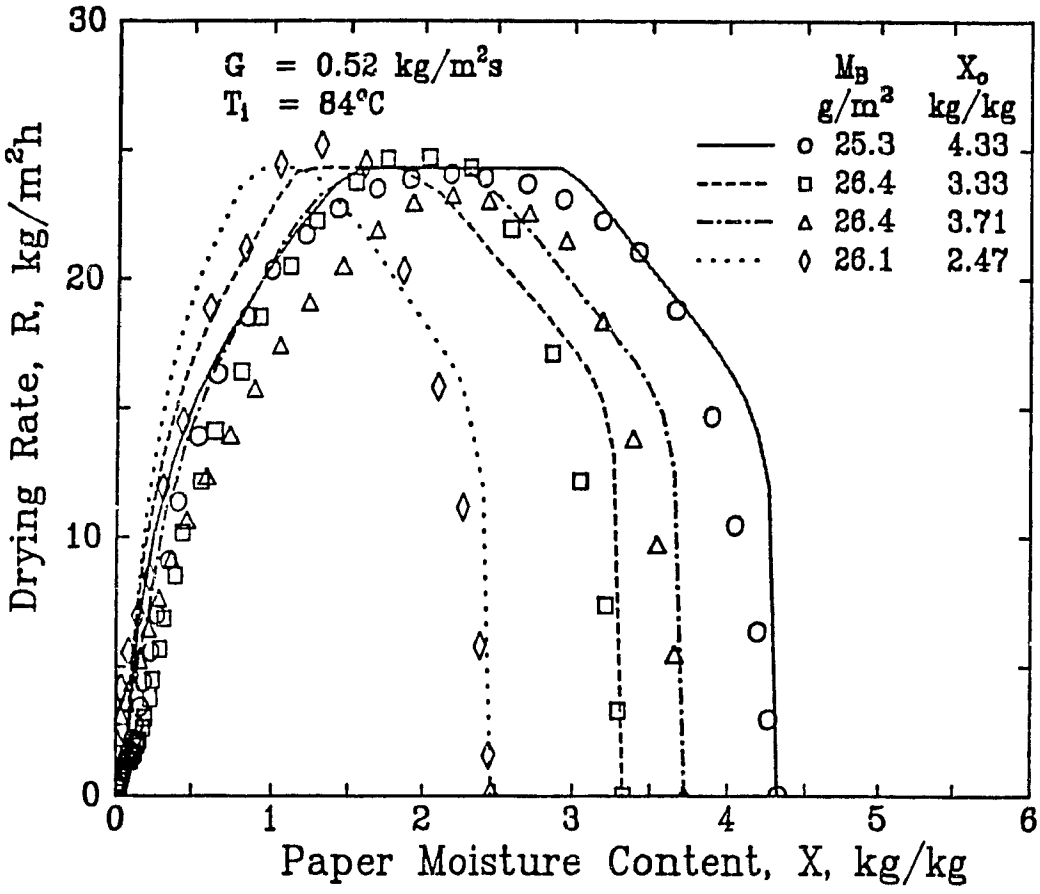

Figure 7.11 Comparison of drying rate curves: experimental and prediction with Table 7.3 model: 25g/m² paper

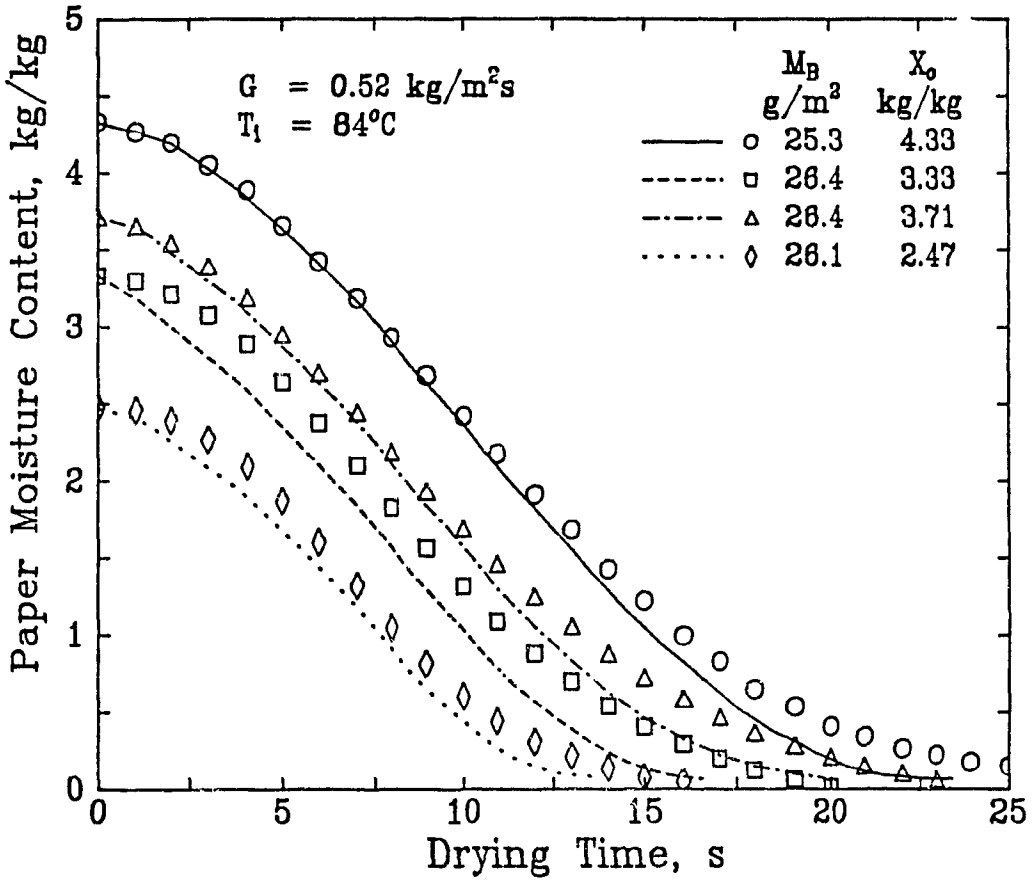

Figure 7.12 Comparison of drying time curves: experimental and prediction with Table 7.3 model: 25g/m² paper

period in particular, where the model overpredicts drying rates. However the model constitutes a sharp break with previous work for the beginning of through drying, where the definition and modelling of the increasing rate period here has resulted in a major improvement in the simulation of drying rate curves. The development through use of momentum transport relations of a sensitively varying specific surface for paper during the increasing rate period is a key feature of the new model.

The complexity of paper structure constitutes a basic obstacle to the simulation of a process such as through drying. The success of the model developed in this chapter confirms the basic concept underlying the entire study, namely, that a fundamental advance in understanding required simultaneous measurement of both momentum and mass transfer aspects of through drying

7.7 SUMMARY

1) When the mass and energy balance equations, one-dimensional in space, are implemented with the initial period of drying treated in what has until now been the standard way, i.e. as a period of heat transfer to bring the paper to the temperature of the constant rate period, the constant drying rate period is shown to be greatly exaggerated, and the resulting drying rate and drying time curves deviate substantially from those measured in the present study. If such a model were used to design a through dryer for 25g/m^2 tissue paper, it would undersize the dryer by about 40%.

2) A new model for the through drying of paper is the first to treat the process as composed of three drying periods, i.e. increasing rate, constant rate and falling rate periods. The evidence supporting

this basic structure of the model is provided by the complete drying rate curves measured for 235 sheets of kraft paper, Chapter 5.

3) The prime focus in this development was on the modelling of the increasing rate period, which can account for 40% of the drying of 25g/m^2 basis weight paper for conditions tested in the present study, Chapter 5. The rapidly increasing rate of drying is attributed to a corresponding increase in interfacial area for heat and mass transfer within the sheet. As pressure drop of the throughflow was monitored here for the first time simultaneously with the instantaneous drying rate, momentum transport was used to model the transient relationship between moisture content and specific surface of paper.

4) The new model was first tested successfully using mass and momentum transport measurements for individual sheets to predict the drying rate history, which was compared with that measured for the same sheets.

5) The final version of the model, that for prediction, was developed using only general correlations of mass and momentum transport which had been successfully tested in Chapters 4, 5 and 6 for the through drying of kraft paper of basis weight 25 to 150g/m^2, in throughflows of from 0.09 to 0.52kg/m^{2}s of 20° to 90°C air.

6) The drying rate and drying time predictions made with the predictive form of the new model, Table 7.3, are in good agreement with the extensive measurements of the present study, in particular for the increasing rate period never before modelled. This success confirms the basic structure of the model, especially the modelling of the rapidly increasing specific surface of paper during the increasing rate period of drying.

CHAPTER 8

CONCLUSIONS

8.1 CONTRIBUTIONS TO KNOWLEDGE

1) Permeability: Dry paper

The permeability of dry paper was determined correctly at industrially relevant throughflow rates for the first time by application of the momentum transport equation, i.e. without the commonly used approximation of Darcy's law which ignores inertial effects. For the combination of minimum basis weight-maximum throughflow rate used, the permeability of dry kraft paper calculated from Darcy's law is shown to be too low by about 40%.

As basis weight is decreased from 250 to 50g/m^2, paper permeability increases gradually, approximately doubling, probably due to widening of the pore size distribution. When basis weight is reduced from 50 to 25g/m^2, permeability increases sharply, by a factor of 2-3, attributed to the associated exponential increase in pin hole count.

2) Permeability: Effect of wetting-drying

The permeability of dry kraft paper, 25-250 g/m^2, approximately doubles when subjected to a wetting-through drying cycle, due to changes in paper microstructure during the wetting, not the drying. As all reported laboratory drying studies begin with rewetting previously dry paper, all physical properties of dry paper used to describe the drying process must be measured after drying, not before.

3) Permeability: Moist paper

The modified permeability, k/L, for moist paper, determined

correctly for the first time by application of the momentum transport equation rather than Darcy's law, is correlated as a function of only paper moisture content and basis weight, i.e. it is not significantly affected by any of the variables which control drying rate.

4) Specific surface: dry paper

The specific surface of dry kraft paper as determined from throughflow measurements using the Kozeny-Carman equation decreases moderately, by about 25%, as basis weight is reduced from 250 to 50g/m^2, then drops by about 1/3 for reduction to 25g/m^2 basis weight. For 25g/m^2 paper, sorption techniques overestimate by about 50% the interfacial area that is effective for throughflow transport processes. Area associated with smaller pores, measured by sorption, scarcely affects the area measured by the throughflow which flows predominantly through large pores and pin holes, leaving the small pores stagnant.

5) Specific surface: Effect of wetting-drying

The specific surface of 25-250 g/m^2 dry kraft paper drops by 2-11% after a wetting-drying cycle. This drop, which occurs during the wetting, not the drying, is attributed to the same irreversible mechanism responsible for the associated doubling of paper permeability, i.e. to collapse of fibre surface fibrillation.

6) Characteristic dimension: dry paper

A new characteristic dimension was determined for flow through paper, $d_p=\beta/\alpha$, where α and β are momentum transport equation parameters. With the new characteristic dimension, Reynolds number becomes rigorously the

ratio of the inertial to the viscous contribution to momentum transport. For kraft paper the theoretically based $d_p=\beta/\alpha$ values are an order of magnitude higher than two widely accepted empirical definitions of characteristic dimension for paper, square root of permeability and reciprocal of specific surface, and are about 1/4-1/2 of the values of the measurements of Bliesner[1964] and of the Hagen-Poiseuille equivalent pore diameter determined by Gummel[1977].

For dry kraft paper of basis weight above 50 g/m^2, d_p is independent of paper thickness while permeability, k, varies significantly. For $25g/m^2$ dry paper, d_p is much higher, by a factor of 3, due to pin holes.

The characteristic dimension, d_p, for Papriformer newsprint is lower, about 2/3 that of kraft paper, as expected for paper from mechanical pulp.

7) Characteristic dimension. Moist paper

With paper moisture content $d_p=\beta/\alpha$ changes between two asymptotic limits. Above about 1.7-2.1kg/kg, d_p is limited by maximum pore size. Below about 0.6-0.9kg/kg, d_p for kraft paper is at its lower limit. The latter moisture content is in the range of the fibre saturation point, 0.72-0.81kg/kg, below which all water is held within the fibres. From the upper to the lower plateaus, d_p-X dependence reflects the opening of progressively smaller pores during through drying. The maximum values of d_p, 44μm and 14μm for 25 and $50g/m^2$ wet kraft paper, correspond to the maximum pore size observed by scanning electron microscopy.

8) Re-f-d_p treatment: Experimental results

With $d_p=\beta/\alpha$, a theoretical relationship between friction factor, $f=(\Delta P/L)/(\beta G^2/\rho)$, and Reynolds number, Gd_p/μ, fits about 700 ΔP measurements for dry paper of basis weight 25-250g/m^2, and about 3000 ΔP measurements for moist paper of two basis weights, 25 and 50g/m^2, for moisture contents from about 250% to dry paper. This analysis is the first treatment of air flow through dry and moist paper based on momentum transport relations.

The ratio between the correct ΔP and that given by the Darcy's law viscous flow simplification is determined to be $\frac{1+1/Re}{1/Re}$. This error is then 5% at Re=0.05 and 100% at Re=1 In industrial practice of through drying of paper, Re=6 may be reached, where this error would be 600%.

9) Re-f-d_p treatment: Comparisons

This form of Re-f definition, the most appropriate for beds of complex porous structure such as paper, also eliminates the need for the still unresolved porosity functions required for the Fanning friction factor alternative. Relations between various friction factor and Reynolds number definitions, essential for comparing results, are provided.

The theoretically sound β/α-d_p-Re-f treatment for air throughflow across moist and dry paper is more powerful than the traditional permeability approach as it yields not only a fluid mechanics characterization of paper for momentum transport, but also provides the basis for theoretical analysis of heat and mass transport phenomena in paper during through drying. This new approach is recommended for paper and other fine particulate media.

10) Re-f-d_p treatment: Application

General procedures for application of the Re-f-d_p method to paper are given.

11) Through drying rates of paper: Complete drying rate curves

Complete drying rate curves were determined for 235 sheets of kraft paper through dried over a wide range of operating variables - temperature and rate of the throughflow, basis weight and initial moisture content of the paper, in the most comprehensive reported investigation of through drying.

The great importance of the "increasing rate period" at the start of through drying, recognized and named in the present study, has been demonstrated. Thus this extensive set of drying rate curves shows a new perspective, i.e three drying periods, those of increasing, constant and falling rate drying.

12) Through drying rates of paper. Increasing rate period

The increasing rate period is associated with a progressive opening of pores which increases drying rate by increasing the area for heat and mass transfer within the web, as documented in the effect of paper moisture content on pore size, d_p, and permeability, k. For 25g/m^2 kraft paper dried at the highest throughflow rate and temperature tested, the amount of water removed during the increasing rate period is large, about 1.25 kg water/kg dry fibre. For these conditions and for X_o=2.5, almost half the water is removed during the increasing rate period, half during the falling rate period, and very little during the constant rate period.

13) Through drying rates of paper: Constant rate period

With initial moisture contents typical of industrial practice, as through drying conditions become more intensive with tissue paper, i.e. with higher throughflow rates and temperatures, the constant drying rate period at first decreases, then disappears. For not such light weight paper the constant rate period remains important.

In the first comprehensive correlation for through drying rates of paper in the constant rate period successfully tested for a wide range of drying conditions, R_C is found to be quite sensitive to throughflow rate and temperature, only weakly dependent on basis weight, and independent of initial moisture content of the paper. R_C may be less than half of R_S, the maximum rate with the air exiting saturated. The extent of this deviation increases as the temperature and rate of throughflow increase, as paper basis weight decreases, but is independent of initial moisture content. The assumption of throughflow air exiting saturated, made in some earlier work due to the lack of data, is therefore not appropriate because drying rate could be overpredicted by more than a factor of two for conditions of industrial relevance.

14) Through drying rates of paper: Drying period diagrams

An original treatment of the relation between drying conditions and the extent of each drying period, i.e. increasing, constant and falling rate periods, was developed in a graphical form denoted "drying period diagrams".

The values of paper moisture content which mark the transition from the increasing to constant drying rate period, and from the constant to falling drying rate period, named here as the "initial" and

"final" critical moisture contents, X_{C_i} and X_{Cf}, are related to the drying conditions.

15) Through drying rates of paper: Drying period diagrams, X_{C_i} and X_{Cf}

Determination for the 235 drying experiments of the initial critical moisture content, X_{C_i}, a drying parameter introduced here, shows that the onset of the constant rate period is sensitive to all through drying variables. By contrast, these determinations show that the final critical moisture content, X_{Cf}, is directly proportional to initial moisture content, X_o, with the proportionality, X_{Cf}/X_o, being independent of throughflow rate and basis weight and only weakly dependent on throughflow temperature. For throughflow temperatures from 23° to 88°C, X_{Cf} varies only between 41 and 49% of X_o.

16) Through drying rates of paper: Drying period diagrams, X_{ICF}

The drying period diagrams show that the amount of drying which occurs in the increasing drying rate period varies considerably with drying conditions, becoming higher with increasing throughflow temperature and rate and with decreasing basis weight. The concept was introduced of an increasing-constant-falling rate triple point, X_{ICF}, where $X_{C_i}=X_{Cf}$. For an initial moisture content $X_o=X_{ICF}$, the constant rate drying condition is reached only momentarily as drying passes directly from the increasing rate to the falling rate period. According to present findings, there is typically no constant rate period for industrial conditions of through drying light weight grades of paper because X_{ICF} is generally higher than X_o values used commercially.

17) Through drying rates of paper: X_{cf} comparison with surface drying

The critical moisture content at the end of the constant rate period, X_{cf}, relates to paper properties and drying conditions completely differently in through drying and surface drying. In surface drying, X_{cf} is reported to depend on paper thickness, drying air temperature, drying rate and initial moisture content. Here X_{cf} is demonstrated to be independent of paper thickness, and the dependence on drying air temperature is in the opposite direction from that for surface drying. With increasing air temperature, X_{cf} decreases in surface drying because of the controlling rate of transport of water through the solid, while X_{cf} increases in through drying paper because of the increasing heat transfer rate to the fibres. Thus theories for surface drying are totally inapplicable to through drying a web of small hygroscopic particles as in paper. The X_{cf} critical moisture content for paper, strongly dependent on drying conditions for surface drying, is nearly independent of throughflow conditions for through drying but is linearly proportional to initial moisture content.

18) Through drying rates of paper: Industrial application

Concerning industrial practice, these findings underline two important facts, that through drying rates are generally less than 50% of the maximum rate corresponding to the throughflow exiting saturated and, that typically the paper remains in the increasing rate period for about half the dryer, in the falling rate period for the remainder. With about half of an industrial through dryer operating in the increasing rate period, with drying rates limited by the development of pore area for heat and mass transfer within the web, the results of the

present work point the way for work to increase the efficiency of through drying of paper.

19) Transport phenomena during constant rate through drying:

Determination of transport parameters

The nondimensional mass transfer coefficient, Sherwood number, for through drying of paper is determined for the first time using the characteristic dimension, d_p, and the interfacial transfer area, a_p, corresponding to actual moisture content and the particular basis weight, and determined from the ΔP across the sheet by momentum transport analysis.

20) Transport phenomena during constant rate through drying:

Experimental results

Experimental results, expressed as Sherwood number, were obtained for drying of kraft paper of basis weight 25, 50, 100 and 150g/m^2, through dried from initial moisture contents of 1.5-4.5kg/kg with air at 23°, 42°, 64° and 88°C, conditions for which the throughflow exits the sheet at humidities from 48% to 99% of that for saturation. Sherwood number was found to be strongly affected by paper basis weight and throughflow inlet temperature driving force.

21) Transport phenomena during constant rate through drying:

Correlation

A correlation of all experimental results was obtained in the form $Sh=aRe^n$ with both coefficients, a and n, functions of paper basis weight and throughflow inlet temperature driving force over the

experimental range of Reynolds number, 0.025-1.5.

For 50-150g/m^2 paper, the Reynolds number exponent, n, approaches unity as M_B increases and as ΔT_1 decreases, consistent with previous studies for packed beds of small particles at low Reynolds number.

The significantly higher Sherwood number obtained for the thinnest paper, 25g/m^2, is believed the consequence of end effects with tissue paper which is effectively a screen, not a bed, being only $1.7d_P$ thick.

22) Transport phenomena during constant rate through drying:

$Sh=f(Re, M_B, \Delta T_1)$ relationship

The complex $Sh=f(Re, M_B, \Delta T_1)$ relationship documented here for paper is believed to result from the effects of channeling, the overlapping of mass and momentum boundary layers, the contributions of convective mass transfer above the sheet, and uneven drying due to micro-scale nonuniformities in momentum, heat and mass transfer in thin beds that are inherently nonuniform at the micro-scale.

23) Through drying model for paper: Feature of increasing rate period

When the initial period of drying is treated as one of pure heat transfer to warm the paper to the temperature of the constant rate period, as in previous models, the constant rate period is shown to be greatly exaggerated. If such a model were used to design a through dryer for tissue paper, it is shown that the dryer would be undersized by about 40%.

A new model was developed which incorporates an additional drying period, that of increasing rate, linked to a rapidly increasing interfacial area for heat and mass transfer. In the new model, the

increasing rate period may account for up to 40% of the drying for tissue paper for conditions run in this study. This through drying model was developed and tested successfully using mass and momentum transport measurements for individual sheets.

24) Through drying model for paper: General predictive form

The final version developed of the new model relies on only general correlations of mass and momentum transport tested sucsessfully in this study. The simulations of drying rate and drying time curves made with this predictive form of the model provide improved agreement with the experimental measurements relative to previous models, especially during the increasing rate period, the importance of which was not recognized in earlier models.

8.2 RECOMMENDATIONS FOR FUTURE STUDIES

1) Never-dried pulp should be used in future drying studies because of the demonstrated effect of rewetting on paper properties.

2) Future experimental studies on through drying of paper should be planned in the light of the importance on drying rate of local micro-scale nonuniformities in flow, heat and mass transfer phenomena.

3) The measurement of local values of velocity, temperature and humidity at the exit of the sheet should be investigated because of the indicated importance of local nonuniformity in all transport phenomena, these small scale nonuniformities resulting from local variability in sheet structure.

4) Although the residence time of air in paper is in the order of milliseconds in through drying, the possibility of measurement of gas

phase axial dispersion in paper should be considered. Experiments at very much lower throughlow rates, with paper of higher basis weight, may provide information relevant to axial dispersion for normal through drying conditions.

5) Theoretical predictions, either numerical or analytical, and/or experimental measurement techniques should be investigated in order to obtain the air temperature and humidity entering the sheet, thereby separating this convective transport from the heat and mass transfer occuring within the sheet.

6) The effect on through drying of varying the flow condition between that of the present study, i.e. a flow of uniform axial velocity, and a that of multiple impinging jets should be investigated.

7) Because the present findings establish that about half of a industrial through dryer operates in conditions of the increasing rate period, for which drying rates are limited by the development of pore area for heat and mass transfer within the web, the possibility of increasing drying rate by combined impingement and through drying should be investigated. In such a general context the present study comprises one limiting case, that of 100% throughflow.

8) The nonuniformity of paper structure should in future be incorporated in models of through drying paper. Statistical description of paper structure may be useful. Such modelling may permit relating pressure drop and drying rate to the progressive opening of pores as drying proceeds. The pressure drop measurements of the present work may aid finding the appropriate function to describe the opening of pores during the increasing rate period

REFERENCES

Ahmed, N., and D.K. Sunada, 1969, "Nonlinear Flow in Porous Media", *J. Hydraul. Div. ASCE*, 95(HY 6): 1847-1857.

Appel, P.W., and J. Newman, 1976, "Application of the Limiting Current Method to Mass Transfer in Packed Beds at Very Low Reynolds Numbers", *AIChE J.*, 22(6): 979-984.

Allerton, J., L.E Brownell, and D.K. Katz, 1949, "Through-Drying of Porous Media", *Chem. Eng. Prog.*, 45(10): 619-635.

Bakhmeteff, B.A., and N V Feodoroff, 1937, "Flow Through Granular Media", *J. Appl Mech.*, 4. A97-A104.

Balazs, T., 1979, "Determination of the Average Heat and Mass Transfer Coefficients for Throughflow Drying", *Period. Polytech Mech. Eng.*, 23(1): 29-39.

Banacki, W.J., Jr., and R.L. Bowers, 1962, "Pore Size Testing of Filter Papers", *Tappi*, 45(10): 805-807.

Bar-Ilan, M., and W. Resnick, 1957, "Gas Phase Mass Transfer in Fixed Beds at Low Reynolds Numbers", *Ind. Eng. Chem.*, 49(2): 313-320.

Bear, J., 1972, *Dynamics of Fluids in Porous Media*, Elsevier Sci. Pub., New York.

Beavers, C.S , and E.M. Sparrow, 1969, "Non-Darcy Flow Through Porous Media", *ASME J Appl. Mech.*, 91(4): 711-714.

Beavers, G.S., T.A. Wilson, and B.A. Masha, 1975, "Flow Through a Deformable Porous Material", *ASME J. Appl. Mech.*, 97(3): 598-602.

Beavers, G.S., A. Hajji, and E.M Sparrow, 1981a, "Fluid Flow Through a Class of Highly-Deformable Porous Media Part 1: Experiments with Air", *ASME J. Fluids Eng*, 103(3). 432-439

Beavers, G.S., K. Wittenberg, and E M. Sparrow, 1981b, "Fluid Flow Through a Class of Highly-Deformable Porous Media Part 2: Experiments with Water", *ASME J. Fluids Eng*, 103(3): 440-444.

Bhattacharyya, D., and D.C.T. Pei, 1975, "Heat Transfer in Fixed Bed Gas-Solid Systems", *Chem. Eng. Sci.*, 30: 293-300.

Bird, R.B., W.E. Stewart, and E.N. Lightfoot, 1960, *Transport Phenomena*, John Wiley & Sons, Inc., New York, NY, U.S.A.

Blake, F.C., 1922, "The Resistance of Packing to Fluid Flow", *Trans. Am. Inst. Chem. Eng.*, 14: 415-421

Bliesner, W.C., 1964, " A Study of the Porous Structure of Fibrous Sheets Using Permeability Techniques", *Tappi*, 47(7): 392-400.

Bradshaw, R.D., and C.O. Bennett. 1961, "Fluid-Particle Mass Transfer in a Packed Bed", *AIChE J.*, 7(1): 48-52.

Bradshaw, R.D., and J.E. Myers, 1963, "Heat and Mass Transfer in Fixed and Fluidized Beds of Large Particles", *AIChE J.*, 9(5): 590-595.

Brown, Jr., J.C., 1950, "Determination of the Exposed Specific Surface of Pulp Fibers from Air Permeability Measurements", *Tappi*, 33(3): 130-137.

Brownell, L.E , and D.L. Katz, 1947, "Flow of Fluids Through Porous Media: I. Single Homegenous Fluids", *Chem. Eng. Prog.*, 43(10): 537-548.

Browning, B.L., 1950, "The Specific Surface of Pulps by the Silvering Method", *Tappi*, 33(8): 410-412.

Brunauer, S., P.H. Emmett, and E. Teller, 1938, "Adsorption of Gases in Multimolecular Layers", *J. Amer. Chem. Soc.*, 60(2): 309-319.

Brundrett, E., and W.D. Baines, 1966, "The Flow of Air Through Wet Paper", *Tappi*, 49(3): 97-101.

Bublitz, W.J., J.W. Dappen, and J.A. van den Akker, 1948, "An Investigation of the Relationship Between the Permeabilities of Paper to Oil and Air", *Tappi*, 31: 305-315.

Burgess, B.W., S.M. Chapman, and W. Seto, 1972a, "The Papridryer Process, Part I, The basic concepts and laboratory results", *Pulp Paper Mag. Can.*, 73(11): T314-323.

Burgess, B.W., W. Seto, E. Koller, and I.T. Pye, 1972b, "The Papridryer Process, Part II, Mill trials", *Pulp Paper Mag. Can.*, 73(11): T323-331.

Burke, S.P., and W.B. Plummer, 1928, "Gas Flow Through Packed Columns", *Ind. Eng. Chem.*, 20: 1196-1200.

Cano, J., and U. Bohm, 1977, "Mass Transfer in Packed Beds of Screens", *Chem. Eng. Sci.*, 32: 213-219.

Carman, P.C., 1937, "Fluid Flow Through Granular Beds", *Trans. Inst. Chem. Eng.*, 15: 150-166.

Carman, P.C., 1938, "Determination of the Specific Surface of Powders I", *J. Soc. Chem. Ind.* (London), 57: 225-234.

Carman, P.C., 1939, "Determination of the Specific Surface of Powders II", *J. Soc. Chem. Ind.* (London), 58: 1-7.

Carman, P.C., 1941, "Capillary Rise and Capillary Movement of Moisture in Fine Solids", *Soil Sci.*, 52: 1-14

Carman, P.C., 1948, "Some Physical Aspects of Water Flow in Porous Media", *Disc. Faraday Soc.*, 3: 72-77

Carman, P.C., 1956, *Flow of Gases Through Porous Media*, Butterworths,

London.

Carson, F.T., 1934, "A Sensitive Instrument for Measuring the Air Permeability of Paper and Other Sheet Materials", *J. Res. Nat. Bur. Stand.*, 12: 567 608.

Carson, F.T.. 1940, "Some Observations on Determining the Size of Pores in Paper", *J. Res. Nat. Bur. Stand.*, 24: 435-442.

Chalmers, J., D.B. Taliaferro, and E L. Rawlins, 1932, "Flow of Air and Gas Through Porous Media", *Trans. Am. Inst. Min. and Met. Eng., Petrol. Div.*, 98: 375-400.

Childs, E.C., and N. Collis-Ceorge, 1950,"The Permeability of Porous Materials", *Proc. Roy. Soc.*, A201: 392-405

Chilton, T.H., and A.P. Colburn, 1934, "Pressure Drop in Packed Tubes", *Ind. Eng. Chem.*, 23: 913-934.

Chu, J.C., J. Kalil, and W.A Wetteroth, 1953, "Mass Transfer in a Fluidized Bed", *Chem. Eng. Prog.*, 49(3): 141-149.

Chu, J.C., and W.L. Kuo, 1967, "The Kinetics of Normal-Through Drying of Paper", *Tappi*, 50(8): 405-415.

Chukhanov, Z.F., 1963, "Heat and Mass Transfer Between Gas and Granular Material", *Int. J. Heat Mass Tr.*, 6: 691-701.

Clark, J D'A., 1942, "A New Method for Measuring Specific Surface of Fibres", *Paper Trade J.*, 115(1). 32-39

Cornell, D, and D.L. Katz, 1953, "Flow of Gases Through Consolidated Porous Media", *Ind. Eng. Chem.*, 45 2145-2152.

Cornish, A.R.H., 1965, "Note on Minimum Possible Rate of Heat Transfer from a Sphere when Other Spheres are Adjacent to It", *Trans. Inst. Chem. Eng.*, 43: T332-T333.

Corte, H., 1958, "The Porous Structure of Paper: Its Measurement, its Importance and Its Modification by Beating", in *Fundamentals of Papermaking Fibres*, F. Bolam, Ed., BPBMA, Kenley, England, 301-331.

Corte, H., 1982, "The Porosity of Paper", in *Handbook of Paper Science*, vol. 2, H.F. Rance, ed., Elsevier Sci. Pub., Amsterdam.

Corte, H., and O.J. Kallmes, 1962, "Statistical Geometry of a Fibrous Network", in *Formation and Structure of Paper*, F. Bolam, Ed., BPBMA, London, England, 13-46.

Corte, H., and E. H. Lloyd, 1966, "Fluid Flow Through paper and Sheet Structure", in *Consolidation of the Paper Web*, F. Bolam. Ed., BPBMA, London. England, 981-1009.

Crotogino, R.H., 1975, "Weiterentwicklung der Trockenpartie; Prallstrom-

und Durchlufttrocknung", *Das Papier*, 29: V127-V133.

Crotogino, R.H., and V. Allenger, 1979, "Mathematical Model of the Papridryer Process", *CPPA Trans. Tech. Sec.*, 5(4): TR84-TR91.

Cybulski, A., M.J. van Dalen, J.W. Verkerk, and P.J. van den Berg, 1975, "Gas-Particle Heat Transfer Coefficients in Packed Beds at Low Reynolds Numbers", *Chem. Eng. Sci.*, 30: 1015-1018.

Darcy, H., 1856, *Les Fontaines Publiques de la Ville de Dijon*, V. Dalmont, Paris.

De Acetis, J., and G. Thodos, 1960, "Mass and Heat Transfer in Flow of Gases Through Spherical Packings", *Ind. Eng. Chem.*, 52(12): 1003-1006.

Dean, J.A., 1979, *Lange's Handbook of Chemistry*, 12. Ed., McGraw Hill, New York, NY.

Donnadieu, G., 1961, "Transmission de la Chaleur dans les Milieux Granulaires", *Revue Inst. Fr Petrole*, 16: 1330.

Dudgeon, C.R., 1966, "An Experimental Study of The Flow of Water Through Coarse Granular Media", *Houille Blanche* 21(7): 785-800.

Dullien, F.A.L., 1975, "Single Phase Flow Through Porous Media and Pore Structure", *Chem. Eng. J.*, 10: 1-34.

Dullien, F.A.L., and M.I.S. Azzam, 1973, "Flow Rate Pressure Gradient Measurements in Periodically Nonuniform Capillary Tubes", *A.I.Ch.E.J.*, 19 (2): 222-229

Dullien, F.A.L , and V.K Batra, 1970, "Determination of the Structure of Porous Media", *Ind. Eng. Chem.*, 62(10): 25-56.

Dwivedi, P.N., and S.N. Upadhyay, 1977, "Particle-Fluid Mass Transfer in Fixed and Fluidized Beds", *Ind. Eng. Chem , Process Des. Dev.*, 16(2): 157-165.

Eichorn, J., and R.R. White, 1952, "Particle-to-Fluid Heat Transfer in Fixed and Fluidized Beds", *Chem Eng. Prog. Symp. Ser.*, 48: 11-18.

Ellis, E.R., K.B. Jewett, K.A. Smith, W.H. Ceckler, and E.V. Thompson, 1983, "Water Retention Ratio and its Use to Study the Mechanism of Water Retention in Paper", *JPPS*, 9(1) · TR12-TR15.

Endo, A., T. Shishido, M Suzuki, and S. Ohtani, 1977, "Estimation of Critical Moisture Content", *A I.Ch.E Symp. Ser.*, 73(163): 57-62.

Ercan, C. 1989, "Gas Phase Axial Dispersion in Mobile Bed and Spray Contacting", *Ph.D. Dissertation*, McGill University, Montreal

Ergun, S., 1952, "Fluid Flow Through Packed Columns", *Chem. Eng. Prog.* 48(2): 89-94

Fancher, G.H., and J.A. Lewis, 1933, "Flow of Simple Fluids Through Porous Materials", *Ind. Eng. Chem* , 25. 1139-1147.

Fedkiw, P., and J Newman, 1978, "Low Peclet Number Behaviour of the Transfer Rate in Packed Beds", *Chem Eng Sci.*, 33: 1043-1048.

Fedkiw, P., and J. Newman, 1982, "Mass Transfer Coefficients in Packed Beds at Very Low Reynolds Numbers", *Int J. Heat Mass Tr.*, 25(7): 935-943.

Fish, J.R., 1975, "Mill Experience of Through Drying", *Paper Tech. and Ind.*, 16: T20-T22.

Forchheimer, P., 1901, "Wasserbewegung durch Boden", *Z. Ver. Deutsch. Ing.*, 45: 1782

Fowler, J.L., and K.L Hertel, 1940, "Flow of Gas Through Porous Media" *J. Appl. Phys.*, 11: 496-502

Galloway, L.R., W. Komarnicky, and N. Epstein, 1957, "Effect of Packing Configuration on Mass and Heat Transfer in Beds of Stacked Spheres", *Can. J. Chem. Eng.*, 35:139-150.

Gamson, B.W., 1951, "Heat and Mass Transfer, Fluid Solid Systems", *Chem. Eng. Prog.*, 47(1): 19-28.

Gamson, B.W., G Thodos, and O A Hougen, 1943, "Heat, Mass and Momentum Transfer in the Flow of Gases Through Granular Solids", *Trans. Am. Inst. Chem. Eng.*, 39: 1-35.

Garner, R.G., and R.J. Kerekes, 1978, "Aerodynamic Characterization of Dry Wood Pulps", *CPPA Trans. Tech. Sec.*, 4(3): TR82-TR89.

Geertsma, J , 1974, *Soc. Pet Eng. J* , 14: 445 (*cited* from Dullien[1975])

Gottsching, L., and D. Rhodius, 1977, "Der Trocknungsverlauf von Papier und Pappe in Abhangigkeit von trocknungstechnischen und papier-technologischen Parametern, Teil I", *Das Papier*, 31: 419-427.

Green, L., and P. Duwez, 1951, "Fluid Flow Through Porous Metals", *J. Appl. Mech.*, 18: 39-44.

Gren, U.B , 1972, "Compressibility and Permeability of Packed Beds of Cellulose Fibers", *Svensk Papperstidn.*, 75(19): 785-793.

Grootenhuis, P., R.C.A. Mackworth, and O.A. Saunders, 1951, "Heat Transfer to Air Passing Through Heated Porous Metals", *Proc. Inst. Mech. Eng.*, 363-366.

Gummel, P., 1977, "Through Drying An Experimental Study of Drying Rate and Pressure Losses in Through-Drying of Textiles and Paper", *Ph.D. Dissertation*, University of Karlsruhe, FRG

Gunn, D.J., and J.F.C. de Souza, 1974, "Heat Transfer and Axial Dispersion in Packed Beds", *Chem. Eng. Sci.*, 29 1363-1371.

Gurnagul, N., and D.G. Gray, 1987, "The Response of Paper Sheet Surface Areas to Changes in Relative Humidity", *JPPS*, 13(5): J159-J164.

Halstrom, A., 1985, *Ph.D. Dissertation*, Lund University, Sweden.

Happel, J., and H. Brenner, *Low Reynolds Number Hydrodynamics, with Special Application to Particulate Media*, Prentice-Hall, Englewood Cliffs, N.J.

Hartler, N., and J. Rennel, 1969, "Opacity in Relation to Strength Properties of Pulps· Part 2 , Light-Scattering Coefficient and Surface Area of Unbonded Pulp Fibres", *Svensk Papperstidn.*, 72(1). 9-13.

Haselton, W.R., 1955, "Gas Adsorption by Wood, Pulp, and Papers, 2. The Application of Gas Adsorption Techniques to the Study of the Area and Structures of Pulps and the Unbonded and Bonded Area of Paper", *Tappi*, 38(12): 716-723.

Hilpert, R., 1933, "Warmeabgabe von geheizten Drahten und Rohren im Luftstrom", *Forsch Gebiete Ing.-Wes* , 4· 215-224.

Hobson, M., and G. Thodos, 1951, "Mass Transfer, Laminar Flow of Gases Through Granular Beds", *Chem. Eng Prog.*, 47(7): 370-375.

Houghton, J.T., and S.D Smith, 1966, *Infra-Red Physics*, Oxford University Press, London, U K

Hsiung, T.H., and G. Thodos, 1977, "Mass-Transfer Factors from Actual Driving Forces for the Flow of Gases Through Packed Beds", *Int. J. Heat Mass Tr.*, 20(4): 331-340.

Huber, M.L., and M.C. Jones, 1988, "A Frequency Response Study of Packed Bed Heat Transfer at Elevated Temperatures", *Int. J. Heat Mass Tr.*, 31(4): 843-853.

Hurt, D.M., 1943, "Principles of Reactor Design, Gas-Solid Interface Reactions", *Ind Eng. Chem.*, 35(5) 522-528

Ingmanson, W.L., 1953, "Filtration Resistance of Compressible Materials", *Chem. Eng. Prog.*, 49: 577-584

Ingmanson, W.L., and B.D. Andrews, 1963, "High-Velocity Water Flow Through Fiber Mats", *Tappi*, 46(3) 150-155.

Ingmanson, W.L , B.D. Andrews, and R.C. Johnson, 1959, "Internal Pressure Distribution in Compressible Mats under Fluid Stresses", *Tappi* 42(10): 840-849.

Jacksor, G.W., and D.F. James, 1986, "The Permeability of Fibrous Porous Media", *Can. J. Chem Eng* , 64: 364-374.

Kaguei, S., B. Shiozawa, and N Wakao, 1977, "Dispersion-Concentric Model for Packed Bed Heat Transfer", *Chem. Eng. Sci.*, 32: 507-513

Kato, K., H. Kubota, and C.Y. Wen, 1970, "Mass Transfer in Fixed and Fluidized Beds", *Chem. Eng. Prog Symp. Ser.*, 66(105): 87-99

Kato, K., and C.Y. Wen, 1970, "Gas-Particle Heat Transfer in Fixed and Fluidized Beds", *Chem Eng Prog Symp Ser.*, 66(105): 100-108

Kehinde, A.J., R.R. Hudgins, and P.L. Silveston, 1983, "Measurement of Mass Transfer in Packed Beds at Low Reynolds Numbers by Imperfect Pulse Chromatography", *J. Chem. Eng. Japan*, 16(6): 483-489.

Keey, R.B., 1972, *Drying Principles and Practice*, Pergamon Press, Oxford, UK.

Keey, R.B., and M. Suzuki, 1974, "On the Characteristic Drying Curve", *Int. J. Heat Mass. Tr.*, 17(12): 1455-1464.

Knauf, G.H., and M R. Doshi, 1986, "Calculation of Aerodynamic Porosity, Specific Surface Area, and Specific Volume from Gurley Seconds Measurement", *Proc. Intl Process & Mat. Qual. Eval. Conf.*, TAPPI Press, Atlanta, 233-239

Knudsen, J.G , and D K. Katz, 1958, *Fluid Dynamics and Heat Transfer*, McGraw-Hill Book Company, Inc., New York, NY, U.S.A.

Kozeny, J., 1927, "Uber Kapillare Leitung des Wassers in Boden", *Sitz. Ber. Akad. Wiss. Wien. Math -naturw Klasse*, Abt. IIA, 136: 271-306.

Krischer, O., 1963, *Die wissenschaftlichen Grundlagen der Trocknungstechnik*, 2. Ed., Springer, Berlin

Krischer, O., and G. Loos, 1958, "Warme- und Stoffaustausch bei erzwungener Stromung an Korpern verschiedener Form, Teil I", *Chem.-Ing.-Tech.*, 30(1): 31-39.

Kumar, S., S N. Upadhyay, and V.K Mathur, 1977, "Low Reynolds Number Mass Transfer in Packed Beds of Cylindrical Particles", *Ind. Eng. Chem., Process Des Dev.*, 16(1) 1-8

Kunii, D , and J.M Smith, 1961, "Heat Transfer Characteristics of Porous Rocks. II. Thermal Conductivities of Unconsolidated Particles with Flowing Fluid", *AIChE J* , 7(1): 29-34.

Kunii, D., and M. Suzuki, 1967, "Particle-to-Fluid Heat and Mass Transfer in Packed Beds of Fine Particles", *Int. J. Heat Mass Tr.*, 10: 845-852.

Kyan, C.P., D T. Wasan, and R C. Kintner, 1970, "Flow of Single-Phase Fluids Through Fibrous Beds", *Ind Eng Chem. Fundam.*, 9(4): 596-603.

Leva, M., M. Weintraub, M Grummer, M Pollchik, and H.H. Storch, 1951, "Fluid Flow Through Packed and Fluidized Systems", *U.S. Bur. of Mines, Bull. 504*

Lewis, W.K., 1921, "The Rate of Drying of Solid Materials", *J. Ind. Eng. Chem.*, 13: 427-432.

Littman, H. , R.G. Barile, and A H. Pulsifer, 1968, "Gas-Particle Heat Transfer Coefficients in Packed Beds at Low Reynolds Numbers", *Ind. Eng. Chem. Fundam.*, 7(4): 554-561.

Macdonald, I.F., M.S. El-Sayed, K Mow, and F.A.L. Dullien, 1979, "Flow Through Porous Media-the Ergun Equation Revisited", *Ind. Eng. Chem. Fundam.*, 18(3): 199-208.

Macdonald, G., and N. Franklin, 1970, *Pulp and Paper Manufacture, Volume 3, Papermaking and Paperboard Making*, 2. ed., McGraw-Hill, NY.

McAdams, W.H., 1954, *Heat Transmission*, 3. Ed., McGraw-Hill, New York.

McConnachie, J.T.L., and G. Thodos, 1963, "Transfer Processes in the Flow of Gases Through Packed and Distended Beds of Spheres", *AIChE J.*, 9(1): 60-64.

McConnell, R.R., 1980, "Literature Review of Drying Research in the Pulp and Paper Industry", *DRYING'80*, A S. Mujumdar, Ed., Vol. 2., Hemisphere Publ. Corp., 330-337

Malling, G.F., and G. Thodos, 1967, "Analogy Between Mass and Heat Transfer in Beds of Spheres: Contributions due to end Effects", *Int. J. Heat Mass Tr.*, 10: 489-498.

Marshall, W.R., and O.A. Hougen, 1942, "Drying of Solids by Through Circulation", *Trans. Am. Inst Chem Eng* , 38· 91-121.

Martin, H., 1978, "Low Peclet Number Particle-to-Fluid Heat and Mass Transfer in packed Beds", *Chem Eng Sci.*, 33: 913-919.

Martin, P.D., 1972, "Through Drying", *Paper Tech.*, 13(2): 114-119.

Mason, S.G., 1950, "The Specific Surface of Fibres- Its Measurement and Application", *Tappi*, 8. 403-409

Menon, A.S., and A S Mujumdar, 1987, "Drying of Solids· Principles, Classification and Selection of Dryers", in *Handbook of Industrial Drying*, A.S. Mujumdar, Ed , Marcel Dekker Inc New York, NY.

Mimura, T., 1963, "Studies on Heat Transfer in Packed Beds", Graduate Thesis, Univ. of Tokyo, (*cited* from Kunii and Suzuki[1967])

Missbach, A., 1937, *Listy Cukrovar.*, 55 293, (*cited* from Scheidegger [1974]).

Miyauchi, T., H Kataoka, and T Kikuchi, 1976, "Gas Film Coefficients of Mass Transfer in Low Peclet Number Region for Sphere Packed Beds", *Chem. Eng. Sci.*, 31. 9-13

Murakami, K, and R. Imamura, 1984, "Porosity and Gas Permeability", Ch. 17 in *Handbook of Physical and Mechanical Testing of Paper and Paperboard*, vol. 2, R.E. Mark, and K Murakami, eds , Marcel Dekker Inc., New York.

Murakami, K., and T. Yamauchi, 1981, "Porous Structure of Pulp Sheets Evaluated by Mercury Intrusion Method", *Proc. Japan Tappi/CPPA Tech. Sec. Papermaking Conf.*, 20-22 Oct., Tokyo, 97-103.

Myklestad, O., 1968, "An Analysis of Transient Flow of Heat and Moisture during Drying of Granular Beds", *Int J. Heat Mass Tr.*, **11**: 675-687.

Nelsen, F.M , and F.T. Eggertsen, 1958, "Determination of Surface Area, Adsorption Measurements by a Continuous Flow Method", *Anal. Chem.*, **30**(8): 1387-1390.

Nelson, P.A., and T.R. Galloway, 1975, "Particle-to-Fluid Heat and Mass Transfer in Dense Systems of Fine Particles", *Chem. Eng. Sci.*, **30**: 1-6.

Nevalainen, A., K. Ebeling, J E. Laine, and K. Knuts, 1983, "The Influence of Pore Structure on Filler Retention", *Paperi ja Puu*, 65(4): 271-277.

Nielsen, R.F., 1951, "Permeability Constancy Range of a Porous Medium", *World Oil*, 132(6): 188-192

Nilson, R.H , 1981, "Transient Fluid Flow In Porous Media: Inertia-Dominated to Viscous-Dominated Transition", *ASME J. Fluids. Eng.*, **103** (2): 339-343.

Nilsson, P., and K.O. Larsson, 1968, "Paper Web Performance in a Press Nip", *Pulp Pap. Mag. Can.*, 69(24)· T438-T445

Ohtake, T., M Usuda, and T Kadoya, 1984, "The Pore Structure of Thermomechanical Pulp Sheets by Mercury Porosimetry", *Japan Tappi*, **38**(10): 47-53

Page, D.H., and P A Tydeman, 1962, "A New Theory of the Shrinkage, Structure and Properties of Paper, in *Formation and Structure of Paper*, F. Bolam, Ed , BPBMA, London, England, 397-413

Patankar, S.V., 1980, *Numerical Heat Transfer and Fluid Flow*, Hemisphere Publ. Corp. Washington, DC

Payatekes, A.C.. C Tien, and R Turian, 1973, "A New Model for Granular Porous Media Parts I and II", *AIChE J* , **19**. 58-76

Petrovic, L J., and G. Thodos, 1968, "Mass Transfer in the Flow of Gases Through Packed Beds", *Ind Eng Chem Fundam.*, 7(2)· 274-280.

Pfeffer, R., 1964, "Heat and Mass Transport in Multiparticle Systems", *Ind. Eng. Chem. Fundam* , 3(4) 380-383

Plain, G.J., and H.L. Morrison, 1954, "Critical Reynolds Number and Flow Permeability", *Am J. Physics*, 22(3) 143-146.

Polat, O., W.J M. Douglas, and R H Crotogino, 1987, "Experimental Study of Through Drying of Paper", *DRYING'87*, A S Mujumdar, Ed., Hemisphere Pub. Corp., New York, N Y 290-295

Polubarinova-Kochina, P.Ya , 1962, *Theory of Groundwater Movement*, Translated by R. de Wiest, Princeton University Press.

Prahl, J.M., 1968, "Thermodynamics of Paaper Fibre and Water Mixtures", *Ph. D. Dissertation*, Harvard University, Cambridge, MA, U.S A.

Raj, P.P.K., and H W Emmons, 1975, "Transpiration Drying of Porous Hygroscopic Materials", *Int. J. Heat Mass Tr.*, **18**: 623-634.

Randall, K.R., 1984, "Using High Velocity Impingement Air to Improve Through Drying Performance on Semi-Permeable Webs", *DRYING'84*, A.S. Mujumdar, Ed., Hemisphere Publ. Corp., New York, 254-263.
Ranz, W E., and W.R. Marshall Jr , 1952, "Evaporation from Drops, I & II", *Chem. Eng. Prog.*, **48**(3)· 141-146, and **43**(4). 173-180.

Resnick W., and R.R White, 1949, "Mass Transfer in Systems of Gas and Fludized Solids", *Chem Eng Prog* , 45(6)· 377-390.

Reynolds, O., 1900, *Papers on Mechanical and Physical Subjects*, Cambridge University Press, London

Robertson, A.A., and S G. Mason, 1949, "Specific Surface of Cellulose Fibers by the Liquid Permeability Method", *Pulp Paper Mag Can.*, **50**(13) 103-110.

Rohrer, J.W., and F J Gardiner, 1976, "Through-Drying: Heat Transfer Mechanism and Machine System Response", *Tappi*, **59**(4): 82-87

Rumpf, H., and A.R. Gupte, 1971, "Einflusse der Porositat und Korngroßenverteilung im Widerstandsgesetz der Porenstromung", *Chem. Ing. Tech.*, **43**(6): 367-375.

Sanborn, I.B., 1962, "A Study of Irreversible, Stress-Induced Changes in the Macrostructure of Paper", *Tappi*, **45**(6): 465-474.

Satterfield, C N , and H Resnick, 1954, "Simultanous Heat and Mass Transfer in a Diffusion Controlled Chemical Reaction-Part 2 Studies in Packed Bed", *Chem Eng Prog* , 50(10) 504-510

Scallan, A.M., and J. Borch, 1976, "Fundamental Parameters Affecting the Opacity and Brightness of Uncoated Paper", in *The Fundamental Properties of Paper Related to Its Use*, vol. 1, F. Bolam, Ed., BPBMA, London, U.K., 152-163.

Scallan, A.M., and J.E. Carles, 1972, "The Correlation of the Water Retention Value with the Fibre Saturation Point", *Svensk Papperstidn.*, 75: 699-703.

Scheidegger, A.E., 1960, *The Physics of Flow Through Porous Media*, 2. edition. Univ. Toronto Press, Toronto

Scheidegger, A.E., 1974, *The Physics of Flow Through Porous Media*, 3. edition, Univ. Toronto Press, Toronto.

Scheneebeli, G., 1955, "Experiences sur la limite de validite de la loi Darcy et l'apparition de la turbulence dans ecoulement de filtration, *La Houille Blanche*, No.2 (March-April): 141-149

Schlunder, E.U , 1976, "Fortschritte und Entwicklungstendenzen bei der Auslegung von Trocknern fur vorgeformte Trocknungsguter", *Chem. Ing. Tech.*, 48(3): 190-198

Schlunder, E.U , 1977, "On the Mechanism of Mass Transfer in Heterogeneous Systems- In Particular in Fixed Beds, Fluidized beds and on Bubble Trays", *Chem. Eng. Sci* , 32: 845-851.

Schlunder, E.U., H. Martin, and P. Gummel, 1977, "Drying Fundamentals and Technology", Intensive Short Course Notes, March 21-23, 1977, Dept. Chem. Eng., McGill University, Montreal, Canada.

Sen Gupta, A., and G. Thodos, 1962, "Mass and Heat Transfer in the Flow of Fluids Through Fixed and Fulidized Beds of Spherical Particles", *AIChE J.*, 8(5): 608-610.

Sen Gupta, A., and G. Thodos, 1963, "Direct Analogy Between Mass and Heat Transfer to Beds of Spheres", *AIChE J.*, 9(6): 751-754.

Sen Gupta, A., and G. Thodos, 1964, "Transitional Behaviour for the Simultaneous Mass and Heat Transfer of Gases Flowing Through Packed and Distended Beds of Spheres", *Ind Eng Chem. Fundam.*, 3(3): 218-220.

Sherman, W.R., 1964, "The Movement of a Soluble Material During the Washing of a Bed of Packed Solids", *A I Ch E.J.*, 10(6): 855-860.

Sherwood, T.K , 1929, "The Drying of Solids, Part I & II", *Ind. Eng. Chem.*, 21(1): 12-26, and 21(10) 976-980.

Slattery, J.C., 1972, *Momentum, Energy, and Mass Transfer in Continua*, Mc-Graw Hill, New York.

Soininen, M , 1987, "Through-Drying Theory", *DRYING'87*, A.S. Mujumdar, Ed., Hemisphere Publ Corp , New York, 218-224

Spielman, L., and S.L. Goren, 1968, "Model for Predicting Pressure Drop and Filtration Efficiency in Fibrous Media", *Envir. Sci. Tech.*, 2(4): 279-287

Stone, J.E., and L.F Nickerson, 1963, "A Dynamic Nitrogen Adsorption Method for Surfaces Area Measurements of Paper", *Pulp Pap. Mag. Can.*, 64(3). T155-T161.

Stone, J.E., and A.M. Scallan, 1965, "A Study of Cell Wall Structure by Nitrogen Adsorption", *Pulp Paper Mag Can.*, 66(8): T407-T414.

Stone, J E., A.M. Scallan, and G M A Aberson, 1966, "The Wall Density of Native Cellulose Fibers", *Pulp Paper Mag Can.*, 67(5): T263-T268.

Suzuki, K., 1964, "Studies on Heat Transfer in Packed Beds", Graduate

Thesis, Univ. of Tokyo, (*cited* from Kunii and Suzuki[1967])

Suzuki, M., R.B. Keey, and S. Maeda, 1975, "On the Characteristic Drying Curvee", *A.I Ch.E. Symp. Ser.*, 73(163): 47-56

Taecker, R.G., and O.A. Hougen, 1949, "Heat, Mass Transfer of Gas Film in Flow of Gases Through Commercial Tower Packings", *Chem. Eng. Prog.*, 45(3): 188-193.

van Brakel, J., 1975, "Pore Space Models for Transport Phenomena in Porous Media", *Powder Tech* , 11· 205-236.

van Brakel, J., 1980, "Heat and Mass Transfer", Lecture notes, Dept. of Chem. Eng., University of New Brunswick, Fredericton, NB.

Villalobos, J.A , 1975, "Engineering Considerations in Through Drying", BPBIF Inter. Water Removal Symp. (109 Conf), London, March 20.

Villalobos, J.A , 1986, "Thru-Drying - A Technology Review", *Proc. PIRA Intl. Conf. on New Tech. in Web Consolidation and Drying*, Brighton, Sussex, UK

Wakao, N., 1976, "Particle-to-Fluid Transfer Coefficients and Fluid Diffusivities at Low Flow Rate in Packed Beds", *Chem. Eng. Sci.*, 31: 1115-1122.

Wakao, N., and T. Funazkri, 1978, "Effect of Fluid Dispersion Coefficients on Particle-to-Fluid Mass Transfer Coefficients in Packed Beds, Correlation of Sherwood Numbers", *Chem Eng. Sci.*, 33: 1375-1384.

Wakao, N., and S Kaguei, 1982. *Heat and Mass Transfer in Packed Beds*, Gordon and Breach Sci. Publ , New York

Wakao, N., and S. Tanisho, 1974, "Chromatographic Measurements of Particle-Gas Mass Transfer Coefficients at Low Reynolds Numbers in Packed Beds", *Chem. Eng Sci* , 29 1991-1994

Wakao, N., K. Tanaka, and H Nagai, 1976, "Measurements of Particle-to-Gas Mass Transfer Coefficients from Chromatographic Adsorption Experiments", *Chem. Eng Sci.*, 31: 1109-1113.

Wakao, N., S. Kaguei, and H Nagai, 1977, "Critique on Determination of Packed Bed Particle-to-Fluid Heat Transfer Coefficients from Steady Radial Heat Transfer Measurements", *Chem Eng. Sci.*, 32· 1261-1265

Walser, R., and R.S. Swenson, 1968, "Air Through-Drying of Paper", *Tappi*, 51(4): 184-190.

Wedel, G.L., and J.L. Chance, 1977, "Analysis of Through-Drying", *Tappi*, 60(7): 82-85.

Whitaker, S., 1967, "Diffusion and Dispersion in Porous Media", *AIChE J.*, 13: 420-427.

Whitaker, S., 1969, "Advances in the Theory of Fluid Motion in Porous Media", *Ind. Eng. Chem.*, 61: 14-28

Whitaker, S., 1977, *Fundamental Principles of Heat Transfer*, Pergamon, New York.

White, A.M., 1935, "Pressure Drop and Loading Velocities in Packed Towers", *Trans. Amer. Inst. Chem. Eng.*, 31: 390-408.

White, R.E., and W.E. Marceau, 1962, "The Capillary Behaviour of Paper", *Tappi*, 45(4): 279-284.

Wilke, C.R., and O A. Hougen, 1945, "Mass Transfer in the Flow of Gases Through Granular Solids Extended to Low Modified Reynolds Numbers", *Trans. Am. Inst. Chem Eng.*, 41· 445-451

Wilkins, G.S , and G. Thodos, 1969, "Mass Transfer Driving Forces in Packed and Fluidized Beds", *AIChE J* , 15(1): 47-50.
Wiseman, N , 1987, personal communication

Yamauchi, T., and K. Murakami, 1983, "Fundamental Studies on Papermaking Properties of Hardwood Pulp III. Pore Structure of Paper Sheets Containing Vessel Elements", *J Japan Wood Res Soc* , 29(2). 158-163.

Yoshida, F., D Ramaswami, and O A Hougen, 1962, "Temperature and Partial Pressures at the Surfaces of Catalyst Particles", *AIChE J.*, 8(1) 5-11.

Zabeschek, G., 1977, *Ph. D Dissertation*, Karlsruhe University, FRG.

APPENDIX 1

RESPONSE OF THE SYSTEM TO MOIST PAPER INSERTION

A1.1 INTRODUCTION

This analysis concerns the system volume from the outlet of the critical flow orifice to the location of the wet sheet, which consists mainly of the air heater and plenum chamber, Fig. 3.1. The mass conservation equation for the drying air in that system is:

$$[\text{Accumulation of air}] = [\text{Air in}] - [\text{Air out}] \qquad (A1.1)$$

The accumulation term is zero for the steady state condition before the wet sheet is inserted and after a sufficient time following its insertion. The "air in" term remains always at a selected constant mass flow rate because the upstream pressure to the critical flow orifice never changes, and although the pressure downstream of this orifice does change during a through drying experiment, that change is always within the limits to maintain critical flow across the orifice. The constancy of the "air out" term, i.e. the flow through the sheet of drying paper, is thus dependent on reducing the "accumulation of air" within the system, which is proportional to changes of pressure within the system and to the system volume. The volume of the air heater and plenum chamber system was minimized by careful design in order to minimize this effect. This appendix provides the analysis which establishes that the moist sheet throughflow rate, i.e. "air out", does not differ in a significant way from the selected, fixed value of the "air in".

On introduction of the wet paper of very low permeability, the pressure upstream of the sheet increases to a very sharp maximum, at which point the air flow through wet sheet ("air out") equals that at

the critical flow orifice ("air in"). During the period of increasing pressure the "accumulation of air" is positive and the "air out" through the drying sheet is therefore less than the set value of "air in" across the critical flow orifice. As the permeability of paper to air throughflow increases greatly during drying. the pressure upstream of the sheet, after reaching its maximum, drops rapidly. During this period the "accumulation" term is negative and the "air out" through the sheet is therefore greater than the set value of "air in". The periods before and after the pressure maximum are for convenience dealt with separately below.

A1.2 INITIAL PERIOD: "Accumulation of air" positive

The objective is to have the system volume sufficiently low that the maximum pressure is reached so quickly that the period of time over which the "air out" through the wet sheet is less than the controlled value of "air in" acceptably short

The pressure-time response of the system immediately after insertion of the moist sheet can be calculated via a simple dynamic analysis.

Assuming ideal gas behaviour, the accumulation term is

$$\text{Accumulation of air} = M \frac{\partial n}{\partial t} = \frac{MV}{RT} \frac{\partial P}{\partial t} \qquad \text{(A1.2)}$$

From Darcy's law, the "air out" term is

$$\text{Air out} = A\, G_{out} = A\, (k/L\nu)\, \Delta P \qquad \text{(A1.3)}$$

Substituting Eqns. A1.2 and A1.3 into Eqn. A1.1 and replacing $(\partial P/\partial t)$ with $(\partial \Delta P/\partial t)$, gives

$$(MV/RTA)(\partial \Delta P/\partial t) = G_{in} - (k/L\nu)\, \Delta P \qquad \text{(A1.4)}$$

which upon integration gives

$$(k/L\nu G_{in})\, \Delta P = 1 - \exp[-(RTAk/L\nu MV)t] \qquad \text{(A1.5)}$$

But $k/L\nu G_{in}=1/\Delta P_{max}$, where ΔP_{max} is the maximum pressure drop attainable for the air flow rate of G_{in} across a bed of permeability k and thickness L. Substitution in Eqn. A1.5 gives

$$\Delta P/\Delta P_f = 1 - \exp[-(RTAk/L\nu MV)t] \qquad (A1.6)$$

Eqn. A1.6 describes the ΔP-t relationship upon insertion of the moist sheet. This equation shows that the pressure build-up follows a first-order response with a time constant, Γ, equal to $L\nu MV/RTAk$. Thus the time constant is proportional to the wet paper permeability term, k/L, to the paper cross-sectional area, A, and to the system volume, V.

The system volume from the critical flow orifice to the wet sheet is $V\simeq 4\times10^{-3}m^3$, and the wet paper cross-sectional area, $A\simeq 8\times10^{-3}m^2$. For ambient air, then

$$\Gamma = [1.5\times10^{-5}\times29\times4\times10^{-3}]/[8314\times293\times8\times10^{-3}]/(k/L)$$

$$= 8.9\times10^{-11}/(k/L) \text{ seconds.}$$

As measurements of the present study indicate that the lowest value of the modified permeability, k/L, for $150g/m^2$ paper with 150% moisture is approximately $3.9\times10^{-10}m$, then Γ=0 23s. The actual value of Γ would be somewhat smaller yet, even for the thickest sheet, because paper permeability increases sharply during through drying, while the above estimate is based on the initial value of permeability. Thus for the worst case of the lowest permeability paper, it takes only 1s to reach 99% approach of the peak pressure at which point the "accumulation of air" term goes to zero and the "air out" rate through the drying paper becomes identical to the "air in" rate across the critical flow orifice. This calculation thus confirms that with the system volume this small, the maximum pressure is reached so quickly that period over which paper throughflow is less than the controlled value of G is very

short, barely 1s in the worst case.

A1.3 FINAL PERIOD: "Accumulation of air" negative

As the sheet dries, its permeability increases and ΔP drops from its maximum value. Thus the "accumulation of air" term in Eqn. A1.1 becomes negative, i.e. $G_{out}>G_{in}$. In order to determine the difference between G_{out} and G_{in}, actual ΔP-t data were fitted to an exponential form, i.e. $\Delta P=a+be^{-ct}$. With this relation substituted in Eqn. A1.4, $(G_{out}-G_{in})$ may be calculated as a function of time. The maximum difference between G_{out} and G_{in} is found to be only 1.1% for the worst case, i.e. for the thickest paper, 150g/m^2.

A1.4 CONCLUSION

It is demonstrated that the system volume is sufficiently small that the selected steady state value of mass flow rate across the wet paper, G, is achieved within 1s and that during the remainder of the drying period this value does not deviate appreciably from the set value.

APPENDIX 2

CALIBRATION OF THE INFRA-RED ANALYZER AS A MOISTURE METER

The IR analyzer is calibrated against an absolute measurement instrument, a chilled-mirror dew point meter (EG&G Model 660) using air of various levels of relative humidity, each fixed by equilibration with a saturated salt solution. During calibration, air is circulated continuously until equilibrium is attained in a closed system which consists of the measuring chamber of the IR analyzer, the saturated salt solution container, the dew point meter and a circulation fan. The salt solutions used in the calibration runs are listed in Table A2.1 with the approximate humidity level of each. Equilibrium relative humidity is a strong function of ambient temperature for some salt solutions. The humidity of the dry compressed air and ambient air were also measured by the dew point meter and used for calibration purposes.

Table A2.1 Solutions used for maintaining constant humidity at 20°C (Dean[1979])

Solid Phase	% Relative Humidity
$LiCl.H_2O$	12.0
$KC_2H_3O_2$ $1.5H_2O$	23.0
$MgCl_2.6H_2O$	33.0
$Mg(NO_3)_2.6H_2O$	55.0
NaCl	75.7
KBr	84.0
KNO_3	93.0
K_2SO_4	97.0

Calibration Procedure

1) Set the IR analyzer wavelength, 2.7μm, time constant, 0.15s, and scale expansion, ×20.

2) Connect the desired salt solution container to the system

3) Start the fan to circulate air and monitor the outputs of the IR analyzer, dew point meter, and circulating air temperature with a 3-pen recorder, YEW Model 3660, until equilibrium is reached, i.e. a steady dew point temperature.

4) After equilibrium is reached, monitor for 5min. the IR analyzer output and the dew point meter temperature via a PC based data acquisition system.

5) Repeat steps 2-4 for each salt solution.

6) Convert dew point temperatures to absolute humidity, and IR outputs to absorbance, and calculate the coefficients of the calibration curve using a statistical package on IBM-PC microcomputer.

This calibration procedure takes approximately 4 hours. Although time consuming, this procedure was repeated on every experiment day prior to the drying experiments in order to avoid error from the slight drift of the IR analyzer output.

APPENDIX 3

EXPERIMENTAL PROCEDURES

Preparation of Test Sheets

Handsheets of all basis weights were prepared from dry, unbleached, unbeaten laboratory kraft pulp, 100% black spruce, according to CPPA Standard C.4. Handsheets were dried, under restraint, in a constant humidity room according to the same Standard and stored in plastic bags until used. Papriformer newsprint, at ~70% moisture, obtained from the Pulp and Paper Research Institute of Canada, was stored in a plastic bag until used.

Through Drying-Permeability Experiments

1) Open the main compressed air line and adjust the air flow rate to the desired value, meanwhile monitor the humidity of the dry, compressed air both by the IR analyzer and, for calibration purposes, by the dew point meter.

2) Connect the measuring chamber of the IR analyzer to the calibration system, and follow the calibration procedure described in Appendix 2.

3) Adjust the air heater controls to the desired inlet air temperature, monitor the air temperature via a recorder and fine tune the heater controls as required.

4) Upon the completion of the calibration runs, reconnect the measuring chamber of the IR analyzer to the drying apparatus.

5) Cut the 104mm diameter test sheet for the sample holder from a 160mm diameter handsheet using a specifically designed carbon steel

punch. Place the test sheet into the sample holder described in Chapter 3, and secure it in place with the six screws of the sample holder to prevent any air by-passing

6) With a spray can, moisten the sheet to the desired moisture content, checked by weighing the sample holder-sheet assembly. Equilibrate in a dessicator charged with distilled water, in order to obtain uniform moisture content in the paper.

7) Start the data acquisition to monitor the drying air conditions prior to the experiment.

8) After 50-60 seconds, weigh the sample holder-sheet assembly on a top-loading electronic balance then insert immediately into the drying system

9) Upon the completion of the experiment, save the acquired data in a file and again weigh the sample holder-sheet assembly.

10) Remove the paper from the sample holder and place in a microwave oven prior to obtaining the bone dry weight for basis weight determination.

11) Convert all thermocouple, pressure transducer and IR readings to temperature, pressure drop and humidity values using the calibration equations, for calculation of drying rate, pressure drop and paper moisture content via a data reduction program.

12) Prepare the calculated data as graphical output, i.e. drying rate and pressure drop as a function of paper moisture content, with a Hewlett Packard Model HP7470A plotter using a modified version of the MGPP (McGill University Plotting Package).

Supplementary Dry Paper Permeability Experiments

Such supplementary experiments were performed using the same apparatus using ambient temperature air. Throughflow temperature and pressure drop across the paper at selected throughflow rates were monitored via the PC-based data acquisition system, with data acquisition and processing as above.

For helium throughflow, a helium cylinder, 18 MPa, was connected to the system.

APPENDIX 4

CHARACTERIZATION OF THE PULP

The freeness the dry, unbleached standard laboratory kraft pulp (100 % black spruce) and the physical properties of handsheets are as follows;

Canadian Standard Freeness, mL	685
Grammage (Basis Weight), g/m^2 (O.D)	59.8
Bulking Caliper, μm	120.1
Bulk, cm^3/g	2 01
Burst Index, kPa m^2/g	1.96
Tear Index, mN m^2/g	21.05
Breaking Length, km	3.30
Stretch, %	1.77
Thoughness Index, mJ	37
Stress-Strain Factor, mJ/g	417
Zero-Span Breaking Length, km (Pulmac)	16.84
Tensile Index, N m/g	32.38
TEA, J/m^2	24.97

APPENDIX 5

TEMPERATURE MEASUREMENT AND CONTROL

Accurate measurements of transient air temperatures upstream and downstream of the paper and within the paper are essential for checking the heat and mass balances, and to document the drying conditions. How the inherent problems of these measurements were solved, or minimized, is summarized here.

A5.1 AIR INLET TEMPERATURE

The volume of the experimental apparatus upstream of the paper sample was minimized in order to keep the time constant of the system as small as possible, as detailed in Appendix 1 The heater and the plenum chamber, i e. the section between the heater and the sample holder, are the main constituents of this volume, are shown in Fig. 3.1. Therefore, uniform heating of the drying air to the maximum temperature of ~95°C, with minimum temperature fluctuation and maximum uniformity of air temperature should be achieved in a small volume. A four-stage electrical heater was designed and built to achieve these objectives

The plenum chamber was a 150mm long, 102mm ID, section of acrylic pipe. The heater unit, 80mm long and 102mm ID, had 6 elements, each a 13mm thick section, 127×127mm square on the outside, cut on the inside for the air flow channel of the same diameter, 102mm, as that of the sheet being dried. Of these six elements, the four elements of diatomaceous earth carried the heating coils. These four were supported at either end for strength by two pieces of aluminum cut to the identical dimensions. Each heater consisted of a grid of 8 parallel

heating wires, made by drilling 8 holes on either side of these elements. Approximately 3.1m of NichromeV wire, 9.85Ω/m, was threaded through each element, so that each of the four units had a capacity of approximately 400W. The 4 heating units were assembled, with the direction of the heating wires in adjacent units set at 90°, supported at each end by an aluminum element Air tight seals between each of the 6 units was obtained with high-temperature resistant gaskets. The whole heater unit was then insulated on the outside. This compact, low contained volume design proved eminently satisfactory.

A perforated plate with 16 holes, 6mm OD, i.e. approximately 6% open area, was placed upstream of the heater in the divergent section, Fig. 3.1, to provide uniform flow over the heater elements. Two sheets of 250g/m^2 blotter paper sandwiched between two fine metal screens were placed 80mm downstream of the heater to eliminate the slight flow and temperature fluctuations and to prevent exposure of the drying paper to radiative heating from the heater resistance wires The inside of the plenum chamber between the heater exit and the sample holder was insulated with a double layer of a plastic insulator sheet with air gaps between the layers. This insulation was glued to the chamber walls with silastic, a silicon based insulating adhesive.

Air temperature profiles were measured at 100mm and 250mm downstream of the heater away from the heater, Fig A5.1. The scanning directions of the two profiles were perpendicular. The small difference between these two profiles, less than 1.5°C, confirms that the objective of having the air inlet temperature uniform over the surface of the drying paper was satisfactorily achieved.

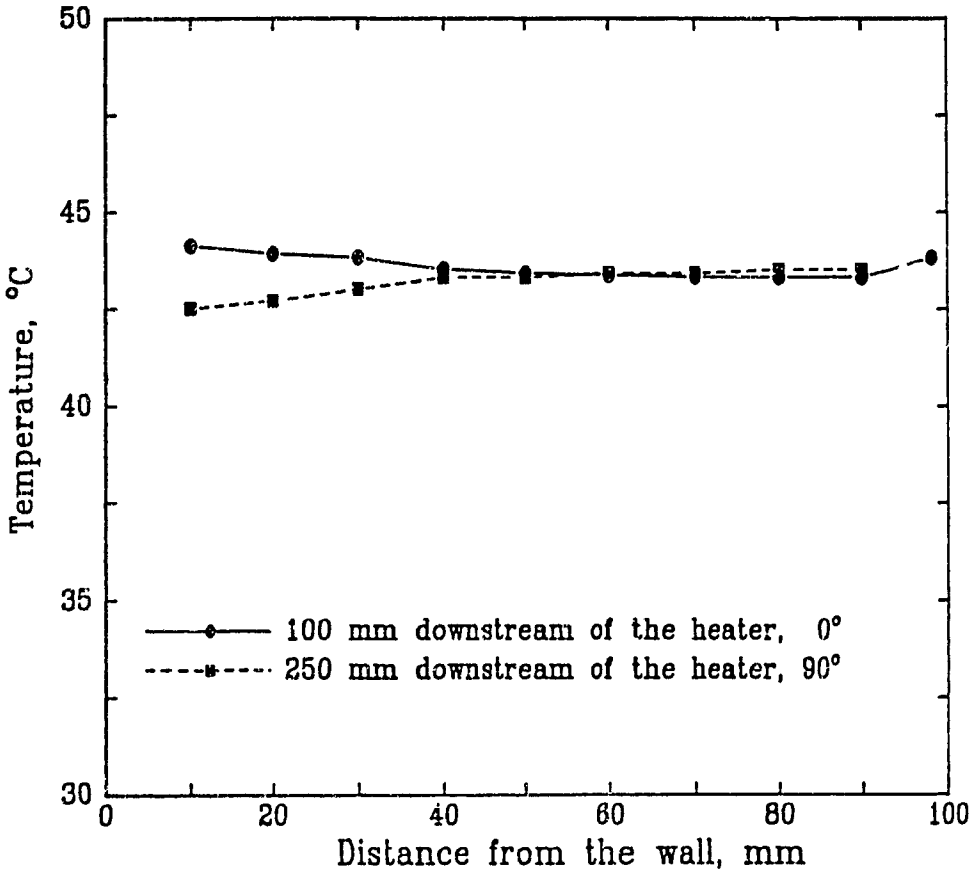

Figure A5.1 Throughflow inlet temperature profiles

A5.2 AIR EXIT TEMPERATURE

In order to minimize heat loss, a convergent plastic section was placed inside the metal adaptor, Fig. 3.1, between the sample insertion mechanism and the measuring chamber of the IR analyzer. The throughflow air exit temperature was measured continuously during the drying experiments at three locations with thermocouples, 15, 35 and 60mm from the wall, placed 3mm below the sample holder. Each thermocouple, of diameter 76μm, was glued on a thin, 1mm OD, polystyrene support. The average of these three measurements was used for the continuous heat and mass balance check during each experiment. These temperatures are displayed in Figs. A5.2a-e for sheets dried in ambient temperature air at various flow rates. The temperature reading of the thermocouple 15mm from the wall is here denoted as T_1, and those 35 and 60mm away as T_2 and T_3 respectively. The differences between the T_1, T_2, T_3 temperatures shown on these figures result from nonuniformity in paper structure. Only the profiles shown in Fig. A5.2d are almost identical, showing the uniformity of the structure, at least at these three locations, of that particular sheet. Results of similar measurements are shown in Figs. A5.3a and b for paper dried at higher temperatures. All these temperatures are higher than the corresponding adiabatic saturation temperature of the drying air. This evidence supplements that presented in the text that the throughflow exit air does not reach saturation except for conditions of low temperature and low throughflow rate below levels of industrial relevance.

A5.3 PAPER TEMPERATURE

A technique was developed to monitor the temperature within the sheet during through drying. For this purpose a very fine thermocouple,

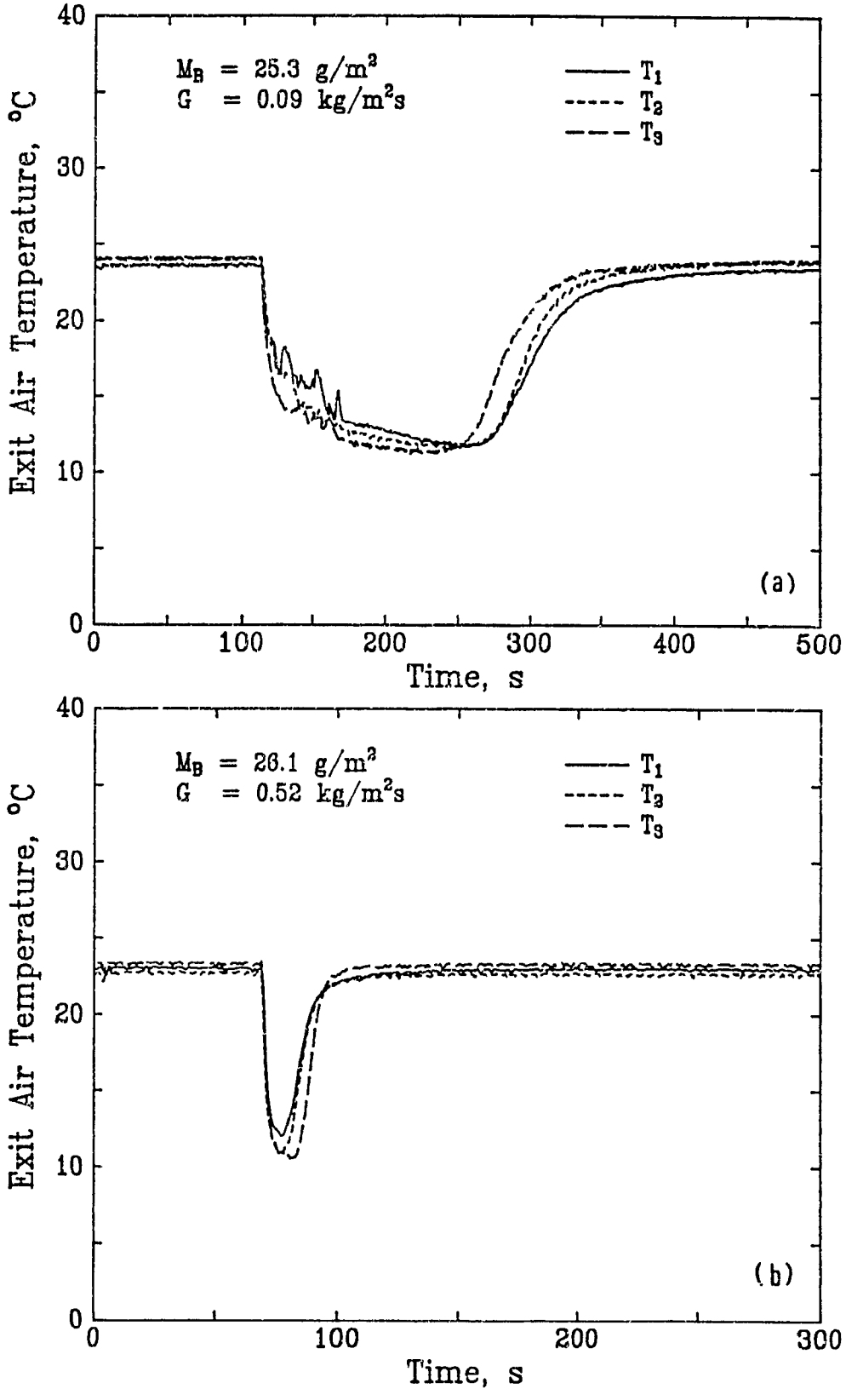

Figure A5.2 Throughflow exit temperature profiles for $T_i \cong 23°C$: a) Low M_B-low G, b) Low M_B-high G, c) Low M_B-high G, d) Medium M_B-medium G, e) Medium M_B-high G

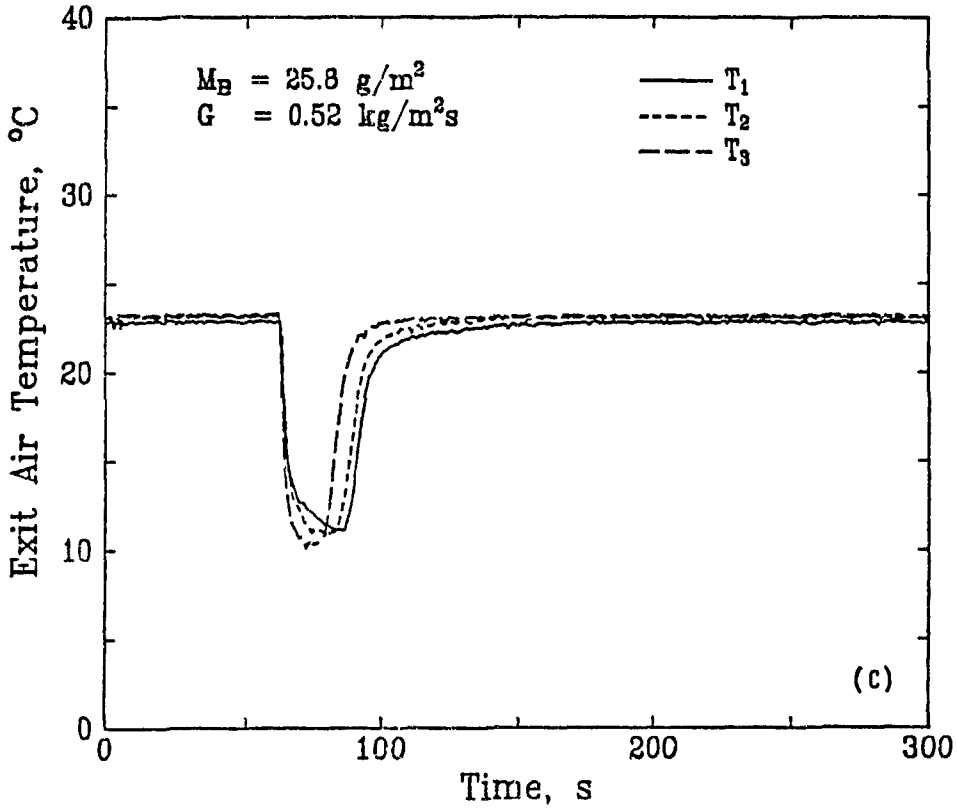

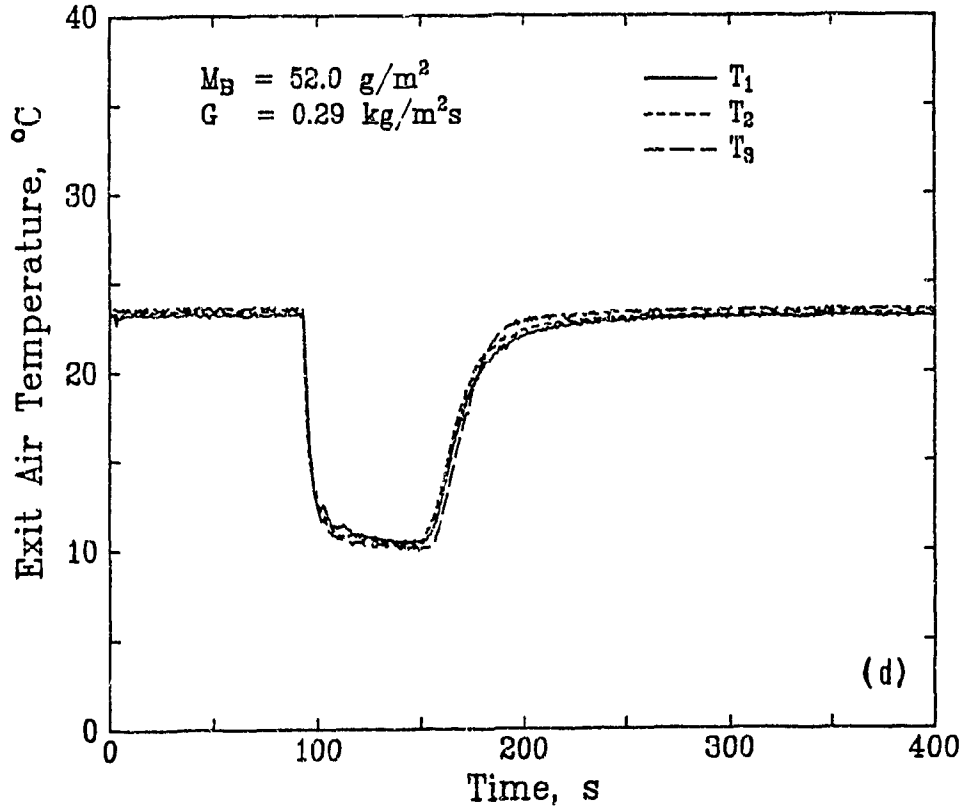

Figure A5.2 continued

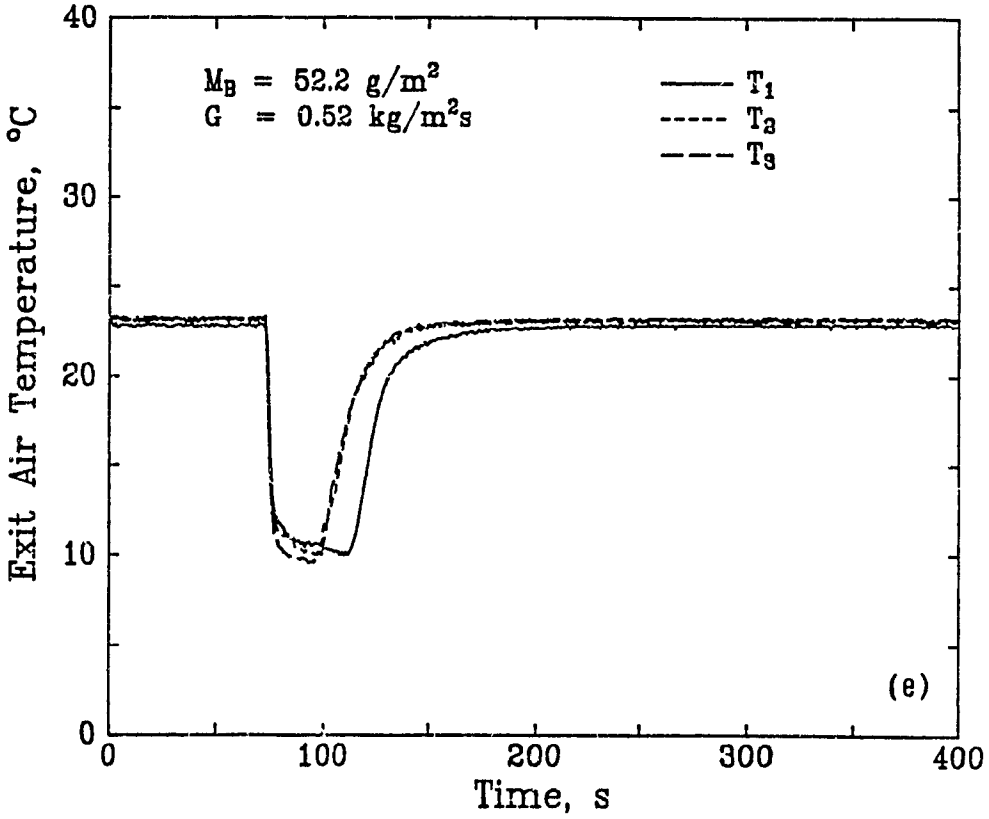

Figure A5.2 continued

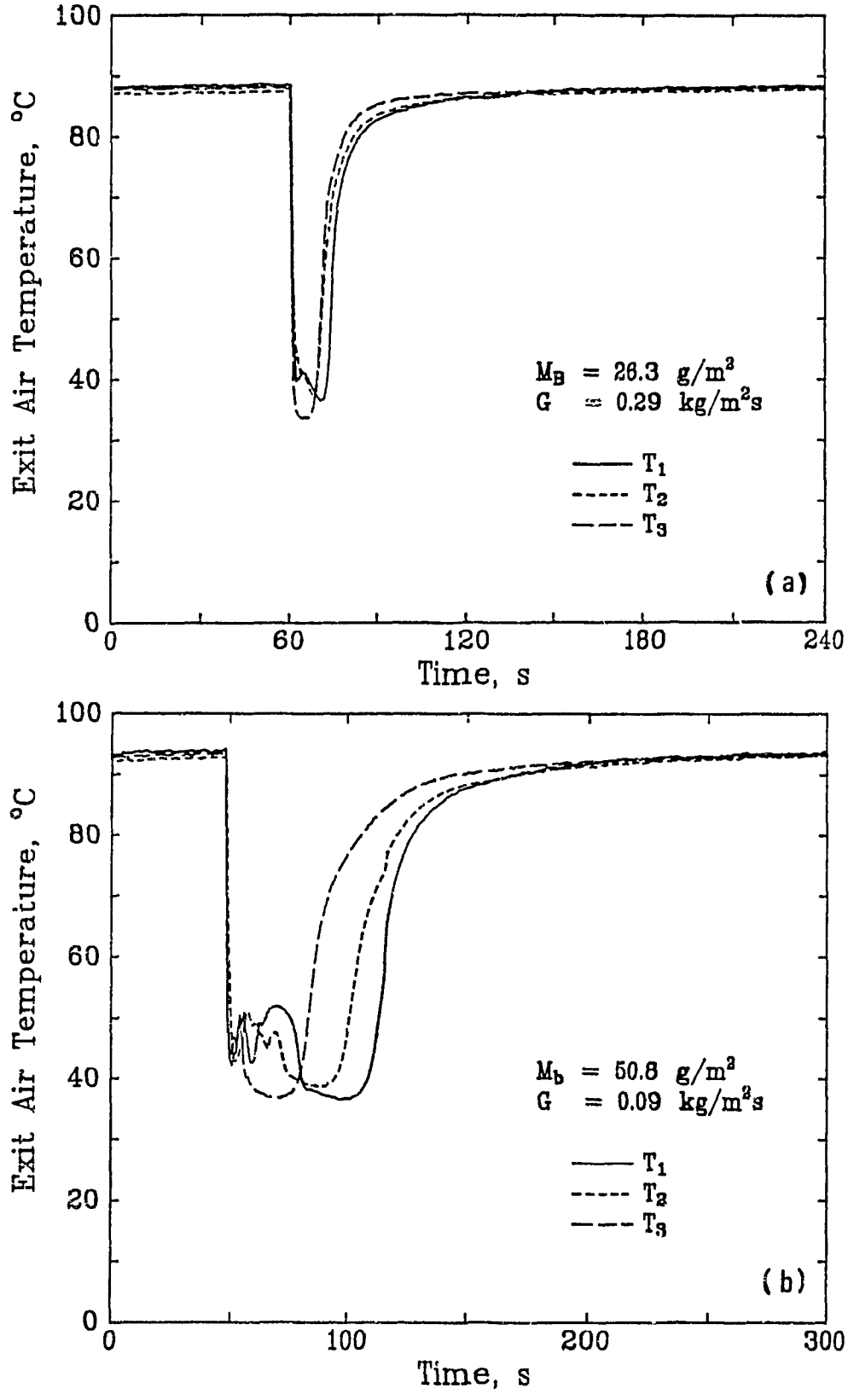

Figure A5.3 Throughflow exit temperature profiles for $T_i \approx 90°C$: a) Low M_B - medium G, b) Medium M_B - low G

made from two adjacent insulated wires, each of 76μm diameter thermocouple wire, was embedded in the middle of the sheet during handsheet preparation This thermocouple size should be viewed relative to the characteristic dimension of the paper pores, d_p, in the range 5-44μm, and with the thickness of the paper, about 0.5mm for the heavy paper used for these tests.

The amount of pulp for the desired basis weight was divided into two equal lots and two handsheets, each of half the desired basis weight, were prepared and the first one couched off the forming screen in the usual manner. The thermocouple was placed between these sheets while the second sheet was still on the forming screen The two sheets were then couched together and removed from the forming screen.

This temperature at the mid-plane of the sheet and the adiabatic saturation temperature for the inlet air conditions are shown in Figs. A5.4a and b for paper dried in ambient temperature air and at $T_1 \cong 46°C$. These temperature profiles reveal that for these conditions of high M_B - low G, paper mid-plane temperature reached saturation during the constant rate period of drying.

Temperatures at the mid-plane and at the exit of the sheet, the temperature defined in Appendix A5 2 as T_3, measured during drying of heavy paper at moderate throughflow rates, are shown in Figs. A5.5a and b. During the constant rate period of drying in both experiments, while the temperature at the exit was as much as 5°C above the adiabatic saturation temperature, the mid-plane paper temperature was at saturation.

For the experiment shown in Fig A5.5a the end of the constant rate period, taken as the point at which temperature starts to increase from its plateau level, occurs at the exit of the sheet very shortly after

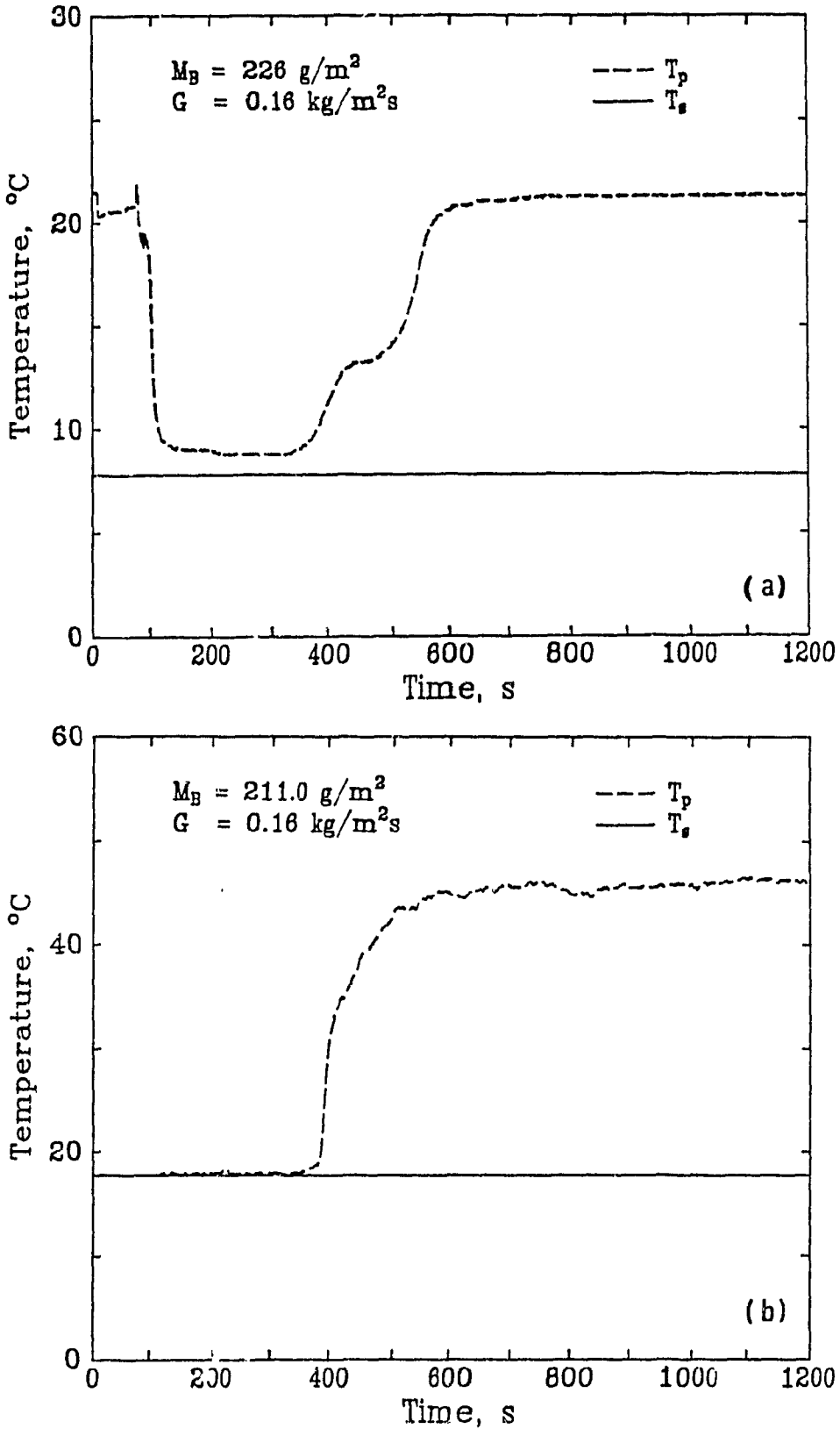

Figure A5.4 Temperature profiles at the mid-plane of the sheet: a) $T_i \cong 23°C$, b) $T_i \cong 46°C$

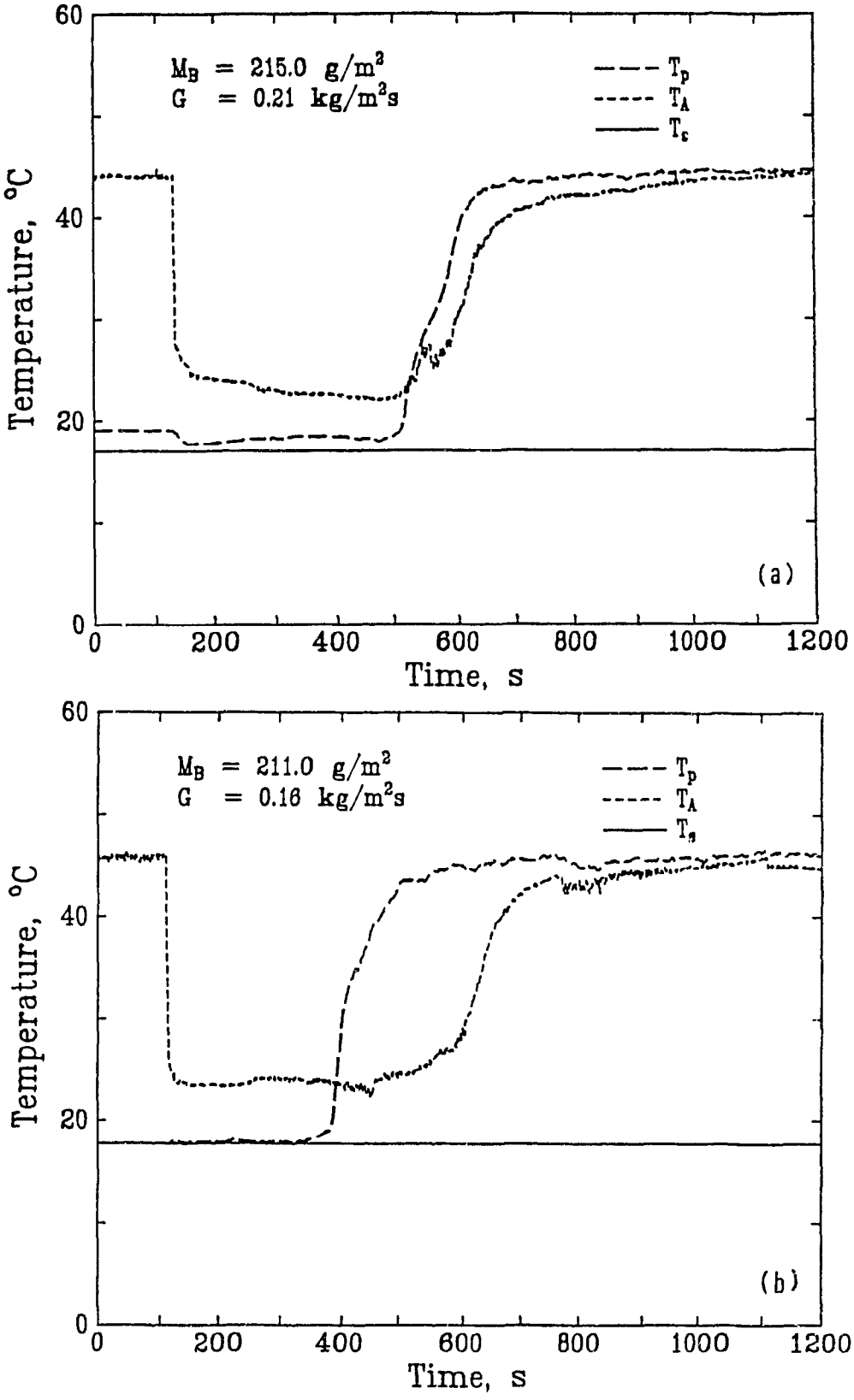

Figure A5.5 Temperature profiles at the mid-plane and exit of the sheet dried in ~46°C air: a) G=0.21kg/m²s, b) G=0.16kg/m²s

it occurs at the mid-plane. However, for the experiment at a lower throughflow rate shown in Fig. A5.5b, the constant rate period lasts almost twice as long at the sheet exit as at the paper mid-plane. The air humidity profile at the exit of the sheet, which is a mixing-cup value, not included in this figure, shows the same behaviour as does the point value of temperature at the exit of the sheet. The differences between these profiles of point temperatures are believed to reflect again the presence of local nonuniformity in paper.

APPENDIX 6

PRESSURE DROP DATA ACROSS MOIST AND DRY PAPER

Pressure drop measurements across dry paper are given in Table A6 1. Momentum transport parameters listed in Table 4.2 are based on this data. Physical properties of air are calculated at the mean pressure, i.e. $\frac{1}{2}(P_1+P_o)=P_o+\frac{\Delta P}{2}$ where $P_o=101.325$kPa

The complete set of momentum transport parameters for moist paper at 0.1kg/kg intervals are given in Table A6 2. The physical properties of air and water vapor are calculated at the mean conditions The viscosity of moist air is calculated using the semiempirical formula of Wilke given by Bird *et al.*[1960]

$$\mu_{mix} = \sum_{i=1}^{n} \frac{x_i \mu_i}{\sum_{j=1}^{n} x_j \Omega_{ij}}$$

in which

$$\Omega_{ij} = \frac{1}{\sqrt{8}} \left(1 + \frac{M_i}{M_j}\right)^{-1/2} \left[1 + \left(\frac{\mu_i}{\mu_j}\right)^{1/2} \left(\frac{M_j}{M_i}\right)^{1/4}\right]^2$$

where n is the number of chemical species in the mixture; x_i and x_j are the mole fractions of species i and j; μ_i and μ_j are the viscosities of species i and j; and M_i and M_j are the corresponding molecular weights Ω_{ij} is dimensionless and, when i=j, $\Omega_{ij}=1$. However the viscosity difference between moist and dry air is always less than 2% for the present experimental conditions

The complete set of Re-f data for dry and moist paper is tabulated in Tables A6.3 and A6.4 respectively

Table A6.1 Pressure drop across dry paper

M_B, g/m^2	G, kg/m^{2}s	ΔP, Pa	G/μ, m^{-1}	$\Delta P/LG\nu$, m^{-2}
		Air flow		
25	0.085	70	4.70×10^3	1.06×10^{12}
	0.144	138	7.97	1.24
	0.269	296	14.83	1.43
	0.381	446	21.01	1.53
	0.483	624	26.65	1.68
	0.612	847	33.79	1.80
25	0.085	70	4.72	1.08
	0.145	132	8.00	1.20
	0.269	284	14.88	1.39
	0.381	450	21.10	1.55
	0.483	615	26.75	1.67
	0.612	839	33 93	1.80
25	0.085	70	4.70	1.07
	0.144	142	8 00	1.28
	0.269	302	14.89	1 47
	0.381	456	21.10	1.57
	0.483	642	26.76	1.73
	0.612	864	33.93	1.85
50	0 085	477	4 70	3.90
	0.145	830	7.97	4.00
	0.270	1580	14.88	4.10
	0.384	2320	21.14	4.25
	0.488	3060	26.91	4.43
	0.621	3970	34.21	4.53
50	0.085	473	4.73	3.91
	0.145	802	8.03	3.98
	0.270	1540	14.98	4.04
	0.384	2280	21.29	4.21
	0.488	2990	27.07	4.38
	0.621	3910	34.44	4.51
50	0.085	482	4.73	3.92
	0.145	817	8.03	3.98
	0.270	1550	14.98	4.06
	0.384	2280	21.29	4.23
	0.488	3030	27.08	4.43
	0.621	3930	34.44	4.53
100	0.085	962	4.69	3.97
	0.145	1710	7.98	4.16
	0.271	3190	14.94	4.18
	0.387	4710	21.31	4.35
	0.494	6200	27.21	4.52
100	0.086	984	4.74	4.06
	0.146	1730	8.07	4.22
	0.272	3240	15.10	4.25
	0.389	4770	21.55	4.41
	0.496	6290	27.50	4.59

Table A6.1 continued

M_B, g/m^2	G, kg/m^{2}s	ΔP, Pa	G/μ, m^{-1}	$\Delta P/LG\nu$, m^{-2}
100	0.086	960	4.74×10^3	3.97×10^{12}
	0.145	1670	8.06	4.08
	0.272	3120	15.09	4.12
	0.389	4650	21.53	4.30
	0.496	6140	27.48	4.49
150	0.086	1700	4.72	4.33
	0.146	2950	8.05	4.43
	0.275	5700	15.16	4.60
	0.394	8080	21.70	4.63
	0.505	10410	27.82	4.69
150	0.086	1750	4.76	4.37
	0.146	3010	8.12	4.43
	0.275	5860	15.29	4.61
	0.394	8270	21.91	4.64
	0.505	10730	28.09	4 73
150	0.086	1750	4.76	4 36
	0.146	3060	8.12	4.48
	0.275	5770	15.29	4.56
	0.394	8190	21.90	4 59
	0.505	10650	28.08	4.69
250	0.086	2850	4.70	4.41
	0.147	4940	8.05	4.51
	0.278	9370	15.27	4.60
	0.402	13610	22 07	4.72
	0.520	17810	28.51	4.87
250	0.086	2810	4.78	4.42
	0.148	4930	8.19	4.56
	0.280	9230	15.54	4.60
	0.405	13560	22 45	4.77
	0.523	17600	28.99	4 89
250	0.086	2890	4.79	4.53
	0 148	4960	8.19	4.59
	0.281	9500	15.56	4.73
	0.405	13660	22 47	4.81
	0.524	18020	29.05	5.00

Table A6.1 continued

M_B, g/m²	G, kg/m²s	ΔP, Pa	G/μ, m⁻¹	ΔP/LGν, m⁻²
		Helium flow		
25	0.024	158	1.19×10³	1.10×10¹²
	0.040	292	2.05	1.19
	0.087	669	4.41	1.27
	0.111	883	5.63	1.31
	0.159	1265	8.06	1.32
25	0.024	159	1.20	1.11
	0.040	280	2.04	1.14
	0.087	641	4.40	1.22
	0.111	890	5.63	1.32
	0.159	1250	8.06	1.31
25	0.024	158	1.19	1.10
	0.040	302	2.06	1.23
	0.087	682	4.41	1.29
	0.111	902	5.63	1.34
	0.159	1300	8.07	1.36
50	0.023	920	1.18	3.51
	0.040	1590	2.04	3.53
	0.078	3120	3.96	3.58
	0.113	4550	5.72	3.64
50	0.023	912	1.17	3.48
	0.040	1540	2.03	3.49
	0.078	3040	3.96	3.51
	0.113	4470	5.71	3.57
50	0.023	930	1.18	3.53
	0.040	1570	2.04	3.55
	0.078	3060	3 96	3.57
	0.113	4480	5.72	3.58
100	0.022	1820	1.14	3 63
	0.031	2500	1.56	3.65
	0.039	3170	1.98	3.65
	0.048	3950	2.45	3.69
	0.061	4880	3.08	3.65
100	0.022	1860	1.15	3.71
	0.031	2530	1.56	3.69
	0.039	3220	1.98	3.71
	0.048	4010	2.45	3.74
	0.061	4950	3.08	3.70
100	0.022	1820	1.14	3.62
	0.031	2440	1.56	3.58
	0.039	3100	1.98	3.58
	0.048	3900	2.45	3.63
	0.061	4840	3.08	3.62
150	0.022	2990	1 12	3 80
	0.041	5580	2.07	3.85
	0.076	10470	3.97	3.84
	0.117	15680	6.10	3.85

Table A6.1 continued

M_B, g/m^2	G, kg/m^{2}s	ΔP, Pa	G/μ, m^{-1}	$\Delta P/LG\nu$, m^{-2}
150	0.022	3080	1.12×10^3	3.89×10^{12}
	0.041	5690	2.07	3.93
	0.076	10770	3.97	3.94
	0.117	16060	6.10	3.94
150	0.022	3070	1.12	3.86
	0.041	5780	2.07	3.96
	0.076	10600	3.97	3.89
	0.117	15890	6.10	3.90
250	0.023	5230	1.15	3.91
	0.040	9030	2.02	3 90
	0.095	20100	4.78	3.87
	0.124	25800	6.27	3 92
250	0.023	5170	1.15	3.86
	0.040	9000	2.02	3 89
	0.095	19810	4.78	3.86
	0.124	25700	6.27	3.91
250	0.023	5290	1.15	3.96
	0.040	9050	2.02	3.91
	0.095	20390	4.78	3.91
	0.124	25890	6.27	3.93

Table A6.2 Momentum transport parameters for moist paper

X	N	α', m^{-1}	$\sigma_{\alpha'}$, m^{-1}	β	$\sigma_{\beta'}$	k/L, m	$C\sqrt{L}=\beta'/\sqrt{\alpha'}$	d_p, μm
				25g/m²				
0.0	65	3.41×10^{7}	2.4×10^{6}	573	58	29.3×10^{-9}	0.098	16 8
0.1	65	3.38	3.1	560	51	29.6	0.096	16.6
0.2	65	3.50	3.7	553	62	28.5	0.093	15.9
0.3	65	3.46	3.6	585	59	28.9	0.099	16.9
0.4	65	3.45	3.2	578	57	29.0	0.098	16 7
0.5	65	3 53	3.4	584	60	28.4	0.098	16.6
0.6	65	3.65	3.2	613	62	27.4	0.101	16 8
0.7	65	3.74	3.4	642	61	26.7	0.105	17.1
0.8	65	4.00	3.7	662	70	25.0	0.105	16.5
0.9	65	4.31	4.3	741	81	23.2	0.113	17.2
1.0	65	4.66	5.8	756	85	21.5	0.111	16 3
1.1	65	4.95	6.3	866	101	20.2	0.123	17 5
1.2	65	5.43	7.1	1041	101	18.4	0.141	19 2
1.3	64	5.87	7.4	1286	120	17.0	0.168	21.9
1 4	64	6.10	8 1	1414	145	16.4	0.181	23.2
1.5	63	6.40	9.0	1704	150	15.6	0.213	26.6
1.6	62	7.12	9.5	2109	180	14.1	0.250	29 6
1.7	60	8.14	11.0	2617	250	12.3	0.286	32.1
1.8	59	8.83	12.0	3264	310	11.3	0.347	37.0
1.9	58	9.50	13.3	3843	350	10.5	0.394	40 4
2.0	55	10 21	14 0	4321	410	9.8	0.428	42 3
2.1	53	11.28	16.0	5012	550	8.9	0.472	44.4
2.2	52	13 95	17.0	6448	580	7.2	0.546	46.2
2.3	49	15 92	18.0	6418	670	6.3	0.509	40 3
2.4	45	15.77	20.0	6855	770	6.3	0.546	43.5
2.5	35	15 98	22 0	7006	850	6.3	0.554	43.8
2.6	30	16.24	22.0	7358	950	6.2	0.577	45.3
2.7	20	16.10	24.0	7426	1100	6.2	0.585	46.1
2.8	17	15.83	25.0	6670	1200	6.3	0.530	42.1
2.9	13	16.59	26.0	7603	1150	6.0	0.590	45.8
3.0	10	16.87	25.0	7062	1130	5.9	0.544	41.9
3.1	7	16.66	28.0	7596	1250	6.0	0.589	45.6
				50g/m²				
0.0	61	1.39×10^{8}	1.2×10^{7}	753	60	7.2×10^{-9}	0.063	5.4
0.1	61	1.45	1.1	584	61	6.9	0.049	4 0
0.2	61	1.38	1.3	639	65	7.3	0.054	4.6
0.3	61	1.37	1.5	691	72	7.3	0.059	5.0
0.4	61	1.42	1.4	831	73	7.0	0.070	5.8
0.5	61	1.49	1.5	739	78	6.7	0.061	5.0
0.6	61	1.53	1.7	1076	96	6.5	0.087	7.0
0.7	61	1.59	1.7	961	120	6.3	0.076	6.0
0.8	61	1.66	1.9	1206	155	6.0	0.094	7.3
0.9	61	1.73	2.0	1387	179	5.8	0.106	8 0
1.0	61	1.91	2 2	1625	198	5.2	0.118	8.5
1.1	61	2.13	2.4	2111	215	4.7	0.145	9 9
1.2	61	2.29	3.1	2639	260	4.4	0.175	11 6
1.3	60	2.54	3.6	3161	350	3.9	0.198	12.5
1.4	59	2.69	3.9	3592	370	3.7	0.219	13 4

Table A6.2 continued

X	N	α', m^{-1}	$\sigma_{\alpha'}$, m^{-1}	β	$\sigma_{\beta'}$	k/L, m	$C\sqrt{L}=\beta'/\sqrt{\alpha'}$	d_p, μm
				$50 g/m^2$				
1.5	58	2.83×10^{8}	4.2×10^{7}	3679	418	3.5×10^{-9}	0.219	13.0
1.6	58	3.28	4.6	4182	510	3.0	0.231	12 7
1.7	58	4.06	5.2	5635	750	2.5	0.280	13 9
1.8	57	4.56	5.1	6578	760	2.2	0.308	14 4
1.9	57	5.44	5.7	8409	810	1.9	0.361	15.5
2.0	57	5.67	6.8	7465	920	1.8	0.313	13 2
2.1	45	5.94	6.9	9202	950	1.7	0.378	15 5
2.2	36	6.94	6.9	8449	1015	1.5	0.321	12.2
2.3	35	7.27	7.0	10551	1150	1.4	0.391	14 5
2.4	33	9 82	8.0	9902	1210	1.0	0.316	10.1
2.5	33	10.60	9.5	10064	1315	0.9	0.309	9 5
2.6	29	9.96	4.5	9483	1080	1.0	0.300	9.5
				$100 g/m^2$				
0.0	61	3.73×10^{8}	4.2×10^{7}			2.68×10^{-9}		
0.1	61	3.82	4.3			2.62		
0.2	61	3.93	4.3			2 54		
0.3	61	4.06	5.0			2.46		
0.4	61	4.22	5.3			2.37		
0.5	61	4.42	5.4			2.26		
0.6	61	4 30	6.5			2.08		
0.7	61	4.82	6.5			2 07		
0 8	61	5.36	7.8			1.87		
0.9	61	5.61	7.9			1.78		
1.0	61	6.08	9.8			1.64		
1.1	61	6.83	12.1			1.46		
1.2	61	7.89	13.1			1.27		
1.3	59	9.67	15.0			1.03		
1.4	58	11.46	17.1			0.87		
1.5	57	12.37	19.0			0.81		
1.6	51	12.88	21.8			0.78		
1.7	43	14.16	23.0			0.71		
1.8	32	17.81	31.0			0.56		
1.9	30	20.22	37.0			0.49		
2.0	27	22.48	23.0			0.44		
2.1	25	24.25	23.7			0.41		
2.2	18	30.08	29.4			0.33		
2.3	12	37.45	39.1			0.27		
2.4	8	39.05	42.0			0.26		
				$150 g/m^2$				
0.0	35	6.70×10^{8}	8.5×10^{7}			1.49×10^{-9}		
0.1	35	6.64	8.6			1.51		
0.2	35	6.66	8.3			1.50		
0.3	35	6.91	8.9			1.45		
0.4	35	7.41	9.5			1.35		
0.5	35	7.84	9.4			1.28		
0.6	35	8.79	10.5			1.14		
0.7	34	9.03	10.7			1.11		

Table A6.2 continued

X	N	α', m^{-1}	$\sigma_{\alpha'}$, m^{-1}	β	$\sigma_{\beta'}$	k/L, m	$C\sqrt{L}=\beta'/\sqrt{\alpha'}$	d_p, μm
				150g/m²				
0.8	34	10.5×10^{8}	17.5×10^{7}			0.96×10^{-9}		
0.9	32	11.7	19.1			0.86		
1.0	30	13.0	21.0			0.77		
1.1	30	14.7	23.1			0.68		
1.2	28	16.7	23.0			0.60		
1.3	23	17.8	31.0			0.56		
1.4	19	23.1	38.9			0.43		
1.5	15	27.0	42.0			0.37		
1.6	9	28.4	32.3			0.35		

Table A6.3 Friction factor for flow through dry paper

Re, Gd_p/μ	f, $\Delta P\rho/\beta G^2 L$	Re, Gd_p/μ	f, $\Delta P\rho/\beta G^2 L$
0.027	38.05	0.046	23.91
0.100	11.82	0.128	9.57
0.183	6.48	0.102	9.87
0.172	6.78	0.320	4.22
0.454	3.17	0.576	2.76
0.730	2.19	0.009	115.81
0.015	67.89	0.029	35.05
0.042	24.76	0.026	39.71
0.044	24.01	0.082	13.19
0.116	9.62	0.148	8.12
0.188	6.33	0.030	34.38
0.051	21.19	0.096	11.36
0.137	8.31	0.174	6.76
0.015	69.04	0.025	41.40
0.047	22.85	0.067	15.71
0.086	12.67	0.020	51.56
0.034	30.79	0.064	16.24
0.093	11.75	0.120	9.39
0.073	13.92	0.123	9.20
0.229	5.33	0.325	4.19
0.412	3.65	0.522	2.87
0.623	2.51	0.069	14.13
0.118	9.83	0.219	5.69
0.310	4.25	0.393	3.79
0.498	2.97	0.594	2.59
0.046	22.31	0.078	13.59
0.145	7.87	0.206	5.99
0.261	5.02	0.331	4.00
0.395	3.45	0.025	41.52
0.041	24.02	0.077	13.21
0.109	9.69	0.138	8.11
0.175	6.39	0.209	5.51
0.024	42.34	0.040	24.55
0.075	13.30	0.106	9.73
0.135	8.23	0.172	6.42
0.205	5.51	0.020	50.81
0.034	30.27	0.064	16.49
0.091	12.00	0.115	10.07
0.146	7.86	0.174	6.76
0.028	36.20	0.047	21.10
0.087	11.68	0.124	8.59
0.157	7.14	0.199	5.61
0.238	4.87	0.030	33.68
0.050	19.72	0.094	10.83
0.134	7.96	0.170	6.54
0.027	36.67	0.046	21.61
0.086	12.09	0.123	8.63
0.156	7.16	0.027	36.82
0.046	21.50	0.086	12.06
0.122	8.58	0.156	7.12
0.031	32.67	0.053	18.83

Table A6.3 continued

Re, Gd_p/μ	f, $\Delta P\rho/\beta G^2 L$	Re, Gd_p/μ	f, $\Delta P\rho/\beta G^2 L$
0.098	10.54	0.139	7.58
0.177	6.32	0.032	31.32
0.055	18.00	0.102	10.11
0.146	7.27	0.185	6.08
0.022	45.49	0.038	26.65
0.070	14.48	0.100	10.61
0.023	43.93	0.039	25.78
0.073	14.10	0.103	10.29
0.030	34.00	0.051	19.46
0.094	10.60	0.135	7.93

Table A6.4 Friction factor for flow through moist paper

Re, Gd_p/μ	f, $\Delta P\rho/\beta' G^2$	Re, Gd_p/μ	f, $\Delta P\rho/\beta' G^2$
	X = 0.1 kg/kg		
0.071	14.34	0.072	16.32
0.076	13.47	0.076	11.54
0.079	10.13	0.080	17.87
0.121	8.12	0.121	9.25
0.128	6.28	0.129	7.96
0.129	8.84	0.131	9.49
0.135	9.16	0.141	9.47
0.228	4.42	0.227	5.35
0.227	5.07	0.230	4.66
0.237	5.24	0.239	4.24
0.240	6.37	0.242	7.74
0.249	4.79	0.249	4.35
0.249	5.15	0.250	3.87
0.264	4.90	0.265	6.03
0.265	5.37	0.266	5.22
0.408	2.72	0.408	3.23
0.408	2.74	0.408	3.30
0.410	3.74	0.425	2.65
0.428	3.76	0.430	4.38
0.430	3.67	0.448	2.40
0.449	3.05	0.449	3.35
0.449	2.45	0.449	3.02
0.449	2.32	0.450	3.02
0.470	2.46	0.471	3.50
0.475	4.03	0.477	3.36
0.017	60.63	0.017	58.25
0.018	53.43	0.018	66.82
0.018	52.98	0.018	57.03
0.018	51.25	0.019	47.19
0.019	59.33	0.019	48.92
0.020	69.88	0.020	47.44
0.029	31.40	0.029	32.46
0.029	35.50	0.029	30.15
0.029	31.06	0.031	37.82
0.031	33.33	0.031	37.25
0.031	38.36	0.031	38.50
0.032	36.03	0.032	35.78
0.034	33.41	0.034	31.34
0.034	37.34	0.054	16.58
0.054	20.06	0.054	15.68
0.054	16.42	0.054	23.70
0.056	15.34	0.056	13.12
0.057	14.55	0.057	18.73
0.057	15.66	0.059	13.98
0.059	17.25	0.060	17.21
0.060	18.73	0.060	15.94
0.062	17.38	0.062	18.75
0.063	18.40	0.063	20.09
0.097	10.53	0.097	11.85

Table A6.4 continued

Re, Gd_p/μ	f, $\Delta P\rho/\beta' G^2$	Re, Gd_p/μ	f, $\Delta P\rho/\beta' G^2$
	X = 0.1 kg/kg		
0.098	8.55	0.098	8.23
0.098	11.22	0.101	7.19
0.102	9.82	0.102	8.12
0.102	7.82	0.103	8.14
0.107	8.39	0.107	9.09
0.107	9.68	0.107	8.09
0.108	10.49	0.112	8.58
0.113	7.79	0.113	11.62
0.113	10.84		
	X = 0.5 kg/kg		
0.073	13.08	0.073	18.83
0.077	12.92	0.077	15.25
0.077	18.71	0.078	19.26
0.079	10.82	0.080	9.47
0.122	9.78	0.123	9.73
0.126	5.57	0.126	9.53
0.127	8.56	0.129	6.39
0.131	8.29	0.132	9.22
0.133	9.73	0.138	9.05
0.143	7.44	0.231	5.18
0.232	5.30	0.235	4.34
0.237	4.72	0.246	5.37
0.246	6.17	0.247	7.49
0.248	4.32	0.251	4.79
0.252	4.97	0.253	4.70
0.255	4.18	0.267	5.86
0.267	5.79	0.267	5.28
0.268	5.18	0.413	2.68
0.415	3.17	0.415	3.22
0.416	2.70	0.424	4.16
0.435	2.75	0.442	3.72
0.446	4.23	0.446	3.54
0.451	2.54	0.453	2.34
0.454	3.00	0.457	3.07
0.457	3.00	0.457	2.61
0.458	3.29	0.478	2.59
0.481	3.58	0.481	3.81
0.481	3.20	0.021	50.95
0.021	53.85	0.022	49.01
0.022	60.47	0.022	46.15
0.022	44.09	0.022	45.19
0.023	41.13	0.023	45.94
0.023	39.13	0.024	52.38
0.024	36.72	0.035	27.28
0.035	29.04	0.036	29.21
0.036	26.29	0.036	24.99
0.037	30.54	0.037	29.47
0.037	30.42	0.038	32.12

Table A6.4 continued

Re, Gd_p/μ	f, $\Delta P\rho/\beta' G^2$	Re, Gd_p/μ	f, $\Delta P\rho/\beta' G^2$
	X = 0.5 kg/kg		
0.038	27.86	0.039	31.97
0.040	28.69	0.041	34.46
0.041	25.74	0.041	27.80
0.041	30.16	0.066	13.77
0.066	17.90	0.066	12.86
0.066	13.29	0.067	18.11
0.068	13.23	0.068	11.59
0.069	11.64	0.069	16.07
0.069	13.27	0.072	12.20
0.072	14.43	0.072	14.06
0.073	12.85	0.074	14.94
0.075	15.02	0.075	13.84
0.076	14.02	0.076	15.63
0.120	6.88	0.120	6.89
0.120	8.94	0.120	9.29
0.122	11.07	0.124	6.24
0.124	8.70	0.124	6.18
0.125	6.56	0.125	6.86
0.129	7.57	0.129	7.12
0.129	8.55	0.130	6.75
0.132	9.27	0.136	7.11
0.136	6.12	0.137	9.50
0.137	9.31		
	X = 1.0 kg/kg		
0.073	13.67	0.075	13.20
0.076	16.74	0.076	17.01
0.076	16.91	0.078	9.15
0.080	13.24	0.120	9.25
0.121	8.96	0.123	8.54
0.125	9.39	0.126	6.17
0.130	7.51	0.130	8.77
0.130	8.00	0.135	10.56
0.135	9.51	0.135	8.26
0.140	8.75	0.228	4.55
0.230	3.87	0.234	5.84
0.234	4.68	0.242	5.14
0.242	4.26	0.242	6.89
0.242	5.65	0.246	4.95
0.247	4.02	0.248	4.06
0.251	4.03	0.261	4.38
0.261	5.07	0.261	5.33
0.262	4.91	0.410	2.48
0.410	2.72	0.411	2.75
0.415	2.69	0.417	5.83
0.433	5.11	0.434	3.02
0.435	3.40	0.436	3.91
0.442	2.73	0.444	2.14
0.445	2.73	0.446	2.68

Table A6.4 continued

Re, Gd_p/μ	f, $\Delta P\rho/\beta' G^2$	Re, Gd_p/μ	f, $\Delta P\rho/\beta' G^2$
	X = 1.0 kg/kg		
0.449	2.90	0.451	2.91
0.451	2.74	0.469	3.85
0.469	3.81	0.469	2.53
0.469	3.15	0.037	33.79
0.038	31.09	0.039	29.72
0.040	25.11	0.040	24.19
0.040	22.62	0.041	27.59
0.041	33.74	0.042	21.30
0.042	18.28	0.043	30.32
0.043	19.56	0.063	15.82
0.064	15.55	0.064	15.05
0.064	14.41	0.064	17.89
0.067	15.30	0.067	16.78
0.067	17.28	0.068	16.41
0.068	18.88	0.070	16.29
0.071	19.29	0.073	18.60
0.073	12.93	0.073	16.69
0.073	14.97	0.118	8.03
0.119	6.97	0.119	7.10
0.120	10.37	0.120	12.62
0.122	7.81	0.123	6.74
0.124	6.28	0.124	7.43
0.124	8.79	0.128	6.82
0.130	8.24	0.131	8.05
0.131	7.35	0.131	8.79
0.134	7.66	0.134	8.26
0.136	7.76	0.136	8.91
0.214	4.01	0.215	5.62
0.215	3.78	0.218	6.36
0.219	9.36	0.223	3.44
0.224	3.59	0.224	3.69
0.225	3.61	0.225	5.91
0.230	4.57	0.230	4.00
0.232	5.60	0.235	4.28
0.236	6.28	0.243	3.90
0.243	3.40	0.245	6.16
0.245	6.07		
	X = 1.5 kg/kg		
0.121	9.50	0.126	10.37
0.126	8.11	0.126	8.81
0.126	9.07	0.130	8.07
0.202	6.45	0.203	5.75
0.204	5.44	0.204	6.67
0.206	8.87	0.208	4.30
0.213	4.52	0.214	6.20
0.214	4.27	0.215	5.68
0.221	7.21	0.222	6.56
0.221	5.76	0.222	5.31

Table A6.4 continued

Re, Gd_p/μ	f, $\Delta P\rho/\beta' G^2$	Re, Gd_p/μ	f, $\Delta P\rho/\beta' G^2$
	X = 1.5 kg/kg		
0.230	6.82	0.376	2.57
0.381	2.32	0.385	3.68
0.386	4.76	0.396	4.19
0.397	4.39	0.397	3.11
0.398	3.54	0.407	2.46
0.408	2.27	0.412	3.61
0.413	2.77	0.428	3.25
0.429	3.36	0.430	3.34
0.430	3.16	0.677	1.71
0.677	1.90	0.677	1.55
0.689	1.78	0.711	3.03
0.714	3.47	0.714	2.59
0.733	1.76	0.733	2.26
0.734	1.55	0.738	1.86
0.741	1.70	0.742	2.29
0.770	2.32	0.771	1.95
0.059	20.67	0.060	22.46
0.061	19.46	0.062	13.40
0.062	12.84	0.062	13.90
0.064	16.79	0.065	13.41
0.065	11.65	0.067	23.97
0.067	12.64	0.100	9.01
0.100	7.95	0.100	8.30
0.101	11.48	0.102	11.50
0.104	9.54	0.104	10.68
0.104	10.21	0.106	15.28
0.106	13.44	0.110	15.92
0.110	15.02	0.113	13.87
0.113	8.42	0.114	10.57
0.185	4.20	0.185	4.43
0.186	6.17	0.189	9.58
0.193	6.15	0.193	4.17
0.193	6.30	0.195	3.98
0.196	4.70	0.201	4.45
0.204	6.82	0.204	7.90
0.204	5.58	0.204	6.26
0.210	5.82	0.210	5.24
0.212	8.15	0.212	6.57
0.333	2.66	0.336	2.28
0.337	4.49	0.340	5.66
0.347	2.15	0.349	2.13
0.351	2.25	0.352	5.32
0.353	2.62	0.359	2.63
0.359	3.30	0.365	3.80
0.366	4.67	0.366	6.28
0.381	2.86	0.381	5.91
0.382	6.46	0.382	2.57

Table A6.4 continued

Re, Gd_p/μ	f, $\Delta P\rho/\beta' G^2$	Re, Gd_p/μ	f, $\Delta P\rho/\beta' G^2$
	X = 2.0 kg/kg		
0.196	7.19	0.204	5.15
0.204	4.37	0.205	7.60
0.205	3.89	0.210	8.18
0.210	5.99	0.210	7.23
0.211	4.60	0.211	5.98
0.329	3.15	0.332	3.47
0.332	4.66	0.333	4.77
0.333	6.32	0.340	2.60
0.343	2.62	0.345	2.18
0.345	3.47	0.347	4.77
0.357	6.15	0.358	5.28
0.358	4.05	0.359	6.17
0.620	1.64	0.640	3.02
0.642	3.51	0.642	2.87
0.662	1.84	0.666	2.35
0.668	3.23	0.694	2.17
0.695	3.33	0.695	2.97
1.113	1.84	1.117	1.47
1.188	0.86	1.190	0.81
1.191	1.29	1.196	1.40
1.197	2.37	1.198	2.79
1.199	1.40	1.244	2.72
1.246	2.23	0.063	12.91
0.064	11.40	0.064	12.15
0.066	22.90	0.066	14.30
0.066	17.16	0.069	21.14
0.102	6.26	0.103	7.08
0.103	9.87	0.103	16.08
0.104	10.94	0.107	11.49
0.107	12.64	0.107	13.25
0.116	11.78	0.190	4.08
0.191	3.85	0.193	6.36
0.198	4.01	0.199	6.75
0.200	3.93	0.200	10.77
0.201	5.83	0.208	6.34
0.208	5.80	0.209	8.99
0.214	7.48	0.215	7.34
0.344	2.27	0.346	1.98
0.346	5.91	0.359	2.96
0.359	2.24	0.371	3.31
0.374	5.98	0.375	2.72
0.375	4.74	0.389	3.94
0.390	3.01		
	X = 2.5 kg/kg		
0.207	4.73	0.208	4.31
0.214	7.68	0.215	7.66
0.223	5.18	0.224	9.01
0.336	3.63	0.347	2.96

Table A6.4 continued

Re, Gd_p/μ	f, $\Delta P\rho/\beta' G^2$	Re, Gd_p/μ	f, $\Delta P\rho/\beta' G^2$
	X = 2.5 kg/kg		
0.351	5.38	0.351	5.20
0.631	2.44	0.676	1.80
0.678	2.83	0.706	4.05
1.125	1.43	1.132	1.31
1.133	2.23	1.214	1.70
1.215	1.89	1.216	2.52
0.043	30.32	0.043	31.22
0.043	32.33	0.044	20.00
0.046	22.00	0.069	13.21
0.069	10.80	0.069	18.01
0.072	22.74	0.072	22.45
0.129	5.83	0.130	5.58
0.130	11.43	0.132	12.98
0.133	6.18	0.135	6.21
0.135	11.32	0.140	12.11
0.235	3.24	0.242	4.24
0.243	3.78	0.252	4.48
0.260	5.49	0.262	4.93

APPENDIX 7

ERROR ANALYSIS

Total rms error is expressed as

$$\delta f = \left[\sum_{i=1}^{n} \left(\frac{\partial f}{\partial x_i} \delta x_i \right)^2 \right]^{1/2}$$

Basis Weight: $M_B = 4W/\pi D^2$

$\partial M_B/\partial W = 4/\pi D^2$; $\partial M_B/\partial D = -8W/\pi D^3$

δM_B is always <1% because δW=0.0005g and δD=0.0005m

Porosity: $\varepsilon = 1 - M_B/(L\rho_f)$

$\partial \varepsilon/\partial M_B = -1/(L\rho_f)$; $\partial \varepsilon/\partial L = M_B/(L^2\rho_f)$, $\partial \varepsilon/\partial \rho_f = M_B/(L\rho_f^2)$

$\delta \varepsilon$ is ~0.013ε because $\delta M_B = 0.01 M_B$, $\delta l = 1\mu m$ and $\delta \rho_f = 50 g/m^3$

Permeability: $k = 1/\alpha$

$\partial k/\partial \alpha = -1/\alpha^2$

$\delta k \approx 0.06k$ because $\delta\alpha \approx 0.06\alpha$ as given in Chapter 4.

Specific Surface: $a_p^2 = \varepsilon^3/(\kappa k(1-\varepsilon)^2)$

$\partial a_p/\partial k = -\varepsilon^3/(2a_p \kappa k^2(1-\varepsilon)^2)$; $\partial a_p/\partial \varepsilon = [3\varepsilon^2/(1-\varepsilon)^2 + 2\varepsilon^3/(1-\varepsilon)^3]/(2a_p\kappa k)$

δa_p is ~6.0% for $\delta k = 0.06k$ and $\delta\varepsilon = 0.013\varepsilon$

Characteristic Dimension: $d_p = \beta/\alpha$

$\partial d_p/\partial \beta = 1/\alpha$; $\partial d_p/\partial \alpha = -\beta/\alpha^2$

δd_p is ~7% for dry paper before wetting-drying because both $\delta\alpha$ and $\delta\beta$ are ~6% as given in Chapter 4. δd_p increases to about 10-12% for dry paper after wetting-drying, and to 10-15% for wet paper.

Drying Rate: $R_C = 3600\ G(Y_o - Y_1)$

$\partial R_C/\partial G = 3600(Y_o - Y_1)$; $\partial R_C/\partial Y_o = 3600\ G$; $\partial R_C/\partial Y_1 = -3600\ G$

δR_C is ~2.5% at high T_1, i.e. 20g/kg$\leq Y_o$, and ~3.5% at low T_1, i.e. 6$\leq Y_o <$7g/kg, because the standard error on Y measurements from the infra

red calibration gives $\delta Y \simeq 0.1 g/kg$.

Number of Transfer Units: $N_G = \ln(R_S/(R_S - R_C))$

$\partial N_G/\partial R_S = -R_C/(R_S(R_S - R_C))$; $\partial N_G/\partial R_C = 1/(R_S - R_C)$

δN_G is highly dependent on the experimental conditions, i.e. the difference between R_S and R_C. The rms error on N_G determination is only 5.0% for $N_G = 0.86$, but as N_G increases to 2 and 3, rms error increases to 10.1% and 23.5%. For N_G greater than 4.5 the rms error is higher than 80%. See section on Sherwood number for use of N_G values.

Mass Transfer Coefficient: $k_G = N_G G/(La_P \rho_a)$

$\partial k_G/\partial N_G = G/(La_P \rho_a)$; $\partial k_G/\partial G = N_G/(La_P \rho_a)$; $\partial k_G/\partial a_P = -N_G G/(La_P^2 \rho_a)$;

$\partial k_G/\partial L = -N_G G/(L^2 a_P \rho_a)$; $\partial k_G/\partial \rho_a = -N_G G/(La_P \rho_a^2)$

For $\delta d_P \simeq 12.5\%$ for wet paper, $\delta a_P \simeq 12.5\%$ thus δk_G is 13% for $N_G = 0.86$. For higher N_G values δk_G is very close to δN_G.

Sherwood Number: $Sh = k_G d_P/D$

$\partial Sh/\partial k_G = d_P/D$; $\partial Sh/\partial d_P = k_G/D$, $\partial Sh/\partial D = -k_G d_P/D^2$

Again for $\delta d_P \simeq 12.5\%$ for wet paper, δSh becomes 18% for the above conditions. For higher N_G values δSh is also very close to δN_G.

As described in Section 6.4.1, Sh was not determined for about 10% of the experiments for which the exiting air was within 1% of saturation, as N_G is then large and subject to excessive error because of the close approach to equilibrium at the exit of the sheet.

Reynolds Number: $Re = Gd_P/\mu$

$\partial Re/\partial G = d_P/\mu$; $\partial Re/\partial d_P = G/\mu$; $\partial Re/\partial \mu = -Gd_P/\mu^2$

δRe is mainly controlled by δd_P, thus $\delta Re \simeq 12.8\%$ for $\delta d_P \simeq 12.5\%$.

APPENDIX 8

EXPERIMENTAL DATA

The experimental data is tabulated in pp. 372-376 followed by the drying rate, pressure drop and exit air temperature plots for all basis weight, throughflow rate and inlet temperature tested in the present study. The exit air temperature is that measured by the third thermocouple, i.e. T_3, described in Appendix 5.

M_g, g/m²	G, kg/m²s	X_o, kg/kg	T_i, °C	T_s, °C	R_s, kg/m²h	R_c, kg/m²h	X_{ci}, kg/kg	X_{cf}, kg/kg	d_p, μm	$4/d_p$, m²/m³	Re	N_G	k_g	Sh
25 8	0 092	3 71	23	7 8	2 08	2 08	3 03	1 51	44 0	0 91×10⁶	0 221	-	-	-
25 5	0 092	3 55	23	7 8	2 08	2 07	3 09	1 38	44 0	0 91	0 220	5 34	0 078	0 136
23 0	0 092	2 71	28	10 5	2 48	2 47	1 83	1 33	30 9	1 30	0 158	5 51	0 056	0 069
51 0	0 092	3 03	23	7 8	2 08	2 06	2 64	1 67	14 0	2 86	0 072	4 64	0 011	0 0061
53 0	0 092	2 27	24	8 6	2 13	2 07	1 75	1 16	12 3	3 24	0 065	3 69	0 0073	0 0039
54 7	0 092	0 63	24	8 6	2.13	2 12	0 55	0 34	5 0	8 05	0 025	5 36	0 0045	0 0009
53 7	0 092	1 32	28	10 2	2 41	2 40	1 10	0 47	7 4	5 37	0 039	5 58	0 0067	0 0021
55 3	0 092	2 92	28	10.2	2 41	2 40	2 27	1 11	14 0	2 86	0 073	5 48	0 0124	0 0074
51 0	0 092	1 13	28	10 2	2 41	2 40	0 97	0 51	6 6	6 02	0 035	6 38	0 0068	0 0019
101 6	0 092	2 08	25	9 7	2.10	2 11	1 64	0 67	11 5	3 47	0 059	-	-	-
97 9	0 092	1 18	25	9 7	2 10	2 06	1 03	0 38	7 1	5 64	0 037	3 99	0 0023	0 0007
102 3	0 092	1 73	25	9 7	2 10	2 02	1 51	0 57	9 6	4 15	0 050	3 29	0 0026	0 0011
149 5	0 092	1 00	28	10 1	2 37	2 30	0 83	0 35	6 5	6 17	0 034	3 57	0 0012	0 0003
152 8	0.092	0 57	28	10.1	2 37	2 30	0 48	0 27	5 0	7 99	0 026	3 61	0 0009	0 0002
147 5	0 092	0 60	27	10 0	2 31	2 26	0.50	0 25	5 1	7 85	0 027	3 74	0 0010	0 0002
26 2	0.156	2 05	23	7 8	3 44	3 37	1 73	1 23	19 5	2 06	0 173	3 88	0 040	0 034
23 5	0 156	3 27	28	10 5	4.15	4 14	2 59	1 42	42 5	0 94	0 368	6 03	0 143	0 240
24 7	0 156	1 59	28	10 5	4 15	4 17	1 05	0 85	16 7	2 40	0 123	-	-	-
51 6	0 156	2 08	23	7.8	3 44	3 35	1 72	0 96	11 0	3 63	0 098	3 69	0 011	0 0052
52 5	0 156	2 51	23	7 8	3 44	3 41	2 51	2 07	13 6	2 95	0 120	4 90	0 018	0 0105
54 0	0 156	2 24	24	8 6	3 60	3 41	1 85	0 83	11 9	3 35	0 106	2 95	0 0095	0 0049
53 6	0 156	2 86	24	8 6	3 60	3 49	2 56	1 16	14 0	2 86	0 124	3 54	0 013	0 0081
100 8	0 156	2 34	23	7 8	3 44	3 40	2 03	0 79	12 9	3 10	0 115	4 56	0 0080	0 0045
94 1	0 156	1 58	25	9 7	3 55	3 45	1 32	0.78	8 7	4 59	0 077	3 49	0 0041	0 0016
100 8	0 156	1 58	25	9 7	3 55	3 52	1 36	0 81	8 7	4 59	0 077	4 55	0 0054	0 0020
101 7	0 156	1 99	25	9.7	3 55	3 43	1.67	0 83	10 9	3 68	0 096	3 35	0 0050	0 0023
152 7	0 156	0 91	27	10 1	3 83	3 44	0 76	0 40	6 1	6 60	0 054	2 29	0 0012	0 0003
149 6	0 156	1 15	27	10 1	3 83	3 74	0 99	0 33	7 0	5 73	0 062	3 74	0 0023	0 0007
26 1	0 289	2 51	23	7 8	6 39	6 03	1 81	1 03	25 3	1 58	0 419	2 87	0 072	0 079
27 2	0 289	2 89	21	7 4	5 92	5 36	2 31	1 36	32 5	1 23	0 538	2 35	0 075	0 106
27 7	0 289	2 69	21	7 3	5 71	5 45	1 93	1 20	28 8	1 39	0 477	3 08	0 088	0 110
53 0	0 289	2 43	23	7 8	6 39	6 12	2 07	1 22	12 8	3 14	0 211	3 18	0 0204	0 011
52 0	0 289	2 20	23	7 8	6 39	6 12	1 85	0 93	11 4	3 51	0 188	3 17	0 018	0 0089
55 3	0 289	2 50	25	9 7	6 65	5 17	1 84	0 89	13 2	3 02	0 217	1 50	0 010	0 0057
55 2	0 289	2 55	25	9 7	6 65	5 44	1 75	1 05	13 5	2 96	0 222	1 70	0 0116	0 0067
102 1	0 289	1 78	23	7 8	6 39	6 09	1 48	1 12	9 5	4 19	0 158	3 05	0 0073	0.0030
102 1	0 289	2 00	23	7 8	6 39	6 08	1 69	0 87	10 7	3 74	0 177	3 02	0 0081	0 0038
105 2	0 289	2 46	25	9 7	6 65	6.01	1 88	0.83	13 4	2 99	0 220	2 34	0 0079	0 0046
153 1	0 289	1 47	23	7 8	6 39	6 08	1 27	0 70	8 2	4 86	0 136	3 01	0 0039	0 0014
154 0	0 289	1 60	23	7 8	6 39	6 05	1 37	0 64	8 8	4 53	0 146	2 93	0 0041	0 0016
26 6	0 518	2 00	23	7 8	11 47	9 65	1.38	0 78	17 2	2 33	0 510	1 84	0 056	0 042
26 3	0 518	2 75	23	7 8	11 47	10 12	1 93	1 08	28 3	1 41	0 840	2 14	0 107	0 132
27 0	0 518	1.94	21	7 4	10 63	9 66	1 31	0 74	16 7	2 40	0 496	2 39	0 071	0.051
27 2	0 518	2 49	21	7 4	10 63	10 06	1.62	1.04	23 9	1 67	0.711	2.92	0 124	0 129
52 9	0 518	2 80	23	7 8	11 47	11 07	2 31	1 14	14 0	2 86	0 415	3 37	0 042	0 026
51 6	0 518	2 98	21	7 4	10 63	10 04	2.43	1 22	14 0	2 86	0 416	2 88	0 036	0 022
51.8	0.518	1.97	21	7 4	10 63	9 15	1.21	0 61	9 9	4 06	0 293	1 97	0 017	0 0075
53 1	0 518	2 06	21	7 4	10 63	9 18	1 26	0 74	10 4	3 86	0 307	1 99	0 018	0 0083
101 2	0 518	1 88	23	7 8	11 47	11 14	1 54	0 90	9 8	4 07	0 291	3 56	0.016	0.0067
104 4	0 518	2 15	23	7 8	11 47	11 06	1 52	0 77	11 3	3 54	0 335	3.34	0.017	0 0084
104 1	0 518	2 16	21	7 4	10 63	9 90	1 54	0 84	11 4	3 52	0 338	2 67	0 014	0 0068
100 9	0 518	1 73	21	7 2	10 41	8 46	1 31	0 71	9 1	4 40	0 270	1 67	0.0068	0 0027
104 4	0 518	1 73	21	7 2	10 41	9 12	1.31	0 71	9 1	4 39	0 271	2 09	0 0085	0 0034

M_B, g/m²	G, kg/m²s	X_o, kg/kg	T_i, °C	T_s, °C	R_s, kg/m²h	R_c, kg/m²h	X_{ci}, kg/kg	X_{cf}, kg/kg	d_p, μm	$4/d_p$, m²/m³	Re	N_G	k_g	Sh
154 0	0 518	1 40	23	7 9	11 77	11 03	0 91	0.64	7 7	5 17×10⁵	0 229	2 77	0 0061	0 0021
159 2	0 518	1 85	23	7 9	11 77	11 51	1 48	0 77	9 9	4 04	0 294	3 80	0 011	0 0047
162 1	0 518	1 52	23	7 9	11 77	10 77	1 15	0 63	8 3	4 82	0 246	2 47	0 0058	0 0021
155 1	0 518	1 88	23	7 8	11 47	9 84	1 41	1 05	10 4	3 83	0 289	1 95	0 0082	0 0024
26 7	0 092	2 90	43	16 5	3.63	3 61	2 47	1 75	34 9	1 14	0 1,9	5.45	0 062	0 088
25 0	0 092	3 28	48	17 9	4 07	4 09	2 68	1 48	41 6	0 91	0 225	-	-	-
51 4	0 092	2 94	39	14 8	3 25	2 94	2 18	0 96	14 0	2 86	0.072	2 35	0 0054	0 0031
50.8	0 092	3 11	40	15 0	3 29	3 15	2 48	1 16	14 0	2 86	0.072	3 19	0 0073	0 0042
50 2	0 092	1 99	48	17 8	4 01	4 00	1 70	0 73	10 6	3 76	0 054	5 99	0 0107	0 0045
94 9	0 092	2 02	39	14 8	3 25	3 05	1 74	0 67	11 2	3 59	0 057	2 78	0 0025	0 0012
99 9	0 092	2 12	40	15 0	3 29	2 85	1 59	0 50	11 8	3 40	0 060	2 01	0 0019	0 0009
99 5	0 092	1 61	37	14 3	3.11	3 15	1 36	0 52	9 0	4 44	0.046	-	-	-
98 4	0 092	1 51	38	14 5	3 15	3 13	1 28	0 64	8 5	4 70	0 043	5 06	0 0036	0 0012
105 7	0 092	2 33	48	18 0	4.08	4 02	1 86	0 60	13 1	3 06	0 067	4 28	0 0046	0 0025
95 7	0 092	2 37	39	14 8	3 25	3 19	1 93	1 14	11.2	3,59	0 057	4 07	0 0037	0 0017
159 1	0 092	0 89	37	14 1	3 07	3 05	0 75	0 34	6 1	6 61	0 031	5 03	0 0016	0 0004
147 9	0 092	0.76	37	14 3	3 11	3 10	0 64	0.33	5 6	7 17	0 029	5 74	0 0017	0 0004
149 9	0 092	1 09	38	14 5	3 15	3 14	0 96	0 40	6 8	5 88	0 035	5.72	0 002	0 0006
26 2	0 156	2 63	43	16 3	6 08	5 65	2 14	1 33	28 0	1 43	0.244	2 64	0 041	0 047
27 5	0 156	2 85	43	16 4	6 18	5 51	2 32	1 16	32 5	1 23	0 282	2 23	0 040	0 053
26 7	0 156	2 68	43	16 4	6 18	5 55	2 17	1 50	28 8	1 39	0 250	2 28	0.036	0 043
26.7	0 156	2 63	43	16.4	6 18	5 54	2 19	1 59	28 0	1 43	0 244	2 27	0 035	0 040
52 6	0 156	2 11	42	15 9	5 95	5 72	1.78	0 91	11 1	3 61	0 096	3 29	0 010	0 0046
52 2	0 156	2 22	42	15 9	5 95	5 95	1 95	1.29	11 7	3 42	0 101	-	-	-
54 5	0 156	3 49	40	15 3	5 62	5 45	3 08	2 28	14 0	2 86	0 122	3 47	0 0135	0 0078
53 7	0 156	3 23	39	14 8	5 51	5 43	2 75	1 42	14 0	2 86	0 122	4 24	0 016	0 0095
99 5	0 156	1 55	39	15 0	5.58	5 52	1.37	0 60	8 5	4 69	0 074	4 59	0 0054	0.0019
100.5	0 156	1 51	39	15 0	5 58	5 60	1 32	0 72	8 3	4 80	0 072	-	-	-
155 0	0 156	1 92	39	14 8	5.51	5 31	1 67	0 43	10 6	3 76	0 093	3 33	0 0031	0 0014
154 6	0 156	1.34	43	16 3	6 08	5 98	1 17	0.85	7 7	5 18	0.067	4 10	0 0028	0 0009
146 6	0 156	2 04	39	15 0	5 58	5 57	1.77	0 46	11 3	3 54	0 098	6 32	0 0059	0 0027
26 4	0 289	2 75	43	16 3	11 31	8 98	2 19	1 65	28 6	1 40	0 462	1 58	0 046	0 054
28 6	0 289	3 49	40	15 3	10 46	8 45	2 86	1 21	44 0	0 91	0 713	1 65	0 074	0 134
26 4	0 289	3 34	43	16 3	11.31	8 50	2 76	1 04	42 1	0 95	0 676	1 39	0 061	0 104
51 1	0 289	3 00	43	16 3	11 31	10 49	2 48	1.93	14 0	2 86	0 226	2 62	0 019	0 0109
50 8	0.289	2 27	43	16 3	11 31	10 03	1 79	0 75	11 6	3 45	0 187	2 18	0 013	0 0062
48 4	0 289	2 21	41	15 7	10 93	8 74	1 68	0 90	11 2	3 57	0 181	1 61	0 0093	0 0043
50 4	0 289	2 70	41	15 7	10 93	8 20	2 00	0 67	14 0	2 86	0 227	1 39	0 010	0 0058
52 0	0 289	2 53	41	15 6	10 75	7 95	1 77	1 14	13 1	3 04	0 213	1 34	0 0091	0 0049
99 2	0 289	1 96	43	16 3	11 31	11 28	1 39	1.15	10 3	3 87	0 167	6 01	0 016	0 0069
99 6	0 289	1 41	43	16 3	11 31	10 22	1 14	0.76	7 6	5 24	0 123	2 33	0 0046	0 0015
103 5	0 289	1 54	41	15 6	10 75	9 18	1 35	0 87	8 3	4 85	0 134	1 92	0 0041	0 0014
104 5	0 289	1 77	41	15 6	10 75	9 96	1 22	0 69	9 4	4 26	0 151	2 61	0 0053	0 0020
103 6	0 289	1 77	41	15 6	10 75	8 77	1 34	0 86	9 4	4 26	0 152	1 69	0 0040	0 0016
156 5	0 289	1 25	43	16 3	11 31	10 72	1 02	0 73	7 2	5 59	0 116	2 96	0 0035	0 0010
149 6	0 289	1.60	43	16 3	11 31	10 45	1 39	0 58	8 7	4 58	0 141	2 57	0 0037	0 0013
156 4	0 289	1 99	41	15 6	10 75	10 00	1.39	0 67	9 6	4 16	0 156	2 66	0 0042	0 0017
27 9	0 518	3 01	42	15 9	19 84	16 48	2 06	1 42	32 5	1 23	0 943	1 77	0 105	0 141
27 5	0 518	2 83	42	15 9	19 84	14 47	2 07	1 10	28 6	1 40	0 829	1 31	0 068	0 080
28 5	0 518	3 55	41	15 6	19 30	13 58	2 70	1 69	44 0	0 91	1 278	1 22	0 097	0 177
28 7	0 518	3 12	42	16 0	20 15	15 68	1 95	1 36	34 9	1 14	1 013	1 51	0 096	0 138
28 8	0 518	3 30	42	16 0	20 15	15 42	1 96	0 81	39 3	1 02	1 138	1 45	0 104	0 168

M_B, g/m²	G, kg/m²s	X_o, kg/kg	T_1, °C	T_S, °C	R_S, kg/m²h	R_C, kg/m²h	X_{C1}, kg/kg	X_{Cf}, kg/kg	d_P, μm	$4/d_P$, m²/m³	Re	N_G	k_G	Sh
52 5	0 518	2.10	42	15 9	19 84	18 27	1 46	0 99	10 3	3 89×10⁵	0 298	2 54	0 024	0 0102
51.6	0 518	2 74	42	15 9	19 84	18 62	2 05	1 28	14 0	2 86	0 406	2 78	0 036	0 0208
52 9	0 518	2 50	42	15 9	19 84	13 77	1 91	0.81	12 6	3 18	0 365	1 18	0 014	0 0072
52 7	0 518	2 60	42	15 9	19 84	11 28	1 96	0 73	13 2	3 03	0 383	0 84	0 010	0 0056
53 1	0 518	2 98	42	15 9	19 84	15 59	2 29	1 32	14 0	2 86	0 406	1 54	0 020	0 0115
99 9	0 518	1 70	42	16 1	20 00	19.93	1 17	0 85	8 7	4 58	0 251	5 65	0 023	0 0081
99 9	0 518	2 03	42	15 9	19 84	15 98	1 17	0 89	10 4	3 83	0 303	1 64	0 0078	0 0034
100 4	0 518	1 92	42	15 9	19 84	14 47	1 16	0 57	9.9	4 06	0 286	1 31	0 0059	0 0024
98 9	0 518	2 23	42	16 0	20 15	17 18	1 68	0 99	11 6	3 46	0.336	1 91	0 0102	0 0049
99 4	0 518	1 97	42	15 9	19 84	18 50	1 43	0 87	10 1	3 95	0 291	2 70	0 0129	0 0053
151 2	0 518	1 31	43	16 2	20 23	20 17	0 98	0.77	7.2	5 56	0 207	5 82	0 0127	0 0036
152 1	0 518	1 81	43	16 2	20 23	20 14	1 48	1 23	9 5	4 19	0.275	5 43	0 0157	0 0058
152 3	0 518	1 82	42	16 0	20 15	16 43	1 27	0 64	9 6	4 16	0 279	1.69	0 0047	0 0019
155 0	0 518	2 27	42	15 9	19 84	19 37	1 41	0 75	12 1	3 29	0 353	3 74	0.0133	0 0068
25 7	0 092	2 57	65	23 3	5 63	5 57	1 99	1 64	27 3	1 47	0 137	4.52	0 041	0 044
25 5	0 092	4 18	62	22 6	5 33	5 30	3 52	1 95	39 3	1 02	0 198	5 18	0 069	0 107
25 5	0 092	4 78	62	22 6	5 33	5 17	4 05	2 39	44 0	0 91	0 219	3.51	0 050	0 087
26 4	0 092	4 68	62	22 6	5.33	5 31	4.03	2 19	44 0	0 91	0 219	5 59	0 084	0 145
25 9	0 092	4 31	65	23 3	5 65	4 90	3.64	2 03	44 0	0 91	0 221	2 02	0 029	0 051
53 1	0 092	2 24	65	23 3	5 61	5 65	1 72	1 06	12 0	3 33	0.061	-	-	
53.1	0 092	2 79	65	23 5	5 68	5 64	2 25	1 38	14 0	2 86	0 072	6 34	0 0149	0.0073
50 3	0 092	3 28	62	22 6	5.33	5.32	2 76	1 53	14 0	2 86	0 071	6.17	0 0145	0 0080
50 3	0 092	3 42	62	22 6	5 33	5 31	2.52	1 49	14 0	2 86	0 072	5 59	0 0131	0 0073
48 7	0 092	3.55	62	22 6	5 33	5 32	3 11	2 16	14 0	2 86	0.072	6 28	0 0148	0 0082
106 7	0 092	2 61	67	23 8	5.86	5 94	2 29	1 31	14 0	2 86	0 072	-	-	-
104 8	0 092	2 14	67	23 8	5 86	5 87	1 73	1 01	11 9	3 37	0 061	-	-	-
97 7	0 092	2 72	63	22 7	5 45	5 35	2 39	1 75	14 0	2 86	0 071	3 96	0 0047	0 0026
100 4	0 092	2 66	62	22 6	5 33	5 30	2.39	1.69	14 0	2 86	0 071	5 34	0 0063	0 0035
99 1	0 092	2.72	63	22 7	5 45	5 50	2 44	1 73	14 0	2 86	0 072	-	-	-
155.6	0 092	1 90	68	24 2	5 94	5 97	1 43	1.10	10 7	3 75	0.055	-	-	-
26 0	0 156	2 92	63	22 7	9 24	8 55	2 29	1 68	33 1	1.21	0 283	2 59	0 048	0 063
26 1	0.156	3 16	64	23 2	9 48	9 43	2 37	1 59	38 8	1 03	0 337	5 24	0.113	0.176
26 0	0 156	4.99	64	23 2	9 48	8.00	4.28	2 29	44 0	0 91	0 375	1 85	0 046	0 079
49 6	0 156	2 21	62	22 6	9 04	8.93	1.7[illegible]	1.18	11 5	3 49	0 098	4 48	0 0146	0.0066
49 9	0 156	2 53	62	22 6	9 04	8 85	2 21	1 29	13 4	2 98	0 115	3 87	0 0148	0.0079
51 8	0.156	2 98	63	22 7	9 24	8.31	2 24	1 34	14 0	2.86	0.120	2 30	0.0091	0 0051
104 9	0 156	1 69	63	22 7	9 24	9 15	1 41	0 94	9 1	4 38	0 078	4 60	0 0060	0 0022
102 5	0 156	2 35	65	23 3	9 57	8 35	1 86	0 93	12 9	3 10	0 110	2 05	0 0038	0 0019
102 8	0 156	2 62	65	23 3	9 57	9 06	1 86	0 81	14 0	2 86	0 119	2 92	0.0058	0 0032
104 1	0 156	2 53	65	23 3	9 57	9 53	1 56	0 85	14 0	2 86	0 119	5 55	0 0111	0 0061
155 8	0 156	1 55	63	22 7	9 24	8 86	1 33	0 91	8 6	4 63	0 074	3 19	0 0025	0 0009
29 3	0 289	2 54	66	23 6	18 10	15 70	1.56	0 99	24 4	1 64	0 387	2 02	0 051	0 049
26 7	0 289	2 83	63	22 7	17 19	12 90	2 17	1 65	29 4	1.36	0 467	1 39	0 043	0.049
26 7	0 289	3 01	63	22 7	17 19	13 90	1 92	1.36	33 7	1 19	0.535	1 66	0.058	0 077
30 0	0 289	3 15	66	23 6	18 10	14 05	2 30	1.10	37 2	1 07	0.590	1 50	0 058	0 085
50 0	0 289	2 52	67	23 8	18 45	15 77	1.87	1 45	12 9	3.11	0 204	1 93	0 013	0 0066
50.5	0 289	3 02	65	23 3	17 80	17 52	2 30	1 56	14 0	2 86	0 222	4 15	0 031	0 017
49 3	0 289	3 31	62	22.6	16 80	13.74	2.22	1 00	14 0	2 86	0.222	1 70	0 0126	0 0070
99 5	0 289	2 06	68	24 2	18 71	17 39	1 57	1.20	10 8	3 72	0.170	2 65	0 0075	0 0032
96 5	0 289	2.67	62	22 6	16 80	14 62	1.66	1 13	14 0	2 86	0 222	2.04	0 0075	0 0042
96 7	0 289	2.59	62	22.6	16 80	14 16	1.72	1.09	14 0	2 86	0 222	1.85	0.0068	0 0038
92 1	0 289	2 48	62	22 6	16 80	13 72	1.69	0 86	13 3	3 01	0 211	1.70	0.0059	0 0031

H_s, g/m²	G, kg/m²s	X_o, kg/kg	T_i, °C	T_s, °C	R_s, kg/m²h	R_c, kg/m²h	X_{ci}, kg/kg	X_{cf}, kg/kg	d_p, μm	$4/d_p$, m²/m³	Re	N_G	k_G	Sh
102 4	0 289	2 15	66	23 6	18 10	16 60	1.59	1 01	11 3	3.54×10^5	0 179	2.48	0 0074	0.0033
152 0	0 289	1 55	67	23 8	18 45	17 34	1 22	0 92	8 4	4 78	0 133	2 81	0 0039	0 0013
152 1	0 289	1 86	67	24 1	18 54	17 69	1 38	0 88	10 0	4 02	0 158	3 21	0 0054	0 0021
28 0	0 518	2 92	66	23 6	32 50	22 56	1 71	1 29	29 4	1 36	0 836	1 18	0 065	0 075
25 1	0 518	3 62	61	22 2	29 68	19 18	2.55	1.34	44 0	0 91	1 256	1 04	0 085	0 149
26 5	0 518	2 43	61	22 2	29 68	19 39	1 53	1 14	26 8	1 49	0 765	1 06	0 053	0 056
25 8	0 518	1 86	61	22 4	29 92	19 17	1 20	0 80	19 6	2 04	0 561	1 02	0 037	0 029
25 1	0 518	2 36	61	22 4	29 92	19 01	1 52	1 14	22 0	1 82	0 628	1 01	0 041	0 036
51 3	0 518	2 41	65	23 3	31 95	24 12	1 85	1.34	11 7	3 41	0.334	1 41	0.016	0 0072
51 1	0 518	3 30	65	23 3	31 95	27 65	2 49	1 92	14 0	2 86	0 399	2 01	0 027	0.015
49 4	0 518	3 12	61	22 4	29 92	22 80	2 43	1 94	14 0	2 86	0 400	1 44	0 019	0 011
47 7	0 518	3 27	61	22 2	29 68	18 64	2 16	1 30	14 0	2 86	0 400	0 99	0 013	0 0073
49 4	0 518	3 40	61	22 2	29 68	18 41	2 06	0 85	14 0	2 86	0 400	0 97	0 013	0 0071
99 5	0 518	2 40	65	23 3	31 95	27 66	1 75	1 13	12 4	3 22	0 353	2.01	0 012	0 0058
99 7	0 518	2 05	65	23 3	31 95	29 38	1 55	0 84	10 4	3 86	0 295	2 52	0 012	0 0051
100 9	0 518	2 58	61	22 4	29 92	22 40	1 81	1 11	13 6	2 94	0 388	1 38	0 0088	0 0048
100 7	0 518	2 74	61	22 4	29 92	25 67	2.32	2.06	14 0	2.86	0 400	1 95	0 013	0 0072
100 1	0 518	2 68	61	22 2	29 68	25 05	2 24	1 25	14 0	2 86	0 400	1 86	0 012	0 0069
149 9	0 518	1 94	64	22 8	31 53	30 15	1 48	1 17	10 1	3 96	0 288	3 13	0 0094	0 0038
150 5	0 518	1 85	65	23 3	3 95	29 15	1 43	1 12	9 6	4 16	0 273	2 44	0 0070	0 0027
27 0	0 092	4 22	90	29 3	8 .7	7 86	3 25	1 95	44 0	0 91	0 218	3 00	0 045	0 075
27 3	0 092	2 51	90	29 3	8 27	7 88	1 88	1 50	26 3	1 52	0 130	3 08	0 027	0 027
27 5	0 092	3 14	92	29 7	8 49	8 39	2.41	1 68	27 5	1 45	0 136	4 48	0 042	0 043
25 7	0 092	4 88	88	28 8	8 06	6 19	4 10	2 41	44 0	0 91	0 218	1 46	0 022	0 036
49.8	0 092	2 57	92	29 7	8 49	8 48	1.96	1 67	15 9	2 87	0 071	6 74	0 015	0 008
51 0	0 092	2 47	92	29 7	8 49	8 43	1 87	1 34	13 3	3 01	0 068	4 95	0 011	0 005
50.9	0 092	1 86	91	29 4	8 36	8 20	1 42	1 08	9 6	4 15	0 048	3 96	0 0065	0 0024
96 8	0 092	2 06	92	29 8	8 51	8 10	1 53	1 00	11 3	3 55	0 056	3 03	0 0029	0 0013
101 5	0 092	1 69	91	29 6	8 40	8 39	1 32	0 82	9 2	4 33	0 047	6 90	0 0044	0 0016
98.3	0 092	1 90	91	29 6	8 40	8 37	1.51	0 88	10 3	3 88	0 053	5 80	0 0041	0 0017
156 8	0 092	2 34	92	29 8	8 51	8 48	1 91	1 36	10 3	3 87	0 052	5 65	0 0013	0 0032
27 8	0 156	3 38	91	29 6	14 24	11 17	2 74	2 10	44 0	0 91	0 369	1 53	0 039	0.064
27 9	0 156	2 95	92	29 7	14 31	11 92	2 10	1 65	33 4	1 20	0 280	1 79	0 034	0 043
25 5	0 156	3 44	88	28 8	13 65	12 04	2.54	1 70	44 0	0 91	0 370	2 14	0 054	0 090
25 3	0 156	3 26	88	28 8	13 65	12 23	2 16	1 51	40 7	0 98	0.342	2 26	0 052	0 081
25 8	0 156	2 90	88	28 8	13 65	12 87	1 92	1 38	31 9	1 25	0 268	2 86	0 052	0 063
51 6	0 156	3 13	92	29 7	14 31	14 04	2 43	1 55	14 0	2 86	0 117	3 98	0 016	0 0086
52 9	0 156	2 97	94	30 0	14 69	12 48	2 17	1 41	14 0	2 86	0 117	1 90	0 0077	0.0041
49 4	0 156	3 53	87	28 6	13 47	12 84	2 83	1.74	14 0	2 86	0 118	3 06	0 012	0 0067
103 8	0 156	2 54	93	29 9	14 62	14.33	1 99	1 26	14 0	2 86	0 117	3 94	0 0080	0 0043
103 4	0 156	2 63	87	28 6	13 47	12 41	1 95	1 03	14 0	2 86	0 121	2 54	0 0044	0 0026
103 0	0 156	2 83	88	28 8	13 65	13 06	1 91	1 22	14 0	2 86	0 118	3 14	0 0064	0 0034
101 8	0 156	2 38	88	28 8	13 65	12 48	1 68	0 92	13 0	2 86	0 109	2 46	0 0046	0 0023
155 5	0.156	1 91	93	29 9	14 57	14 41	1 53	1 17	9 5	4 23	0 082	4 51	0 0039	0 0015
152 1	0 156	2 18	87	28 6	13 56	13 42	1.71	1 07	11 0	3 62	0 096	4 57	0.0021	0 0046
26 4	0 289	2 45	85	28 2	24 34	17 99	1 52	1 33	26 5	1 51	0 416	1 34	0 038	0 038
26 3	0 289	2 44	85	28 2	24 34	18 51	1 33	1 33	21 7	1 85	0 348	1 43	0 032	0 028
26 3	0 289	2 59	85	28 2	24 34	15 85	1.71	1 23	31 6	1 27	0 495	1 05	0 035	0 043
26 4	0 289	2 57	85	28 2	24 34	16 29	1 55	1 23	23 7	1 69	0 381	1.11	0 027	0 026
24 1	0 289	3 62	86	28 2	24 77	19 82	2 32	1 67	44 0	0 91	0 689	1 61	0 075	0 126
26 3	0 289	3 59	87	28 6	25 04	18 55	2 10	1 67	44 0	0 91	0 706	1 35	0 062	0 110
23 4	0 289	2 80	84	28 1	23 96	18 19	1 70	1 49	27 3	1 47	0 427	1 43	0 041	0 043

H_E, g/m²	G, kg/m²s	X_o, kg/kg	T_i, °C	T_s, °C	R_S, kg/m²h	R_C, kg/m²h	X_{ci}, kg/kg	X_{cf}, kg/kg	d_p, μm	$4/d_p$, m²/m³	Re	N_G	k_G	Sh
26 4	0 289	2 75	87	28 6	25 12	18 15	1 49	1 49	26 8	1 49×10⁵	0 430	1 28	0 036	0 039
51 7	0 289	3 13	85	28 2	24 34	16 14	2 10	0 95	14 0	2 86	0 219	1 09	0 0082	0 0044
52 1	0 289	2 14	85	28 2	24 34	21 41	1 47	1 15	10 5	3 82	0 164	2 11	0 012	0 0048
44 9	0 289	2 20	87	28 6	25 04	20 04	1 43	1 19	10 6	3 77	0 166	1 61	0 0092	0 0037
50 7	0 289	2 13	87	28 7	25.21	21 14	1 19	1 19	10 3	3 87	0.166	1 82	0 010	0 0042
46.3	0 289	3 34	87	28.6	25 04	16.45	2 30	1 29	14 0	2 86	0 225	1 07	0 0079	0 0045
100 7	0 289	2 30	86	28 2	24 77	22 06	1 31	0.70	12 1	3 31	0 189	2 21	0 0072	0 0033
101 8	0.289	2 27	86	28 2	24 77	21.72	1 64	1.12	11 9	3 36	0 187	2 09	0 0067	0 0031
100 4	0 289	2 62	87	28 6	25 04	20 73	1 63	1.06	14 0	2 86	0 219	1 76	0 0066	0 0036
102 6	0 289	2.75	87	28 6	25.04	22.41	2 13	1 34	14 0	2 86	0 219	2 19	0 0082	0 0044
155 2	0 289	1 74	86	28 2	24 56	23 12	1 35	1.19	9 2	4 33	0 145	2 84	0 0045	0 0016
156 1	0 289	2.13	86	28.2	24 77	22 92	1.28	0 61	11 4	3 50	0 179	2 60	0 0051	0 0022
28 4	0 518	3 49	88	28 8	45 57	26 63	2 36	1.86	39 6	1 01	1 192	0 88	0 061	0 107
25 4	0 518	3 45	83	27 8	42 45	24 90	2.33	2 06	40 0	1 00	1 125	0 88	0 067	0 103
25 1	0 518	3 40	83	27 8	42 45	25 64	2 06	2 06	40 0	1 00	1 125	0 93	0 070	0 108
26 4	0 518	3 33	83	27 8	42 45	24 22	2.32	1.59	37.2	1 07	1.047	0 85	0 060	0 085
25 4	0 518	3 29	83	27 8	42 45	24 69	2 07	1 58	37 2	1 07	1 047	0 87	0 062	0.088
26.1	0.518	2 47	83	27 8	42 45	24 42	1 53	1 03	26 8	1 49	0 754	0 86	0 043	0 045
25 4	0 518	3 71	83	27 8	42 45	22 87	2 69	1 97	44 0	0 91	1 238	0 77	0 065	0 109
24 9	0 518	3 69	83	27 8	42 47	23 23	2 58	1 95	44 0	0 91	1 238	0 79	0 066	0 112
25 3	0 518	4 33	84	28 1	43 00	24 05	2 68	1 68	44 0	0 91	1 237	0 82	0 068	0 115
52 5	0 518	1 99	87	28 6	44 95	32 39	1 17	1 00	9.1	4 38	0 262	1 28	0.011	0 0041
51.5	0 518	1 95	87	28 6	44 95	34 23	1 00	1 00	9 1	4 39	0 262	1 43	0 012	0 0046
52 3	0 518	2 51	87	28 6	44 95	32 38	1 63	1 13	12 1	3 31	0 348	1 27	0 015	0 0069
50 5	0 518	2 49	89	29 1	46 04	32 41	1 46	1 11	11 9	3 36	0 342	1 22	0 014	0 0066
49 9	0 518	2 28	83	27 8	42 45	24 90	1 61	1 08	10.7	3 38	0.301	0 88	0 0091	0 0037
49 1	0 518	3 23	83	27 8	42 45	25 85	2 42	1 87	14 0	2 86	0 394	0 94	0 013	0 0068
47 9	0 518	2 90	83	27 8	42 45	22 34	2 23	1 01	14.0	2 86	0 403	0 75	0 0099	0 0056
101 1	0 518	2 18	87	28 6	44 95	37 98	1 58	1 18	10 9	3 66	0 307	1 87	0 0098	0 0041
100 6	0 518	2 21	85	28 2	43 70	36 18	1 54	0 97	11.1	3 60	0 312	1 76	0 0094	0 0040
99 6	0 518	2 57	82	27.6	41 83	29 81	1.84	1 25	13 4	2 99	0.376	1 26	0 0081	0 0042
100 5	0 518	2 38	83	27 8	43 45	31 87	1.91	1.25	12.2	3 29	0 342	1 43	0 0083	0 0039
150 8	0 518	1 55	85	28 2	43 70	35 22	1.19	0 63	8 0	5 02	0.224	1.64	0 0039	0 0012
150 7	0 518	1 86	85	28 2	43 70	34.91	1 50	1.13	9 5	4 20	0 268	1 60	0 0046	0 0017
151 3	0 518	1 65	87	28.6	45.10	35 34	1 01	0 81	8 4	4 74	0 243	1 52	0 0039	0 0013
149 9	0.518	1 81	87	28 6	45 18	35 12	1 17	0 89	9.2	4 32	0.266	1.50	0 0042	0.0016

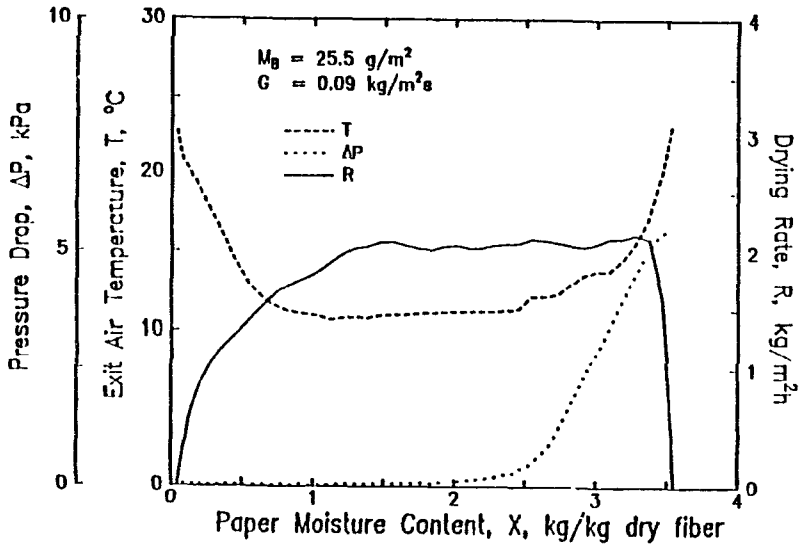
M_B = 25.5 g/m²
G = 0.09 kg/m²s
T
ΔP
R
Pressure Drop, ΔP, kPa
Exit Air Temperature, T, °C
Drying Rate, R, kg/m²h
Paper Moisture Content, X, kg/kg dry fiber

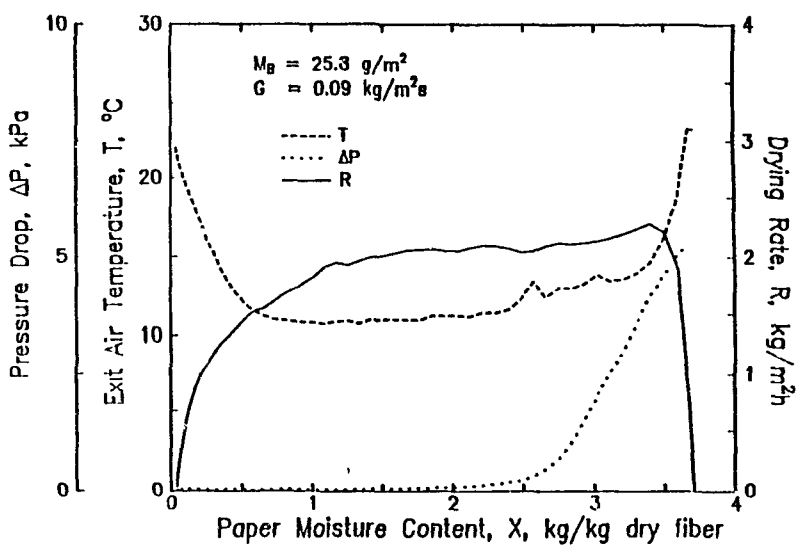
M_B = 25.3 g/m²
G = 0.09 kg/m²s
T
ΔP
R
Pressure Drop, ΔP, kPa
Exit Air Temperature, T, °C
Drying Rate, R, kg/m²h
Paper Moisture Content, X, kg/kg dry fiber

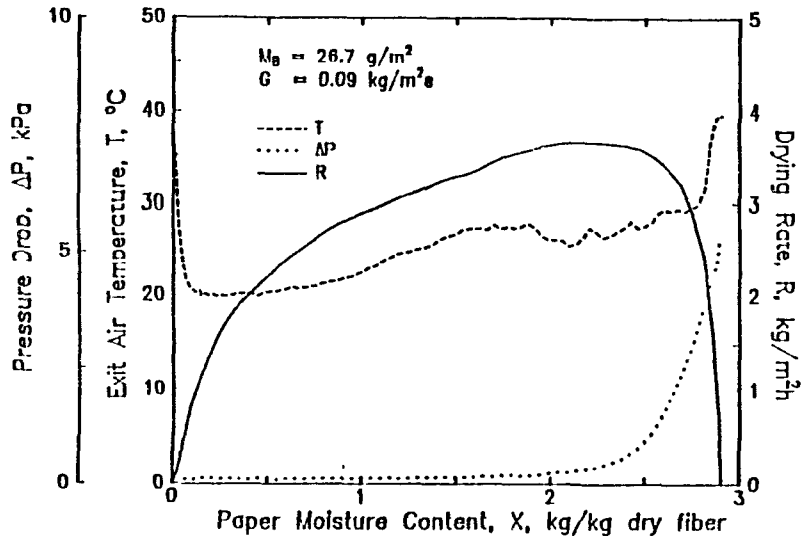
M_B = 26.7 g/m²
G = 0.09 kg/m²s
T
ΔP
R
Pressure Drop, ΔP, kPa
Exit Air Temperature, T, °C
Drying Rate, R, kg/m²h
Paper Moisture Content, X, kg/kg dry fiber

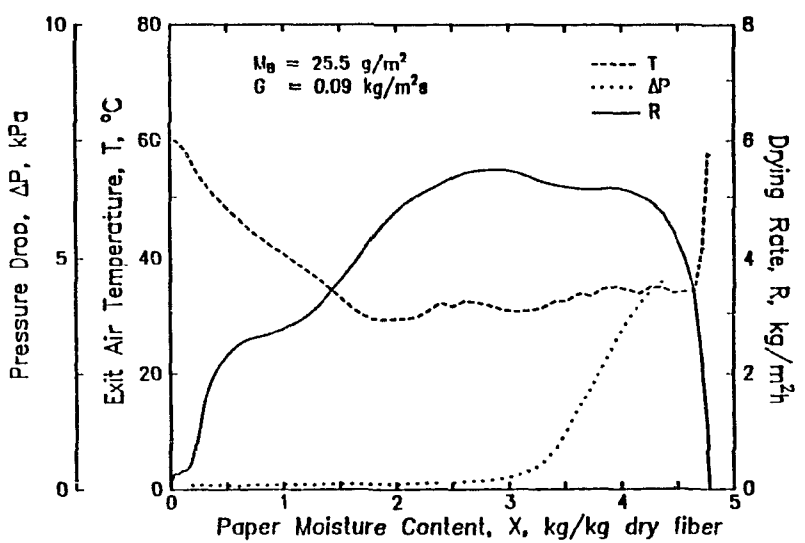
M_B = 25.5 g/m²
G = 0.09 kg/m²s
T
ΔP
R
Pressure Drop, ΔP, kPa
Exit Air Temperature, T, °C
Drying Rate, R, kg/m²h
Paper Moisture Content, X, kg/kg dry fiber

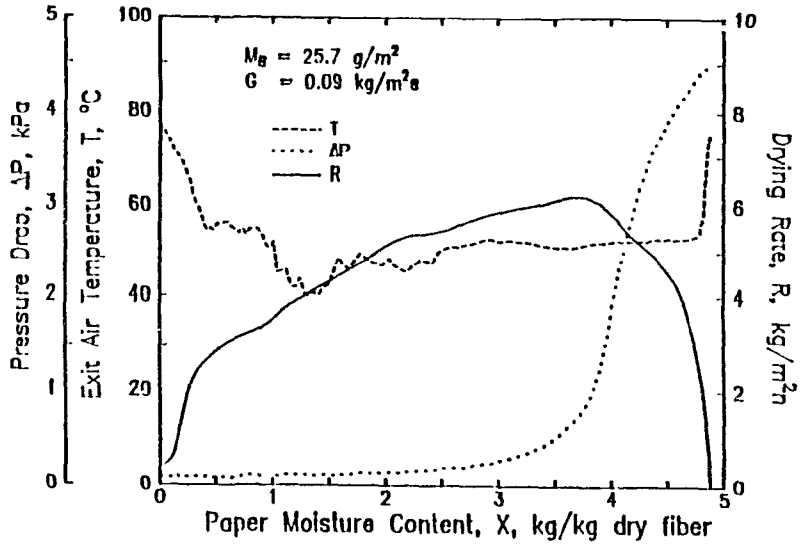
M_B = 25.7 g/m²
G = 0.09 kg/m²s
T
ΔP
R
Pressure Drop, ΔP, kPa
Exit Air Temperature, T, °C
Drying Rate, R, kg/m²h
Paper Moisture Content, X, kg/kg dry fiber

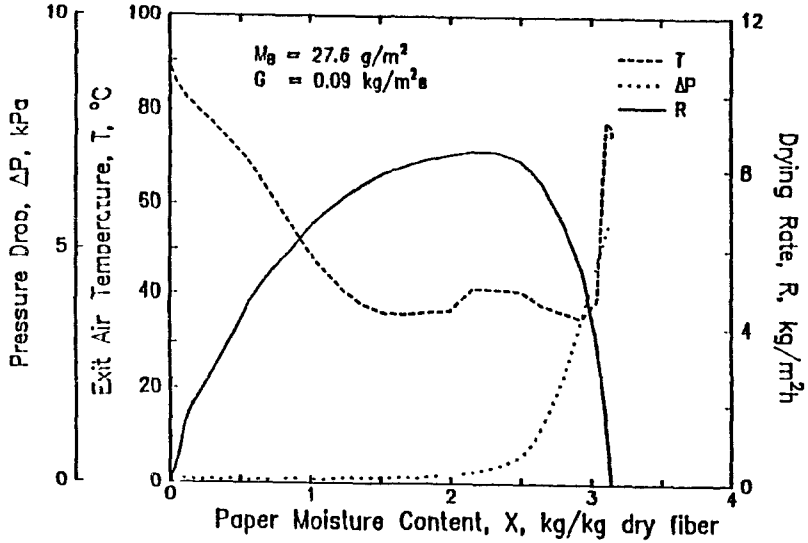
M_B = 27.6 g/m²
G = 0.09 kg/m²s
T
ΔP
R
Pressure Drop, ΔP, kPa
Exit Air Temperature, T, °C
Drying Rate, R, kg/m²h
Paper Moisture Content, X, kg/kg dry fiber

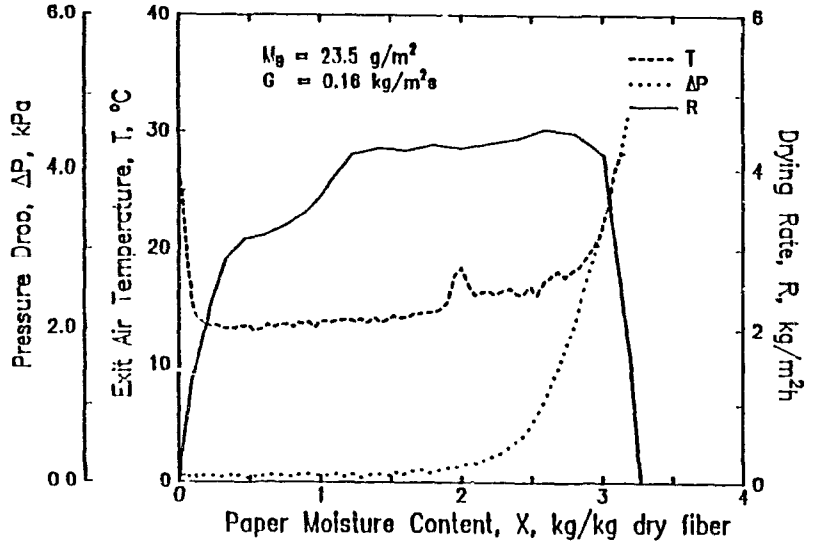
M_B = 23.5 g/m²
G = 0.16 kg/m²s
T
ΔP
R
Pressure Drop, ΔP, kPa
Exit Air Temperature, T, °C
Drying Rate, R, kg/m²h
Paper Moisture Content, X, kg/kg dry fiber

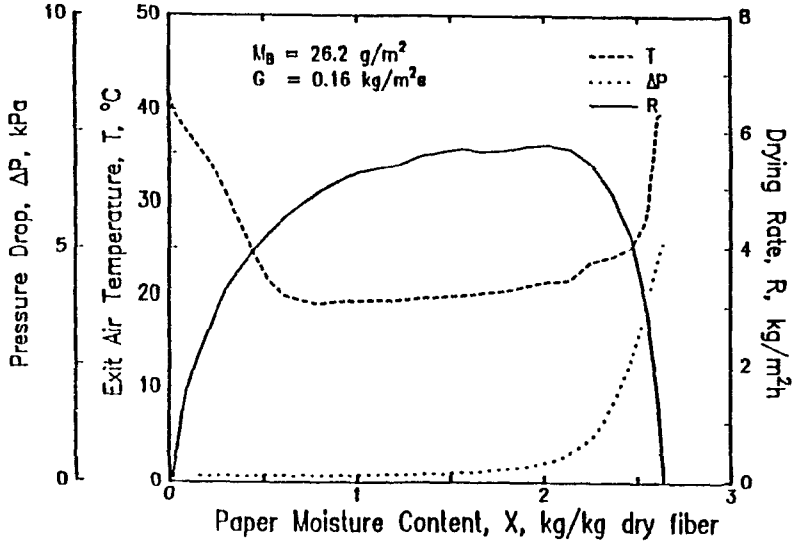
M_B = 26.2 g/m²
G = 0.16 kg/m²s
T
ΔP
R
Pressure Drop, ΔP, kPa
Exit Air Temperature, T, °C
Drying Rate, R, kg/m²h
Paper Moisture Content, X, kg/kg dry fiber

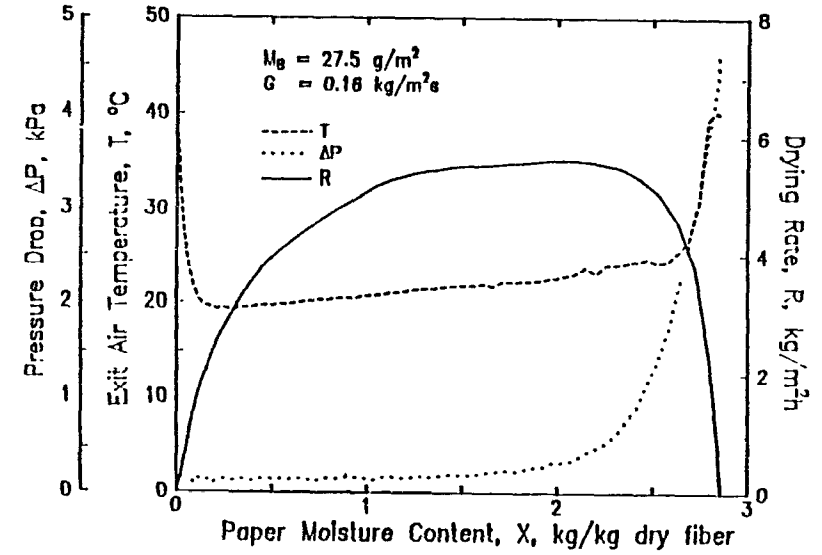
M_B = 27.5 g/m²
G = 0.16 kg/m²s
T
ΔP
R
Pressure Drop, ΔP, kPa
Exit Air Temperature, T, °C
Drying Rate, R, kg/m²h
Paper Moisture Content, X, kg/kg dry fiber

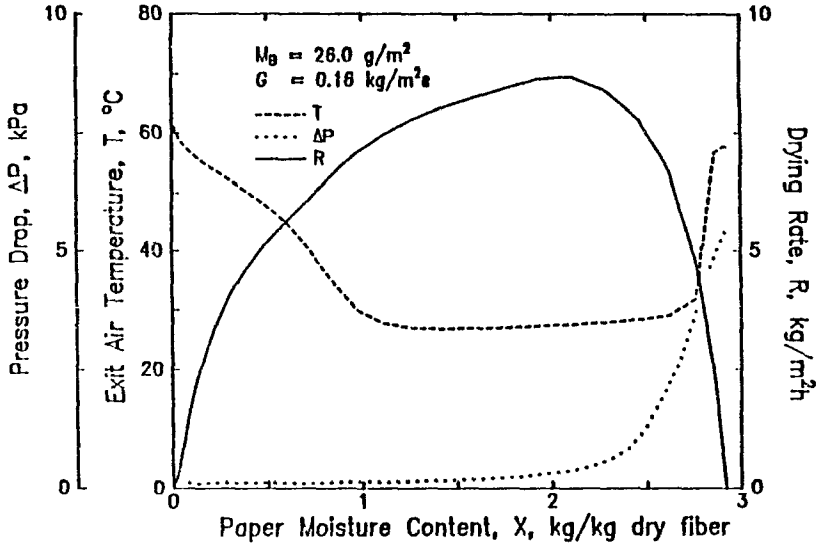
M_B = 26.0 g/m²
G = 0.16 kg/m²s
T
ΔP
R
Pressure Drop, ΔP, kPa
Exit Air Temperature, T, °C
Drying Rate, R, kg/m²h
Paper Moisture Content, X, kg/kg dry fiber

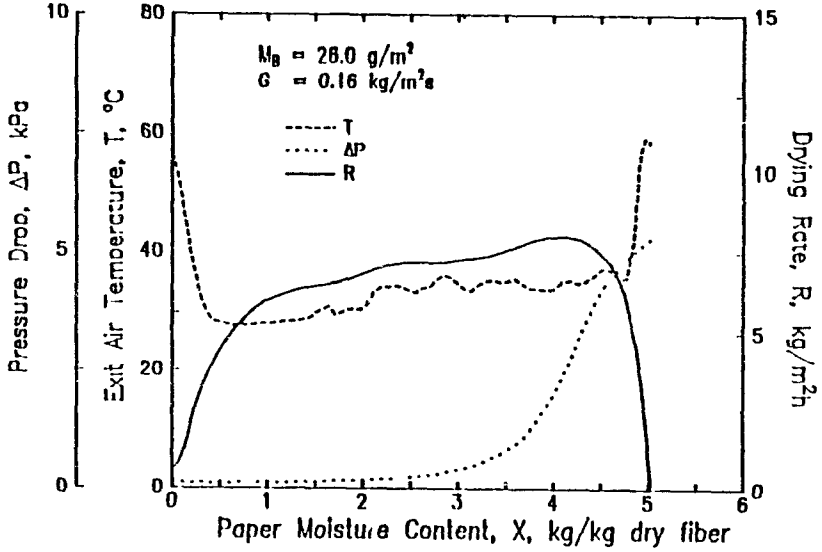
M_B = 26.0 g/m²
G = 0.16 kg/m²s
T
ΔP
R
Pressure Drop, ΔP, kPa
Exit Air Temperature, T, °C
Drying Rate, R, kg/m²h
Paper Moisture Content, X, kg/kg dry fiber

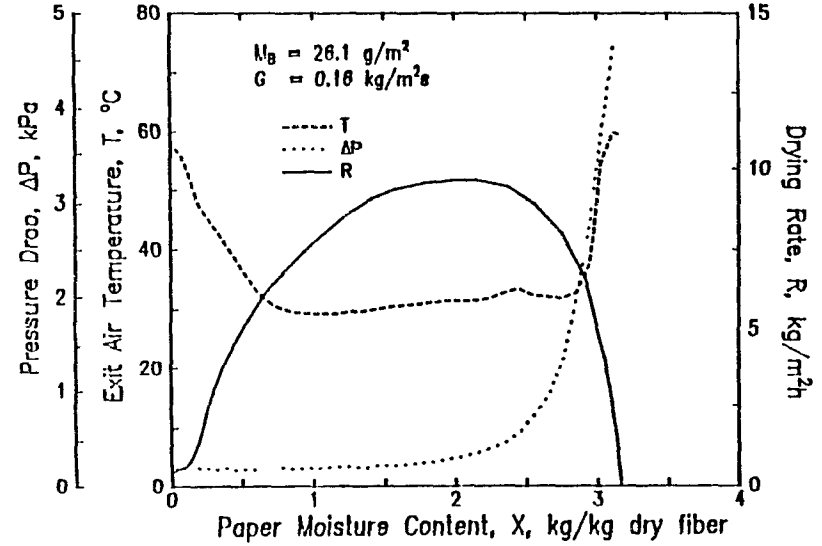
M_B = 26.1 g/m²
G = 0.16 kg/m²s
T
ΔP
R
Pressure Drop, ΔP, kPa
Exit Air Temperature, T, °C
Drying Rate, R, kg/m²h
Paper Moisture Content, X, kg/kg dry fiber

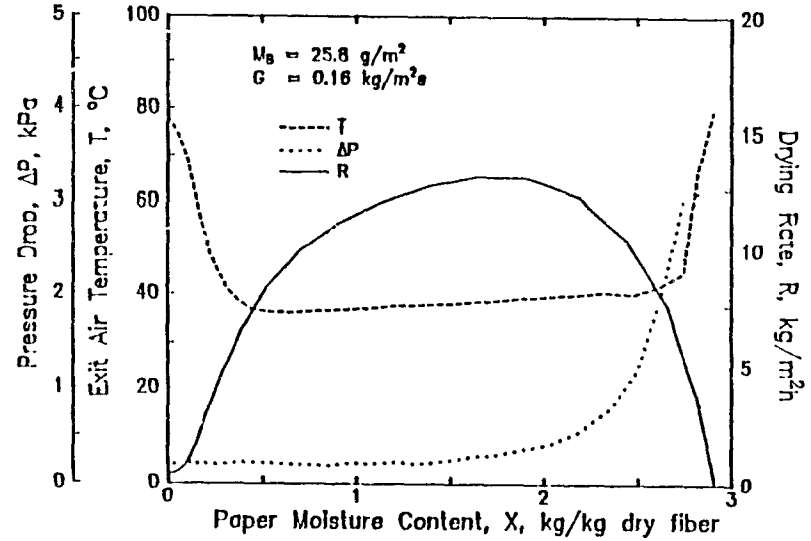
M_B = 25.8 g/m²
G = 0.16 kg/m²s
T
ΔP
R
Pressure Drop, ΔP, kPa
Exit Air Temperature, T, °C
Drying Rate, R, kg/m²h
Paper Moisture Content, X, kg/kg dry fiber

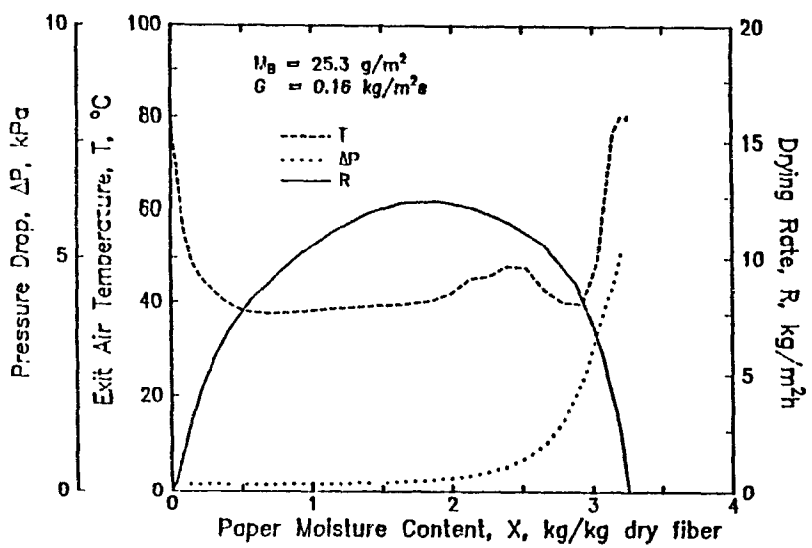
M_B = 25.3 g/m²
G = 0.16 kg/m²s
T
ΔP
R
Pressure Drop, ΔP, kPa
Exit Air Temperature, T, °C
Drying Rate, R, kg/m²h
Paper Moisture Content, X, kg/kg dry fiber

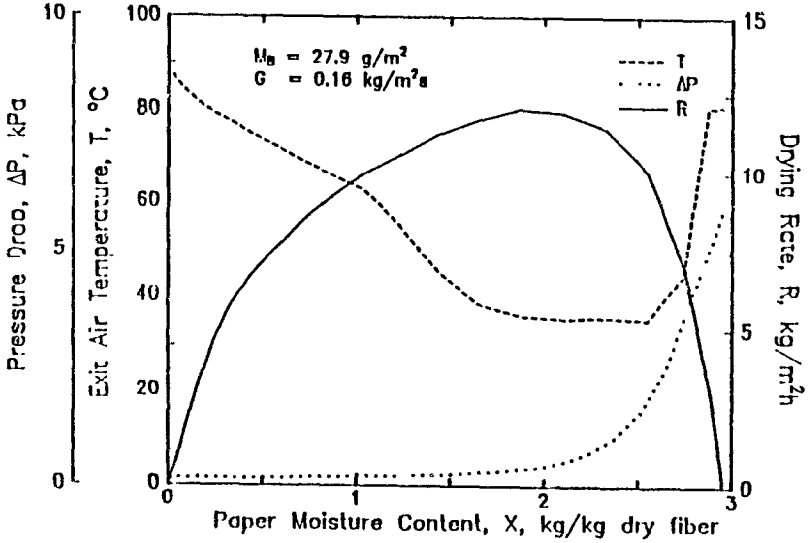
M_B = 27.9 g/m²
G = 0.16 kg/m²s
T
ΔP
R
Pressure Drop, ΔP, kPa
Exit Air Temperature, T, °C
Drying Rate, R, kg/m²h
Paper Moisture Content, X, kg/kg dry fiber

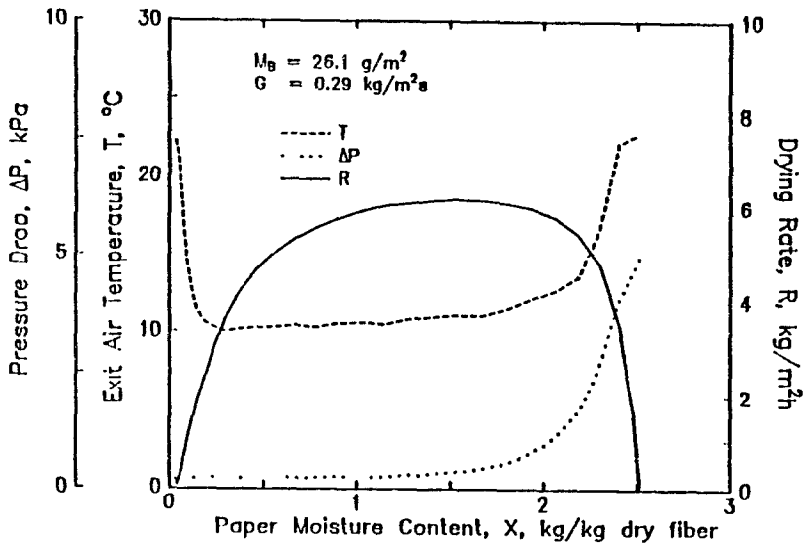
M_B = 26.1 g/m²
G = 0.29 kg/m²s
T
ΔP
R
Pressure Drop, ΔP, kPa
Exit Air Temperature, T, °C
Drying Rate, R, kg/m²h
Paper Moisture Content, X, kg/kg dry fiber

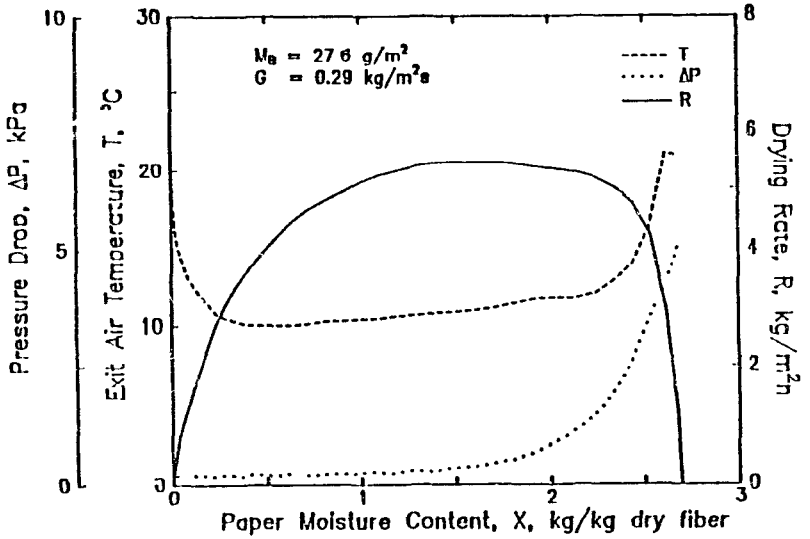
M_B = 27.6 g/m²
G = 0.29 kg/m²s
T
ΔP
R
Pressure Drop, ΔP, kPa
Exit Air Temperature, T, °C
Drying Rate, R, kg/m²h
Paper Moisture Content, X, kg/kg dry fiber

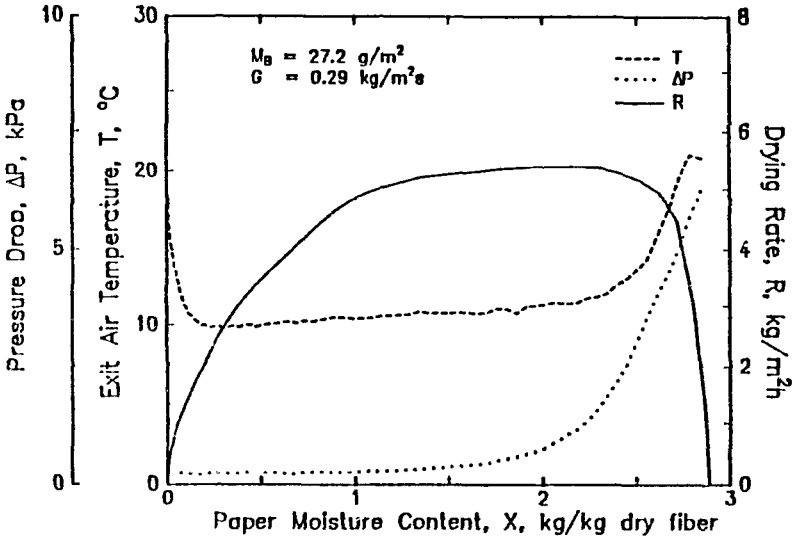
M_B = 27.2 g/m²
G = 0.29 kg/m²s
T
ΔP
R
Pressure Drop, ΔP, kPa
Exit Air Temperature, T, °C
Drying Rate, R, kg/m²h
Paper Moisture Content, X, kg/kg dry fiber

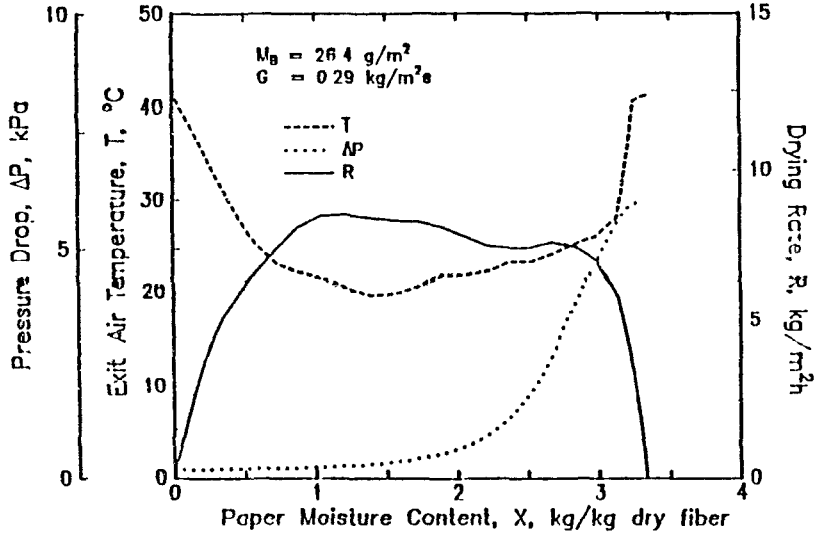
M_B = 26.4 g/m²
G = 0.29 kg/m²s
T
ΔP
R
Pressure Drop, ΔP, kPa
Exit Air Temperature, T, °C
Drying Rate, R, kg/m²h
Paper Moisture Content, X, kg/kg dry fiber

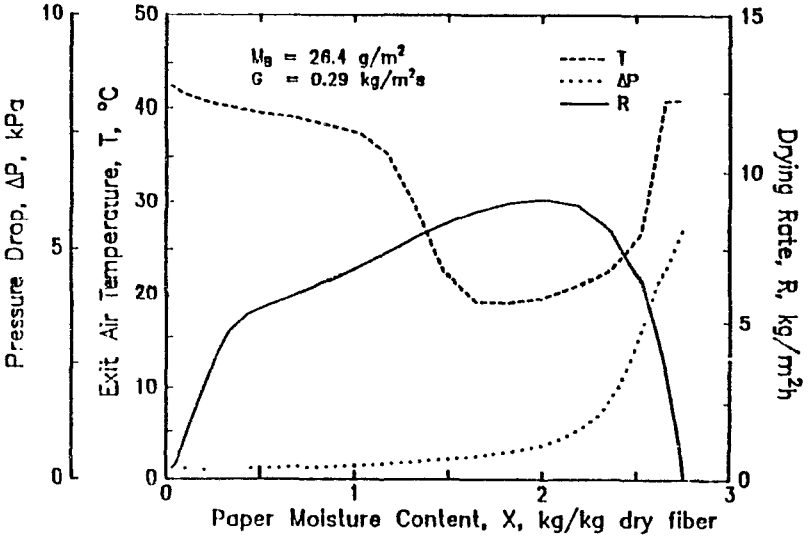
M_B = 26.4 g/m²
G = 0.29 kg/m²s
T
ΔP
R
Pressure Drop, ΔP, kPa
Exit Air Temperature, T, °C
Drying Rate, R, kg/m²h
Paper Moisture Content, X, kg/kg dry fiber

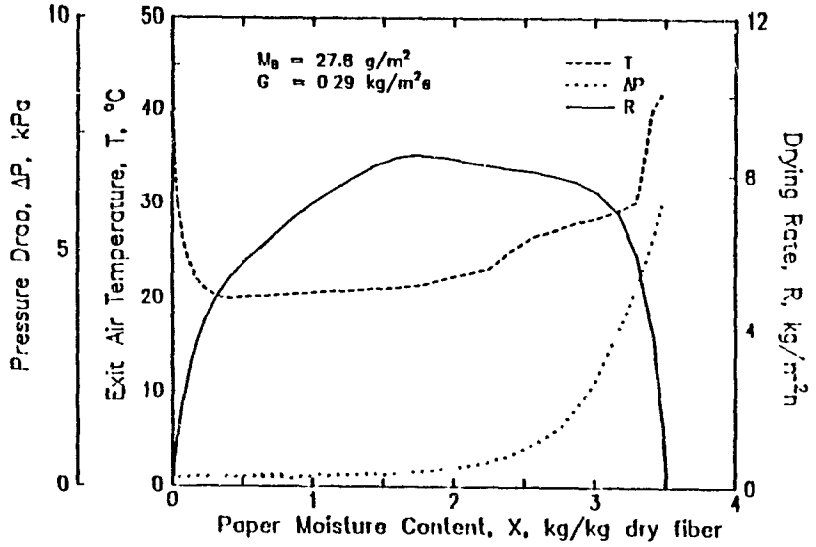
M_B = 27.8 g/m²
G = 0.29 kg/m²s
T
ΔP
R
Pressure Drop, ΔP, kPa
Exit Air Temperature, T, °C
Drying Rate, R, kg/m²h
Paper Moisture Content, X, kg/kg dry fiber

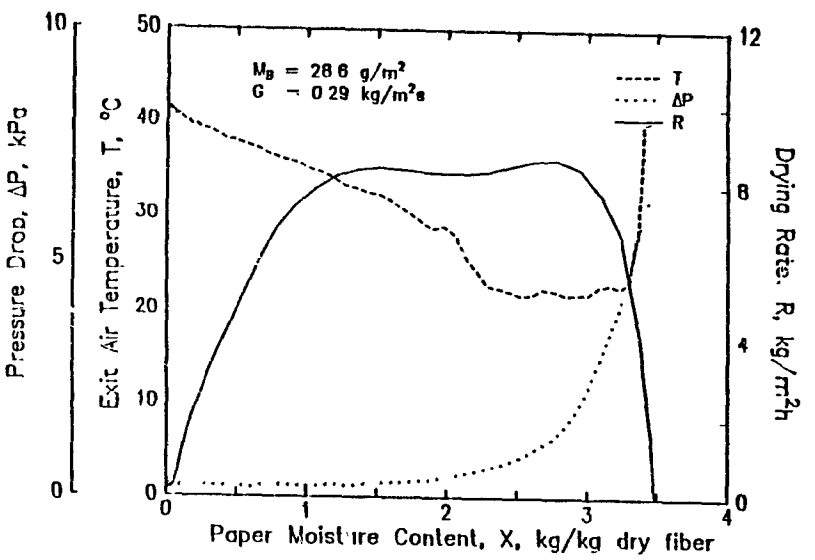
M_B = 28.6 g/m²
G = 0.29 kg/m²s
T
ΔP
R
Pressure Drop, ΔP, kPa
Exit Air Temperature, T, °C
Drying Rate, R, kg/m²h
Paper Moisture Content, X, kg/kg dry fiber

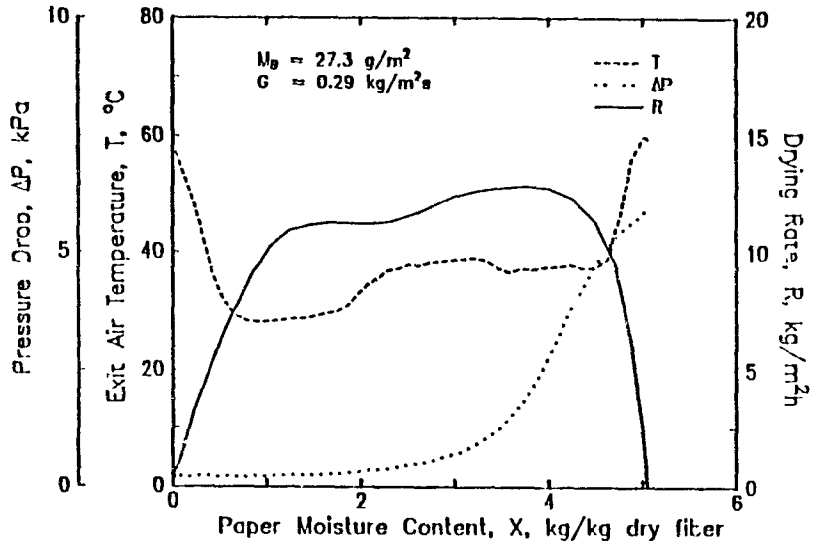
M_B = 27.3 g/m²
G = 0.29 kg/m²s
T
ΔP
R
Pressure Drop, ΔP, kPa
Exit Air Temperature, T, °C
Drying Rate, R, kg/m²h
Paper Moisture Content, X, kg/kg dry fiber

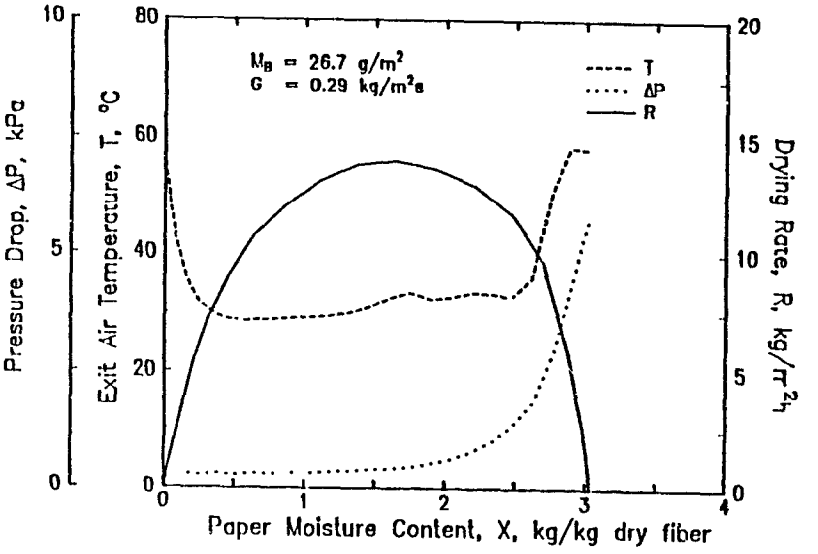
M_B = 26.7 g/m²
G = 0.29 kg/m²s
T
ΔP
R
Pressure Drop, ΔP, kPa
Exit Air Temperature, T, °C
Drying Rate, R, kg/m²h
Paper Moisture Content, X, kg/kg dry fiber

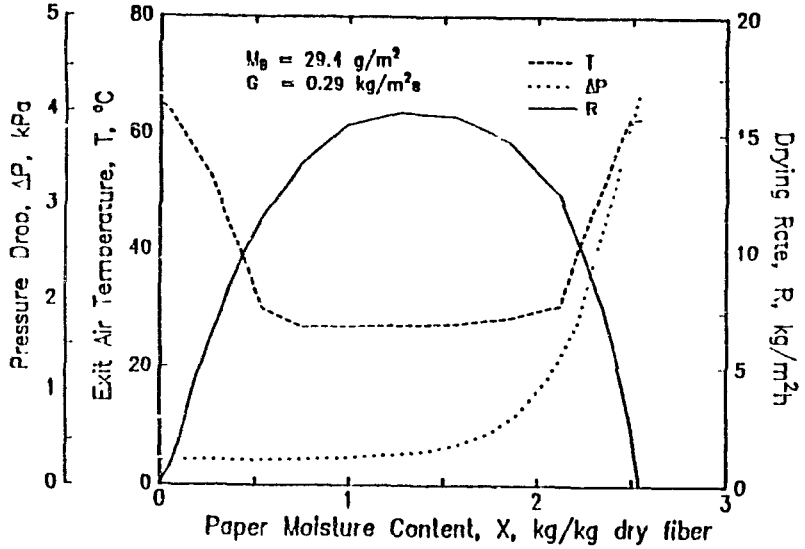
M_B = 29.4 g/m²
G = 0.29 kg/m²s
T
ΔP
R
Pressure Drop, ΔP, kPa
Exit Air Temperature, T, °C
Drying Rate, R, kg/m²h
Paper Moisture Content, X, kg/kg dry fiber

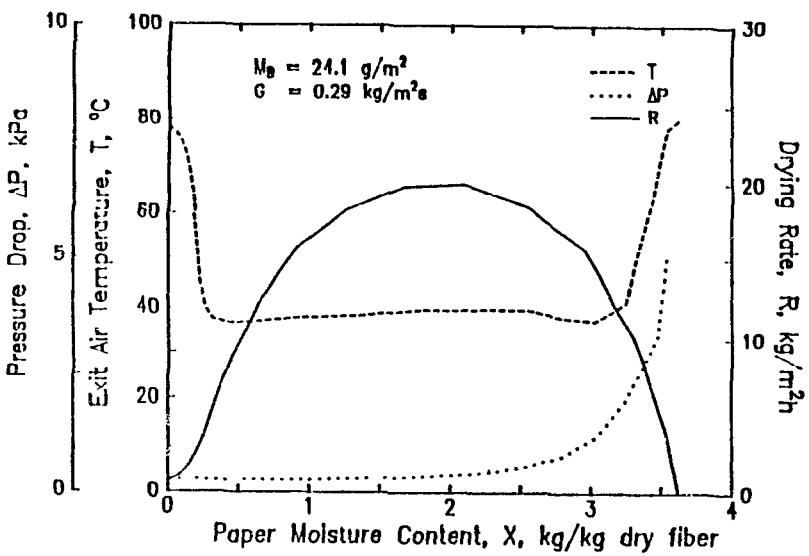
M_B = 24.1 g/m²
G = 0.29 kg/m²s
T
ΔP
R
Pressure Drop, ΔP, kPa
Exit Air Temperature, T, °C
Drying Rate, R, kg/m²h
Paper Moisture Content, X, kg/kg dry fiber

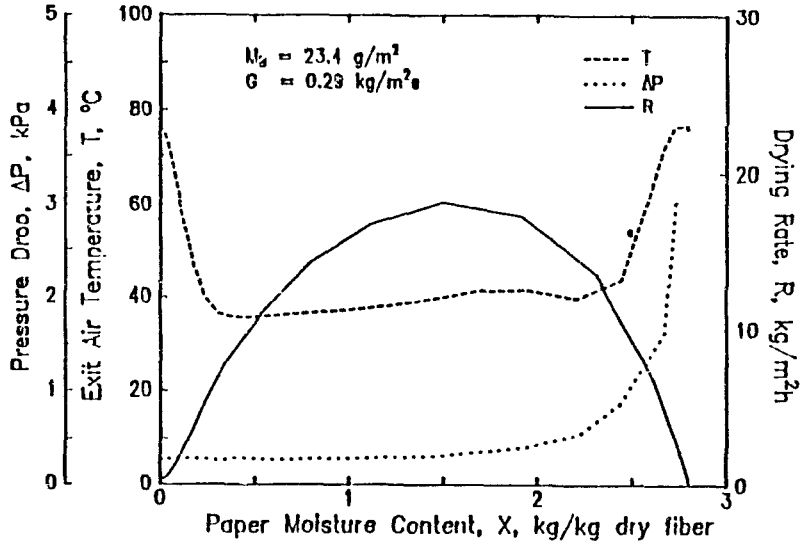
M_B = 23.4 g/m²
G = 0.29 kg/m²s
T
ΔP
R
Pressure Drop, ΔP, kPa
Exit Air Temperature, T, °C
Drying Rate, R, kg/m²h
Paper Moisture Content, X, kg/kg dry fiber

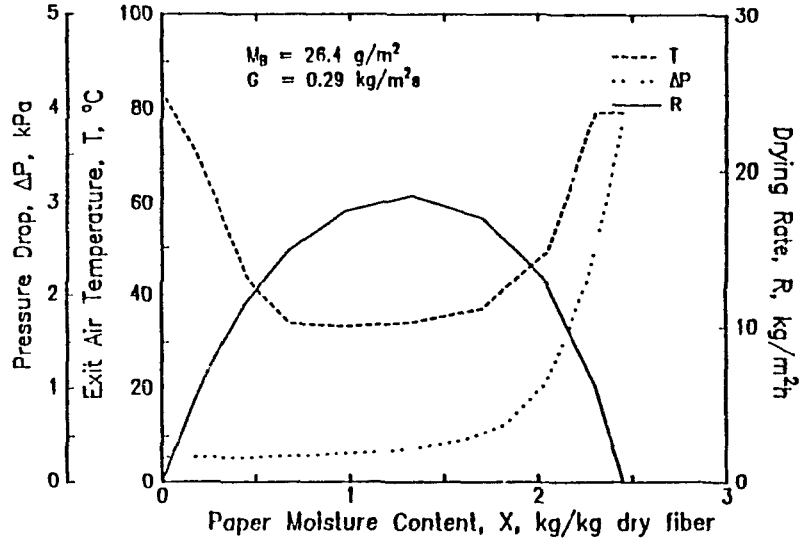
M_B = 26.4 g/m²
G = 0.29 kg/m²s
T
ΔP
R
Pressure Drop, ΔP, kPa
Exit Air Temperature, T, °C
Drying Rate, R, kg/m²h
Paper Moisture Content, X, kg/kg dry fiber

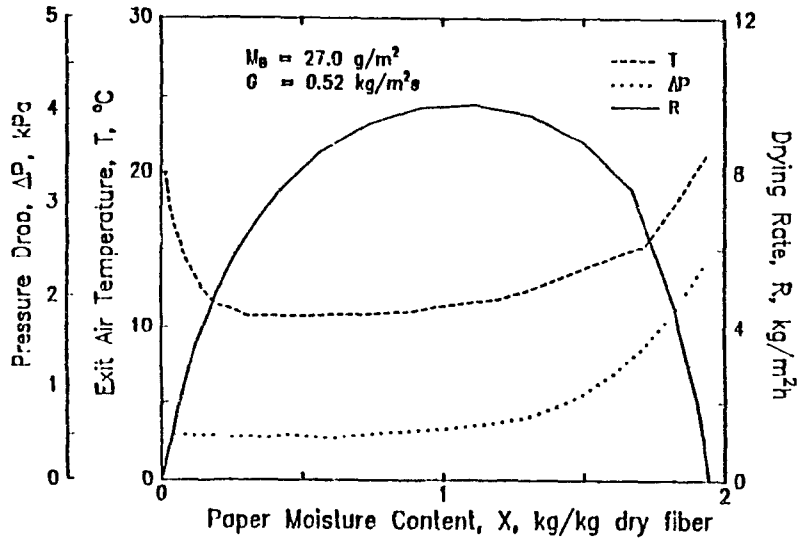
M_B = 27.0 g/m²
G = 0.52 kg/m²s
T
ΔP
R
Pressure Drop, ΔP, kPa
Exit Air Temperature, T, °C
Drying Rate, R, kg/m²h
Paper Moisture Content, X, kg/kg dry fiber

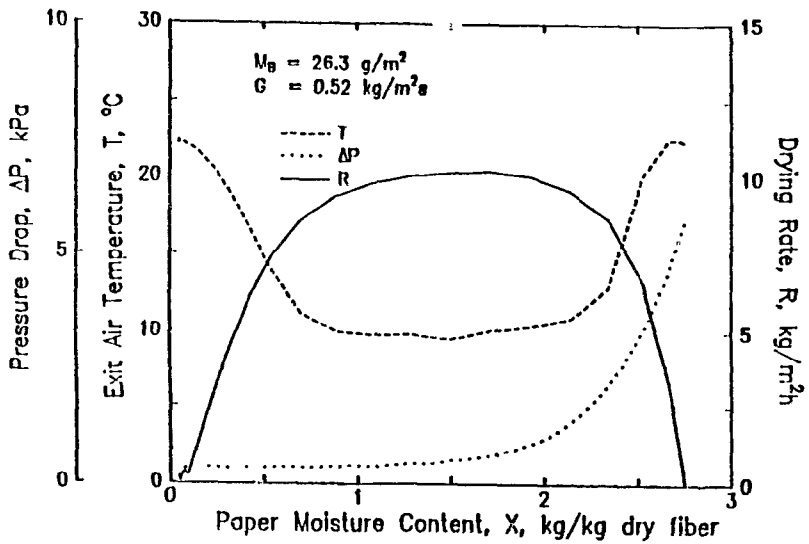
M_B = 26.3 g/m²
G = 0.52 kg/m²s
T
ΔP
R
Pressure Drop, ΔP, kPa
Exit Air Temperature, T, °C
Drying Rate, R, kg/m²h
Paper Moisture Content, X, kg/kg dry fiber

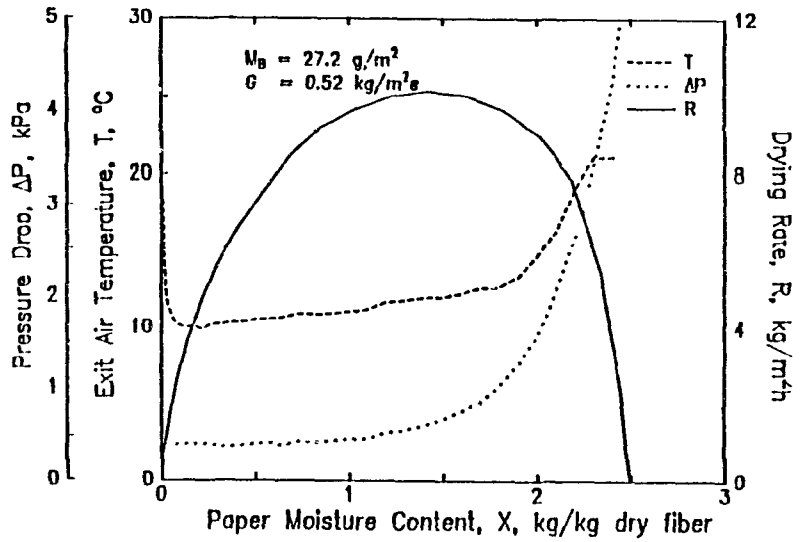
M_B = 27.2 g/m²
G = 0.52 kg/m²s
T
ΔP
R
Pressure Drop, ΔP, kPa
Exit Air Temperature, T, °C
Drying Rate, R, kg/m²h
Paper Moisture Content, X, kg/kg dry fiber

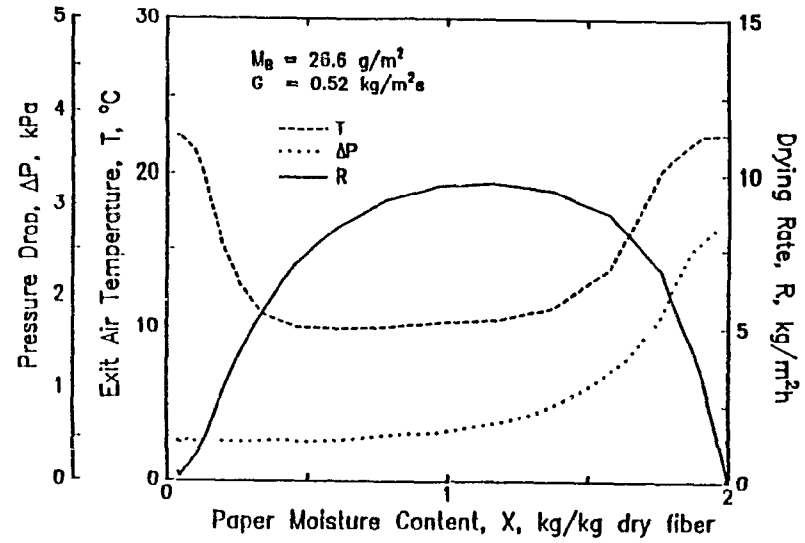
M_B = 26.6 g/m²
G = 0.52 kg/m²s
T
ΔP
R
Pressure Drop, ΔP, kPa
Exit Air Temperature, T, °C
Drying Rate, R, kg/m²h
Paper Moisture Content, X, kg/kg dry fiber

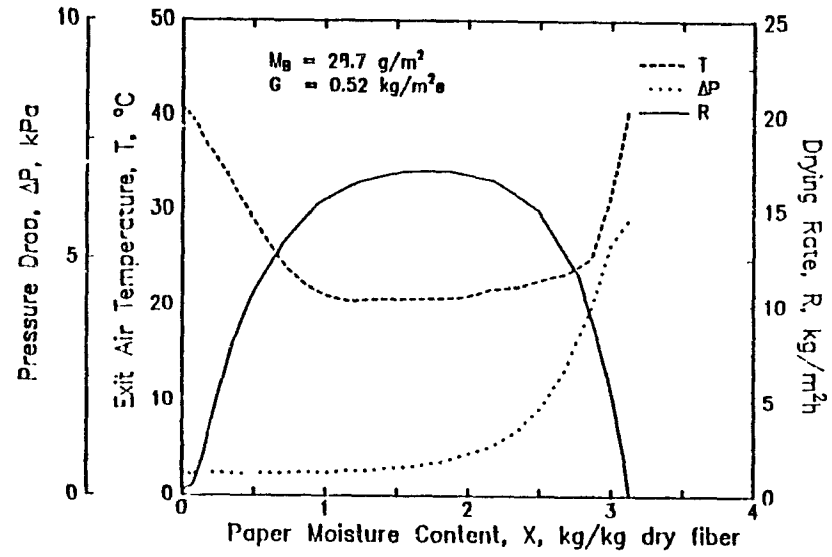
M_B = 29.7 g/m²
G = 0.52 kg/m²s
T
ΔP
R
Pressure Drop, ΔP, kPa
Exit Air Temperature, T, °C
Drying Rate, R, kg/m²h
Paper Moisture Content, X, kg/kg dry fiber

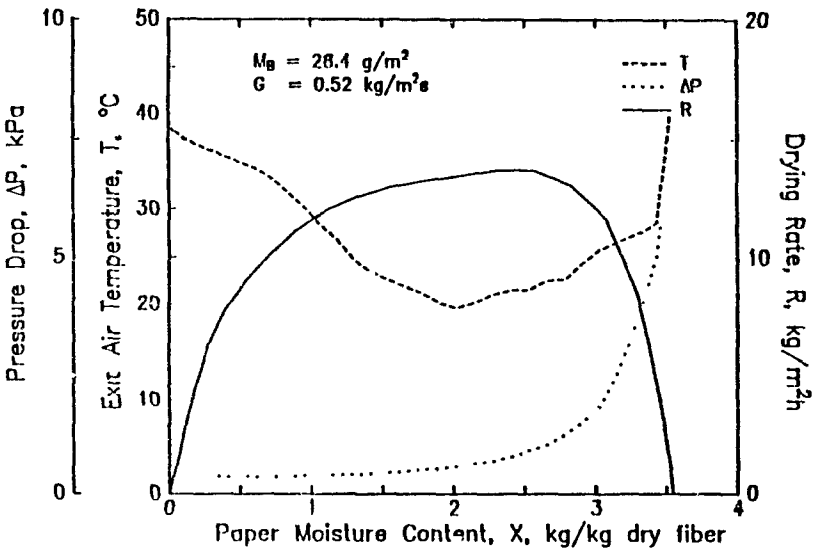
M_B = 28.4 g/m²
G = 0.52 kg/m²s
T
ΔP
R
Pressure Drop, ΔP, kPa
Exit Air Temperature, T, °C
Drying Rate, R, kg/m²h
Paper Moisture Content, X, kg/kg dry fiber

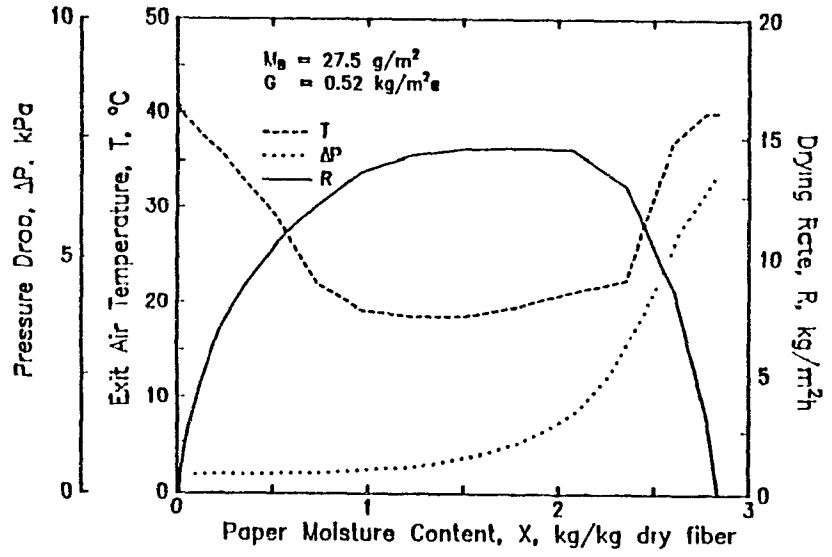
M_B = 27.5 g/m²
G = 0.52 kg/m²s
T
ΔP
R
Pressure Drop, ΔP, kPa
Exit Air Temperature, T, °C
Drying Rate, R, kg/m²h
Paper Moisture Content, X, kg/kg dry fiber

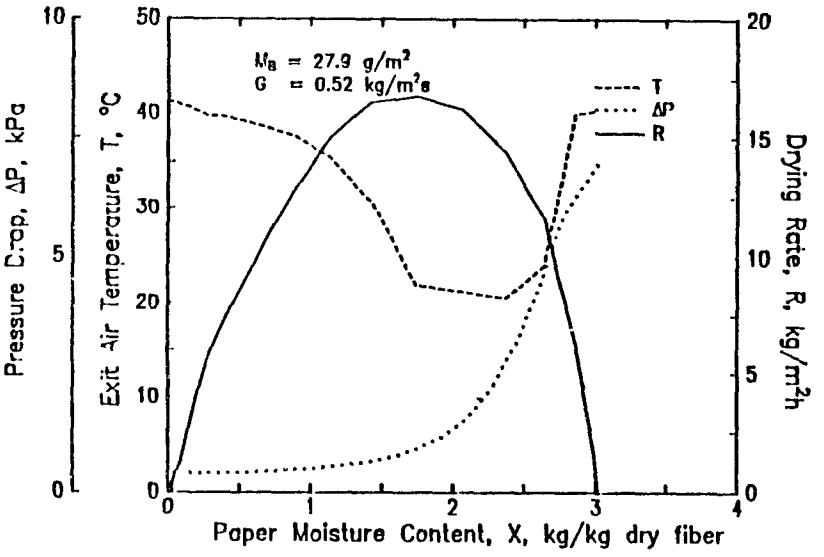
M_B = 27.9 g/m²
G = 0.52 kg/m²s
T
ΔP
R
Pressure Drop, ΔP, kPa
Exit Air Temperature, T, °C
Drying Rate, R, kg/m²h
Paper Moisture Content, X, kg/kg dry fiber

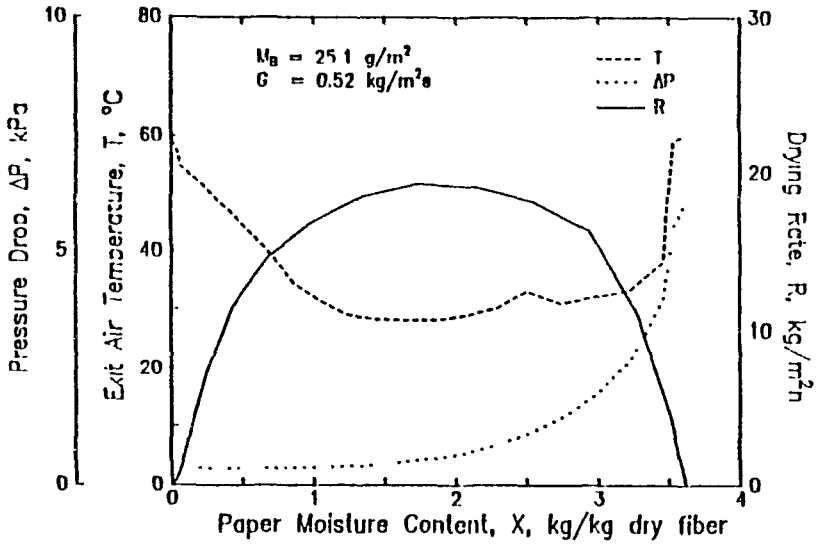
M_B = 25.1 g/m²
G = 0.52 kg/m²s
T
ΔP
R
Pressure Drop, ΔP, kPa
Exit Air Temperature, T, °C
Drying Rate, R, kg/m²h
Paper Moisture Content, X, kg/kg dry fiber

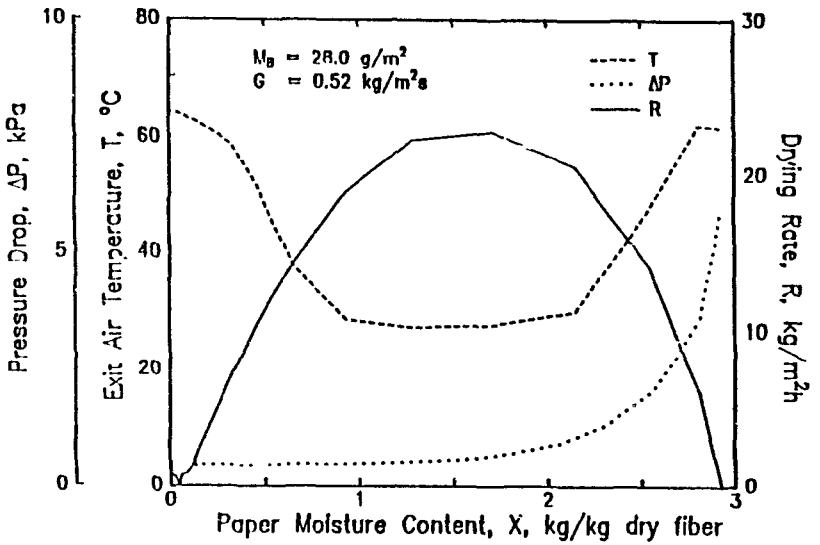
M_B = 28.0 g/m²
G = 0.52 kg/m²s
T
ΔP
R
Pressure Drop, ΔP, kPa
Exit Air Temperature, T, °C
Drying Rate, R, kg/m²h
Paper Moisture Content, X, kg/kg dry fiber

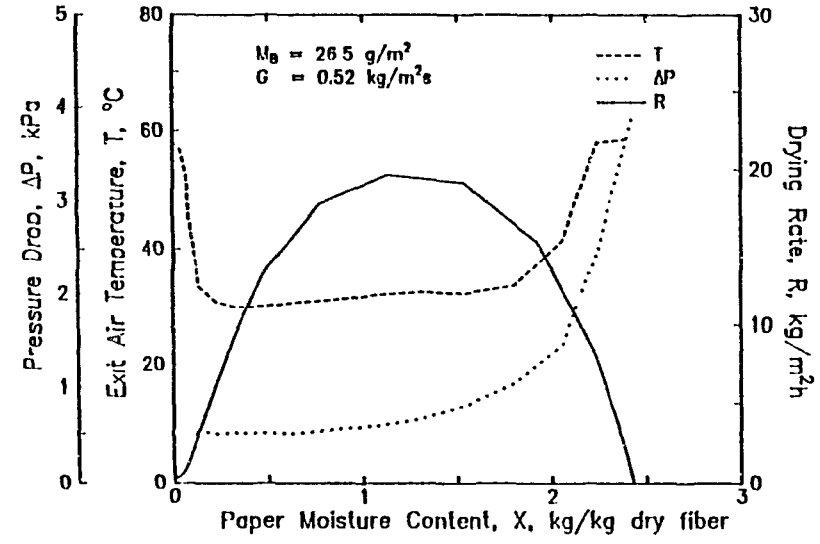
M_B = 26.5 g/m²
G = 0.52 kg/m²s
T
ΔP
R
Pressure Drop, ΔP, kPa
Exit Air Temperature, T, °C
Drying Rate, R, kg/m²h
Paper Moisture Content, X, kg/kg dry fiber

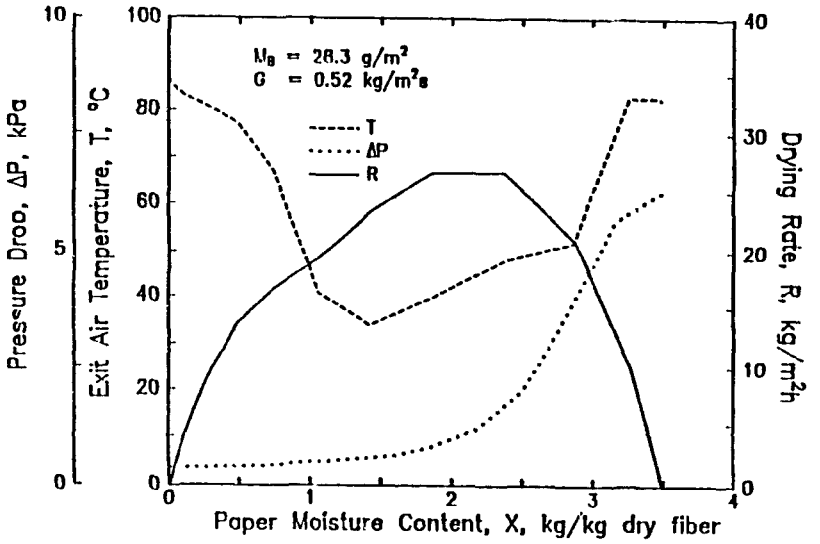
M_B = 28.3 g/m²
G = 0.52 kg/m²s
T
ΔP
R
Pressure Drop, ΔP, kPa
Exit Air Temperature, T, °C
Drying Rate, R, kg/m²h
Paper Moisture Content, X, kg/kg dry fiber

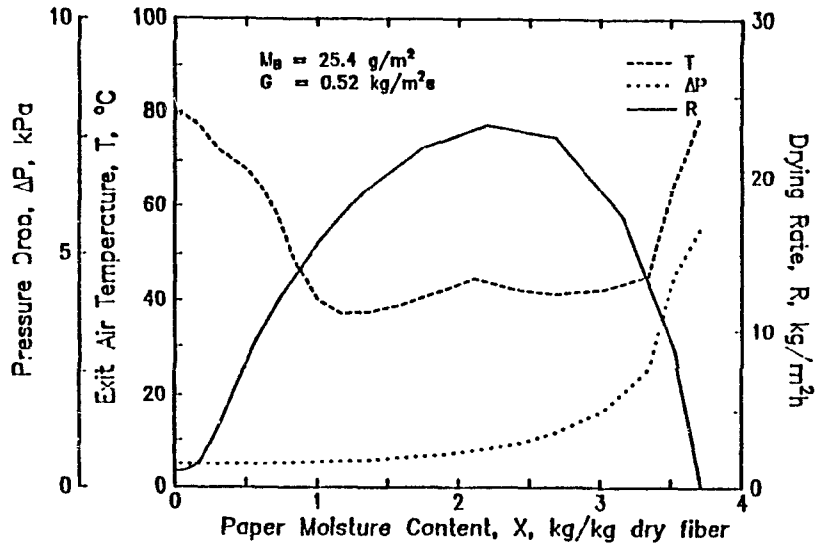
M_B = 25.4 g/m²
G = 0.52 kg/m²s
T
ΔP
R
Pressure Drop, ΔP, kPa
Exit Air Temperature, T, °C
Drying Rate, R, kg/m²h
Paper Moisture Content, X, kg/kg dry fiber

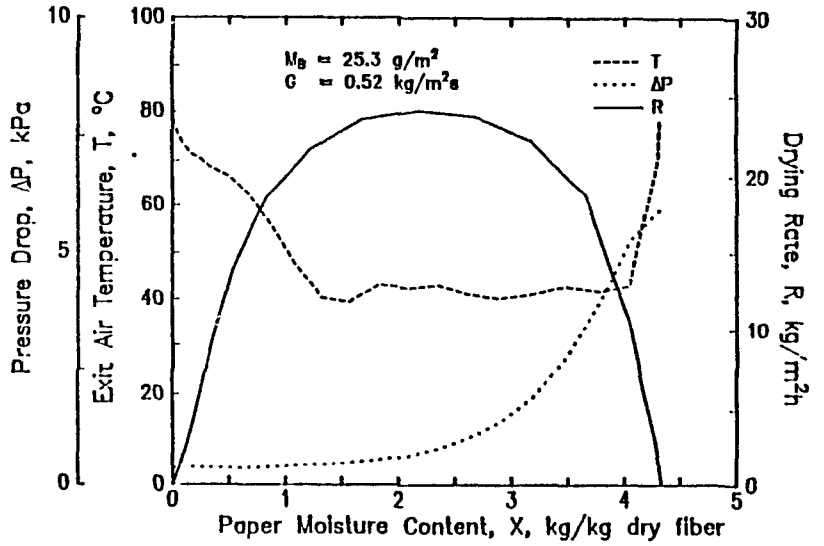
M_B = 25.3 g/m²
G = 0.52 kg/m²s
T
ΔP
R
Pressure Drop, ΔP, kPa
Exit Air Temperature, T, °C
Drying Rate, R, kg/m²h
Paper Moisture Content, X, kg/kg dry fiber

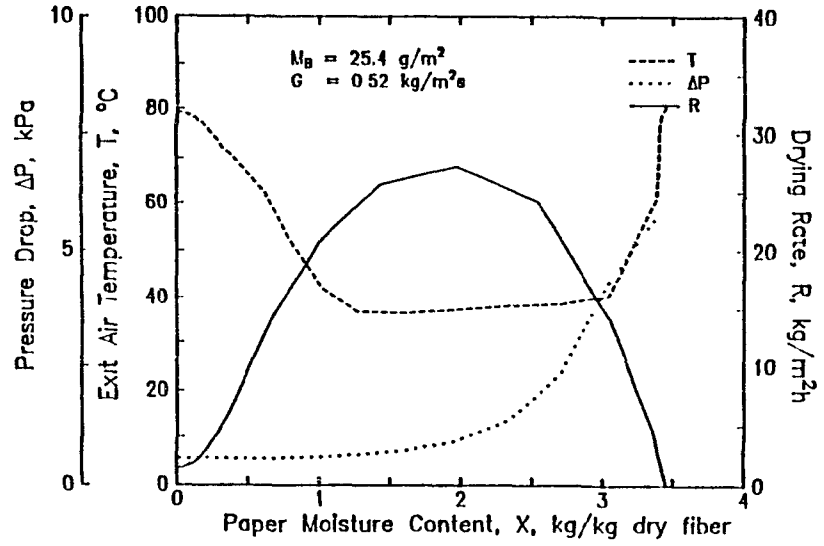
M_B = 25.4 g/m²
G = 0.52 kg/m²s
T
ΔP
R
Pressure Drop, ΔP, kPa
Exit Air Temperature, T, °C
Drying Rate, R, kg/m²h
Paper Moisture Content, X, kg/kg dry fiber

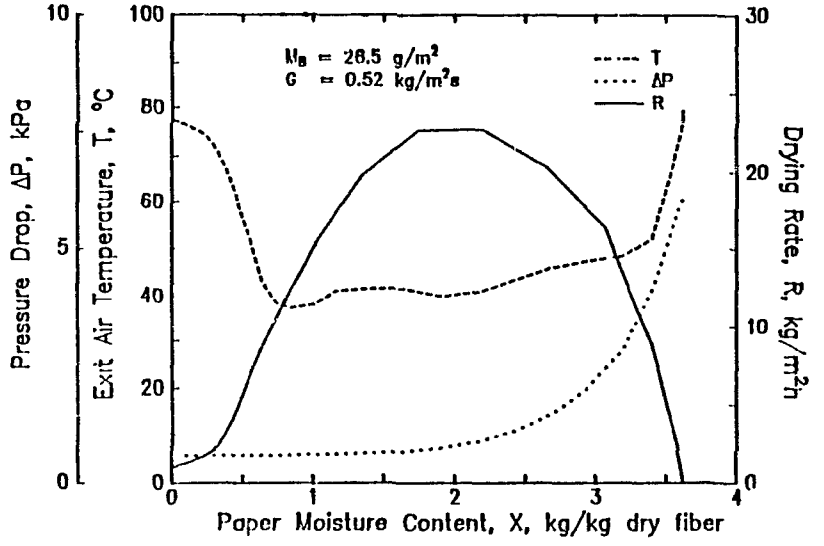
M_B = 26.5 g/m²
G = 0.52 kg/m²s
T
ΔP
R
Pressure Drop, ΔP, kPa
Exit Air Temperature, T, °C
Drying Rate, R, kg/m²h
Paper Moisture Content, X, kg/kg dry fiber

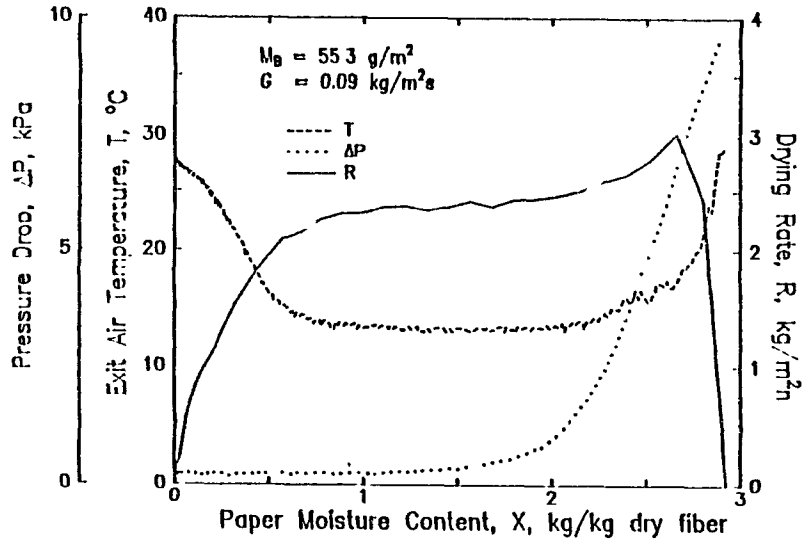
M_B = 55.3 g/m²
G = 0.09 kg/m²s
T
ΔP
R
Pressure Drop, ΔP, kPa
Exit Air Temperature, T, °C
Drying Rate, R, kg/m²h
Paper Moisture Content, X, kg/kg dry fiber

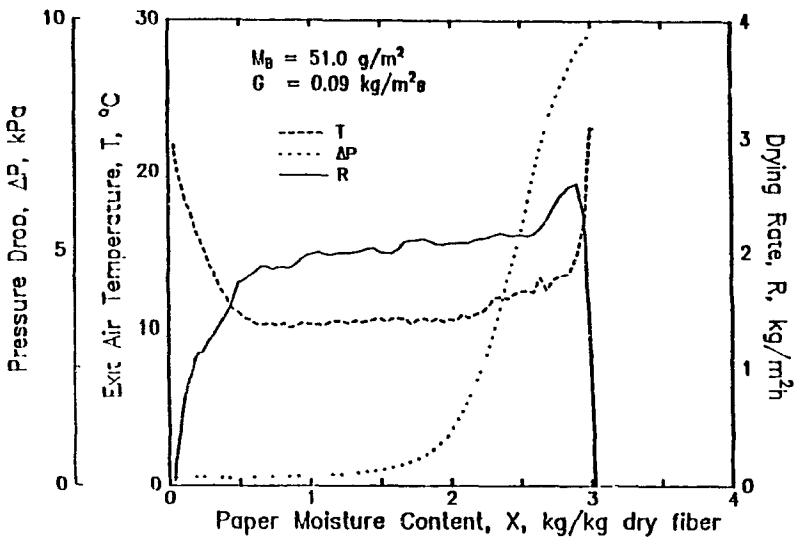
M_B = 51.0 g/m²
G = 0.09 kg/m²s
T
ΔP
R
Pressure Drop, ΔP, kPa
Exit Air Temperature, T, °C
Drying Rate, R, kg/m²h
Paper Moisture Content, X, kg/kg dry fiber

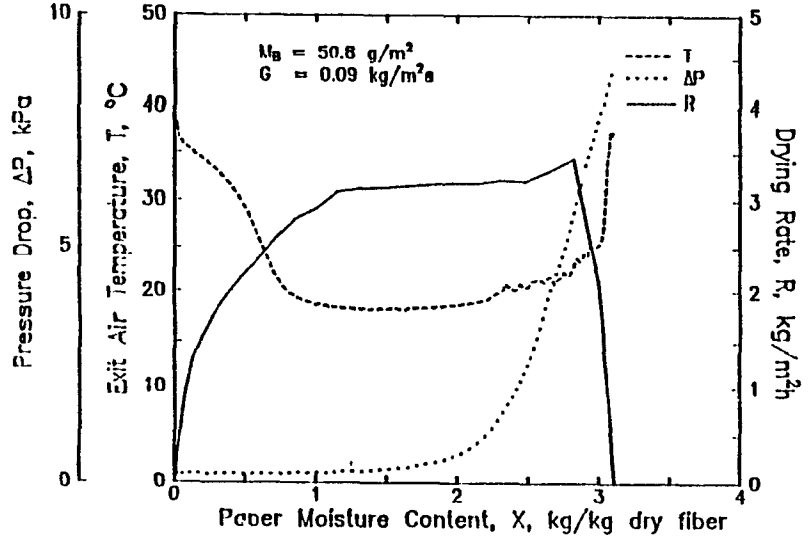
M_B = 50.6 g/m²
G = 0.09 kg/m²s
T
ΔP
R
Pressure Drop, ΔP, kPa
Exit Air Temperature, T, °C
Drying Rate, R, kg/m²h
Paper Moisture Content, X, kg/kg dry fiber

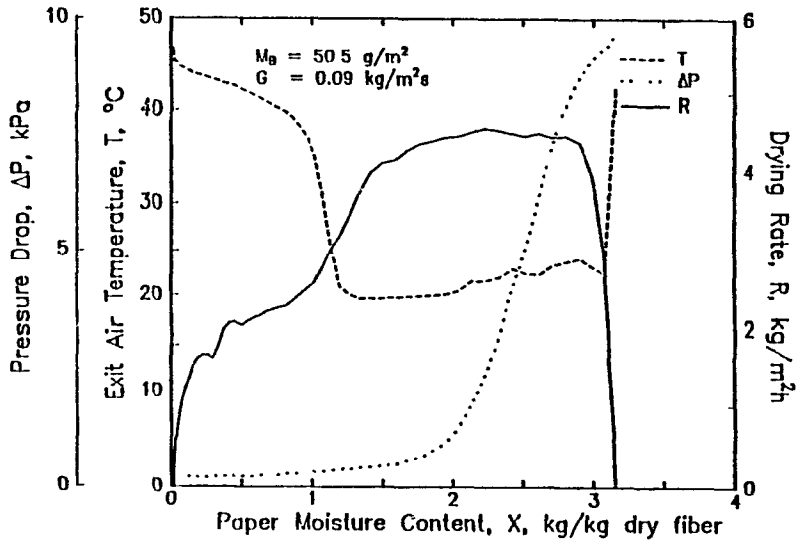
M_B = 50.5 g/m²
G = 0.09 kg/m²s
T
ΔP
R
Pressure Drop, ΔP, kPa
Exit Air Temperature, T, °C
Drying Rate, R, kg/m²h
Paper Moisture Content, X, kg/kg dry fiber

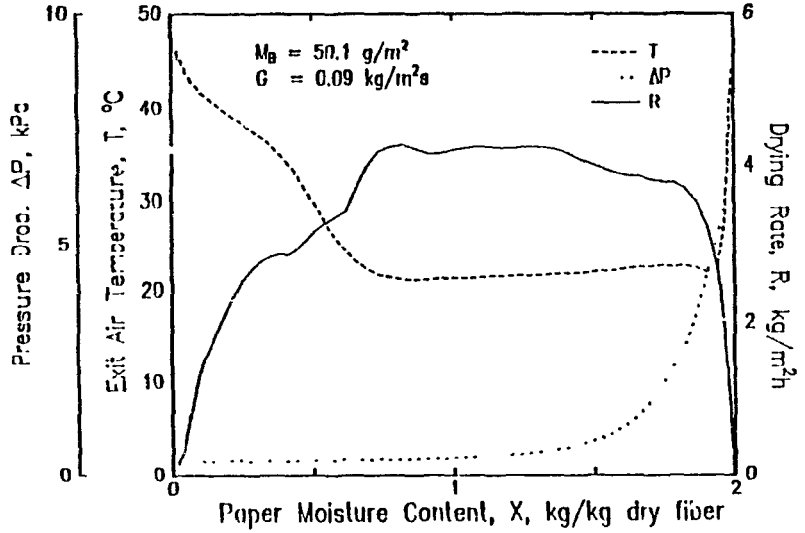
M_B = 50.1 g/m²
G = 0.09 kg/m²s
T
ΔP
R
Pressure Drop, ΔP, kPa
Exit Air Temperature, T, °C
Drying Rate, R, kg/m²h
Paper Moisture Content, X, kg/kg dry fiber

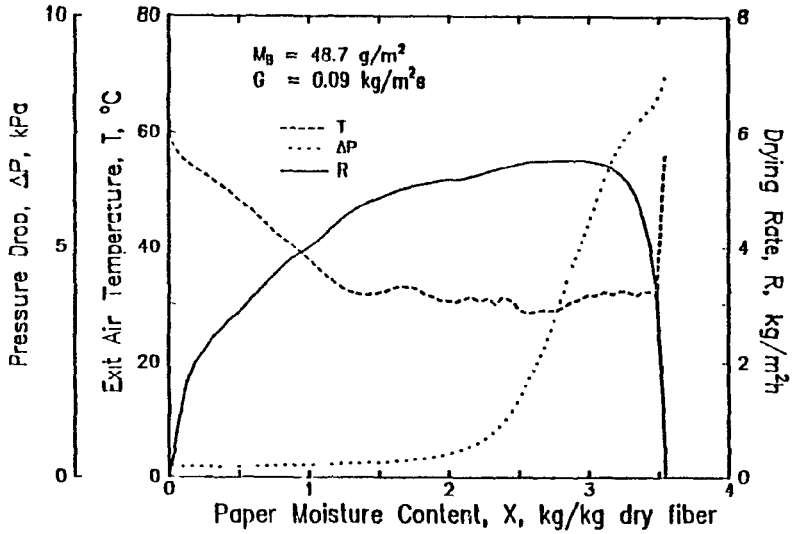
M_B = 48.7 g/m²
G = 0.09 kg/m²s
T
ΔP
R
Pressure Drop, ΔP, kPa
Exit Air Temperature, T, °C
Drying Rate, R, kg/m²h
Paper Moisture Content, X, kg/kg dry fiber

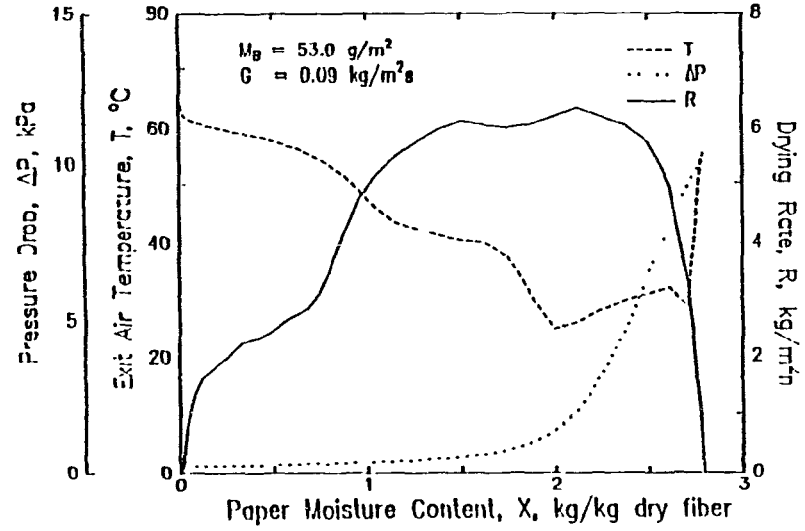
M_B = 53.0 g/m²
G = 0.09 kg/m²s
T
ΔP
R
Pressure Drop, ΔP, kPa
Exit Air Temperature, T, °C
Drying Rate, R, kg/m²h
Paper Moisture Content, X, kg/kg dry fiber

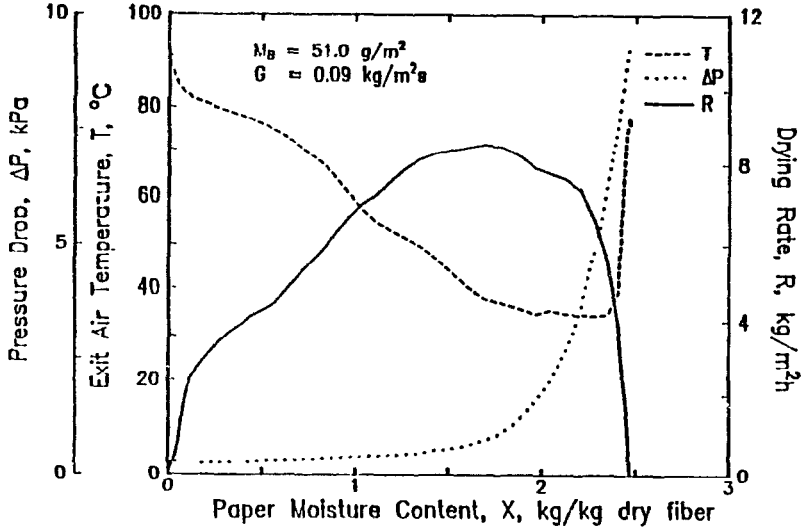
M_B = 51.0 g/m²
G = 0.09 kg/m²s
T
ΔP
R
Pressure Drop, ΔP, kPa
Exit Air Temperature, T, °C
Drying Rate, R, kg/m²h
Paper Moisture Content, X, kg/kg dry fiber

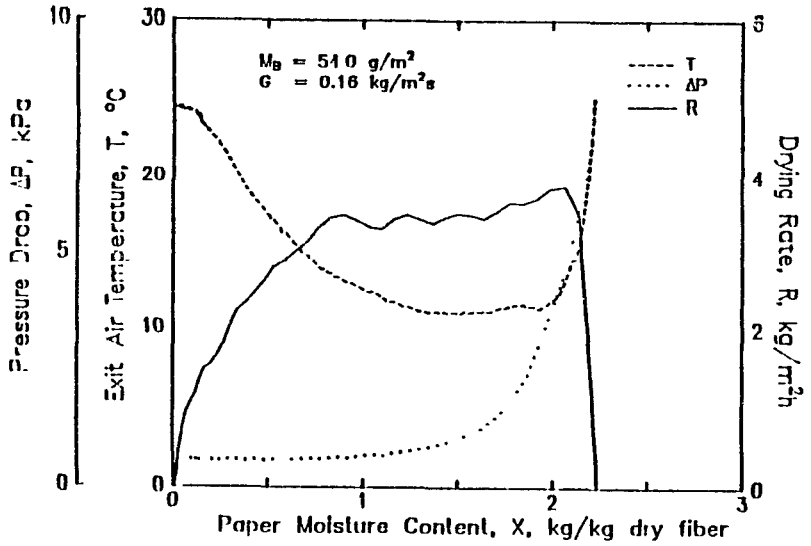
M_B = 54.0 g/m²
G = 0.16 kg/m²s
T
ΔP
R
Pressure Drop, ΔP, kPa
Exit Air Temperature, T, °C
Drying Rate, R, kg/m²h
Paper Moisture Content, X, kg/kg dry fiber

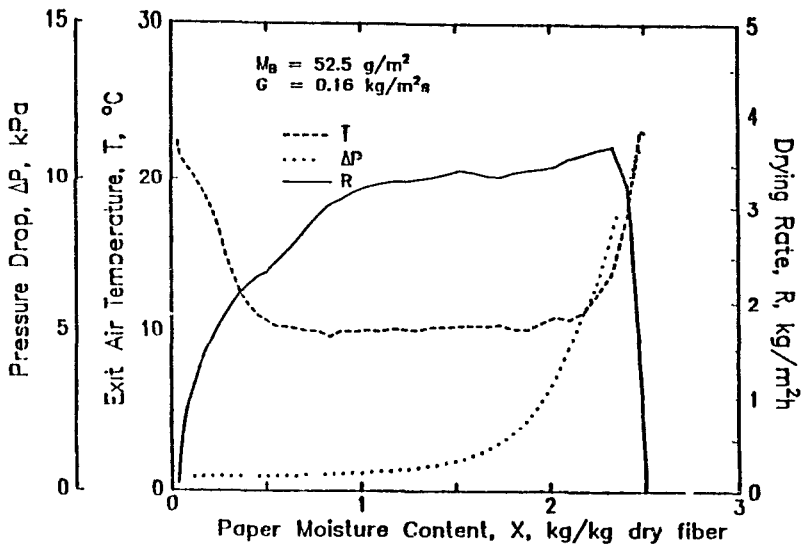
M_B = 52.5 g/m²
G = 0.16 kg/m²s
T
ΔP
R
Pressure Drop, ΔP, kPa
Exit Air Temperature, T, °C
Drying Rate, R, kg/m²h
Paper Moisture Content, X, kg/kg dry fiber

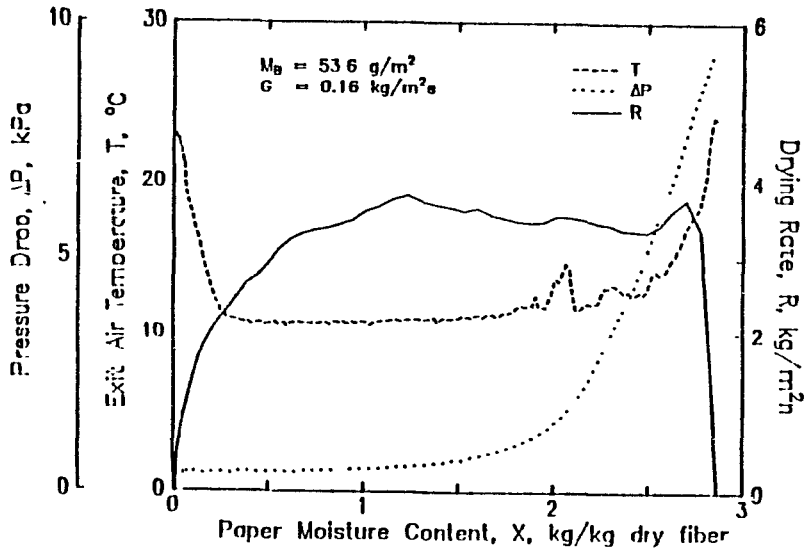
M_B = 53.6 g/m²
G = 0.16 kg/m²s
T
ΔP
R
Pressure Drop, ΔP, kPa
Exit Air Temperature, T, °C
Drying Rate, R, kg/m²h
Paper Moisture Content, X, kg/kg dry fiber

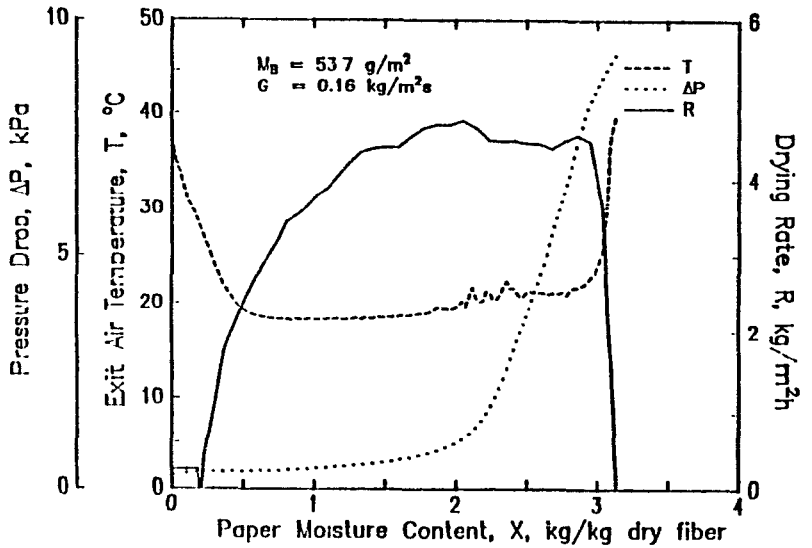
M_B = 53.7 g/m²
G = 0.16 kg/m²s
T
ΔP
R
Pressure Drop, ΔP, kPa
Exit Air Temperature, T, °C
Drying Rate, R, kg/m²h
Paper Moisture Content, X, kg/kg dry fiber

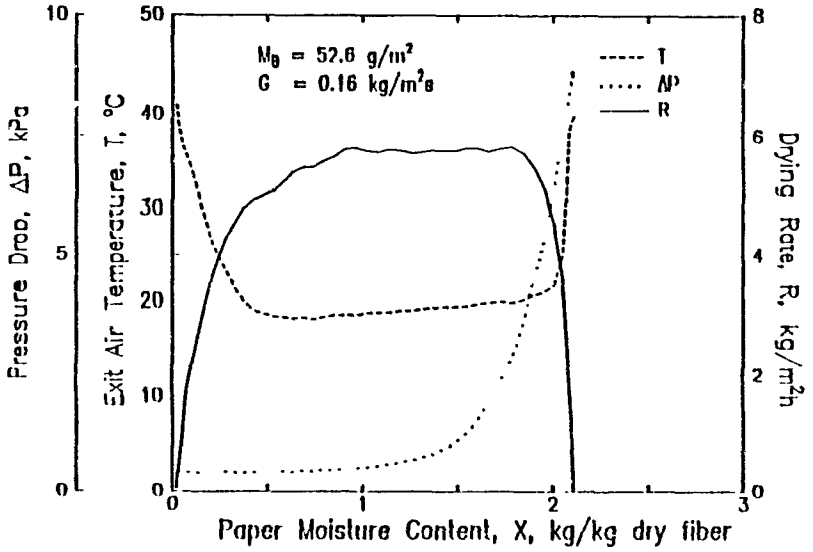
M_B = 52.6 g/m²
G = 0.16 kg/m²s
T
ΔP
R
Pressure Drop, ΔP, kPa
Exit Air Temperature, T, °C
Drying Rate, R, kg/m²h
Paper Moisture Content, X, kg/kg dry fiber

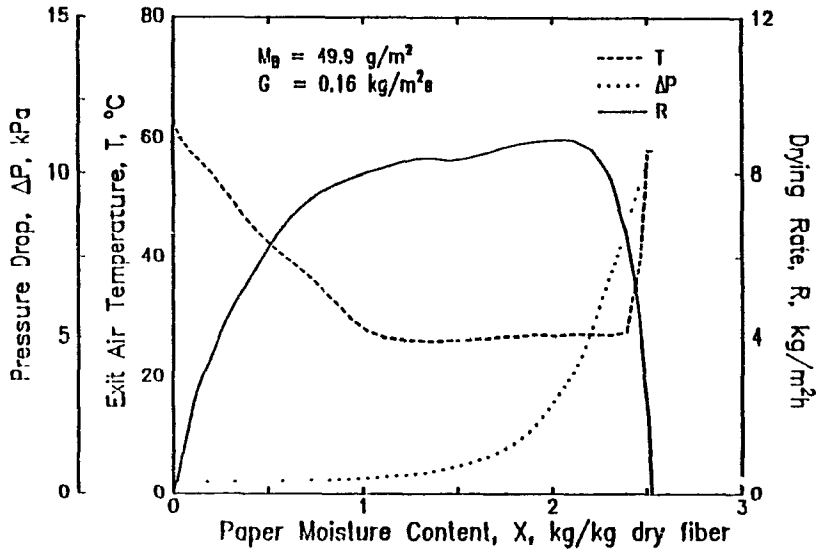
M_B = 49.9 g/m²
G = 0.16 kg/m²s
T
ΔP
R
Pressure Drop, ΔP, kPa
Exit Air Temperature, T, °C
Drying Rate, R, kg/m²h
Paper Moisture Content, X, kg/kg dry fiber

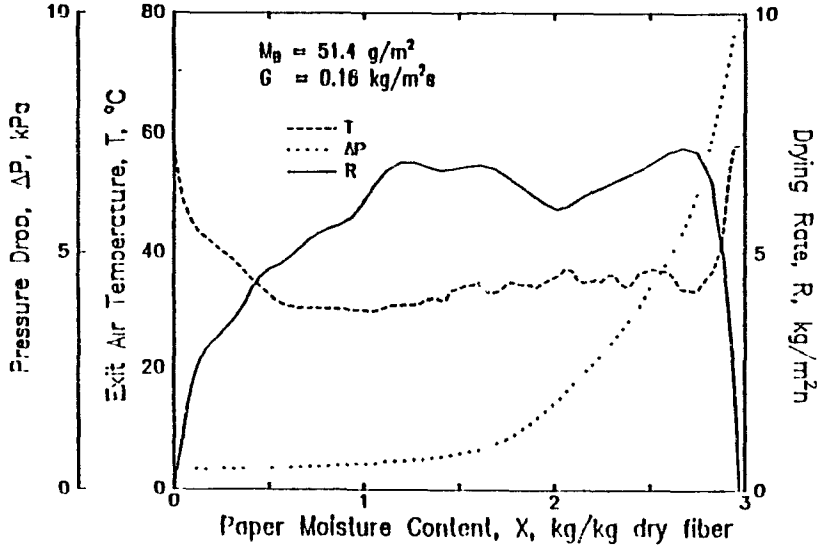
M_B = 51.4 g/m²
G = 0.16 kg/m²s
T
ΔP
R
Pressure Drop, ΔP, kPa
Exit Air Temperature, T, °C
Drying Rate, R, kg/m²h
Paper Moisture Content, X, kg/kg dry fiber

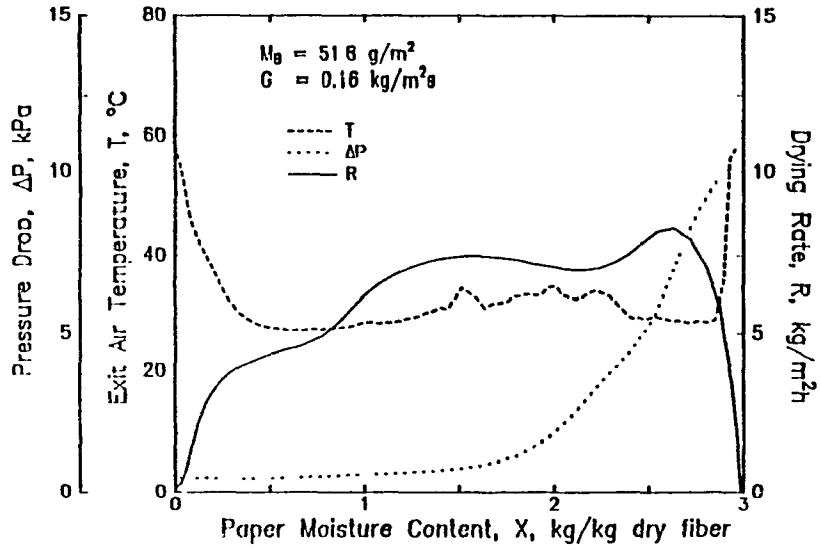
M_B = 51.6 g/m²
G = 0.16 kg/m²s
T
ΔP
R
Pressure Drop, ΔP, kPa
Exit Air Temperature, T, °C
Drying Rate, R, kg/m²h
Paper Moisture Content, X, kg/kg dry fiber

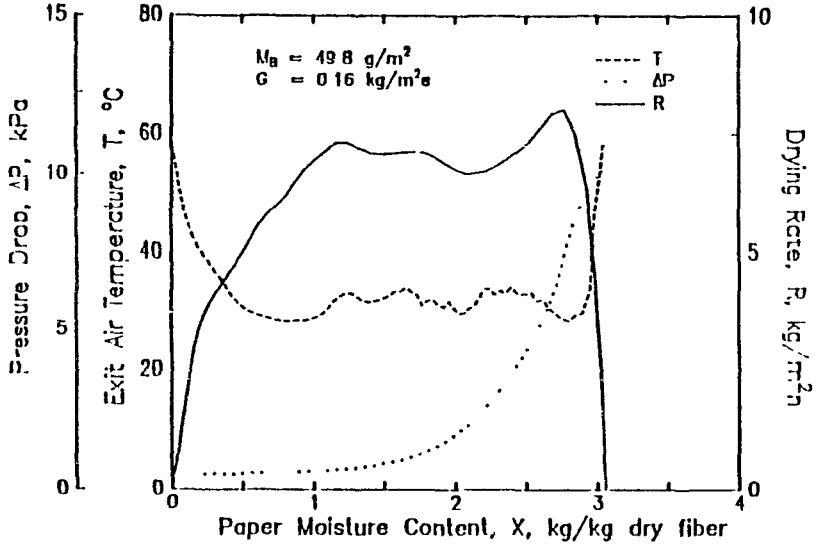
M_B = 49.8 g/m²
G = 0.16 kg/m²s
T
ΔP
R
Pressure Drop, ΔP, kPa
Exit Air Temperature, T, °C
Drying Rate, R, kg/m²h
Paper Moisture Content, X, kg/kg dry fiber

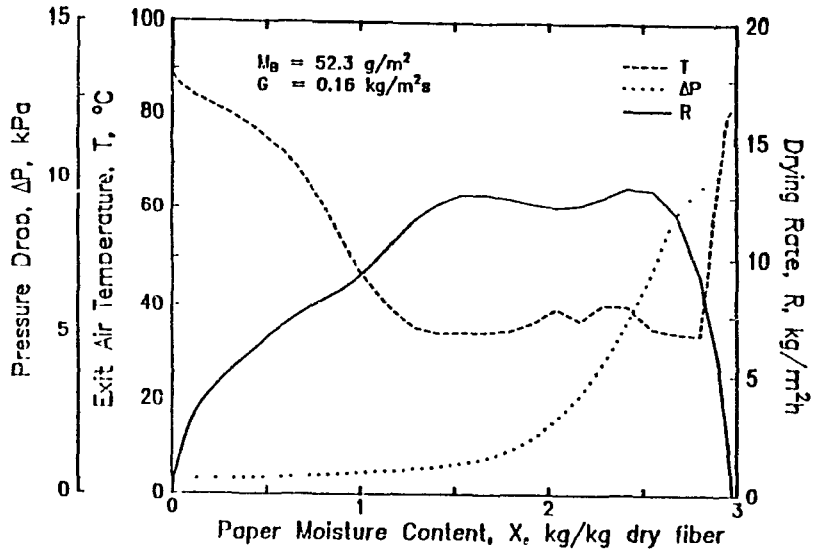
M_B = 52.3 g/m²
G = 0.16 kg/m²s
T
ΔP
R
Pressure Drop, ΔP, kPa
Exit Air Temperature, T, °C
Drying Rate, R, kg/m²h
Paper Moisture Content, X, kg/kg dry fiber

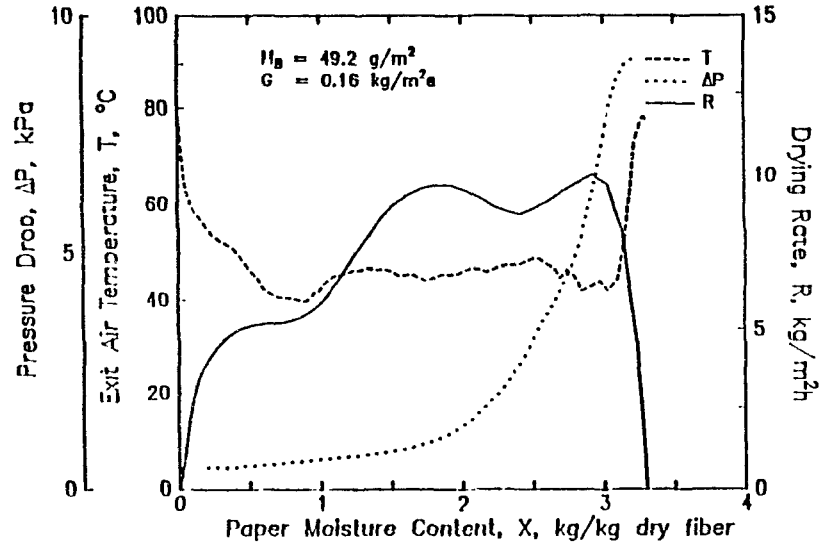
M_B = 49.2 g/m²
G = 0.16 kg/m²s
T
ΔP
R
Pressure Drop, ΔP, kPa
Exit Air Temperature, T, °C
Drying Rate, R, kg/m²h
Paper Moisture Content, X, kg/kg dry fiber

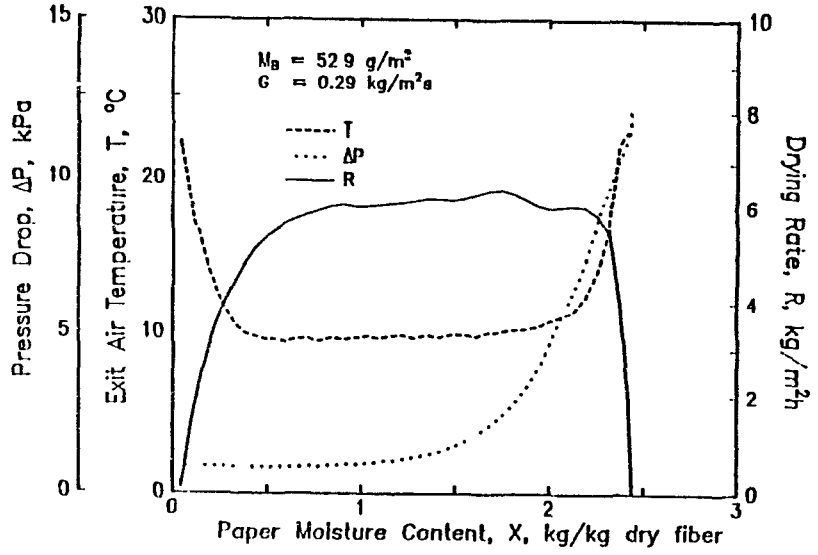
M_B = 52.9 g/m²
G = 0.29 kg/m²s
T
ΔP
R
Pressure Drop, ΔP, kPa
Exit Air Temperature, T, °C
Drying Rate, R, kg/m²h
Paper Moisture Content, X, kg/kg dry fiber

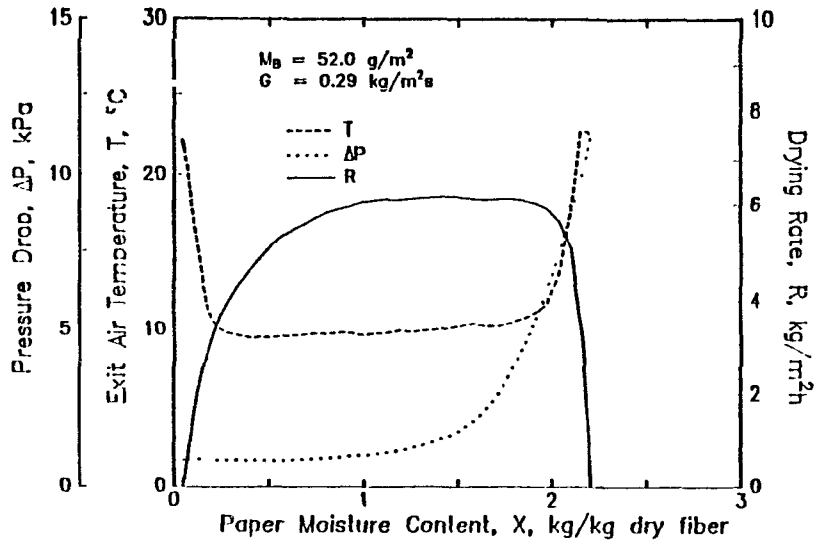
M_B = 52.0 g/m²
G = 0.29 kg/m²s
T
ΔP
R
Pressure Drop, ΔP, kPa
Exit Air Temperature, T, °C
Drying Rate, R, kg/m²h
Paper Moisture Content, X, kg/kg dry fiber

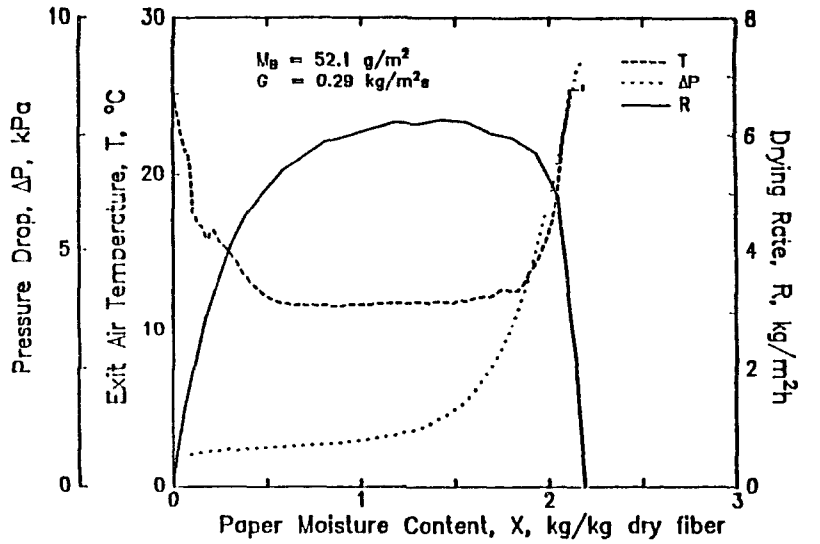
M_B = 52.1 g/m²
G = 0.29 kg/m²s
T
ΔP
R
Pressure Drop, ΔP, kPa
Exit Air Temperature, T, °C
Drying Rate, R, kg/m²h
Paper Moisture Content, X, kg/kg dry fiber

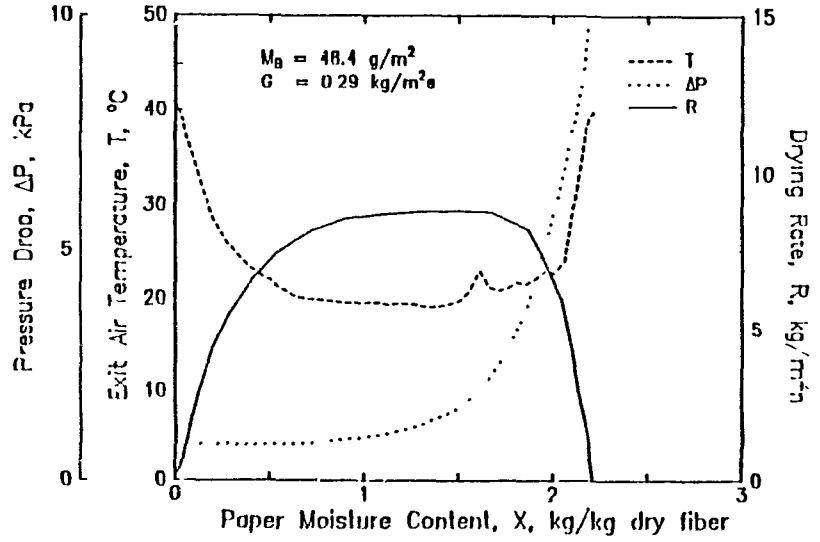
M_B = 48.4 g/m²
G = 0.29 kg/m²s
T
ΔP
R
Pressure Drop, ΔP, kPa
Exit Air Temperature, T, °C
Drying Rate, R, kg/m²h
Paper Moisture Content, X, kg/kg dry fiber

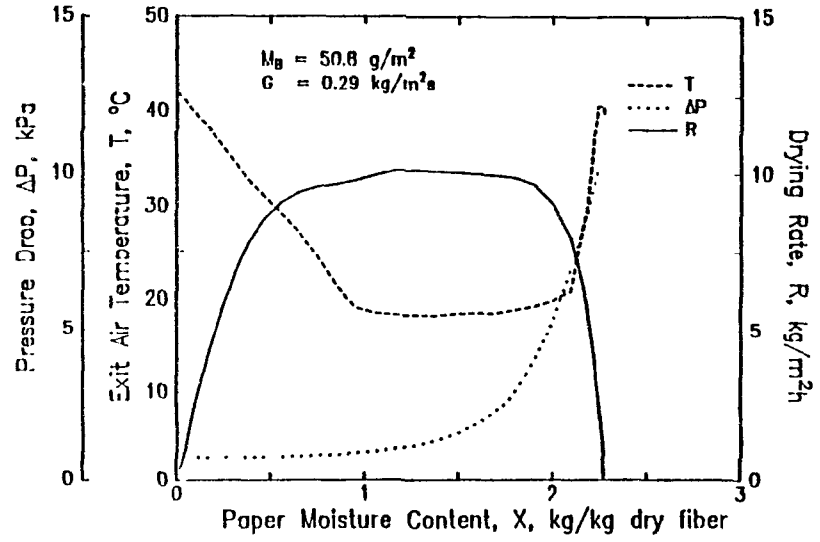
M_B = 50.8 g/m²
G = 0.29 kg/m²s
T
ΔP
R
Pressure Drop, ΔP, kPa
Exit Air Temperature, T, °C
Drying Rate, R, kg/m²h
Paper Moisture Content, X, kg/kg dry fiber

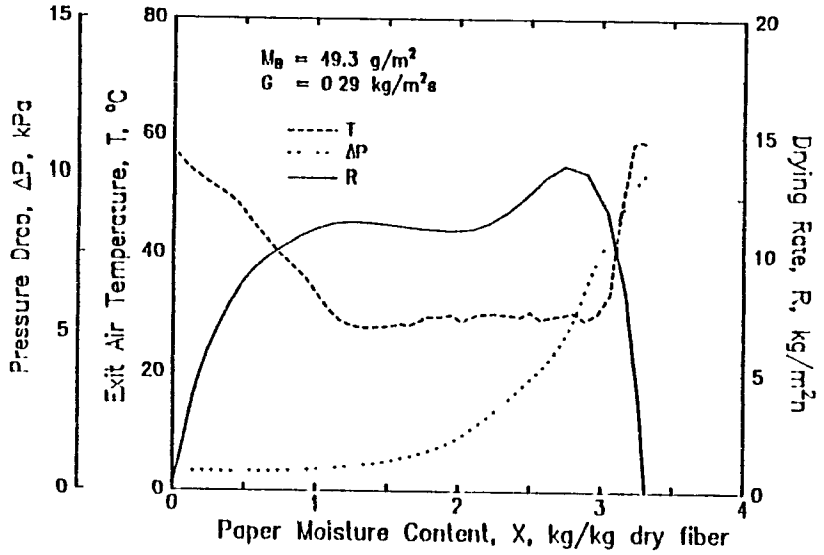
M_B = 49.3 g/m²
G = 0.29 kg/m²s
T
ΔP
R
Pressure Drop, ΔP, kPa
Exit Air Temperature, T, °C
Drying Rate, R, kg/m²h
Paper Moisture Content, X, kg/kg dry fiber

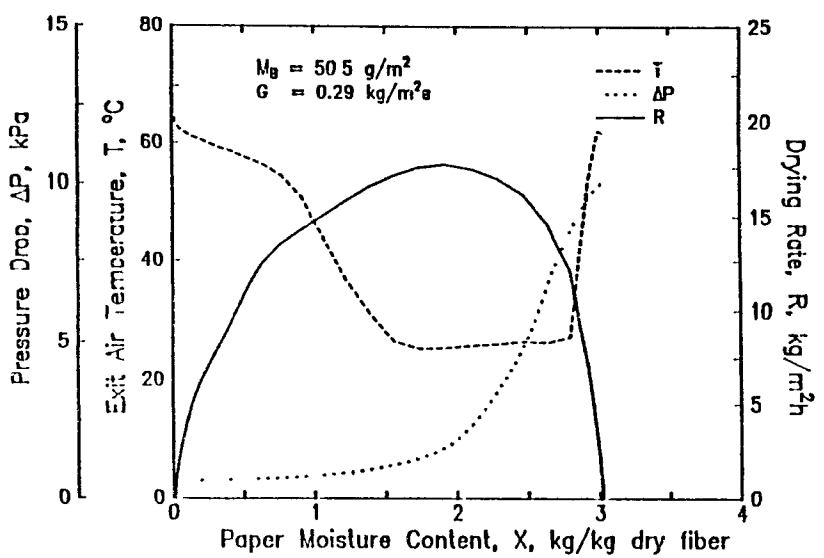
M_B = 50.5 g/m²
G = 0.29 kg/m²s
T
ΔP
R
Pressure Drop, ΔP, kPa
Exit Air Temperature, T, °C
Drying Rate, R, kg/m²h
Paper Moisture Content, X, kg/kg dry fiber

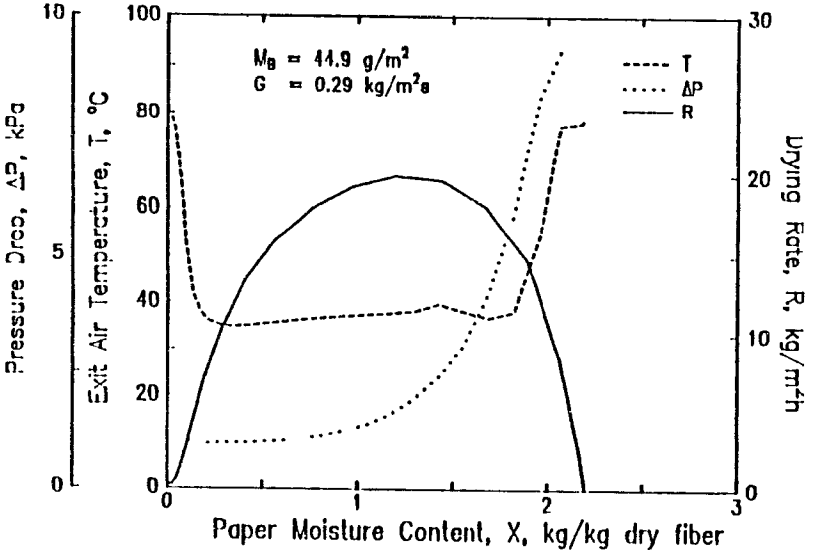
M_B = 44.9 g/m²
G = 0.29 kg/m²s
T
ΔP
R
Pressure Drop, ΔP, kPa
Exit Air Temperature, T, °C
Drying Rate, R, kg/m²h
Paper Moisture Content, X, kg/kg dry fiber

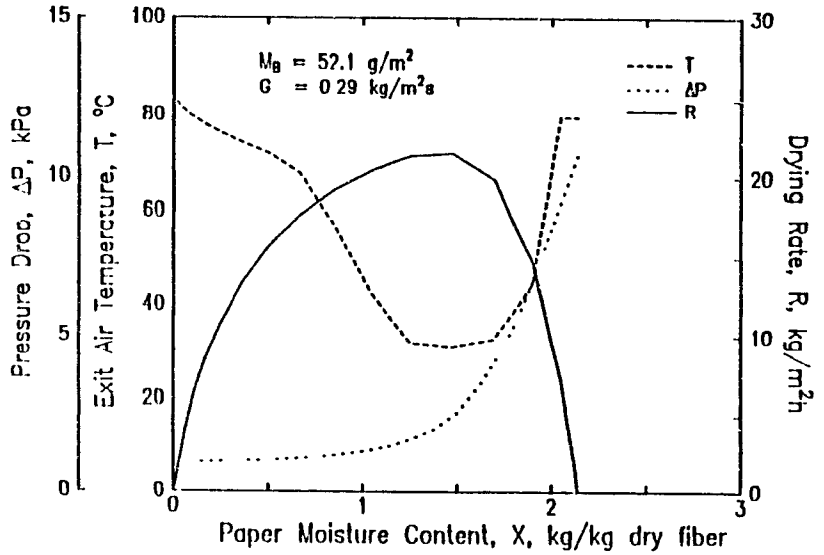
M_B = 52.1 g/m²
G = 0.29 kg/m²s
T
ΔP
R
Pressure Drop, ΔP, kPa
Exit Air Temperature, T, °C
Drying Rate, R, kg/m²h
Paper Moisture Content, X, kg/kg dry fiber

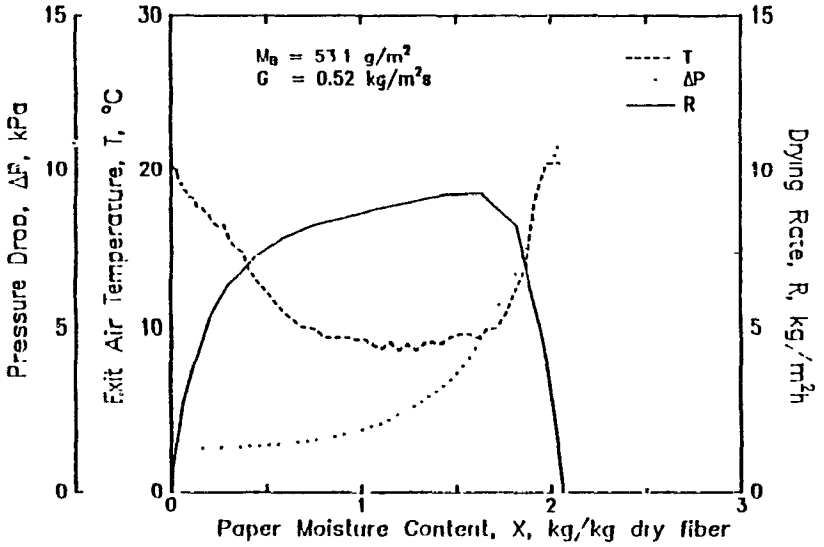
M_B = 53.1 g/m²
G = 0.52 kg/m²s
T
ΔP
R
Pressure Drop, ΔP, kPa
Exit Air Temperature, T, °C
Drying Rate, R, kg/m²h
Paper Moisture Content, X, kg/kg dry fiber

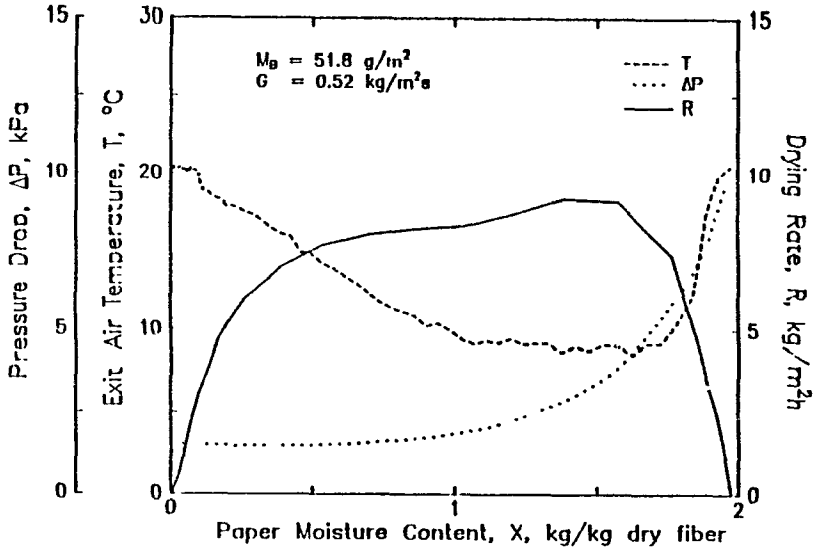
M_B = 51.8 g/m²
G = 0.52 kg/m²s
T
ΔP
R
Pressure Drop, ΔP, kPa
Exit Air Temperature, T, °C
Drying Rate, R, kg/m²h
Paper Moisture Content, X, kg/kg dry fiber

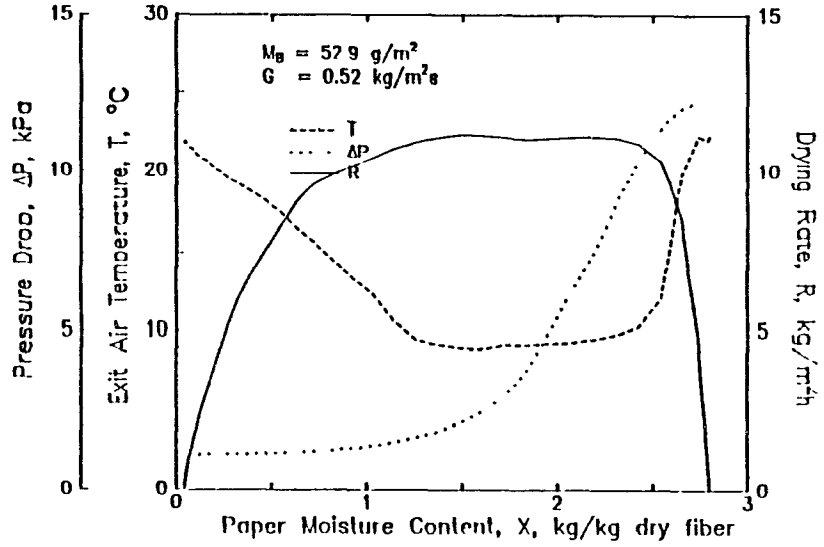
M_B = 57.9 g/m²
G = 0.52 kg/m²s
T
ΔP
R
Pressure Drop, ΔP, kPa
Exit Air Temperature, T, °C
Drying Rate, R, kg/m²h
Paper Moisture Content, X, kg/kg dry fiber

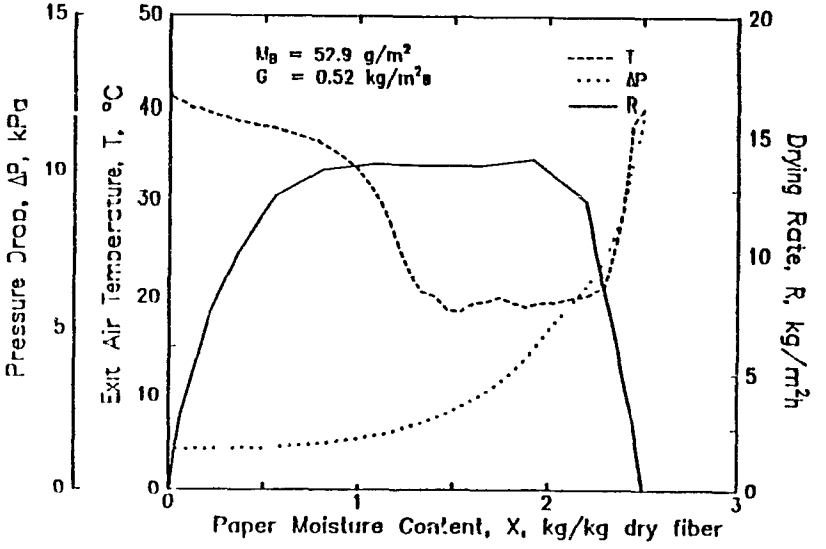
M_B = 57.9 g/m²
G = 0.52 kg/m²s
T
ΔP
R
Pressure Drop, ΔP, kPa
Exit Air Temperature, T, °C
Drying Rate, R, kg/m²h
Paper Moisture Content, X, kg/kg dry fiber

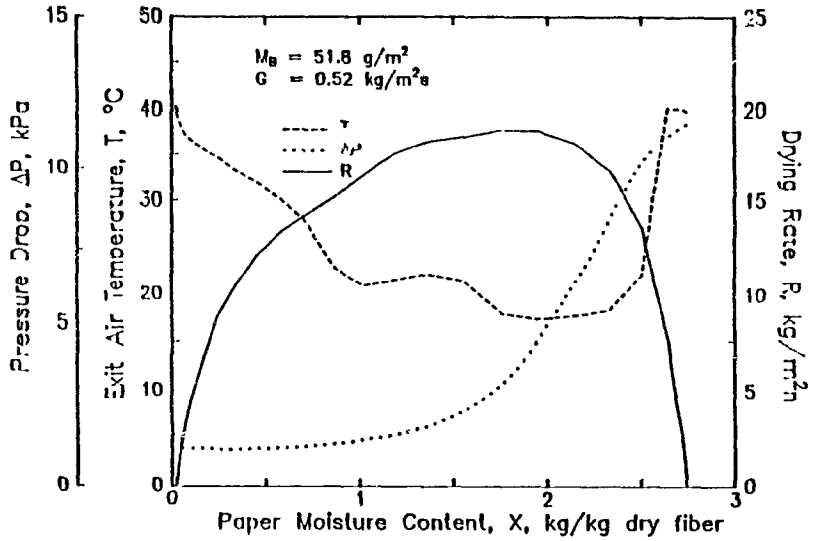
M_B = 51.6 g/m²
G = 0.52 kg/m²s
T
ΔP
R
Pressure Drop, ΔP, kPa
Exit Air Temperature, T, °C
Drying Rate, R, kg/m²h
Paper Moisture Content, X, kg/kg dry fiber

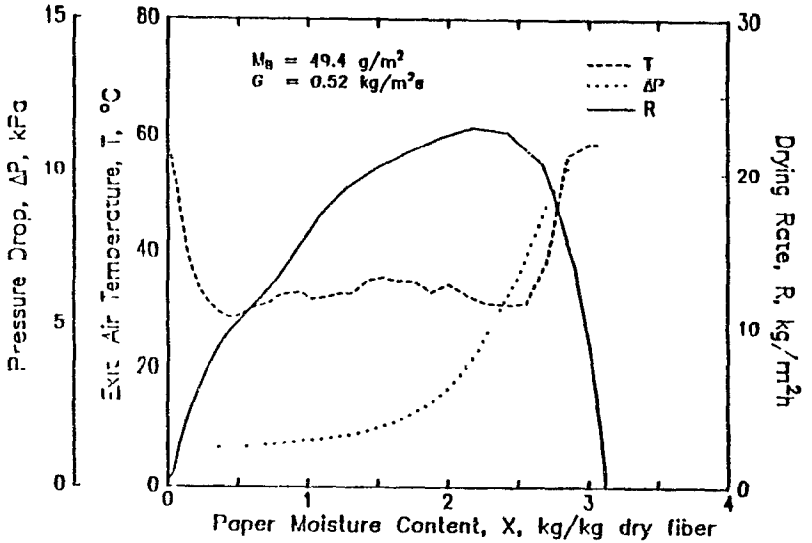
M_B = 49.4 g/m²
G = 0.52 kg/m²s
T
ΔP
R
Pressure Drop, ΔP, kPa
Exit Air Temperature, T, °C
Drying Rate, R, kg/m²h
Paper Moisture Content, X, kg/kg dry fiber

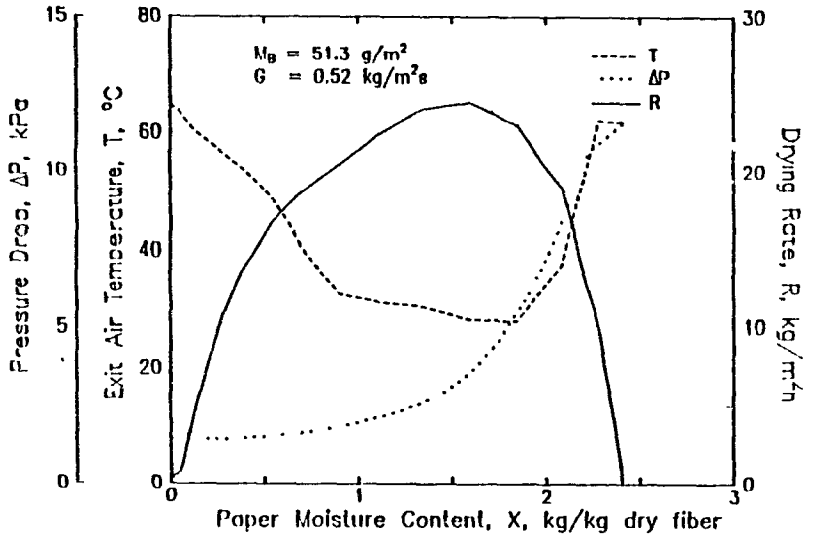
M_B = 51.3 g/m²
G = 0.52 kg/m²s
T
ΔP
R
Pressure Drop, ΔP, kPa
Exit Air Temperature, T, °C
Drying Rate, R, kg/m²h
Paper Moisture Content, X, kg/kg dry fiber

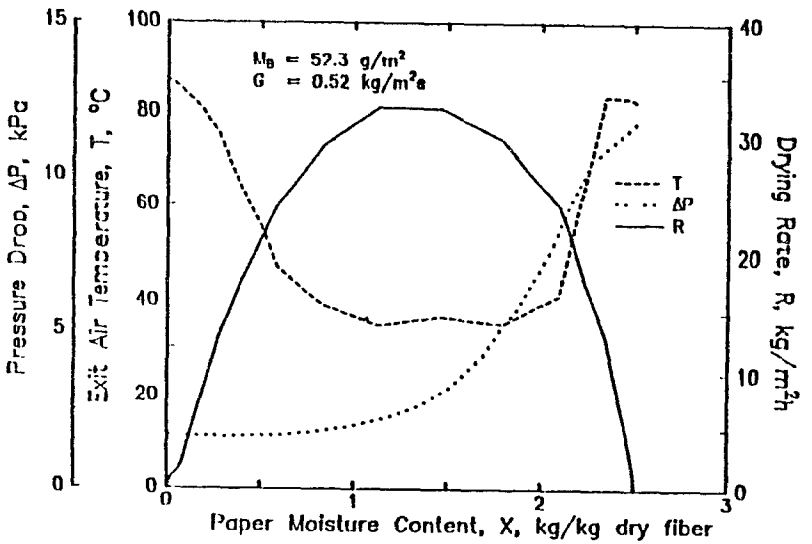
M_B = 52.3 g/m²
G = 0.52 kg/m²s
T
ΔP
R
Pressure Drop, ΔP, kPa
Exit Air Temperature, T, °C
Drying Rate, R, kg/m²h
Paper Moisture Content, X, kg/kg dry fiber

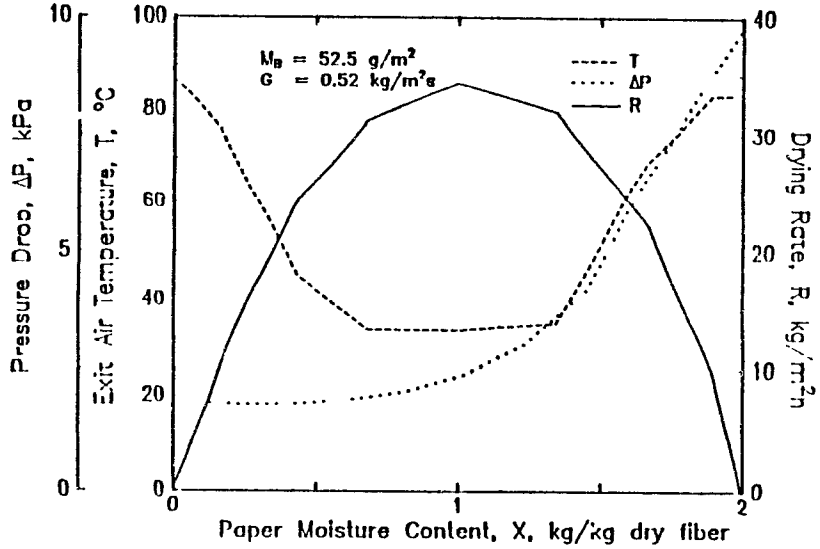
M_B = 52.5 g/m²
G = 0.52 kg/m²s
T
ΔP
R
Pressure Drop, ΔP, kPa
Exit Air Temperature, T, °C
Drying Rate, R, kg/m²h
Paper Moisture Content, X, kg/kg dry fiber

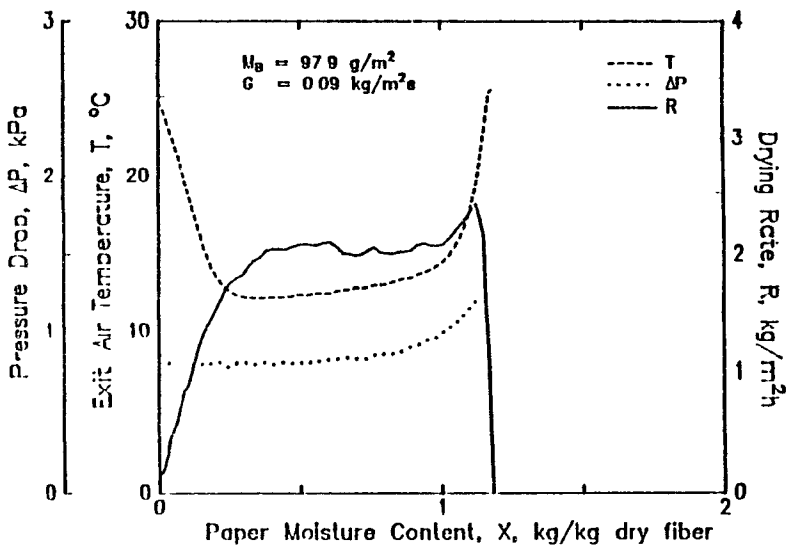
M_B = 97.9 g/m²
G = 0.09 kg/m²s
T
ΔP
R
Pressure Drop, ΔP, kPa
Exit Air Temperature, T, °C
Drying Rate, R, kg/m²h
Paper Moisture Content, X, kg/kg dry fiber

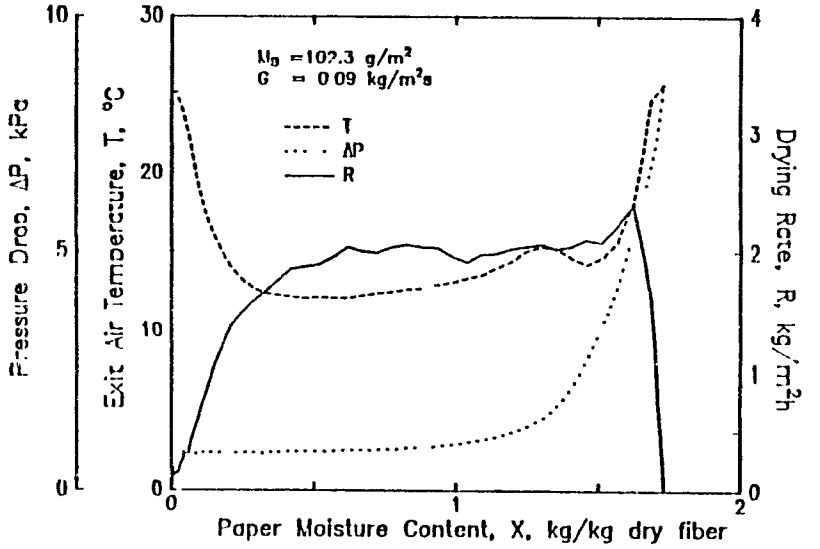
M_B =102.3 g/m²
G = 0.09 kg/m²s
T
ΔP
R
Pressure Drop, ΔP, kPa
Exit Air Temperature, T, °C
Drying Rate, R, kg/m²h
Paper Moisture Content, X, kg/kg dry fiber

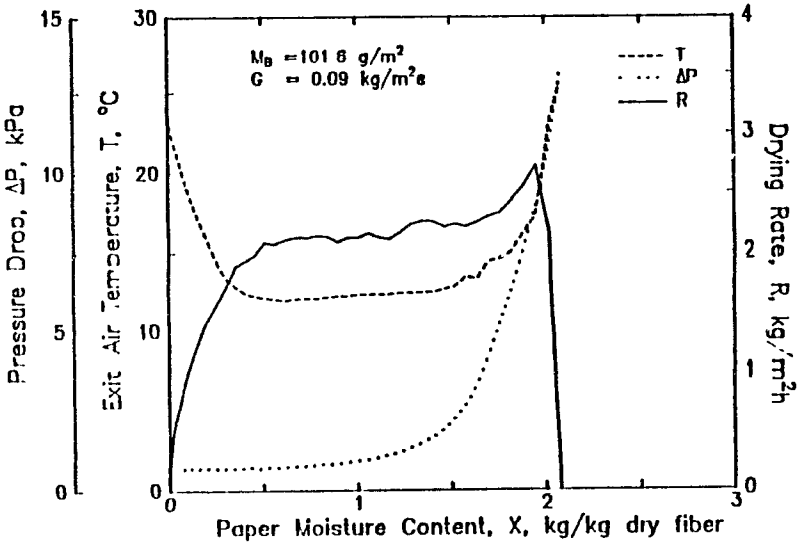
M_B =101.6 g/m²
G = 0.09 kg/m²s
T
ΔP
R
Pressure Drop, ΔP, kPa
Exit Air Temperature, T, °C
Drying Rate, R, kg/m²h
Paper Moisture Content, X, kg/kg dry fiber

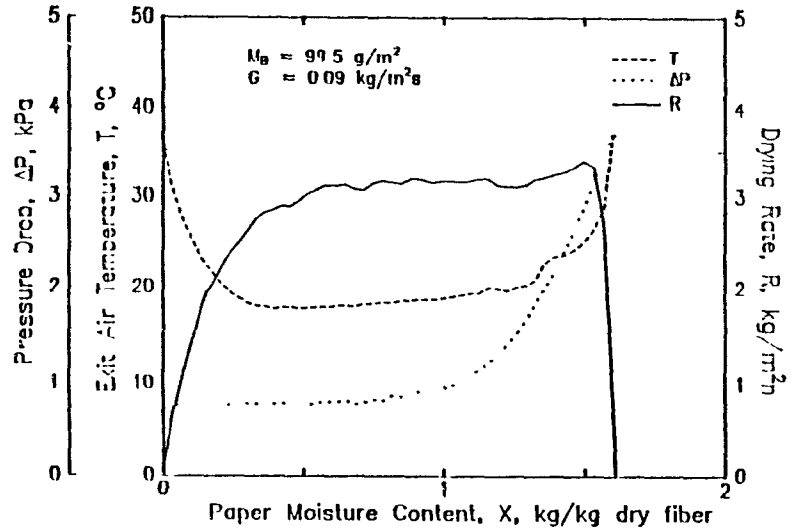
M_B = 99.5 g/m²
G = 0.09 kg/m²s
T
ΔP
R
Pressure Drop, ΔP, kPa
Exit Air Temperature, T, °C
Drying Rate, R, kg/m²h
Paper Moisture Content, X, kg/kg dry fiber

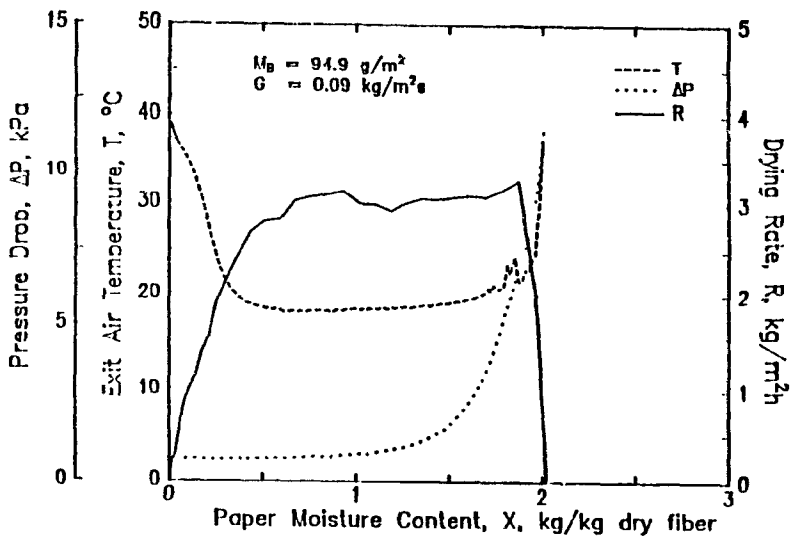
M_B = 94.9 g/m²
G = 0.09 kg/m²s
T
ΔP
R
Pressure Drop, ΔP, kPa
Exit Air Temperature, T, °C
Drying Rate, R, kg/m²h
Paper Moisture Content, X, kg/kg dry fiber

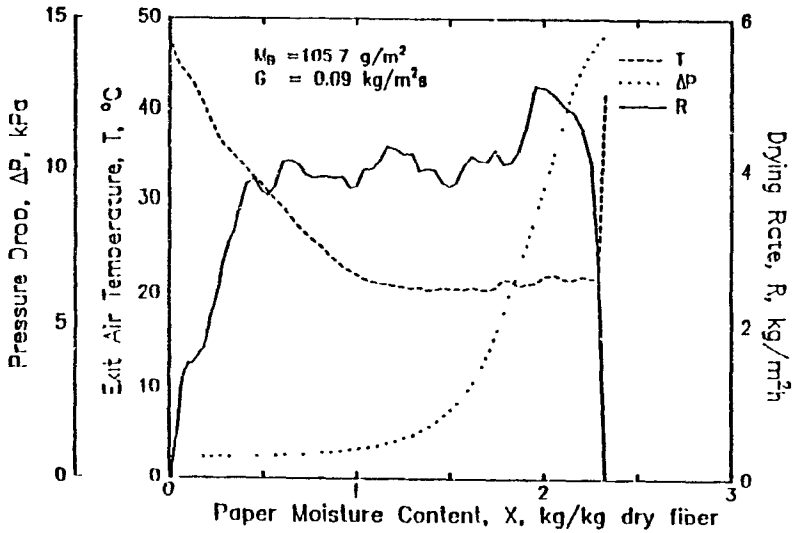
M_B = 105.7 g/m²
G = 0.09 kg/m²s
T
ΔP
R
Pressure Drop, ΔP, kPa
Exit Air Temperature, T, °C
Drying Rate, R, kg/m²h
Paper Moisture Content, X, kg/kg dry fiber

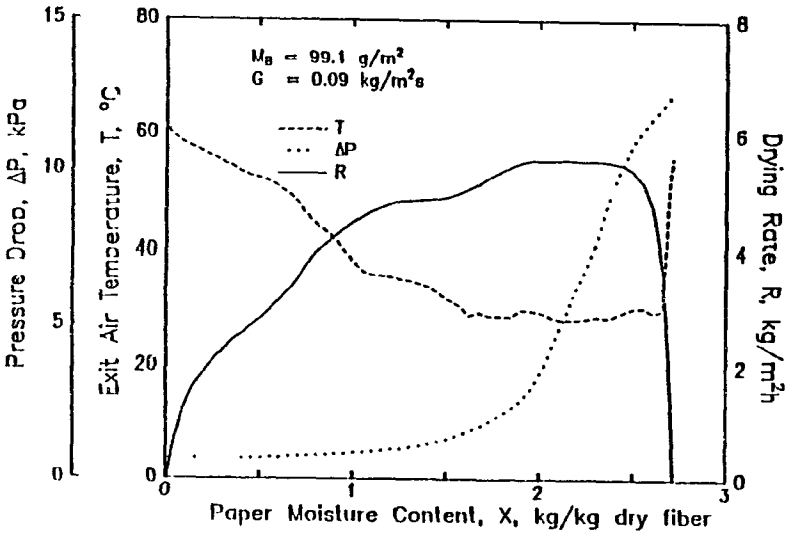
M_B = 99.1 g/m²
G = 0.09 kg/m²s
T
ΔP
R
Pressure Drop, ΔP, kPa
Exit Air Temperature, T, °C
Drying Rate, R, kg/m²h
Paper Moisture Content, X, kg/kg dry fiber

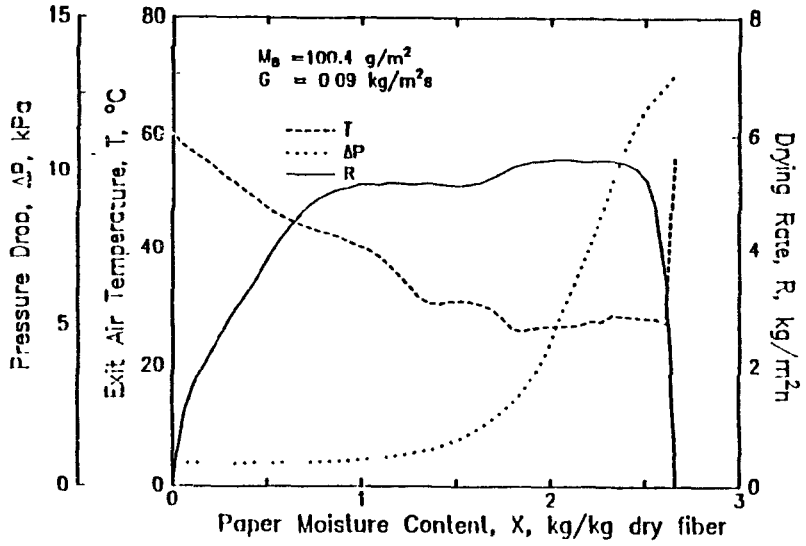
M_B =100.4 g/m²
G = 0.09 kg/m²s
T
ΔP
R
Pressure Drop, ΔP, kPa
Exit Air Temperature, T, °C
Drying Rate, R, kg/m²h
Paper Moisture Content, X, kg/kg dry fiber

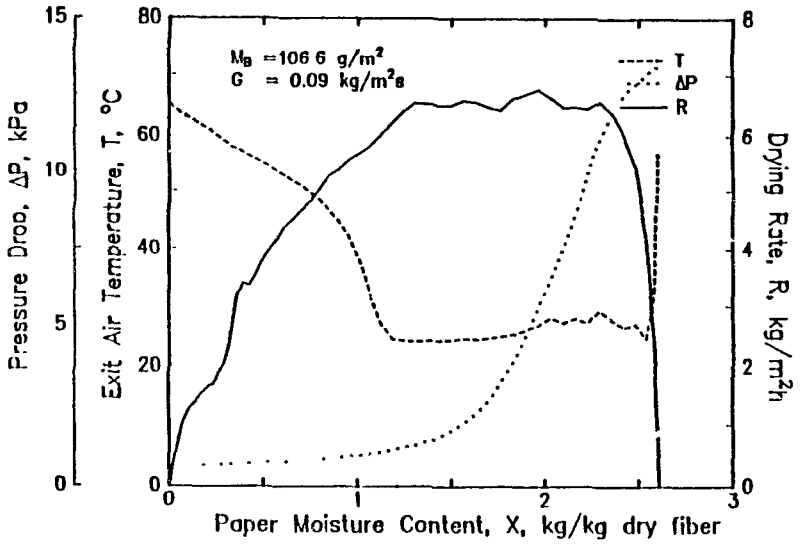
M_B =106.6 g/m²
G = 0.09 kg/m²s
T
ΔP
R
Pressure Drop, ΔP, kPa
Exit Air Temperature, T, °C
Drying Rate, R, kg/m²h
Paper Moisture Content, X, kg/kg dry fiber

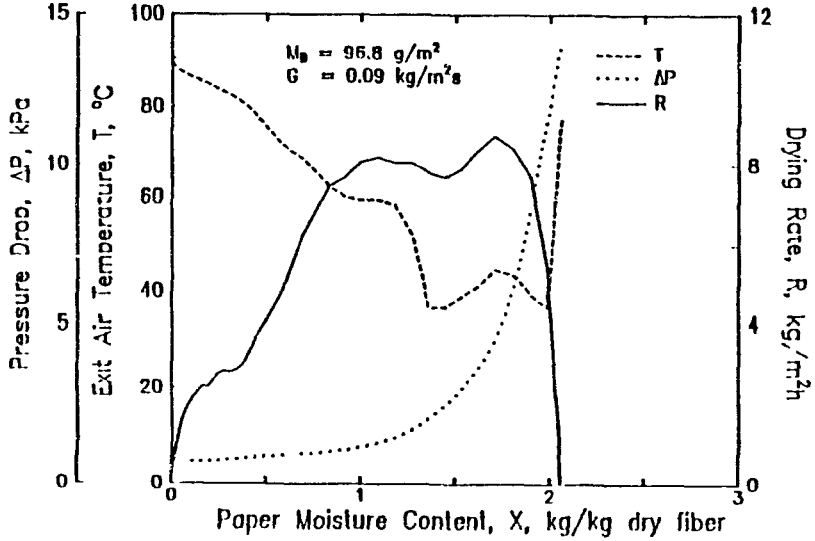
M_B = 96.8 g/m²
G = 0.09 kg/m²s
T
ΔP
R
Pressure Drop, ΔP, kPa
Exit Air Temperature, T, °C
Drying Rate, R, kg/m²h
Paper Moisture Content, X, kg/kg dry fiber

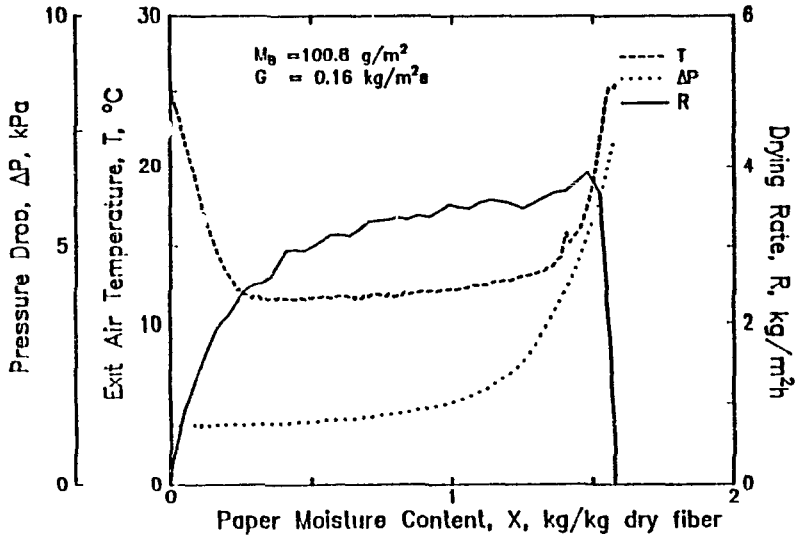
M_B =100.8 g/m²
G = 0.16 kg/m²s
T
ΔP
R
Pressure Drop, ΔP, kPa
Exit Air Temperature, T, °C
Drying Rate, R, kg/m²h
Paper Moisture Content, X, kg/kg dry fiber

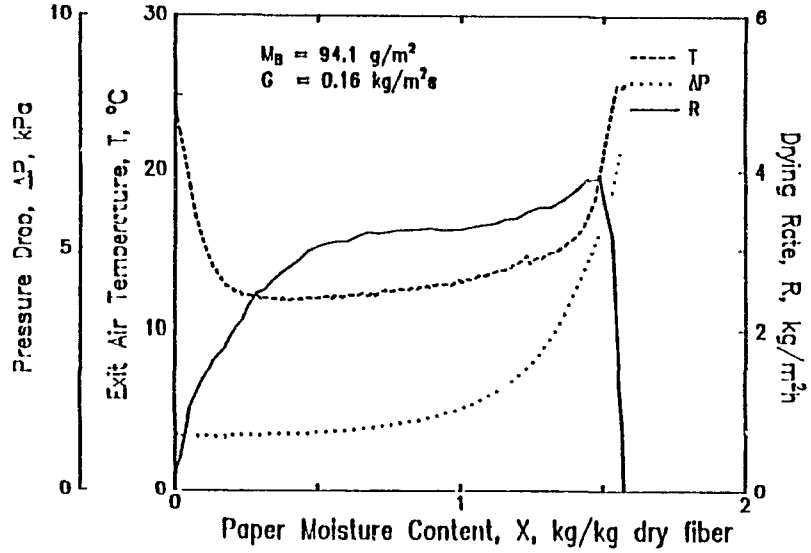
M_B = 94.1 g/m²
G = 0.16 kg/m²s
T
ΔP
R
Pressure Drop, ΔP, kPa
Exit Air Temperature, T, °C
Drying Rate, R, kg/m²h
Paper Moisture Content, X, kg/kg dry fiber

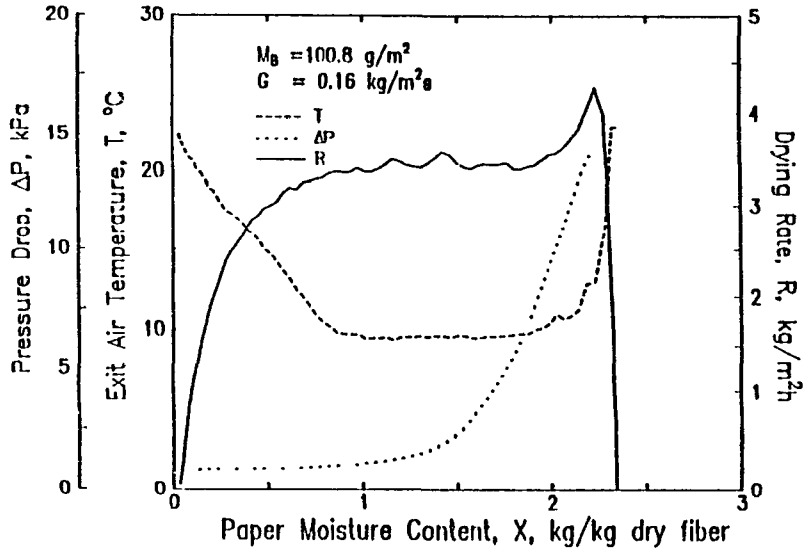
M_B =100.8 g/m²
G = 0.16 kg/m²s
T
ΔP
R
Pressure Drop, ΔP, kPa
Exit Air Temperature, T, °C
Drying Rate, R, kg/m²h
Paper Moisture Content, X, kg/kg dry fiber

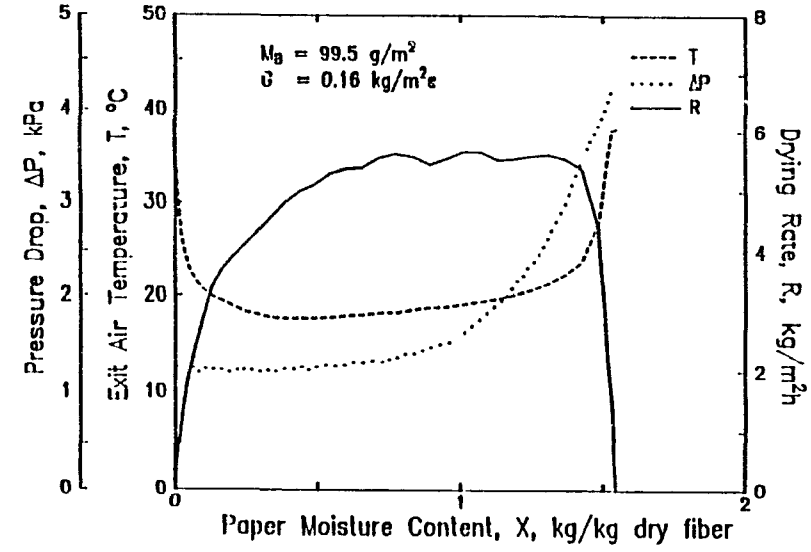
M_B = 99.5 g/m²
G = 0.16 kg/m²s
T
ΔP
R
Pressure Drop, ΔP, kPa
Exit Air Temperature, T, °C
Drying Rate, R, kg/m²h
Paper Moisture Content, X, kg/kg dry fiber

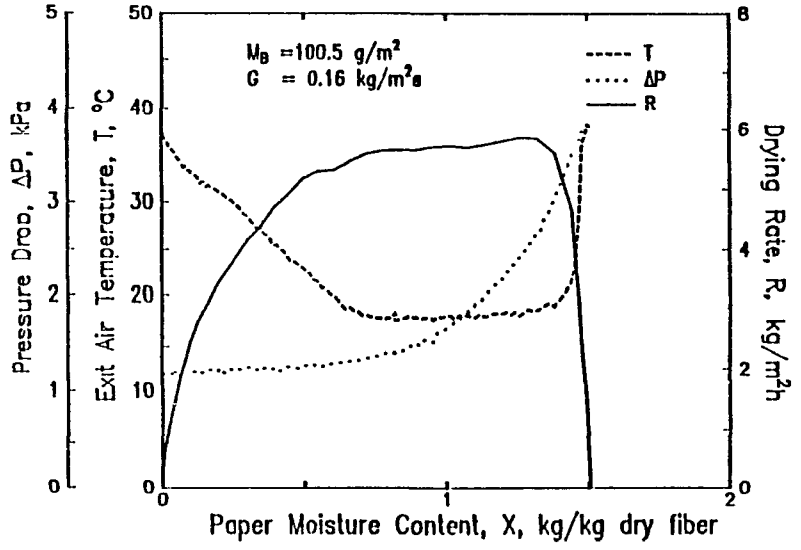
M_B =100.5 g/m²
G = 0.16 kg/m²s
T
ΔP
R
Pressure Drop, ΔP, kPa
Exit Air Temperature, T, °C
Drying Rate, R, kg/m²h
Paper Moisture Content, X, kg/kg dry fiber

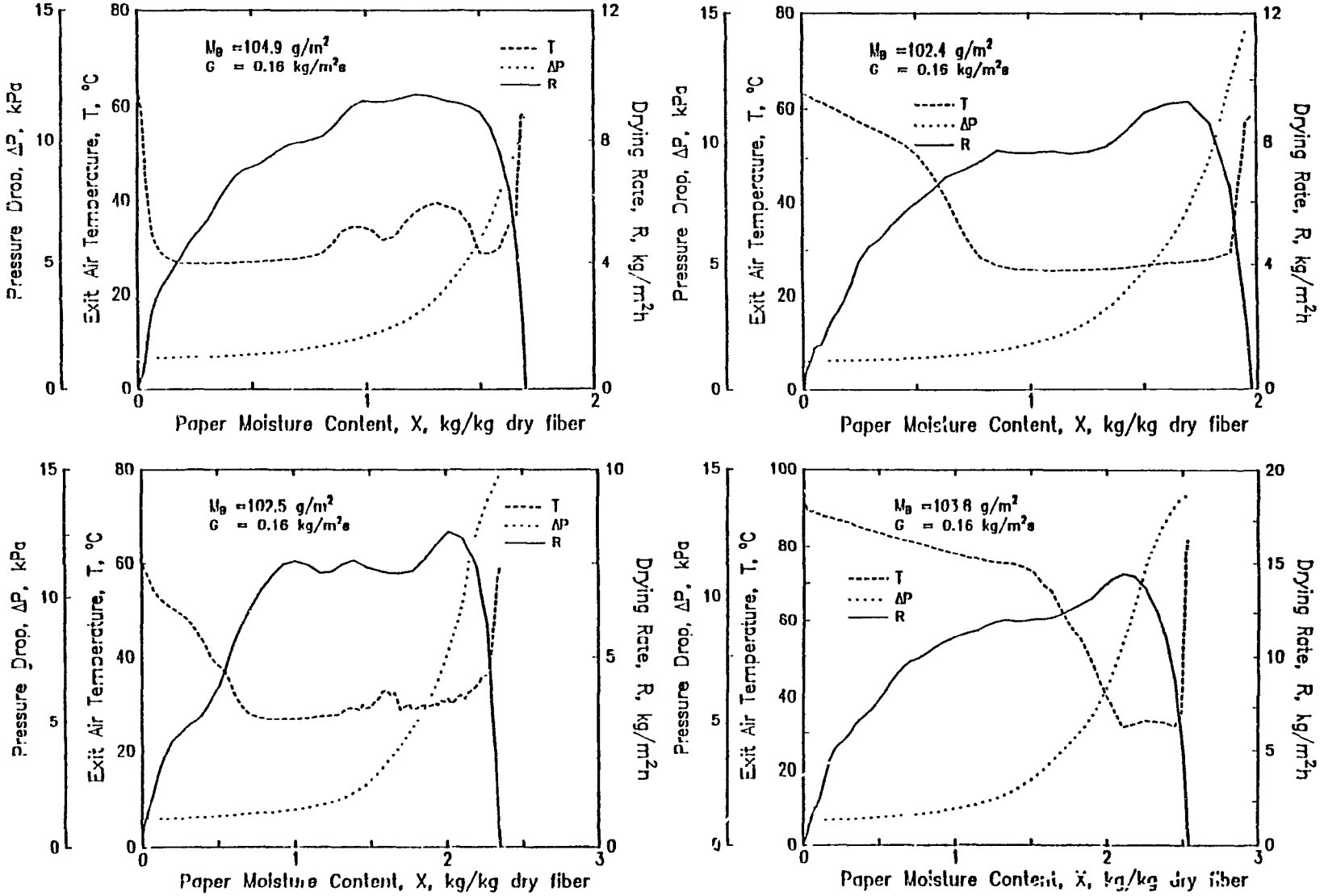
M_B =104.9 g/m²
G = 0.16 kg/m²s
T
ΔP
R
Pressure Drop, ΔP, kPa
Exit Air Temperature, T, °C
Drying Rate, R, kg/m²h
Paper Moisture Content, X, kg/kg dry fiber
M_B =102.4 g/m²
G = 0.16 kg/m²s
T
ΔP
R
Pressure Drop, ΔP, kPa
Exit Air Temperature, T, °C
Drying Rate, R, kg/m²h
Paper Moisture Content, X, kg/kg dry fiber
M_B =102.5 g/m²
G = 0.16 kg/m²s
T
ΔP
R
Pressure Drop, ΔP, kPa
Exit Air Temperature, T, °C
Drying Rate, R, kg/m²h
Paper Moisture Content, X, kg/kg dry fiber
M_B =103.8 g/m²
G = 0.16 kg/m²s
T
ΔP
R
Pressure Drop, ΔP, kPa
Exit Air Temperature, T, °C
Drying Rate, R, kg/m²h
Paper Moisture Content, X, kg/kg dry fiber

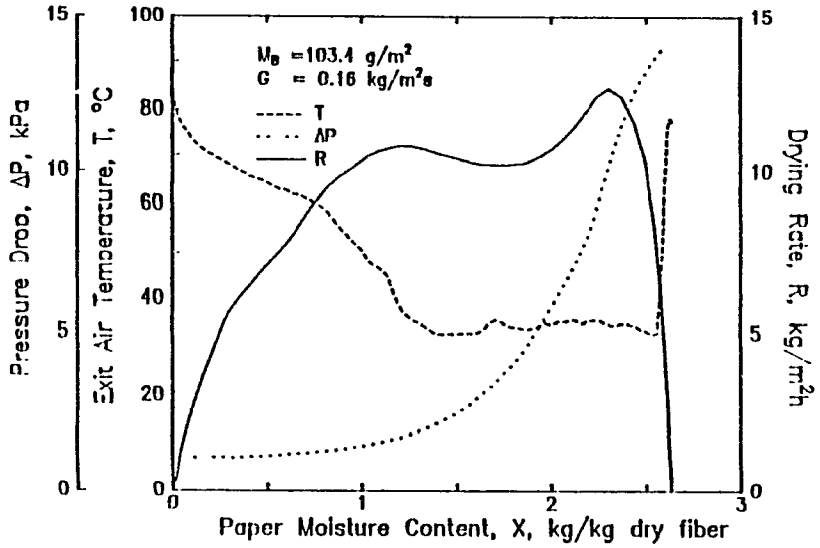
M_B =103.4 g/m²
G = 0.16 kg/m²s
T
ΔP
R
Pressure Drop, ΔP, kPa
Exit Air Temperature, T, °C
Drying Rate, R, kg/m²h
Paper Moisture Content, X, kg/kg dry fiber

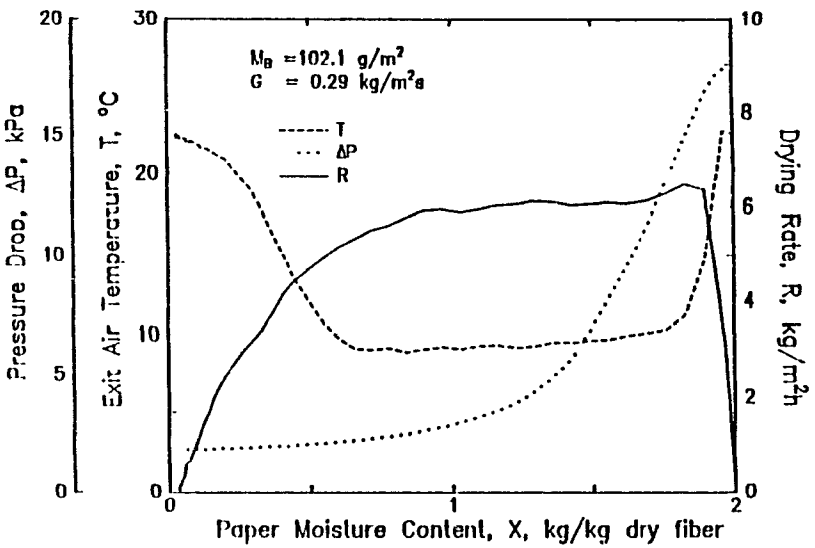
M_B =102.1 g/m²
G = 0.29 kg/m²s
T
ΔP
R
Pressure Drop, ΔP, kPa
Exit Air Temperature, T, °C
Drying Rate, R, kg/m²h
Paper Moisture Content, X, kg/kg dry fiber

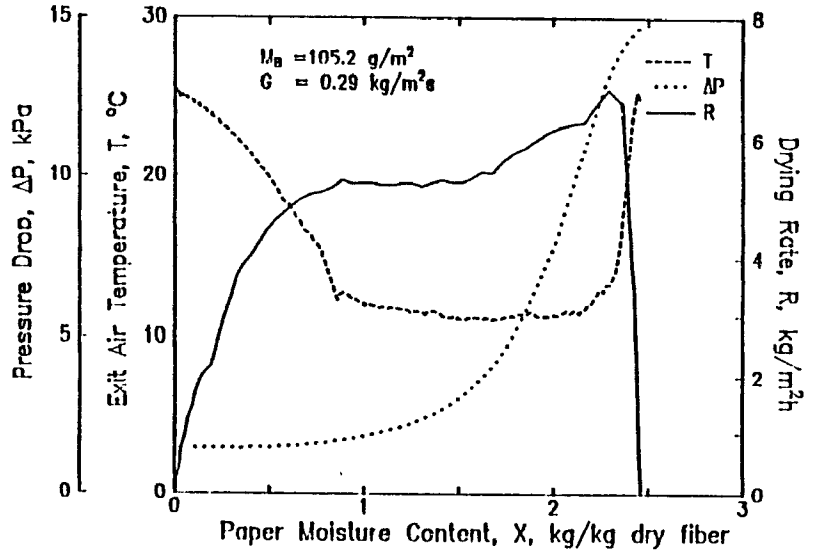
M_B =105.2 g/m²
G = 0.29 kg/m²s
T
ΔP
R
Pressure Drop, ΔP, kPa
Exit Air Temperature, T, °C
Drying Rate, R, kg/m²h
Paper Moisture Content, X, kg/kg dry fiber

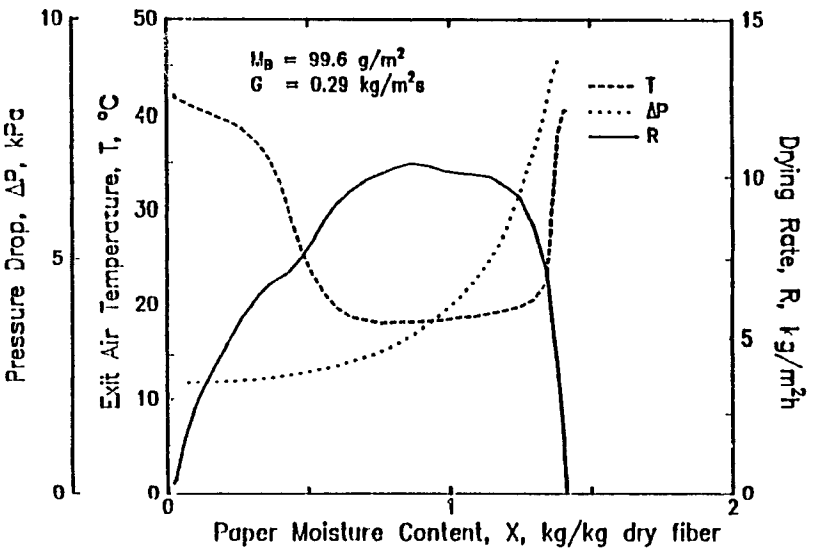
M_B = 99.6 g/m²
G = 0.29 kg/m²s
T
ΔP
R
Pressure Drop, ΔP, kPa
Exit Air Temperature, T, °C
Drying Rate, R, kg/m²h
Paper Moisture Content, X, kg/kg dry fiber

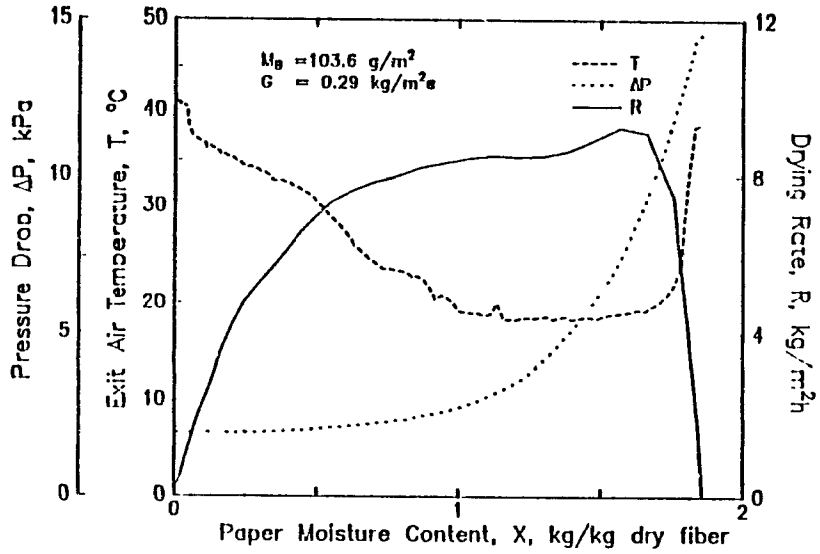
M_B =103.6 g/m²
G = 0.29 kg/m²s
T
ΔP
R
Pressure Drop, ΔP, kPa
Exit Air Temperature, T, °C
Drying Rate, R, kg/m²h
Paper Moisture Content, X, kg/kg dry fiber

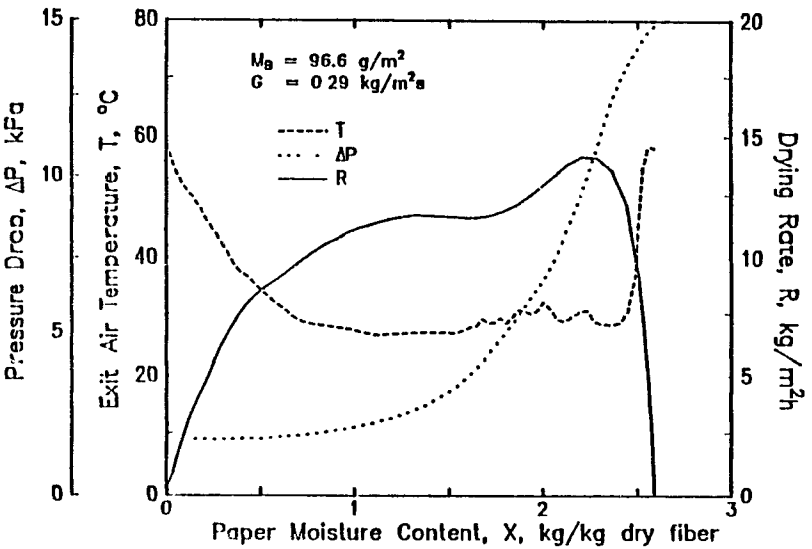
M_B = 96.6 g/m²
G = 0.29 kg/m²s
T
ΔP
R
Pressure Drop, ΔP, kPa
Exit Air Temperature, T, °C
Drying Rate, R, kg/m²h
Paper Moisture Content, X, kg/kg dry fiber

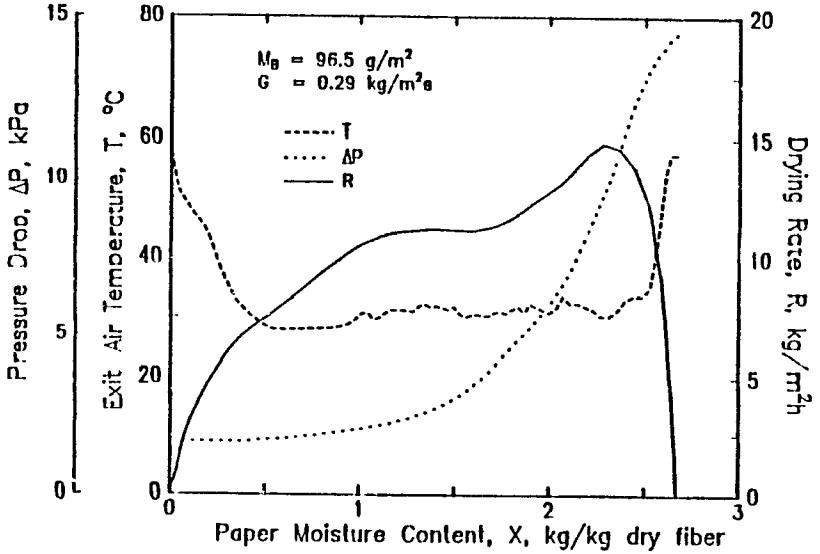
M_B = 96.5 g/m²
G = 0.29 kg/m²s
T
ΔP
R
Pressure Drop, ΔP, kPa
Exit Air Temperature, T, °C
Drying Rate, R, kg/m²h
Paper Moisture Content, X, kg/kg dry fiber

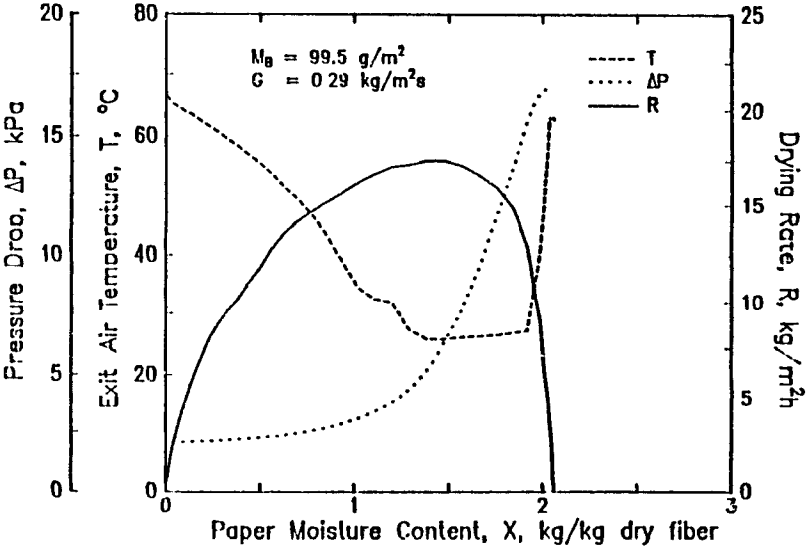
M_B = 99.5 g/m²
G = 0.29 kg/m²s
T
ΔP
R
Pressure Drop, ΔP, kPa
Exit Air Temperature, T, °C
Drying Rate, R, kg/m²h
Paper Moisture Content, X, kg/kg dry fiber

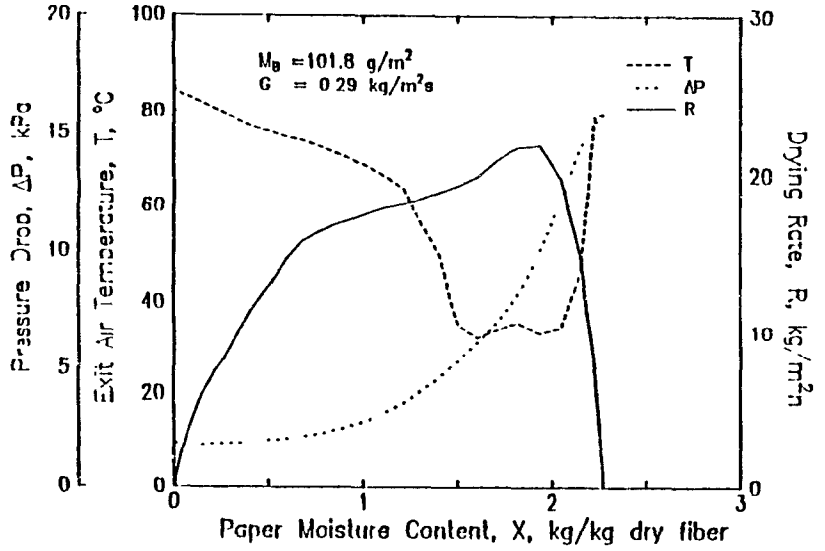
M_B =101.8 g/m²
G = 0.29 kg/m²s
T
ΔP
R
Pressure Drop, ΔP, kPa
Exit Air Temperature, T, °C
Drying Rate, R, kg/m²h
Paper Moisture Content, X, kg/kg dry fiber

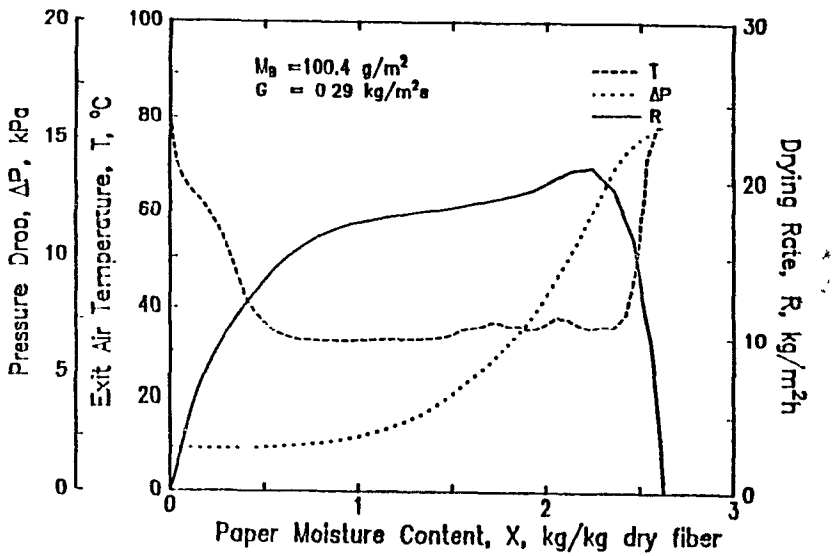
M_B =100.4 g/m²
G = 0.29 kg/m²s
T
ΔP
R
Pressure Drop, ΔP, kPa
Exit Air Temperature, T, °C
Drying Rate, R, kg/m²h
Paper Moisture Content, X, kg/kg dry fiber

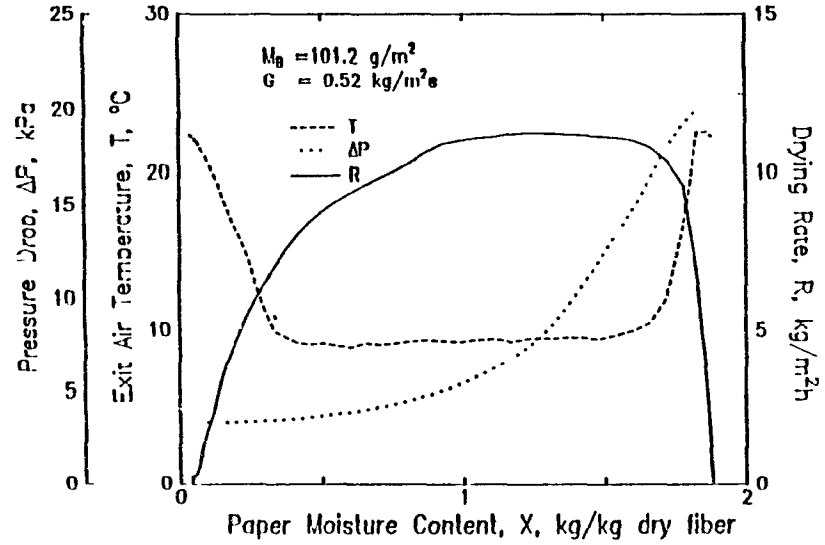
M_B =101.2 g/m²
G = 0.52 kg/m²s
T
ΔP
R
Pressure Drop, ΔP, kPa
Exit Air Temperature, T, °C
Drying Rate, R, kg/m²h
Paper Moisture Content, X, kg/kg dry fiber

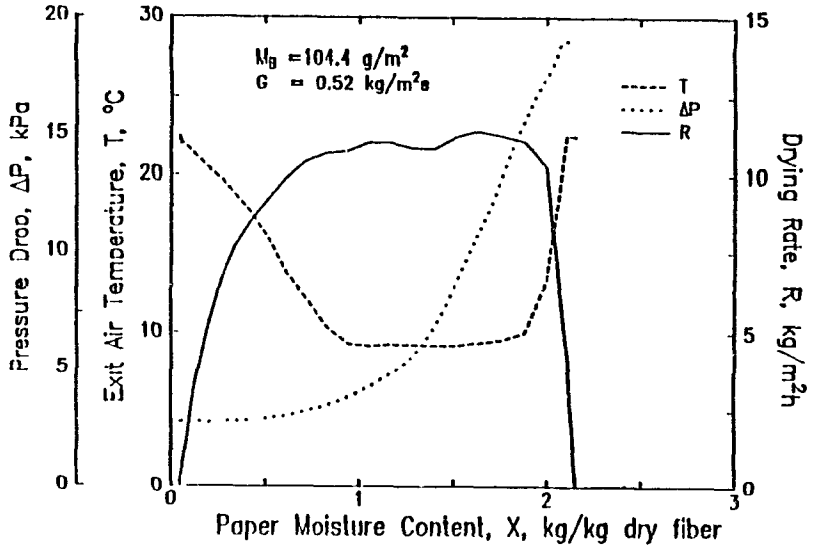
M_B =104.4 g/m²
G = 0.52 kg/m²s
T
ΔP
R
Pressure Drop, ΔP, kPa
Exit Air Temperature, T, °C
Drying Rate, R, kg/m²h
Paper Moisture Content, X, kg/kg dry fiber

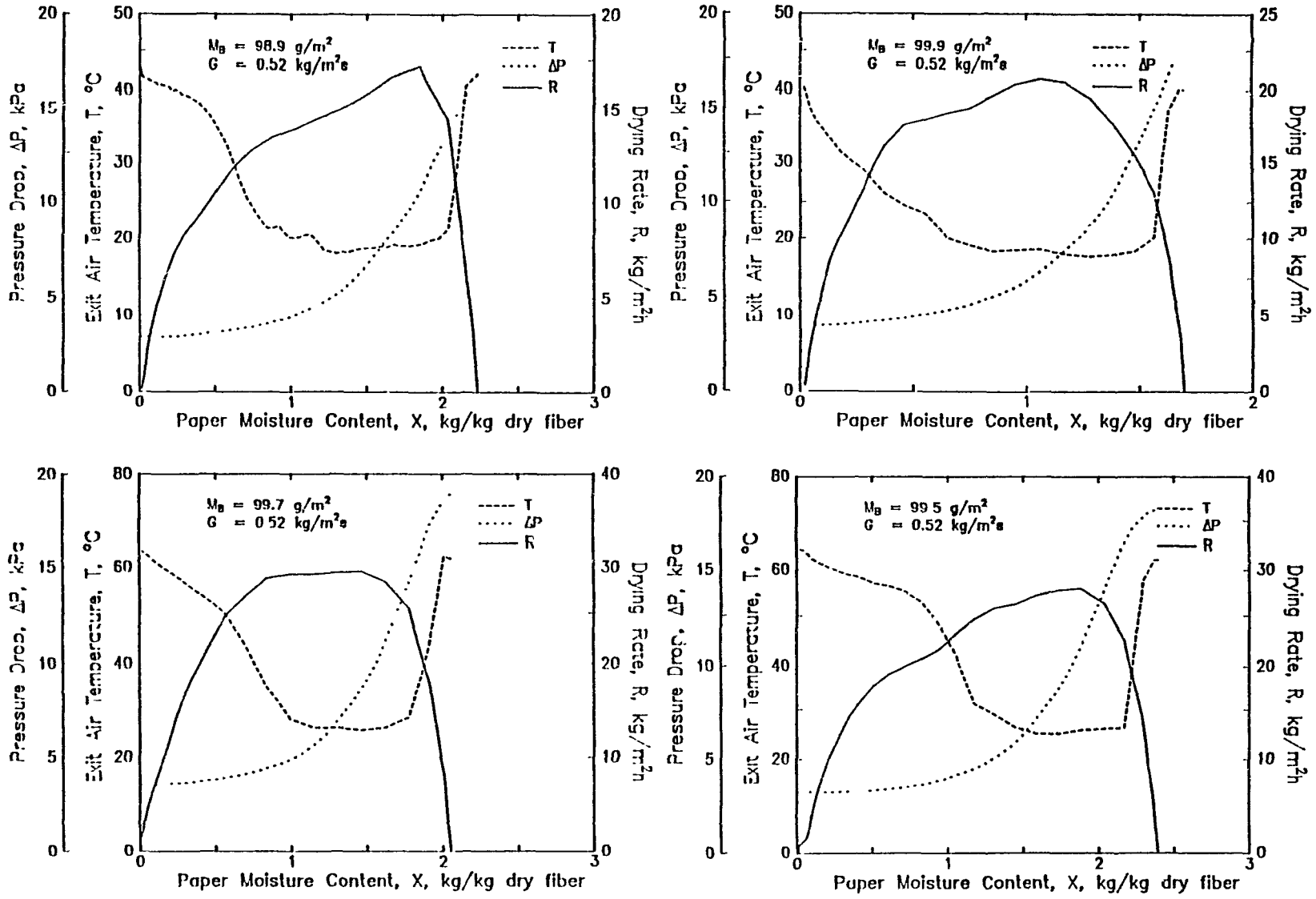
M_B = 98.9 g/m²
G = 0.52 kg/m²s
T
ΔP
R
Pressure Drop, ΔP, kPa
Exit Air Temperature, T, °C
Drying Rate, R, kg/m²h
Paper Moisture Content, X, kg/kg dry fiber
M_B = 99.9 g/m²
G = 0.52 kg/m²s
T
ΔP
R
Pressure Drop, ΔP, kPa
Exit Air Temperature, T, °C
Drying Rate, R, kg/m²h
Paper Moisture Content, X, kg/kg dry fiber
M_B = 99.7 g/m²
G = 0.52 kg/m²s
T
ΔP
R
Pressure Drop, ΔP, kPa
Exit Air Temperature, T, °C
Drying Rate, R, kg/m²h
Paper Moisture Content, X, kg/kg dry fiber
M_B = 99.5 g/m²
G = 0.52 kg/m²s
T
ΔP
R
Pressure Drop, ΔP, kPa
Exit Air Temperature, T, °C
Drying Rate, R, kg/m²h
Paper Moisture Content, X, kg/kg dry fiber

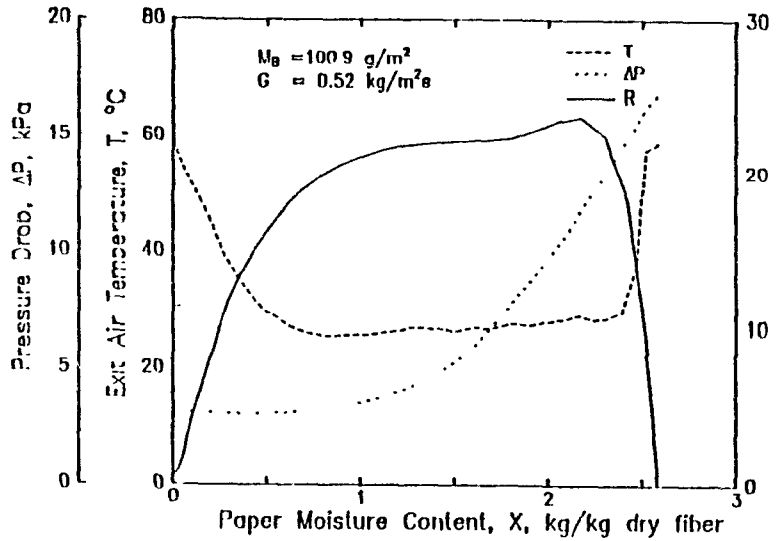
M_B =100 9 g/m²
G = 0.52 kg/m²s
T
ΔP
R
Pressure Drop, ΔP, kPa
Exit Air Temperature, T, °C
Drying Rate, R, kg/m²h
Paper Moisture Content, X, kg/kg dry fiber

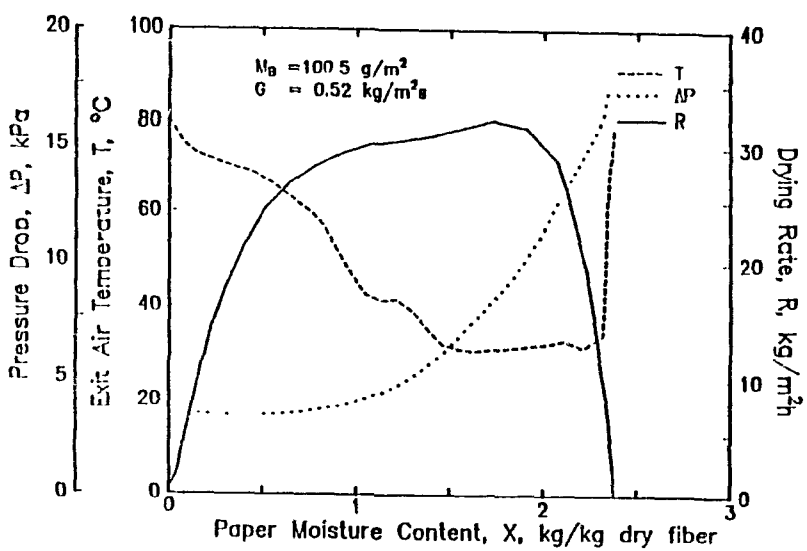
M_B =100 5 g/m²
G = 0.52 kg/m²s
T
ΔP
R
Pressure Drop, ΔP, kPa
Exit Air Temperature, T, °C
Drying Rate, R, kg/m²h
Paper Moisture Content, X, kg/kg dry fiber

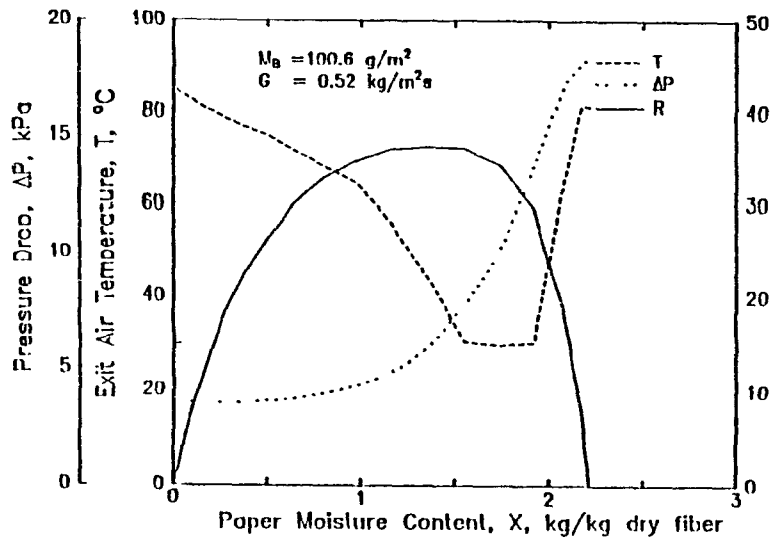
M_B =100.6 g/m²
G = 0.52 kg/m²s
T
ΔP
R
Pressure Drop, ΔP, kPa
Exit Air Temperature, T, °C
Drying Rate, R, kg/m²h
Paper Moisture Content, X, kg/kg dry fiber

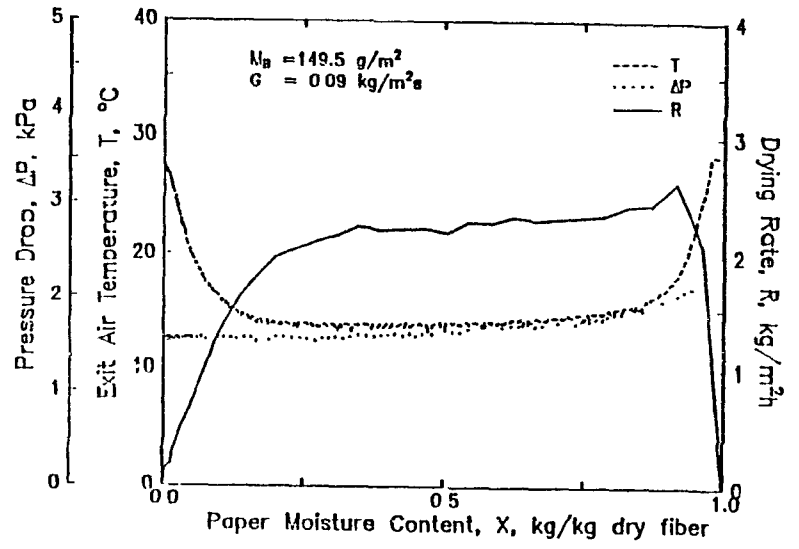
M_B =149.5 g/m²
G = 0 09 kg/m²s
T
ΔP
R
Pressure Drop, ΔP, kPa
Exit Air Temperature, T, °C
Drying Rate, R, kg/m²h
Paper Moisture Content, X, kg/kg dry fiber

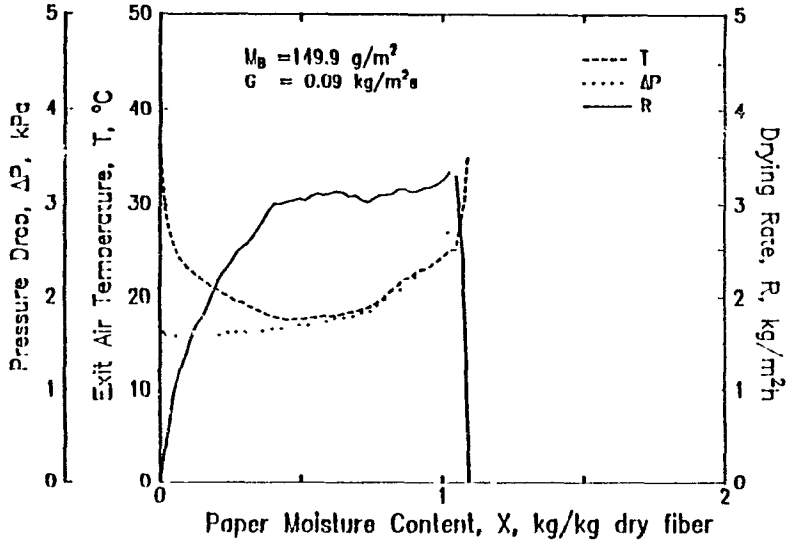
M_B =149.9 g/m²
G = 0.09 kg/m²s
T
ΔP
R
Pressure Drop, ΔP, kPa
Exit Air Temperature, T, °C
Drying Rate, R, kg/m²h
Paper Moisture Content, X, kg/kg dry fiber

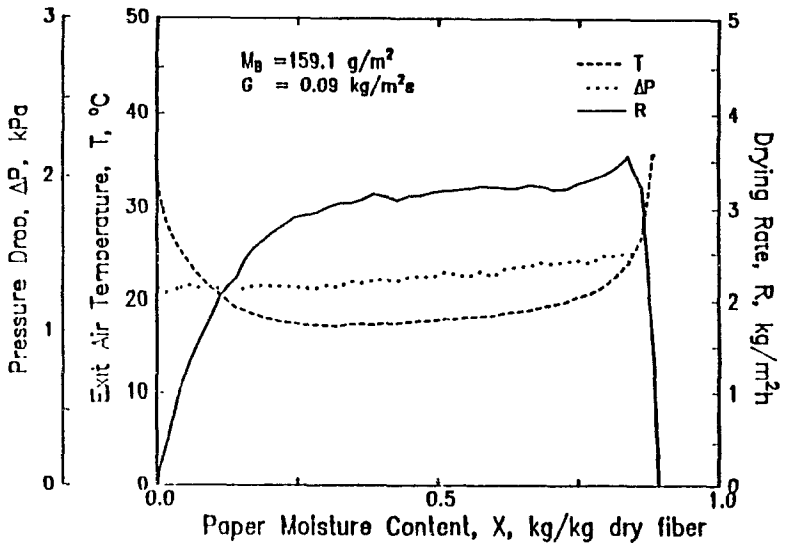
M_B =159.1 g/m²
G = 0.09 kg/m²s
T
ΔP
R
Pressure Drop, ΔP, kPa
Exit Air Temperature, T, °C
Drying Rate, R, kg/m²h
Paper Moisture Content, X, kg/kg dry fiber

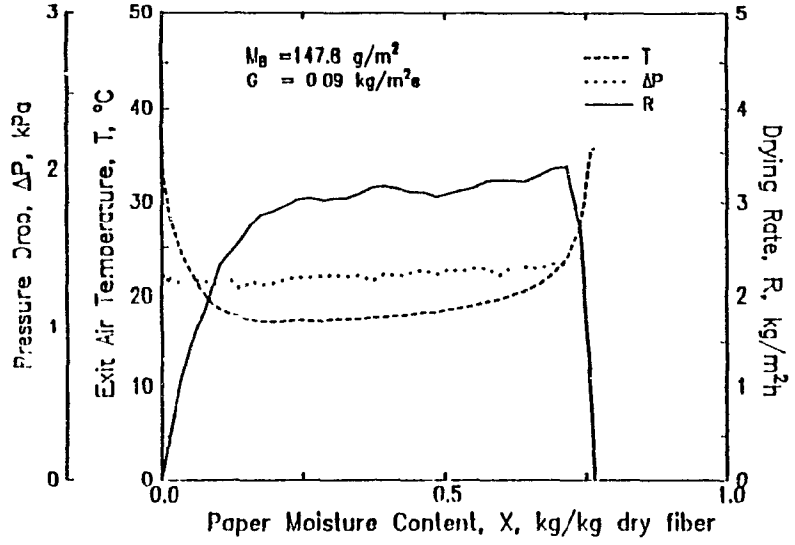
M_B =147.6 g/m²
G = 0.09 kg/m²s
T
ΔP
R
Pressure Drop, ΔP, kPa
Exit Air Temperature, T, °C
Drying Rate, R, kg/m²h
Paper Moisture Content, X, kg/kg dry fiber

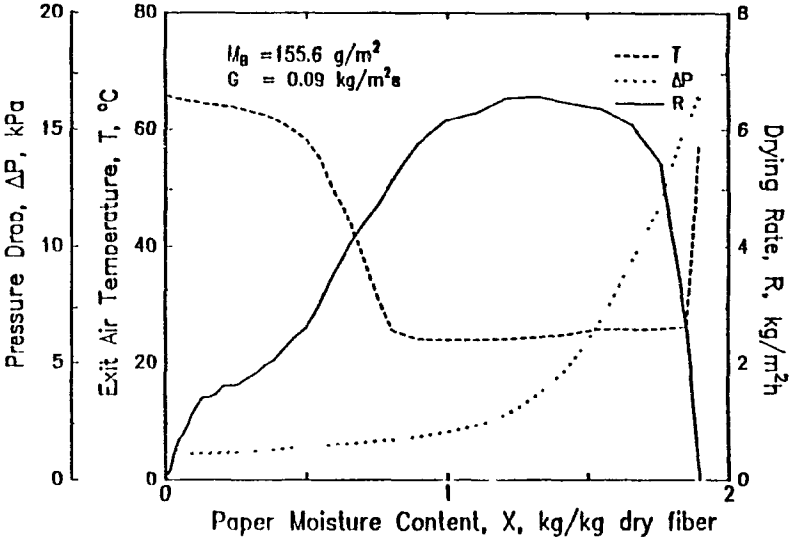
M_B =155.6 g/m²
G = 0.09 kg/m²s
T
ΔP
R
Pressure Drop, ΔP, kPa
Exit Air Temperature, T, °C
Drying Rate, R, kg/m²h
Paper Moisture Content, X, kg/kg dry fiber

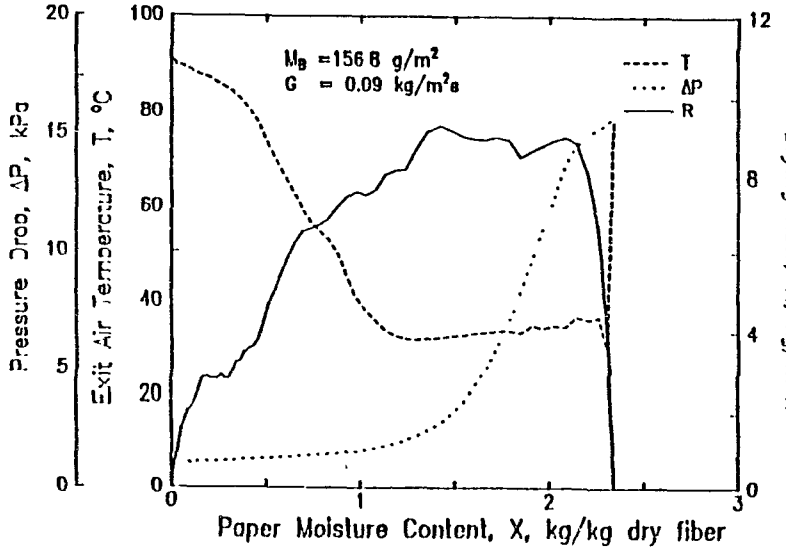
M_B =156.8 g/m²
G = 0.09 kg/m²s
T
ΔP
R
Pressure Drop, ΔP, kPa
Exit Air Temperature, T, °C
Drying Rate, R, kg/m²h
Paper Moisture Content, X, kg/kg dry fiber

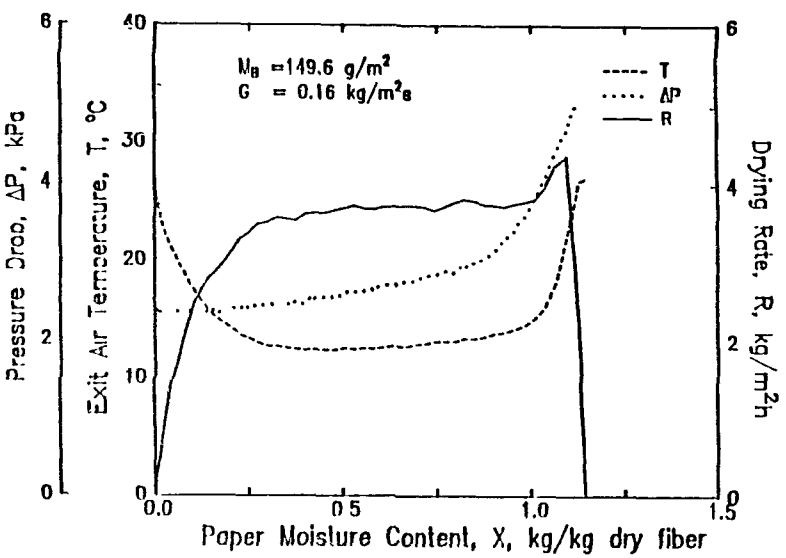
M_B =149.6 g/m²
G = 0.16 kg/m²s
T
ΔP
R
Pressure Drop, ΔP, kPa
Exit Air Temperature, T, °C
Drying Rate, R, kg/m²h
Paper Moisture Content, X, kg/kg dry fiber

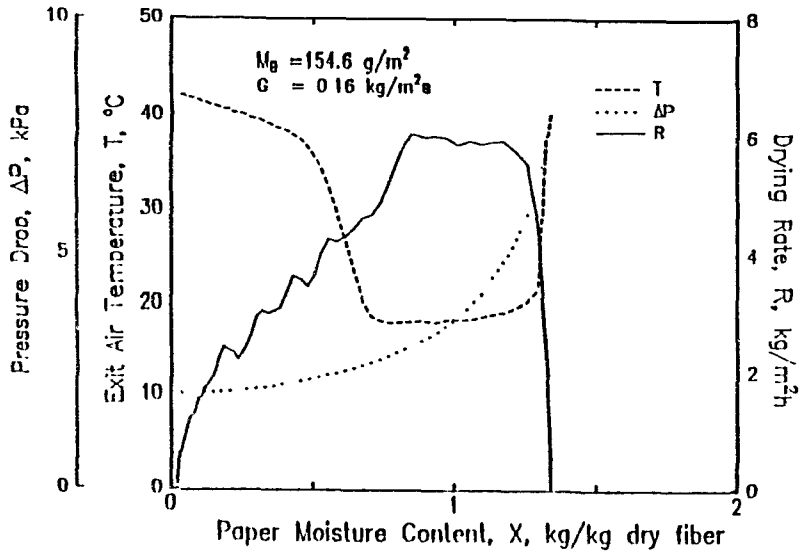
M_B =154.6 g/m²
G = 0.16 kg/m²s
T
ΔP
R
Pressure Drop, ΔP, kPa
Exit Air Temperature, T, °C
Drying Rate, R, kg/m²h
Paper Moisture Content, X, kg/kg dry fiber

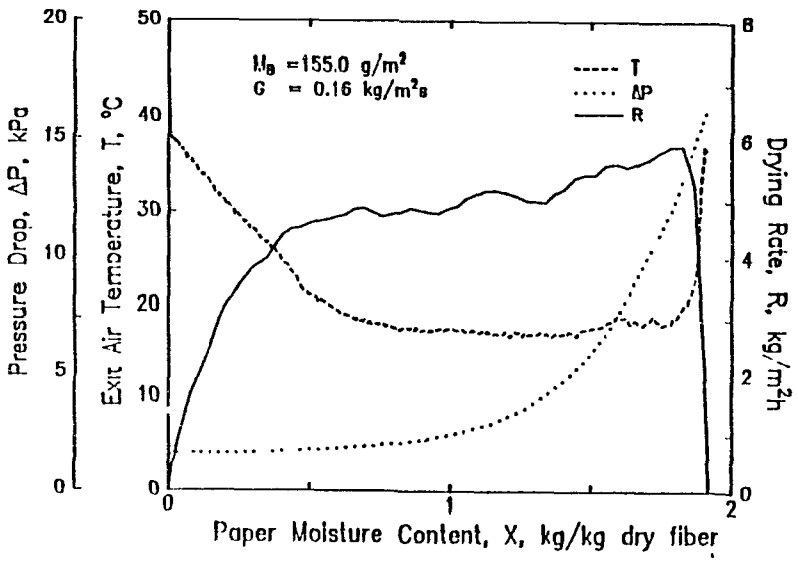
M_B =155.0 g/m²
G = 0.16 kg/m²s
T
ΔP
R
Pressure Drop, ΔP, kPa
Exit Air Temperature, T, °C
Drying Rate, R, kg/m²h
Paper Moisture Content, X, kg/kg dry fiber

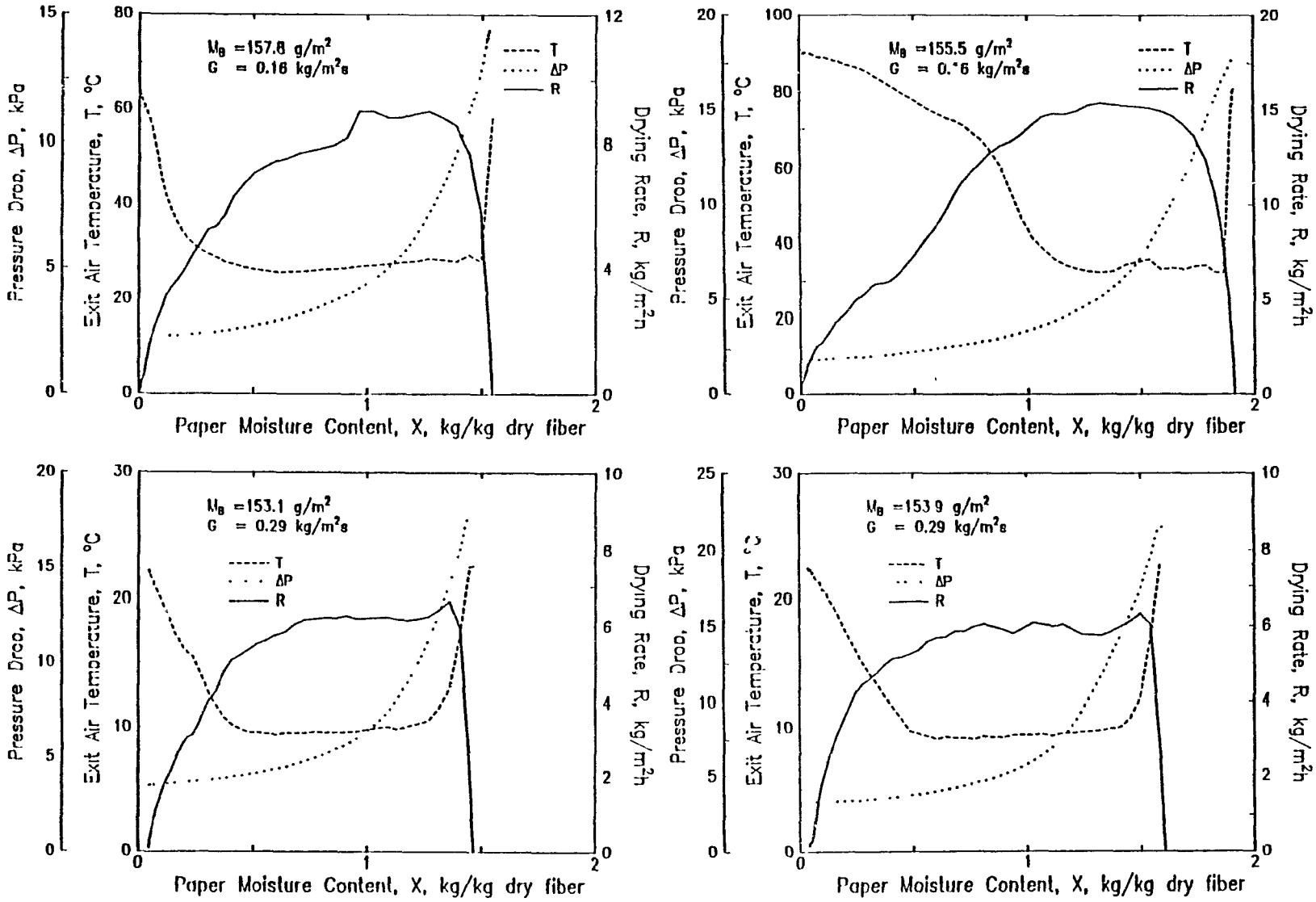
M_B =157.8 g/m²
G = 0.16 kg/m²s
T
ΔP
R
Pressure Drop, ΔP, kPa
Exit Air Temperature, T, °C
Drying Rate, R, kg/m²h
Paper Moisture Content, X, kg/kg dry fiber
M_B =155.5 g/m²
G = 0.16 kg/m²s
M_B =153.1 g/m²
G = 0.29 kg/m²s
M_B =153.9 g/m²
G = 0.29 kg/m²s

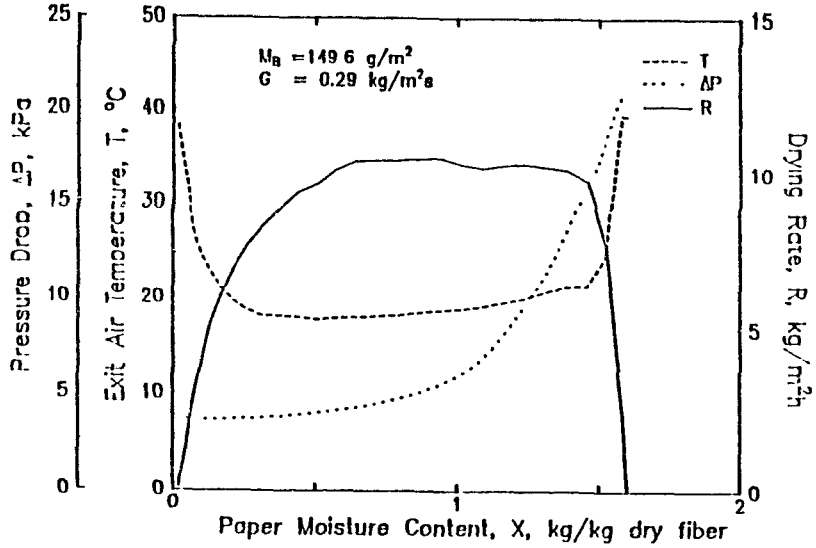
M_B =149.6 g/m²
G = 0.29 kg/m²s
T
ΔP
R
Pressure Drop, ΔP, kPa
Exit Air Temperature, T, °C
Drying Rate, R, kg/m²h
Paper Moisture Content, X, kg/kg dry fiber

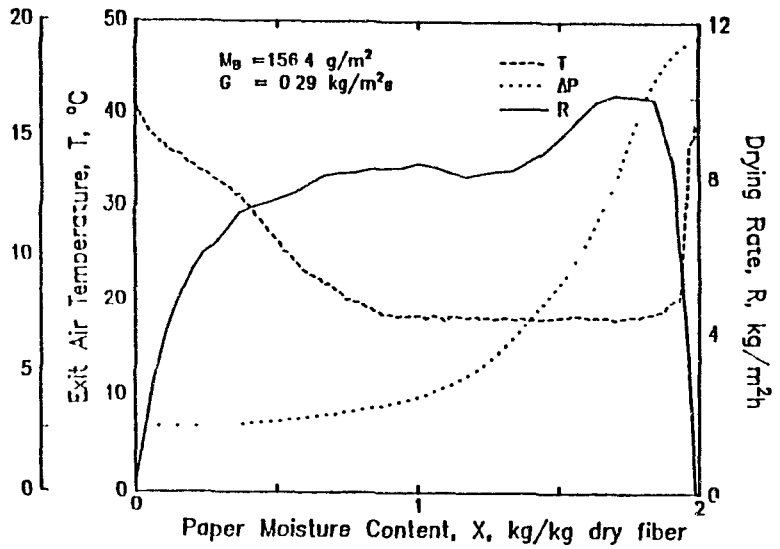
M_B =156.4 g/m²
G = 0.29 kg/m²s
T
ΔP
R
Pressure Drop, ΔP, kPa
Exit Air Temperature, T, °C
Drying Rate, R, kg/m²h
Paper Moisture Content, X, kg/kg dry fiber

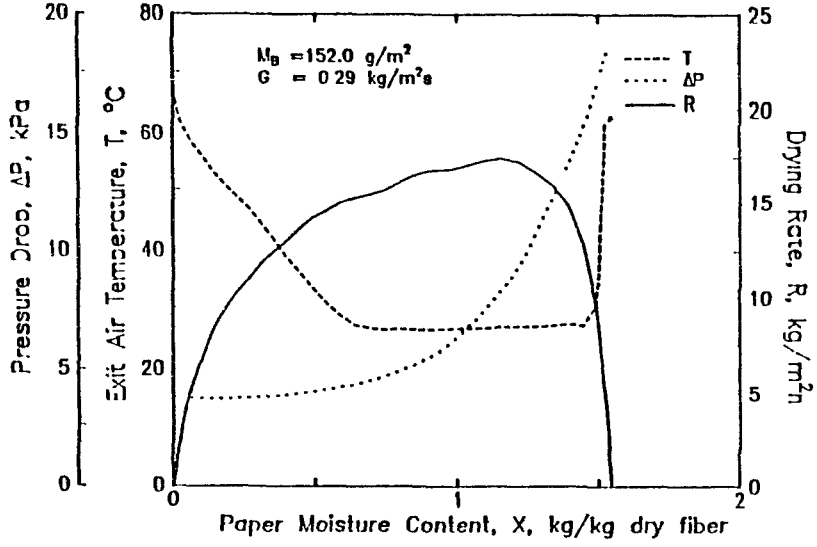
M_B =152.0 g/m²
G = 0.29 kg/m²s
T
ΔP
R
Pressure Drop, ΔP, kPa
Exit Air Temperature, T, °C
Drying Rate, R, kg/m²h
Paper Moisture Content, X, kg/kg dry fiber

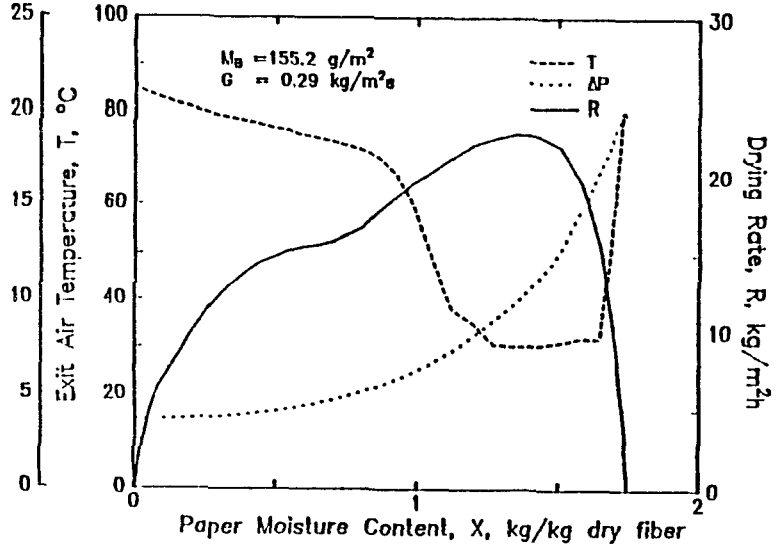
M_B =155.2 g/m²
G = 0.29 kg/m²s
T
ΔP
R
Pressure Drop, ΔP, kPa
Exit Air Temperature, T, °C
Drying Rate, R, kg/m²h
Paper Moisture Content, X, kg/kg dry fiber

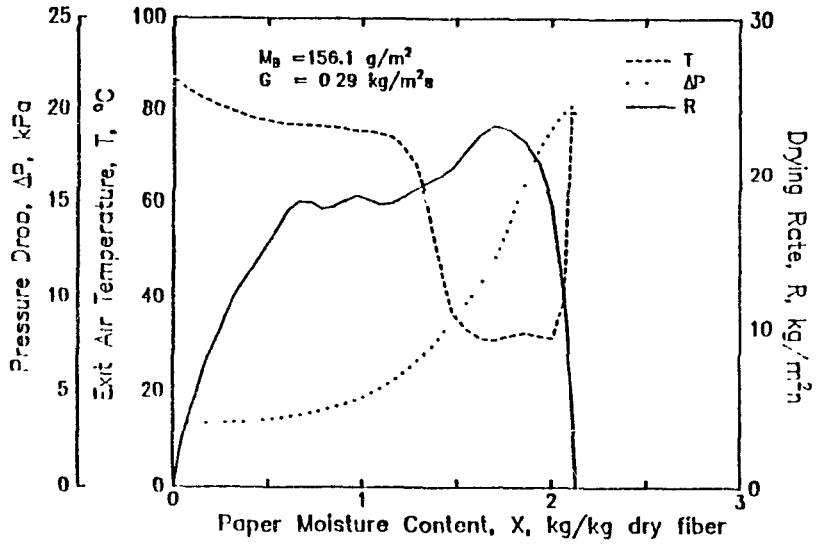
M_B =156.1 g/m²
G = 0.29 kg/m²s
T
ΔP
R
Pressure Drop, ΔP, kPa
Exit Air Temperature, T, °C
Drying Rate, R, kg/m²h
Paper Moisture Content, X, kg/kg dry fiber

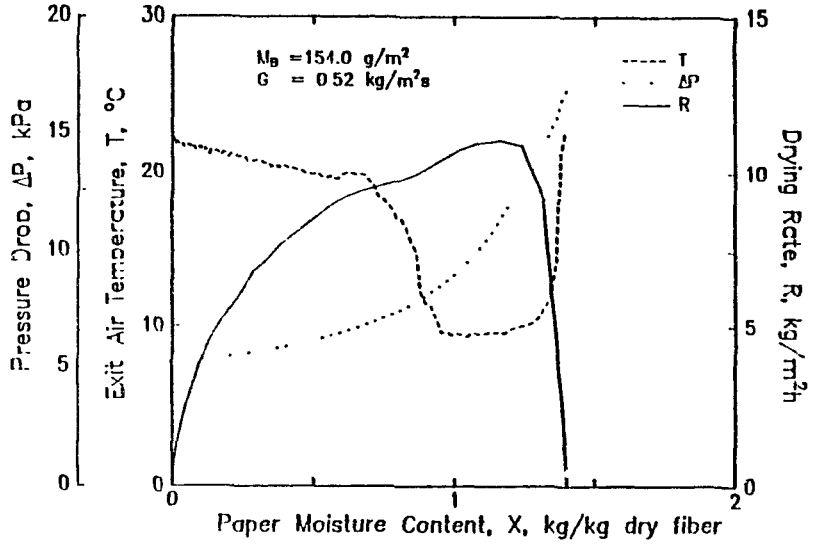
M_B =154.0 g/m²
G = 0.52 kg/m²s
T
ΔP
R
Pressure Drop, ΔP, kPa
Exit Air Temperature, T, °C
Drying Rate, R, kg/m²h
Paper Moisture Content, X, kg/kg dry fiber

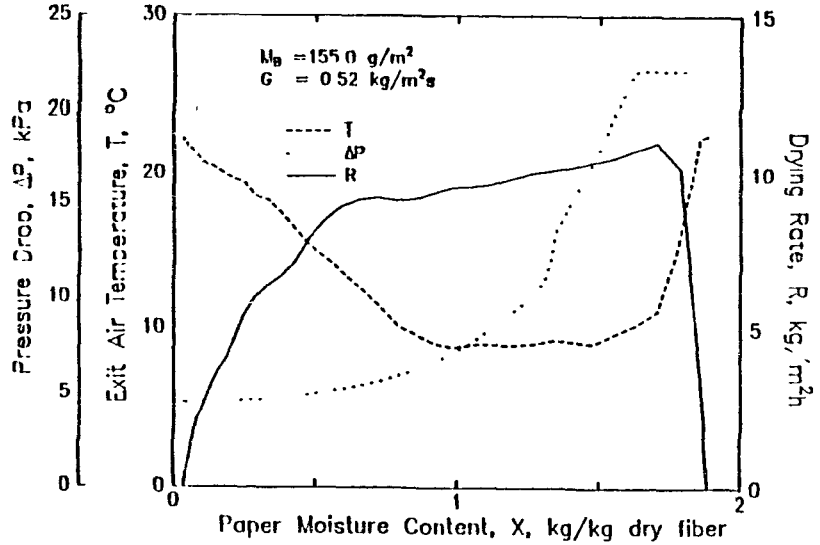
M_B =155.0 g/m²
G = 0.52 kg/m²s
T
ΔP
R
Pressure Drop, ΔP, kPa
Exit Air Temperature, T, °C
Drying Rate, R, kg/m²h
Paper Moisture Content, X, kg/kg dry fiber

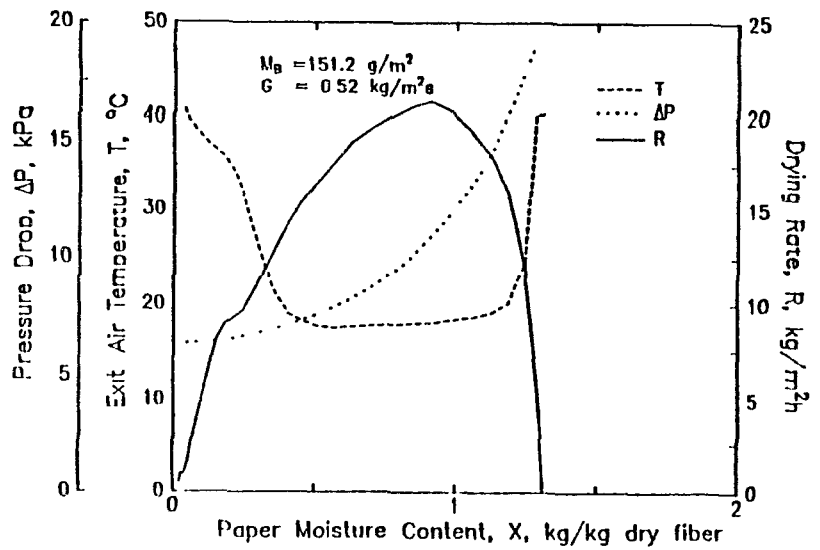
M_B =151.2 g/m²
G = 0.52 kg/m²s
T
ΔP
R
Pressure Drop, ΔP, kPa
Exit Air Temperature, T, °C
Drying Rate, R, kg/m²h
Paper Moisture Content, X, kg/kg dry fiber

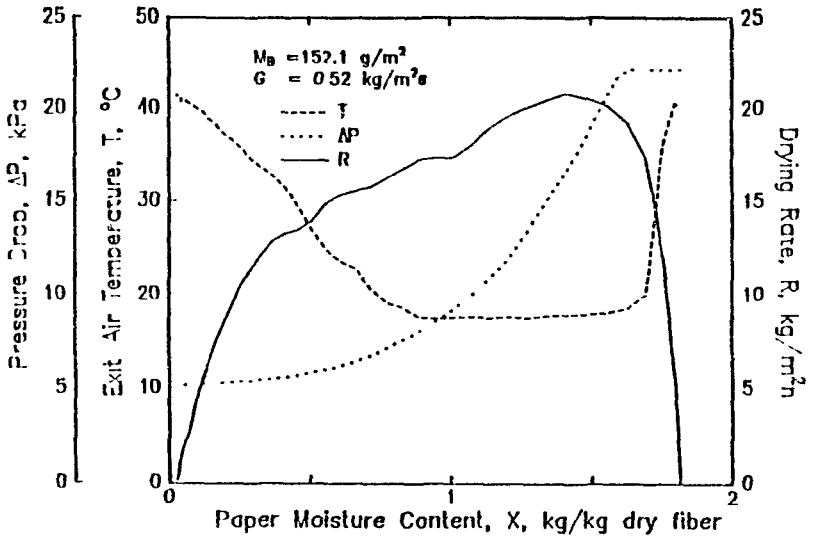
M_B =152.1 g/m²
G = 0.52 kg/m²s
T
ΔP
R
Pressure Drop, ΔP, kPa
Exit Air Temperature, T, °C
Drying Rate, R, kg/m²h
Paper Moisture Content, X, kg/kg dry fiber

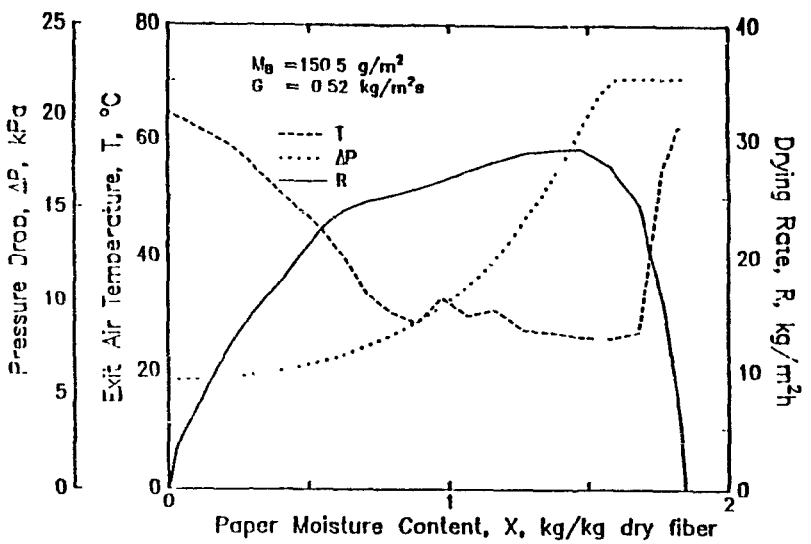
M_B =150.5 g/m²
G = 0.52 kg/m²s
T
ΔP
R
Pressure Drop, ΔP, kPa
Exit Air Temperature, T, °C
Drying Rate, R, kg/m²h
Paper Moisture Content, X, kg/kg dry fiber

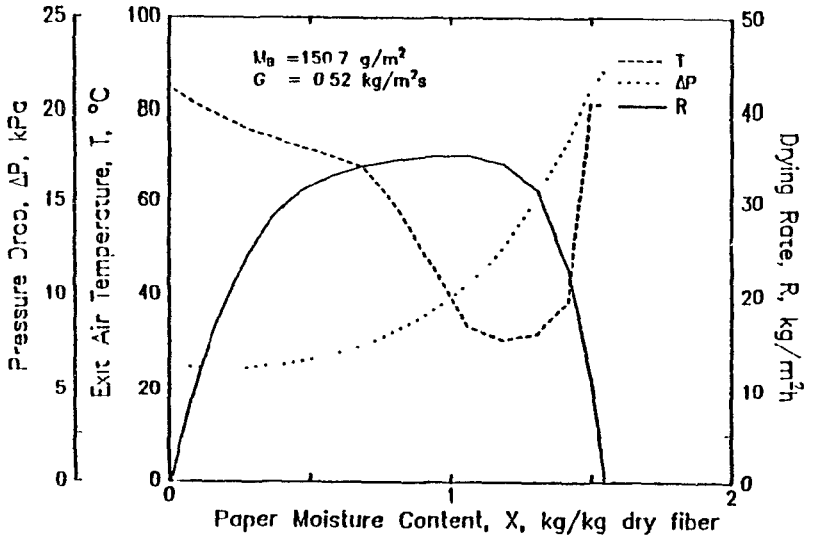
M_B =150.7 g/m²
G = 0.52 kg/m²s
T
ΔP
R
Pressure Drop, ΔP, kPa
Exit Air Temperature, T, °C
Drying Rate, R, kg/m²h
Paper Moisture Content, X, kg/kg dry fiber

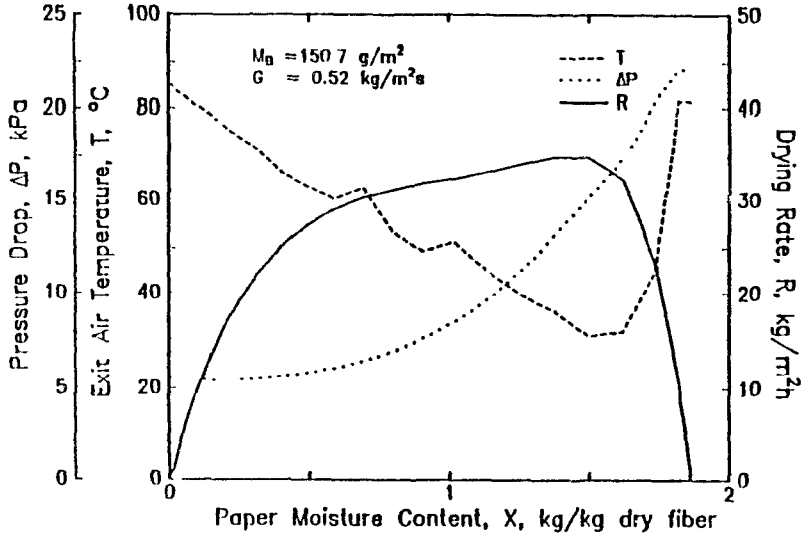
M_B =150.7 g/m²
G = 0.52 kg/m²s
T
ΔP
R
Pressure Drop, ΔP, kPa
Exit Air Temperature, T, °C
Drying Rate, R, kg/m²h
Paper Moisture Content, X, kg/kg dry fiber

APPENDIX 9

ALGORITHM OF THE THROUGH DRYING MODEL